ABSTRACT

Title of Document: LARGE-SCALE CONTROLLED-CONDITION EXPERIMENT TO EVALUATE LIGHT WEIGHT DEFLECTOMETERS FOR MODULUS DETERMINATION AND COMPACTION QUALITY ASSURANCE OF UNBOUND PAVEMENT MATERIALS

Sadaf Khosravifar, Doctor of Philosophy, 2015

Directed By: Professor Charles W. Schwartz,
Department of Civil and Environmental Engineering

Compaction control using lightweight deflectometers (LWD) is currently being evaluated in several states and countries and fully implemented for pavement construction quality assurance (QA) by a few. Broader implementation has been hampered by the lack of a widely recognized standard for interpreting the load and deflection data obtained during construction QA testing. More specifically, reliable and practical procedures are required for relating these measurements to the fundamental material property—modulus—used in pavement design.

This study presents a unique set of data and analyses for three different LWDs on a large-scale controlled-condition experiment. Three 4.5x4.5 m^2 test pits were designed and constructed at target moisture and density conditions simulating acceptable and unacceptable construction quality. LWD testing was performed on the constructed layers along with static plate loading testing, conventional nuclear gauge moisture-density testing, and non-nuclear gravimetric and volumetric water content measurements.

Additional material was collected for routine and exploratory tests in the laboratory. These included grain size distributions, soil classification, moisture-density relations, resilient modulus testing at optimum and field conditions, and an advanced experiment of LWD testing on top of the Proctor compaction mold.

This unique large-scale controlled-condition experiment provides an excellent high quality resource of data that can be used by future researchers to find a rigorous, theoretically sound, and straightforward technique for standardizing LWD determination of modulus and construction QA for unbound pavement materials.

LARGE-SCALE CONTROLLED-CONDITION EXPERIMENT TO EVALUATE LIGHT WEIGHT DEFLECTOMETERS FOR MODULUS DETERMINATION AND COMPACTION QUALITY ASSURANCE OF UNBOUND PAVEMENT MATERIALS

Sadaf Khosravifar

Dissertation submitted to the Faculty of the Graduate School of the
University of Maryland, College Park, in partial fulfillment
of the requirements for the degree of
Doctor of Philosophy
2015

Advisory Committee:
Professor Charles W. Schwartz, Chair
Professor M. Sherif Aggour
Professor Dimitrios G. Goulias
Professor Ahmet Aydilek
Professor Wenlu Zhu

Dedication

To my loving parents Parivash and Asgar, for giving me the support I needed to build a dream to chase after.

To Shahin, my soul mate, best friend and the love of my life.

Acknowledgments

This dissertation would have been far from reach without the guidance, support, knowledge and help of many individuals and institutes to whom I owe the greatest of gratitude.

First and foremost, to my advisor and mentor, Professor Charles Schwartz for his brilliant thoughts, inspiring discussions, crucial technical advices, and unwavering support throughout my graduate career at University of Maryland.

I am also very grateful to my dissertation committee, Professor M. Sherif Aggour, Professor Dimitrios Goulias, Professor Ahmet Aydilek and Professor Wenlu Zhu for their valuable comments, advices and discussions.

I am truly thankful to the eight Departments of Transportation—MD, VA, NY, MI, MO, NC, SC, and FL—for their participation in funding this research through Federal Highway Administration's (FHWA) Transportation Pooled Fund study program—TPF 5(825). Special thanks goes to Dan Sajedi from Maryland State Highway Administration (MDSHA) for his continuous support and technical leadership of the project. I am also thankful to the advisory committee of TPF 5(825), Shabbir Hossain of Virginia DOT, David Horhota of Florida DOT, David Gauthier of Michigan DOT, John Donahue of Missouri DOT, Brett Dening of New York DOT, K.J. Kim of North Carolina DOT, Jesse Thompson of South Carolina DOT, Micheal Arasteh and Azmat Hussain of FHWA and Rodney Wynn of MDSHA.

I would also like to express my special gratitude to Mr. John Siekmeier of Minnesota DOT, and Nayyar Zia Siddiki of Indiana DOT for their competent suggestions in this research work, Dr. Marco Bassani of University of Torino Italy for interesting discussions during the early stages of the project and Alfredo Bituin our lab manager for his support during the laboratory experimental work.

To Virginia and Garry Aicken of Kessler Soils Engineering Products Inc. representative of Zorn Instruments in the US, Larry Olson and Pat Miller of Olson Engineering and Dr. Regis Carvalho and Dr. Kurt Keifer of Dynatest Consulting Inc., I owe the greatest appreciation for allowing us the use of their equipment, pro bono, during this study and sharing with us their valuable technical knowledge. Special thanks goes to Mr. Larry Olson for sharing his clever idea of ‘LWD testing on mold’ which was adopted in this study. I am also grateful to Luck Stone Company for donating us the test material needed for this research work.

My sincere thanks also go to FHWA, and specially Dr. Nelson Gibson, for providing us with the unique testing facility at Turner- Fairbank Highway Research (TFHRC) Center and the great people at TFHRC who helped with the construction and testing: Dennis

Sixbey, Mario Tinio, Jan Li, Mike Adams, Karl, and Chris. It would have not been possible to conduct this research without their support.
I am truly grateful to my dear current and previous lab-mates Niosha Afsharikia, Gregory Koepping, Ramiz Vatan, Marcus Lapa Watson, Mateus Coelho, Luca Tefa, Chris Leininger, Azadeh Farzaneh, and Ali Rahjoo for their help and assistance in performing the extensive laboratory and field experiments. This work could have never been done without your dedication, help, and friendship. Your friendship made the journey a lot more enjoyable.

Finally, completing this important step of my academic life could have not been possible without support and love from my family and friends. I would like to thank my parents, Parivash and Asgar, for being my inspiration in life. I am also very thankful to my elder brother, Arash, for having my back in life and my dearest in-laws Amanda and Shahriar for their companionship and sweet friendship. Sahar Nabaee, Sahar Akram, Mersedeh Tariverdi, Naeem Masnadi, Endri Mustafa, Yanshu Sun, Negin Kananizadeh, Giti Malek, Saena Nejadi and the rest of my dear friends who have been there for me throughout the tough times and good times; I am truly thankful to your friendship.

Last but not least—Shahin Sefati—my best friend, and the love and joy of my life. Words cannot express my gratitude. So, I keep it short. Thanks!

Table of Contents

List of Tables

List of Figures

Chapter 1. Introduction

Modulus-based compaction quality assurance (QA) of unbound material is gaining attention in the pavement industry. The conventional method of using nuclear moisture-density gauge as the compaction QA method of unbound material is no longer desirable. Density, although an easy property to measure in the field and one that is correlated to more fundamental engineering properties of interest, is not a direct input in design of the pavements and is not directly linked to pavement performance. Modulus is the fundamental material input required for the structural design of pavements.

On the other hand, Lightweight Deflectometers (LWD) are gaining attention since they can be used to measure modulus directly. LWDs are being implemented for pavement construction QA in a few states and countries but their broader implementation has been hampered by the lack of a widely recognized standard for interpreting the load and deflection data obtained during the construction QA testing. The challenges in establishing a standard specification for interpreting the LWD data are broad and include the differences in the various commercial LWD devices, the nonlinearity of the soil modulus under different moisture and stress conditions, and the differences in the stress states and boundary conditions between typical laboratory tests and field conditions. Despite these challenges, LWDs are a promising tool for performance based construction QA testing that will not only result in a better product but will also provide the quantitative measures critical for better understanding the connection between pavement design and long term pavement performance.

In this study, the dynamic responses of three different LWDs were carefully studied through a unique large-scale, controlled experimental setting. Three large 4.5x4.5 m^2 test pits were designed and constructed at target moisture and density conditions simulating scenarios of acceptable and failing construction quality. The pits were carefully constructed using two different cohesive and noncohesive subgrade soils and one type of granular aggregate base to provide a wide range of material selection. The test pits were equipped with in-situ environmental sensors to monitor the post-compaction variations in water content and temperature and pressure cells to evaluate the zone of influence of the LWD loading. LWD testing was performed on the constructed layers along with static plate loading tests, conventional nuclear gauge moisture-density testing, and non-nuclear gravimetric and volumetric water content measurements. In addition to evaluation of the LWDs, the two non-nuclear water content measurement techniques, namely a volumetric water content sensor and gravimetric moisture analyzer, were assessed. Additional material was collected for further routine and advanced tests in the laboratory. These include grain size distributions, soil classification, moisture-density relations, resilient modulus tests on samples prepared at optimum and field conditions, and finally LWD testing directly on the Proctor compaction mold.

In addition to the test pit construction and the documentation of all field and supplementary routine and advanced laboratory testing data, material models, structural stress-strain models (layered elastic versus finite element method), and techniques for LWD signal analysis (peak method and spectral analysis) were also evaluated with the intent to overcome some of the challenges in interpreting and standardizing LWD data for QA. More specifically, soil resilient modulus constitutive models based on unsaturated soil mechanics principles were evaluated using the data collected by Andrei (2003) on several cohesive and non-cohesive soils. The models were assessed for their suitability in setting the target modulus in LWD-based QA work.

Frequency domain spectral analysis was performed on the force and deflection signals from LWD tests performed on a four-point steel beam with known stiffness properties. The results were used to distinguish the inherent variabilities between the three LWD devices and to endorse the sufficiency of peak method in LWD stiffness determination.

1.1. Key objectives of this study

The main objective of this study was to collect a unique set of high quality data through construction and LWD testing on a "large enough" test pit truly representative of field boundary conditions and yet a "small enough" pit to assure uniformity and the lowest spatial variability. The primary aim of this dissertation was to comprehensively describe and document the construction, testing conditions, and results from all field and laboratory tests to provide a valuable resource for future researches in standardizing the LWD for compaction QA of unbound materials.

This study had two other secondary objectives: (1) Evaluation of several soil modulus constitutive models rooted in unsaturated soil mechanics using the data from Andrei (2003) for their suitability to be utilized in LWD based QA work; and (2) Evaluation of frequency domain analysis of LWD test data to assess whether it is necessary to perform full spectral analysis in an LWD-based procedure.

1.2. Organization of the dissertation

Chapter 1 provides the summary of the dissertation, the key objectives, and a review of the state of practice on modulus-based QA of unbound material using LWD.

Chapter 2 describes the preparation work prior to test pit construction. This chapter describes in detail the properties of the materials used in the test pit construction as well as the laboratory tests, statistical models, and simulations performed to understand the (a) material behavior, (b) LWD device behavior and (c) pavement structure response. The related background and literature review on each subtopic are also presented.

Chapter 3 presents the details of test pits construction and testing schedule.

Chapter 4 presents the data from the test pits including structural (LWD and plate loading tests), moisture (nuclear and non-nuclear moisture and density measurements), and weather data.

Chapter 5 summarizes the findings and conclusions of the study and provides recommendations for future the research.

1.3. **Background**

Work by Fleming et al. (2000), Vennapusa and White (2009), Senseney et al. (2009, 2012, and 2014), and Stamp and Mooney (2013) showed the potential of LWDs for determining the moduli of compacted soil layers. A few of these studies along with a recent NCHRP Synthesis 382 *Estimating Stiffness of Subgrade and Unbound Materials for Pavement Design* noted the important research need to evaluate the ability of LWDs to determine the moduli of prototype test sections and also to address the effects of stress dependency and layering on the moduli predictions. The ASTM Standard Test Methods *Method for Measuring Deflections with a Light Weight Deflectometer* (ASTM E2583-07) and *Measuring Deflections using a Portable Impulse Plate Load Test Device* (ASTM E2835-11) only provide standards for measuring deflections using an LWD. They do not provide a standardized way to interpret those deflection measurements for the calculation of stiffness or modulus.

Two recently published project reports served as the main resources in the literature review: NCHRP Project 10-84 *Modulus-Based Construction Specification for Compaction of Earthwork and Unbound Aggregate* and NCHRP Synthesis 20-05/Topic 44-10 *Non-Nuclear Methods for Compaction Control*. A thorough review was conducted of past investigations and case studies in the US, Europe, and elsewhere involving modulus based construction QA procedures. A review of current LWD based quality control specifications is provided in the following subsections.

1.3.1 MNDOT

The MNDOT specification for using LWD for QA of geomaterials suggests defining the target LWD deflection based on the grading number (GN) (Equation 1-1) and field moisture content for granular materials and on the plastic limit and field moisture content for fine-grained soils. The MNDOT specification requires testing immediately after compaction. Table 1-1 and

Table 1-2 provide the target LWD deflection and modulus for granular materials and fine soils, respectively. The specification is provided in the following link: http://www.dot.state.mn.us/materials/gblwd.html.

Equation 1-1

$$GN(\%\text{passing}) = \frac{25mm + 19mm + 9.5mm + 4.75mm + 2.00mm + 425\mu m + 75\mu m}{100}$$

Table 1-1. LWD Target Values for Granular Material (Siekmeier et al. 2009)

GN	Moisture Content	Target LWD Modulus		Target LWD Deflection Zorn
		Keros/Dynatest	Zorn	
	%	MPa	MPa	mm
3.1 – 3.5	5 -7	120	80	0.38
	7- 9	100	67	0.45
	9 - 11	75	50	0.60
3.6 – 4.0	5 -7	120	80	0.38
	7- 9	80	53	0.56
	9 - 11	63	42	0.71
4.1 – 4.5	5 -7	92	62	0.49
	7- 9	71	47	0.64
	9 - 11	57	38	0.79
4.6 – 5.0	5 -7	80	53	0.56
	7- 9	63	42	0.71
	9 - 11	52	35	0.86
5.1 – 5.5	5 -7	71	47	0.64
	7- 9	57	38	0.79
	9 - 11	48	32	0.94
5.6 – 6.0	5 -7	63	42	0.71
	7- 9	50	33	0.90
	9 - 11	43	29	1.05

Table 1-2. LWD Target Values for Fine Grained Soil (Siekmeier et al. 2009)

Plastic Limit	Estimated Optimum Moisture	Field Moisture as a % of Optimum Moisture	Zorn Deflection Target at Field	
			Minimum	Maximum
%	%	%	mm	mm
Non-plastic	10-14	70 – 74	0.5	1.1
		75 - 79	0.6	1.2
		80 - 84	0.7	1.3
		85 - 89	0.8	1.4
		90 - 94	1.0	1.6
15 – 19	10 - 14	70 – 74	0.5	1.1
		75 - 79	0.6	1.2
		80 - 84	0.7	1.3
		85 - 89	0.8	1.4
		90 - 94	1.0	1.6
20 – 24	15 - 19	70 – 74	0.8	1.4
		75 - 79	0.9	1.6
		80 - 84	1.0	1.7
		85 - 89	1.2	1.9
		90 - 94	1.4	2.1
25 – 29	20 - 24	70 – 74	1.0	1.7
		75 - 79	1.2	1.9
		80 - 84	1.4	2.1
		85 - 89	1.6	2.3
		90 - 94	1.8	2.6
30 – 34	25 - 29	70 – 74	1.3	2.0
		75 - 79	1.5	2.2
		80 - 84	1.7	2.4
		85 - 89	1.9	2.7
		90 - 94	2.2	3.0

1.3.2 INDOT

The Indiana DOT also developed a test method for "Field Determination of Deflection Using
Light Weight Deflectometer." The INDOT specification can be used on granular soils, coarse aggregates and chemical modified soils.

The INDOT specification provides two options to determine the LWD target deflection value (LWD-TV): (1) Control strip and (2) Comparison. In the first method, the specification requires: (a) construction of a control strip to meet the specified requirements; (b) LWD testing during the control strip construction at specified rates; and (c) plotting the

average LWD deflection against the roller pass count. The minimum deflection is set as LWD-TV. LWD test on the compacted layer should not exceed 1.1 * LWD-TV.

In the second method, LWD-TV is selected based on comparisons with Dynamic Penetration Index for granular base or the INDOT-specified density method for fine-grained soils. LWD-TV is defined as the average LWD deflection at which minimum DPI or density values pass their respective criteria.

1.3.3 Europe

The European Union (EU) also has developed a specification for LWD implementation (CEN ICS 93.020). In this specification two parameters are determined through LWD testing: (1) dynamic modulus, which is calculated based on the Bousinesq equation ((Equation 2-1); and (2) dynamic compactness (T_{rd}), which shows the quality of the compaction and is equal to:

Equation 1-2

$$T_{rd} = T_{rE}.T_{rw}$$

where T_{rE} is site relative compaction at a given water content and T_{rw} is the moisture correction coefficient to adjust for differences between the measured moisture content and optimum moisture content. Follows the process to obtain T_{rE}, and T_{rw}.

The testing process involves six sequences of LWD testing, each consisting of three LWD drops (total of 18 drops) on the loose, non-compacted material at the site. The average deformation of the 2nd sequence is used to determine the initial dynamic modulus. The final dynamic modulus is calculated from the 6th testing sequence.

According to the standard, the work imparted on the material during the six LWD sequences is equivalent to that applied in the modified Proctor test. The relative compactness rate (T_{rE}) at the field moisture content is therefore determined from the compaction curve using the following equation:

$$T_{rE}\% = 100 - \Phi_0 \times D_m$$ **Equation 1-3**

where Φ_0 is a linear coefficient calculated from the Proctor-test results, typically assumed to be 0.365 ± 0.025, and D_m is the deformation index, calculated from sum of the elements of the data line formed from the difference of the subsequent deflections up to the drop.

where T_{rE} is site relative compaction at a given water content and T_{rw} is the moisture correction coefficient to adjust for differences between the measured moisture content and optimum moisture content:

$$T_{rw} = \frac{\rho_{di}}{\rho_{d\max}} \qquad \textbf{Equation 1-4}$$

In Equation 1-4, ρ_{dmax} is the maximum dry density value obtained in the modified Proctor test and ρ_{di} is the dry density value on compaction curve of the modified Proctor tests corresponding to the in situ moisture content.

1.3.4 UK

The UK specification defines four foundation classes according to the long term in-service foundation surface modulus values. For construction quality control, the target mean and minimum modulus values are specified for the four foundation classes as shown in Table 1-3. The moving mean of five consecutive in-situ foundation surface modulus measurements must equal or exceed the target mean foundation surface modulus. All individual in-situ foundation surface modulus measurements must equal or exceed the target minimum foundation surface modulus.

Table 1-3. UK specification. Target pavement foundation surface modulus

Long-Term In-Service Modulus (MPa)			**Class I**	**Class II**	**Class III**	**Class IV**
			≥50	≥100	≥200	≥400
Target Mean Modulus (MPa)	Unbound		40	80	…	…
	Bound	Fast Curing	50	100	300	600
		Slow Curing	40	80	150	300
Target Minimum Modulus (MPa)	Unbound		25	50	…	…
	Bound	Fast Curing	25	50	150	300
		Slow Curing	25	50	75	150

1.3.5 NCHRP 10-84

NCHRP 10-84 project report (2014) proposed a framework for modulus based specification using LWD. The procedure is as follows:

1. After conducting the test, the LWD effective modulus (E_{eff}) is determined from the Bousinesq equation (Equation 2-1).
2. Next, E_{eff} is adjusted using the following formula:

$$E_{adj} = E_{eff} \times K_{lab-field} \times K_{moist} \qquad \textbf{Equation 1-5}$$

where $K_{lab-field}$ is an adjustment factor that accounts for differences in lab and field moduli at the same moisture content and density:

$$K_{lab-field} = \left(F_{env}\right)^{\lambda} \quad \textbf{Equation 1-6}$$

where λ= -0.36 and F_{env} is the relationship proposed by Cary and Zapata (2010) simplified by replacing wPI with zero.

$$\log(F_{env}) = \left(-0.40535 + \frac{1.20693}{1+e^{\left(0.68184+1.33194\cdot\left(\frac{S-S_{opt}}{100}\right)\right)}}\right) \quad \textbf{Equation 1-7}$$

where S_{opt} = degree of saturation at optimum moisture content and S = degree of saturation at compaction moisture content.

K_{moist} is an adjustment factor for differences in the compaction and testing moisture contents:

$$K_{moist} = e^{\eta(w_C - w_T)} \quad \textbf{Equation 1-8}$$

where η=0.18 for fine-grained soils and 1.19 for unbound aggregates, w_T is moisture content at time of testing (in percent); and w_C is moisture content at time of compaction (in percent).

3. The target modulus is established For this, the specification suggests direct measurement of the resilient modulus of the geomaterial according to AASHTO T-307 (Equation 2-20). The pavement section is then modeled in a nonlinear structural pavement algorithm that simulates the center deflection under the LWD load the Bousinesq equation (Equation 2-1) and using that to calculate the E_{target}.

The evaluation of the proposed specification showed that achieving adequate layer modulus is weakly associated with achieving density. Changes in the assumed Poisson's ratio will highly affect the acceptance rate. Different LWDs estimate different moduli at the same test spot, suggesting the necessity for LWD specific specification. NCHRP 10-84 also found that it is very important to consider the properties of the underlying layers in setting the LWD target values, which is in line with findings from Khosravifar et al. (2013). A common concern regarding the modulus-based devices was the variability of the measurements. Based on tests on 20 independent specimens, Nazarian et al. (2014) found

that the repeatability of the LWD devices is better than 15% and their reproducibility is better than 12%. More than 70% of variability in the LWD devices measurements was attributed to the variation in the materials properties.

The online survey circulated among state Departments of Transportation (DOTs) as part of the NCHRP 10-84 project revealed that, while DOTs are interested in implementing a practical modulus-based specification, the incorporation of laboratory resilient modulus tests is not desirable.

Finally, NCHRP 10-84 recommended modulus-based acceptance tests to be implemented in conjunction with moisture measurements. Ironically, the nuclear density gauge was determined as the most reasonable moisture measurement tool in this study.

All the previous work on standardizing the data from LWD lack validation under large scale controlled conditions. Nazarian et al. (2013) only performed small scale testing in which specimens were compacted in a 90 cm diameter PVC pipe to a thickness of less than 0.55 m; these are much different conditions than in the field. Grasmick (2013) performed LWD testing on a large free-standing soil box structure with inside dimensions of 2.4m x 2.4m x 1.2m constructed out of timber. One significant issue reported in this work was the reflection of the LWD induced waves off the wood/soil box.

Chapter 2. Pre-construction Preparations: Testing and Modeling

This chapter describes in detail the Lightweight Deflectometer (LWD) working principles, properties of the materials used in the test pits construction, the associated laboratory tests, statistical models, and simulations performed to understand the (a) material, (b) LWD device and (c) and pavement structure response which are the necessary steps for standardizing the data acquired by LWD for compaction quality control of unbound material.

First, the details of LWD working principles for the LWDs selected for the study and stiffness and modulus determination techniques are discussed. More specifically, the Beam Verification Test (BVT)—a test performed to evaluate the LWD devices—is elaborated in detail.

Next, the routine properties of the test material were characterized followed by two advanced tests to characterize the stress and moisture dependency of the modulus; namely (1) resilient modulus (M_R) testing and modeling explained in Sections 2.6 to 2.8 and (2) LWD testing on Proctor molds explained in detail in Section 2.9.

The chapter concludes by describing the instrumentation used in test pits and their calibration process. The Decagon GS1 volumetric water content (VWC) sensors,

thermocouples, Geokon pressure cells, and the Ohaus MB45 gravimetric moisture analyzer were among the instruments and sensors used in this study.

2.1. LWD working principles

The Light-Weight Deflectometer (LWD) is a dynamic plate loading test developed for the determination of the modulus (E_{LWD}) of soils and unbound fill materials.

The test consists of subjecting the soil to a pulse load applied via a disk-shaped steel or aluminum plate. The loading mechanism consists of a drop weight that, once released, falls along a rod until it hits a spring dashpot unit. The spring dashpot unit is attached to the plate, which is in contact with ground. Once the drop weight hits the spring dashpot unit, the LWD and ground move together in coupled mode. The LWD-ground system is analogous to a two degree of freedom (DOF) mass-spring-damper system (Figure 2.2) during the loading and rebound until the moment that the impact load becomes zero, after which the system decouples.

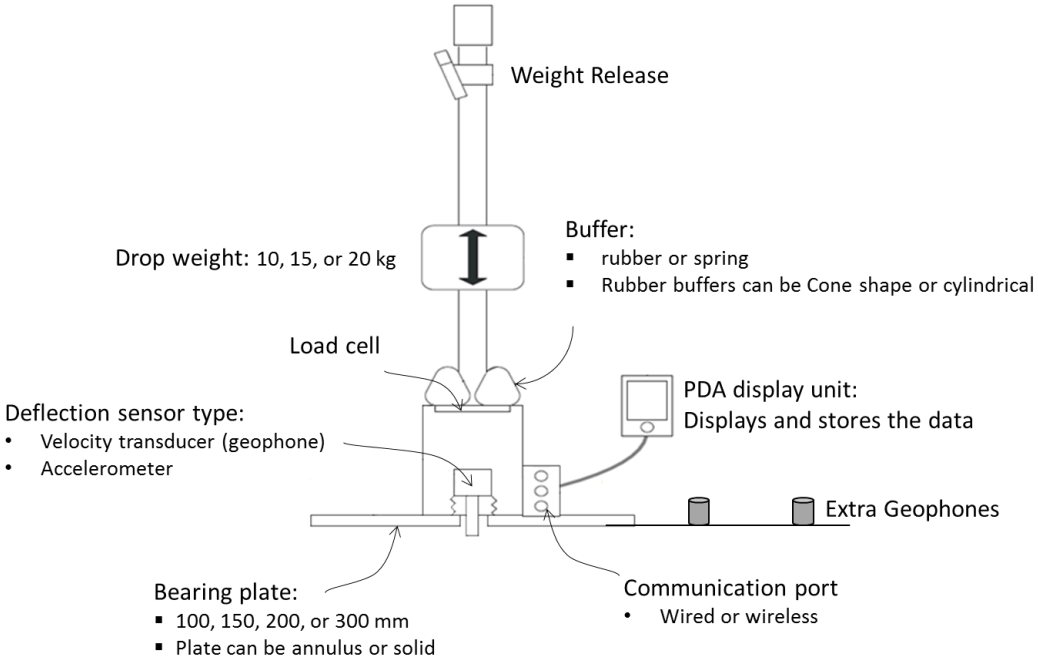

Figure 2.1. Diagram of LWD and its parts

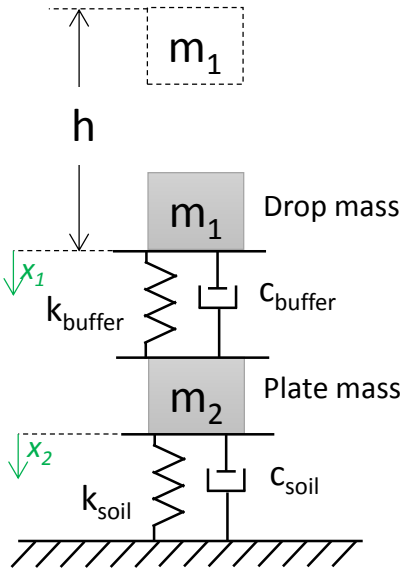

Figure 2.2. Schematic of the LWD-ground movement: 2 DOF system

A velocity sensor or accelerometer records the speed or acceleration of the movements of the plate or ground depending on the position of the sensor. The position and type of the deflection sensor is different in different LWD devices. After completion of the test, the maximum displacement is calculated by means of double/single integrals of the accelerations/velocities. The load history and peak load are either assumed or measured by a load cell. Some types of LWDs also provide additional geophones to measure the surface deflection at several radial distances from the center of the load.

Figure 2.3 and Figure 2.4 present an example of the load and deflection time history and hysteresis, respectively. The area in the hysteresis loop represents the energy loss due to material damping in the soil.

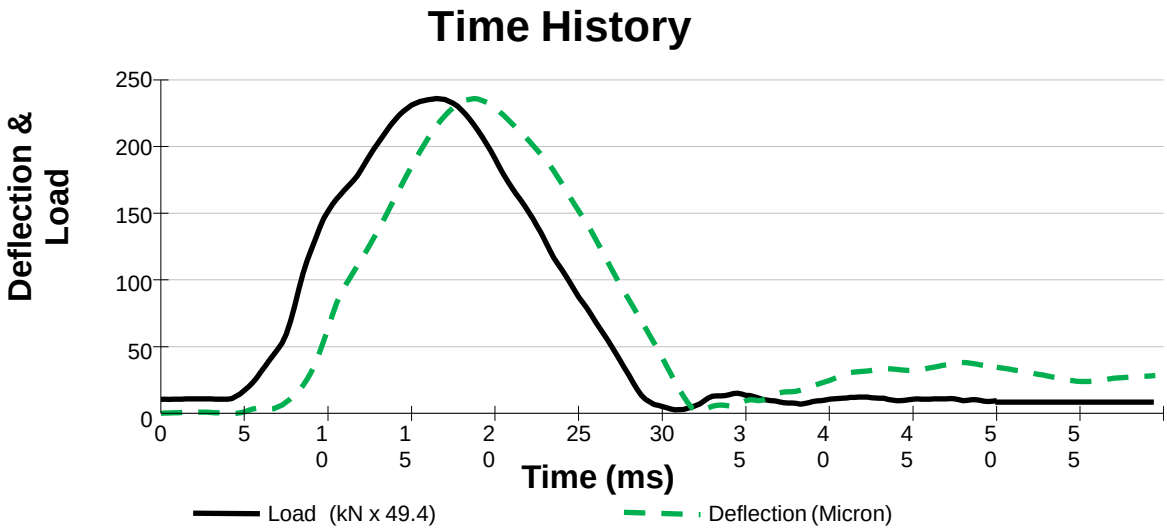

Figure 2.3. An example of load and deflection time history. (From LWDmod Software- Dynatest)

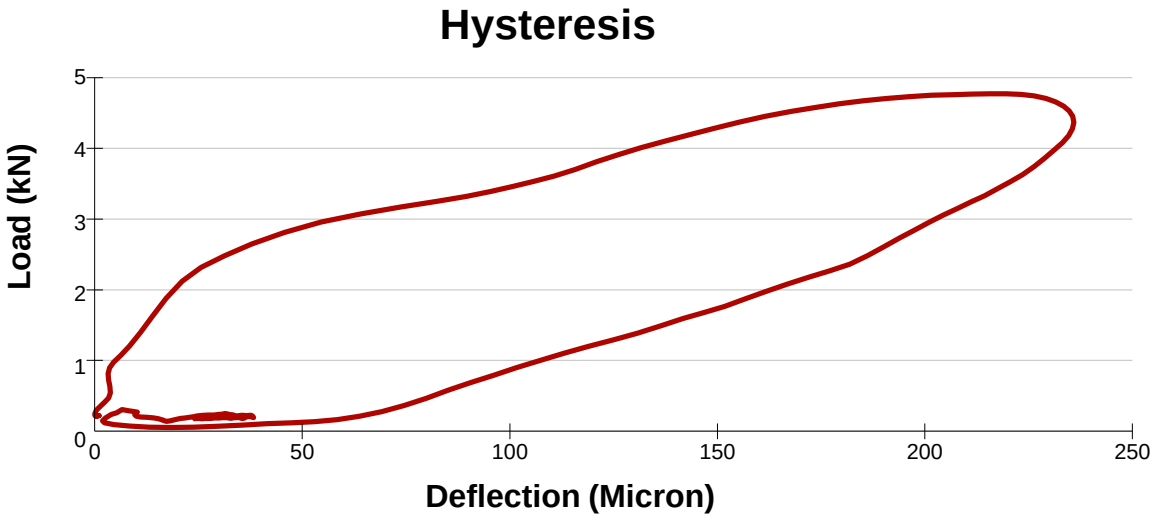

Figure 2.4. An example of load vs deflection hysteresis. (From LWDmod Software- Dynatest)

LWD is generally used to determine the modulus of subgrade or base layers; in other words, one or two layer systems (Figure 2.5).

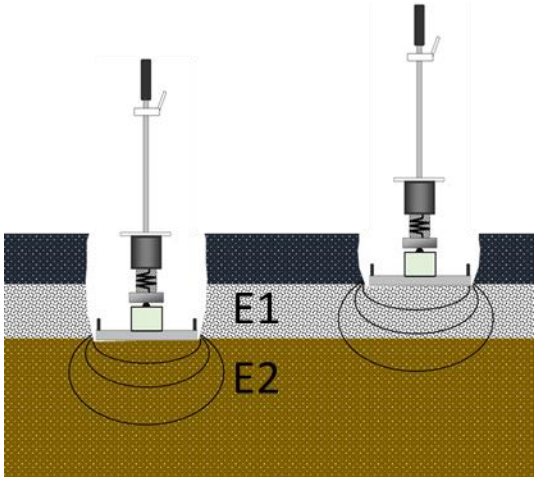

Figure 2.5. LWD testing on one layer and two layer system

The modulus is then calculated using the Bousinesq equation (Equation 2-1):

Equation 2-1

$$E = \frac{2k_s\left(1-\upsilon^2\right)}{Ar_0}$$

where $k_s = \left|\frac{F_{peak}}{w_{peak}}\right|$, A is the stress distribution factor, ν is the Poisson's ratio, and r_0 is the plate radius.

This equation assumes the test media to be linear elastic, isotropic, homogeneous semi-infinite continuum. Other parameters required for determining the modulus, including the distribution of the contact stress between the plate and the soil (A) and Poisson's ratio (ν), are assumed. Some LWD manufacturers (i.e., Dynatest and Olson) give users the option of selecting the shape factor and ν, others (i.e., Zorn) assume a fixed stress distribution factor of π and ν of 0.5.

Terzaghi, Peck and Mesri (1996) defined the stress distribution under a plate as a function of plate rigidity and soil type. Table 2-1 denotes the stress distribution coefficients (A) typical of different kinds of soils under the LWD plate.

Table 2-1. Stress distribution factor for different types of soil

Soil type	Factor (A)	Stress distribution Shape
Uniform (mixed soil)	π	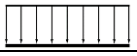
Granular material (parabolic)	3π/4	
Cohesive (inverse-parabolic)	4	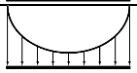

The following formula is used to calculate the surface modulus at radial distance (d_0):

Equation 2-2

$$E = \frac{k_s\left(1-\upsilon^2\right)}{\pi d_0}$$

For a two layer system, Burmister (1945) proposed the following formula where E_1 is the modulus of the top layer with the thickness of h and E_2 is the modulus of the underlying layer.

Equation 2-3

$$w_{0,0} = w_{0,h_e} + \left(w_{0,0} - w_{0,h}\right) = \frac{2\left(1-\upsilon^2\right)F_{peak}}{\pi r_0}\left\{\frac{1}{E_2\sqrt{1+\left(\frac{h}{r_0}\sqrt[3]{\frac{E_1}{E_2}}\right)^2}} + \frac{\left[1-\frac{1}{\sqrt{1+\left(\frac{h}{r_0}\right)^2}}\right]}{E_1}\right\}$$

2.2. **Selected LWD equipment**

A variety of LWDs were investigated during the literature review. Three representative LWDs were selected for the study: the Zorn ZGF 3.0 (Figure 2.6), Dynatest 3031 (Figure 2.7), and Olson 01 (Figure 2.8). These LWDs cover the typical differences in the device. Table 2-2 summarizes the characteristics of the selected LWDs. The Zorn LWD has no

load cell, while the Dynatest and Olson LWDs include a load cell. Zorn and Olson have a solid plate, while Dynatest has an annulus plate (plate with a small central hole). The Olson LWD measures velocities using a geophone sensor on the top of the plate while the Dynatest LWD measures velocities using a geophone sensor extending through the annular hole. The Zorn LWD measures accelerations using an accelerometer on the top of the plate. Zorn and Olson LWD follow ASTM E 2835, and Dynatest follows ASTM E 2583.

Table 2-2. Charactrisitics of the studied LWDs

LWD	**Total weight with 10 kg falling weight and plate**				**Falling weight**	**Max height**
	100 mm	150 mm	200 mm	300 mm		
	[kg]	[kg]	[kg]	[kg]	[kg]	[cm]
Zorn 3000	30.1	30.2	30.4	30.2	10	72.4
Dynatest 3031	19.8	20.1	20.5	23.3	10 (adjustable)	83.8
Olson 01	27.1	24.8	26.7	26.0	10	61.0

LWD	**Load cell**	**Deformation sensor**		**Plate type**	**Type of buffer**
		type	range		
	[-]	[-]	[mm]	[-]	[-]
Zorn 3000	No	Accelerometer	0.2–30 (±0.02)	Solid	Spring
Dynatest 3031	Yes	Geophone +2 additional	0–2.2 (±0.002)	Annulus	Flat Rubber-adjustable
Olson 01	Yes	Geophone		Solid	Spring

Figure 2.6. Zorn ZFG 3.0 LWD

Figure 2.7. Dynatest LWD 3031- Pictures courtesy of Dynatest Consulting Inc.

Figure 2.8.Olson LWD-01

2.2.1 Force versus height assumptions for Zorn LWD

As mentioned in the previous section, the Zorn LWD does not have a load cell and assumes a constant applied load of 7.07 kN when dropped from full height of 72.4 cm on soils with different stiffness values.

The load of Zorn LWD at drops other than the full height was estimated based on a single DOF mechanical model assumption illustrated in Figure 2.9.

A linear relationship can be derived between the square root of the drop height and the impact force. Upon releasing the falling weight, the gravitational potential energy (E) stored in the falling weight transforms to kinetic energy and then to elastic potential energy in the spring when the mass hits the spring, as shown in the following equations:

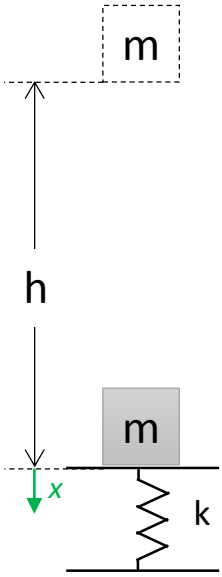

Figure 2.9. Similified schematic of LWD- soil motion as a one DOF mass-spring system.

Equation 2-4

$$E = m.g.h = \frac{1}{2}k.\Delta x^2$$

Equation 2-5

$$F = k.\Delta x$$

therefore

Equation 2-6

$$F = \sqrt{2.m.g.h.k}$$

Equation 2-6 was used to estimate the impact force of Zorn LWD at heights other than the full height when necessary.

2.3. **LWD testing on four-point steel beam**

The performance of the three LWD devices was examined with the beam verification tester (BVT) developed by Hoffman et al. (2004). The BVT is a simply supported steel beam under two symmetric loads, also known as a four-point beam. The schematic of the beam is shown below:

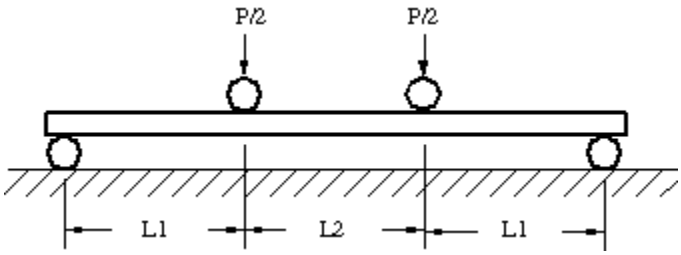

Figure 2.10. Schematic of the BVT

L2 was 10 cm while, *2L1+L2* was changed from 40 cm to 70 cm in 10 cm intervals to produce a linear elastic structure with different stiffness values. The static stiffness of the beam (k_s) was measured by applying a ramp load at a slow rate of 0.2 mm/sec using an Instron Machine (Figure 2.13). The k_s was subsequently compared to the peak stiffness derived from LWD testing on the beam ($k_{p\text{-}LWD}$). Figure 2.11 shows the Dynatest LWD on the beam as an example.

Using the LWD test data, the beam stiffness was calculated through two methods:
Peak stiffness ($k_{p\text{-}LWD}$) based on the ratio of peak load (F_{peak}) to peak deflection (d_{peak}) as reported by LWD ($k_{p\text{-}LWD}= F_{peak}/d_{peak}$).
Static Stiffness ($k_{s\text{-}LWD}$). Based on the frequency response function and assumption of a single-degree-of-freedom mechanical model.

Figure 2.11. Dynatest LWD test performed on BVT

The most important objective of the BVT tests were to (1) verify the calibration and reliability of the three test equipment on a linear elastic structure with known stiffness properties; and (2) assess the necessity to perform a full frequency domain analysis of the load and deflection signals for future LWD testing on soil. This study was based on a study performed by Hoffmann et al. (2004), who found significant systematic errors of up to 278% between the $k_{p\text{-}LWD}$ calculated from a Prima-100 LWD and the true stiffness of the beam (k_s).

Tests were performed using the 300 mm diameter plate and the drop heights listed in Table 2-4, Table 2-5, and Table 2-6 for the Olson, Zorn, and Dynatest LWD respectively. Figure 2.12 presents the $k_{p\text{-}LWD}$ versus the beam span for the evaluated LWDs. Tests were highly repeatable with coefficients of variation (CV) of less than 3% for all devices. The $k_{p\text{-}LWD}$ for all three devices was overall in the same ballpark of the true stiffness of the beam, contrary to the finding of Hoffmann et al. (2004).

For Zorn and Olson, the $k_{p\text{-}LWD}$ results were in line with true k_s of the beam at beam spans of 60 and 70 cm. As the beam span decreased, the $k_{p\text{-}LWD}$ underestimated the stiffness. In case of the Dynatest LWD, k_p was close to the true stiffness of the beam at beam spans 40 and 50 cm and only slightly underestimated at higher beam spans. One of the reasons of the under-estimation of the beam stiffness by Olson and Zorn in this experiment could be justified by the fact that these two LWDs measure the deflection of the plate where as in Dynatest, the deflection of the beam in the center of the plate is measured. The underestimation was more significant for Zorn, which could be attributed to the error from assuming the peak load.

Table 2-3 provides the k_s measured by the Instron machine. Table 2-4, Table 2-5, and Table 2-6 present $k_{p\text{-}LWD}$ and the $k_{p\text{-}LWD}/k_s$ ratio for the Olson, Zorn, and Dynatest LWDs, respectively.

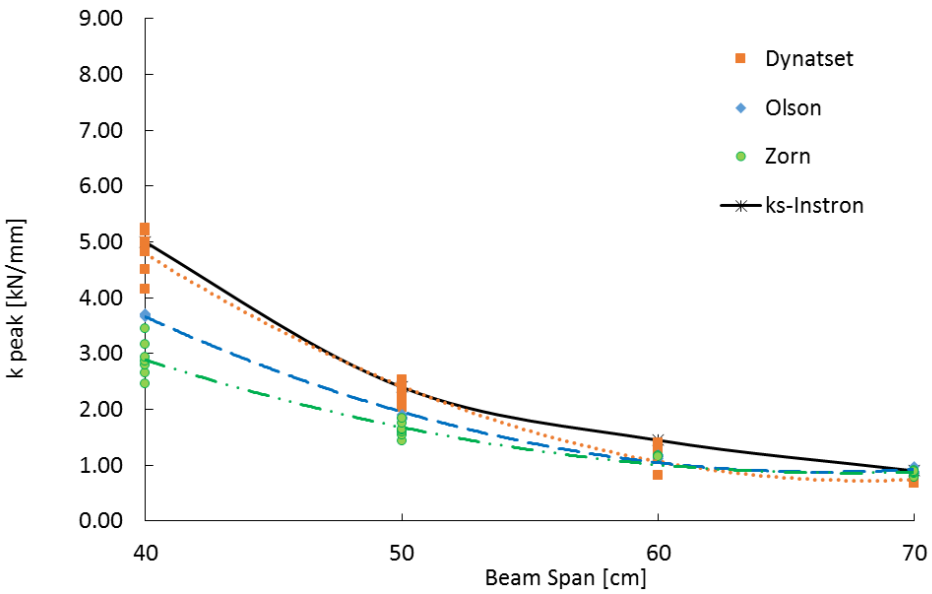

Figure 2.12.k_p as a function of beam span for the all the evaluated devices.

Figure 2.13. measurement of BVT static stiffness (k_s) with the Instron machine

Table 2-3. True static stiffness of the 4-point beam as measured by Instron

Span	**ks-true**
[cm]	[MN/m]
30	7.92
40	5.01
50	2.42
60	1.45
70	0.91

Table 2-4. Peak stiffness (k_p) from Olson LWD testing on 4 point beam

Span	Drop height	Force	d	k_p	$k_{p\text{-}LWD}/k_s$
[cm]	[cm]	[kN]	[mm]	[MN/m]	[-]
40	2.5	1.70	0.463	3.68	0.7
40	5.1	2.20	0.594	3.70	0.7
40	7.6	2.80	0.752	3.72	0.7
40	10.2	3.09	0.837	3.69	0.7
40	12.7	3.38	0.923	3.66	0.7
40	21.6	4.72	1.268	3.72	0.7
50	2.5	1.51	0.814	1.86	0.8
50	5.1	1.96	1.075	1.82	0.8
50	7.6	2.37	1.285	1.85	0.8
50	10.2	2.80	1.503	1.86	0.8
50	12.7	3.17	1.680	1.89	0.8
50	21.6	4.13	2.162	1.91	0.8
60	2.5	1.47	1.311	1.12	0.8
60	5.1	1.88	1.620	1.16	0.8
60	7.6	2.23	1.925	1.16	0.8
60	10.2	2.58	2.214	1.17	0.8
60	12.7	2.90	2.453	1.18	0.8
60	21.6	3.85	2.861	Deflection sensor overload	
70	2.5	1.45	1.705	0.85	0.9
70	5.1	1.81	2.108	0.86	0.9
70	7.6	2.22	2.489	0.89	1.0
70	10.2	2.48	2.818	0.88	1.0
70	12.7	2.77	2.837	0.98	1.1
70	21.6	3.65	2.899	Deflection sensor overload	

Table 2-5. Peak stiffness (k_p) from Zorn LWD testing on 4 point beam

Span	Drop height	Force	d	$k_{p\text{-}LWD}$	$k_{p\text{-}LWD}/k_s$
[cm]	[cm]	[kN]	[mm]	[MN/m]	[-]
40	2.54	1.32	0.537	2.47	0.5
40	5.08	1.87	0.707	2.65	0.5
40	7.62	2.29	0.818	2.80	0.6
40	10.16	2.65	0.922	2.87	0.6
40	12.7	2.96	1.011	2.93	0.6
40	31.75	4.68	1.482	3.16	0.6
40	72.4	7.07	2.028	3.46	0.7
50	2.54	1.32	0.918	1.44	0.6
50	5.08	1.87	1.215	1.54	0.6
50	7.62	2.29	1.436	1.60	0.7
50	10.16	2.65	1.616	1.64	0.7
50	12.7	2.96	1.804	1.64	0.7
50	31.75	4.68	2.666	1.76	0.7
50	72.4	7.07	3.792	1.85	0.8
60	31.75	4.68	4.011	1.17	0.8
60	72.4	7.07	3.253	1.16	0.8
70	2.54	1.32	1.683	0.79	0.9
70	5.08	1.87	2.179	0.86	0.9
70	7.62	2.29	2.643	0.87	1.0
70	10.16	2.65	3.049	0.87	1.0
70	12.7	2.96	3.288	0.90	1.0
70	31.75	4.68	5.228	0.90	1.0
70	72.4	7.07	8.406	0.83	0.9

Table 2-6. Peak stiffness (k_p) from Dynatest LWD testing on 4 point beam

Span	Drop height	Force	d	k_p	$k_{p\text{-}LWD}/k_s$
[cm]	[cm]	[kN]	[mm]	[MN/m]	[-]
40	2.54	0.78	0.150	5.25	1.0
40	5.08	1.15	0.229	5.00	1.0
40	7.62	1.58	0.303	5.20	1.0
40	10.16	1.95	0.403	4.82	1.0
40	12.7	2.27	0.503	4.51	0.9
40	17.78	2.86	0.687	4.16	0.8
50	2.54	0.80	0.315	2.53	1.0
50	5.08	1.17	0.490	2.39	1.0
50	7.62	1.64	0.666	2.45	1.0
50	10.16	1.97	0.863	2.28	0.9
50	12.7	2.28	1.037	2.20	0.9
50	17.78	2.77	1.362	2.04	0.8
60	2.54	0.82	0.586	1.40	1.0
60	5.08	1.22	0.929	1.31	0.9
60	7.62	1.51	1.222	1.24	0.9
60	10.16	1.82	1.589	1.15	0.8
60	12.7	2.08	1.889	1.10	0.8
70	2.54	0.75	0.923	0.81	0.9
70	5.08	1.11	1.616	0.69	0.8
70	7.62	1.41	1.986	0.71	0.8
70	10.16	1.65	2.439	0.68	0.7
70	12.7	1.97	2.825	0.70	0.8

2.3.1 Frequency domain analysis

To account for the transient load and displacement data recorded on the BVT, the response was analyzed in the frequency domain using the Fast Fourier transform (FFT) algorithm in MATLAB. The technique has already been used by several researchers e.g. Hoffmann (2004).

In a linear system with *y(t)* and *u(t)* as the output and input of the system, respectively, the transient response of the linear system can be analyzed by the Frequency Response Function (FRF) defined as the ratio of the Fourier transform of the output, *Y(f)* and the Fourier transform of the input, *U(f)*:

$$FRF(f) = \frac{Y(f)}{U(f)}$$ **Equation 2-7**

where *f* is the frequency in Hz.

Assuming a linear model, the FRF of the dynamic stiffness, *K(f)* and mobility, *M(f)* are defined as follows:

$$K(f) = \frac{F(f)}{X(f)}$$ **Equation 2-8**

$$M(f) = \frac{\dot{X}(f)}{F(f)}$$ **Equation 2-9**

where F(*f*), X(*f*), and $\dot{X}$ (*f*) are the respective Fourier transforms of the force f(t), the displacement x(t), and the velocity $\dot{x}$(t).

The static stiffness, k_s, of this linear model can therefore be computed as the magnitude of the dynamic stiffness, *K(f),* at zero frequency. The geophone or accelerometer measurements are not reliable at low frequencies and thus the static stiffness cannot directly be calculated from the measurements (Hoffmann, 2004). Alternatively, the experimental data corresponding to the FRF of the dynamic stiffness at higher frequencies can be extrapolated to zero frequency. To get a more accurate extrapolation to zero frequency, the single degree of freedom (SDOF) mass (*m*), spring (with stiffness *k*), and damper (with damping coefficient *c)* linear system was considered to explain the LWD-beam movement. The ordinary differential equation (ODE) of motion for the SDOF mass-spring-damper system is as follows:

Equation 2-10

$$m\ddot{x}(t) + c\dot{x}(t) + kx(t) = f(t)$$

where $\ddot{x}$(t) is the acceleration, *m* is summation of the mass of the LWD, including the receptacle and any other part on top of the verification beam, *c* represents the damping of the beam, and stiffness *k* is equal to the static stiffness of the verification beam (k_s).

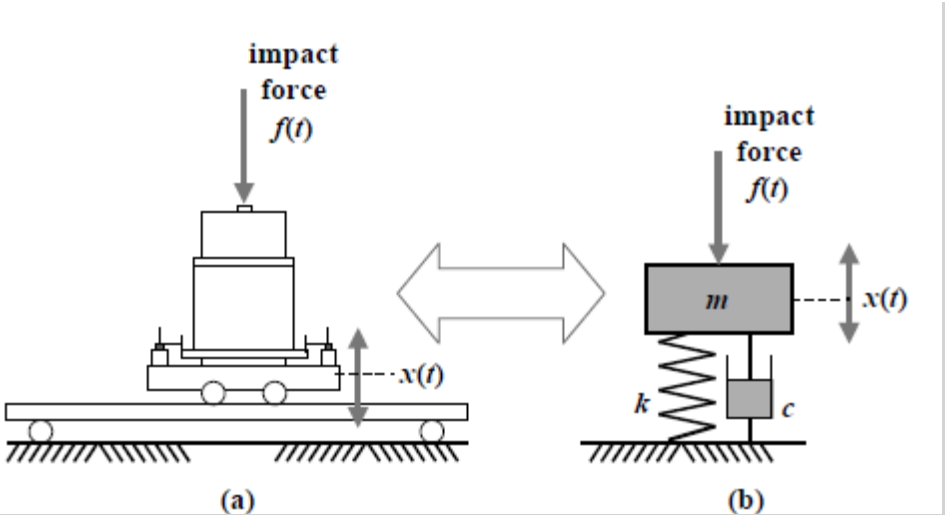

Figure 2.14. SDOF analog for the BVT: (a) four-point beam testing configuration; (b) corresponding SDOF analog (after Hoffmann, 2004).

The *K(f)* and *M(f)* functions can be derived by taking the Fourier transform from Equation 2-10 in the time domain. The functions as shown in Equation 2-11 and Equation 2-12, for *K(f)* and *M(f)*, respectively, can be used for curve fitting and extrapolation of the experimental data to zero frequency. Since the force and deflection data were readily available in the tested LWDs, the spectral analysis using the dynamic stiffness function, *K(f)*, was utilized.

Equation 2-11

$$K(f) = k\left[\left(1-\beta^2\right)+2i\xi\beta\right]$$

Equation 2-12

$$M(f) = \frac{1}{k}\frac{2i\pi f}{(1-\beta^2)+2i\xi\beta}$$

where $\beta = \frac{f}{f_n}$ is the tuning ratio, $\xi = \frac{c}{4\pi m f_n}$ is the damping ratio, and $f_n = \frac{1}{2\pi}\sqrt{\frac{k}{m}}$ is the undamped natural frequency.

To reduce the effects of experimental noise and minimize the errors, a spectral average technique was used. This technique was effectively used by Bendat and Piersol (2011), and Guzina and Osburn (2002) for backcalculating the FWD modulus on layered systems and by Hoffmann (2004) for the spectral analysis of the Prima-100 LWD impact load on BVT. In the averaging technique, the dynamic stiffness function is estimated as:

Equation 2-13

$$K(f) = \frac{G_{xf}(f)}{G_{xx}(f)}$$

where G_{xf} (f) is the one-sided cross-spectral density function of the deflection and force records and G_{xx} (f) is the one-sided auto-spectral density function of the deflection record. G_{xf} (f) and G_{xx} (f) were calculated using the built-in functions in MATLAB. The spectral averaging approach also allows for assessing the quality of the measurements and validity of the linearity assumption via the coherence function:

Equation 2-14

$$\gamma^2(f) = \frac{\left|G_{xf}(f)\right|^2}{G_{ff}(f)G_{xx}(f)}$$

where G_{ff} (f) is the one-sided auto-spectral density function of the force record. The coherence function ranging from 0 to 1. A value for γ^2(f) of zero shows no correlation between the input and output, while γ^2(f) equal to 1 shows the system is perfectly linear and noise free. The spectral analysis was not possible for the Zorn LWD since the load is not measured and a fixed load is assumed. An example of the spectral analysis on the Dynatest and Olson LWDs is shown in Figure 2.15 and Figure 2.16, respectively. Figure 2.17 depicts the strong agreement of the $k_{p\text{-}LWD}$ and k_s values from the spectral analysis for the Dynatest LWD. Appendix 10 reports the detailed results on the Dynatest LWD.

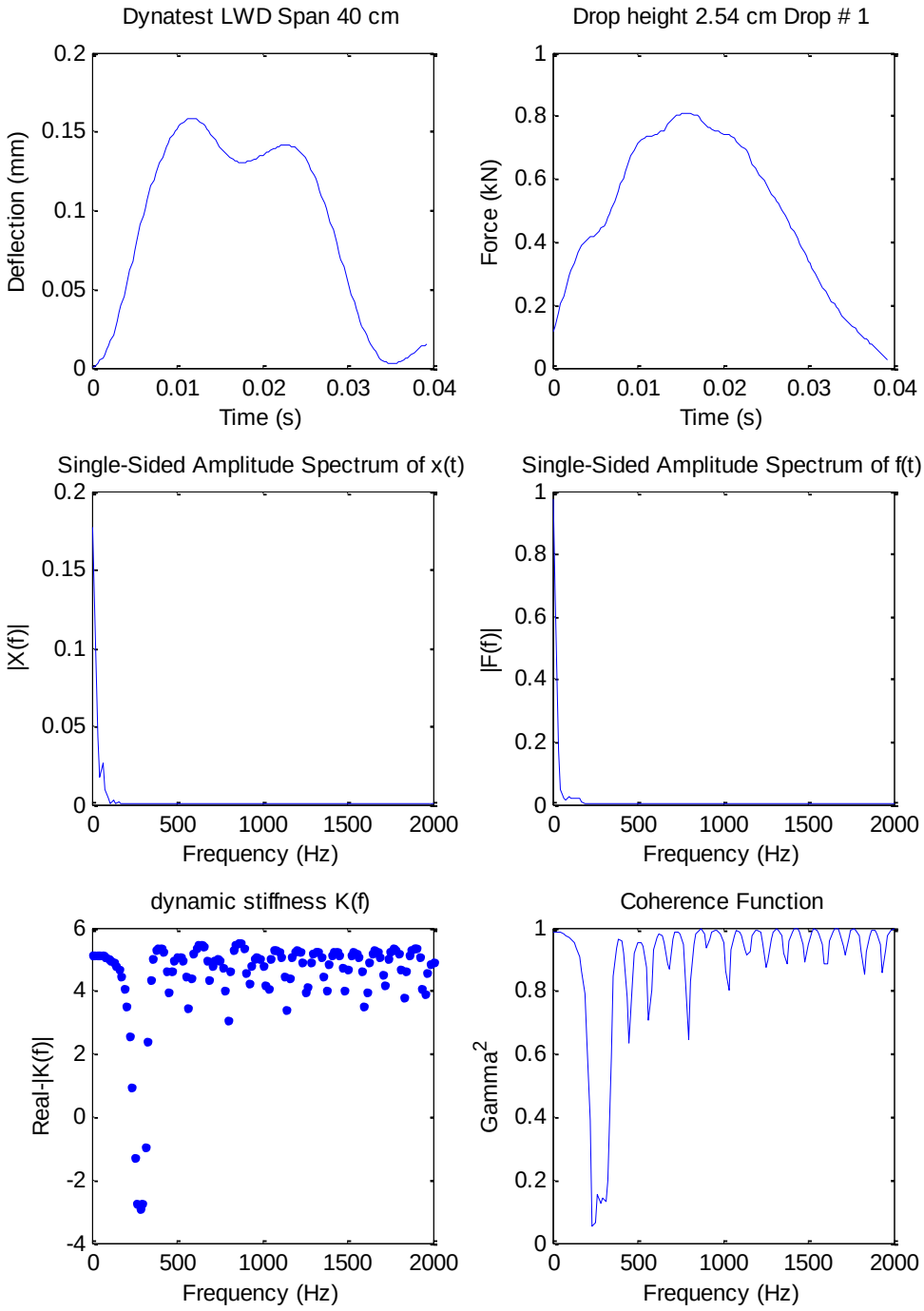

Figure 2.15. Spectral analysis on Dyantest LWD

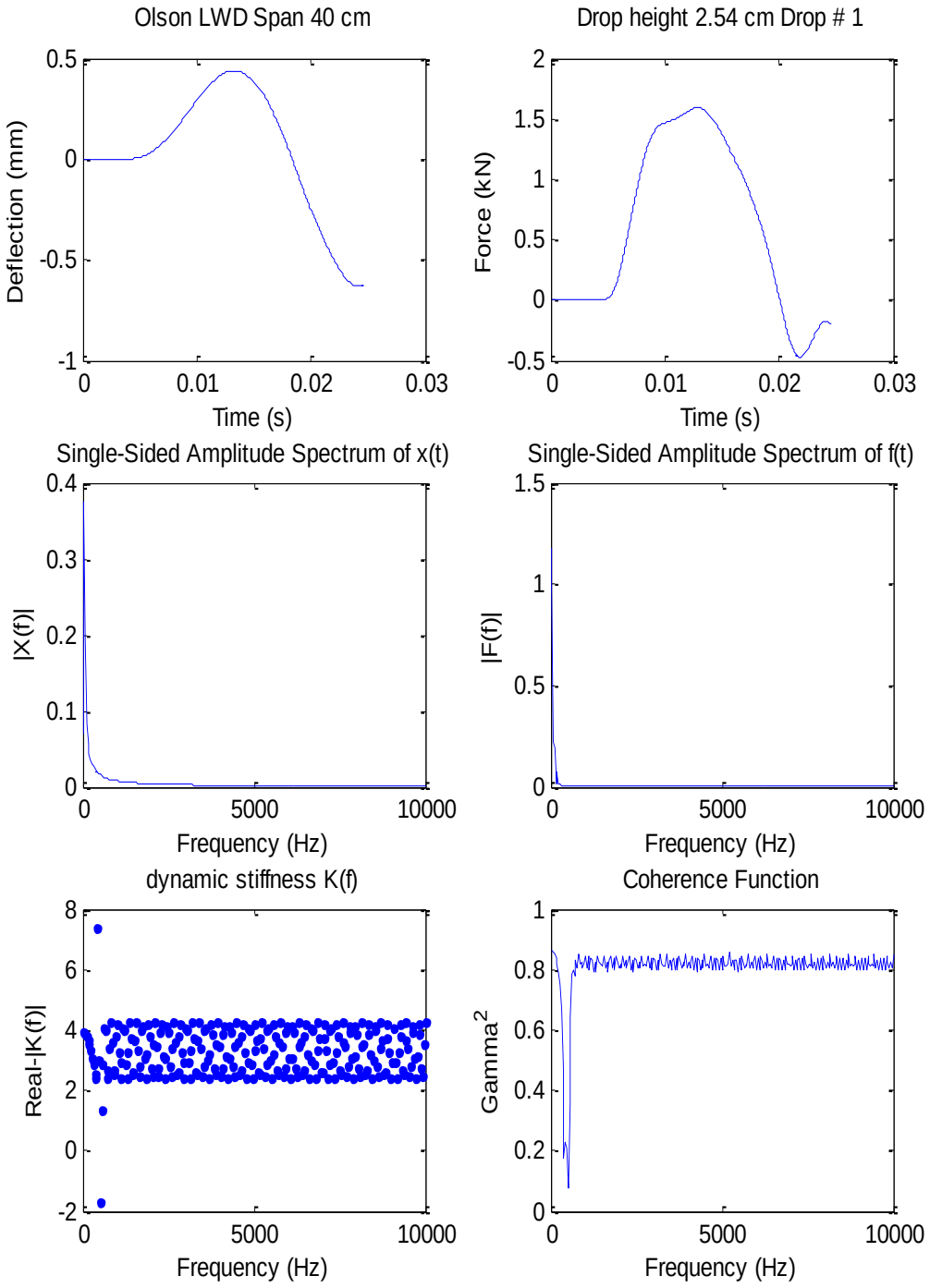

Figure 2.16. Spectral analysis on Olson LWD

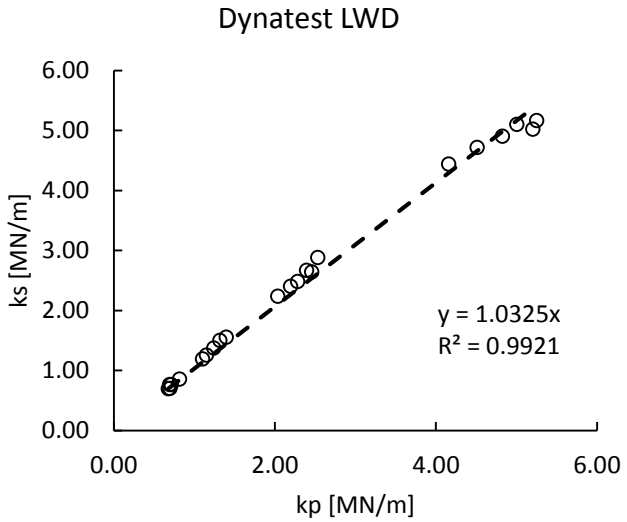

Figure 2.17. k_s from spectral analysis versus k_p of conventional peak method

Overall, contrary to Hoffmann et al. (2004) it was found that the conventional, peak-based method of stiffness determination produces estimates in line with true static stiffness of the BVT. Zorn and Olson LWD expressed a slight underestimation because of the fact that deflection of the plate is measured. It was found that the spectral-based data interpretation method only marginally improves the results. Therefore, it is not required to perform full spectral analysis on the LWD data.

2.4. **Material characteristics**

In this section, the properties of the materials used in the test pits are described.

The three materials used in this study included: (1) a well graded aggregate base commonly used in state of Virginia designated as VA21a stone; (2) a non-cohesive silty sand subgrade soil, which was the local subgrade soil used at the TFHRC accelerated loading facility (ALF); and (3) a cohesive high plasticity clay (HPC) subgrade soil. The ALF soil used in the study was excavated from a hill at TFHRC and the VA21a stone and HPC were donated by the Luck Stone Company. The Unified Soil Classification and Atterberg Limits (AASHTO T-89 and T-90) of the studied soils are summarized in Table 2-7.

Table 2-7. Material description

Material	Soil classification	PL	LL	PI	D_{90}	D_{60}	D_{30}	D_{20}	D_{10}	P_{200}	C_U	C_C
[-]	[-]	[%]	[%]	[%]						[%]		
VA21a	GW	-	-	-	13.8	6.6	1.7	0.8	0.3	3.3	25.1	1.7
ALF	SM	27	31	5		0.2				41.6		
HPC	CH-MH	38	65	27						81.7		

Figure 2.18 shows the gradation of the materials. The gradations were obtained according to AASHTO T-27 for VA21a and according to AASHTO T-11 and T-27 (wet and dry sieve analysis) for the ALF and HPC soils. The gradations were monitored throughout all phases of the project to ensure uniformity.

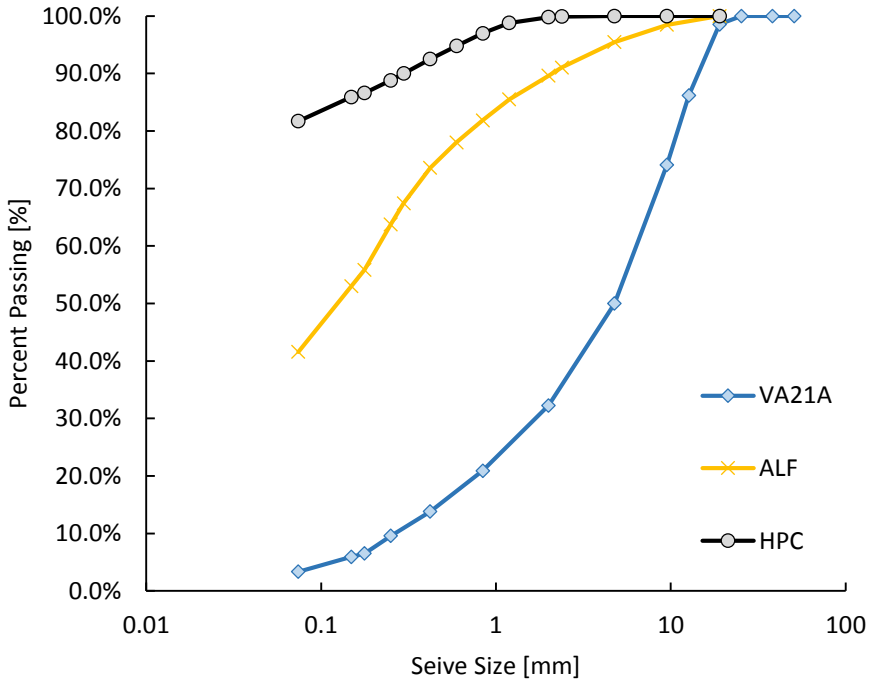

Figure 2.18. Gradation of the materials used in this study

The moisture-density relationships were determined for all three materials. Table 2-8 presents the optimum moisture content (OMC), maximum dry density (MDD) and bulk specific gravity of the test material. Figure 2.19 presents the moisture- density curves for all soils.

Table 2-8. OMC, MDD and Specific gravity of the test material

Soil Type	AASHTO Procedure	Method	Compaction energy	MDD	OMC	Specific Gravity(1)
[-]	[-]	[-]	[-]	kg/m^3 (pcf)	[%]	[-]
VA21a	T-99	D	Standard	2307.7 (144.0)	5.0	2.77
VA21a	T-180	D	Modified	2435.9 (152.0)	4.5	
ALF	T-99	C	Standard	1923.1 (120.0)	11.5	2.71
ALF	-	C	Semi Modified(2)	2003.2 (125.0)	10.5	
ALF	T-180	C	Modified	2083.3 (130.0)	9.5	
HPC	T-99	A	Standard	1522.4 (95.0)	24.0	2.66

(1) Specific gravity test according to AASHTO T-84 and T-85
(2) Customized compaction energy: 3 layers, 25 drops per layer using a 4.54 kg rammer and a 457 mm drop

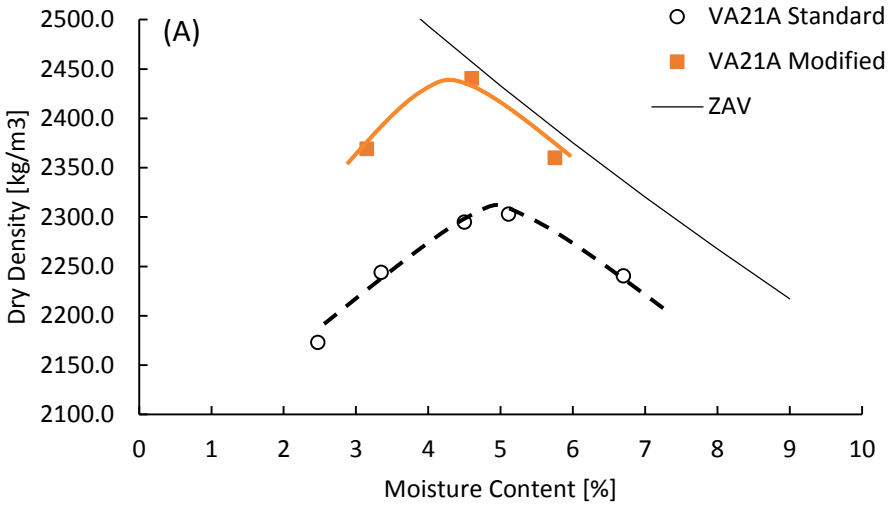
(A)
VA21A Standard
VA21A Modified
ZAV
Dry Density [kg/m3]
2500.0
2450.0
2400.0
2350.0
2300.0
2250.0
2200.0
2150.0
2100.0
0
1
2
3
4
5
6
7
8
9
10
Moisture Content [%]

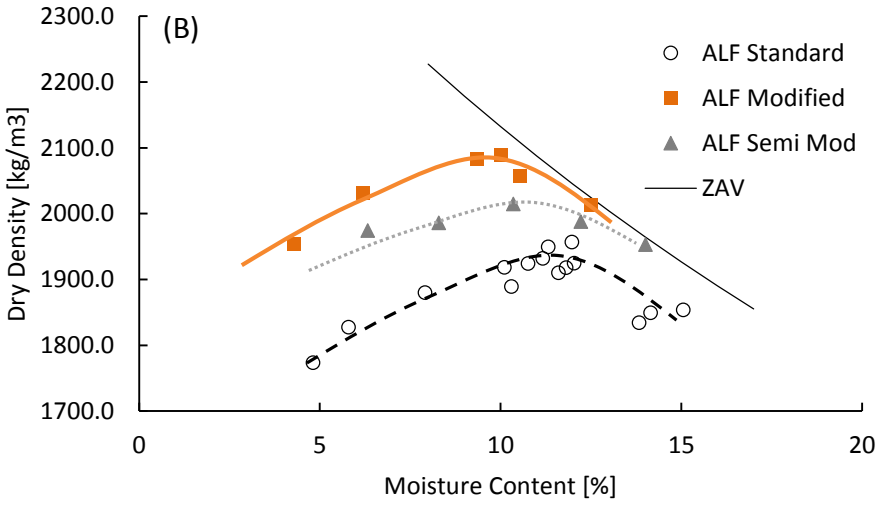
(B)
ALF Standard
ALF Modified
ALF Semi Mod
ZAV
Dry Density [kg/m3]
2300.0
2200.0
2100.0
2000.0
1900.0
1800.0
1700.0
0
5
10
15
20
Moisture Content [%]

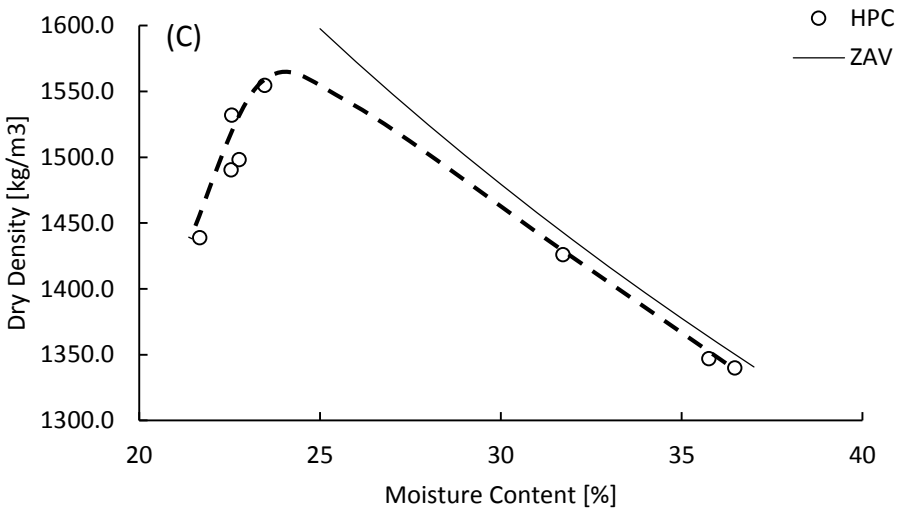

Figure 2.19. Moisture-Density relationships for (A) VA21a, (B) ALF, and (C) HPC.

2.5. **Soil-water characteristic curve (SWCC)**

The SWCC is the constitutive relationship existing between the degree of saturation of a soil (S) or volumetric water content and the associated matric suction. The degree of saturation is expressed by:

$$S = \frac{V_w}{V_v}$$ **Equation 2-15**

The SWCC is an important constitutive relationship for unsaturated soils. The typical shape of the soil-water characteristic curve is showed in Figure 2.20. The suction (usually in logarithmic scale) increases as the degree of saturation (S) increases. SWCC consists of three different zones as shown in Figure 2.20.

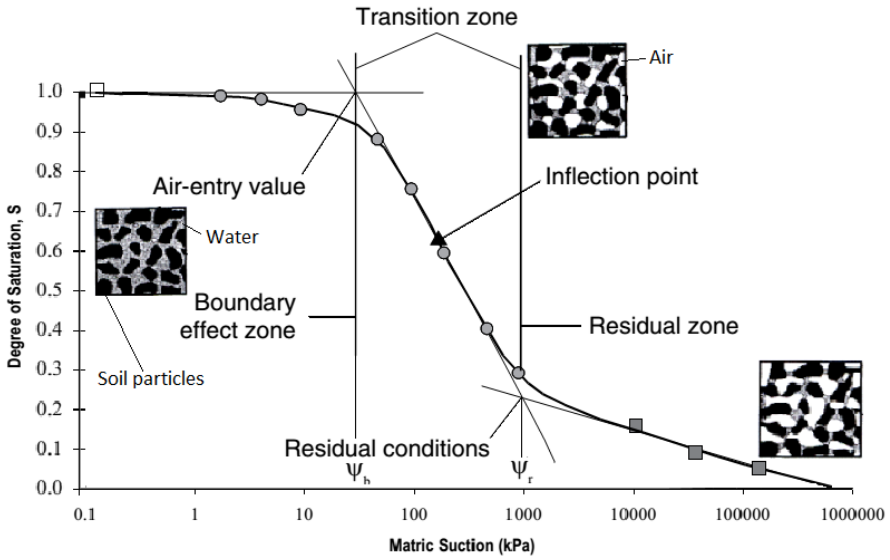

Figure 2.20. Schematic of the 3 zones of SWCC (Fredlund and Xing, 1994)

In the first zone, known as the boundary effect zone, the suction is low and the soil is in a completely saturated condition. An increment of reduction in degree of saturation (S) does not generate a substantial increase in suction. This situation continues until some air bubbles start to appear in the soil skeleton. The suction associated with this point is known as air-entry value, indicated as $(u_a\text{-}u_w)_b$ or ψ_b.

The second part of SWCC is called the transition zone. It starts at the air-entry value. In this zone, an increment of reduction in degree of saturation is associated with a considerable increase in suction.

In the third part of curve, called the residual zone, a very significant reduction in degree of saturation is required for any further reduction of suction. The suction value at the start of the third zone is marked as ψ_r and the associated S is known as the residual degree of saturation (S_r).

The SWCC is commonly formulated as a nonlinear sigmoid function using the four-parameter equation proposed by Fredlund and Xing (1994):

$$\theta_w = c(h) \times \left[\frac{\theta_{sat}}{\left[\ln\left[\exp(1) + \left(\frac{h}{a_f} \right)^{b_f} \right] \right]^{c_f}} \right] \quad \textbf{Equation 2-16}$$

$$c(h) = \left[1 - \frac{\ln\left(1 + \frac{h}{h_r} \right)}{\ln\left(1 + \frac{10^6}{h_r} \right)} \right] \quad \textbf{Equation 2-17}$$

where θ_w = volumetric water content,
h = matric suction in kPa,
a_f = fitting parameter, which is primarily a function of the air entry value of the soil,
b_f = fitting parameter, which is primarily a function of the rate of water extraction from the soil, once the air entry value has been exceeded,
c_f = fitting parameter, which is primarily a function of the residual water content,
h_{rf} = fitting parameter, which is primarily a function of the suction at which residual water content occurs, and
C(h) = correction factor which is a function of matric suction.

While SWCC can be directly measured in the lab, there are several studies that predict the SWCC parameters based on the gradation and soil index properties. In this study, the empirical model in the Mechanistic-Empirical Pavement Design Guide (MEPDG) was used to obtain the fitting parameters of the Fredlund and Zing SWCC equation. These equations are as follows:

i.

if $P_{200}PI > 0$

$$a_f = 0.00364\left(P_{200}PI\right)^{3.35} + 4\left(P_{200}PI\right) + 11,\ \text{kPa}$$

$$\frac{b_f}{c_f} = -2.313\left(P_{200}PI\right)^{0.14} + 5 \qquad \textbf{Equation 2-18}$$

$$c_f = 0.0514\left(P_{200}PI\right)^{0.465} + 0.5$$

$$\frac{h_r}{a_f} = 32.44e^{0.0186\left(P_{200}PI\right)}$$

ii.

if $P_{200}PI = 0$

$$a_f = 0.8627\left(D_{60}\right)^{-0.751},\ \text{kPa}$$

$$\bar{b}_f = 7.5 \qquad \textbf{Equation 2-19}$$

$$c_f = 0.1772\ln\left(D_{60}\right) + 0.7734$$

$$\frac{h_r}{a_f} = \frac{1}{D_{60} + 9.7e^{-4}}$$

The predicted SWCC for the test soils is shown in Figure 2.21.

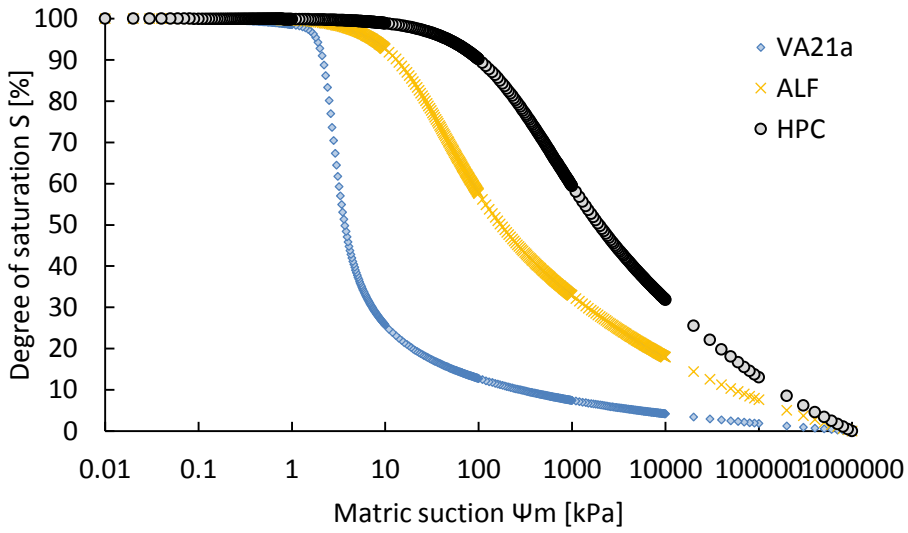

Figure 2.21. SWCC for the material used in this study

2.6. **Resilient Modulus testing**

Resilient modulus (M_R), a measure of stiffness, is a fundamental material property for unbound pavement materials. It is the most important material input for subgrade and base soils required by MEPDG. The resilient modulus for an individual soil can significantly vary with changes in density, moisture content, gradation, plasticity index, and the stress levels (Vanapalli et al., 1999).

The M_R of unbound materials is determined in the laboratory by repeated load triaxial compression tests according to the AASHTO T-307 procedure.

Fifteen combinations of different axial and confining pressures are applied during the test. The load combinations are chosen based on the location of the material in the pavement structure—whether it is a subgrade or base. Table 2-9 and Table 2-10 present the test sequences for subgrade and base soils, respectively.

Each cycle of the axial stress is a haversine shape pulse with the duration of 0.1 second and the rest period of 0.9 second. During the rest period, a contact stress equal to 10% of the maximum axial stress (σ_{max}) is maintained. The cyclic stress (σ_{cyclic}) is therefore equal to σ_{max}- $\sigma_{contact}$= 90% σ_{max}. M_R is defined as the ratio of the amplitude of the repeated axial cyclic stress (σ_{cyclic}) to the amplitude of the resultant recoverable axial strain (ε_r). Figure 2.22 shows the terms of a load pulse in M_R test and Figure 2.23 shows the stress- strain relation for a given cycle in the test.

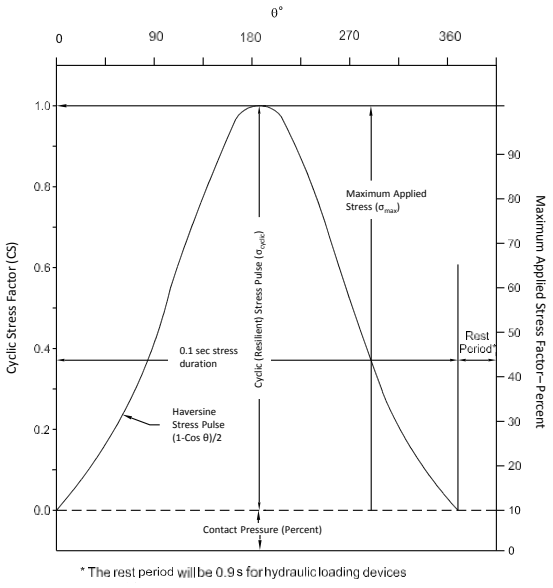

Figure 2.22. Resilient Modulus Terms: Contact stress, Cyclic Axial stress, and maximum (Resilient Vertical stress, σ_{cyclic}) (AASHTO T-307)

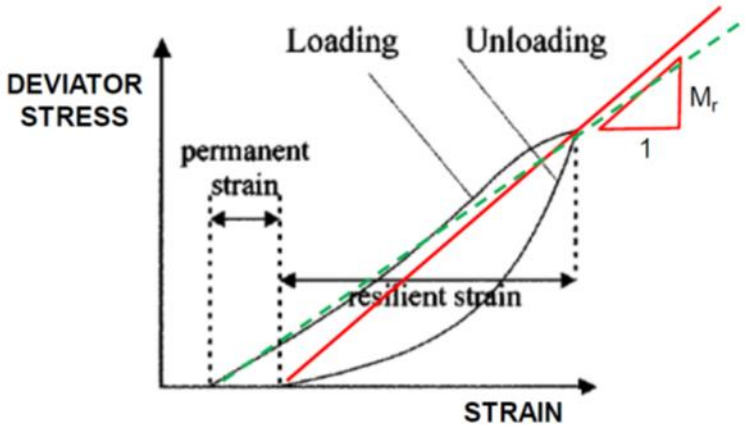

Figure 2.23. Stress-strain relationship in M_R test

Table 2-9. Testing sequence for subgrade soils

Sequence No.	Confining Pressure, σ_3		Max. Axial Stress, σ_{max}		Cyclic Stress, σ_{cyclic}		Constant Stress, 0.1 σ_{max}		No. of Load Applications
-	kPa	psi	kPa	psi	kPa	psi	kPa	psi	-
0	41.4	6	27.6	4	24.8	3.6	2.8	0.4	500–1000
1	41.4	6	13.8	2	12.4	1.8	1.4	0.2	100
2	41.4	6	27.6	4	24.8	3.6	2.8	0.4	100
3	41.4	6	41.4	6	37.3	5.4	4.1	0.6	100
4	41.4	6	55.2	8	49.7	7.2	5.5	0.8	100
5	41.4	6	68.9	10	62.0	9.0	6.9	1.0	100
6	27.6	4	13.8	2	12.4	1.8	1.4	0.2	100
7	27.6	4	27.6	4	24.8	3.6	2.8	0.4	100
8	27.6	4	41.4	6	37.3	5.4	4.1	0.6	100
9	27.6	4	55.2	8	49.7	7.2	5.5	0.8	100
10	27.6	4	68.9	10	62.0	9.0	6.9	1.0	100
11	13.8	2	13.8	2	12.4	1.8	1.4	0.2	100
12	13.8	2	27.6	4	24.8	3.6	2.8	0.4	100
13	13.8	2	41.4	6	37.3	5.4	4.1	0.6	100
14	13.8	2	55.2	8	49.7	7.2	5.5	0.8	100
15	13.8	2	68.9	10	62.0	9.0	6.9	1.0	100

Table 2-10. Testing sequence for base soils

Sequence No.	Confining Pressure, σ_3		Max. Axial Stress, σ_{max}		Cyclic Stress, σ_{cyclic}		Constant Stress, 0.1 σ_{max}		No. of Load Applications
-	kPa	psi	kPa	psi	kPa	psi	kPa	psi	-
0	103.4	15	103.4	15	93.1	13.5	10.3	1.5	500–1000
1	20.7	3	20.7	3	18.6	2.7	2.1	0.3	100
2	20.7	3	41.4	6	37.3	5.4	4.1	0.6	100
3	20.7	3	62.1	9	55.9	8.1	6.2	0.9	100
4	34.5	5	34.5	5	31.0	4.5	3.5	0.5	100
5	34.5	5	68.9	10	62.0	9.0	6.9	1.0	100
6	34.5	5	103.4	15	93.1	13.5	10.3	1.5	100
7	68.9	10	68.9	10	62.0	9.0	6.9	1.0	100
8	68.9	10	137.9	20	124.1	18.0	13.8	2.0	100

9	68.9	10	206.8	30	186.1	27.0	20.7	3.0	100
10	103.4	15	68.9	10	62.0	9.0	6.9	1.0	100
11	103.4	15	103.4	15	93.1	13.5	10.3	1.5	100
12	103.4	15	206.8	30	186.1	27.0	20.7	3.0	100
13	137.9	20	103.4	15	93.1	13.5	10.3	1.5	100
14	137.9	20	137.9	20	124.1	18.0	13.8	2.0	100
15	137.9	20	275.8	40	248.2	36.0	27.6	4.0	100

The tests were performed using a 100 kN Servo Hydraulic Dynamic Universal Testing Machine (UTM-100) from IPC Global in the University of Maryland Pavement Materials Laboratory. The original 100 kN capacity load cell of the machine was replaced with a smaller and hence more delicate load cell with a 6 kN capacity. Two external linear variable differential transformers (LVDT)s were used to record the deformations under the cyclic dynamic haversine load.

Figure 2.24. UTM- 100 apparatus

The M_R tests were performed at similar moisture and density conditions as during the test pit construction as well as at optimum moisture content and maximum dry density conditions.

The samples were prepared in molds with a height to diameter ratio of 2 using the Proctor hammer. These molds are taller than those used in a conventional Proctor compaction test. The number of layers and drops per layer were adjusted for the tall M_R molds to achieve the densities similar to that of the Proctor test. Table 2-11 lists the adjusted numbers of

layers and drops per layer used in compaction of the M_R samples unless otherwise stated (i.e., for the case of less than standard compaction for ALF Pit 1 material).

Table 2-11. The mold dimensions, number of layers and drops per layer for Proctor molds and M_R molds for standard and modified compaction energy

Proctor Mold		**Standard (T-99)**		**Modified (T-180)**	
		100 mm mold	150 mm mold	100 mm mold	150 mm mold
Weight of the hammer	[kg]	2.495	2.495	4.54	4.54
Height of drop	[m m]	305	305	457	457
Number of drops per layer	[-]	25	56	25	56
Number of layers	[-]	3	3	5	5
Diameter of mold	[mm]	101.6	152.4	101.6	152.4
Height of mold	[mm]	116.3	116.3	116.3	116.3
Volume of mold	[cm^3]	0.94	2.12	0.94	2.12
Compaction energy/volume	[kNm/m^3]	594	591	2698	2686
M_R Mold		**Standard**		**Modified**	
		100 mm mold	150 mm mold	100 mm mold	150 mm mold
Weight of the hammer	[kg]	2.495	2.495	4.54	4.54
Height of drop	[mm]	305	305	457	457
Number of drops per layer	[-]	26	48	31	59
Number of layers	[-]	5	9	7	12
Diameter of mold	[mm]	101.6	152.4	101.6	152.4
Height of mold	[mm]	203.2	295.02	203.2	295.02
Volume of mold	[cm^3]	1.65	5.38	1.65	5.38
Compaction energy/volume	[kNm/m^3]	589	599	2681	2678

Table 2-12 summarizes the testing plan for the M_R tests performed in the lab.

Table 2-12. Testing plan for M_R testing according to AASHTO T-307

Soil Type	Target MC	Target DD	Mold diameter	Compaction energy	Condition	# of Replicate	Base or Subgrade Procedure
[-]	[%]	[kg/m^3 (pcf)]	[mm]	[-]	[-]	[-]	[-]
VA21a	4.5	2435 (152)	150	Modified	Optimum- Pit 2, Pit 3	2	Base
ALF	11.5	1922.2 (120.0)	100	Standard	Optimum	3	Subgrade+Base
ALF	15.3	1837.3 (114.7)	100	Standard	Pit 2	2	Subgrade+8 cycles of Base
ALF	10.0	1771.2 (110.6)	100	<standard[1]	~Pit 1	2	Subgrade+Base
HPC	24.0	1521.8 (95.0)	100	Standard	Optimum	2	Subgrade+Base
HPC	29.0	1457.7 (91.0)	100	Standard	Pit 3	2	Subgrade+8 cycles of Base

(1) 3 layers- 15 drops per layer

The MEPDG universal constitutive model was fit to the experimental data.

Equation 2-20

$$M_R = k_1 . p_a \left(\frac{\theta}{p_a} \right)^{k_2} . \left(\frac{\tau_{oct}}{p_a} + 1 \right)^{k3}$$

where:

- M_R = resilient modulus;
- $\theta = \sigma_1 + \sigma_2 + \sigma_3 = \sigma_1 + 3 \cdot \sigma_3$ = bulk stress;
- $\tau_{oct} = \frac{1}{3} \cdot \sqrt{(\sigma_1 - \sigma_2)^2 + (\sigma_1 - \sigma_3)^2 + (\sigma_2 - \sigma_3)^2}$ = octahedral shear stress;
- p_a = atmospheric pressure used to normalize the equation;
- k_1, k_2, k_3 = regression constants determined from the laboratory tests.

The regression coefficient k_1 is a positive number that is directly proportional to the modulus. The coefficient k_2 is a positive value and is known as the stress hardening term; this is most significant in granular material. The coefficient k_3 is a negative value, known as the stress softening term. The k_3 coefficient is more significant in clay, showing a reduction of modulus with an increase of the octahedral shear stress.

Table 2-14, Table 2-15, and Table 2-13 summarize the average test results and the coefficients of the M_R universal constitutive model for the ALF, HPC, and VA21a soils, respectively. The individual results for each test specimen are provided in Appendix 9.

Table 2-13. ALF M_R test results

Sample ID	[-]	OPT	Pit 2	~Pit 1
Achieved MC	[%]	11.9%	14.6%	9.4%
Achieved DD	[pcf]	118.9	116.5	110.6
	[kg/m3]	1904.3	1867.0	1771.2
Pa	[kPa]	101.3	101.3	101.3
k1	[-]	1437.4	177.6	793.9
k2	[-]	0.429	0.485	0.601
k3	[-]	-3.717	0.000	-2.023
SSE	[MPa^2]	131.6	384.1	1635.8
Sqr(SSE)	[MPa]	11.5	19.60	40.44
R^2	[MPa^2]	98.1%	58.7%	66.2%
R^2_adj	[MPa^2]	97.6%	52.8%	61.4%
Max Sample-to-Sample CV of M_R at different stress states	[%]	32.5%	27.9%	5.0%
Average Sample-to-Sample CV of M_R at different stress states	[%]	16.2%	13.2%	1.8%

Table 2-14. HPC M_R test results

Test Condition/ Material	[-]	OPT	Pit 3
Achieved MC	[%]	24.5	30.8
Achieved DD	[pcf]	93.6	89.4
	[kg/m3]	1499.2	1432.1
Pa	[kPa]	101.3	101.3
k1	[-]	888.8	583.4
k2	[-]	0.378	0.095
k3	[-]	-0.843	-1.789
SSE	[MPa^2]	2261.6	259.0
Sqr(SSE)	[MPa]	47.56	16.09
R^2	[MPa^2]	26.8	81.0
R^2_adj	[MPa^2]	16.4	78.3
Max Sample-to-Sample CV of M_R at different stress states	[%]	6.4	18.7
Average Sample-to-Sample CV of M_R at different stress states	[%]	2.4	5.3

Table 2-15. VA21a M_R test results

Sample ID	[-]	VA21a__Ave OMC
Achieved MC	[%]	3.7
Achieved DD	[pcf]	153.4
	[kg/m3]	2458.0
Pa	[kPa]	101.3
k1	[-]	590.6
k2	[-]	0.824
k3	[-]	0.000
SSE	[MPa2]	2765.0
Sqr(SSE)	[MPa]	52.58
R2	[MPa2]	96.6
R2_adj	[MPa2]	95.7
Max Sample-to-Sample CV of MR at different stress states	[%]	47.9
Average Sample-to-Sample CV of MR at different stress states	[%]	17.6

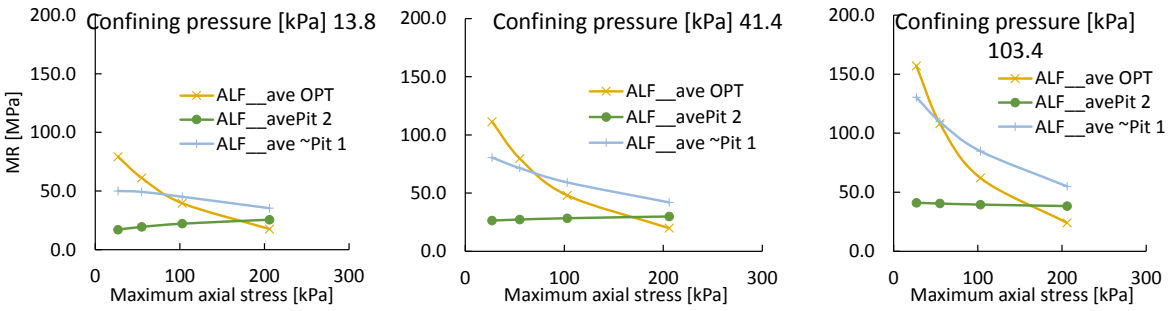

Figure 2.25. M_R for ALF at optimum, and Pit 1 and Pit 2 condition

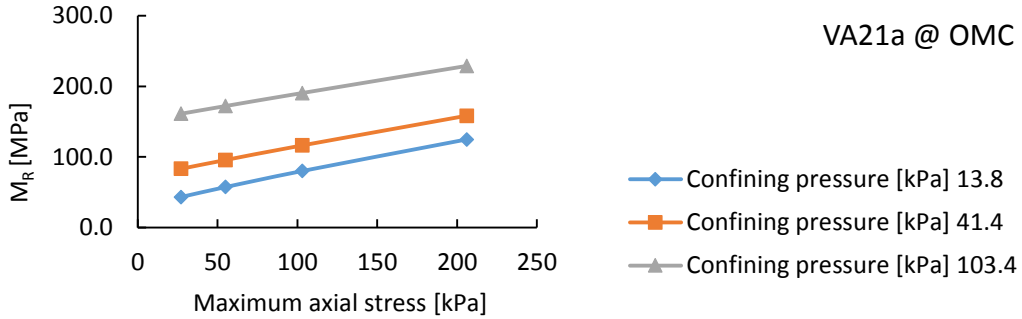

Figure 2.26. M_R for VA21a at optimum, as well as Pit 2 and Pit 3 construciton condition

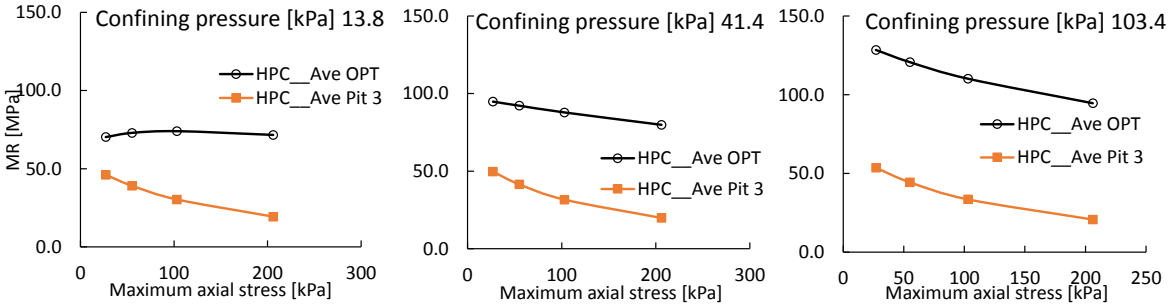

Figure 2.27. M_R for HPC soil at optimum and Pit 3 construction condition

2.7. Factors affecting the resilient modulus

The resilient modulus of geomaterials is influenced by several factors. The stress and moisture dependency of geomaterials are widely accepted among researchers (e.g. Lekarp et al. 2000, Smith and Nair 1973, Vuong 1992, Haynes and Yoder 1963, Hicks and Monismith 1971, Barksdale and Itani 1989, Dawson et al. 1996, and Heydinger et al. 1996, Wolfe and Butalia (2004), Hopkins et al. (2004) and Ooi et al. (2006), Richter (2006), Kung et al. (2006), Gupta et al. (2007), and Cary and Zapata (2010)). However, the effects of other factors including dry density are found relatively inconsistent.

Even though there is a great amount of information on the effect of moisture on resilient modulus of unbound material, most of the previous studies had looked at the long term and seasonal effects of moisture. Few studies differentiate the effect of compaction and post-compaction moisture variations due to surface drying. In addition, the shortest study span of moisture effects found in literature are on daily basis while QA testing is typically performed immediately or within a few hours after compaction.

In NCHRP 10-84, Nazarian et al. (2013) tried to capture the effect of compaction MC, testing MC, and density on modulus using the free-free resonant column (FFRC) test. FFRC showed that the higher the difference between the MC at compaction and testing, the higher will be the seismic modulus which in turn is correlated with M_R. They also found that the effect of density is negligible as compared to MC. M_R tests performed on specimens compacted at 96% MDD, 98% MDD and 100% MDD and all to a similar OMC did not show an increasing stiffness due to higher density.

The effect of moisture is usually modeled in two different approaches among past researchers: (a) separate from stresses in form of an empirical environmental factor (e.g. Cary and Zapata (2010), Nazarian et al. (2013); and (b) based on unsaturated soil mechanics considering suction and its effect on effective stresses. This approach is elaborated in detail in Section 2.8).

As an example of the first approach, Cary and Zapata (2010) found that the effect of moisture on modulus of soils is similar at different stress states and thus separable. The

environmental factor (F_U) was introduced as the function of the degree of saturation to estimate the effect of moisture and density on resilient modulus:

Equation 2-21

$$M_R = F_U \times M_{R@opt}$$

where $M_{R@opt}$ is the resilient modulus at optimum moisture content and maximum dry density at any given stress state.

Equation 2-22 presents the enhanced version of F_U parameter from the study by Cary and Zapata (2010), which combines the effects of percent compaction (PC) and degree of saturation (S):

$$F_U = 10^{\left(a + \frac{b-a}{1+e^{\left(\ln\left(\frac{-b}{a}\right) + k_m \cdot \left(\frac{S - S_{opt}}{100}\right)\right)}} \right)} . 10^{C_2 \cdot (PC - 100)}$$

Equation 2-22

where $a = -0.40535$, $b = 0.80158$, $k_m = 1.33194$ and $C_2 = 0.03223$;
$(S - S_{opt})$ is the variation in the degree of saturation S expressed as a decimal fraction with respect to the degree of saturation at optimum conditions S_{opt}.

Figure 2.28 shows contours of F_U versus PC and S based on this equation.

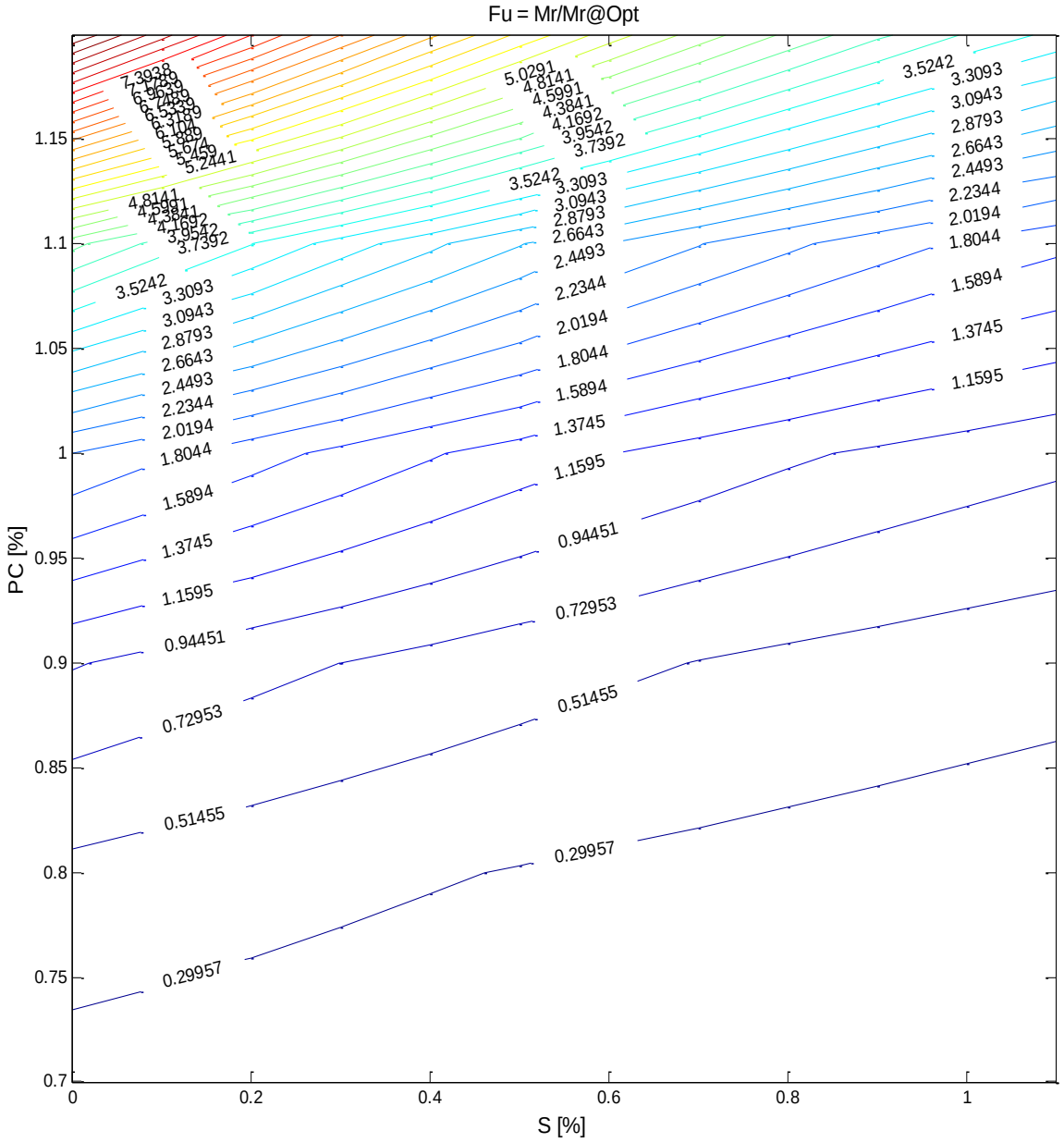

Figure 2.28. Contour of F_U as a function of PC and S.

2.8. Evaluation of measured M_R vs. predictive models

2.8.1 Background on unsaturated soil mechanics

For soils in saturated or unsaturated conditions, the mechanical response is a function of effective stresses rather than total stresses (Bishop, 1960; Terzaghi, 1996). In unsaturated soils, two main factors define the effective stresses; (1) pore air pressure (u_a) which is often insignificant, and (2) the difference between u_a and the pore water pressure (u_w), designated as matric suction ($u_a - u_w$) or simply u as referred to in this study. Bishop (1960) formulated the effective stress of unsaturated soils as:

Equation 2-23

$$\sigma' = (\sigma - u_a) + \chi (u_a - u_w)$$

Matric suction (u) is a function of pore size geometry, pore size distribution, and the soil water content and can be predicted from the soil-water characteristic curve (SWCC) (Fredlund and Xing, 1994) as described earlier in Section 2.5. The effective stress parameter χ—also known as pore suction resistance factor—in Equation 2-23 is a material variable that shows the contribution of the matric suction in the effective stress and is generally considered to vary between zero and unity, corresponding to a completely dry and fully saturated condition, respectively. At the fully saturated condition, the equation reduces to Terzaghi's classic effective stress equation.

While several researchers, e.g. Lytton (1995), Khalili and Khabbaz (1998), and Roberson and Siekmeier (2002), have proposed different models to quantify the pore suction resistance factor, these have not been well accepted to date and χ equal to 1 is often preferred by researchers (Morgenstern, 1979).

To characterize the nonlinear modulus of soils, tests at various conditions—in particular stress and moisture—may be required. Yet, routine testing is usually only performed at optimum moisture and density condition. Therefore, implementation of an accurate constitutive model based on mechanics of unsaturated soils capable of predicting the nonlinear M_R at other moisture and density condition is of great interest. In this study several resilient modulus constitutive models and two empirical predictive models were evaluated on independent cohesive and noncohesive soils. The models were compared in terms of their rationality, accuracy of prediction, and applicability to the widest range of soils.

In this study, 4 types of subgrade and 4 types of granular base soil data from Andrei (2003) were used to evaluate the models. The soil type and description for each material is presented in Table 2-16. More information about the volumetric and mechanical properties of the soils can be found in Andrei (2003).

Table 2-16- Soil Type and Description (From Andrei, 2003)

	Soil Types	Description
Subgrade	Phoenix Valley Subgrade (PVSG)	Clayey Sand, SC
	Yuma Sand Subgrade (YSSG)	Poorly Graded Gravel with Sand, GP, Non Plastic
	Flagstaff Clay Subgrade (FCSG)	Clayey Sand, SC
	Sun City Subgrade (SCSG)	Clayey Sand, SC
Base	Grey Mountain Base (GMAB2)	Well Graded Gravel with Sand, GW, Non Plastic
	Salt River Base (SRAB2)	Poorly Graded Sand with Gravel, SP, Non Plastic
	Globe Base (GLAB2)	Poorly Graded Sand with Silt and Gravel, SP-SM, Non Plastic
	Prescott Base (PRAB2)	Poorly Graded Sand with Silt and Gravel, SP-SM, Non Plastic

All base materials and one of the subgrade soils were non-plastic. The soil water characteristic curves, which were key inputs to the evaluated models, were predicted from the gradation and soil indices using the Fredlund and Xing (1994) procedure as implemented in the MEPDG. The unconfined compression (U_C), which was input to one of the predictive models, was estimated from CBR values according to Black (1962).

For all of the soils, the M_R tests were performed on specimens compacted with standard and modified Proctor energies at their corresponding optimum moisture content as well as above and below optimum. This resulted in a total of 6 scenarios for each soil.

2.8.2 Evaluated unsaturated resilient modulus constitutive models

The 9 following models were selected for evaluation. The parameters of the following models were calibrated—except for M4 and M6 predictive models—based on the measured data at optimum moisture content and maximum dry density of the standard Proctor compaction test scenario.

The models where subsequently used to predict the M_R at the other moisture-density conditions. The evaluated models are explained below:

M1 is the general nonlinear model implemented in the MEPDG and is a function of total bulk stresses. This model does not consider the effect of suction *u.*

Equation 2-24

M1: $$M_R = K_1 P_a \left(\frac{\sigma_{bulk}}{P_a}\right)^{K_2} \left(\frac{\tau_{oct}}{P_a} + 1\right)^{K_3}$$

in which $\sigma_{bulk} = \sigma_1 + \sigma_2 + \sigma_3 = \sigma_d + 3\sigma_c$, $\sigma_1, \sigma_2, \sigma_3$ = three principal stresses, σ_d= deviatoric stress, σ_c= confining stress, τ_{oct}= octahedral shear stress = $\frac{\sqrt{3}}{2}\sigma_d$, and the coefficients K_1, K_2, and K_3 are regression coefficients.

M2, the second evaluated model, is similar to M1, with the bulk effective stress ($\sigma_{bulk} + 3u$) replacing σ_{bulk}. The reason for the multiplication of suction by 3 is that suction adds to each of the three principal effective stresses.

Equation 2-25

$$\textbf{M2}: M_R = K_1 P_a \left(\frac{\sigma_{bulk}+3u}{P_a}\right)^{K_2} \left(\frac{\tau_{oct}}{P_a}+1\right)^{K_3}$$

M3, proposed by Liang et al (2008) adds a suction dependency term (χ) to the effective stress term. The suction dependency term was proposed by Khalili and Khabbaz (1998). In this model the suction term (u) is not multiplied by 3.

Equation 2-26

$$\textbf{M3}: M_R = K_1 P_a \left(\frac{\sigma_{bulk}+\chi\, u}{P_a}\right)^{K_2} \left(\frac{\tau_{oct}}{P_a}+1\right)^{K_3}$$

Equation 2-27

$$\chi = \left(\frac{(u_a - u_w)_b}{u_a - u_w}\right)^{0.55} = \frac{u_{air-entry}}{u}$$

The $u_{air-entry}$ term is the suction at air entry level where air starts to enter the largest pores in the soil. The upper limit of χ is equal to 1.

M4, proposed by Siekmeier (2011), has been found a suitable predictive model for subgrade and fine soils. The K_1-K_3 coefficients are also predicted as a function of suction and volumetric moisture content from SWCC of the soils. The equations are as follows:

Equation 2-28

$$\textbf{M4:}\ M_R = K_1 P_a \left(\frac{\sigma_{bulk}+\theta_w f\, u}{P_a}\right)^{K_2} \left(\frac{\tau_{oct}}{P_a}+1\right)^{K_3}$$

in which $K_1 = 800 \times \left(\frac{1}{5\theta_{sat}}\right)^{1.5} \times \left(\frac{1}{log_{10}(u)}\right)$, $K_2 = log_{10}(u) - 1$, $K_3 = -8\theta_{sat}$, $f = \theta_w^{10\theta_{sat}^3}$, θ_w= volumetric water content, θ_{sat}= volumetric water content at saturation, and $\chi = \theta_w f$.

The χ in M4 model is not bracketed by the upper bound of 1. The M4 predictive model was re-evaluated as model M5, in which the K values were calibrated for each soil through nonlinear regression. The formula for *f* was kept the same.

Yan et al. (2013) proposed two predictive models for subgrade soils based on gene expression programming (GEP) to correlate M_R with routine properties of subgrade soils

and state of stress. GEP I was computationally unstable for nonplastic soils and was found erroneous for plastic soil and has thus been excluded from the comparisons. The GEP II model, selected for evaluation as model M6—is displayed below:

Equation 2-29

$$\textbf{M6}: M_R = \operatorname{atan}\left\{\gamma_d * \left[\frac{\gamma_d - U_c}{PI}\right]\right\} + \left\{2 * \left[\frac{sqrt(PI)}{P_{200}}\right]\right\} + \sigma_d + \left\{2 * \sin\left[\frac{\gamma_d * \exp\{\operatorname{atan}[\sin(P_{200})]\}}{P_{200}}\right]\right\} + (\sigma_d * \operatorname{atan}\{sqrt(P_{200}) - [(\sigma_d * P_{200})/\gamma_d]\}) + \{\operatorname{atan}[sqrt(U_c) - \gamma_d] + \operatorname{atan}(\gamma_d)\}$$

in which U_c = unconfined compressive strength, *PI* = Plasticity Index, *P200* = percentage passing the No. 200, γ_d= dry density, and σ_d= deviatoric stress.

Recently, Gu et al. (2014) evaluated a model proposed by Lytton (1995) and reported satisfactory predictions for base course aggregates. The model is:

Equation 2-30

$$M_R = K_1 P_a \left(\frac{\sigma_{bulk} - 3\theta_w f u}{P_a}\right)^{K_2} \left(\frac{\tau_{oct}}{P_a}\right)^{K_3}$$

The *f* parameter in this model is a function of θ_a and θ_u, which are the volumetric water contents of the soil at air entry and unsaturation, respectively. The parameter *f* is bracketed by the upper and lower bounds below:

Equation 2-31

$$f_{upper\ bound} = \left[\left(\frac{\theta_a - \theta_w}{\theta_a - \theta_u}\right) + \frac{1}{\theta_w}\left(\frac{\theta_w - \theta_u}{\theta_a - \theta_u}\right)\right]$$

Equation 2-32

$$f_{lower\ bound} = \left[\frac{1}{\left(\frac{\theta_a - \theta_w}{\theta_a - \theta_u}\right) + \theta_w\left(\frac{\theta_w - \theta_u}{\theta_a - \theta_u}\right)}\right]$$

Three *f* values were evaluated in the Lytton model to predict the resilient modulus, resulting in the following models. $\chi = \theta_w f$ ranges from $\theta_u$to 1 and therefore is theoretically sound.

M7 based on $f = \frac{f_{upper\ bound} + f_{lower\ bound}}{2}$, **M8** based on $f = f_{upper\ bound}$, and **M9** based on $f = f_{lower\ bound}$. Figure 2.29 shows the bounds of the pore suction for Lytton (1995) model.

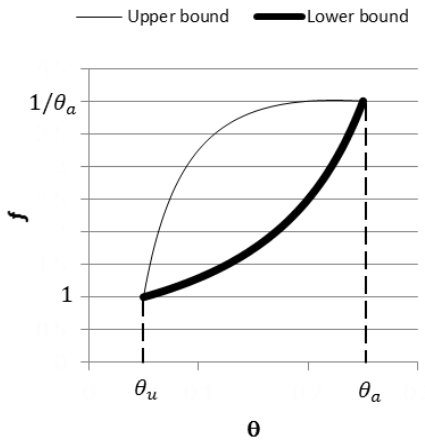

Figure 2.29. The bounds of pore suction for Lytton (1995)

2.8.3 Comparison of evaluated M_R predictive models

Least squares analysis was applied to the measured data at optimum moisture content and maximum standard dry density for all models except for the M4 and M6 predictive models to find the best model. To evaluate the performance of the models, the root mean square error (RMSE) and average relative error (RE) of model prediction were calculated at each moisture condition (wet, dry, optimum), each compaction energy effort (standard and modified Proctor compaction effort), and overall for each soil and every model. RMSE, a measure of model accuracy, reflects both systematic and nonsystematic error variation and has the same units as M_R, here reported in ksi. RE measures the systematic error or bias of the models. The definitions of these evaluation criteria are given as follows:

Equation 2-33

$$\mathrm{RMSE} = \sqrt{\frac{1}{n}\sum_{i=1}^{n}\left((M_{R-predicted} - M_{R-measured})^2\right)}$$

Equation 2-34

$$\mathrm{RE} = \frac{\frac{1}{n}\sum_{i=1}^{n}\left(M_{R-predicted} - M_{R-measured}\right)}{\frac{1}{n}\sum_{i=1}^{n}(M_{R-measured})} = \bar{e}/\overline{M_R}$$

Figure 2.30 shows the distribution of RMSE of the evaluated models at different moisture and compaction energy conditions. As expected, all the models performed well at the optimum moisture and density, the condition at which was the model parameters were calibrated. Prediction errors were the highest at dry of optimum at both compaction efforts.

Figure 2.31 presents the prediction bias of the models for the plastic and nonplastic soils. Overall, all models underpredicted at dry of optimum for nonplastic soils.

The overall RMSE of prediction of the models per soil is shown in Table 2-17. The shaded cells in the table present the most accurate model. Overall, model M8—Lytton (1995) with $f_{upper\ bound}$—outperformed the other models for both plastic and neoplastic soils. The M2 model, which in fact is the effective stress model with f=1, performed very well for nonplastic soils but did not provide an acceptable prediction accuracy for plastic soils. An example of the measured vs. predicted M_R by M2 for a plastic soil (PVSG) is shown in Figure 2.32. Table 2-18 shows the RE for each model and soil type. Again, model M8 was overall the most consistent model for both plastic and nonplastic soils. Model M4 and M2, while outperformed in several soil types, were erroneous in several others and did not provide a consistent prediction over the range of the evaluated soils.

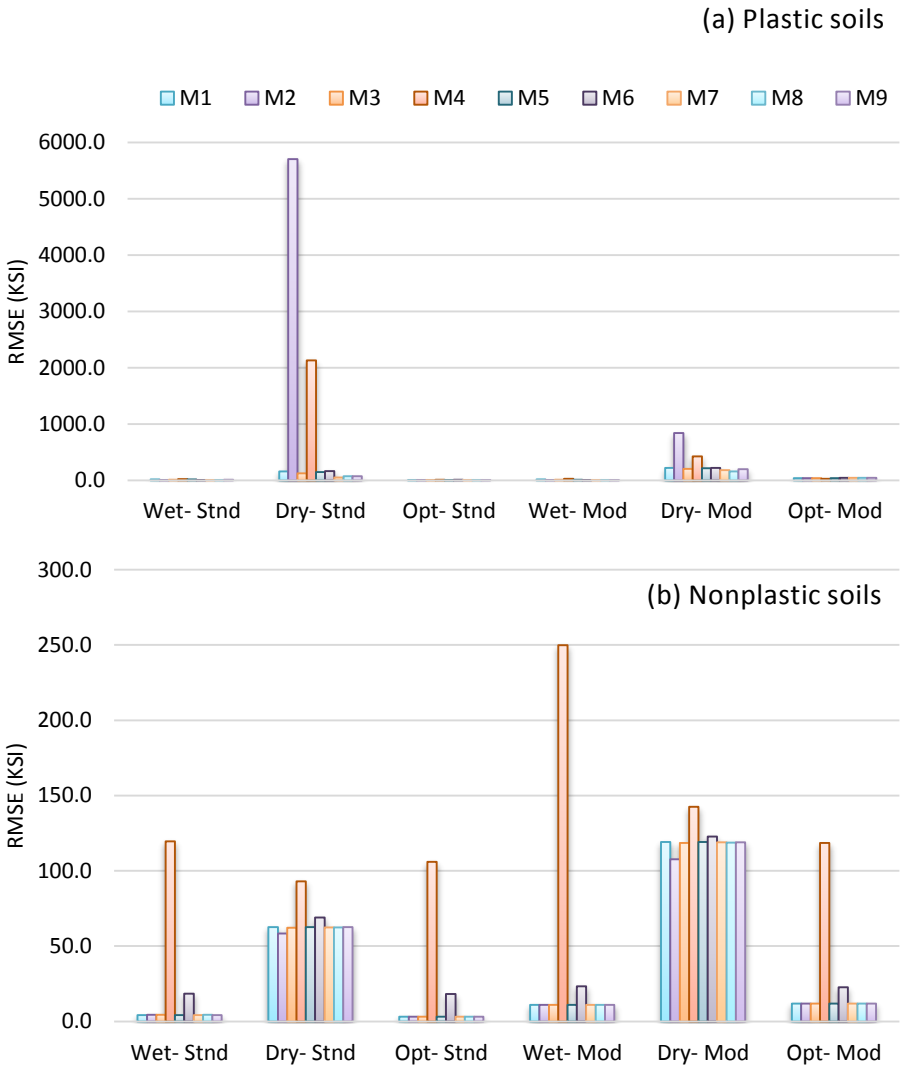

Figure 2.30. RMSE of evaluated models at different moisture and compaction energy condition for (a) Plastic, and (b) Nonplastic soils.

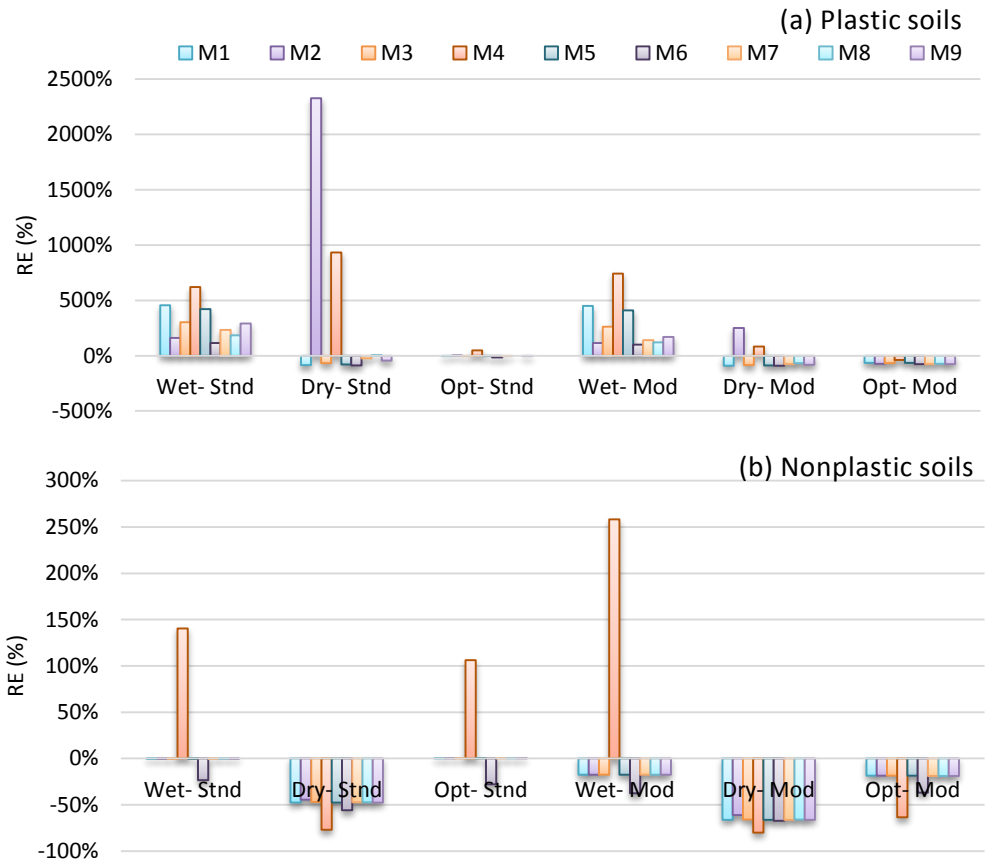

Figure 2.31. Average RE of evaluated models at different moisture and compaction energy condition for (a) Plastic, and (b) Nonplastic soils.

Table 2-17. Overall RMSE of the evaluated models for each soil.

RMSE (ksi)	M1	M2	M3	M4	M5	M6	M7	M8	M9
1.PVSG	143.0	3452.0	129.8	292.4	139.8	141.9	99.9	90.3*	118.0
2.YSSG	88.0	67.9	87.1	268.4	87.9	96.8	87.5	87.4	87.5
3.FCSG	49.6	49.6	49.2	46.2	49.7	55.0	51.4	50.9	52.1
4.SCSG	107.7	2964.4	86.9	2138.2	102.7	110.4	57.8	60.4	64.9
5.GMAB	26.9	26.8	26.9	196.0	26.9	37.5	26.9	26.9	26.9
6.SRAB	48.3	44.5	48.0	81.6	48.3	50.3	48.3	48.1	48.4
7.GLAB	41.1	39.9	40.9	67.3	41.1	43.3	41.0	40.9	41.1
8.PRAB	47.0	46.0	46.9	208.7	47.0	47.7	47.0	47.0	47.1
Plastic	100.1	2155.3	88.6	825.6	97.4	102.4	69.7	67.2	78.3
NonPlastic	50.3	45.0	49.9	164.4	50.2	55.1	50.1	50.1	50.2
All	69.0	836.4	64.5	412.3	67.9	72.9	57.5	56.5	60.8

* The shaded cells show the model yielded the lowest RMSE of prediction for each Soil type.

Table 2-18. Overall relative bias of the evaluated Models for each soil.

RE, %	M1	M2	M3	M4	M5	M6	M7	M8	M9
1.PVSG	-83%	1310%	-76%	85%	-81%	-86%	-53%	-30%	-68%
2.YSSG	-55%	-43%	-55%	127%	-55%	-80%	-55%	-55%	-55%
3.FCSG	-58%	-66%	-65%	-51%	-60%	-75%	-70%	-69%	-71%
4.SCSG	-71%	1789%	-58%	1240%	-67%	-83%	-21%	-5%	-35%
5.GMAB	-23%	-23%	-23%	16%	-23%	-40%	-23%	-23%	-23%
6.SRAB	-36%	-34%	-36%	-28%	-36%	-41%	-36%	-36%	-36%
7.GLAB	-32%	-31%	-32%	-36%	-32%	-38%	-32%	-32%	-32%
8.PRAB	-35%	-34%	-35%	-50%	-35%	-41%	-35%	-35%	-35%

* The shaded cells show the model yielded the lowest RMSE of prediction for each Soil type.

Figure 2.33 presents the RMSE and RE for model M8 at different moisture and compaction effort conditions. M8, albeit better than the other models, underpredicted the moduli at dry of optimum and optimum moisture at the modified compaction condition for all soils and overpredicted at wet of optimum for the standard and modified compaction conditions of the plastic soils.

Figure 2.34 shows the measured vs. predicted M_R for GMAB and PVSG for the M8 model. These two soils provided the most and least accurate predictions, respectively.
Overall, model M8—the model proposed by Lytton (1995) using the upper bound of the suction resistance factor ($\theta_w f$) based on Equations 8 and 9—was found to be the most accurate model over a wide range of fine and coarse and plastic and nonplastic soils used in pavements subgrades and bases. However, the RMSE for all models were high and far from acceptable. Local biases existed in all the evaluated models. The models tended to systematically underpredict the moduli at dry of optimum.

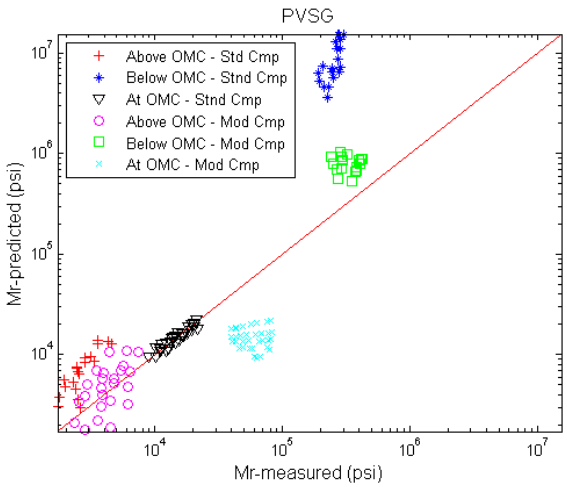

Figure 2.32. $M_{R\text{-predicted}}$ VS. $M_{R\text{-measured}}$ - Model M2 for Soil PVSG.

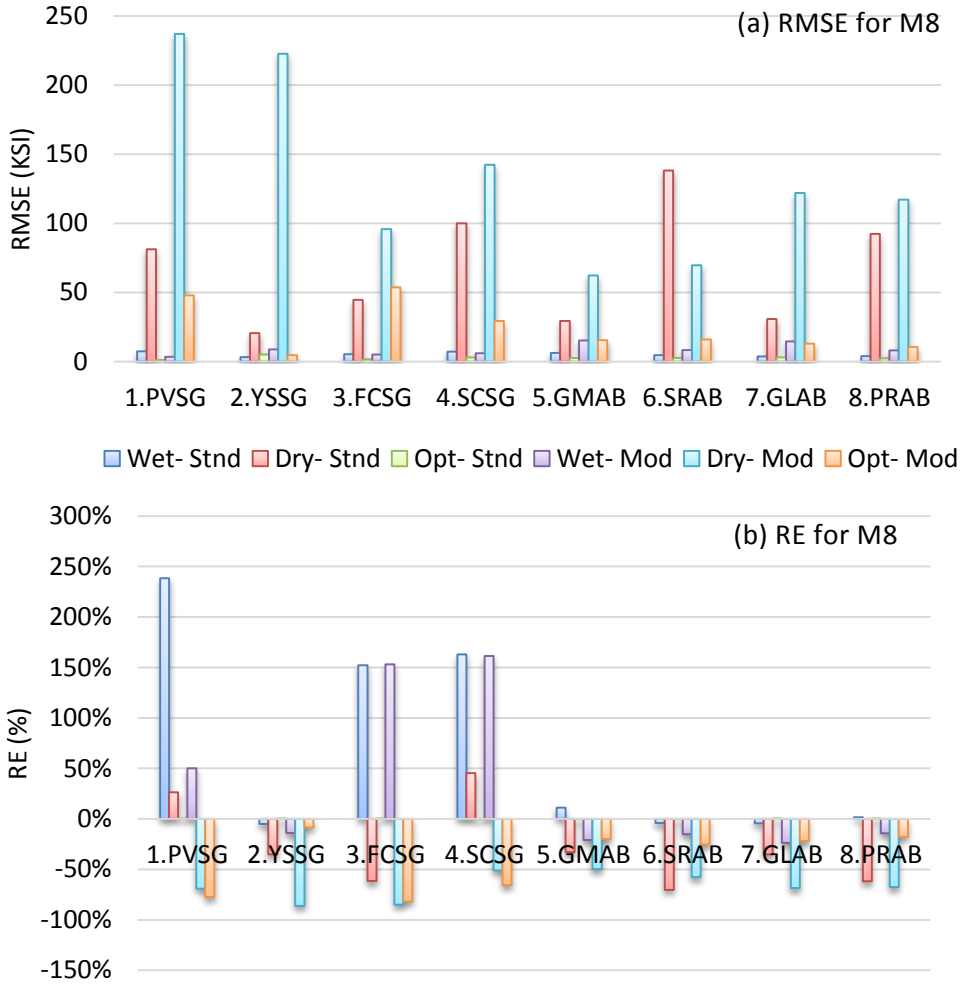

Figure 2.33. (a) RMSE and (b) RE at different moisture and compaction energy conditions for Model 8.

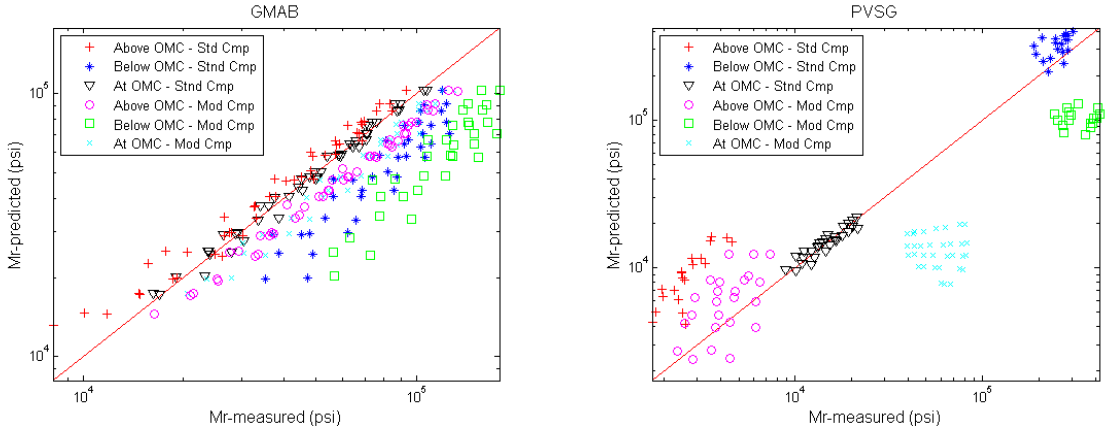

Figure 2.34. $M_{R\text{-predicted}}$ from model M8 VS. $M_{R\text{-measured}}$ for GMAB and PVSG soils.

2.8.4 Findings from evaluation of M_R predictive models

In order to standardize the LWD data, it is important to be capable of characterizing the nonlinear modulus of soils, at various stresses and moisture contents, which requires an extensive amount of testing.

Yet, routine M_R testing (if performed) is usually performed only at the optimum moisture and density condition. Therefore, an accurate model based on mechanics of unsaturated soils that can predict the nonlinear M_R at other test conditions is of a great interest.

In this study, several resilient modulus constitutive models and two empirical predictive models were evaluated on independent cohesive and noncohesive soils obtained from Andrei (2003). The statistical analysis of accuracy and bias on the predicted moduli at various moisture and density conditions found that the model proposed by Lytton (1995), designated here as model M8, provided the most accurate predictions of the nine evaluated models and is rationally founded on the principals of unsaturated soil mechanics. While the model performed better than the rest in terms of rationality, accuracy of prediction, and applicability to the widest range of cohesive and noncohesive soils, the predictions were far from acceptable and perhaps cannot be used by confidence for LWD target modulus.

Although the ability to predict M_R at different moisture and density conditions would represent a significant advance in the state of the art, the present inability to do this reliably using current models is fortunately not a major issue for the purposes of the present study. LWD testing for compaction QA in the field will usually be performed immediately or very shortly (within 2 hours) after material placement. Any surface drying from the as-placed moisture condition will be minimal during this short time interval for most soils.

2.9. **LWD testing on Proctor Molds**

LWD tests were performed directly on the Proctor compacted molds on top of a concrete foundation in laboratory as can be seen in Figure 2.36. The diameter of the LWD plate was almost equal to that of the mold. The data from the first three seating drops were not included in the calculations. The maximum deformation (δ), and maximum impact load (F), and maximum peak stiffness (k) which is equal to F/δ were averaged for the last three drops and used in the analysis.

The modulus of the soil was derived from the theory of elasticity for a cylinder of elastic material with constraint lateral movement imposed by the rigid mold. In this analysis it was assumed that (a) soil is an elastic material, (b) the deformation occurred in the soil material only and not in the underlying stiff concrete foundation, and (c) the impact load was static as opposed to dynamic.

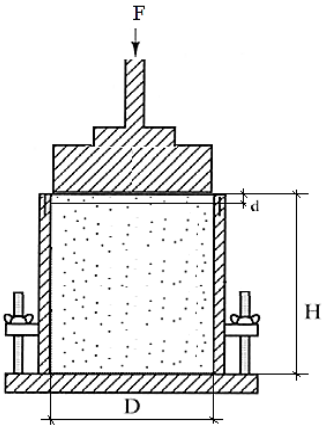

Figure 2.35. Schematic of LWD testing on Mold. (Tefa, 2015)

The obtained equation is as follows:

Equation 2-35

$$E = (1 - \frac{2v^2}{1 - v}) \frac{4H}{\pi D^2} k$$

where μ = poison's ratio, H = height of the mold, D = the diameter of the plate or mold, and k = soil stiffness =F/δ as calculated by LWD device .

The lateral pressure is as follows:

Equation 2-36

$$\sigma_r = \sigma_z \times \frac{v}{1 - v}$$

Figure 2.36. Configuration of Olson LWD test on top of the Proctor mold. (Tefa, 2015)

The tests were performed concurrent to the Proctor testing using the three LWDs. 3 to 4 different drop heights were used to assess the stress dependency of the test material. Initially, the drop heights in Table 2-19 were used. Later, the drop heights were modified to include heights as low as 2.5 cm. Table 2-20 tabulates the revised drop heights. It is important to note that the magnitude of the peak load is correlated with $h^{0.5}$ based on Equation 2-6. The testing order with each LWD device was switched in turns to avoid any systematic differences in the results due to the order in which LWD devices were tested on molds and potential sample destruction. Similar to the field projects, six LWD drops were executed at each drop height and the average modulus of the last three drops were obtained.

Table 2-19. Initial drop heights for LWD testing on molds

Drop height ID	Zorn	Dynatest	Olson
[-]	[cm]	[cm]	[cm]
h1	5	10	11
h2	17	23	20
h3	30	30	31
h4	72	38	61
h5		61	
h6		84	

Table 2-20. Revised drop heights for LWD testing on molds

Drop Height ID	Zorn	Dynatest	Olson
[-]	[cm]	[cm]	[cm]
h7	2.5	2.5	2.5
h8	5.1	5.1	5.1
h9	7.6	7.6	7.6
h10	10.2	10.2	10.2
h11	12.7	12.7	12.7
h12	31.8	17.8	21.6

This test is an easy add-on to the routine Proctor test and can serve as a measure to find the target LWD modulus in field. The LWD modulus on mold is derived from Equation 2-35 and is designated as *E_ZM*, *E_DM*, and *E_OM* for Zorn, Dynatest, and Olson LWDs, respectively. P/Pa is the ratio of the induced stress to the air pressure (101.325 kPa).

Prior to any analysis, the force and deflection signals were screened using the available software for each LWD device. The poor signals (e.g. Figure 2.37- B for Zorn, Figure 2.38A and B for Olson, and Figure 2.39B for Dynatest) were detected and deleted prior to any further analysis. Moreover, data with higher than 5% CV in the modulus of last three drops were also excluded.

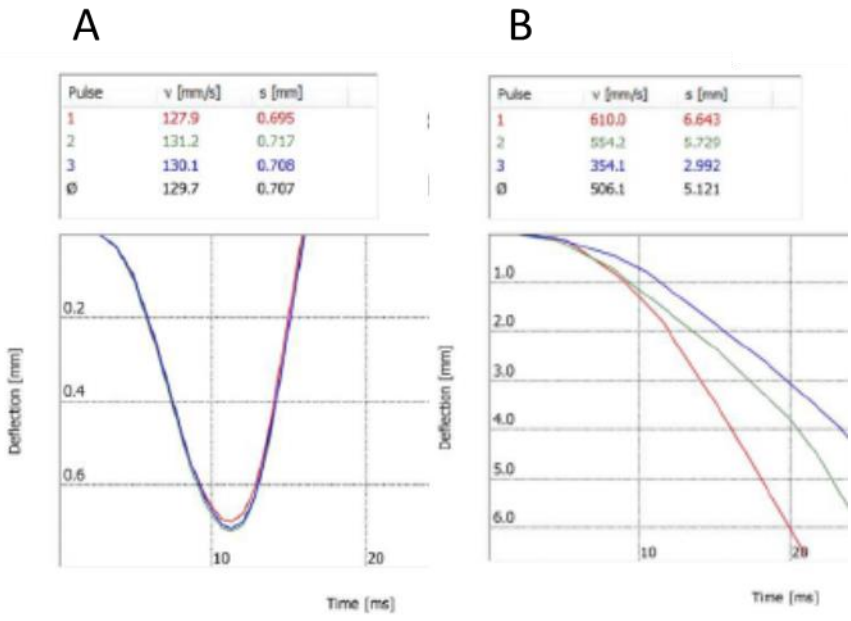

Figure 2.37. Example of (A) good signal and (B) poor LWD Zorn deflection data. Poor signals ommited prior to any further analysis. Graphs obtained from ZornZFG software

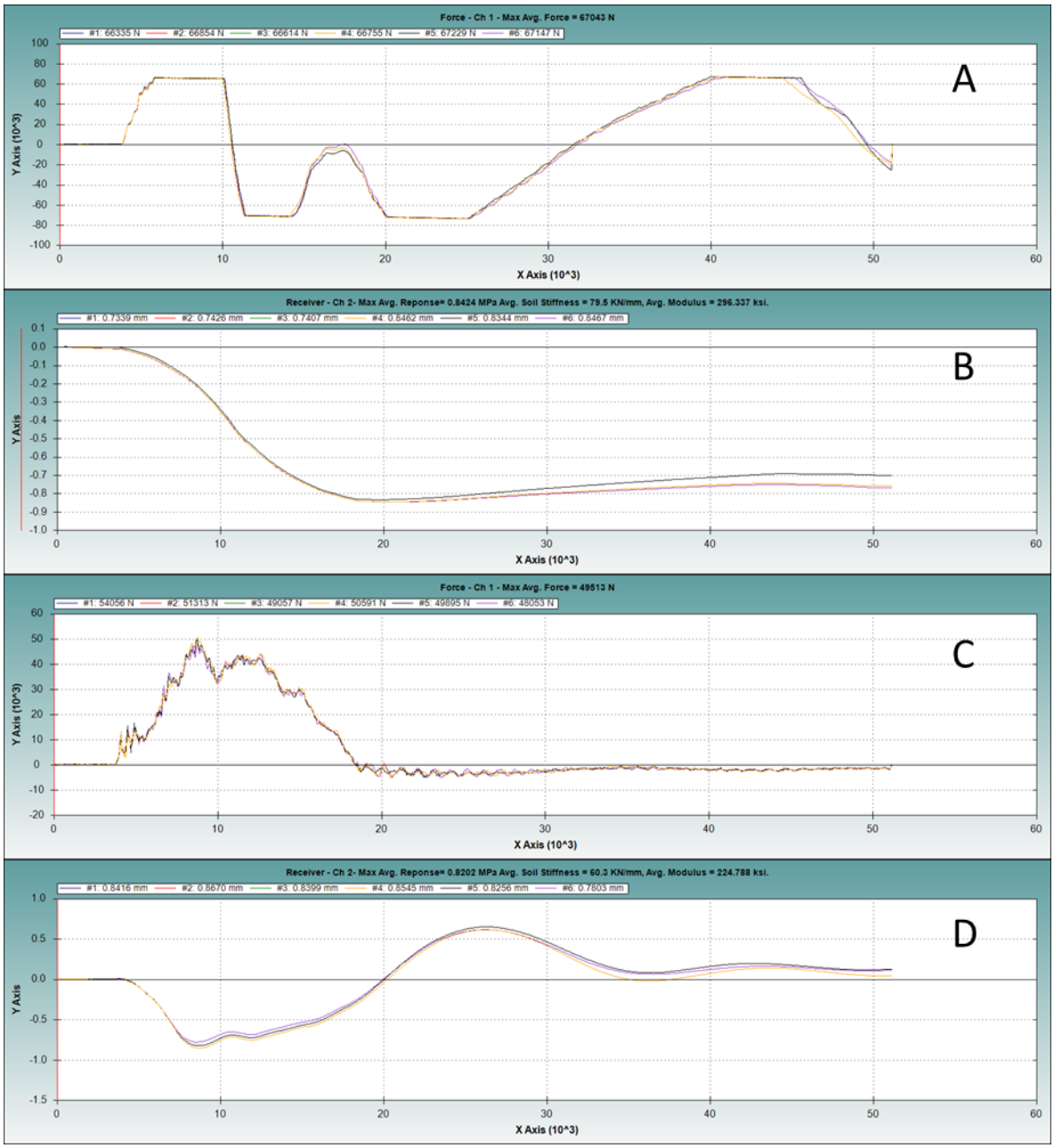

Figure 2.38. An example of (A) poor clipped force signal; (B) poor deflection signal with no rebound; (C) a good force signal; and (D) good deflection signal in Olson LWD. Poor signals ommited prior to any further analysis. Graphs obtained from WinLWD Olson software

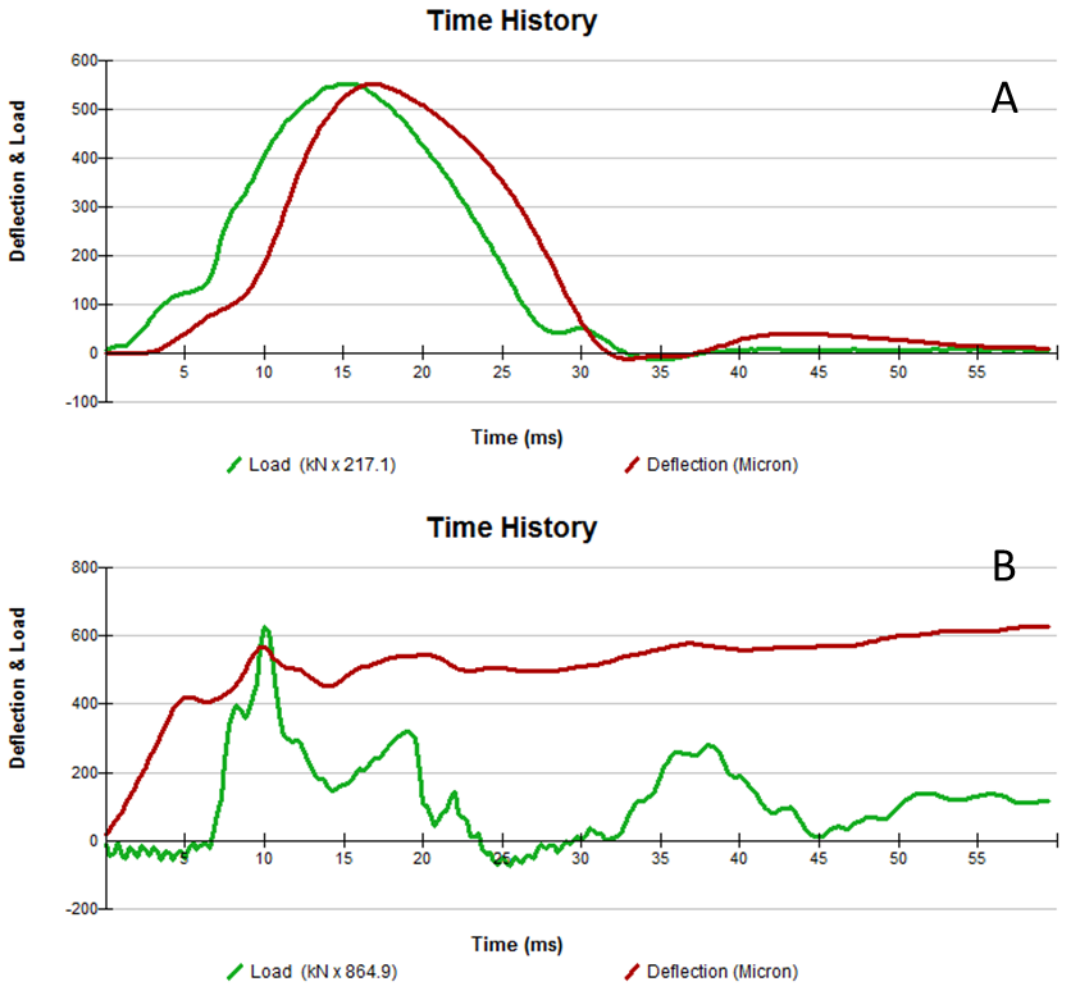

Figure 2.39. Example of (A) good and (B) poor signal in Dynatest LWD- Poor signals ommited prior to any further analysis. Graphs obtained from LWDmod Dynatest software

The LWD moduli was plotted in three layouts:

i. Versus GWC for different stress states (P/Pa) superimposed by Dry density plots versus the GWC.
ii. Versus VWC for different stress states (P/Pa) superimposed by Dry density plots versus the VWC.
iii. Versus P/Pa at different GWC. The plots are color coded from highest GWC to the lowest—with black representing the highest GWC, followed by Pink, Blue, and Green.

An example of (i) and (ii) plots is shown in Figure 2.40 for Zorn LWD testing on HPC soil. There was not a noticeable difference between the trends of the modulus when plotted against GWC or VWC. Due to the compaction condition of the samples, there was a strong correlation between the GWC and VWC of the tested samples and therefore the plots of modulus versus GWC and modulus versus VWC were similar for all soils. Subsequently, only plots of modulus versus GWC are presented for brevity. However, it is not valid to conclude that the trend of the modulus is similar versus gravimetric or volumetric water contents in all cases.

Figure 2.41, Figure 2.42, and Figure 2.43 present the modulus of HPC, ALF, and VA21a soil versus GWC at different P/Pa values as measured by the three LWDs, respectively.

Figure 2.44, Figure 2.45, and Figure 2.46 present the modulus of HPC, ALF, and VA21a soil versus P/Pa at different GWC values as measured by the three LWDs, respectively. Olson LWD induced higher stresses than the two other LWDs at a similar height which is due to the higher stiffer of the spring.

Tests were capable of capturing the stress and moisture dependency trends for the different types of soils. The sample-to-sample variability and variability in the modulus of last three drops was higher in this laboratory testing than the field data (discussed in Section 4.10). One of the reasons could be the physical instability of the test setup especially for the drops from higher heights, permanent deformation and sample destruction due to multiple drops.

For HPC and ALF soil, the modulus was a more significant function of water content and it increased by a reduction in water content. For VA21a soil, there was more variability in the data at different moisture contents and a significant descending or ascending trend was not observed. All three soils generally showed increase in modulus with increase in P/Pa.

LWD on mold modulus at OPT and Pits compaction condition were interpolated from the data from Zorn, Olson and Dynatest LWD for HPC, ALF, and VA21a soils at P/Pa equal to 1 and is presented in Table 2-21. In general, Dynatest and Zorn respectively calculated the highest and lowest modulus values for a given material/condition (Figure 2.48). There was a good correlation between the modulus calculated from each device (Figure 2.47).

In comparison to resilient modulus test results at the same deviatoric stress ($\sigma_d = p_a$) and confining pressure of $\sigma_3 = \frac{\upsilon}{1-\upsilon}\sigma_1$, all LWDs underestimated the modulus; nonetheless the correlation was fairly good.

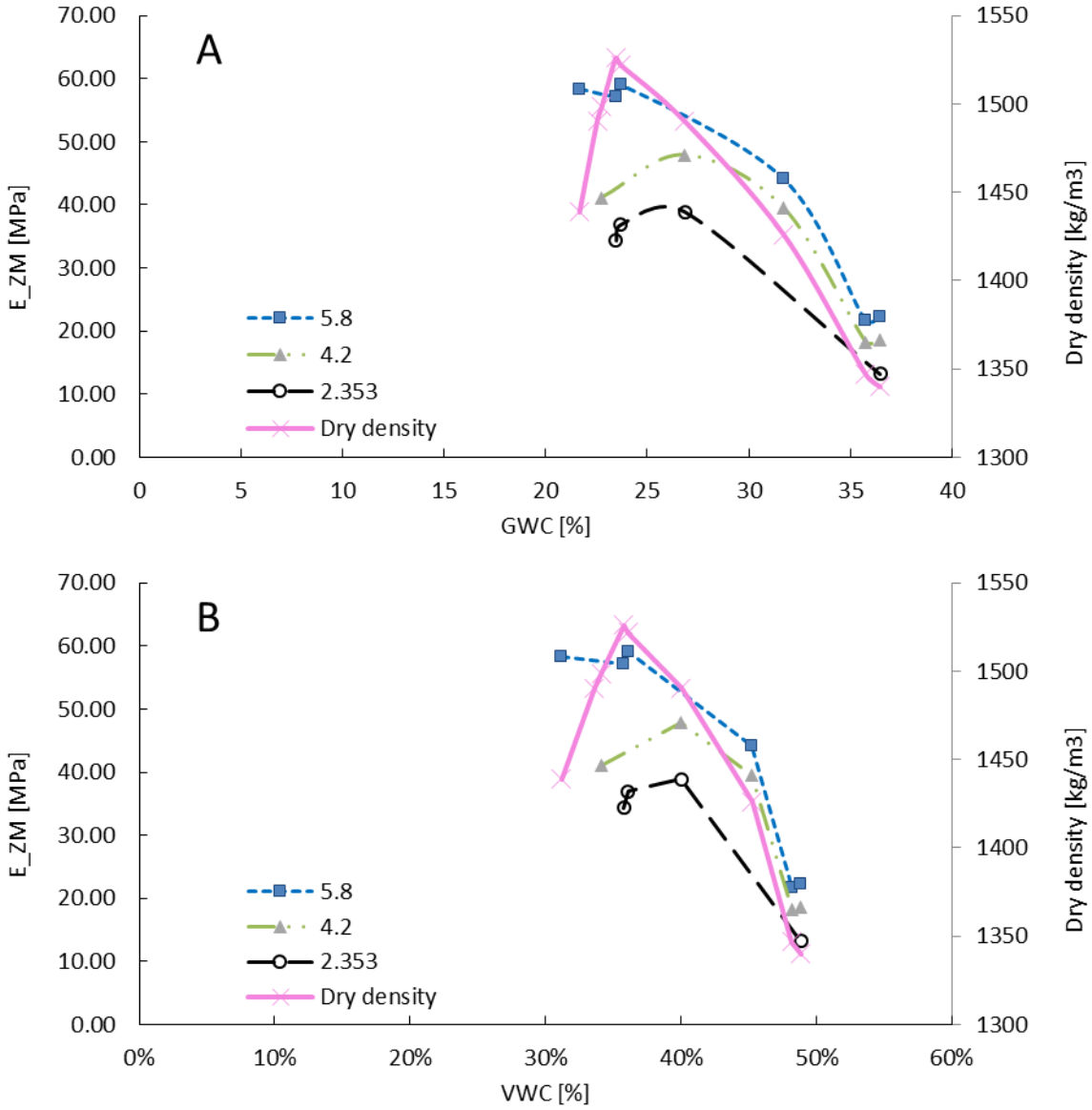

Figure 2.40. E_ZM and dry density versus (A) GWC and (B) VWC.

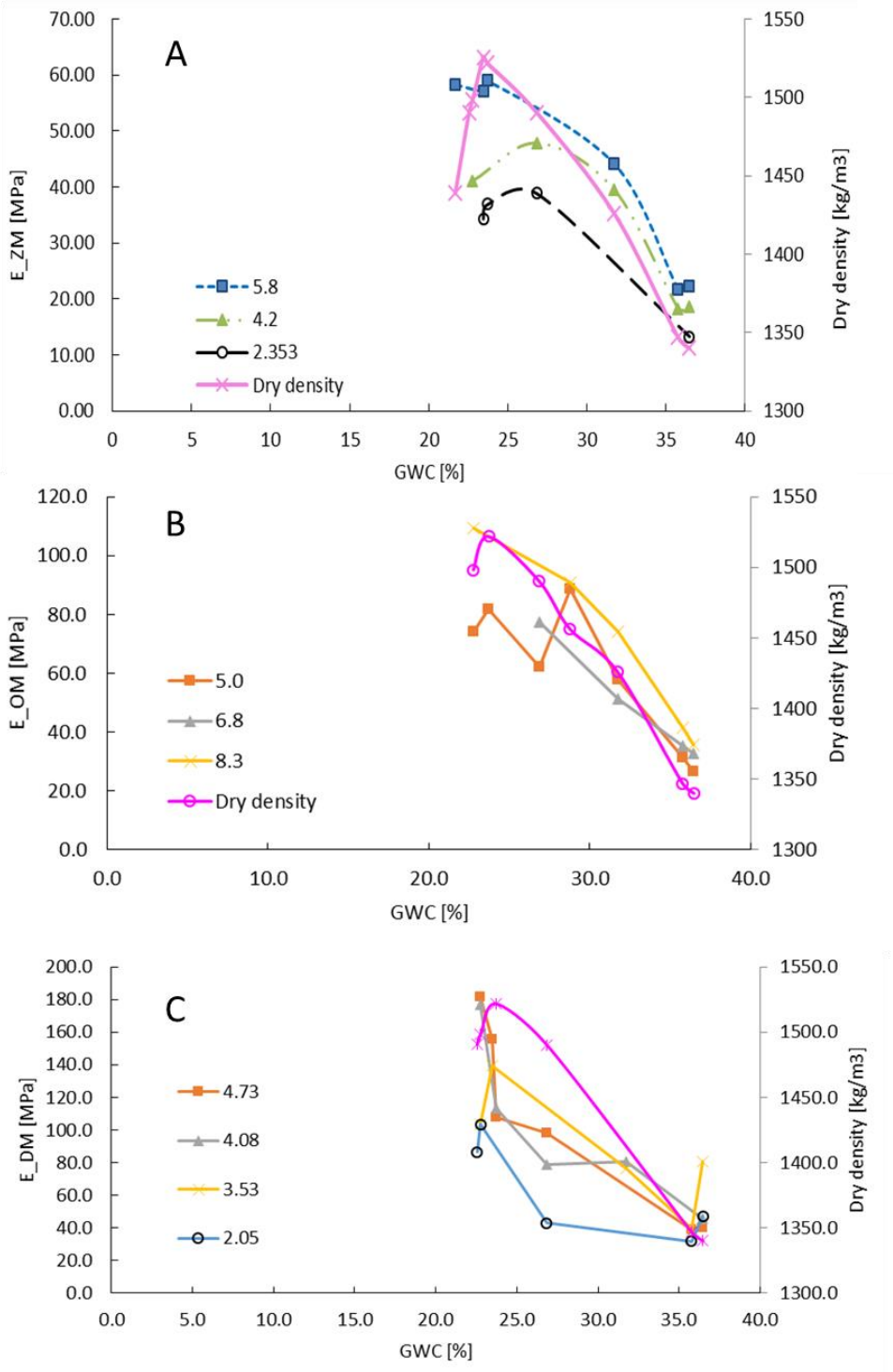

Figure 2.41. LWD modulus on Mold versus GWC superimposed by Dry density versus GWC for HPC soil at variable P/Pa for (A) Zorn, (B) Olson, and (C) Dynatest LWD. Legend specifies P/Pa.

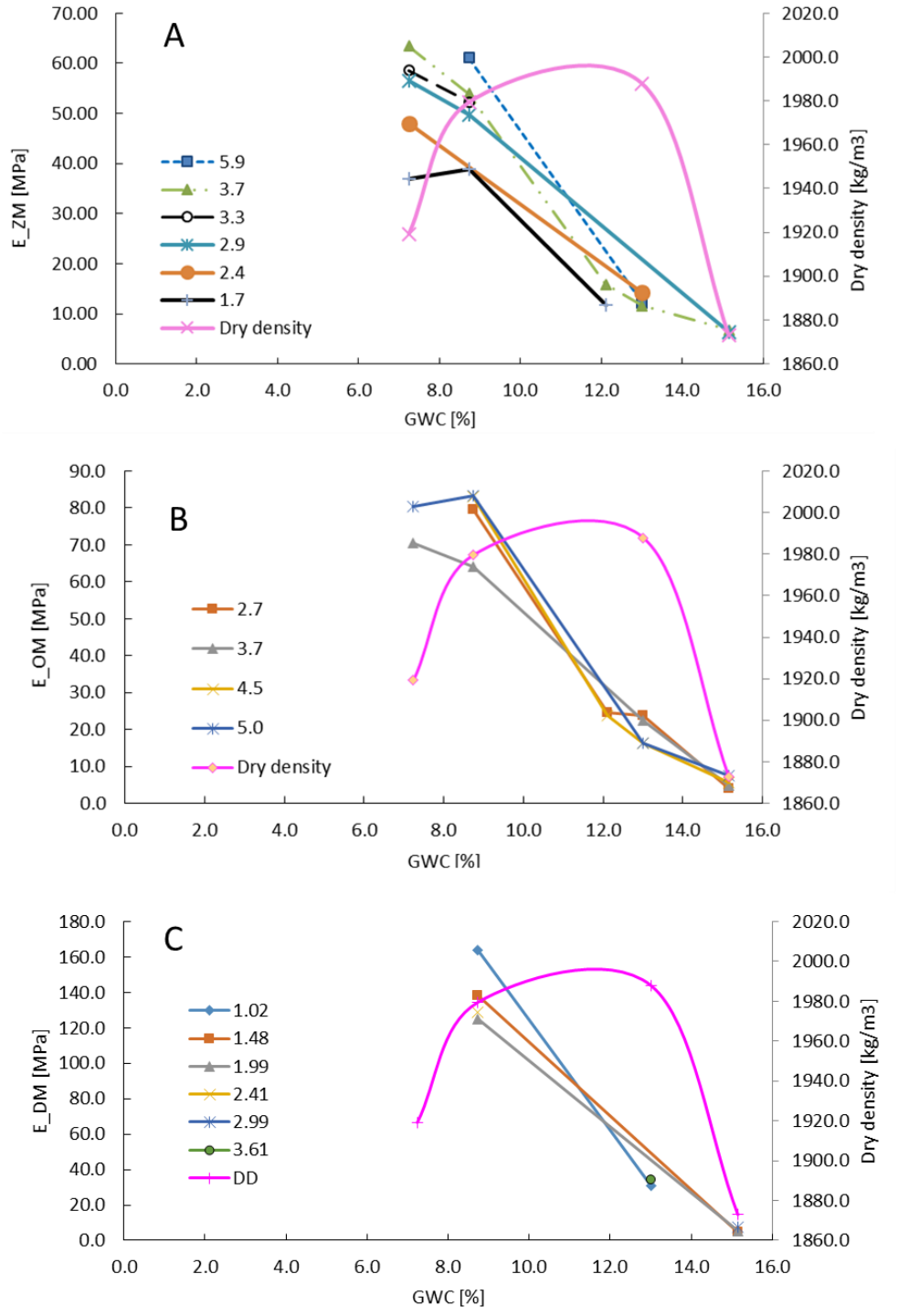

Figure 2.42. LWD modulus on Mold versus GWC superimposed by Dry density versus GWC for ALF soil at variable P/Pa for (A) Zorn, (B) Olson, and (C) Dynatest LWD. Legend specifies P/Pa.

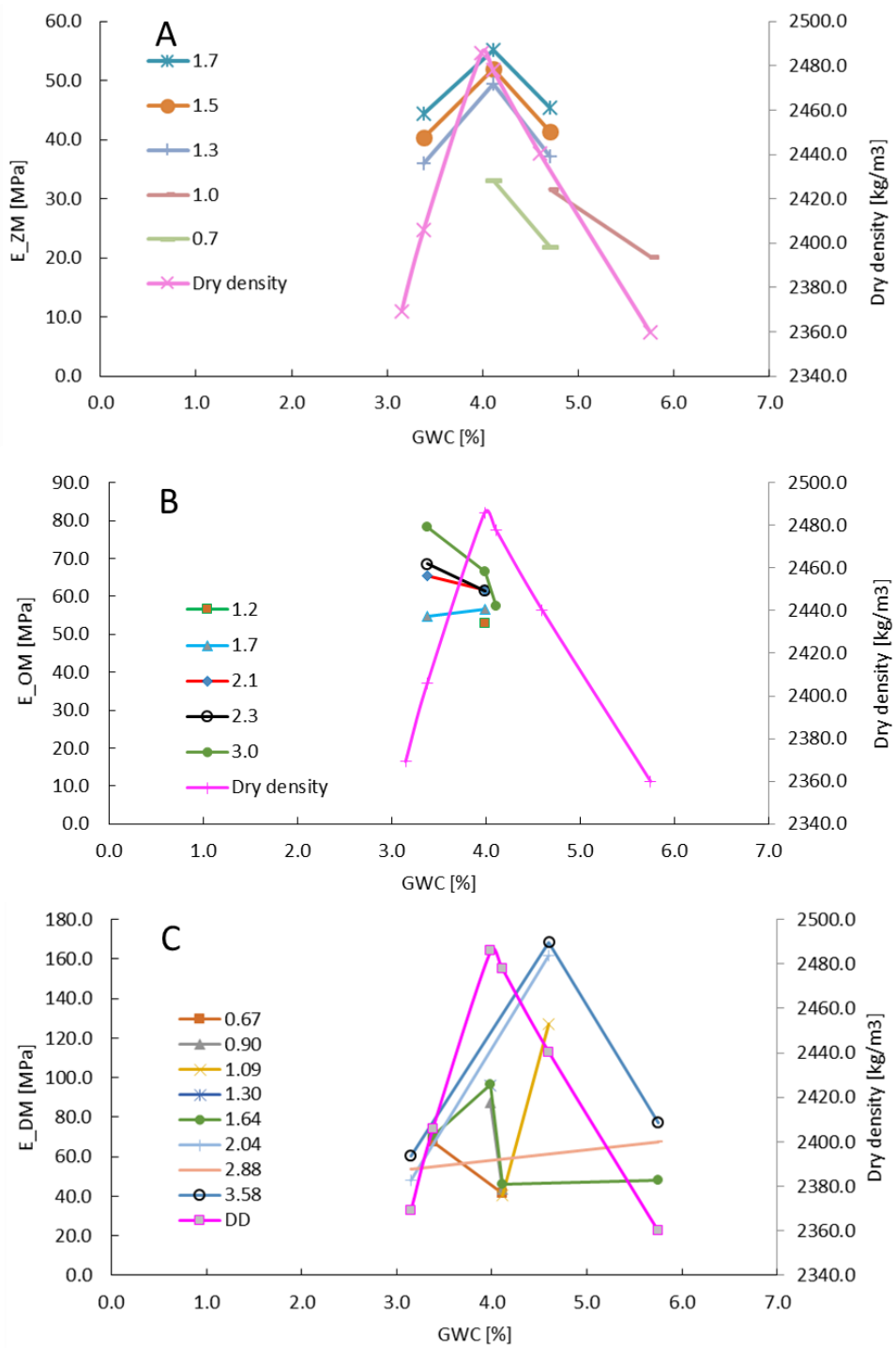

Figure 2.43. LWD modulus on Mold versus GWC superimposed by Dry density versus GWC for VA21a soil compacted at modified compaction energy at variable P/Pa for (A) Zorn, (B) Olson, and (C) Dynatest LWD. Legend specifies P/Pa.

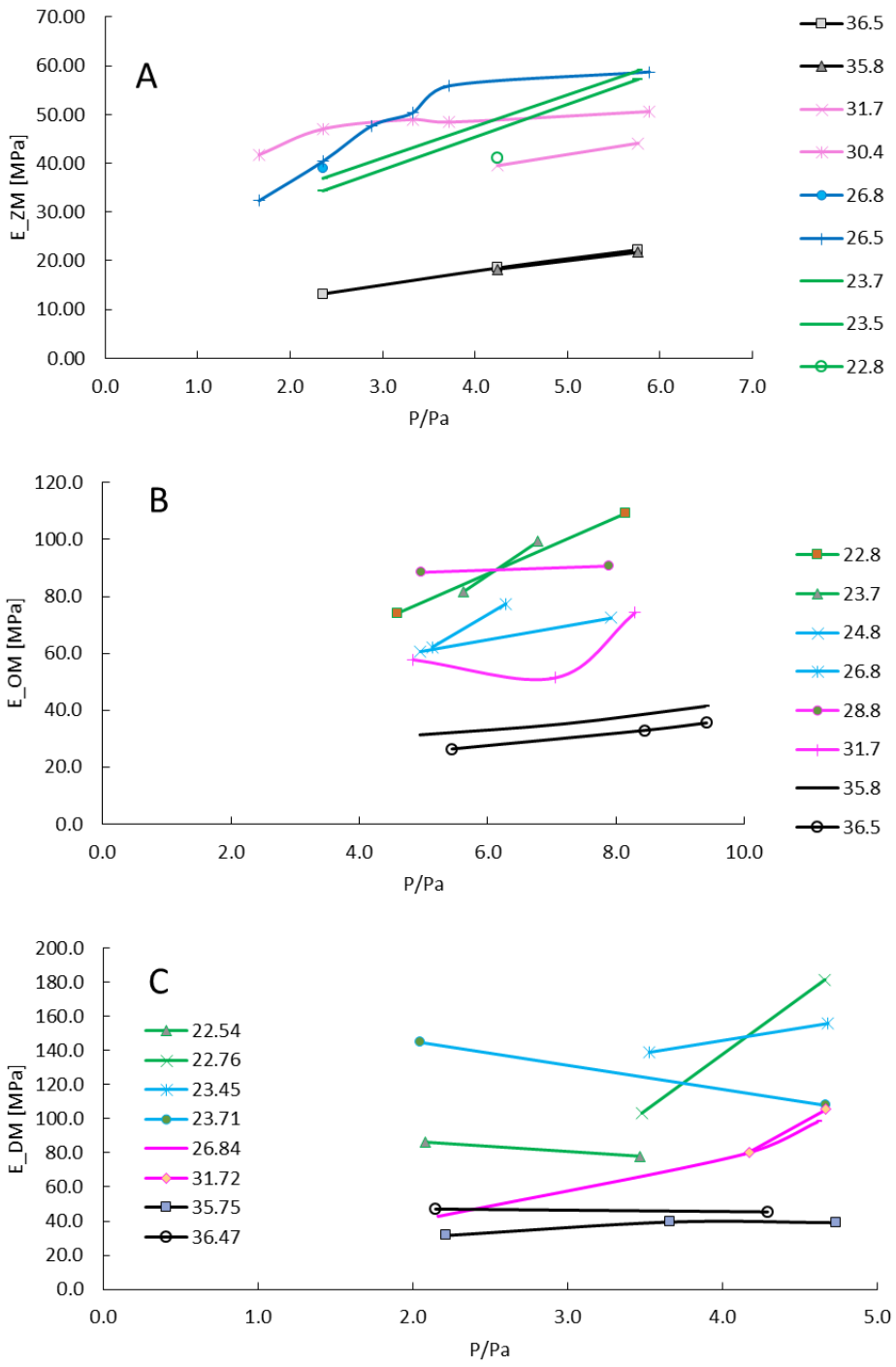

Figure 2.44. LWD modulus on Mold versus P/Pa for HPC soil at variable GWCs for (A) Zorn, (B) Olson, and (C) Dynatest LWD. Legend specifies GWC.

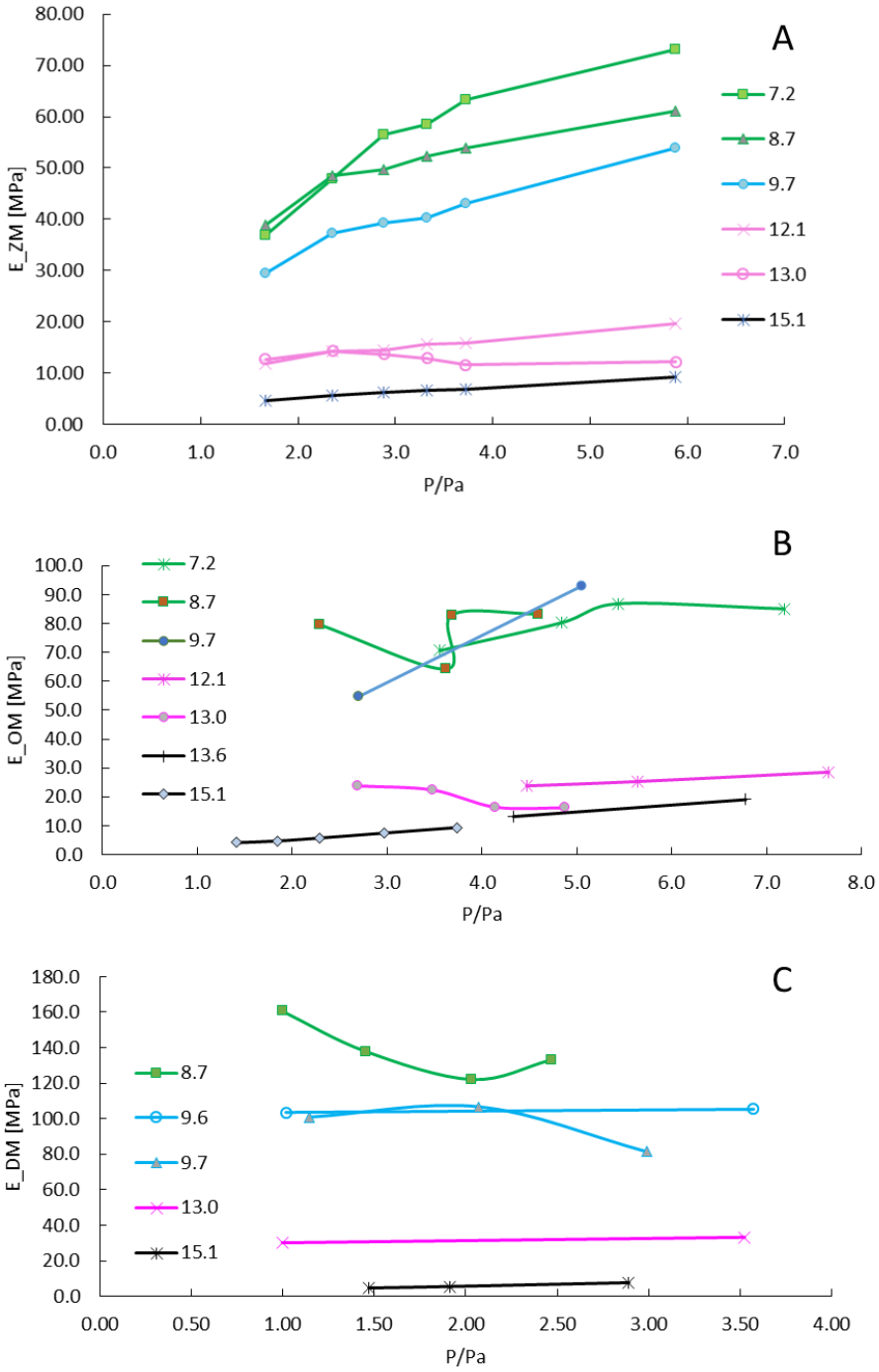

Figure 2.45. LWD modulus on Mold versus P/Pa for ALF soil at variable GWCs for (A) Zorn, (B) Olson, and (C) Dynatest LWD. Legend specifies GWC.

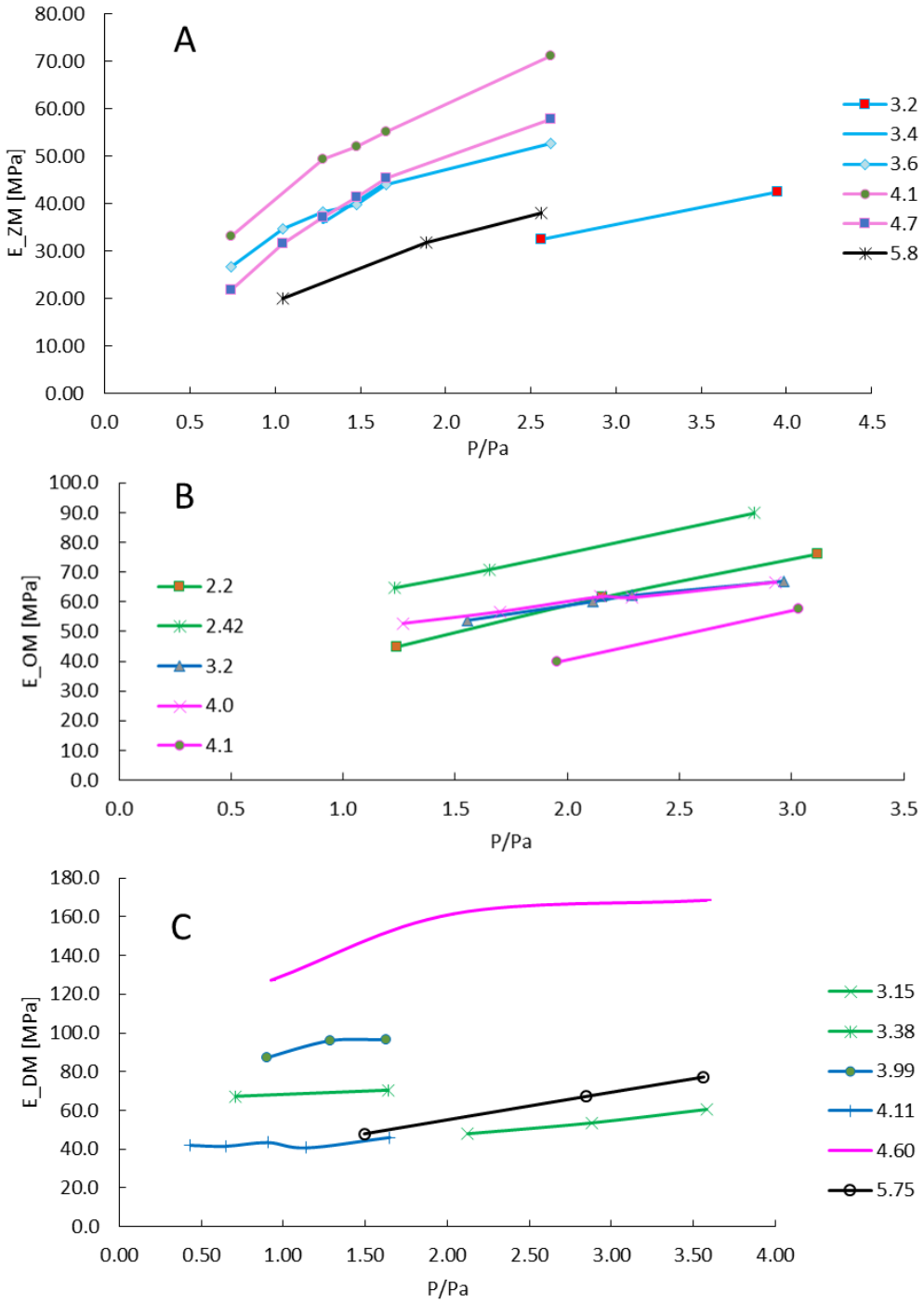

Figure 2.46. LWD modulus on Mold versus P/Pa for VA21a soil at variable GWCs for (A) Zorn, (B) Olson, and (C) Dynatest LWD. Legend specifies GWC.

Table 2-21. E_M at OPT and Pits condition for HPC, ALF, and VA21a soil as measured by Zorn, Olson, and Dynatest LWD at P/Pa=1

Material		HPC		ALF			VA21a
Test condition		OMC	Pit 3	OMC	~Pit 1	Pit 2	OMC/ Pit 2/ Pit 3
GWC [%]		24.5	29.5	11.5	10	14.5	4
PC [%]		100	95	100	98	95	100
Resilient modulus		100.6	44.5	95.8	-	25.6	109.3
LWD	Zorn	31.8	20.7	16.4	27.2	6.3	32.6
	Olson	66.1	44.2	42.7	59.1	9.9	43.0
	Dynatest	78.3	49.1	56.0	76.1	15.9	68.3

*~Pit 1: Compacted at WC equal to Pit 1 condition but to 98% PC

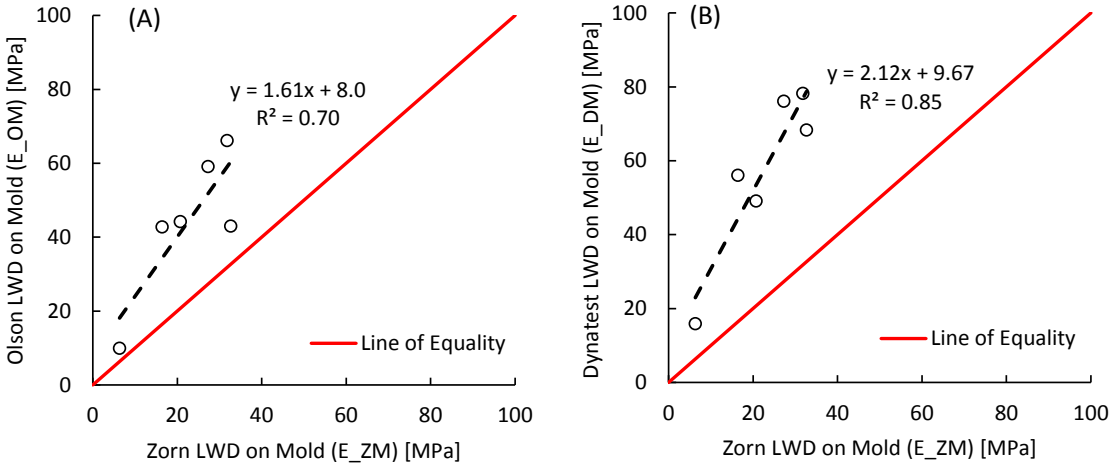

Figure 2.47. (A) E_OM versus E_ZM and (B) E_DM versus E_ZM

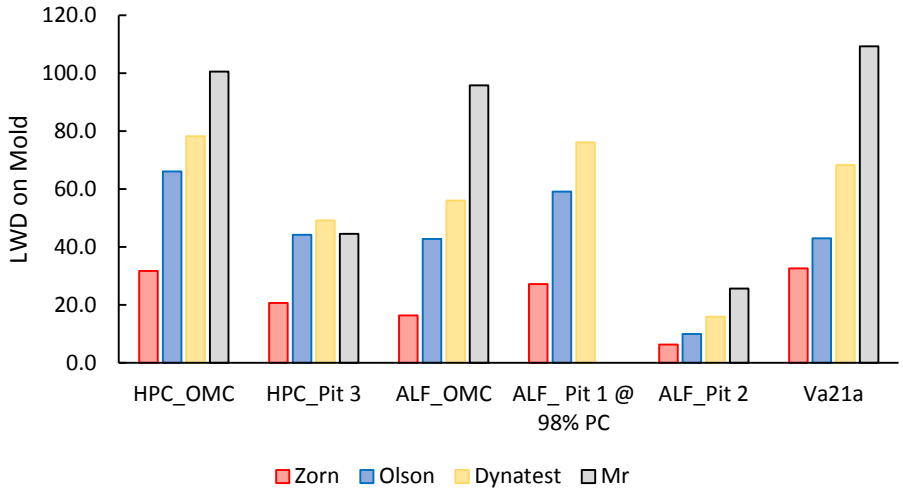

Figure 2.48. Resilient modulus and LWD on mold modulus as measured by different LWDs at P/Pa=1.

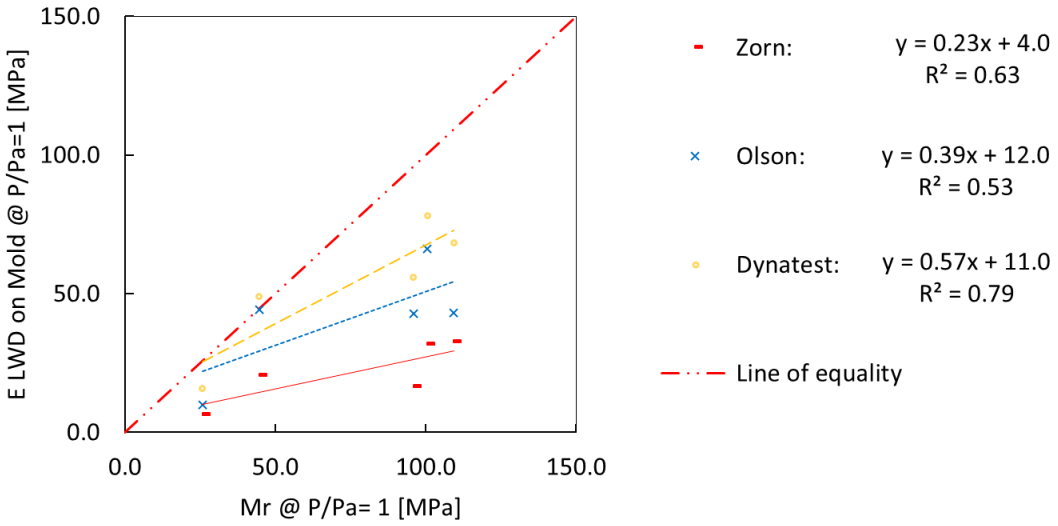

Figure 2.49. LWD on mold modulus versus resilient modulus at P/Pa=1.

2.10. **LWD modulus on mold versus triaxial resilient modulus**

The resilient modulus test results can be different from the LWD modulus on Proctor mold for three reasons: (1) different stress paths in the two tests; (2) assumption of Poisson's ratio in determination of LWD modulus; and (3) resilient versus total strain measurements in M_R test versus LWD test on mold.

2.10.1 Different stress paths in LWD modulus on mold versus triaxial resilient modulus

In the laboratory M_R test a constant confining pressure (σ_3) is applied throughout the test all around the sample. Application of the axial deviatoric stress (σ_d) increases σ_1 from σ_3 to $\sigma_3 + \sigma_d$. In LWD testing on the mold, σ_1 and σ_3 both start from zero and rapidly rise to their maximum values (Figure 2.50). The confining stress σ_3 is a reaction of the rigid walls of the mold to the applied axial stress σ_1.

It is possible to correct for the differences in the stress paths by integrating the strains at each load step to find the ultimate cumulative strain at the end of each test according to Equation 2-37.

Equation 2-37

$$\varepsilon_{peak} - \varepsilon_0 = \int_{t=0}^{t=n} (\varepsilon_{t+1} - \varepsilon_t).dt = \int_{t=0}^{t=n} \frac{1}{M_R\left\{ f\left(\frac{\sigma^{\theta,r}{}_{t+1} + \sigma^{\theta,r}{}_{t}}{2}\right)\right\}} \left[\left(\sigma^1{}_{t+1} - \sigma^1{}_{t}\right) - 2\upsilon\left(\sigma^3{}_{t+1} - \sigma^3{}_{t}\right)\right].dt$$

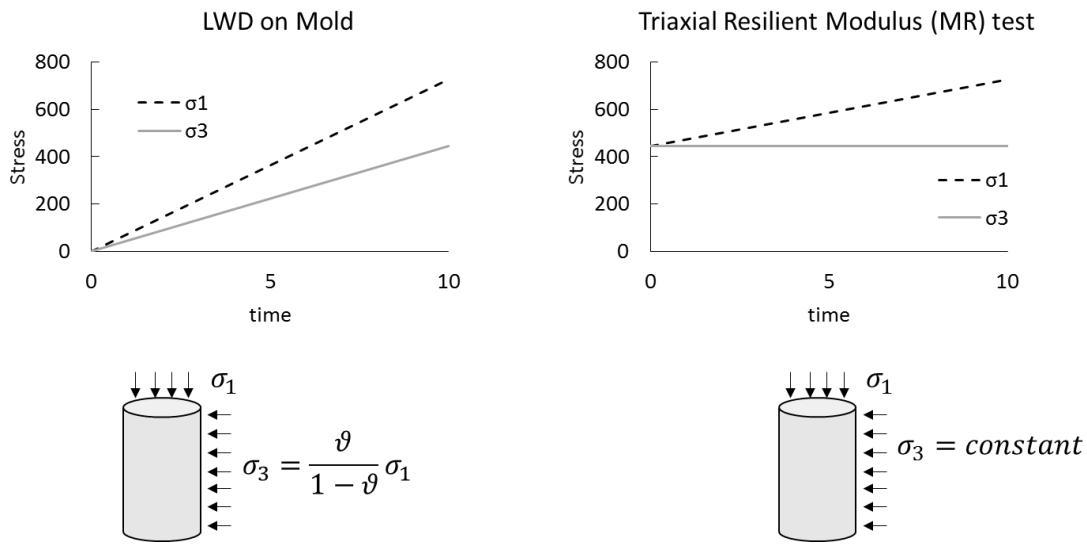

Figure 2.50. The different stress paths in LWD test on mold versus M_R

Figure 2.51 to Figure 2.58 present the variations of M_R/E_{LWD} versus ν or σ_1/P_a for the evaluated soils in the field condition. The simulation shows that M_R/E_{LWD} is a function of k_2, and k_3, ν, and P. The ratio M_R/E_{LWD} is independent of k_1 but significantly dependent on k_2. When k_2 equals zero, M_R/E_{LWD} equals to 1; as k_2 increases, M_R/E_{LWD} increases. This is why the highest discrepancy between E_{LWD} and M_R is for the granular aggregate base VA21a, which has the highest k_2 value. The M_R/E_{LWD} ratio increases with higher ν or P/Pa. At P/Pa equal to 1 and ν of 0.35, the ratio was close to 1 for all tested material. Therefore, correction for this discrepancy in the data cannot improve the systematic underestimation of LWD on mold modulus with respect to M_R test results.

Therefore, the main reason of the systematic underestimation of LWD on mold modulus as compared to M_R test (Figure 2.49) is believed to be the resilient versus total strain measurements in M_R test versus LWD test on mold.

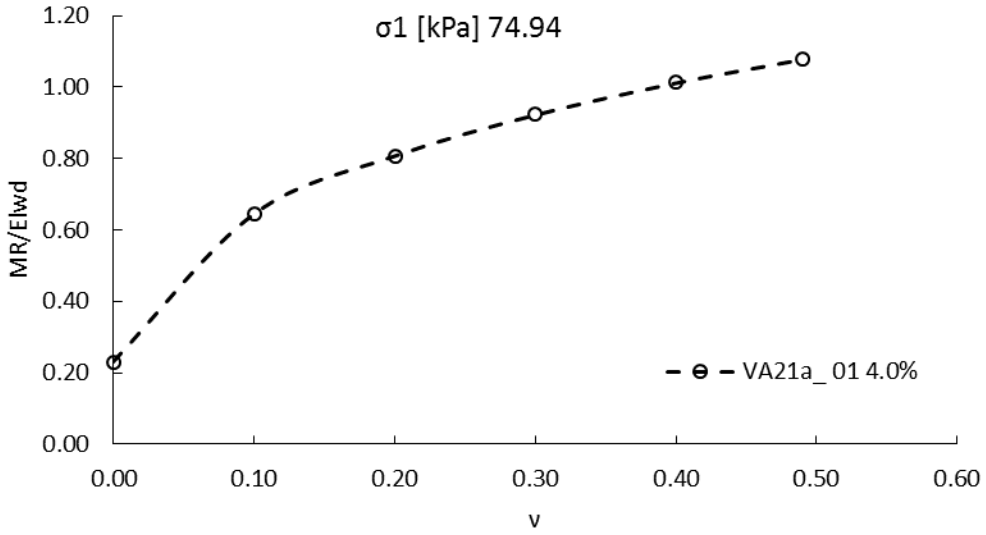

Figure 2.51. M_R/E_{LWD} versus ν at P/Pa of 0.7 for VA21a soil at OPT, Pit 2, and Pit 3 field condition

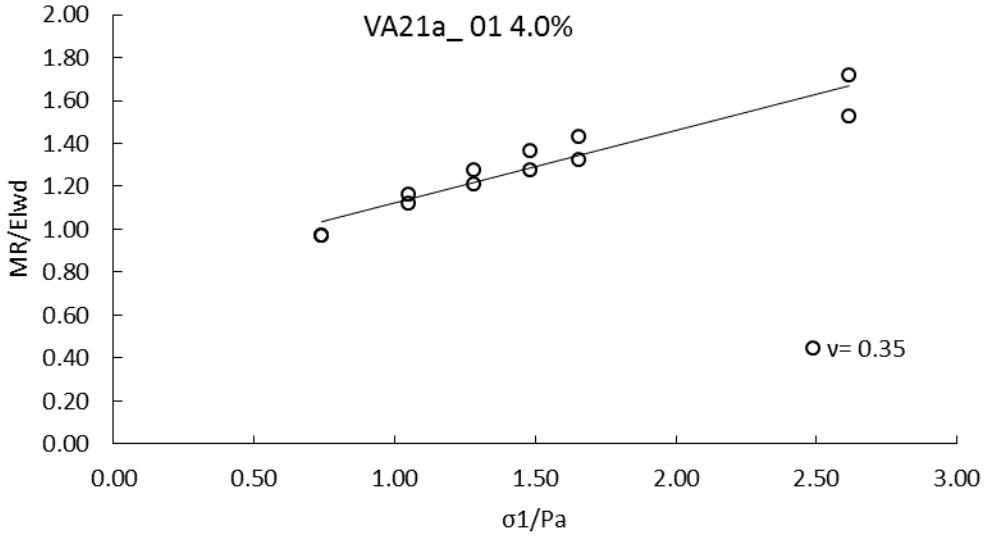

Figure 2.52. M_R/E_{LWD} versus P/Pa for ν= 0.35- VA21a soil at OPT, Pit 2, and Pit 3 field condition

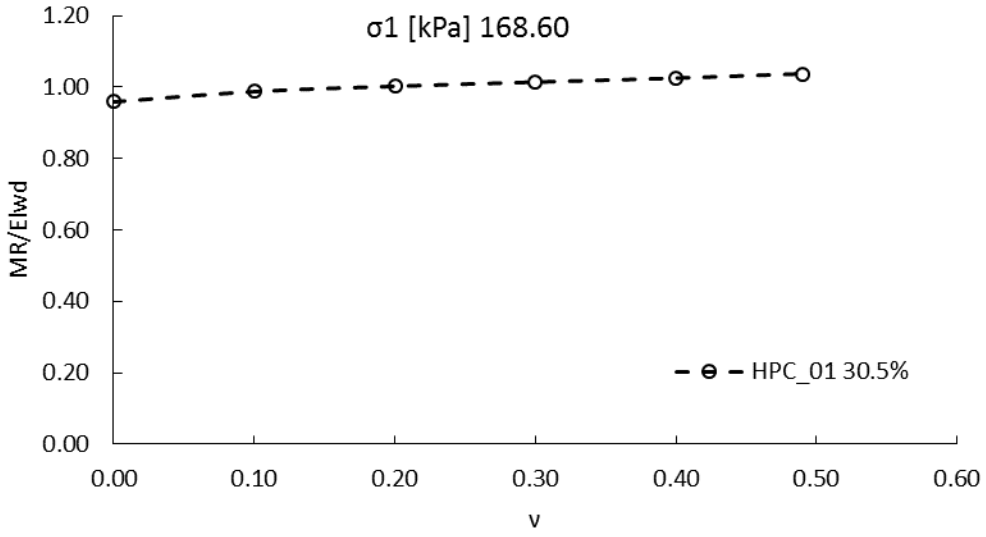

Figure 2.53. M_R/E_{LWD} versus ν at P/Pa of 1.7 for HPC soil at Pit 3 field condition

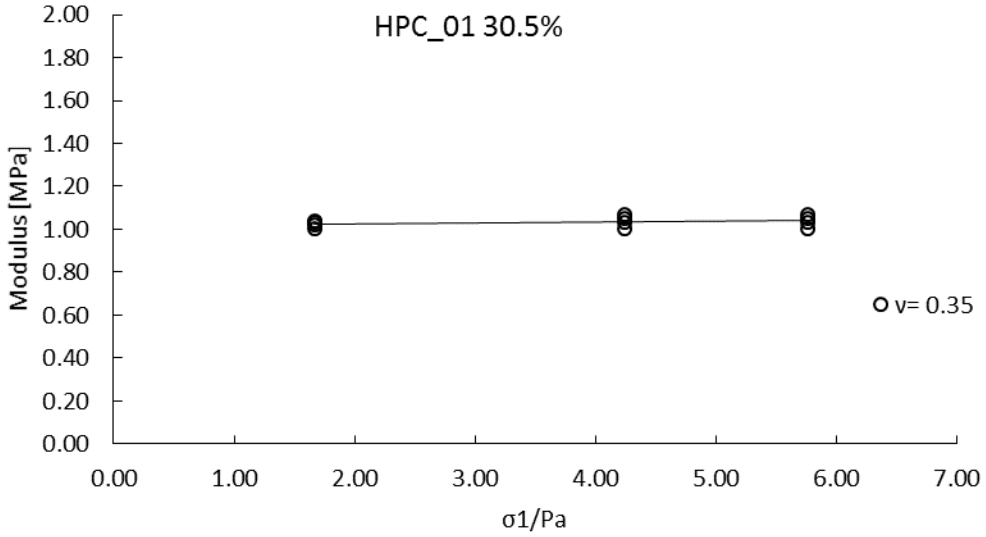

Figure 2.54. M_R/E_{LWD} versus P/Pa for ν= 0.35- HPC soil at Pit 3 field condition

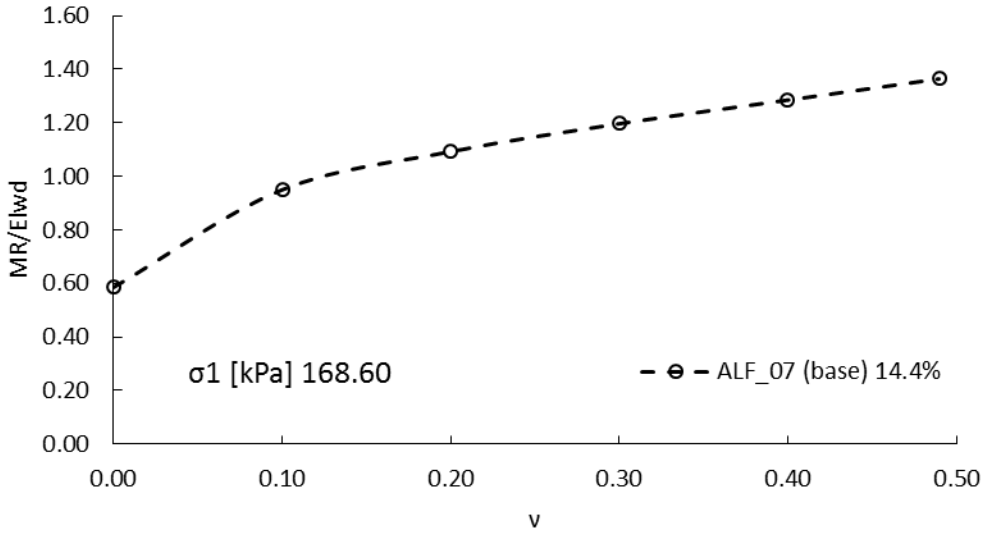

Figure 2.55. M_R/E_{LWD} versus ν at P/Pa of 1.7 for ALF soil at Pit 2 field condition

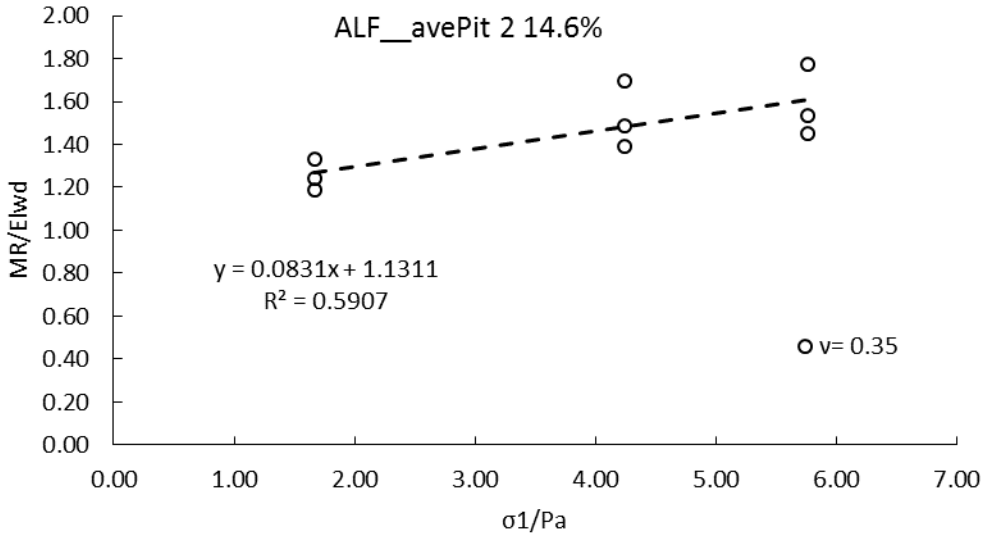

Figure 2.56. M_R/E_{LWD} versus P/Pa for ν= 0.35- ALF soil at Pit 2 field condition

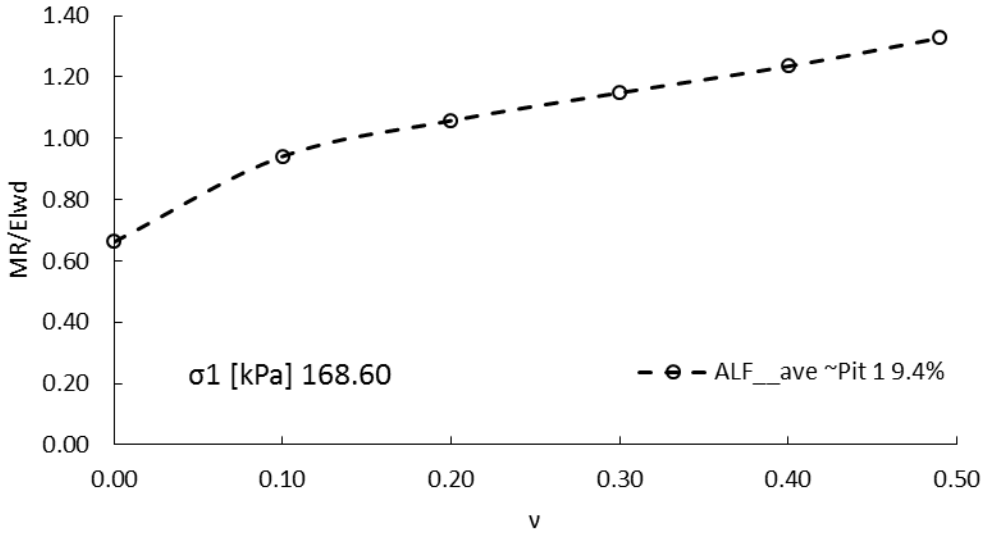

Figure 2.57. M_R/E_{LWD} versus ν at P/Pa of 1.7 for ALF soil at Pit 1 field condition

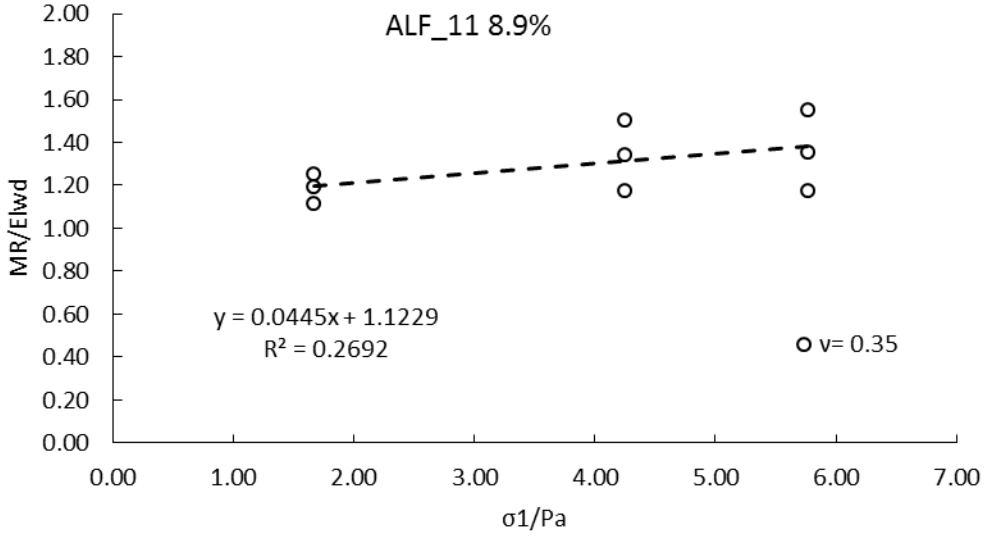

Figure 2.58. M_R/E_{LWD} versus P/Pa for ν= 0.35- ALF soil at Pit 1 field condition

2.11. Ohaus MB45 moisture analyzer

Moisture content is one of the main factors influencing soil modulus. The ability to quickly measure the soil moisture content in field is of particular importance. The Ohaus MB45 moisture analyzer shown in Figure 2.59 was evaluated for the purpose of quick moisture measurements during construction of the pits.

The Ohaus MB45 operates on the thermogravimetric principle. First, the moisture analyzer determines the weight of the sample; then the sample is quickly heated by the integral halogen dryer unit and the moisture evaporates. During drying, the instrument continuously determines the weight of the sample and displays the results as % moisture content, % or solids weight. The MB45 takes about 15 minutes to dry the samples.

Ohaus MB45 Moisture Analyzer was evaluated against oven-drying measurements for four different kinds of soil—gravel, sand, silty sand, and clayey sand. For each soil, 20 to 26 tests at various moisture contents were performed.

Results from the evaluation are shown in Figure 2.60. The results showed a very high correlation (R = 0.98) between the moisture contents measured using the two techniques for all evaluated soils. The moisture content measured by MB45 was generally slightly lower (by a factor of approximately 0.9) than the moisture measured using the standard oven drying technique which could be due to the shorter drying period in MB45. A default factor of 1.11 can be applied to correct for the underestimation of moisture content by the MB45. For higher accuracy, a soil-specific calibration can be developed.

The MB45 was found to be a robust device, especially for fine soils. A few drawbacks of the MB45 are its low capacity (45 gr), which makes it less suitable for larger aggregates, and the need for a generator to power the device in the field.

Figure 2.59. Ohaus MB45 moisture analyzer

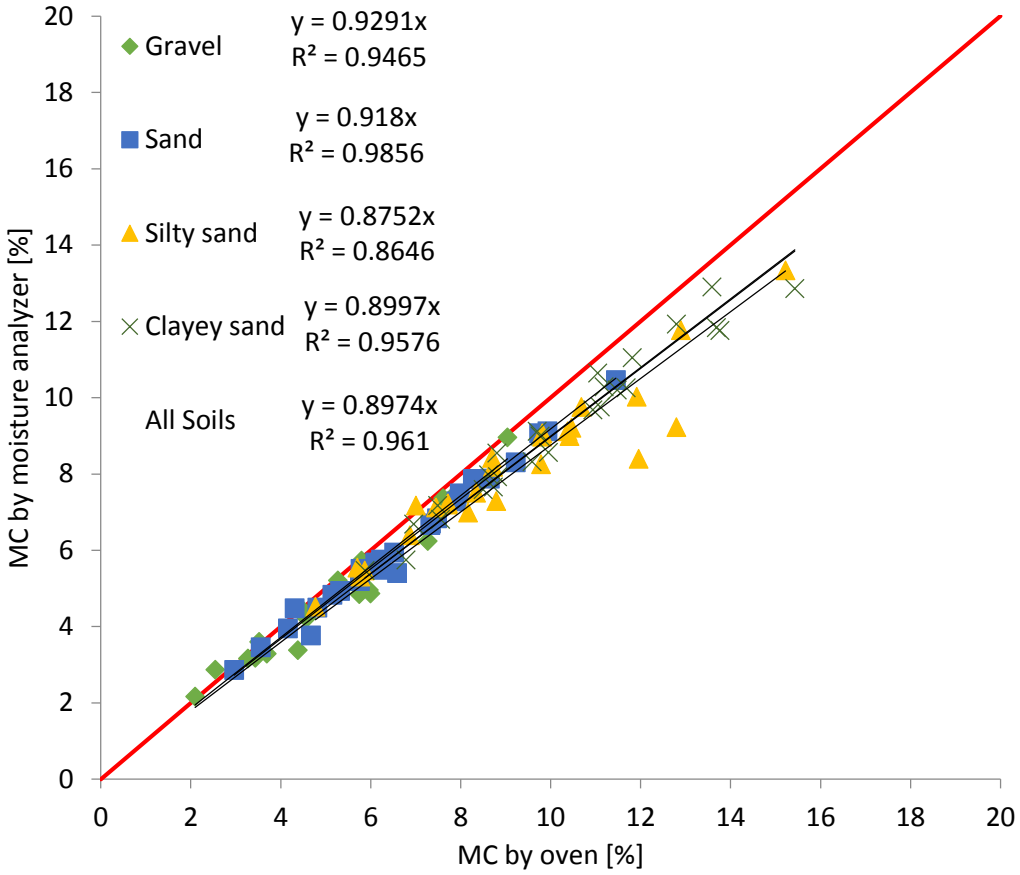

Figure 2.60. Comparison of water content measurement by Ohaus MB45 moisture analyzer and oven drying for gravel, sand, silty sand, and clayey sand soil.

2.12. **Instrumentation and Calibration**

The test pits were instrumented with 6 thermocouples, 6 volumetric water content (VWC) sensors, and 2 earth pressure cells to record the environmental and load-related responses during the time of construction and testing.

2.12.1 Data acquisition system and software

The data acquisition system shown in Figure 2.61 included an NI SCXI-1001 (Signal Conditioning eXtensions for Instrumentation) compact 12-slot chassis housing an NI SCXI-1600 USB Data Acquisition and Control Module, two SCXI-1102 32-channel thermocouple amplifier modules and several SCXI-1520 8-channel universal strain/bridge modules.

The sensors were connected to terminal blocks mounted on the corresponding modules on the chassis. Table 2-22 lists all the modules that the chassis housed with their associated terminal blocks and sensors. LabVIEW SignalExpress, an interactive data-logging software, was used for quickly acquiring, analyzing, and presenting the data from the instruments.

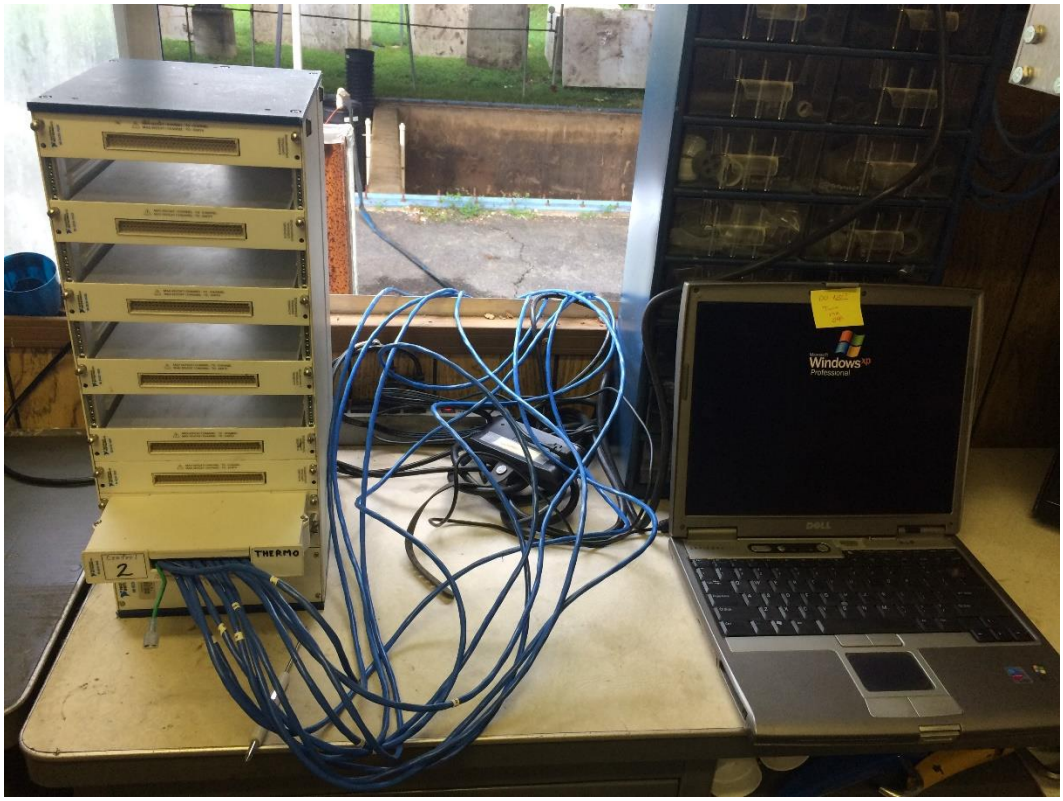

Figure 2.61. NI SCXI- 1001 Rugged, compact 12-slot chassis

Table 2-22. Summary of the modules and terminal blocks used for sensors in the chassis

Module	Terminal block	Sensor
SCXI -1520 (8-Channel Universal Strain/ Bridge)	SCXI-1314	VWC, earth pressure cell
SCXI-1102 (32-Channel Thermocouple Amplifier)	SCXI-1303	Thermocouple

2.12.2 Thermocouple sensors

The Omega EXPP-T-20-TWSH-SLE wire thermocouples consisted of a pair of solid constantan and copper shielded wires twisted and soldered (Figure 2.62). The ground wire was folded back as can be seen in Figure 2.62. No lead wire splicing was performed on the

thermocouples as they were cut to the full required length (15 m each), as shown in Figure 2.63.

Thermocouples operate on the principle that dissimilar metals generate a voltage when in contact with one another. Each combination of metal yields a known voltage related to the temperature of the junction.

Thermocouples were connected to the NI SCXI-1303 terminal block mounted to the front of the SCXI-1102 module, as shown in Figure 2.64. Connecting a thermocouple to a data acquisition board will add more dissimilar metal junctions, called cold junctions, to the circuit that may skew the temperature measurement. Cold junction compensation (CJC) removes the effect of the voltages generated by these cold junctions for a more accurate temperature measurement. A built-in CJC setting was applied to remove the unwanted voltages. A VWR Traceable Digital Thermometer was used to measure the temperature of a pan of water along with the thermocouple as a check of the accuracy of the thermocouples.

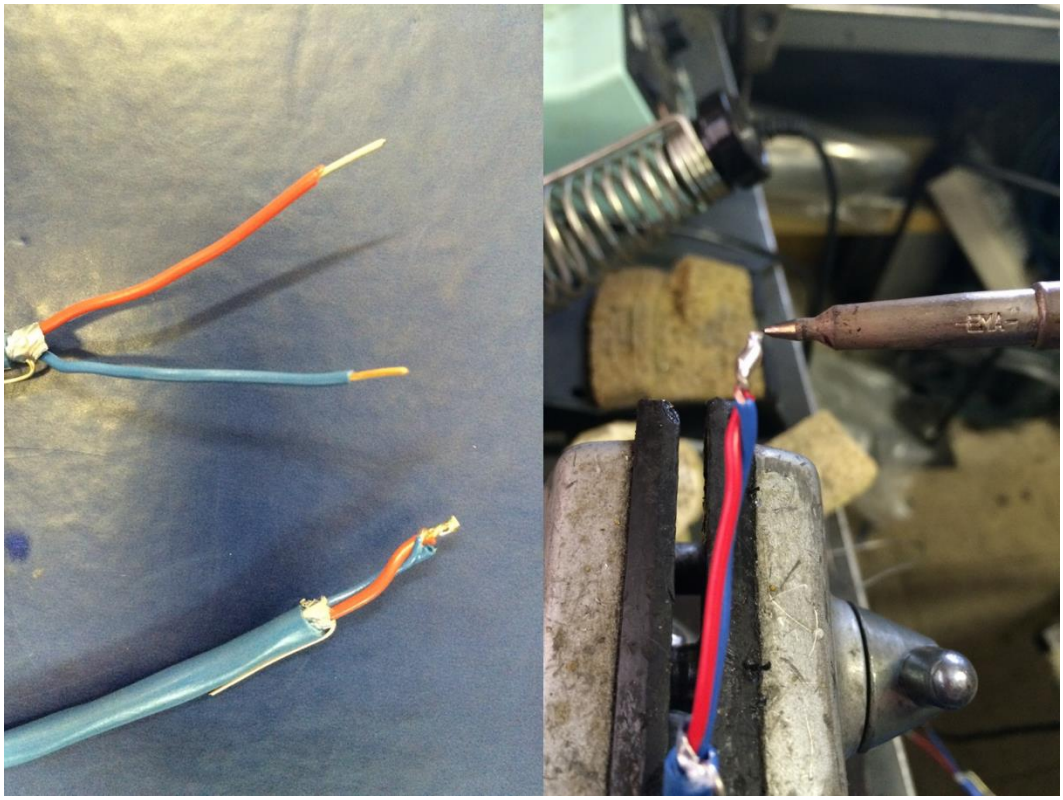

Figure 2.62. Theromcouple fabrication

Figure 2.63. Thermocouple wires cut to length

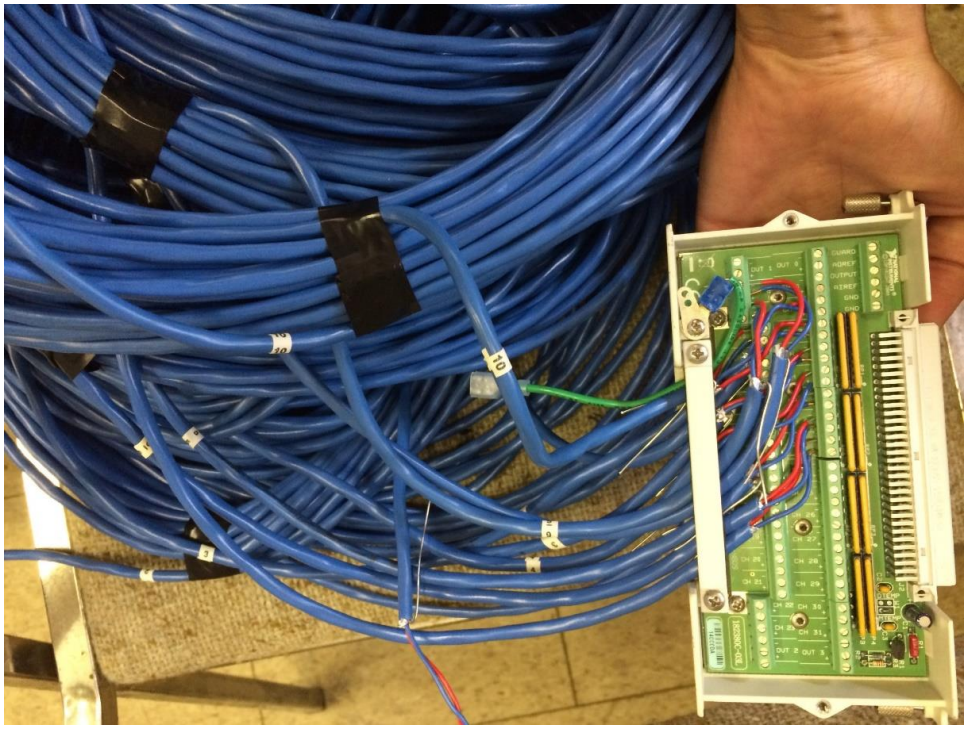

Figure 2.64. Connecting the thermocouples to the NI SCXI-1303 terminal block

2.12.3 Volumetric water content (VWC) Sensor

VWC in the test pits was measured using Decagon ruggedized GS-1 sensors (Figure 2.65). The GS-1 measures the dielectric constant of the soils using capacitance and frequency domain technology.

The dimensions of the GS-1 sensor are 8.9 cm x 1.8 cm x 0.7 cm. Its zone of influence is shown in Figure 2.66; the maximum volume of the zone of influence is 1430 mL. The default length of the sensors was 5 m and therefore splicing of the wires was performed to develop the required length for the test pits.

The GS-1 sensor requires 3 to 15 VDC excitation power. The sensor supplies a 70 MHz oscillating wave to the sensor prongs that changes according to the dielectric constant of the material. The GS-1 measures the charge and outputs a voltage between 1000 mV to 2500 mV (or RAW value) that strongly correlates to the VWC. The output setting being mV or RAW value depends on the data logger. With a non-Decagon data logger such as the NI data acquisition system used for the embedded sensors in the test pits, the output is mV while with ProCheck, the handheld sensor read-out and storage system from Decagon, the RAW value is displayed instead. Therefore two different sets of calibration equations must be used as appropriate. The difference between the two is the slope constant (RAW=1.365*mV).

The factory default calibration of the GS-1 sensor is not relevant to the levels of compaction achieved in pavements. Therefore, a soil-specific calibration was performed in the laboratory. Samples were compacted at OMC and MDD and ±2% of OMC according to AASHTO T-99—Method C for the HPC and ALF soils and according to AASHTO T-180—Method D for the VA21a aggregate.

The sensor prongs were inserted from the top while the soil was still inside the solid-wall metal Proctor mold. Since the zone of influence of the GS-1 sensor is non-symmetric along its prongs, the sensor was inserted at a 7.5 cm radial distance from the center of the mold to maximize the extent of the influence of the sensor inside the soil and minimize the effect of the metal walls of the mold. ProCheck was used to read the output RAW value. The RAW data was correlated with measured VWC of the soil samples. The constructed linear calibration equations are presented in Table 2-23 for each soil as a function of RAW and mV.

Figure 2.65. Decagon GS-1 ruggedized volumetric water content (VWC) sensor— www.Decagon.com

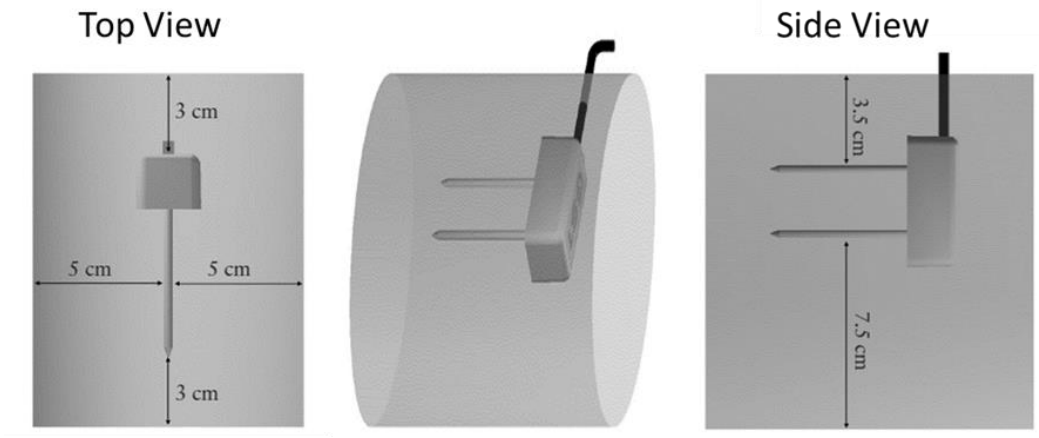

Figure 2.66. The influence zone of GS-1 sensor—GS-1 sensor manual

Table 2-23. Calibration equations for the implemented instrumentations

Device	Calibration equation
Decagon GS-1 Volumetric Moisture Content VMC sensor (θ)	$\theta\ VA21a = 1.92E-04 \times mVol - 0.1348$ $\theta\ VA21a = 1.40E-04 \times RAW - 0.1348$
	$\theta\ ALF = 4.53E-04 \times mVol - 0.539$ $\theta\ ALF = 3.32E-04 \times RAW - 0.539$
	$\theta\ HPC = 3.34E-04 \times mVol - 0.3357$ $\theta\ HPC = 2.44E-04 \times RAW - 0.3357$
Earth Pressure Cell	$\sigma\ (kPa) = 120.0 \times Vol$ $\sigma\ (psi) = 17.4 \times Vol$

2.12.4 Earth pressure cell

Pressure was measured by a GEOKON pressure cell Model 3515 in test pits #1 and 2. The earth pressure cell consists of two stainless steel plates welded together around their edges so as to leave a narrow gap in between. The gap is filled with de-aired hydraulic oil. As the two plates get squeezed, pressure builds up in the hydraulic oil. The pressure cell is connected to a transducer that converts the mechanical input, pressure, into an electrical output, voltage, ranging from 0-5 volts. An excitation voltage of 10 VDC was used to power the sensor. Figure 2.67 presents a schematic of earth pressure cell. The calibration equation is provided in Table 2-23.

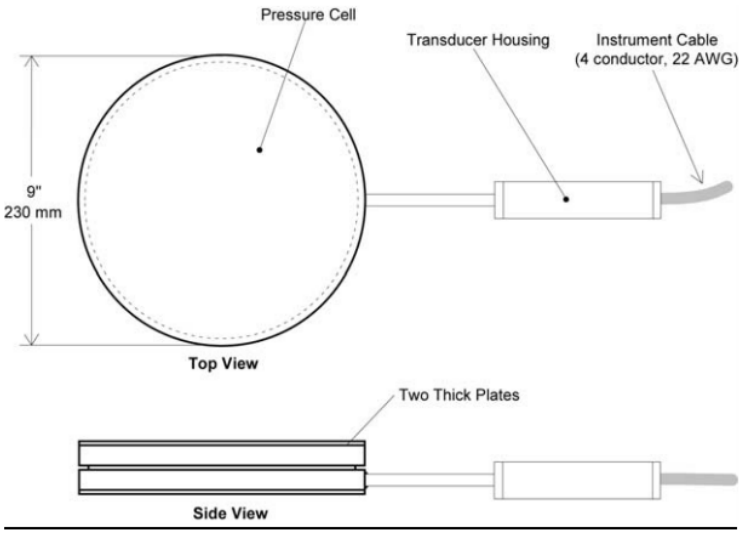

Figure 2.67. Schematic of model 3515 Granular materials pressure cell (Geokon manual)

Figure 2.68. Earth pressure cell

Chapter 3. Construction of Test Pits

This chapter summarizes the construction of the test pits including subgrade, and base layers. The details of the construction of each pit are provided in Appendices 1, 2, and 3 for Pit 1, Pit 2, and Pit 3, respectively.

3.1. **Test pit properties**

The test pits at TFHRC were approximately $4.6 \times 4.6 \times 2.4\ m^3$ ($15 \times 15 \times 8\ ft^3$). Half of the depth of the pits (~1.2 m) was already filled with a uniform crushed stone (Figure 3.1). The elevation of each pit was measured at multiple locations inside and across the walls before placing the test material (Table 3-1). The low coefficient of variation (CV) of less than 1.3% indicates the uniformity of the test pits.

Table 3-1. Elevation of pits before material placement

Pit #	Depth of Pit	
	Average [cm (in)]	CV [%]
1	120.5 (47.5)	0.9
2	123.0 (48.4)	1.3
3	120.2 (47.3)	1.1

The test pits were equipped with a reaction frame with a pneumatic pulsed loading capability that was used for static plate load testing. The pits also included infrastructure to control and change the water table. Prior to the construction, water was pumped out of the pits and a geotextile was placed to preserve the existing crushed stone from potential contamination (Figure 3.2).

Figure 3.1. Crushed stone

Figure 3.2. Placement of geotextile on top of the 1.2 m crushed stone

3.2. Design of the test pits

To achieve the objectives of the study, the subgrade and base layers in each test pit were designed to different target moisture, density, and layer thickness values. The material used in each pit and the design values for each layer are listed in Table 3-2.

The ALF subgrade of Pit 1 was designed to be placed at slightly dry of OMC at a target MC of $(-10\% \times OMC)$, which is within the current moisture-density based specification limits, but at a lower density of below 90% of the MDD (90% Percent compaction, PC) from standard compaction energy.

The ALF subgrade of Pit 2 was designed to be placed at wet of OMC and at the minimum density of 95% PC at standard compaction energy.

Similar to Pit 2, The HPC subgrade of Pit 3 was designed to be placed at wet of OMC and at the minimum density of 95% PC at standard compaction energy.

The VA21a base of Pit 2 and 3 were designed to be placed at OMC and at 95% MDD from modified compaction energy.

Table 3-2. Target MC, Density, and layer thickness

Pit #	Layer	Material	Moisture condition	Target MC [%]		Target PC*	Target Layer thickness [cm (in)]	Sub layers
1	Subgrade	ALF	Dry of OMC	10	$-10\% \times OMC$	≤ 90	508.0 (20.0)	3
	Base	-	-	-	-	-	-	-
2	Subgrade	ALF	Wet of OMC	15	$+30\% \times OMC$	≥ 95	609.6 (24.0)	6
	Base	VA21a	At OMC	4.5	OMC	≥ 95	203.2 (8.0)	2
3	Subgrade	HPC	Wet of OMC	29	$+20\% \times OMC$	≥ 95	508.0 (20.0)	5
	Base	VA21a	At OMC	4.5	OMC	≥ 95	101.6 (4.0)	1

3.3. **Tent setup**

A tent was set up on top of the test pits to preserve them from the frequent summer rains during the time of construction and testing and to reduce the potential environmental effects for this large scale controlled-condition testing (Figure 3.3).

Figure 3.3. Tent setup on top of the test pits

3.4. **Soil preparations for compaction**

The soils were transported and stockpiled in an open area close to the test pits. Figure 3.4 to Figure 3.9 show the soil stockpiles for the ALF, HPC and VA21a soils.

Preparations prior to placement and compaction included regular moisture content checking and consequential wetting or drying of the soils to reach the target moisture condition; removing organic and other deleterious materials from the soil—especially in the case of the locally obtained ALF soil as shown in Figure 3.4; breaking the very large chunks of soil—especially in case of the HPC soil as Figure 3.7—using a skid-steer loader; and covering the stockpiles with tarps in case of any anticipated rain (Figure 3.9).

To efficiently dry the soils, a skid-steer and backhoe loader were used to spread the soils. In case of the ALF soil used in Pit 1, which was intended to be compacted dry of optimum, the soil for each sublayer was transferred and spread inside the pit and was dried prior to compaction using a portable oscillating fan.

The material for each sublayer—around 7-10 half-full buckets of skid-steer loader with 0.73 m^3 capacity—was transferred to the pits. To expedite the transfer and distribution of

the soils in pits, a ramp was made as shown in Figure 3.10. To assure a uniform compaction, extra care was taken to evenly spread and distribute each load of soil poured in the pits using shovels and rakes for the ALF and VA21a soils and by hand for chunks of the HPC soil prior to compaction. The nominal thickness of the loose layer was 5 cm above the target thickness for the ALF and HPC sublayers placed in Pit 2 and Pit 3 and 2.5 cm above the target thickness in case of the VA21a sublayers placed in Pit 2 and 3 and the ALF soil sublayers in Pit 1.

Figure 3.4. ALF stockpile--removing the organinc soil from ALF soil

Figure 3.5. Spreading the ALF stockpile for drying prior to compaction

Figure 3.6. Stockpile of HPC soil

Figure 3.7. Use of skid-steer loader for breaking and spreading the HPC soil for furthur drying

Figure 3.8. Stockpile of VA21a stone

Figure 3.9. Covering the stockpiles

Figure 3.10. Use of ramp for transferring the material into the pits

3.5. **Compaction**

Two compactors were used in the project:
(1) Sheep foot trench roller with remote control (Figure 3.11)
(2) Vibratory plate compactor (Figure 3.12).

The sheep foot trench roller had a drum width of 81.3 cm and weighed 1370 kg. It induced an impact force of up to 62.3 kN. The plate compactor had a plate size of 50 x 56 cm^2 and weighed 88 kg. It induced an impact force of up to 15 kN.

The sheep foot trench roller was mainly used for compaction of the ALF soil in Pit 2 and the HPC soil in Pit 3. The plate compactor was mainly used for compaction of ALF soil in Pit 1 and the VA21a stone in Pit 2 and 3. The compaction method for each sublayer is listed in Table 3-3, Table 3-4, and Table 3-5 for Pits 1, 2, and 3, respectively. As can be seen, the compaction method and numbers of passes were adjusted to some extent throughout the construction process to achieve the desired levels of compaction. The construction of each sublayer took around 3 hours to complete.

Figure 3.11. Sheep foot trench roller with remote control

Figure 3.12. Vibratory plate compactor

Table 3-3. Construction timeline and compaction procedure for Pit 1

Lift	Date	time	Compaction method
1	22-Jul	13:30	3 passes of sheep foot compactor with high vibration
2	24-Jul	8:00	2 passes of plate compactor with medium vibration
3	24-Jul	13:00	2 passes of plate compactor with medium vibration

Table 3-4. Construction timeline and compaction procedure for Pit 2

Lift	Date	time	Compaction method
1	9-Jul	13:00	2 coverages of sheep foot compactor with high vibration
2	9-Jul	16:00	2 coverages of sheep foot compactor with high vibration
	10-Jul	9:00	Additional 2 coverages of sheep foot compactor with high vibration and 1 pass of plate compactor with high vibration
3	10-Jul	13:00	2x2 coverages of sheep foot compactor with high vibration and 1 pass of plate compactor with high vibration
4	10-Jul	16:00	2x2 coverages of sheep foot compactor with high vibration
5	13-Jul	10:00	2x2 coverages of sheep foot compactor with high vibration
6	13-Jul	15:00	2x2 coverages of sheep foot compactor with high vibration
7	14-Jul	13:00	2x2 coverages of sheep foot compactor with high vibration
	14-Jul	14:00	additional 2x2 passes of plate compactor with high vibration
	14-Jul	15:00	Water spray and 6 extra passes of plate compactor with high vibration
8	15-Jul	11:00	2x2 coverages of sheep foot compactor with high vibration and 3 passes of plate compactor with high vibration

Table 3-5. Construction timeline and compaction procedure for Pit 3

Lift	Date	time	Compaction method
1	17-Jul	11:00	2x2 coverages of sheep foot compactor with high vibration
2	17-Jul	16:00	2x2 coverages of sheep foot compactor with high vibration
3	20-Jul	11:00	3x3 coverages of sheep foot compactor with high vibration
4	20-Jul	15:00	3x3 coverages of sheep foot compactor with high vibration
5	21-Jul	11:00	3x3 coverages of sheep foot compactor with high vibration
6	22-Jul	10:00	2x2 coverages of sheep foot compactor with high vibration and 3 passes of plate compactor with high vibration
	22-Jul	11:00	Water spray and 2 extra passes of plate compactor with high vibration

Chapter 4. Test Pit Testing Program

4.1. **Nuclear moisture and density measurements**

The compaction effort was monitored with a Troxler 3440 nuclear moisture-density gauge (Figure 4.1). The measurements were performed in direct transmission mode (Figure 4.2). In direct transmission mode, the rod containing the Cesium-137 source is lowered to the desired depth. The detectors in the gauge base measure the radiation emitted by the source rod. This gives an estimate of the average density of the material from the source to the surface.

Table 4-1, Table 4-2, and Table 4-3 summarize the dry density (DD), gravimetric water content (w), percent compaction (PC), and VWC (θ) on each sublayer for Pit 1, Pit 2, and Pit 3, respectively. Nuclear gauge measurements were taken at a minimum of 3 random

spots on each sublayer. The measurements on the final sublayer of each layer were taken at the same locations as where the LWD tests were performed. For example, Figure 4.1 shows the testing performed on the final sublayer of base in Pit 3.

A uniform compaction with very low spatial variability was achieved throughout the construction, as can be inferred from the low CV values reported in Table 4-1, Table 4-2, and Table 4-3.

Figure 4.1. Troxler 3440 Nuclear moisture-density gauge.

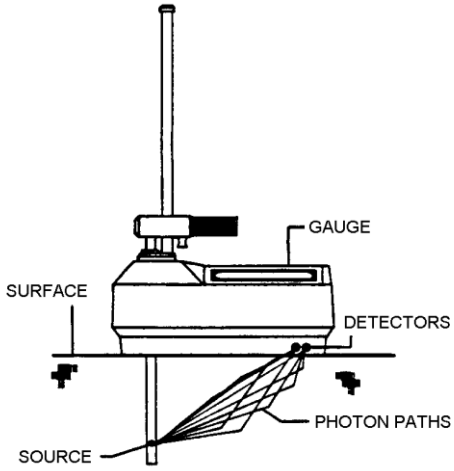

Figure 4.2. Nuclear gauge in direct transmission geometry (Troxler 3440 Manual, 2015).

Table 4-1. Nuclear moisture-density test results for Pit 1

Lift #	Soil type	Penetration depth	Dry density		w		PC	θ	
			Average	CV	Average	Sd	Average	Average	Sd
[-]	[-]	[cm]	[kg/m^3 (pcf)]	[%]	[%]	[%]	[%]	[%]	[%]
1	ALF	10.2	1904.6 (118.9)	-	11.9	-	99.1	22.7	-
2	ALF	15.2	1648.0 (102.9)	3.8	9.7	1.1	85.7	16.0	1.4
3	ALF	20.3	1593.3 (99.5)	1.3	10.2	0.6	82.9	16.2	1.0

Table 4-2. Nuclear moisture-density test results for Pit 2

Lift #	Soil type	Penetration depth	Dry density		w		PC	θ	
			Average	CV	Average	Sd	Average	Average	Sd
[-]	[-]	[cm]	[kg/m3 (pcf)]	[%]	[%]	[%]	[%]	[%]	[%]
1	ALF	5.1	1800.9 (112.4)	4.3	14.4	1.3	93.7	26.0	2.4
2	ALF	7.6	1809.6 (113.0)	1.8	16.5	0.7	94.1	29.8	0.8
3	ALF	10.2	1836.0 (114.6)	1.8	16.1	0.4	95.5	29.6	0.3
4	ALF	10.2	1874.6 (117.0)	1.4	14.9	0.5	97.5	27.8	0.9
5	ALF	10.2	1879.8 (117.4)	1.8	13.7	0.3	97.8	25.8	0.7
6	ALF	10.2	1834.8 (114.5)	4.2	15.4	0.7	95.5	28.2	1.1
7	VA21a	10.2	2306.3 (144.0)	1.5	5.9	1.6	94.7	13.6	2.9
8	VA21a	10.2	2388.8 (149.1)	4.3	4.7	0.2	98.1	11.2	0.6

Table 4-3. Nuclear moisture-density test results for Pit 3

Lift #	Soil type	Penetration depth	Dry density		w		PC	θ	
			Average	CV	Average	Sd	Average	Average	Sd
[-]	[-]	[cm]	[kg/m3 (pcf)]	[%]	[%]	[%]	[%]	[%]	[%]
1	HPC	10.2	1408.7 (87.9)	3.3	30.6	2.7	92.6	43.0	2.8
2	HPC	10.2	1485.4 (92.7)	5.3	29.3	3.6	97.6	43.4	2.9
4	HPC	10.2	1450.7 (90.6)	4.4	29.0	3.8	95.3	41.9	3.9
4	HPC	20.3	1497.2 (93.5)	2.1	27.3	2.0	98.4	40.9	3.0
5	HPC	10.2	1419.2 (88.6)	4.0	29.9	1.6	93.3	42.3	2.0
6	VA21a	10.2	2364.6 (147.6)	1.2	3.6	0.4	97.1	8.5	0.9

4.2. Layer thicknesses

The final thicknesses of the subgrade and base layer in each pit was measured at multiple points inside and across the walls of the pits as shown in Table 4-4. The thicknesses of the layers were fairly even throughout the pit area with a CV of less than 4%. The highest CV was for the HPC soil, which was the hardest soil to handle.

Table 4-4. Final Layer thicknesses

Pit	Subgrade		Base	
	Average	CV	Average	CV
[-]	[cm (in)]	[%]	[cm (in)]	[%]
1	50.8 (20.0)	1.1	-	-
2	59.9 (23.6)	2.6	19.3 (7.6)	2.4
3	50.5 (19.9)	4.0	10.7 (4.2)	2.5

4.3. Weather data and surface temperature

Weather data, evaporation rate, and soil surface temperatures were collected several times during the construction and testing of the pits using the Kestrel portable weather station and Fluke Infrared Thermometer, respectively (Figure 4.3). The weather data captured with these two devices during the time of construction and testing is provided in Appendices 1 to 3 for Pits 1 to 3, respectively.

The temperature was in the mid to high 20°C during the construction of Pit 2 and in the high 20°C to low 30°C range during the construction of Pits 1 and 3. Relative humidity was about 50-60% during the construction period. Table 4-5 provides the weather data from Weather Underground website (http://www.wunderground.com). The important factor to bear in mind is that degree of sunshine and wind speed were essentially zero, since the pits were covered with a tent.

The temperature of the constructed layers were monitored via the embedded thermocouples at the locations shown in Figure 4.8. The temperature plots for thermocouples are presented in Figure 4.13.

Figure 4.3. Kestrel portable weather station (right) and Fluke Infrared Thermometer (left)

Table 4-5. Weather data from http://www.wunderground.com/

2015	Temp. (°C)			Humidity (%)			Precip. (cm)	Events
Jul	high	avg	low	high	avg	low	sum	
1	31.1	26.1	20.6	90	67	43	3.30	Rain , Thunderstorm
2	25.0	22.8	20.6	87	76	64	0.05	Rain
3	28.3	23.9	18.9	93	72	51	0.08	Fog , Rain
4	29.4	26.1	22.2	87	76	65	2.16	Rain , Thunderstorm
5	30.6	26.1	21.7	87	71	55	T	
6	31.7	28.3	24.4	88	74	59	0.05	Rain
7	32.8	28.3	23.9	87	66	44	0.00	
8	33.3	29.4	25.6	85	71	56	2.84	Rain , Thunderstorm
9	33.3	29.4	25.6	85	70	55	0.08	Rain
10	31.1	28.3	25.0	69	58	46	T	Rain
11	31.1	27.8	23.9	82	64	45	0.23	Rain
12	31.1	26.1	21.1	79	58	37	0.00	
13	27.8	25.6	23.3	82	75	67	0.08	Rain
14	31.7	28.3	24.4	82	71	59	T	
15	31.1	26.7	22.2	79	65	51	0.03	Rain
16	30.6	25.0	18.9	66	51	35	0.00	
17	29.4	25.6	21.7	84	70	55	0.00	
18	31.1	28.3	25.0	82	73	63	0.10	Rain
19	36.7	31.7	26.1	91	70	48	0.00	
20	36.1	32.2	27.8	85	64	43	0.00	
21	33.3	30.0	26.1	74	63	52	T	Rain
22	31.7	27.2	22.2	68	50	31	0.00	
23	31.1	26.7	21.7	66	51	35	0.00	
24	32.2	26.7	20.6	73	51	28	0.00	
25	32	27	22.2	71	57	43	0	
26	33	28	23.3	67	60	52	0	
27	32	28	22.8	85	72	59	0.94	Rain , Thunderstorm
28	34	30	25.0	82	67	52	0	Thunderstorm
29	33	29	25.6	85	71	56	0	
30	33	29	25.6	85	75	64	0.53	Rain , Thunderstorm
31	33	28	23.3	69	51	32	0	

4.4. **Gravimetric water content (GWC) measurements**

The Ohaus MB45 moisture analyzer and oven drying were used to monitor the GWC of the stockpiles and to control construction quality in conjunction with nuclear moisture-density gauge during material spreading and after compaction.

The Ohaus MB45 in particular was being evaluated for its feasibility as a tool for rapid gravimetric water content measurements. The switch-off was done manually when the MC versus time curve became a flat line.

It took about 10-13 minutes to completely dry the VA21a aggregate. The drying time was about 20-23 minutes for the ALF soil and 60-70 minutes for the HPC soil.

There was a good correlation between the GWC measured by the Ohaus MB45 and the nuclear moisture-density gauge after applying the 1.11 correction factor to MB45 as previously obtained in laboratory. Figure 4.4 presents the comparison.

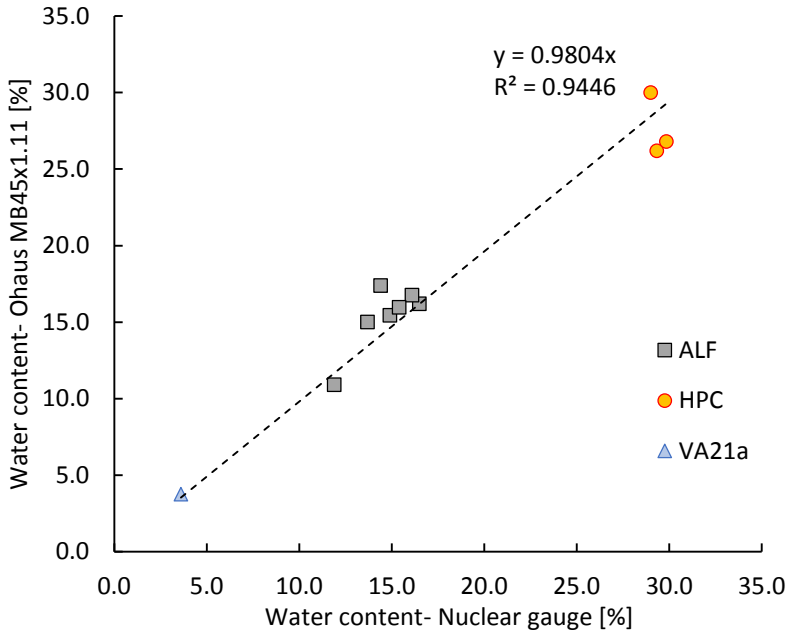

Figure 4.4. GWC by Ohaus MB45 moisture analyzer versus GWC by Nuclear moisture-density gauge.

4.5. **Decagon GS1 Volumetric Water Content (VWC) surface measurements with ProCheck**

The GS1 VWC sensors were used in two different ways in the pits:

1. VWC spot check by inserting the sensor from the top of the layer
2. Drying profile monitoring through sensors embedded within the layers

VWC was measured at various locations and sublayers in the ALF, HPC and VA21a soils with the GS1 sensors and nuclear density gauges. For the GS1 sensor, the calibration equations listed in Table 2-23 were used. The GS1 sensor was inserted from top as shown in Figure 4.5 to spot check the VWC of the layer using ProCheck, the handheld sensor read-out and storage system by Decagon.

The spot checking worked the best on ALF soil in Pit 1 due to the lower compaction levels of the soil. In ALF pit 2 and especially in HPC soil in Pit 3, it was difficult to insert the sensor due to the higher density of the soil. The usage of the sensor was even less practical on VA21a soil given the large particle sizes.

Through try and error it was found that the sensor is not practical for VA21a soil given its large nominal maximum size. It was also found that using a drill or a placebo sensor for prefabricating holes is necessary when using the sensor on fine grained soils such as ALF and HPC as shown in Figure 4.6.

Figure 4.5. Decagon GS1 VWC sensor inserted from the top on the ALF soil; VWC reading with ProCheck

Figure 4.6. Use of drill to prefabricate holes for the Decagon GS1 VWC sensor insertion into HPC soil

The VWC was also calculated from nuclear gauge measurements using the following formula:

$$\theta = \frac{w.\gamma_d}{\gamma_{water}} \qquad \textbf{Equation 4-1}$$

where $\theta = VWC, w = gravimetric\ water\ content,\ \gamma_d = dry\ density, and\ \gamma_{water} = density\ of\ water$. Despite the difficulties with the sensor insertion and its unsuitability for use on base soils, there was a fairly acceptable agreement between the two techniques. Table 4-6 shows the average VWC measured with the two methods. The VWC of the different soils at different pits were segregated and distinguishable with the sensor. A strong correlation was found between the two methods as shown in Figure 4.7. Decagon sensor slightly underestimated the VWC by the factor of 0.9 on average.

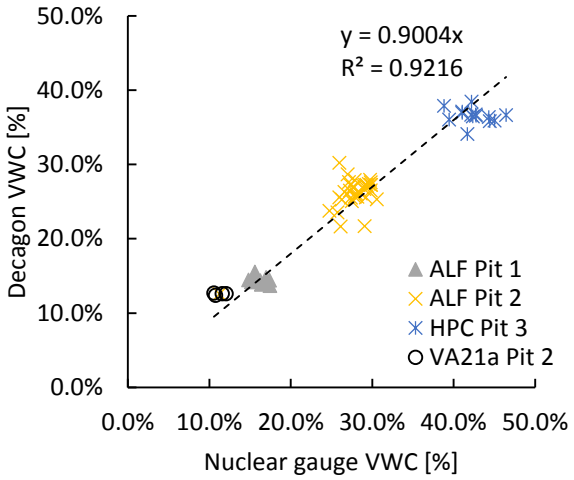

Figure 4.7. VWC measurements: Decagon versus nuclear gauge

Table 4-6. VWC as measured by Nuclear gauge and Decagon GS1 sensor

Pit number	Lift number	Material type	Nuclear gauge VWC		Decagon GS1 VWC	
			Average	Std Dev	Average	Std Dev
[-]	[-]	[-]	[%]	[%]	[%]	[%]
Pit 1	Lift 3	ALF	16.2%	1.0%	14.4%	0.6%
Pit 2	Lift 2	ALF	27.1%	0.6%	27.6%	1.2%
Pit 2	Lift 2	ALF	29.8%	0.8%	26.5%	1.1%
Pit 2	Lift 3	ALF	29.6%	0.3%	27.4%	0.3%
Pit 2	Lift 4	ALF	27.8%	0.9%	25.7%	0.6%
Pit 2	Lift 5	ALF	25.7%	0.8%	23.6%	1.8%
Pit 2	Lift 6	ALF	28.1%	1.0%	26.0%	1.6%
Pit 2	Lift 8	VA21a	11.2%	0.7%	12.6%	0.1%
Pit 3	Lift 1	HPC	42.7%	3.4%	36.7%	1.0%
Pit 3	Lift 5	HPC	42.3%	2.0%	36.5%	1.2%

4.6. Decagon GS1 Volumetric Water Content (VWC) embedded sensor

The second application of the GS1 sensors was to monitor the drying profile of the soils through embedded sensors. Six GS1 VWC sensors designated as M# were embedded in the three test pits. The sensor locations are shown in Figure 4.8. Figure 4.9 illustrates the steps in the GS1 sensor installation in test pits.

The GS1 VWC sensors were used to monitor the drying profile in the soils. After applying the calibration equations in Table 2-23, there was a disagreement between the VWC calculated from the embedded sensors and concurrent measurements with nuclear gauge and GS1 VWC spot checks with ProCheck. This is due to the fact that the sensors were

calibrated based on top-insertion (not embedded) mode as explained in Chapter 2. Correction factors as shown in Table 4-7 were applied to each sensor to match the VWC with concurrent measurements.

Table 4-7. Correction factor applied to GS1 VWC sensor to match the initial value measured by nuclear gauge

Sensor	Location	Correction factor
M0	Pit 2- ALF	0.95
M1	Pit 2- VA21a	0.64
M2	Pit 2- VA21a	0.75
M3	Pit 3- HPC	1.51
M4	Pit 3- VA21a	0.60
M5	Pit 1- ALF	1.30

The sensors were disconnected and connected several times during construction for safety reasons. This discontinuity led to alterations in the connection resistance and fluctuations in the voltages. An example of this false fluctuation in VWC is shown in Figure 4.10. Figure 4.11presents the VWC from embedded sensors. Table 4-8, Table 4-9, and Table 4-10 shows the VWC at time of LWD and plate load testing for Pit 1, Pit 2, and Pit 3, respectively.

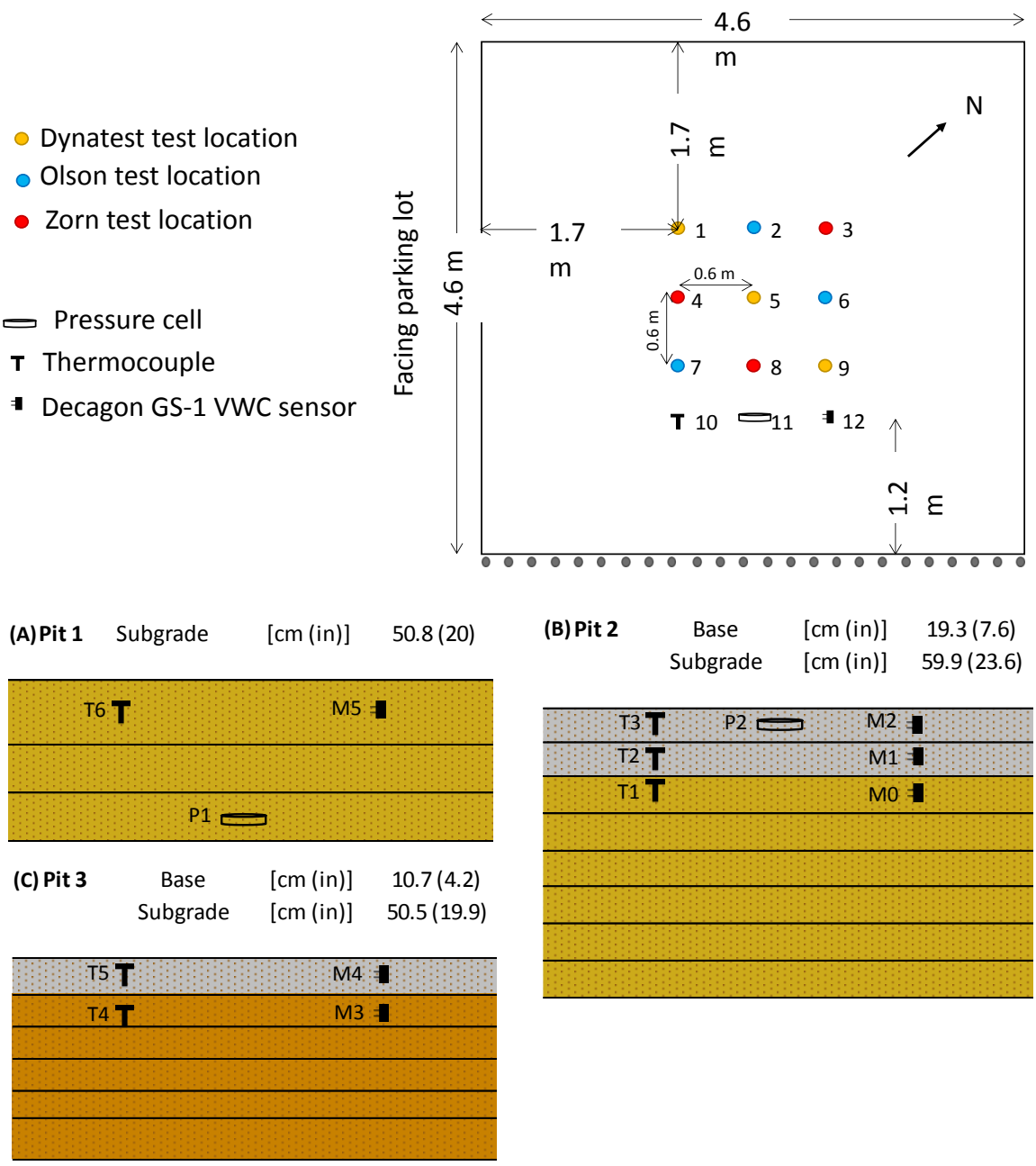

Figure 4.8. LWD test locations and embedded sensor locations.

Figure 4.9. Embedding the GS1 VWC sensor in ALF and VA21a soil

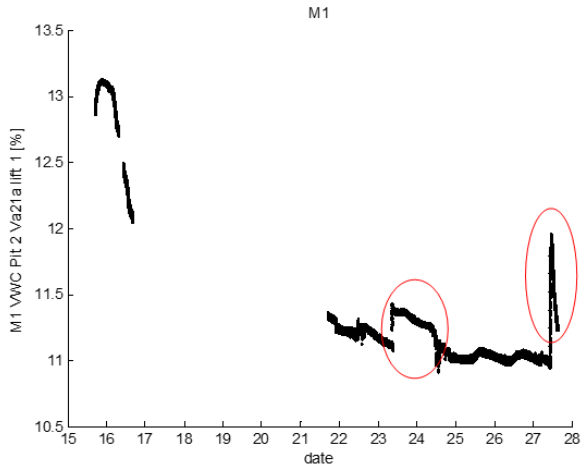

Figure 4.10. M1 sensor voltage fluctuation due to disconnection and reconnection of the sensor

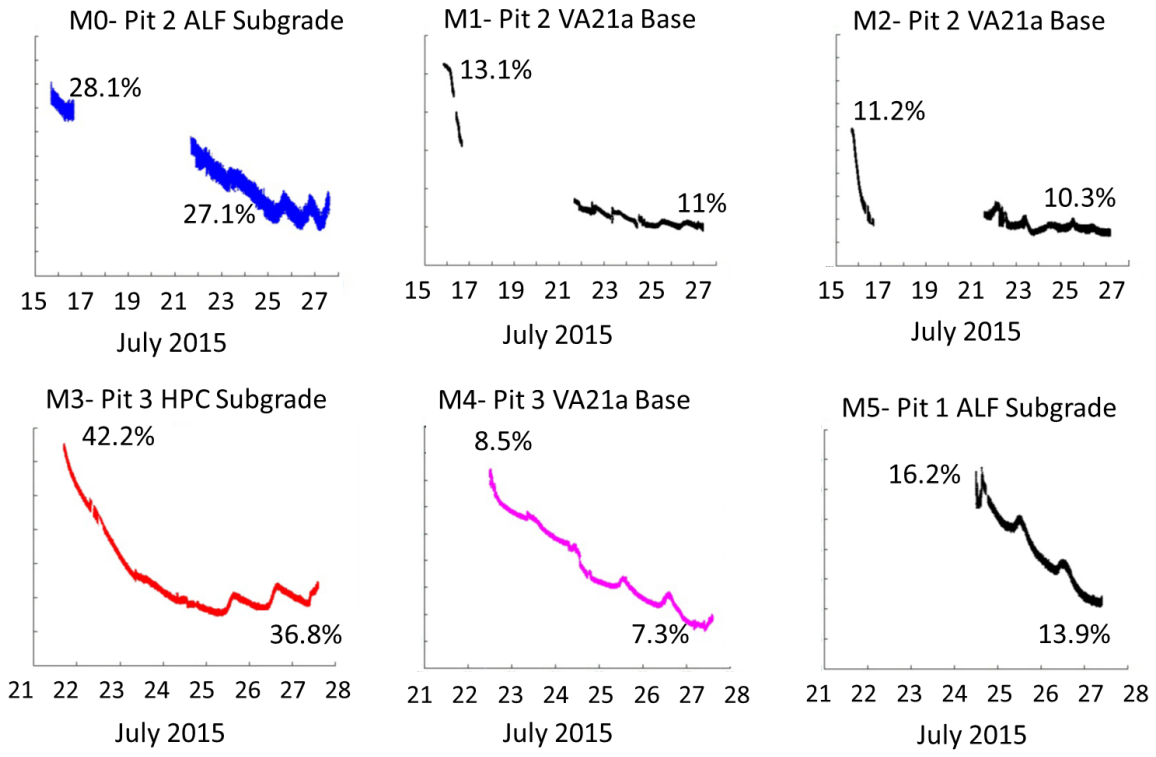

Figure 4.11. GS-1 embedded VWC sensors. The data lables on the plots are associated with the initial and final VWC.

Table 4-8. Volumetric water content at times of LWD and plate load testing on Pit 1

Date and time	test	M5
7/24/15 3:00 PM	LWD 2 hr after compaction, Plate load test	16.2
7/28/15 1:00 PM	LWD Zorn 4 days after compaction	13.9

Table 4-9. Volumetric water content at times of LWD and plate load testing on Pit 2

Date and time	test	M0	M1	M2
7/13/15 4:00 PM	LWD 1 hr after compaction	28.9	-	-
7/14/15 7:30 AM	LWD 16 hr after compaction, plate load test	28.5	-	-
7/14/15 12:30 PM	LWD Zorn and Olson 21 hr after compaction	28.4	-	-
7/15/15 7:30 AM	LWD 16 hr after final series of compaction	28.3	13.1	-
7/15/15 12:00 PM	LWD 1 hr after compaction	28.2	13.0	11.2
7/15/15 3:00 PM	LWD 5 hr after compaction, plate load test	28.1	13.0	11.1
7/20/15 1:00 PM	LWD Zorn 5 days after compaction	27.7	11.4	10.4
7/24/15 8:30 AM	LWD 9 days after compaction	27.3	11.1	10.3
7/28/15 1:00 PM	LWD Zorn 13 days after compaction	27.0	11.0	10.3

Table 4-10. Volumetric water content at times of LWD and plate load testing on Pit 3

Date and time	test	M3	M4
7/21/15 11:00 AM	LWD right after compaction, plate load test	42.3	-
7/22/15 10:30 AM	LWD right after compaction	39.6	8.2
7/22/15 12:30 PM	LWD 1.5 hr after 2nd compaction	39.4	8.5
7/22/15 3:00 PM	LWD 4 hr after 2nd compaction, plate load test	39.2	8.3
7/24/15 7:30 AM	LWD 45 hr after compaction	36.9	7.9
7/28/15 1:00 PM	LWD Zorn 6 days after compaction	36.8	7.3

4.7. Embedded thermocouple sensors

Six thermocouples were embedded in the pits to monitor the temperature in the subgrade and base layers. Figure 4.12 shows the sensor installment in HPC soil. The thermocouple locations are shown in Figure 4.8. Temperature data from thermocouples are shown in Figure 4.13. The increase in the temperature after July 26th was due to covering the pits with tarp at the end of the project.

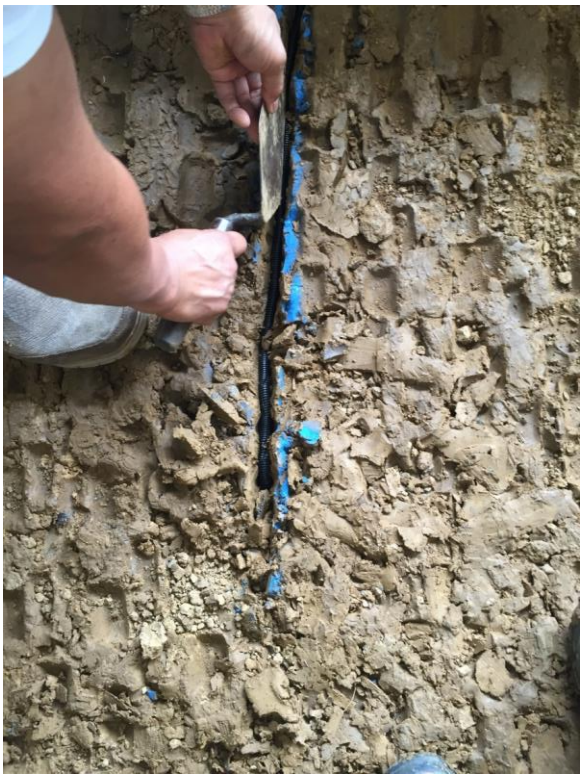

Figure 4.12. Cutting the HPC soil for embedding the thermocouple sensor

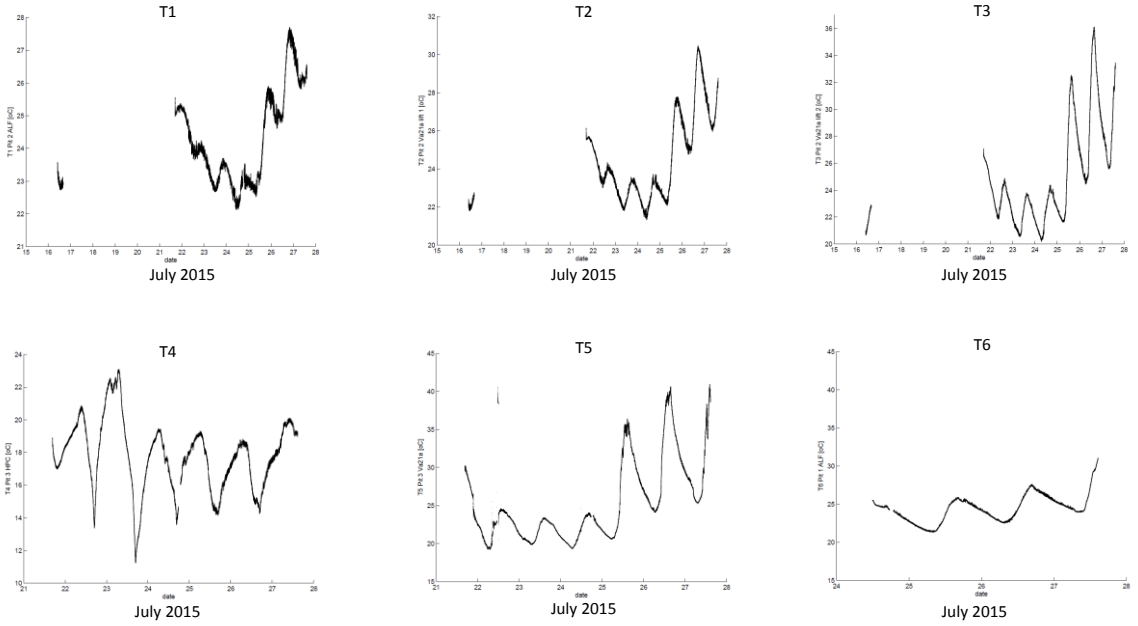

Figure 4.13. Temperature from embedded thermocouple sensors.

4.8. **Embedded pressure cells**

Two pressure cells were embedded in Pits 1 and 2 to assess the zone of influence of the LWDs. Figure 4.14 shows the pressure cell installation in Pit 1. The locations of the pressure cells are shown in Figure 4.8.

Figure 4.15 and Figure 4.16 show the sensors' response to overburden pressure and the LWD dynamic load in Pit 1 and 2, respectively. The calibration files for the pressure cells were questionable and therefore the absolute data is not trustworthy. However, it could be seen from the graphs that Pit 1 with the sensor embedded in the depth of 45 cm measured more overburden pressure than the one in Pit 2, which was embedded only 5 cm deep from the surface. Moreover, the pressure cell in Pit 1 did not record any pulse from the LWD drop.

Figure 4.14. Embedding the pressure cell in the ALF soil Pit 1

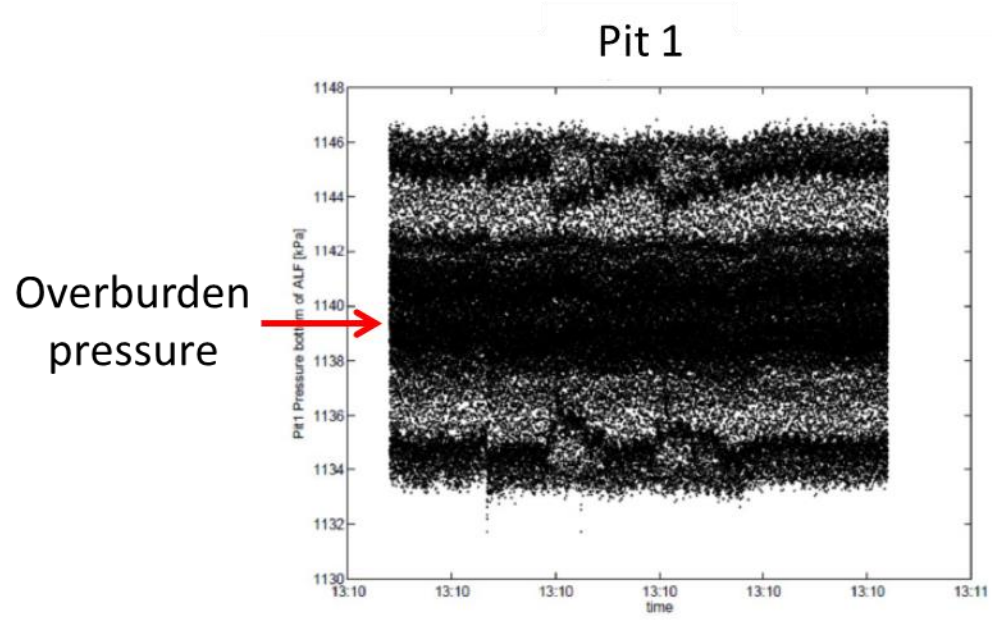

Figure 4.15. Pressure cell P1, embedded in the subgrade of Pit 1, 45 cm from the surface

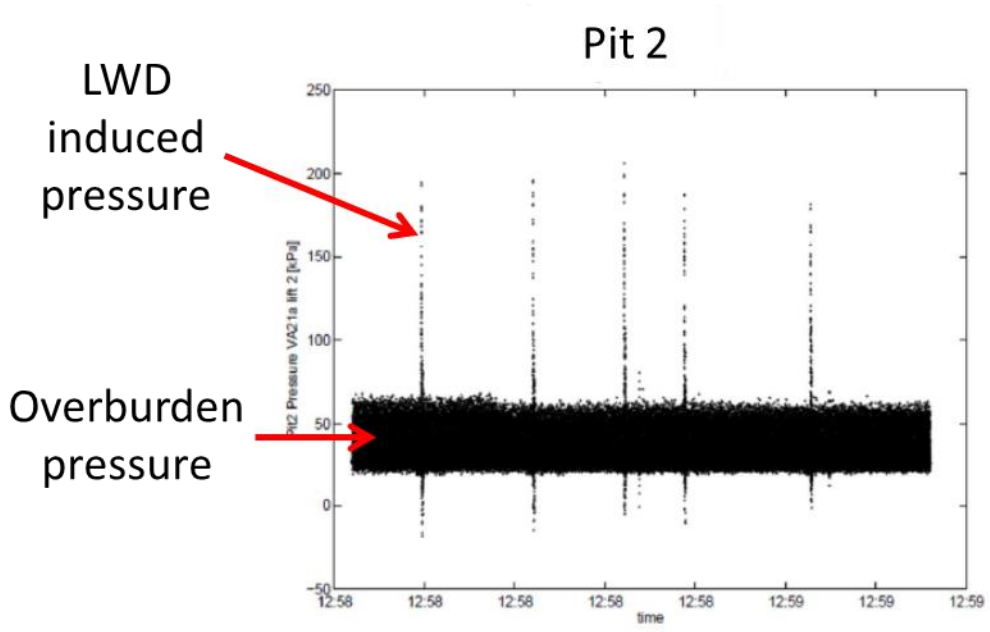

Figure 4.16. Pressure cell P2, embedded in the Base of Pit 2, 5 cm from the surface

4.9. Static Plate loading testing

Static Plate loading test was performed concurrent to LWD testing on the final grade of the subgrade and base course of each pit according to ASTM 1196 with some modifications. The reaction frame shown in Figure 4.17 was used to produce the desired reaction. Load was applied and released using a hydraulic jack assembly in increments. A proving ring was accurately calibrated (Equation 4-2) and set up to measure the magnitude of the applied load. A 300 mm rigid steel plate was used as bearing plate. One dial gauge was used to record the deflection on the plate. The deflection beam upon which the dial gauge was mounted rested on two supports more than 2.4 m away from the circumference of the bearing plate. Tests were performed at two different locations per test layer. On Pit 1 and 3, two sets of tests were performed at each location without moving the bearing plate. After arrangement of the equipment, a seating and recovery was performed by quick application and release of a load sufficient to produce a deflection between 0.25 mm and 0.51 mm. After the recovery, the dial gauge was zeroed for the start the next test. Table 4-11 shows the testing timeline.

Six increments of load—1.6 kN, 3.0 kN, 4.3 kN, 5.9 kN, 7.5 kN, and 8.9 kN—similar to the range of load levels achieved by the LWDs were applied. The corresponding deflections were measured by the dial gauge. Upon reaching the maximum load, load was released to zero. The deflection at the end of the test—an indicator of the permanent deformation—was recorded. Figure 4.18 to Figure 4.22 present the load versus deflection for the subgrade and base layers.

Equation 4-2

$$F = 20.827 \times def + 0.842$$

where *F*= applied load [kN], and *def*= deflection [mm].

Table 4-11. Plate load testing condition

Pit #	Material	Time	Test condition
1	ALF	7/24/15 3:00 PM	2 hr after compaction
2	ALF	7/14/15 7:30 AM	16 hr after compaction
2	VA21a	7/15/15 2:30 PM	3 hr after compaction
3	HPC	7/21/15 11:00 AM	right after compaction
3	VA21a	7/22/15 3:00 PM	4 hr after 2nd round compaction

Figure 4.17. Static plate load test

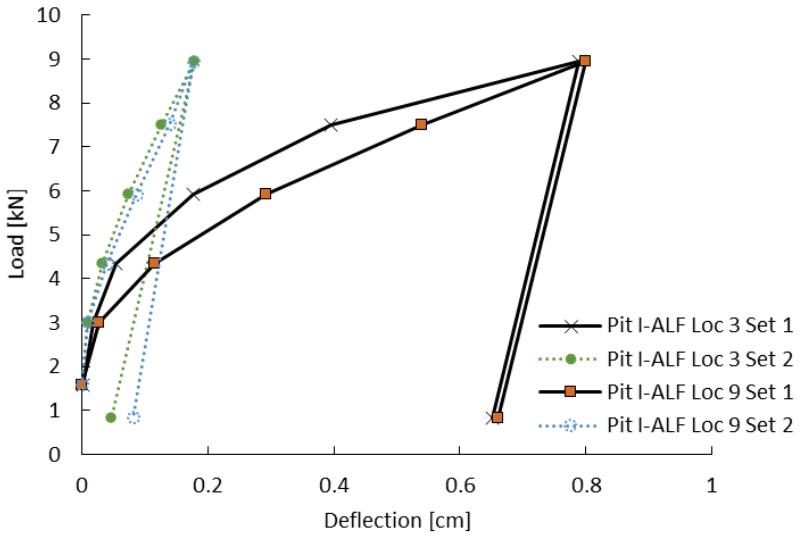

Figure 4.18. Static plate loading test: Load versus deformation for Pit I ALF Subgrade

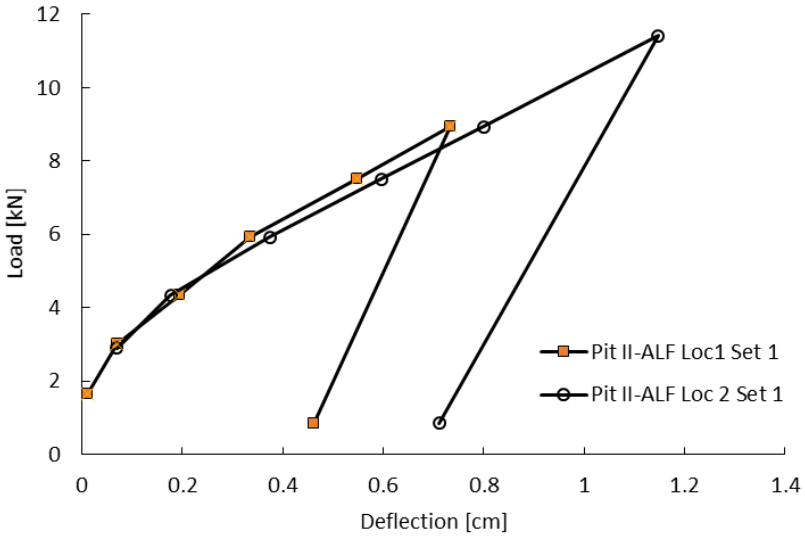

Figure 4.19. Static plate loading test: Load versus deformation for Pit II ALF Subgrade

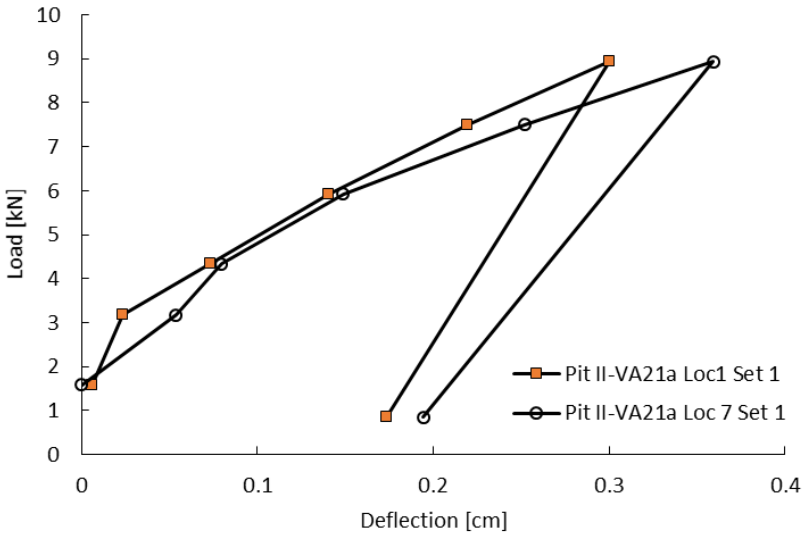

Figure 4.20. Static plate loading test: Load versus deformation for Pit II VA21a Base

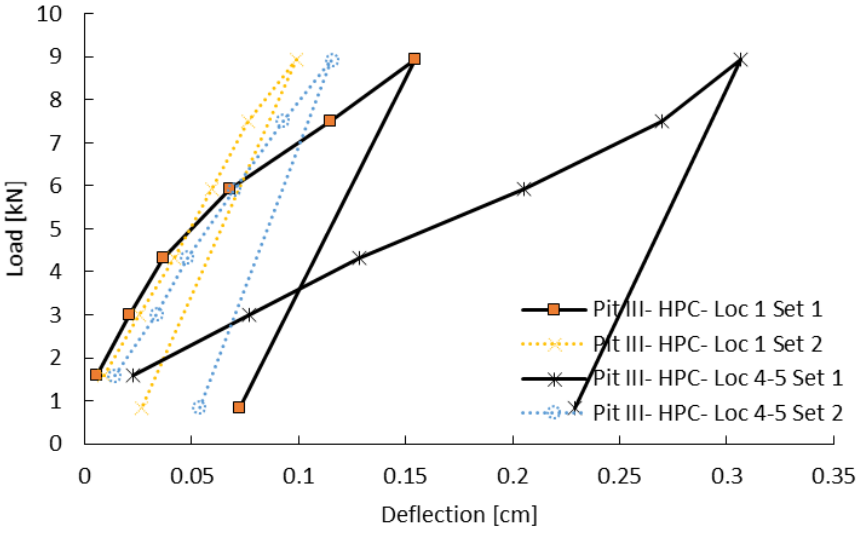

Figure 4.21. Static plate loading test: Load versus deformation for Pit III HPC Subgrade

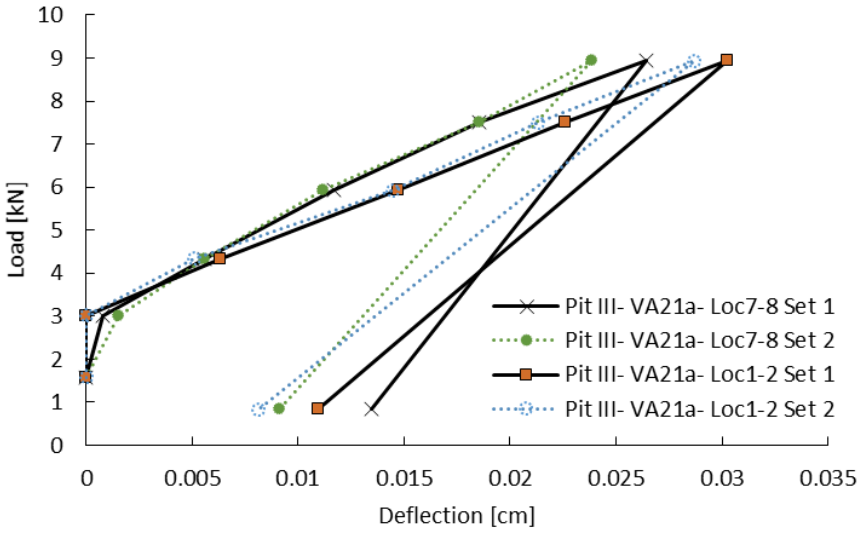

Figure 4.22. Static plate loading test: Load versus deformation for Pit III VA21a Base

The Bousinesq equation (Equation 2-1) was used to calculate the modulus of the test layer under the circular static load. The stress distribution factor used in modulus calculation was assumed as uniform ($A=\pi$) for all soils except for the HPC subgrade, which was assumed as inverse parabolic ($A=4$). The stiffness k input in modulus definition was determined from the loading and unloading Figure 4.23.

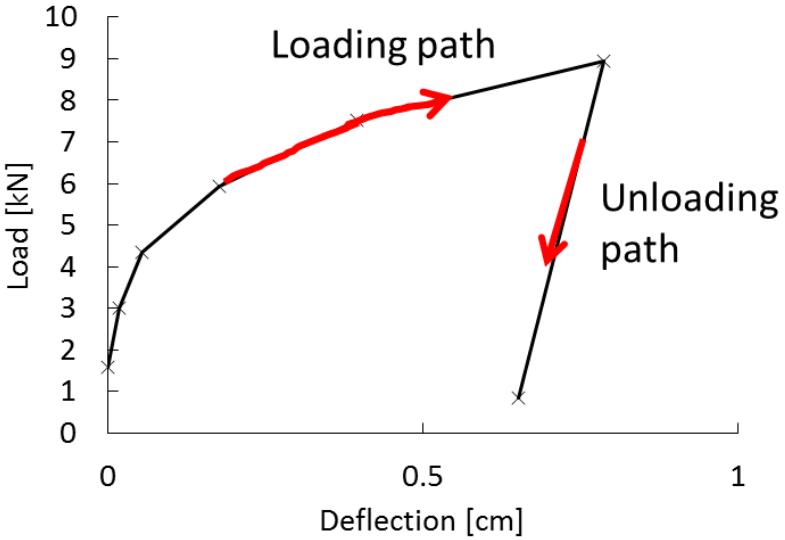

Figure 4.23. Loading and unloading paths in static plate loading test.

To precisely determine the modulus at a given stress level within the range of the test rseults, a quadratic equation was fit to the load versus deflection curves before unloading:

$$F = ax^2 + bx + c$$ **Equation 4-3**

Where F is the applied load and x is the corresponding deflection measured by dial gauge. By solving the above equation for a given F, x can be obtained by solving the above equation for a given F.

Equation 4-4

$$x = \frac{-b + \sqrt{b^2 - 4a(c - F)}}{2a}$$

Stiffness, k is determined by taking the differential of the Equation above.

Equation 4-5

$$k = \frac{dF}{dx} = 2ax + b$$

By replacing Equation 4-4 in Equation 4-5, k is obtained as a function of force, F.

Equation 4-6

$$k = \sqrt{b^2 - 4a(c - F)}$$

The static modulus was then determined during loading at the 6.3 kN load equivalent to a 90 kPa average plate pressure (E_S @ 90 kPa), and during unloading ($E_{S\text{-unload}}$). The static plate loading test results including the permanent deformation at the end of the test (d_P), resilient deflection (d_R), $E_{S\text{-unload}}$, the coefficients and R^2 of the quadratic fit, and E_S @ 90 kPa are presented for each test location in Table 4-12. Table 4-13 provides the average loading and unloading modulus, the spatial CV of the test results, and the moisture content (MC) and PC (percentage compaction) of the associated test layer.

Table 4-12. Static plate loading test results

Pit #_Material_Location	Set	d_P	d_R	Es-unload	a	b	c	R^2	Es @ 90 kPa
[-]	[-]	[mm]	[mm]	[MPa]	[-]	[-]	[-]	[%]	[MPa]
Pit I-ALF Loc 9	1	6.599	1.389	24.0	-5.33	11.79	2.86	100	3.0
	2	0.810	0.960	34.7	-17.78	37.69	2.74	100	12.7
Pit I-ALF Loc 3	1	6.507	1.367	24.4	-11.09	16.02	3.15	98	4.0
	2	0.457	1.321	25.2	-83.71	49.86	2.67	100	13.2
Pit II-ALF Loc1	1	4.503	2.723	12.2	-6.66	14.57	1.73	99	3.5
	2								
Pit II-ALF Loc 2	1	6.419	4.364	9.7	-1.47	9.42	2.48	100	3.0
	2								
Pit II-VA21a Loc1	1	1.671	1.273	26.1	-38.93	34.95	1.86	99	8.5
	2								
Pit II-VA21a Loc 7	1	1.943	1.648	20.2	-38.28	33.85	1.63	100	7.6
	2								
Pit III- HPC- Loc 1	1	0.665	0.823	31.8	-213.56	81.11	1.34	99	14.0
	2	0.178	0.721	36.2	-105.31	94.79	0.69	100	23.8
Pit III- HPC- Loc 4-5	1	2.068	0.775	33.7	8.86	21.85	1.19	100	7.5
	2	0.396	0.620	42.2	-116.70	88.17	0.32	100	20.6
Pit III- VA21a- Loc1-2	1	0.109	0.193	172.4	-224.39	202.52	3.02	100	72.6
	2	0.081	0.206	161.7	-116.73	206.45	3.10	100	75.5
Pit III- VA21a- Loc7-8	1	0.135	0.130	256.9	-2513.77	300.60	2.76	100	86.7
	2	0.091	0.147	225.9	-2151.25	313.77	2.59	100	95.7

Table 4-13. Average static plate loading test results at each Pit and layer

Pit #_Material	Set	MC	PC	Ave Es-unload	CV	Ave Es @ 90 kPa	CV
[-]	[-]	[%]	[%]	[MPa]	[%]	[MPa]	[%]
Pit 1_ ALF	1	10.0	84.3	24.2	1.2%	3.5	20%
	2			29.9	22.4%	12.9	3%
Pit 2_ ALF	1	15.3	95.6	11.0	16%	3.3	11%
	2						
Pit 2_ VA21a	1	5.3	96.4	23.2	18%	8.1	7%
	2						
Pit 3_ HPC	1	28.9	96.1	32.7	4%	10.8	43%
	2			39.2	11%	22.2	10%
Pit 3_ VA21a	1	3.6	97.1	214.6	28%	79.6	12%
	2			193.8	23%	85.6	17%

Figure 4.24 presents an interesting takeaway from the static plate loading test regarding the degree of compaction. The E_unload /E_load ratio is significantly higher for the ALF material in Pit 1 than the rest of the materials. This ratio can be interpreted as an indicator of the degree of resiliency in the response. The ratio significantly drops for Pit 1, indicating undercompaction and densification under the load during the test.

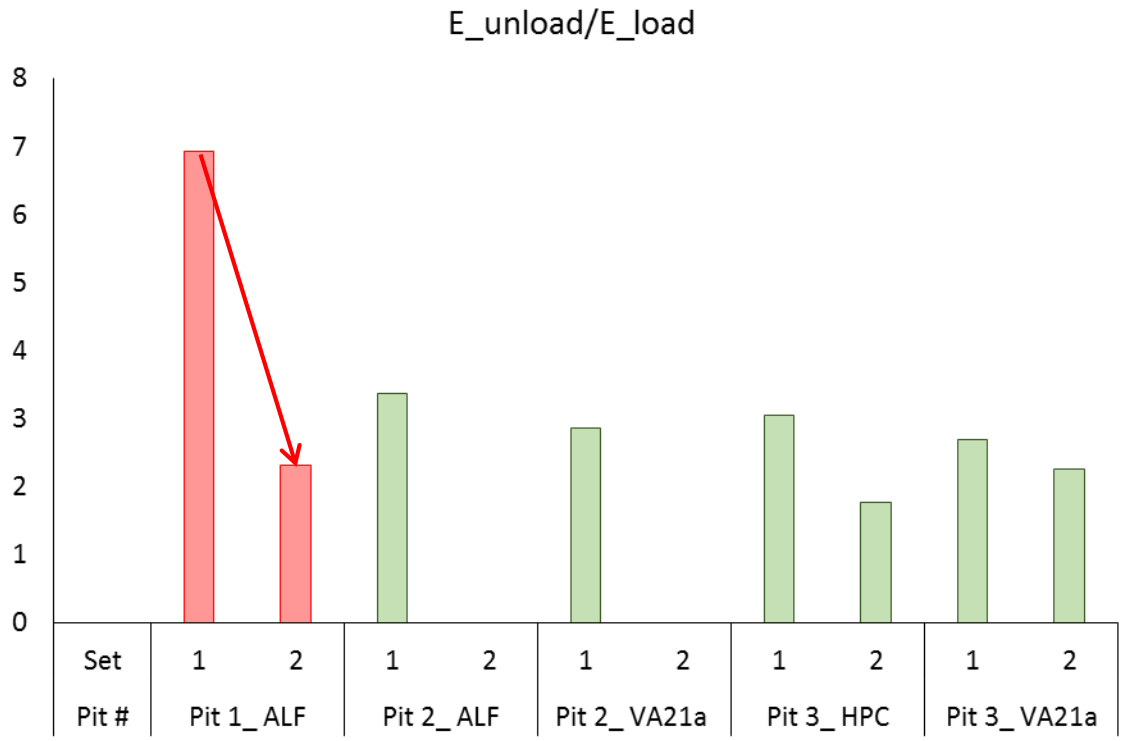

Figure 4.24. E_unload/E_load@90kPa average for the sets 1 and 2 of testing at each layer

4.10. **LWD measurements**

A comprehensive LWD testing was performed on the final grade of the compacted subgrade and base layers in test pits using the three LWD devices. Figure 4.8 shows the 9 LWD test locations (3 per LWD device). The test locations were at least 1.7 m away from the walls of the pits to avoid any boundary effects and simulate a half space condition. The test locations were at least 0.6 m (2 ft) apart. LWD testing on intermediate lifts were performed occasionally on random locations to avoid undue delays in construction process. The tests on intermediate lifts were performed in simplest form with the main objective of getting an assessment of the zone of influence of the device. The random locations were designated as alphabet letters (A, B, C…) to differentiate from testing on final layers which were named with numbers. As shown in Figure 4.8, Dynatest LWD was tested on locations

1, 5, and 9, Zorn on 3, 4, and 8; and Olson on 2, 6, and 7. The testing time is summarized in Table 4-14, Table 4-15, and Table 4-16 for Pit 1, 2, and 3, respectively. Data from Dynatest LWD is provided in Appendices 4, 5, 6 for Pits 1 to 3, in order; for Olson LWD in appendix 7; and Zorn LWD in Appendix 8.

Tests were performed using the 300 mm plate diameter. The drop heights were varied to get a grasp of stress dependency of the test material moduli in field (Table 4-17).

The bousinesq Equation (Equation 2-1) was used to calculate the surface (composite) modulus based on the peak load (F_{peak}) and peak deflection (d_{peak}) under the centerline of the applied load. Distribution factors of π, π, and 4 were used for the ALF, VA21a, and HPC soil, respectively. The surface modulus for Olson, Zorn, and Dynatest LWD is designated as E_Os, E_Zs, and E_Ds, respectively.

Table 4-14. LWD testing at Pit 1

Lift number	Material	LWD testing on constructed layer and time	
0	Crushed stone	7/17/15 2:00 PM	On top of geotextile and crushed stone
1	ALF	7/22/15 1:30 PM	right after compaction
2	ALF	7/24/15 8:00 AM	right after compaction
3	ALF	7/24/15 3:00 PM	2 hr after compaction- Concurrent to plate load test
3	ALF	7/28/15 1:00 PM	4 days after compaction- Zorn only

Table 4-15. LWD testing at Pit 2

Lift number	Material	LWD testing on constructed layer and time	
5	ALF	7/13/15 10:00 AM	Zorn and Olson only
6	ALF	7/13/15 4:00 PM	1 hr after compaction
		7/14/15 7:30 AM	16 hr after compaction- Concurrent to plate load test
		7/14/15 12:30 PM	21 hr after compaction- Zorn only
7	VA21a	7/15/15 7:30 AM	16 hr after final series of compaction
8	VA21a	7/15/15 12:00 PM	0.5 hr after compaction
		7/15/15 2:30 PM	3 hr after compaction- Concurrent to plate load test
		7/20/15 1:00 PM	5 days after compaction- except Dynatest
		7/24/15 8:30 AM	9 days after compaction
		7/28/15 1:00 PM	13 days after compaction- Zorn only

Table 4-16. LWD testing at Pit 3

Lift number	Material	LWD testing on constructed layer and time	
1	HPC	7/17/15 11:00 AM	right after compaction
2	HPC	7/17/15 4:00 PM	Only with Zorn
		7/20/15 9:00 AM	65 hr after compaction
4	HPC	7/20/15 1:00 PM	right after compaction
5	HPC	7/21/15 11:00 AM	right after compaction- Concurrent to plate load test
6	VA21a	7/22/15 10:30 AM	right after compaction
		7/22/15 12:30 PM	1.5 hr after 2nd compaction
		7/22/15 3:00 PM	4 hr after 2nd compaction- Concurrent to plate load test
		7/24/15 7:30 AM	45 hr after compaction
		7/28/15 1:00 PM	6 days after compaction- Zorn only

Table 4-17. Drop heights for each LWD device

Drop Height [cm]	Zorn	Dynatest	Olson
h1	32	20	20
h2	-	56	48
h3	72	84	61
h4	32	20	20

4.10.1 Summary of results from LWD testing on pits

Table 4-18 summarizes the CV of the modulus of last three drops as measured by Zorn, Dynatest, and Olson LWD. The Olson LWD had the highest variability among all. In Zorn, a constant force is assumed, therefore all the variability in E_Zs is attributed to CV of surface deflection. For Dynatest, even though force is measured, the CV of the force channel in last three drops was essentially zero; so, all the variability in E_Ds was attributed to the variability in deflection data. In the other hand, Olson showed higher variability in E_Os.

The variability of a given LWD was not similar in all soils, either. This is attributed to the stiffness, degree of compaction, saturation, plasticity, evenness, and quality of the contact stress. Overall, ALF in Pit 2 showed the lowest variability; VA21a in Pit 3 and stone in Pit 1 showed the highest.

Table 4-18. CV in the surface modulus of the last three drops in LWD testing in Pits

	CV of last 3 drops	Stone pit 1	Alf Pit 1	ALF Pit 2	VA21a Pit 2	HPC Pit 3	VA21a Pit 3
Zorn	Max	4.0%	4.3%	1.9%	4.7%	4.5%	5.1%
	Ave	2.7%	2.0%	0.7%	1.4%	1.5%	2.1%
Dynatest	Max	3.0%	3.0%	3.9%	7.2%	4.2%	8.0%
	Ave	2.0%	1.5%	1.2%	1.7%	1.3%	2.5%
Olson	Max	6.5%	10.5%	6.4%	6.5%	6.9%	18.3%
	Ave	4.9%	2.8%	1.4%	1.5%	2.8%	3.4%

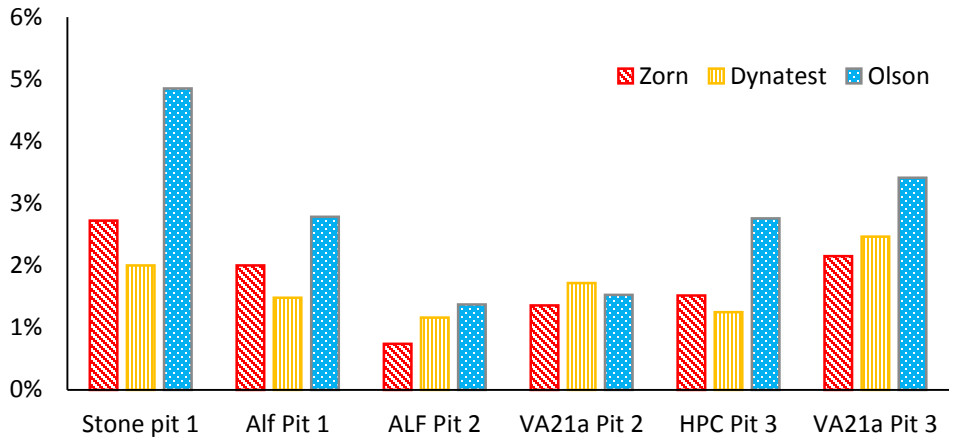

Figure 4.25. Average CV in the last three drops

Figure 4.26 to Figure 4.33 show the surface modulus as the function of P/Pa measured on the final grade of the subgrade and base layers in the pits using the Zorn, Dynatest, and Olson LWDs. Error bars indicate 1 standard deviation spatial variability. Overall, Dynatest LWD showed the higher spatial variability than the other two and a declining trend versus P/Pa. Zorn and Olson LWDs showed an increase in modulus with an increase in the induced pressure. The average GWC, DD, and VWC of the layers at the time of testing was derived from a combination of resources including the embedded sensors, spot check VWC testing, and GWC measurements from MA and oven drying and is summarized in a table under each graph.

In order to be able to compare the modulus values at a given stress level, power law model $E = a\left(\frac{P}{P_a}\right)^b$ was fit to the data obtained from each LWD on the 3 test locations on each lift or layer. Average modulus at each lift was also predicted at P/Pa=0.9 corresponding to average force of 6.4 kN and 90 kPa induced pressure. Average spatial CV was also obtained from the measurements at each lift and stress level. For cases were enough measurements were not taken to fit the power law model, the measurements at P/Pa close

to 0.9 is reported. For cases that test was only performed at one location, average spatial CV is not applicable (NA).

Table 4-19 to Table 4-27 summarize the coefficients of the power law model, the R^2 of the fit model over the multiple test locations, predicted surface modulus at P/Pa of 0.9 and spatial CV for the LWD devices at each pit on sublayers and final grades of each layer and at several times after compaction.

Table 4-19. Power law model ($E=a(P/Pa)^b$) for Zorn LWD measurements in Pit 1

Material	Lift	time	a	b	R2	P/Pa	Predicted Ave E_Zs	Ave spatial CV
[-]	[-]	[hr]	[MPa]	[-]	[%]	[-]	[MPa]	[%]
Stone	0	0	40.87	0.32	37.3%	0.9	39.4	5.0%
ALF	1	0	14.83	0.30	60.3%	0.9	14.3	NA
ALF	2	0	9.99	0.07	12.4%	0.9	9.9	4.4%
ALF	3	2	6.94	-0.19	59.5%	0.9	7.1	8.6%

Table 4-20. Power law model ($E=a(P/Pa)^b$) for Dynatest LWD measurements in Pit 1

Material	Lift	time	a	b	R2	P/Pa	Ave E_Ds	Ave spatial CV
[-]	[-]	[hr]	[MPa]	[-]	[%]	[-]	[MPa]	[%]
ALF	1	0	33.97	-0.06	5.0%	0.9	34.2	NA
ALF	2	0	13.24	-0.32	89.3%	0.9	13.8	36.4%
ALF	3	2	9.63	-0.63	95.8%	0.9	10.4	11.4%

Table 4-21. Power law model ($E=a(P/Pa)^b$) for Olson LWD measurements in Pit 1

Material	Lift	time	a	b	R2	P/Pa	Ave E_Os	Ave spatial CV
[-]	[-]	[hr]	[MPa]	[-]	[%]	[-]	[MPa]	[%]
ALF	1	0	20.76	0.30	82.6%	0.9	20.0	NA
ALF	2	0	13.13	0.21	76.6%	0.9	12.8	19.0%
ALF	3	2	11.32	0.38	91.1%	0.9	10.8	2.6%

Table 4-22. Power law model ($E=a(P/Pa)^b$) for Zorn LWD measurements in Pit 2

Material	Lift	time	a	b	R2	P/Pa	Ave E_Zs	Ave spatial CV
[-]	[-]	[hr]	[MPa]	[-]	[%]	[-]	[MPa]	[%]
ALF	5	0	7.73	-0.17	98.8%	0.9	7.9	2.4%
ALF	6	0.5	6.40	-0.10	95.1%	0.9	6.5	9.2%
ALF	6	16	8.02	-0.05	49.6%	0.9	8.1	13.6%
ALF	6	21	7.51	-0.08	92.2%	0.9	7.6	4.7%
VA21a	7	16	7.98	-0.09	55.5%	0.9	8.1	12.2%
VA21a	8	1	11.28	0.03	2.2%	0.9	11.2	9.0%
VA21a	8	4	12.23	0.02	34.1%	0.9	12.2	6.4%
VA21a	8	122				1.0	31.6	NA
VA21a	8	216	48.46	-0.09	89.0%	0.9	49.0	6.2%
VA21a	8	316				1.0	54.0	NA

Table 4-23. Power law model ($E=a(P/Pa)^b$) for Dynatest LWD measurements in Pit 2

Material	Lift	time	a	b	R2	P/Pa	Ave E_Ds	Ave spatial CV
[-]	[-]	[hr]	[MPa]	[-]	[%]	[-]	[MPa]	[%]
ALF	6	0.5	7.39	-0.41	64.6%	0.9	7.8	33.8%
ALF	6	16	9.03	-0.44	79.2%	0.9	9.5	33.5%
VA21a	7	16	8.99	-0.17	38.5%	0.9	9.2	3.2%
VA21a	8	1	9.63	-0.11	60.6%	0.9	9.8	10.5%
VA21a	8	4	12.06	-0.12	48.0%	0.9	12.2	20.5%
VA21a	8	216	64.34	-0.46	90.3%	0.9	67.9	6.6%

Table 4-24. Power law model ($E=a(P/Pa)^b$) for Olson LWD measurements in Pit 2

Material	Lift	time	a	b	R^2	P/Pa	Ave E_Os	Ave spatial CV
[-]	[-]	[hr]	[MPa]	[-]	[%]	[-]	[MPa]	**[%]**
ALF	5	0	10.88	0.46	63.1%	0.9	10.3	8.3%
ALF	6	0.5	10.98	0.63	100.0%	0.9	10.2	3.4%
ALF	6	16	10.80	0.00	0.6%	0.9	10.8	4.4%
VA21a	7	16	11.09	0.21	61.0%	0.9	10.8	21.0%
VA21a	8	1	15.05	0.13	94.8%	0.9	14.8	23.7%
VA21a	8	4	16.05	0.27	87.4%	0.9	15.5	14.9%
VA21a	8	122				1.1	38.1	NA
VA21a	8	216	67.72	0.03	22.3%	0.9	67.5	4.7%

Table 4-25. Power law model ($E=a(P/Pa)^b$) for Zorn LWD measurements in Pit 3

Material	Lift	time	a	b	R^2	P/Pa	Ave E_Zs	Ave spatial CV
[-]	[-]	[hr]	[MPa]	[-]	[%]	[-]	[MPa]	[%]
HPC	5	0.0	17.87	0.28	71.1%	0.9	17.3	5.0%
VA21a	6	0.0	43.57	0.26	43.0%	0.9	42.3	11.6%
VA21a	6- 2nd rnd	0.0	39.52	0.35	43.0%	0.9	37.9	14.4%
VA21a	6- 2nd rnd	4.0	48.73	0.31	60.9%	0.9	46.9	16.6%
VA21a	6- 2nd rnd	45.0	44.43	0.29	65.0%	0.9	42.9	9.3%
VA21a	6- 2nd rnd	144.0				1.0	37.5	

Table 4-26. Power law model ($E=a(P/Pa)^b$) for Dynatest LWD measurements in Pit 3

Material	Lift	time	a	b	R2	P/Pa	Ave E_Ds	Ave spatial CV
[-]	[-]	[hr]	[MPa]	[-]	[%]	[-]	[MPa]	[%]
HPC	5	0.0	41.69	-0.16	91.1%	0.9	42.5	9.5%
VA21a	6	0.0	69.93	-0.16	96.7%	0.9	71.2	17.3%
VA21a	6- 2nd rnd	0.0	46.93	-0.07	3.9%	0.9	47.3	20.3%
VA21a	6- 2nd rnd	4.0	66.16	-0.18	90.2%	0.9	67.6	39.1%
VA21a	6- 2nd rnd	45.0	56.79	-0.02	28.1%	0.9	56.9	20.8%

Table 4-27. Power law model ($E=a(P/Pa)^b$) for Olson LWD measurements in Pit 3

Material	Lift	time	a	b	R2	P/Pa	Ave E_Os	Ave spatial CV
[-]	[-]	[hr]	[MPa]	[-]	[%]	[-]	[MPa]	[%]
HPC	5	0.0	27.54	0.42	99.5%	0.9	26.2	9.2%
VA21a	6	0.0	51.86	0.48	87.0%	0.9	49.0	19.6%
VA21a	6- 2nd rnd	0.0	39.95	0.59	75.6%	0.9	37.3	11.8%
VA21a	6- 2nd rnd	4.0	57.89	0.67	52.0%	0.9	53.5	13.3%
VA21a	6- 2nd rnd	45.0	47.58	0.41	87.1%	0.9	45.3	6.2%

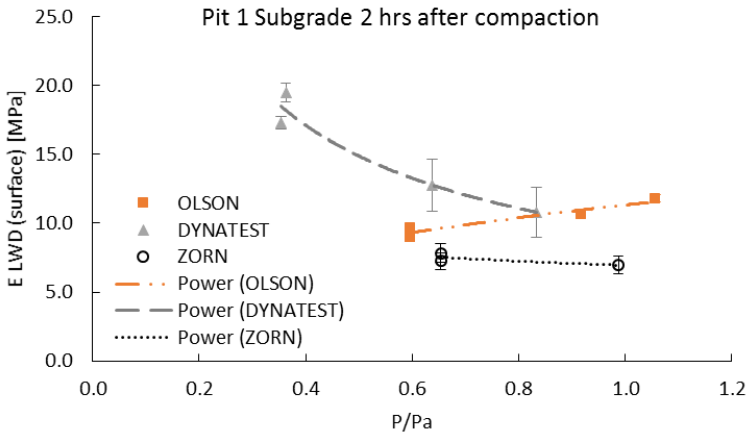

Average Subgrade		
GWC	DD	VWC
10.0	1621.4	16.2

Figure 4.26. LWD surface modulus on the final grade of the subgrade soil in Pit 1 as measured by Zorn, Dynatest, and Olson LWD. Error bars indicate 1 standard deviation spacial variability.

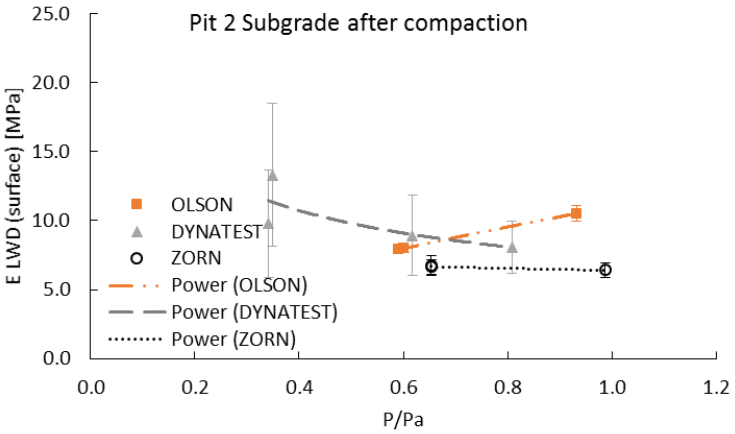

Average Subgrade		
GWC	DD	VWC
15.3	1838.2	28.1

Figure 4.27. LWD surface modulus on the final grade of the subgrade soil in Pit 2 as measured by Zorn, Dynatest, and Olson LWD. Error bars indicate 1 standard deviation spacial variability.

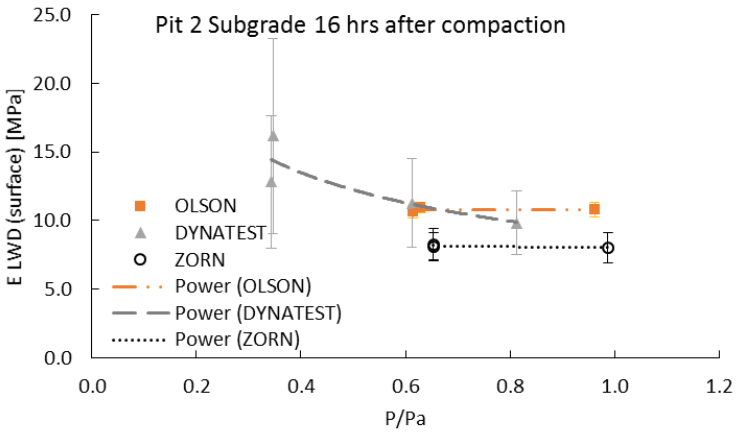

Average Subgrade		
GWC	DD	VWC
15.0	1838.2	27.7

Figure 4.28. LWD surface modulus on the final grade of the subgrade soil in Pit 2 16 hours after compaction as measured by Zorn, Dynatest, and Olson LWD. Error bars indicate 1 standard deviation spacial variability.

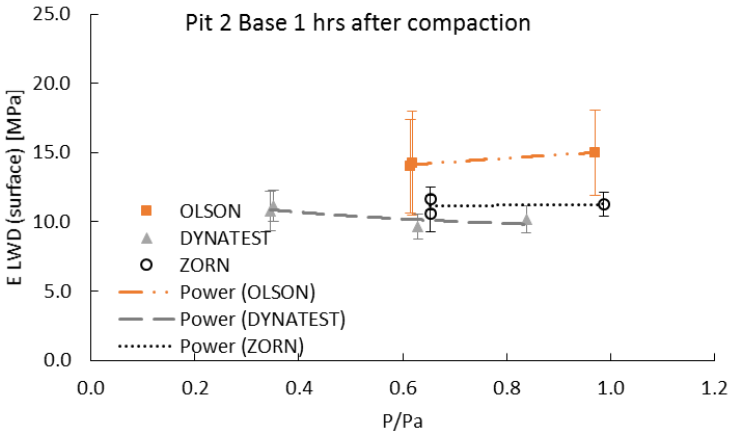

Average Subgrade			Average Base		
GWC	DD	VWC	GWC	DD	VWC
14.9	1838.2	27.4	5.3	2348.6	12.5

Figure 4.29. LWD surface modulus on the final grade of the base layer in Pit 2 1 hour after compaction as measured by Zorn, Dynatest, and Olson LWD. Error bars indicate 1 standard deviation spacial variability.

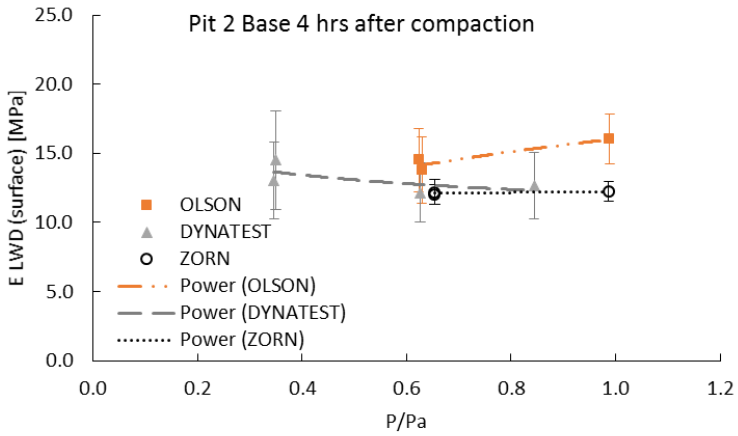

Average Subgrade			Average Base		
GWC	DD	VWC	GWC	DD	VWC
14.9	1838.2	27.3	5.3	2348.6	12.4

Figure 4.30. LWD surface modulus on the final grade of the base layer in Pit 2 4 hour afters compaction as measured by Zorn, Dynatest, and Olson LWD. Error bars indicate 1 standard deviation spacial variability.

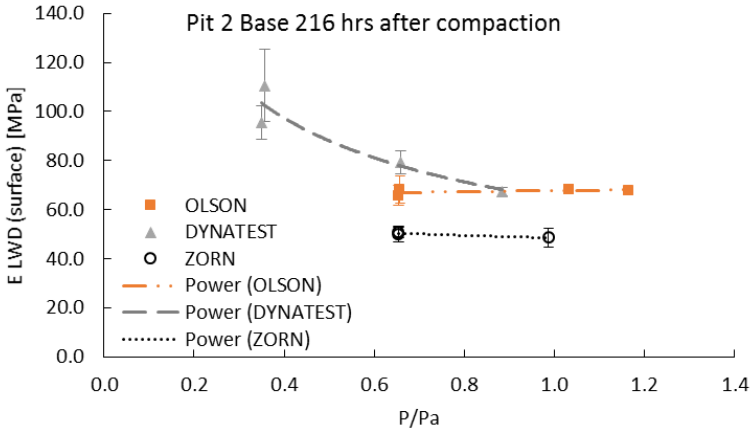

Average Subgrade			Average Base		
GWC	DD	VWC	GWC	DD	VWC
14.4	1838.2	26.5	4.7	2348.6	11.0

Figure 4.31. LWD surface modulus on the final grade of the base layer in Pit 2 216 hours after compaction as measured by Zorn, Dynatest, and Olson LWD. Error bars indicate 1 standard deviation spacial variability.

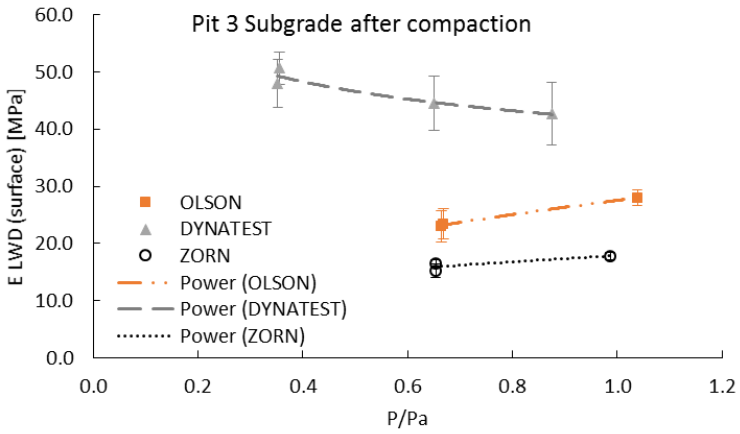

Average Subgrade		
GWC	DD	VWC
28.9	1463.8	42.3

Figure 4.32. LWD surface modulus on the final grade of the subgrade soil in Pit 3 as measured by Zorn, Dynatest, and Olson LWD. Error bars indicate 1 standard deviation spacial variability.

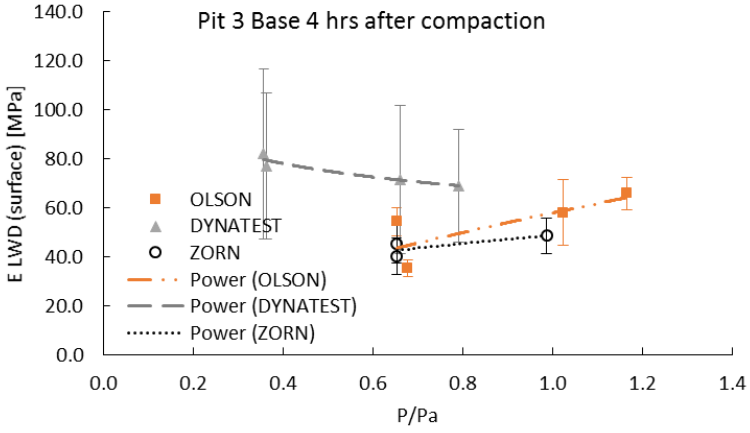

Average Subgrade			Average Base		
GWC	DD	VWC	GWC	DD	VWC
26.7	1463.8	39.1	3.5	2365.7	8.4

Figure 4.33. LWD surface modulus on the final grade of the base layer in Pit 3 4 hours after compaction as measured by Zorn, Dynatest, and Olson LWD. Error bars indicate 1 standard deviation spacial variability.

Consecutive testing on the pits revealed the changes in surface modulus due to drying as shown in Figure 4.34 to Figure 4.37.

ALF material in Pit 1 and Pit 2 both had an initial surface modulus of about 7 MPa even though Pit 1 was compacted at much lower WC (10%). At such low WC higher modulus is anticipated given a good compaction. The low modulus as compared to the compaction condition of Pit 2 (higher WC, higher PC) clearly indicates the poor compaction in Pit 1. In addition, ALF material in Pit 1 did not show any increase in modulus even after 3 days as shown in Figure 4.34. ALF material in Pit 2 however, demonstrated about 24%, 23%, and 6% increase in modulus after 16 hours as measured by Zorn, Dynatest, and Olson LWD respectively (Figure 4.35).

The surface modulus measured on top of the VA21a base material in Pit 2 and 3 were significantly different right after compaction. Material in Pit 2, compacted at higher WC of 5.3% had an initial modulus of about 10-15 MPa as measured by different LWD devices. However, after 9 days drying to WC of 4.7%, the surface modulus increased by the factor of 4.8, 7.0, and 4.6 as measured by Zorn, Dynatest, and Olson LWD (Figure 4.36). In the other hand, in Pit 3, with lower compaction WC of 3.5%, the initial modulus was much higher than Pit 2 at around 37-47 MPa as measured by different devices. After 45 hrs, there was an increase of 13-22% in the modulus as measured by different devices.

It is important to consider that the aforementioned values are the surface modulus. In order to obtain the layer modulus for VA21a material in Pit 2 and Pit 3, Equation 2-3 can be used.

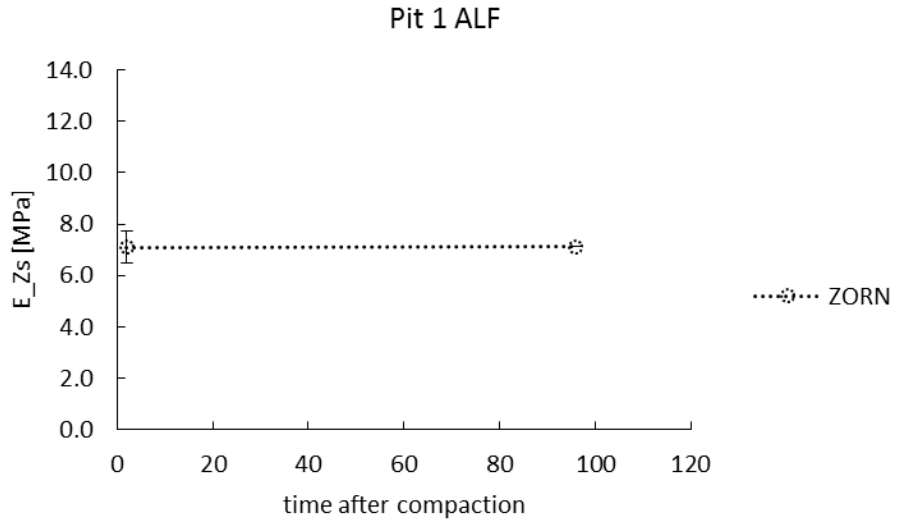

Figure 4.34. Variation in surface modulus of ALF soil in Pit 1 after compaction

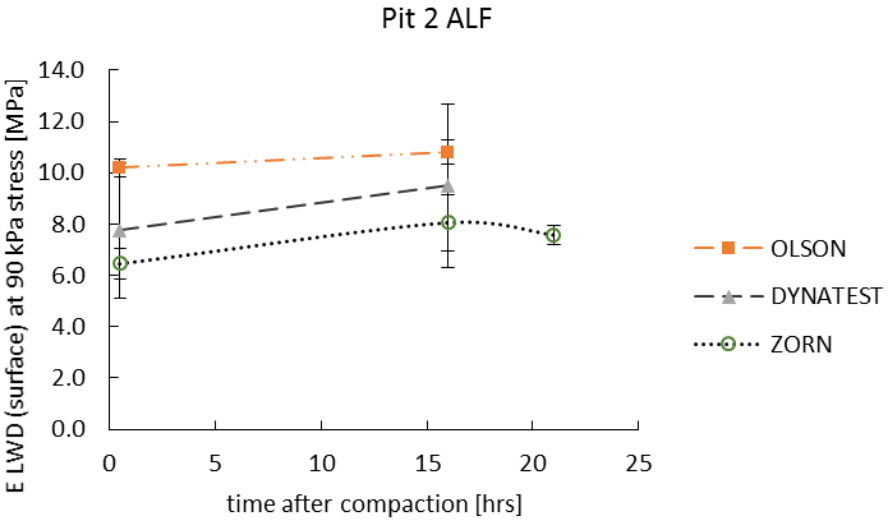

Figure 4.35. Variation in surface modulus of ALF soil in Pit 2 after compaction

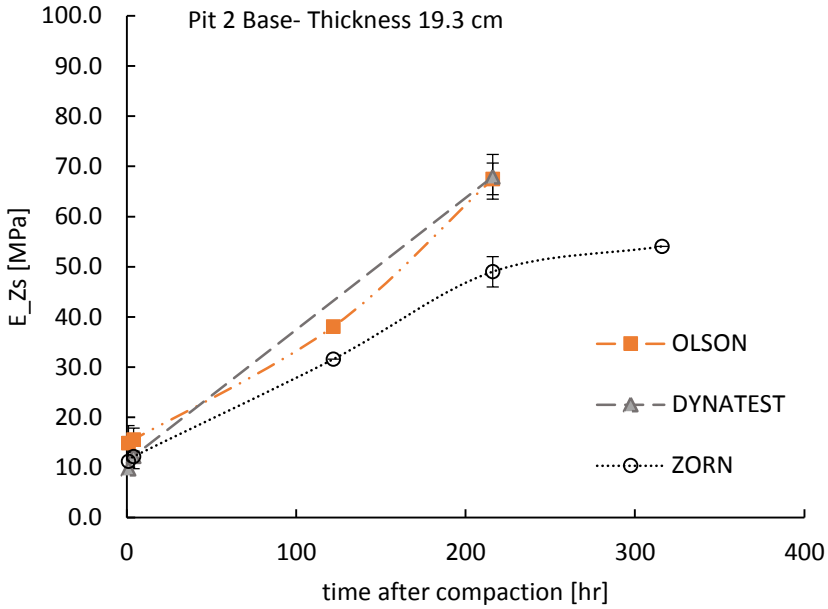

Average Subgrade			Average Base		
GWC	DD	VWC	GWC	DD	VWC
14.9	1838.2	27.4	5.3	2348.6	12.5
14.3	1838.2	26.3	4.7	2348.6	10.9

Figure 4.36. Variation in surface modulus of VA21a base soil in Pit 2 after compaction. Table shows the volumetric properties of the base and subgrade layers after compaction and after nine days.

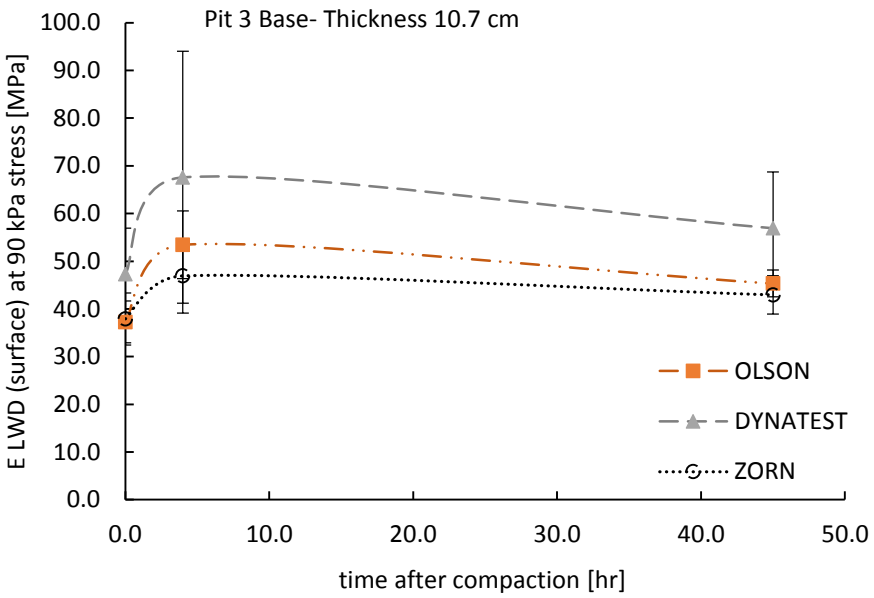

Average Subgrade			Average Base		
GWC	DD	VWC	GWC	DD	VWC
26.7	1463.8	39.1	3.5	2365.7	8.4
25.1	1463.8	36.7	3.1	2365.7	7.3

Figure 4.37. Variation in surface modulus of VA21a base soil in Pit 3 after compaction. Table shows the volumetric properties of the base and subgrade layers after compaction and after 45 hrs.

The LWD modulus on mold ($E_{LWDonMold}$) tabulated in Table 2-21 was compared to the field surface modulus ($E_{field\text{-}Surface}$) at P/Pa=0.9 for each testing device and material. LWD on mold lab tests were conducted at the same field water content as Pits but to the minimum of 95% PC. $E_{LWDonMold}$ is used as the target modulus and the $E_{field\text{-}Surface}$ is normalized by this target value. Figure 4.38 presents the modulus ratio ($E_{field\text{-}Surface}/ E_{LWDonMold}$) for the different materials and pits. It could be seen that for the ALF material in Pit 1, the ratio was much lower than the other scenarios, suggesting the poor compaction of Pit 1. VA21a soil in Pit 2 was in borderline (shown in yellow) but its modulus and therefore the ratio increased substantially after 216 hours as shown in Figure 4.38. Figure 4.39 (A) compares the lab LWD on mold and field surface modulus measured on the subgrade and base layers of Pit 2 and 3. There was a poor correlation between the lab and field results. However, after excluding the average surface modulus measured on VA21a layer at Pit 2, the correlation became stronger with R^2 values of 0.883, 0.995, and 0.529 for Zorn, Dynatest, and Olson LWD, respectively. In Pit 2, as previously discussed, the surface modulus measured on the base layer was initially very low due to high water content but quickly increased. The results showed that LWD testing on mold can serve as a promising testing tool to find the target modulus values in the field at a given water content and density condition. More testing is required to validate the outcomes of this study.

Moreover, upon comparison of the two modulus values for ALF material in Pit 1, poor compaction of Pit 1 was clearly observed. The LWD modulus on mold was conducted on ALF material in the same field water content as Pit 1 but to 95% PC. As expected, the modulus values of the LWD on mold were well above the numbers achieved in the field.

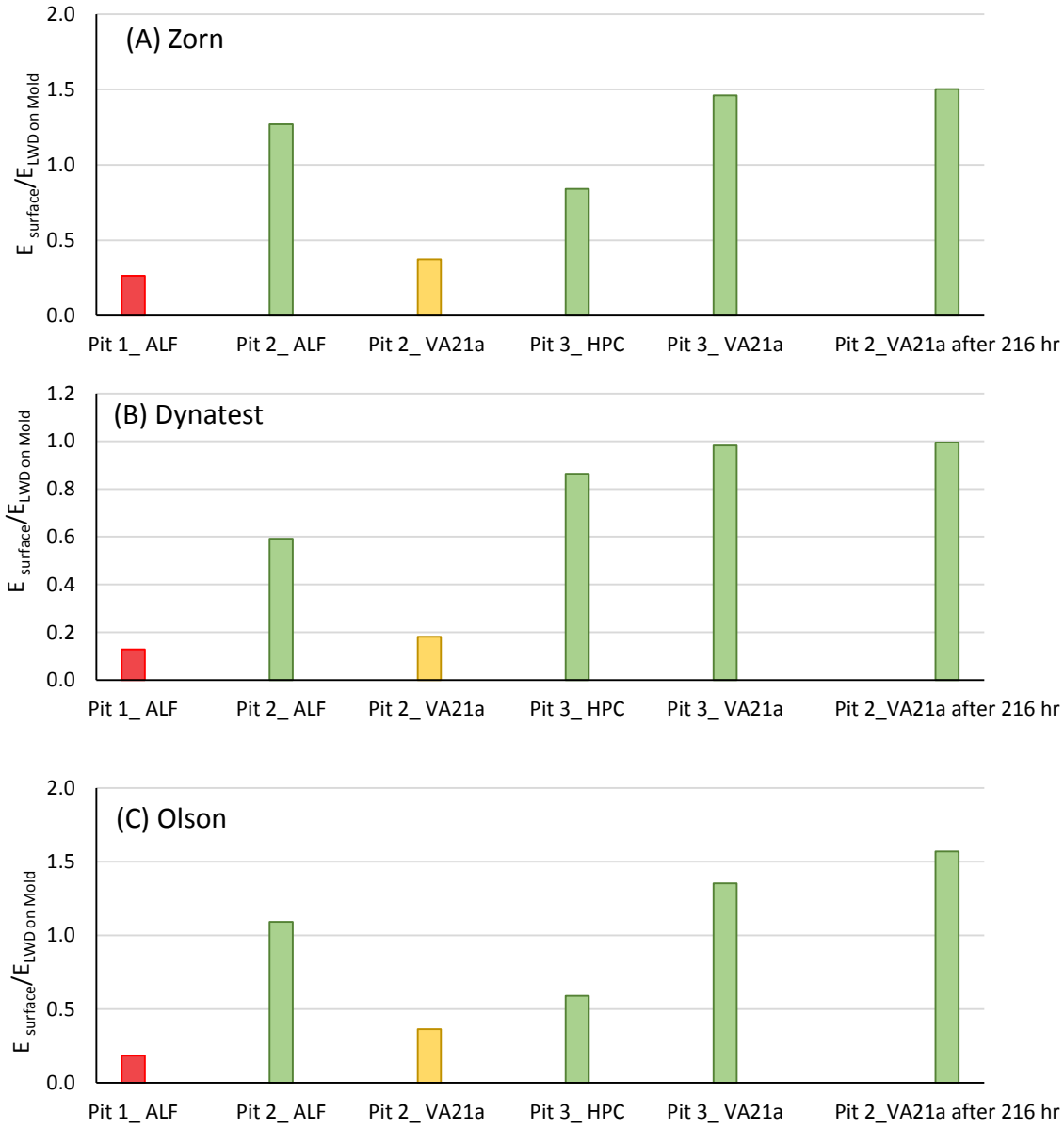

Figure 4.38. Ratio of $E_{Field\ surface}$ / $E_{LWD\ on\ Mold}$ for different materials and Pits.

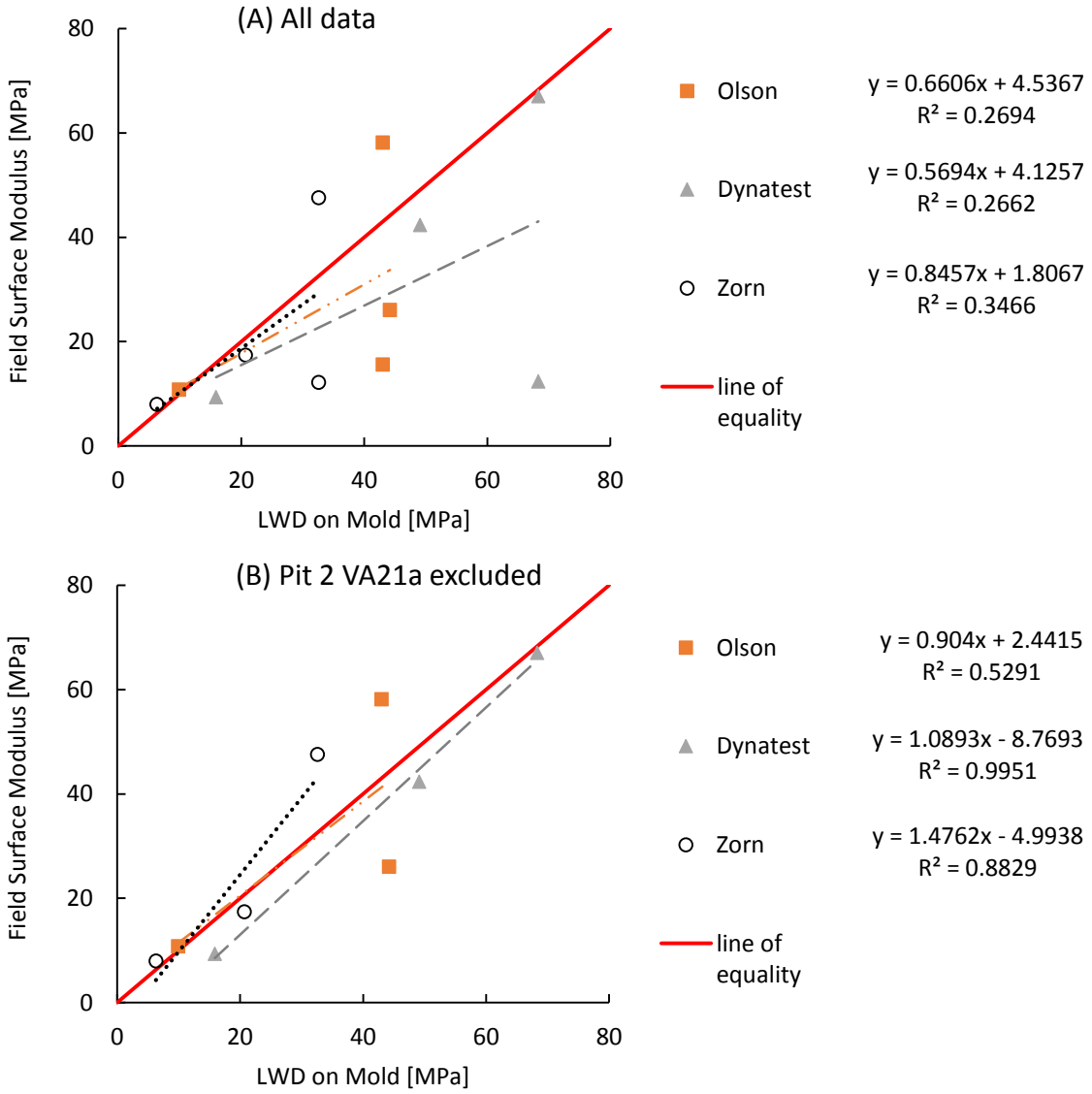

Figure 4.39. Comparison of Field LWD surface modulus and LWD on mold modulus for Zorn, Dynatest, and Olson LWD (A) data from Pit 2 ALF and VA21a, Pit 3 HPC and VA21a; (B) data from Pit 2 ALF, and Pit 3 HPC and VA21a.

Figure 4.40 (A) presents the moduli at the same induced stress level of 90 kPa from all the LWD devices and the plate load tests. The details of LWD testing and analysis are presented later in Section 4.10.

Figure 4.41 depicts the modulus of each LWD versus that of the static plate test. A fair correlation was observed between LWDs and static plate load test. It was observed that all LWDs over-predicted the surface moduli as compared to static plate test except for the case of base layer in Pit 3.

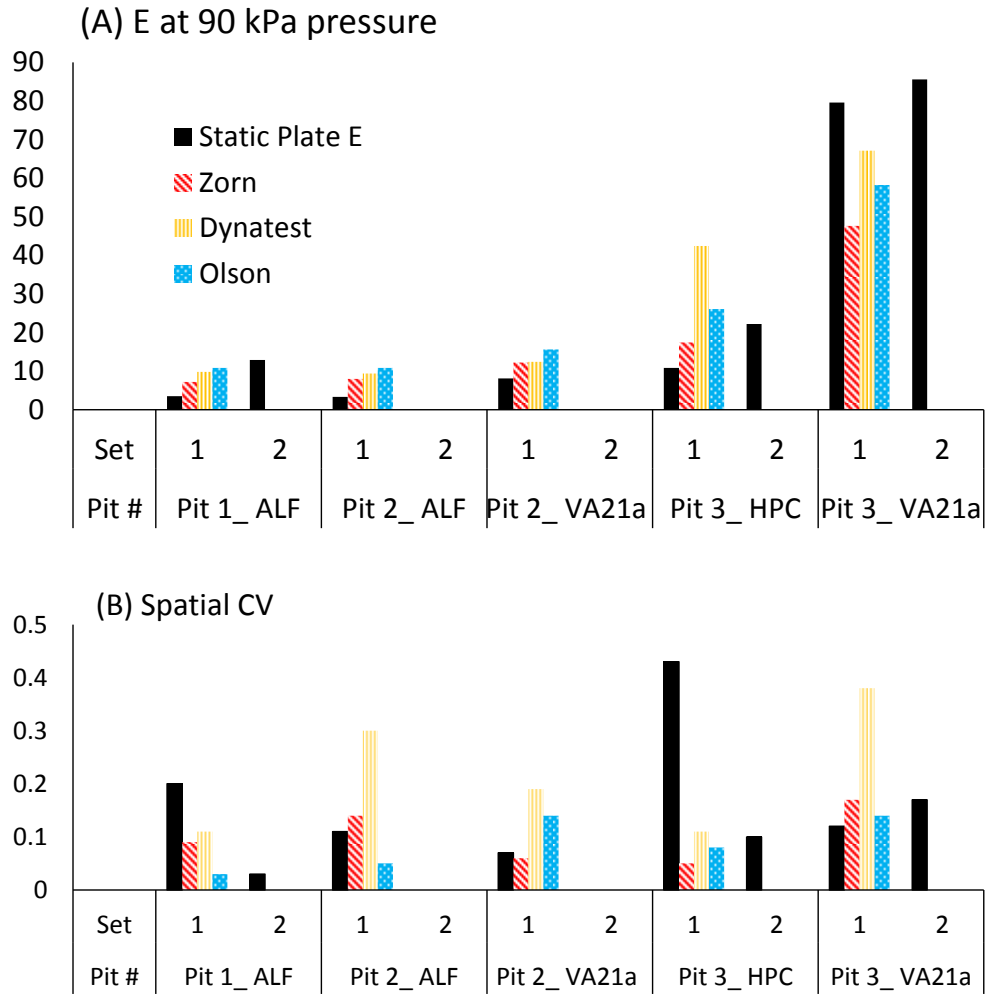

Figure 4.40. (A) Surface modulus from LWD testing and plate load testing (set 1 and 2) at 90 kPa; (B) Spatial variability from LWD testing and plate load testing (set 1 and 2) at 90 kPa.

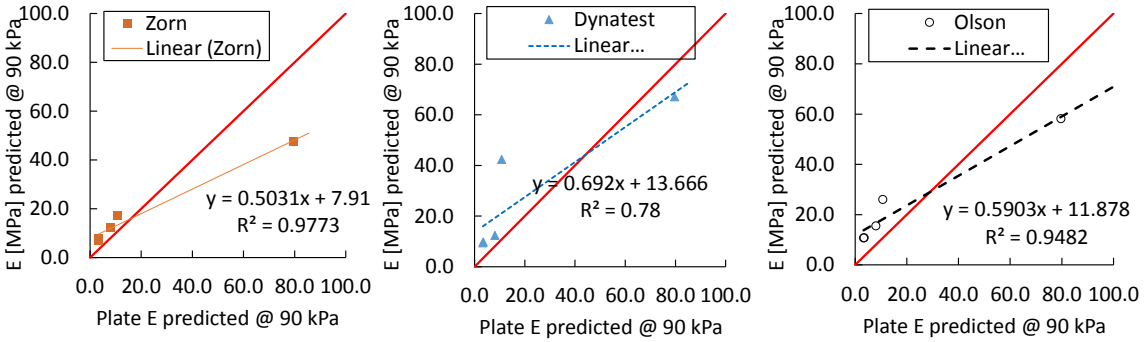

Figure 4.41. Surface modulus from LWD testing versus plate load testing (set 1) at 90 kPa

Chapter 5. Conclusions

Lightweight deflectometers (LWD) are gaining attention for compaction quality assurance because they can directly measure modulus, which is a primary input for pavement structural design. LWDs have been implemented for pavement construction QA in a few states and countries but their broader implementation has been hampered by the lack of a widely recognized standard for interpreting the load and deflection data obtained during testing. The challenges in establishing a standard specification for interpreting the LWD data are broad and include the differences among the various LWD devices, the nonlinearity of the soil modulus under different moisture and stress conditions, and the differences in the stress states and boundary conditions between typical laboratory tests and field conditions. Despite the challenges, LWDs are promising tools for performance based construction QA testing that will not only result in a better product but also provide the quantitative measures critical for better understanding the connection between pavement design and long term pavement performance.

In this study, the dynamic responses of three different LWDs were carefully studied through a unique large-scale controlled experimental setting. Three large 4.5x4.5 m^2 test pits were designed and constructed at target moisture and density conditions to simulate scenarios of acceptable (Pits 2 and 3) and failing construction quality (Pit 1). The pits were carefully constructed using two different cohesive (HPC) and noncohesive (ALF) subgrade soils and one type of granular aggregate base (VA21a). The test pits were equipped with in-situ environmental sensors to monitor the post-compaction variations in volumetric water content and temperature and pressure cells to evaluate the zone of influence of the LWD loading.

LWD testing on intermediate lifts were performed occasionally at random locations to avoid undue delays in construction process. The tests on intermediate lifts were performed in their simplest form with the main objective of getting an assessment of the zone of influence of the device. Samples were taken for moisture content measurements using Ohaus MB45 moisture analyzer. Nuclear moisture- density measurements were also performed as the traditional quality check. The nuclear gauge results demonstrated a very uniform and homogeneous construction with less than a 4% coefficient of variation in the dry density in all the test pits. The nuclear gauge testing also confirmed that the target moisture and densities were achieved.

On the final lift of the subgrade or base layer in each pit, a complete set of stiffness tests were performed using the LWDs and a static plate loading. The maximum load, maximum deflection, load vs. time, and deflection vs. time data were recorded, depending on device capabilities. The external sensors on the Dynatest LWD were used to measure the deflection bowl. The LWD testing included testing at different induced stress levels via changing the drop height to assess the stress dependency of the material.

The LWD results showed that: (1) at the full drop height, the Dynatest LWD (with the intermediate buffer stiffness setting) induced the lowest stresses and the Olson LWD induced the highest stress levels; (2) the Dynatest surface modulus exhibited stress softening for all the evaluated soils while Zorn and Olson demonstrated stress hardening or an increase in modulus with increasing induced stress/drop height; (3) overall, the Dynatest LWD showed the highest spatial variability while the Olson LWD showed the higher variability in the last three drops while tested in one spot.

Static plate load testing was performed concurrent to LWD testing. Results showed a strong correlation between the modulus values measured in the static plate loading test with the values measured by the LWDs with R values of 0.88, 0.99, and 0.97 for Dynatest, Zorn, and Olson LWD, respectively. Overall, LWDs over predicted the modulus relative to the static plate loading value except for the case of the base layer in Pit 3.

It was found that Ohaus MB45 moisture analyzer is sufficiently accurate to replace nuclear gauge determination of moisture content. In addition, the Decagon GS1 volumetric water content sensor was found suitable for spot check testing in fine soils.

Additional material was collected for routine and advanced tests in the laboratory. These tests include grain size distributions, soil classification, moisture-density relations, resilient modulus test at optimum and field conditions, and LWD testing on top of the Proctor compaction mold.

Resilient modulus testing was performed on the material compacted at optimum condition as well as at the field construction condition. Material constitutive models rooted in unsaturated soil mechanics were evaluated on several cohesive and non-cohesive soils to test their suitability for LWD based QA work. The results showed that none of the existing models is accurate enough to be used as the basis for target modulus determination. This led to the new approach of using LWD testing directly on the Proctor compaction mold to find the target field modulus at a given moisture condition.

The LWD testing on mold is an easy add-on to the routine Proctor test. The benefits of the test in spite of its higher variability are significant. The summary of these benefits are as followed.

(1) The test provides valuable insights into the soils response to moisture, density and stresses which can be used to tailor the compaction criteria in field. It was found from the testing that HPC subgrade soil showed an increase in modulus with decrease in moisture up to a point (lower than OMC), after which the modulus declined. The ALF subgrade soil, on the other hand, exhibited a continuous increase in modulus with decreasing moisture content. The VA21a granular base material did not demonstrate a clear trend with changes in moisture.

(2) A strong correlation with laboratory resilient modulus test was found from the results. M_R values at the same stress levels were higher that LWD testing on mold mainly due to the assumptions in Poisson's ratio. However, the correlation was very strong with R values of 0.89, 0.79, and 0.73 for Dynatest, Zorn, and Olson LWD, respectively.

(3) The most important benefit gained from the test is to find the target field modulus at a given moisture and density condition. The LWD on mold moduli were interpolated at the corresponding compaction water content of pits and regarded to as the target LWD modulus. The target modulus was compared to the field achieved surface modulus. The test was capable of detecting the poor compaction of Pit 1 with field moduli much lower than the target modulus and relatively lower modulus ratios ($E_{surface}/E_{LWDonMold}$). There was a strong correlation between the Lab and field test for the three LWD devices on Pit 2 and Pit 3 which had acceptable compaction, except for the initial modulus of base in Pit 2 which had excess water content. After excluding Pit 2 base initial modulus, a high R value of 1, 0.94, and 0.73 was achieved for Dynatest, Zorn, and Olson LWD, respectively. Surface modulus on base of Pit 2 stiffened very fast after several hours after compaction. The results showed the potential benefit of the laboratory LWD test on mold in identifying the field target modulus. Further testing is required to validate this approach.

The last laboratory testing objective of the research was to distinguish the inherent differences in the LWD devices. In order to accomplish this task, LWD testing was performed on a four-point linear elastic steel beam with known stiffness properties. The stiffness from LWD was measured from (1) conventional peak method (k_{peak}), by normalizing the peak force by peak deflection; and (2) through frequency domain spectral analysis to find the static k (k_s). The results showed that the LWDs provide a good estimate of the beam stiffness through peak method and spectral analysis can only slightly improve the results.

The new approach of using LWD testing on mold to find the target LWD modulus in field at a given compaction moisture and density was encouraging, showing a strong correlation between the LWD testing on mold and field moduli at P/Pa of 0.9. Further testing is required to validate this approach. This unique large-scale controlled condition experiment provides an excellent high quality resource of field and comprehensive laboratory data, which can serve the future researchers on route to find a rigorous, theoretically sound and straightforward technique for standardizing the LWD measurements for construction QA of unbound pavement materials.

Finally, FHWA is preserving the pits at Turner-Fairbanks for potential use in future studies. The data collected here and the embedded sensors in the pits will be a valuable complement to these future studies for advancement of the state-of-the-art.

Chapter 6. Appendices

Appendix 1

Pit 1- Construction and testing schedule

Pit I

	Max γd	OMC	Compaction Energy
	[pcf]	[%]	[-]
ALF Subgrade	120	11.5	Standard
VA21a Base	152	4.5	modified
HPC Subgrade	95	24	Standard

Date	7/17/2015	11:00 AM			
Lift number	[-]	0			
Material	[-]	HPC			
Compaction	[-]	0	Coverage of sheeps foor roller compactor	with	vibration
	[-]	0	passes of plate	with	vibration
Nominal lift thickness	[in]				
Compacted lift thickness	[in]				

LWD test Data

Dynatest

Location	h1	h2	h3	h4	Comment
A			Lift0_A		File name: PIT I
B			Lift0_B		on geotextile

Zorn

Location	h1	h2	h3
A	394	395	396
B		397	

Olson

Location	h1	h2	h3- Full height	h4
A			PITI 1	
B			PITI 2	

Date	7/22/2015	1:30 PM			
Lift number	[-]	1			
Material	[-]	ALF			
Compaction	[-]	3	Coverage of sheeps foor roller compactor	with	high vibration
	[-]	0	passes of plate	with	high vibration
Nominal lift thickness	[in]				
Compacted lift thickness	[in]				

LWD test Data

Dynatest

Location	h1	h2	h3	h4	Comment
5	loc 5_lift 1	loc 5_lift 1	loc 5_lift 1	loc 5_lift 1	File name: PIT I
11			loc 11_lift 1		22-Jul
					1:30 PM

right after compaction

Zorn

Location	h1	h2	h3
4	434	435	436

Olson

Location	h1	h2	h3- Full height	h4
6	PITI 4	PITI 5	PITI 6	PITI 7

Nuclear Gauge Readings

Location	Transmission mode	Penetration depth	γd	γt	w	PC	Comments	θ
[-]	[-]	[in]	[pcf]	[pcf]	[%]	[%]	[-]	[%]
5	Direct	4	118.9	133	11.9	99.1%	22-Jul 1:30 PM right after compaction	22.7%
Average			118.9	133.0	11.9	99.1%		22.7%

Date	7/24/2015	8:00 AM			
Lift number	[-]	2			
Material	[-]	ALF			
Compaction	[-]		Coverage of sheeps foor roller compactor	with	high vibration
	[-]	2	passes of plate	with	medium vibration
Nominal lift thickness	[in]				
Compacted lift thickness	[in]				

LWD test Data

Dynatest

Location	h1	h2	h3	h4
C	loc C_lift 2	loc C_lift 2	loc C_lift 2	loc C_lift 2
D	locD_lift 2	locD_lift 2	locD_lift 2	locD_lift 2

Zorn

Location	h1	h2	h3
A	452	453	454
E	455	456	457

Olson

Location	h1	h2	h3- Full height	h4
B	PITI 8	PITI 9	PITI 10	PITI 11
F	PITI 12	PITI 13	PITI 14	PITI 15

Comment

File name: PIT I
24-Jul
8:00 AM
right after compaction

Nuclear Gauge Readings

Location	Transmission mode	Penetration depth	γd	γt	w	PC	Comments	θ
[-]	[-]	[in]	[pcf]	[pcf]	[%]	[%]	[-]	[%]
A	Direct	6	101.2	110.9	9.6	84.3%	24-Jul	15.6%
B	Direct	6	103.6	113	9.1	86.3%	8:00 AM	15.1%
C	Direct	6	100.1	110.8	10.7	83.4%	right after compaction	17.2%
D	Direct	6	110.1	120	8.9	91.8%		15.7%
E	Direct	6	103.1	112.1	8.7	85.9%		14.4%
F	Direct	6	99.2	110.6	11.4	82.7%		18.1%
Average			102.9	112.9	9.7	85.7%		16.0%
Standard Deviation			3.9	3.6	1.1	3.3%		1.4%

Date	7/24/2015	12:45 PM			
Lift number	[-]	3			
Material	[-]	ALF			
Compaction	[-]				
	[-]	2	passes of plate	with	medium vibration
Nominal lift thickness	[in]				
Compacted lift thickness	[in]				

Nuclear Gauge Readings

Location	Transmission mode	Penetration depth	γd	γt	w	PC	Comments	θ
[-]	[-]	[in]	[pcf]	[pcf]	[%]	[%]	[-]	[%]
1	Direct	8	101.8	112.8	10.7	84.8%	24-Jul	17.5%
2	Direct	8	100.7	111.3	10.5	83.9%	ALF	16.9%
3	Direct	8	97.9	108.8	11.1	81.6%	3rd lift	17.4%
4	Direct	8	99.6	109.3	9.7	83.0%	1:00 PM	15.5%
5	Direct	8	98.2	107.5	9.4	81.8%	right after compaction	14.8%
6	Direct	8	98.9	109.4	10.7	82.4%		17.0%
7	Direct	8	99.3	109	9.8	82.8%		15.6%
8	Direct	8	98.3	108.5	10.4	81.9%		16.4%
9	Direct	8	100.5	110	9.4	83.8%		15.1%
Average			99.5	109.6	10.2	82.9%		16.2%
Spatial Sd			1.3	1.6	0.6	1.1%		1.0%

Decagon Moisture sensor

Location	ave RAW	Voltage	Aveθ Alf	Sd θ Alf	Comments
[-]	[-]	[mV]	[%]	[%]	[-]
1	2036		14%	0.7%	24-Jul
2	2048		14%	1.0%	ALF
3	2058		14%	0.4%	3rd lift
4	2051		14%	0.6%	1:40 PM
5	2059		14%	0.4%	1 hr after compaction
6	2070		15%	1.1%	Before LWD testing
7	2092		16%	0.3%	
8	2041		14%	0.8%	
9	2051		14%	0.5%	
Average	2056.3		14.4%	0.7%	
Spatial Sd	16.7		0.6%	0.3%	

Plate load testing

	24-Jul
	ALF
	3rd lift
	2:30 PM
	1.5 hr after compaction
	before LWD testing

LWD test Data

Dynatest

Location	h1	h2	h3	h4
1	loc1_lift 3	loc1_lift 3	loc1_lift 3	loc1_lift 3
5	loc5_lift3	loc5_lift3	loc5_lift3	loc5_lift3
9	loc9_lift 3	loc9_lift 3	loc9_lift 3	loc9_lift 3

Zorn

Location	h1	h2	h3
3	467	468	469
4	470	471	472
8	473	474	475

Comment
Pit 1
7/24/2015
3rd lift
3:00 PM
2 hr after compaction
ALF

Olson				
Location	h1	h2	h3	h4
2	PITI 16	PITI 17	PITI 18	PITI 19
6	PITI 20	PITI 21	PITI 22	PITI 23
7	PITI 24	PITI 25	PITI 26	PITI 27

Decagon Moisture sensor					
Location	ave RAW	Voltage	Aveθ Alf	Sd θ Alf	Comments
[-]	[-]	[mV]	[%]	[%]	[-]
1	2079		15%	1.0%	24-Jul
2	2083		15%	0.3%	ALF
3	2093		16%	1.3%	3rd lift
4	2061		15%	0.8%	4:00 PM
5	2058		14%	0.8%	3 hr after compaction
6	2099		16%	0.7%	After LWD testing
7	2070		15%	1.0%	
8	2106		16%	0.7%	
9	2055		14%	0.8%	
Average	2078.1		15.1%	0.8%	
Spatial Sd	18.6		0.6%	0.3%	

Weather data					
Wind Speed	Air Temperature	Relative Humidity	Soil Surface Temperature	Evaporation Rate	Time/Date/Comment
[km/hr]	[°C]	[%]	[°C]	[kg/m2/hr]	Pit 1
0	27.5	0.495	23.5	0.09	7/24/2015
					3rd lift
					4:00 PM
					3 hr after compaction

Appendix 2

Pit 2- Construction and testing schedule

Pit II

	Max γd	OMC	Compaction Energy
	[pcf]	[%]	[-]
ALF Subgrade	120	11.5	Standard
VA21a Base	152	4.5	modified
HPC Subgrade	95	24	Standard

Date	7/9/2015

Lift number	[-]	1			
Material	[-]	ALF			
Compaction	[-]	2	Coverage of sheeps foor roller compactor	with	vibration
Nominal lift thickness	[in]	6			
Compacted lift thickness	[in]	4.1	average of the following points		
			4	3.125	
			4.125	5	
			3.625	4.625	

Nuclear Gauge Readings

Location	Transmission mode	Penetration depth	γd	γt	w	PC	Comments	θ
[-]	[-]	[in]	[pcf]	[pcf]	[%]	[%]	[-]	[%]
Center	Direct	2	107	122.6	14.5	89.2%	non-flattened surface	24.9%
Center	Direct	2	113.8	130.5	14.7	94.8%	9-Jul	26.8%
SW Corner	Direct	2	115	129.5	12.7	95.8%		23.4%
NW Center	Direct	2	113.9	131.9	15.8	94.9%		28.8%
Average	Direct	2	112.4	128.6	14.4	93.7%		26.0%
Spatial Sd			3.7	4.1	1.3	3.0%		2.4%

Decagon Moisture sensor

Location	RAW	Voltage	θ Alf	Sd θ Alf	Comments
[-]	[-]	[mV]	[%]	[%]	[-]
random			31.0%		These points
random			30.2%		are not from
random			34.3%		the same
random			30.7%		position of
random			25.0%		Nuclear gauge
Average			30.2%		
Spatial Sd			3.3%		

Date	7/9/2015					
Lift number	[-]	2				
Material	[-]	ALF				
Compaction	[-]	2	Coverage of sheeps foor roller compactor	with	vibration	
Nominal lift thickness	[in]	6				
Compacted lift thickness	[in]	4.0				

Nuclear Gauge Readings

Location	Transmission mode	Penetration depth	γd	γt	w	PC	Comments	θ
[-]	[-]	[in]	[pcf]	[pcf]	[%]	[%]	[-]	[%]
SW Center	Direct	3	107	124.5	15.5	89.2%	right after compaction of lift 2	26.6%
NE Center	Direct	3	111.5	128.4	15.1	92.9%	7/9/2015	27.0%
N Center	Direct	3	116.6	134	14.9	97.2%		27.8%
Average	Direct	3	111.7	129.0	15.2	93.1%		27.1%
Spatial Sd			4.8	4.8	0.3	4.0%		0.6%

Decagon Moisture sensor

Location	RAW	Voltage	θ Alf	Sd θ Alf	Comments
[-]	[-]	[mV]	[%]	[%]	[-]
SW Center			26.3%	1.6%	right after first compaction of lift 2
NE Center			28.7%	0.5%	7/9/2015
N Center			27.9%	1.7%	
Average			27.6%	1.2%	
Spatial Sd			1.2%	0.7%	

Date	7/10/2015					
Lift number	[-]	2				
Material	[-]	ALF				

Weather data

Wind Speed	Air Temperature	Relative Humidity	Soil Surface Temperature	Evaporation Rate	Time/Date/Comment
[km/hr]	[°C]	[%]	[°C]	[kg/m2/hr]	7/10/2015
1.5-3	22.8-23.6	71.9-69.2	21.8-22.3	0.1-0.06	7:20 AM
					One day after initial compaction of lift 2

Decagon Moisture sensor

Location	RAW	Voltage	θ Alf	Sd θ Alf	Comments
[-]	[-]	[mV]	[%]	[%]	[-]
SW Center			25.6%	1.9%	The day after initial compaction of lift 2
NE Center			28.6%	2.1%	7/10/2015
N Center			27.7%	0.9%	7:20 AM
Average			27.3%	1.6%	
Spatial Sd			1.5%	0.6%	

Date	7/10/2015					
Lift number	[-]	2				
Material	[-]	ALF				
Compaction	[-]	+2	additional Coverage of sheeps foor roller compactor	with	vibration	
	[-]	+1	plate roller	with	vibration	
Nominal lift thickness	[in]	6				
Compacted lift thickness	[in]	4.0				

Nuclear Gauge Readings

Location	Transmission mode	Penetration depth	γd	γt	w	PC	Comments	θ
[-]	[-]	[in]	[pcf]	[pcf]	[%]	[%]	[-]	[%]
W	Direct	3	110.7	129.3	16.8	92.3%		29.8%
NE	Direct	3	115.3	133.4	15.7	96.1%	right after second set compaction of lift 3	29.0%
SE	Direct	3	112.9	132	16.9	94.1%		30.6%
							7/10/2015	
Average	Direct	3	113.0	131.6	16.5	94.1%		29.8%
Spatial Sd			2.3	2.1	0.7	1.9%		0.8%

Decagon Moisture sensor

Location	RAW	Voltage	θ Alf	Sd θ Alf	Comments
[-]	[-]	[mV]	[%]	[%]	[-]
W			27.6%	1.9%	right after second set compaction of lift 2
NE			26.7%	1.9%	
SE			25.3%	1.3%	
					7/10/2015
Average			26.5%	1.7%	
Spatial Sd			1.1%	0.3%	

Date	7/10/2015					
Lift number	[-]	3				
Material	[-]	ALF				
Compaction	[-]	4(2x2)	Coverage of sheeps foor roller compactor	with	vibration	
	[-]	1	plate roller	with	vibration	
Nominal lift thickness	[in]	6				
Compacted lift thickness	[in]	4.0				

Nuclear Gauge Readings

Location	Transmission mode	Penetration depth	γd	γt	w	PC	Comments	θ
[-]	[-]	[in]	[pcf]	[pcf]	[%]	[%]	[-]	[%]
SW	Direct	4	114.9	133.1	15.8	95.8%		29.1%
SW	Direct	8	114.9	133.5	16.2	95.8%		29.8%
Center E	Direct	4	116.5	134.8	15.7	97.1%	right after compaction of lift 3	29.3%
SE	Direct	4	111.1	129.6	16.7	92.6%		29.7%
Center	Direct	4	115.7	134.3	16.1	96.4%		29.9%
Average	Direct	4	114.6	133.1	16.1	95.5%		29.6%
Spatial Sd			2.1	2.0	0.4	1.7%		0.3%

Decagon Moisture sensor

Location	RAW	Voltage	θ Alf	Sd θ Alf		Comments
[-]	[-]	[mV]	[%]	[%]		[-]
SW			27.3%	1.3%	right after compaction of lift 3	
SW			27.3%	1.3%		
Center E			27.3%	2.1%		
SE			28.0%	1.4%	7/10/2015	
Center			27.3%	3.4%		
Average			27.4%	1.9%		
Spatial Sd			0.3%	0.9%		

Weather data

Wind Speed	Air Temperature	Relative Humidity	Soil Surface Temperature	Evaporation Rate	Time/Date/Comment
[km/hr]	[°C]	[%]	[°C]	[kg/m2/hr]	7/10/2015
0	28+/-0.3	60+/-0.5	25.6-25.8	0.08	3rd lift/pit 2

Date	7/10/2015				
Lift number	[-]	4			
Material	[-]	ALF			
Compaction	[-]	4(2x2)	Coverage of sheeps foor roller compactor	with	vibration
	[-]	0	plate roller	with	vibration
Nominal lift thickness	[in]	6			
Compacted lift thickness	[in]	4.0			

Nuclear Gauge Readings

Location	Transmission mode	Penetration depth	γd	γt	w	PC	Comments	θ
[-]	[-]	[in]	[pcf]	[pcf]	[%]	[%]	[-]	[%]
A center	Direct	4	117	134.1	14.6	97.5%		27.4%
B N	Direct	4	119.2	136.4	14.4	99.3%	right after compaction of lift 4	27.5%
C E	Direct	4	114.2	131.2	14.9	95.2%		27.3%
D S	Direct	4	117.7	135.9	15.5	98.1%	7/10/2015	29.2%
Average			117.0	134.4	14.9	97.5%		27.8%
Spatial Sd			2.1	2.4	0.5	1.7%		0.9%

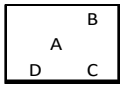

Decagon Moisture sensor

Location	RAW	Voltage	θ Alf	Sd θ Alf		Comments
[-]	[-]	[mV]	[%]	[%]		[-]
A center			25.5%	2.1%	right after compaction of lift 4	
B N			25.1%	1.1%		
C E			26.5%	1.1%		
D S			25.6%	1.3%	7/10/2015	
Average			25.7%	1.4%		
Spatial Sd			0.6%	0.5%		

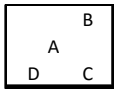

Weather data					
Wind Speed	Air Temperature	Relative Humidity	Soil Surface Temperature	Evaporation Rate	Time/Date/Comment
[km/hr]	[°C]	[%]	[°C]	[kg/m2/hr]	7/10/2015
0	27.9-28.1	58.6-59.3	26.6	0.09	4:00 PM
					4th lift/ pit 2

Date	7/13/2015	
Lift number	[-]	4
Material	[-]	ALF

Weather data					
Wind Speed	Air Temperature	Relative Humidity	Soil Surface Temperature	Evaporation Rate	Time/Date/Comment
[km/hr]	[°C]	[%]	[°C]	[kg/m2/hr]	7/13/2015
0	22.1	82.2	22.3	0.04	7:30 AM
					4th lift/ pit 2/ after 3days 60 hr after compaction
					Rain over weekend

Decagon Moisture sensor					
Location	RAW	Voltage	θ Alf	Sd θ Alf	Comments
[-]	[-]	[mV]	[%]	[%]	[-]
A center			22.0%		3days after compaction of lift 4
B N	B		24.6%	1.7%	
C E	A		24.6%	2.3%	7/13/2015
D S	D C				
Average			23.7%	2.0%	
Spatial Sd			1.5%	0.4%	

Date	7/13/2015				
Lift number	[-]	5			
Material	[-]	ALF			
Compaction	[-]	4(2x2)	Coverage of sheeps foor roller compactor	with	vibration
	[-]	0	plate roller	with	vibration
Nominal lift thickness	[in]	6			
Compacted lift thickness	[in]	4.0			

Nuclear Gauge Readings									
Location		Transmission mode	Penetration depth	γd	γt	w	PC	Comments	θ
[-]		[-]	[in]	[pcf]	[pcf]	[%]	[%]	[-]	[%]
A	A C	Direct	4	119.7	136	13.7	99.8%		26.3%
B		Direct	4	116.1	131.6	13.3	96.8%	right after compaction of lift 5	24.7%
C		Direct	4	116.4	132.8	14	97.0%		26.1%
D	B D	Direct	4	117.2	133.3	13.8	97.7%	7/13/2015	25.9%
Average				117.4	133.4	13.7	97.8%		25.8%
Spatial Sd				1.6	1.9	0.3	1.4%		0.7%

Decagon Moisture sensor						
Location	RAW	Voltage	θ Alf	Sd θ Alf		Comments
[-]	[-]	[mV]	[%]	[%]		[-]
A			25.3%	1.6%	right after compaction of lift 5	
B			23.8%	1.5%		
C			21.6%	2.3%		
D			25.3%	0.8%	7/13/2015	
Average			23.6%	1.5%		
Spatial Sd			1.7%	0.6%		

Weather data					
Wind Speed	Air Temperature	Relative Humidity	Soil Surface Temperature	Evaporation Rate	Time/Date/Comment
[km/hr]	[°C]	[%]	[°C]	[kg/m2/hr]	7/13/2015
0	22.9	89.7	23.4	0.02	5th lift/ pit 2

LWD test Data					
Dynatest					
	h1	h2	h3	h4	Comment
A	-	-	-	-	Lost connection
B	-	-	-	-	
C	-	-	-	-	
Zorn					
	h1	h2	h3	h4	
A	-	-	-		
B	319	320	321		
C	322	323	324		
D	316	317	318		
Olson					
Drop Height	h1	h2	h3	h4	
A	Pitii 1	-	Pitii 2	Pitii 3	
B	Pitii 4	Pitii 6	Pitii 5	Pitii 7	
C	Pitii 8	Pitii 9	-	Pitii 10	
D	-	-	-	-	

Date	7/13/2015	2:00 PM			
Lift number	[-]	6			
Material	[-]	ALF			
Compaction	[-]	4(2x2)	Coverage of sheeps foor roller compactor	with	vibration
	[-]	1	plate roller	with	vibration
Nominal lift thickness	[in]	6			
Compacted lift thickness	[in]	4.0			

Nuclear Gauge Readings								
Location	Transmission mode	Penetration depth	γd	γt	w	PC	Comments	θ
[-]	[-]	[in]	[pcf]	[pcf]	[%]	[%]	[-]	[%]
1	Direct	4	114.1	130.3	14.2	95.1%		26.0%
2	Direct	4	115.3	133.7	15.9	96.1%	right after compaction of lift 6	29.4%
3	Direct	4	114.5	132.5	15.8	95.4%		29.0%
4	Direct	4	113.4	131.6	16	94.5%	7/13/2015	29.1%
5	Direct	4	118	135.4	14.8	98.3%		28.0%
6	Direct	4	110.6	128.2	15.9	92.2%		28.2%
7	Direct	4	116.5	113.7	14.8	97.1%		27.6%
8	Direct	4	116	133	14.7	96.7%		27.3%
9	Direct	4	113.2	130.5	15.3	94.3%		27.8%
10	Direct	4	112.6	131.9	16.4	93.8%		29.6%
11	-	-	-	-	-		-	-
12	Direct	4	115.8	133.7	15.4	96.5%		28.6%
Average			114.5	130.4	15.4	95.5%		28.2%
Spatial Sd			2.1	5.9	0.7	1.7%		1.1%

Decagon Moisture sensor					
Location	RAW	Voltage	θ Alf	Sd θ Alf	Comments
[-]	[-]	[mV]	[%]	[%]	[-]
1			25.6%	1.3%	right after compaction of lift 6
2			27.1%	1.1%	
3			27.1%	1.5%	
4		1669.0	21.7%	6.1%	7/13/2015
5		1759.3	25.8%	2.7%	
6		1756.3	25.7%	5.3%	
7		1784.5	26.9%	6.7%	
8		1790.8	27.2%	2.3%	
9		1783.5	26.9%	2.4%	
10					
11					
12		1766.0	26.1%	3.1%	
Average			26.0%	3.3%	
Spatial Sd			1.6%	2.0%	

Thickness			
Location	**Elevation from top**	**Total Thickness=49.5-elv**	**Average sublayer thickness**
1	25.5	24.0	4.0
2	26.5	23.0	3.8
3	26.875	22.6	3.8
4	26.75	22.8	3.8
5	26	23.5	3.9
6	26	23.5	3.9
7	25.75	23.8	4.0
8	25.375	24.1	4.0
9	25.25	24.3	4.0
10	26.625	22.9	3.8
11	25	24.5	4.1
12	25.5	24.0	4.0
13	24.875	24.6	4.1
Average	25.8	23.7	3.94
Spatial Sd	0.67	0.67	0.11

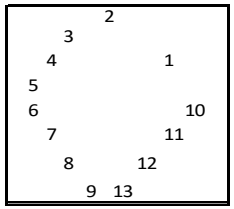

Weather data					
Wind Speed	Air Temperature	Relative Humidity	Soil Surface Temperature	Evaporation Rate	Time/Date/Comment
[km/hr]	[°C]	[%]	[°C]	[kg/m2/hr]	7/13/2015
0-2.6	26	73.3	24-24.4	0.07-0.1	5:22 PM
					6th lift/ pit 2

LWD test Data					
Dynatest					**Comment**
	h1	h2	h3	h4	
1	1 (1-6)	1 (7-12)	1 (13-18)	1 (19-24)	File name: PIT II
5	5 (1-6)	5 (7-12)	5 (13-18)	5 (19-24)	7/13/2015
9	9 (1-6)	9 (7-12)	9 (13-18)	9 (19-24)	4:00 PM
Zorn					**1.5 hr after compaction**
	h1	h2	h3		
3	325	326	327		
4	328	329	330		
8	331	332	333		
Olson					
Drop Height	h1	h2	h4		
2	Pitii 11	Pitii 12	Pitii 13		
6	Pitii 14	Pitii 15	Pitii 16		
7	Pitii 17	Pitii 18	Pitii 19		

Date	7/14/2015	
Lift number	[-]	6

LWD test Data					
Dynatest					**Comment**
Location	h1	h2	h3	h4	File name: PIT II
1	1-16h (1-6)	1-16h (7-12)	1-16h (13-18)	1-16h (19-24)	7/14/2015
5	5-16h (1-6)	5-16h (7-12)	5-16h (13-18)	5-16h (19-24)	16 hr after compaction
9	9-16h (1-6)	9-16h(7-12)	9-16h (13-18)	9 -16h(19-24)	7:30 AM
Zorn					
Location	h1	h2	h3		
3	334	335	336		
4	337	338	339		
8	340	341	342		
Olson					
Location	h1	h2	h4		
2	Pitii 20	Pitii 21	Pitii 22		
6	Pitii 23	Pitii 24	Pitii 25		
7	Pitii 26	Pitii 27	Pitii 28		

Decagon Moisture sensor						
Location	RAW	Voltage	θ Alf	Sd θ Alf		Comments
[-]	[-]	[mV]	[%]	[%]		[-]
1		1720.5	24.0%	6.2%	16 hr after compaction of lift 6	
2		1819.0	28.5%	1.4%		
3		1775.0	26.5%	1.6%		
4		1772.3	26.4%	3.3%	7/14/2015	
5		1804.7	27.9%	1.6%		
6		1779.7	26.7%	3.8%		
7		1751.7	25.5%	7.2%		
8		1774.3	26.5%	5.9%		
9 (before LWD)		1749.3	25.4%	5.9%		
12		1764.7	26.1%	3.0%		
9 (after LWD)		1771.8	26.4%	3.1%		
Average			26.3%	3.9%		
Spatial Sd			1.2%	2.1%		

Weather data						
Wind Speed	Air Temperature	Relative Humidity	Soil Surface Temperature	Evaporation Rate		Time/Date/Comment
[km/hr]	[°C]	[%]	[°C]	[kg/m2/hr]		7/14/2015
0	24.6	82.6	22.9	0.01		7:30 AM
						6th lift/ pit 2
						16 hr after compaction

Effect of LWD testing on VMC								
Location	h1	h2	h3	VMC before Zorn	+/- Sd	VMC after Zorn	+/- Sd	
A	343	344	345	24.0%	0.00%	22.2%	0.00%	21 hr
B	346	347	348	23.1%	0.00%	23.5%	0.00%	after
C	349	350	351	22.3%	0.00%	22.9%	0.00%	compacti
Not statistically different	21 hr after compaction							

Decagon Moisture sensor						
Location	RAW	Voltage	θ Alf	Sd θ Alf		Comments
[-]	[-]	[mV]	[%]	[%]		[-]
A- Before Zorn		1718.7	24.0%	1.5%	16 hr after compaction of lift 6	
B- Before Zorn		1699.8	23.1%	0.6%		
C- Before Zorn		1681.3	22.3%	2.2%		
A- After Zorn		1680.3	22.2%	3.1%	7/14/2015	
B- After Zorn		1707.4	23.5%	1.3%		
C- After Zorn		1694.4	22.9%	1.5%		
Average			23.0%	1.7%		
Spatial Sd			0.7%	0.8%		

Date	7/14/2015					
Lift number	[-]	7				
Material	[-]	VA21a				
Compaction	[-]	4(2x2)	Coverage of sheeps foor roller compactor	with	vibration	
	[-]	0	plate roller	with	vibration	
Nominal lift thickness	[in]	6				
Compacted lift thickness	[in]	4.0				

Nuclear Gauge Readings

Location	Transmission mode	Penetration depth	γd	γt	w	PC	Comments	θ
[-]	[-]	[in]	[pcf]	[pcf]	[%]	[%]	[-]	[%]
A	Direct	4	133.2	140.4	5.4	87.6%	right after compaction of lift 7 w/ 4 passes of sheep foot	11.5%
B	Direct	4	137	143.3	4.6	90.1%		10.1%
Average			135.1	141.9	5.0	88.9%		10.8%
Spatial Sd			2.7	2.1	0.6	1.8%		1.0%

Date	7/14/2015					
Lift number	[-]	7				
Material	[-]	VA21a				
Compaction	[-]	0	Coverage of sheeps foor roller compactor	with	vibration	
	[-]	4	plate roller	with	vibration	
Nominal lift thickness	[in]	6				
Compacted lift thickness	[in]	4.0				

Nuclear Gauge Readings

Location	Transmission mode	Penetration depth	γd	γt	w	PC	Comments	θ
[-]	[-]	[in]	[pcf]	[pcf]	[%]	[%]	[-]	[%]
A	Direct	4	140.3	147.9	5.4	92.3%	right after compaction of lift 7 w/ additional 4 passes of plate compactor	12.1%
B	Direct	4	145.6	152.1	4.4	95.8%		10.3%
Average			143.0	150.0	4.9	94.0%		11.2%
Spatial Sd			3.7	3.0	0.7	2.5%		1.3%

Date	7/14/2015					
Lift number	[-]	7				
Material	[-]	VA21a				
Compaction	[-]	0	Coverage of sheeps foor roller compactor	with	vibration	
	[-]	+2	after two additional passes of plate and spraying water	with	vibration	
Nominal lift thickness	[in]	6				
Compacted lift thickness	[in]	4.0				

Nuclear Gauge Readings

Location	Transmission mode	Penetration depth	γd	γt	w	PC	Comments	θ
[-]	[-]	[in]	[pcf]	[pcf]	[%]	[%]	[-]	[%]
A	Direct	4	144.2	152.2	5.2	94.9%	after two additional passes of plate and spraying water	12.0%
B	Direct	4	146	153.5	5.2	96.1%		12.2%
Average			145.1	152.9	5.2	95.5%		12.1%
Spatial Sd			1.3	0.9	0.0	0.8%		0.1%

Nuclear Gauge Readings

Location	Transmission mode	Penetration depth	γd	γt	w	PC	Comments	θ
[-]	[-]	[in]	[pcf]	[pcf]	[%]	[%]	[-]	[%]
A	Direct	4	144.1	152.2	5.6	94.8%	After additional 4 passes of plate compactor	12.9%
Average			144.1	152.2	5.6	94.8%		12.9%

Nuclear Gauge Readings

Location	Transmission mode	Penetration depth	γd	γt	w	PC	Comments	θ
[-]	[-]	[in]	[pcf]	[pcf]	[%]	[%]	[-]	[%]
A	Direct	4	147.1	156	6.1	96.8%		14.4%
B	Direct	4	148.4	155.7	4.9	97.6%		11.7%
C	Direct	4	145.4	152.4	4.8	95.7%	after additional 4 passes of plate compactor	11.2%
D	Direct	4	145.5	153.2	5.3	95.7%		12.4%
E	Direct	4	133.5	145	8.6	87.8%		18.4%
Average			144.0	152.5	5.9	94.7%		13.6%
Spatial Sd			6.0	4.5	1.6	3.9%		2.9%

Date	7/15/2015	
Lift number	[-]	7

LWD test Data

Dynatest

Location	h1	h2	h3	h4
A	VA21A_sub1_A (1-6)	VA21A_sub1_A(7-12)	VA21A_sub1_A (13-18)	VA21A_sub1_A (19-24)
B	VA21A_sub1_B (1-6)	VA21A_sub1_B (7-12)	VA21A_sub1_B (13-18)	VA21A_sub1_B (19-24)

Zorn

Location	h1	h2	h3
B	354	355	356
C	357	358	359

Olson

Location	h1	h2	h4
A	Pitii 29	Pitii 30	Pitii 31
B	Pitii 32	Pitii 33	Pitii 34

Comment

File name: PIT II

7/15/2015

16 hr after compaction of 1st lift of Base

7:16:00 AM- 7:45:00 AM

Random locations

Decagon Moisture sensor

Location	RAW	Voltage	θ Alf	Sd θ Alf	Comments
[-]	[-]	[mV]	[%]	[%]	[-]
A	1946		14%		16 hr after compaction of lift 7
B	1910		13%		VA21a material- lift 1
C	1933		14%		7/15/2015
D	1912		13%		7:45 AM
Average	1925.3		13.6%		
Spatial Sd	17.30847577		0.2%		

Weather data

Wind Speed	Air Temperature	Relative Humidity	Soil Surface Temperature	Evaporation Rate	Time/Date/Comment	
[km/hr]	[°C]	[%]	[°C]	[kg/m2/hr]	7/15/2015	7:45 AM
0	23.6	77.5-79	21.9	0.03	7th lift/ pit 2 16 hr after compaction	

Date	7/15/2015	11:00 AM			
Lift number	[-]	8			
Material	[-]	VA21a			
Compaction	[-]	4	Coverage of sheeps foor roller compactor	with	vibration
	[-]	3	passes of plate	with	vibration
Nominal lift thickness	[in]	6			
Compacted lift thickness	[in]	4.0			

Nuclear Gauge Readings

Location	Transmission mode	Penetration depth	γd	γt	w	PC	Comments		θ
[-]	[-]	[in]	[pcf]	[pcf]	[%]	[%]	[-]		[%]
1	Direct	4	149.7	156.3	4.4	98.5%	right after compaction of 8th lift		10.6%
2	Direct	4	149.1	155.8	4.5	98.1%	2nd sublayer of Base		10.8%
3	Direct	4	150.6	157.8	4.8	99.1%		15-Jul	11.6%
4	Direct	4	150.6	158	5	99.1%		11:00 AM	12.1%
5	Direct	4	151.3	158.4	4.7	99.5%	till		11.4%
6	Direct	4	152.1	159.3	4.8	100.1%		11:50 AM	11.7%
7	Direct	4	144.6	151.5	4.8	95.1%			11.1%
7'	Direct	4	146.7	154.3	5.1	96.5%			12.0%
8	Direct	4	147.6	154.6	4.7	97.1%			11.1%
9	Direct	4	148.9	155.4	4.4	98.0%			10.5%
A	Direct	4	149.2	155.7	4.4	98.2%			10.5%
Average			149.1	156.1	4.7	98.1%			11.2%
Spatial Sd			2.2	2.2	0.2	1.4%			0.6%

Decagon Moisture sensor

Location	RAW	Voltage	θ Alf	Sd θ Alf	Comments
[-]	[-]	[mV]	[%]	[%]	[-]
1	1865		13%	0.2%	50 min after compaction of 8th lift
2	1842		12%	0.3%	2nd sublayer of Base
3	1857		13%	0.4%	7/15/2015
4	1858		13%	0.4%	11:50 AM
5					At Nuk locations
					It was not easy to make the holes
					test terminated
Average	1855.5		12.6%	0.3%	
Spatial Sd	9.6		0.1%	0.1%	

LWD test Data

	Dynatest				
Location	h1	h2	h3	h4	**Comment**
					File name: PIT II
1	VA21A-sub2-1 (1-6)	VA21A-sub2-1(7-12)	VA21A-sub2-1 (13-18)	VA21A-sub2-1(19-24)	7/15/2015
5	VA21A-sub2-5 (1-6)	VA21A-sub2-5 (7-12)	VA21A-sub2-5(13-18)	VA21A-sub2-5(19-24)	1 hr after compaction of 2nd lift of Base
9	VA21A-sub2-9 (1-6)	VA21A-sub2-9(7-12)	VA21A-sub2-9(13-18)	VA21A-sub2-9(19-24)	12:15 PM

Zorn			
Location	h1	h2	h3
3	360	361	362
4	363	364	365
8	366	367	368

Olson			
Location	h1	h2	h4
2	Pitii 35	Pitii 36	Pitii 37
6	Pitii 38	Pitii 39	Pitii 40
7	Pitii 41	Pitii 42	Pitii 43

Weather data

Wind Speed	Air Temperature	Relative Humidity	Soil Surface Temperature	Evaporation Rate	Time/Date/Comment
[km/hr]	[°C]	[%]	[°C]	[kg/m2/hr]	7/15/2015
0	26.4	74%	23.2-23.8	0.03	12:45 PM
					8th lift/ pit 2
					2 hr after compaction

LWD test Data

Dynatest					Comment
Location	h1	h2	h3	h4	File name: PIT II
1	VA21A-sub2-3h-1 (1-6)	VA21A-sub2-3h-1(7-12)	VA21A-sub2-3h-1 (13-18)	VA21A-sub2-3h-1(19-24)	7/15/2015
5	VA21A-sub2-3h-5 (1-6)	VA21A-sub2-3h-5 (7-12)	VA21A-sub2-3h-5(13-18)	VA21A-sub2-3h-5(19-24)	~4 hr after compaction of 2nd lift of Base
9	VA21A-sub2-3h-9 (1-6)	VA21A-sub2-3h-9(7-12)	VA21A-sub2-3h-9(13-18)	VA21A-sub2-3h-9(19-24)	2:40 PM

Zorn			
Location	h1	h2	h3
3	369	370	371
4	372	373	374
8	375	376	377

Olson			
Location	h1	h2	h4
2	Pitii 44	Pitii 45	Pitii 46
6	Pitii 47	Pitii 48	Pitii 49
7	Pitii 50	Pitii 51	Pitii 52

Weather data

Wind Speed	Air Temperature	Relative Humidity	Soil Surface Temperature	Evaporation Rate	Time/Date/Comment
[km/hr]	[°C]	[%]	[°C]	[kg/m2/hr]	7/15/2015
1.3-->2.1-->0	27.7	66-68%	24.6	0.04-0.07	3:30 PM
					8th lift/ pit 2
					4.5 hr after compaction

Plate load testing

7/15/2015

Date	7/15/2015	
Lift number	[-]	8
Final thickness	31.2	

Thickness measurements on LWD and Sensor Locations			
Location	**Elevation from top**	**Total Thickness**	**Average Base layer thickness**
1	18.125	31.375	8.175
2	18.25	31.25	8.05
3	19.125	30.375	7.175
4	18.25	31.25	8.05
5	18.5	31	7.8
6	19	30.5	7.3
7	18.125	31.375	8.175
8	18.375	31.125	7.925
9	18.25	31.25	8.05
10	17.75	31.75	8.55
11	17.75	31.75	8.55
12	17.75	31.75	8.55
Average	18.3	31.2	8.0
Spatial Sd	0.45	0.45	0.45

LWD test Data					
Dynatest					**Comment**
Location	h1	h2	h3	h4	File name: PIT II
1					7/20/2015
5					5 days after compaction of 2nd lift of Base
9					1:00 PM
Zorn					
Location	h1	h2	h3		
3		402			
4					
8					
Olson					
Location	h1	h2	h3	h4	
2					
6			Pitii 56		
7					

LWD test Data					
Dynatest					**Comment**
Location	h1	h2	h3	h4	File name: PIT II
1		VA21A-sub2-9days-1			7/24/2015
5		VA21A-sub2-9days-5			9 days after compaction of 2nd lift of Base
9		VA21A-sub2-9days-9			8:30 AM
Zorn					
Location	h1	h2	h3		
3	458	459	460		
4	461	462	463		
8	464	465	466		
Olson					
Location	h1	h2	h3	h4	
2	Pitii 57	Pitii 58	Pitii 59	Pitii 60	
6	Pitii 61	Pitii 62	Pitii 63	Pitii 64	
7	Pitii 65	Pitii 66	Pitii 67	Pitii 68	

Appendix 3

Pit 3- Construction and testing schedule

Pit III

	Max γd	OMC	Compaction Energy
	[pcf]	[%]	[-]
ALF Subgrade	120	11.5	Standard
VA21a Base	152	4.5	modified
HPC Subgrade	95	24	Standard

Date	7/17/2015	11:00 AM			
Lift number	[-]	1			
Material	[-]	HPC			
Compaction	[-]	4	Coverage of sheeps foor roller compactor	with	vibration
	[-]	0	passes of plate	with	vibration
Nominal lift thickness	[in]	6			
Compacted lift thickness	[in]	5.6	*calucalation in "Elevations" sheet		

LWD test Data

Dynatest					**Comment**
Location	h1	h2	h3	h4	File name: PIT III
5	VA21A-sub2-5 (1-6)	VA21A-sub2-5 (7-12)	VA21A-sub2-5(13-18)	VA21A-sub2-5(19-24)	right after compaction
Zorn					1st lift
Location	h1	h2	h3		HPC
4	388	389	390		7/17/2015
Olson					
Location	h1	h2	h4		
6	pIII 1	pIII 2	pIII 3		
7	pIII 4	pIII 5	pIII 6		

Nuclear Gauge Readings

Location	Transmission mode	Penetration depth	γd	γt	w	PC	Comments	θ
[-]	[-]	[in]	[pcf]	[pcf]	[%]	[%]	[-]	[%]
4	Direct	4	86.4	114.5	32.5	90.9%	File name: PIT III	45.0%
5	Direct	4	88.1	112.3	27.5	92.7%	2 hrs after compaction	38.8%
6	Direct	4	86.4	114	32	90.9%	1st lift	44.3%
A	Direct	4	85.9	114.3	33	90.4%	HPC	45.4%
B	Direct	4	92.9	118.7	27.8	97.8%	1:23 PM	41.4%
							7/17/2015	
Average	Direct	4	87.9	114.8	30.6	92.6%		43.0%
Spatial Sd			2.9	2.4	2.7	3.0%		2.8%

Decagon Moisture sensor						
Location	RAW	Voltage	θ Alf	Sd θ Alf		Comments
[-]	[-]	[mV]	[%]	[%]		[-]
1						
2					2 hrs after compaction	
3					1st lift	
4	2843		36%	1.3%	HPC	
5	2924		38%	1.1%	1:23 PM	
6	2863		36%	2.3%	7/17/2015	
7	2892		37%	0.1%		
8	2784		34%	1.2%		
9	2915		38%	0.4%		
Average	2870		36.6%	1.1%		
Spatial Sd	52.0		1.3%	0.8%		

Weather data						
Wind Speed	Air Temperature	Relative Humidity	Soil Surface Temperature	Evaporation Rate		Time/Date/Comment
[km/hr]	[°C]	[%]	[°C]	[kg/m2/hr]		7/17/2015
0-3.4	24.6	69-70%	22.4	0.04-0.11		2 hrs after compaction
						1st lift
						HPC
						1:23 PM
Date	7/17/2015					
Lift number	[-]	2				
Material	[-]	HPC				
Compaction	[-]	4	Coverage of sheeps foor roller compactor	with	vibration	
	[-]	0	passes of plate	with	vibration	
Nominal lift thickness	[in]	6				
Compacted lift thickness	[in]	3.1	*calucalation in "Elevations" sheet			

LWD test Data				
	Zorn			Comment
Location	h1	h2- Full height	h3	File name: PIT III
random A		398		right after compaction
Random B		399		17-Jul
				4:00 PM

Nuclear Gauge Readings								
Location	Transmission mode	Penetration depth	γd		γt	w	PC	Comments	θ
[-]	[-]	[in]	[pcf]		[pcf]	[%]	[%]	[-]	[%]
A	Direct	4	87.1		116.1	33.3	91.7%	File name: PIT III	46.5%
B	Direct	4	94.8		121.6	28.3	99.8%	65 hrs after compaction	43.0%
C	Direct	4	96.3		121.7	26.4	101.4%	2st lift	40.7%
								20-Jul	
Average	Direct	4	92.7		119.8	29.3	98%		43%
Spatial Sd			4.9		3.2	3.6	5.2%		2.9%

LWD test Data						
Dynatest						**Comment**
Location	h1	h2	h3	h4		File name: PIT III
D			LocD_lift2			
E			LocE_lift2			65 hrs after compaction
Zorn						2st lift
Location	h1	h2	h3			20-Jul
D		400				
E		401				
Olson						
Location	h1	h2	h4			
D		pIII 7				
E		PIII 8				
F		PitI3				******PitI3 renamed to pIII0

Date	7/20/2015				
Lift number	[-]	3			
Material	[-]	HPC			
Compaction	[-]	6	Coverage of sheeps foor roller compactor	with	vibration
	[-]	0	passes of plate	with	vibration
Nominal lift thickness	[in]	6			
Compacted lift thickness	[in]	3.9			

No tests performed on the third lift

Date	7/20/2015				
Lift number	[-]	4			
Material	[-]	HPC			
Compaction	[-]	6	Coverage of sheeps foor roller compactor	with	vibration
	[-]	0	passes of plate	with	vibration
Nominal lift thickness	[in]	6			
Compacted lift thickness	[in]	3.9			

Decagon Moisture sensor						
Location	RAW	Voltage	θ Alf	Sd θ Alf		Comments
[-]	[-]	[mV]	[%]	[%]		[-]
A	2901		37%	1.4%	right fter compaction	
B	2833		36%	1.5%	4th lift	
C	2911		38%	1.5%	HPC	
					3:00 PM	
					7/20/2015	
Average	2881.6		36.9%	1.5%		
Spatial Sd	42.7		1.0%	0.1%		

Weather data						
Wind Speed	Air Temperature	Relative Humidity	Soil Surface Temperature	Evaporation Rate	Time/Date/Comment	
[km/hr]	[°C]	[%]	[°C]	[kg/m2/hr]	right fter compaction	
0	30.4	68%	29	0.09	3:00 PM	4th lift
					7/20/2015	HPC

LWD test Data					
Dynatest					**Comment**
Location	h1	h2	h3	h4	File name: PIT III
A			LocA_lift4		
B			LocB_lift4		right fter compaction
C			LocC_lift4		2nd lift
Zorn					HPC
Location	h1	h2	h3		3:00 PM
A		403			7/20/2015
B		404			
C		405			
Olson					
Location	h1	h2	h4		
A		PIII 9			
B		PIII 10			
C		PIII 11			

Nuclear Gauge Readings								
Location	Transmission mode	Penetration depth	γd	γt	w	PC	Comments	θ
[-]	[-]	[in]	[pcf]	[pcf]	[%]	[%]	[-]	[%]
A	Direct	4	94.5	117.9	24.7	99.5%	17 hrs after compaction	37.4%
B	Direct	4	86.5	114.1	31.9	91.1%	4th lift	44.2%
C	Direct	4	90.7	118.4	30.4	95.5%	21-Jul	44.2%
							9:00 AM	
Average	Direct	4	90.6	116.8	29.0	95%		42%
Spatial Sd			4.0	2.4	3.8	4.2%		3.9%

Nuclear Gauge Readings								
Location	Transmission mode	Penetration depth	γd	γt	w	PC	Comments	θ
[-]	[-]	[in]	[pcf]	[pcf]	[%]	[%]	[-]	[%]
A	Direct	8	92.7	116.2	25.3	97.6%	17 hrs after compaction	37.6%
B	Direct	8	92.0	118.9	29.3	96.8%	4th lift	43.2%
C	Direct	8	95.7	122	27.4	100.7%	21-Jul	42.0%
							9:15 AM	
Average	Direct	8	93.5	119.0	27.3	98%		41%
Spatial Sd			2.0	2.9	2.0	2.1%		3.0%

Date	7/21/2015	10:30 AM			
Lift number	[-]	5			
Material	[-]	HPC			
Compaction	[-]	6	Coverage of sheeps foor roller compactor	with	vibration
	[-]	0	passes of plate	with	vibration
Nominal lift thickness	[in]	6			
Compacted lift thickness	[in]	3.9			

Nuclear Gauge Readings								
Location	Transmission mode	Penetration depth	γd	γt	w	PC	Comments	θ
[-]	[-]	[in]	[pcf]	[pcf]	[%]	[%]	[-]	[%]
1	Direct	4	90.2	115.8	28.4	94.9%	right after compaction	41.1%
2	Direct	4	92.9	119.5	28.7	97.8%	5th lift	42.7%
3	Direct	4	80.5	106.5	32.3	84.7%	21-Jul	41.7%
4	Direct	4	88	113.6	29.1	92.6%	11:00 AM	41.0%
5	Direct	4	87.5	113.8	30.1	92.1%		42.2%
6	Direct	4	91.3	117.5	28.8	96.1%		42.1%
7	Direct	4	90	117.7	30.8	94.7%		44.4%
8	Direct	4	89.4	118.4	32.4	94.1%		46.4%
9	Direct	4	87.6	112.3	28.1	92.2%		39.4%
Average	Direct	4	88.6	115.0	29.9	93%		42%
Spatial Sd			3.5	4.0	1.6	4%		2%

Decagon Moisture sensor						
Location	RAW	Voltage	θ Alf	Sd θ Alf		Comments
[-]	[-]	[mV]	[%]	[%]		[-]
1	2886		37%	0.7%	right after compaction	After LWD
2	2870		37%	2.1%	5th lift	After LWD
3	2770		34%	3.5%	21-Jul	After LWD
4	2892		37%	2.1%	11:00 AM	After LWD
5	2948		38%	1.0%	HPC	After LWD
6	2875		37%	2.6%		After LWD
7	2840		36%	0.8%		After LWD
8	2874		37%	2.2%		After LWD
9	2848		36%	1.2%		After LWD
8	2935		38%	1.6%		Before LWD
9	2820		35%	1.9%		Before LWD
Average	2873.8		37%	1.8%		
Spatial Sd	49.9		1%	0.8%		

Weather data					
Wind Speed	Air Temperature	Relative Humidity	Soil Surface Temperature	Evaporation Rate	Time/Date/Comment
[km/hr]	[°C]	[%]	[°C]	[kg/m2/hr]	right after compaction
0	27.8	80%	26	0.03	5th lift
					21-Jul
					11:00 AM

LWD test Data						
Dynatest						**Comment**
Location	h1 (1-6)	h2 (7-12)	h3 (13-18)	h4 (19-24)		File name: PIT III
1	loc 1-lift 5	loc 1-lift 5	loc 1-lift 5	loc 1-lift 5		right after compaction
5	loc 5-lift 5	loc 5-lift 5	loc 5-lift 5	loc 5-lift 5		5th lift
9	loc 9-lift 5	loc 9-lift 5	loc 9-lift 5	loc 9-lift 5		21-Jul
Zorn						11:00 AM
Location	h1	h2	h3			
3	406	407	408			
4	409	410	411			
8	412	413	414			
Olson						
Location	h1	h2	h3	h4		
2	PIII 12	PIII 13		PIII 14		
6	PIII 15	PIII 16		PIII 17		
7	PIII 18	PIII 19		PIII 20		
Date	7/22/2015	10:00 AM				
Lift number	[-]	6				
Material	[-]	VA21a				
Compaction	[-]	4	Coverage of sheeps foor roller compactor	with	vibration	
	[-]	3	passes of plate	with	vibration	
Nominal lift thickness	[in]					
Compacted lift thickness	[in]					

LWD test Data						
Dynatest						**Comment**
Location	h1 (1-6)	h2 (7-12)	h3 (13-18)	h4 (19-24)		File name: PIT III
1	loc 1-lift 6	loc 1-lift 6	loc 1-lift 6	loc 1-lift 6		right after compaction
5	loc 5-lift 6	loc 5-lift 6	loc 5-lift 6	loc 5-lift 6		6th lift
9	loc 9-lift 6	loc 9-lift 6	loc 9-lift 6	loc 9-lift 6		22-Jul
Zorn						10:00 AM
Location	h1	h2	h3			VA21a
3	416	417	418			MC ~3.5-4%
4	419	420	421			
8	422	423	424			
Olson						
Location	h1	h2	h3	h4		
2	PIII 21	PIII 22	PIII 23	PIII 24		
6	PIII 25	PIII 26	PIII 27	PIII 28		
7	PIII 29	PIII 30	PIII 31	PIII 32		
Date	7/22/2015	11:00 AM				
Lift number	[-]	6	WATER ADD+ RECOMPACT			
Material	[-]	VA21a				
Compaction	[-]			with	vibration	
	[-]	2	Added water + plate load compactor	with	vibration	
Nominal lift thickness	[in]					
Compacted lift thickness	[in]					

LWD test Data					
Dynatest					**Comment**
Location	h1 (1-6)	h2 (7-12)	h3 (13-18)	h4 (19-24)	File name: PIT III
1			loc 1-lift 6-2nd compaction		1.5 after second compaction
5			loc 5-lift 6- 2nd compaction		2.5 after first round of compaction
9			loc 9-lift 6- 2nd compaciton		6th lift
Zorn					22-Jul
Location	h1	h2	h3		12:30 PM
3	425	426	427		VA21a
4	428	429	430		added water- recompacted @11 AM
8	431	432	433		
Olson					
Location	h1	h2	h3	h4	
2	PIII 33	PIII 34	PIII 35	PIII 36	
6	PIII 37	PIII 38	PIII 39	PIII 40	
7	PIII 41	PIII 42	PIII 43	PIII 44	

Nuclear Gauge Readings								
Location	Transmission mode	Penetration depth	γd	γt	w	PC	Comments	θ
[-]	[-]	[in]	[pcf]	[pcf]	[%]	[%]	[-]	[%]
1	Direct	4	147.5	153.2	3.8	97.0%	2.5 after second compaction	9.0%
2	Direct	4	149.4	153.9	3	98.3%	3.5 after first round of compaction	7.2%
3	Direct	4	149.9	154.6	3.2	98.6%	6th lift	7.7%
4	Direct	4	147.5	152.7	3.5	97.0%	22-Jul	8.3%
5	Direct	4	148.1	152.8	3.2	97.4%	1:30 PM	7.6%
6	Direct	4	145.8	150.5	3.2	95.9%	VA21a	7.5%
7	Direct	4	143.6	149.2	3.9	94.5%	First round compaction@10 AM	9.0%
8	Direct	4	148.2	154.1	4	97.5%	added water+recompact @11 AM	9.5%
9	Direct	4	148.4	154.4	4	97.6%		9.5%
1'	Direct	4	147.8	153.8	4	97.2%		9.5%
Average	Direct	4	147.6	152.9	3.6	97%		8%
Spatial Sd			1.8	1.8	0.4	1.2%		0.9%

Plate load testing		
	two locations	6th lift
	3 hr after second compaction	22-Jul
	4 hr after first fompaction	2:00 PM
		VA21a

LWD test Data					
Dynatest					**Comment**
Location	h1 (1-6)	h2 (7-12)	h3 (13-18)	h4 (19-24)	File name: PIT III
1&2			loc 5-lift 6- 2nd compaction		4 hr after second compaction
7&8			loc 9-lift 6- 2nd compaciton		5 hr after first fompaction
Zorn					6th lift
Location	h1	h2	h3		22-Jul
1&2	440	441	442		3:18 PM
7&8	437	438	439		VA21a
Olson					
Location	h1	h2	h3	h4	
1&2	PIII 49	PIII 50	PIII 51	PIII 52	
7&8	PIII 45	PIII 46	PIII 47	PIII 48	

LWD test Data					
Dynatest					**Comment**
Location	h1 (1-6)	h2 (7-12)	h3 (13-18)	h4 (19-24)	File name: PIT III
1			loc 1-lift 6-44 hr		2 days after compaction
5			loc 5-lift 6-44 hr		45 hr
9			loc 9-lift 6-44 hr		6th lift
Zorn					24-Jul
Location	h1	h2	h3		7:30 AM
3	443	444	445		VA21a
4	446	447	448		
8	449	450	451		
Olson					
Location	h1	h2	h3	h4	
2	PIII 53	PIII 54	PIII 55	PIII 56	
6	PIII 57	PIII 58	PIII 59	PIII 60	
7	PIII 61	PIII 62	PIII 63	PIII 64	

Appendix 4

Dynatest 3031 LWD
Data Report

Project: Pit 1
Data File: pit 1

Test Results

Location: lift0-A

Drop	Radius	Load	Stress	Dist. 1	Dist. 2	Dist. 3	Def. 1	Def. 2	Def. 3	Eo	Offset	Energy
	mm	kN	kPa	mm	mm	mm	Micron	Micron	Micron	MPa	Micron	Joule
1	150	6.3	90	0	300	600	120	56	14	197	-14	0.196
2	150	6.4	90	0	300	600	123	53	15	193	-14	0.154
3	150	6.3	89	0	300	600	140	54	15	167	-23	0.172
4	150	6.3	89	0	300	600	148	53	15	158	-13	0.185
5	150	6.4	90	0	300	600	151	53	15	157	-17	0.212
6	150	6.3	89	0	300	600	157	54	15	149	-9	0.208

Location: lift0-B

Drop	Radius	Load	Stress	Dist. 1	Dist. 2	Dist. 3	Def. 1	Def. 2	Def. 3	Eo	Offset	Energy
	mm	kN	kPa	mm	mm	mm	Micron	Micron	Micron	MPa	Micron	Joule
1	150	6.4	90	0	300	600	190	55	16	125	-67	0.321
2	150	6.4	90	0	300	600	258	57	17	92	-13	0.469
3	150	6.3	89	0	300	600	259	53	18	90	-20	0.421
4	150	6.3	90	0	300	600	267	52	18	89	-9	0.440
5	150	6.3	90	0	300	600	265	55	17	89	2	0.439
6	150	6.3	89	0	300	600	263	54	18	89	-8	0.421

Location: loc11-lift1

Drop	Radius	Load	Stress	Dist. 1	Dist. 2	Dist. 3	Def. 1	Def. 2	Def. 3	Eo	Offset	Energy
	mm	kN	kPa	mm	mm	mm	Micron	Micron	Micron	MPa	Micron	Joule
1	150	6.1	86	0	300	600	867			26	836	3.678
2	150	6.3	89	0	300	600	542			43	71	1.653
3	150	6.3	89	0	300	600	509			46	66	1.446
4	150	6.3	89	0	300	600	491			48	192	1.323
5	150	6.4	90	0	300	600	494			48	32	1.301
6	150	6.3	89	0	300	600	481			49	83	1.232

Location: **loc5-lift1**

Drop	Radius	Load	Stress	Dist. 1	Dist. 2	Dist. 3	Def. 1	Def. 2	Def. 3	Eo	Offset	Energy
	mm	kN	kPa	mm	mm	mm	Micron	Micron	Micron	MPa	Micron	Joule
1	150	2.6	37	0	300	600	442			22	126	0.602
2	150	2.6	37	0	300	600	292			33	16	0.268
3	150	2.6	37	0	300	600	275			35	-1	0.231
4	150	2.6	36	0	300	600	271			35	-5	0.214
5	150	2.6	37	0	300	600	271			36	-3	0.216
6	150	2.6	37	0	300	600	269			36	-6	0.214
7	150	4.7	67	0	300	600	646			27	75	1.473
8	150	4.8	68	0	300	600	616			29	24	1.296
9	150	4.8	68	0	300	600	610			29	20	1.257
10	150	4.8	68	0	300	600	614			29	19	1.264
11	150	4.8	68	0	300	600	608			29	13	1.234
12	150	4.8	67	0	300	600	597			30	9	1.187
13	150	6.3	89	0	300	600	871			27	80	2.645
14	150	6.3	89	0	300	600	852			27	50	2.480
15	150	6.3	90	0	300	600	845			28	35	2.429
16	150	6.4	90	0	300	600	845			28	10	2.422
17	150	6.3	90	0	300	600	837			28	9	2.367
18	150	6.4	90	0	300	600	825			29	2	2.298
19	150	2.6	36	0	300	600	297			32	24	0.290
20	150	2.6	36	0	300	600	271			35	6	0.245
21	150	2.5	36	0	300	600	265			36	14	0.245
22	150	2.5	36	0	300	600	244			39	-1	0.204
23	150	2.5	36	0	300	600	239			40	-8	0.187
24	150	2.5	36	0	300	600	243			39	-1	0.197

Location: **locC-lift2**

Drop	Radius	Load	Stress	Dist. 1	Dist. 2	Dist. 3	Def. 1	Def. 2	Def. 3	Eo	Offset	Energy
	mm	kN	kPa	mm	mm	mm	Micron	Micron	Micron	MPa	Micron	Joule
1	150	2.5	36	0	300	600	1493	62	22	6	715	2.303
2	150	2.6	36	0	300	600	884	58	22	11	164	1.049
3	150	2.6	36	0	300	600	809	60	22	12	120	0.906
4	150	2.6	37	0	300	600	828	61	22	12	140	0.949
5	150	2.6	37	0	300	600	804	62	24	12	122	0.905
6	150	2.6	37	0	300	600	816	63	24	12	127	0.923
7	150	4.3	61	0	300	600	1751	103	38	9	549	4.560
8	150	4.4	62	0	300	600	1612	113	42	10	387	3.874
9	150	4.4	62	0	300	600	1514	116	44	11	302	3.501
10	150	4.4	62	0	300	600	1470	120	46	11	250	3.312
11	150	4.4	62	0	300	600	1438	121	46	11	234	3.214
12	150	4.4	62	0	300	600	1402	122	47	12	207	3.100
13	150	6.0	85	0	300	600	2177	150	56	10	585	7.855
14	150	6.1	86	0	300	600	2206	157	58	10	611	7.748
15	150	6.1	86	0	300	600	2132	168	62	11	497	7.311
16	150	6.1	87	0	300	600	2106	172	62	11	456	7.117
17	150	6.1	86	0	300	600	2245	186	65	10	539	8.197
18	150	6.1	87	0	300	600	2128	190	64	11	418	7.447
19	150	2.5	36	0	300	600	847	62	23	11	110	0.989
20	150	2.5	36	0	300	600	716	61	22	13	68	0.796
21	150	2.5	36	0	300	600	665	60	23	14	46	0.709
22	150	2.6	36	0	300	600	652	60	23	15	39	0.683
23	150	2.6	36	0	300	600	634	60	23	15	30	0.643
24	150	2.5	36	0	300	600	627	60	22	15	24	0.632

Location: **locD-lift2**

Drop	Radius	Load	Stress	Dist. 1	Dist. 2	Dist. 3	Def. 1	Def. 2	Def. 3	Eo	Offset	Energy
	mm	kN	kPa	mm	mm	mm	Micron	Micron	Micron	MPa	Micron	Joule
1	150	2.5	35	0	300	600	430	71	18	21	38	0.493
2	150	2.5	36	0	300	600	374	68	20	25	26	0.400
3	150	2.6	36	0	300	600	375	70	21	25	24	0.399
4	150	2.6	36	0	300	600	371	72	22	26	17	0.390
5	150	2.6	36	0	300	600	366	70	21	26	13	0.377
6	150	2.6	37	0	300	600	362	70	21	27	17	0.375
7	150	4.3	61	0	300	600	809	114	34	20	120	1.944
8	150	4.3	62	0	300	600	844	126	38	19	110	2.013
9	150	4.4	62	0	300	600	821	128	39	20	82	1.862
10	150	4.4	62	0	300	600	815	127	38	20	67	1.808
11	150	4.4	62	0	300	600	805	128	39	20	56	1.767
12	150	4.4	62	0	300	600	797	130	40	20	43	1.702
13	150	6.0	85	0	300	600	1302	159	48	17	223	4.670
14	150	6.1	86	0	300	600	1399	171	52	16	260	5.022
15	150	6.1	87	0	300	600	1374	173	52	17	212	4.771
16	150	6.1	87	0	300	600	1374	178	53	17	220	4.755
17	150	6.2	87	0	300	600	1344	183	54	17	149	4.525
18	150	6.1	87	0	300	600	1336	181	54	17	109	4.415
19	150	2.5	36	0	300	600	513	66	20	18	64	0.581
20	150	2.5	36	0	300	600	471	63	20	20	36	0.462
21	150	2.5	36	0	300	600	474	65	20	20	27	0.453
22	150	2.5	36	0	300	600	478	64	20	20	29	0.438
23	150	2.5	36	0	300	600	461	64	21	21	5	0.420
24	150	2.5	36	0	300	600	476	65	21	20	-7	0.416

Location: **loc1-lift3**

Drop	Radius	Load	Stress	Dist. 1	Dist. 2	Dist. 3	Def. 1	Def. 2	Def. 3	Eo	Offset	Energy
	mm	kN	kPa	mm	mm	mm	Micron	Micron	Micron	MPa	Micron	Joule
1	150	2.6	36	0	300	600	707	83	24	13	150	0.983
2	150	2.6	37	0	300	600	555	84	24	18	55	0.684
3	150	2.6	37	0	300	600	493	78	22	20	6	0.534
4	150	2.6	37	0	300	600	492	80	22	20	7	0.525
5	150	2.6	37	0	300	600	491	80	23	20	5	0.518
6	150	2.6	37	0	300	600	485	80	23	20	0	0.503
7	150	4.6	65	0	300	600	1212	160	41	14	198	3.370
8	150	4.7	67	0	300	600	1060	163	45	17	39	2.595
9	150	4.8	68	0	300	600	1176	179	49	15	111	2.949
10	150	4.7	66	0	300	600	1169	181	50	15	82	2.874
11	150	4.7	67	0	300	600	1169	182	50	15	64	2.826
12	150	4.7	67	0	300	600	1189	187	51	15	115	2.905
13	150	6.0	85	0	300	600	1590	228	59	14	189	5.712
14	150	6.1	86	0	300	600	1739	250	64	13	351	6.265
15	150	6.0	85	0	300	600	1757	256	65	13	250	6.253
16	150	6.0	85	0	300	600	1730	259	66	13	263	5.993
17	150	6.1	86	0	300	600	1749	267	67	13	290	6.069
18	150	6.0	85	0	300	600	1738	265	67	13	237	5.920
19	150	2.6	36	0	300	600	656	88	25	14	67	0.820
20	150	2.6	36	0	300	600	573	82	24	17	-2	0.635
21	150	2.6	36	0	300	600	562	83	24	17	-1	0.609
22	150	2.6	36	0	300	600	553	84	24	17	-10	0.579
23	150	2.6	36	0	300	600	543	82	24	17	-20	0.557
24	150	2.6	37	0	300	600	540	84	24	18	-8	0.558

Location: **loc5-lift3**

Drop	Radius	Load	Stress	Dist. 1	Dist. 2	Dist. 3	Def. 1	Def. 2	Def. 3	Eo	Offset	Energy
	mm	kN	kPa	mm	mm	mm	Micron	Micron	Micron	MPa	Micron	Joule
1	150	2.5	35	0	300	600	653	91	23	14	139	0.963
2	150	2.5	36	0	300	600	505	83	22	19	23	0.639
3	150	2.5	36	0	300	600	493	85	24	19	16	0.604
4	150	2.6	36	0	300	600	478	84	23	20	5	0.573
5	150	2.5	36	0	300	600	476	85	24	20	8	0.560
6	150	2.6	36	0	300	600	482	85	24	20	9	0.571
7	150	4.5	63	0	300	600	1423	166	38	12	388	4.427
8	150	4.5	64	0	300	600	1277	174	42	13	209	3.737
9	150	4.5	64	0	300	600	1470	193	45	11	336	4.417
10	150	4.5	64	0	300	600	1466	194	47	11	291	4.340
11	150	4.5	64	0	300	600	1420	196	46	12	237	4.066
12	150	4.5	64	0	300	600	1413	200	47	12	219	3.998
13	150	5.9	83	0	300	600	2126	241	55	10	595	9.100
14	150	5.9	83	0	300	600	2328	263	58	9	768	9.950
15	150	5.9	83	0	300	600	2321	271	61	9	718	9.759
16	150	5.9	84	0	300	600	2285	274	63	10	571	9.492
17	150	5.9	84	0	300	600	2268	280	64	10	610	9.349
18	150	6.0	85	0	300	600	2207	276	64	10	411	8.989
19	150	2.5	36	0	300	600	648	83	23	15	52	0.873
20	150	2.5	36	0	300	600	563	80	22	17	-9	0.671
21	150	2.5	36	0	300	600	555	81	23	17	-13	0.627
22	150	2.5	36	0	300	600	551	82	23	17	0	0.607
23	150	2.5	36	0	300	600	546	83	23	17	-4	0.604
24	150	2.5	36	0	300	600	531	82	23	18	-5	0.5

Location: **loc9-lift3**

Drop	Radius	Load	Stress	Dist. 1	Dist. 2	Dist. 3	Def. 1	Def. 2	Def. 3	Eo	Offset	Energy
	mm	kN	kPa	mm	mm	mm	Micron	Micron	Micron	MPa	Micron	Joule
1	150	2.5	36	0	300	600	510	98	24	19	8	0.632
2	150	2.5	36	0	300	600	515	97	24	18	4	0.630
3	150	2.6	36	0	300	600	517	97	25	18	5	0.614
4	150	2.6	36	0	300	600	524	98	25	18	5	0.622
5	150	2.6	36	0	300	600	518	100	25	18	4	0.611
6	150	2.6	36	0	300	600	509	97	25	19	-3	0.586
7	150	4.5	64	0	300	600	1337	196	42	13	264	3.923
8	150	4.6	65	0	300	600	1264	197	45	14	89	3.517
9	150	4.5	64	0	300	600	1409	224	50	12	211	4.015
10	150	4.5	64	0	300	600	1443	228	52	12	199	4.106
11	150	4.5	64	0	300	600	1431	225	51	12	196	4.043
12	150	4.5	64	0	300	600	1451	233	53	12	179	4.117
13	150	5.9	84	0	300	600	2156	287	60	10	529	9.191
14	150	6.0	84	0	300	600	2292	313	67	10	683	9.801
15	150	6.0	84	0	300	600	2391	324	70	9	782	10.329
16	150	5.9	84	0	300	600	2321	326	70	10	539	9.754
17	150	6.0	84	0	300	600	2293	333	73	10	596	9.577
18	150	6.0	85	0	300	600	2268	335	73	10	489	9.420
19	150	2.5	36	0	300	600	570	95	25	17	4	0.667
20	150	2.5	36	0	300	600	572	97	26	17	4	0.669
21	150	2.5	36	0	300	600	563	96	26	17	9	0.656
22	150	2.5	36	0	300	600	555	95	26	17	3	0.625
23	150	2.5	36	0	300	600	546	96	26	17	5	0.612
24	150	2.5	36	0	300	600	550	97	26	17	11	0.622

Appendix 5

Dynatest 3031 LWD
Data Report

Project: Pit 2
Data File: pit 2

Test Results

Location: 1

Drop	Radius	Load	Stress	Dist. 1	Dist. 2	Dist. 3	Def. 1	Def. 2	Def. 3	Eo	Offset	Energy
	mm	kN	kPa	mm	mm	mm	Micron	Micron	Micron	MPa	Micron	Joule
1	150	2.5	36	0	300	600	499	197	43	19	67	1.016
2	150	2.5	35	0	300	600	474	182	36	19	39	0.910
3	150	2.5	36	0	300	600	493	195	44	19	58	0.964
4	150	2.5	36	0	300	600	481	194	44	20	38	0.950
5	150	2.5	36	0	300	600	490	188	43	19	46	0.954
6	150	2.5	36	0	300	600	487	189	46	19	40	0.946
7	150	4.7	66	0	300	600	1261	462	75	14	157	4.877
8	150	4.6	65	0	300	600	1278	443	76	13	44	5.050
9	150	4.5	64	0	300	600	1317	444	78	13	35	5.184
10	150	4.5	64	0	300	600	1346	443	79	13	46	5.307
11	150	4.5	63	0	300	600	1370	450	79	12	8	5.411
12	150	4.5	64	0	300	600	1371	458	81	12	23	5.411
13	150	5.9	83	0	300	600	1991	616	84	11	148	10.190
14	150	5.9	83	0	300	600	2067	653	94	11	147	10.530
15	150	5.9	83	0	300	600	2150	679	97	10	196	10.933
16	150	5.9	83	0	300	600	2081	665	95	10	91	10.482
17	150	5.9	84	0	300	600	2150	681	104	10	89	10.912
18	150	5.9	83	0	300	600	2200	688	104	10	90	11.134
19	150	2.5	35	0	300	600	655	207	42	14	46	1.320
20	150	2.5	35	0	300	600	653	207	43	14	29	1.310
21	150	2.5	35	0	300	600	651	208	44	14	22	1.293
22	150	2.5	35	0	300	600	657	210	44	14	29	1.312
23	150	2.5	35	0	300	600	649	207	44	14	20	1.290
24	150	2.5	35	0	300	600	656	209	45	14	29	1.306

Location: 5

Drop	Radius	Load	Stress	Dist. 1	Dist. 2	Dist. 3	Def. 1	Def. 2	Def. 3	Eo	Offset	Energy
	mm	kN	kPa	mm	mm	mm	Micron	Micron	Micron	MPa	Micron	Joule
1	150	2.5	35	0	300	600	708	212	42	13	37	1.462
2	150	2.5	36	0	300	600	741	220	44	13	13	1.563
3	150	2.5	35	0	300	600	762	222	44	12	13	1.610
4	150	2.4	35	0	300	600	770	219	45	12	0	1.607
5	150	2.5	35	0	300	600	798	219	44	12	35	1.613
6	150	2.5	35	0	300	600	802	221	44	11	29	1.596
7	150	4.4	62	0	300	600	1979	467	61	8	206	7.424
8	150	4.4	62	0	300	600	2084	489	51	8	241	7.871
9	150	4.4	62	0	300	600	2158	503	58	8	225	8.244
10	150	4.4	62	0	300	600	2209	511	61	7	168	8.491
11	150	4.4	62	0	300	600	2235	511	61	7	136	8.554
12	150	4.4	62	0	300	600	2270	516	62	7	65	8.699
13	150	5.7	80	0	300	600	3074	700	66	7	340	15.278
14	150	5.6	80	0	300	600	3120	719	64	7	600	15.079
15	150	5.7	81	0	300	600	2918	720	78	7	225	14.401
16	150	5.8	81	0	300	600	2943	722	79	7	132	14.539
17	150	5.8	82	0	300	600	2981	732	80	7	187	14.640
18	150	5.7	81	0	300	600	2963	731	81	7	195	14.423
19	150	2.4	34	0	300	600	1118	257	46	8	39	2.224
20	150	2.4	34	0	300	600	1123	261	47	8	32	2.239
21	150	2.4	35	0	300	600	1106	261	48	8	21	2.218
22	150	2.4	35	0	300	600	1090	260	48	8	10	2.182
23	150	2.4	35	0	300	600	1091	259	46	8	13	2.177
24	150	2.4	35	0	300	600	1093	258	47	8	13	2.178

Location: 9

Drop	Radius	Load	Stress	Dist. 1	Dist. 2	Dist. 3	Def. 1	Def. 2	Def. 3	Eo	Offset	Energy
	mm	kN	kPa	mm	mm	mm	Micron	Micron	Micron	MPa	Micron	Joule
1	150	2.4	34	0	300	600	1242	231	8	7	540	2.478
2	150	2.4	35	0	300	600	1040	234	31	9	247	2.079
3	150	2.4	35	0	300	600	1005	233	36	9	198	1.998
4	150	2.4	35	0	300	600	986	233	40	9	166	1.943
5	150	2.5	35	0	300	600	1011	241	41	9	188	1.992
6	150	2.5	35	0	300	600	1010	240	42	9	186	2.003
7	150	4.3	61	0	300	600	2261	520	42	7	501	8.536
8	150	4.3	61	0	300	600	2368	569	43	7	473	9.052
9	150	4.3	61	0	300	600	2331	573	51	7	362	8.868
10	150	4.4	62	0	300	600	2324	610	63	7	285	8.744
11	150	4.4	62	0	300	600	2327	627	54	7	412	8.320
12	150	4.4	62	0	300	600	2215	604	66	7	194	7.915
13	150	5.7	81	0	300	600	2941	777	60	7	332	14.263
14	150	5.7	81	0	300	600	3131	822	53	7	443	15.419
15	150	5.7	81	0	300	600	3183	846	60	7	466	15.527
16	150	5.7	81	0	300	600	3159	853	61	7	399	15.344
17	150	5.7	81	0	300	600	3156	859	66	7	359	15.335
18	150	5.7	81	0	300	600	3179	861	67	7	352	15.508
19	150	2.4	34	0	300	600	1346	281	43	7	118	2.561
20	150	2.4	34	0	300	600	1348	303	45	7	163	2.575
21	150	2.4	34	0	300	600	1302	288	45	7	119	2.521
22	150	2.4	34	0	300	600	1300	284	44	7	181	2.576
23	150	2.4	34	0	300	600	1279	282	44	7	164	2.526
24	150	2.4	34	0	300	600	1277	285	45	7	146	2.509

Location: 1-16h

Drop	Radius	Load	Stress	Dist. 1	Dist. 2	Dist. 3	Def. 1	Def. 2	Def. 3	Eo	Offset	Energy
	mm	kN	kPa	mm	mm	mm	Micron	Micron	Micron	MPa	Micron	Joule
1	150	2.5	35	0	300	600	393	168	34	23	59	0.762
2	150	2.5	35	0	300	600	358	156	35	26	17	0.661
3	150	2.5	35	0	300	600	364	162	42	25	21	0.674
4	150	2.5	35	0	300	600	400	167	35	23	46	0.745
5	150	2.5	35	0	300	600	373	163	37	25	20	0.664
6	150	2.5	35	0	300	600	374	161	37	25	15	0.674
7	150	4.2	60	0	300	600	943	354	65	17	151	3.314
8	150	4.2	59	0	300	600	996	384	71	16	137	3.505
9	150	4.2	60	0	300	600	1018	394	75	16	126	3.577
10	150	4.2	59	0	300	600	1025	397	76	15	112	3.593
11	150	4.2	60	0	300	600	1049	398	76	15	138	3.663
12	150	4.2	59	0	300	600	1056	402	77	15	130	3.676
13	150	5.9	83	0	300	600	1614	600	95	14	199	7.994
14	150	5.8	82	0	300	600	1684	626	103	13	183	8.362
15	150	5.8	82	0	300	600	1710	632	107	13	209	8.348
16	150	5.8	83	0	300	600	1730	636	106	13	174	8.508
17	150	5.9	83	0	300	600	1757	636	108	12	231	8.656
18	150	5.9	83	0	300	600	1754	647	114	12	207	8.598
19	150	2.5	35	0	300	600	516	192	41	18	74	0.971
20	150	2.5	35	0	300	600	507	190	42	18	63	0.926
21	150	2.5	35	0	300	600	499	190	42	18	51	0.922
22	150	2.5	35	0	300	600	504	191	42	18	49	0.932
23	150	2.5	35	0	300	600	509	192	43	18	56	0.937
24	150	2.5	35	0	300	600	505	193	43	18	52	0.938

Location: 5-16h

Drop	Radius	Load	Stress	Dist. 1	Dist. 2	Dist. 3	Def. 1	Def. 2	Def. 3	Eo	Offset	Energy
	mm	kN	kPa	mm	mm	mm	Micron	Micron	Micron	MPa	Micron	Joule
1	150	2.5	35	0	300	600	723	201	49	13	119	1.461
2	150	2.5	35	0	300	600	699	200	53	13	66	1.417
3	150	2.4	34	0	300	600	703	185	52	13	-3	1.343
4	150	2.5	35	0	300	600	733	193	55	13	117	1.469
5	150	2.5	35	0	300	600	730	200	54	13	107	1.463
6	150	2.4	35	0	300	600	708	192	54	13	80	1.405
7	150	4.4	62	0	300	600	1781	492	94	9	350	6.777
8	150	4.4	62	0	300	600	1758	493	100	9	209	6.749
9	150	4.4	62	0	300	600	1787	502	103	9	179	6.883
10	150	4.4	62	0	300	600	1817	510	106	9	200	6.979
11	150	4.4	63	0	300	600	1821	510	106	9	184	7.010
12	150	4.4	62	0	300	600	1802	509	107	9	159	6.912
13	150	5.7	81	0	300	600	2467	694	127	9	400	12.316
14	150	5.7	81	0	300	600	2420	706	132	9	228	12.110
15	150	5.7	81	0	300	600	2479	720	133	9	275	12.382
16	150	5.7	81	0	300	600	2495	702	132	9	224	12.449
17	150	5.8	82	0	300	600	2558	719	131	8	262	12.915
18	150	5.7	80	0	300	600	2536	719	132	8	247	12.564
19	150	2.4	34	0	300	600	838	224	58	11	53	1.643
20	150	2.4	34	0	300	600	858	230	57	10	48	1.702
21	150	2.4	34	0	300	600	852	228	57	11	40	1.681
22	150	2.4	34	0	300	600	859	229	58	10	42	1.701
23	150	2.4	34	0	300	600	856	226	57	10	48	1.690
24	150	2.4	34	0	300	600	865	232	58	10	45	1.717

Location: 9-16h

Drop	Radius	Load	Stress	Dist. 1	Dist. 2	Dist. 3	Def. 1	Def. 2	Def. 3	Eo	Offset	Energy
	mm	kN	kPa	mm	mm	mm	Micron	Micron	Micron	MPa	Micron	Joule
1	150	2.5	36	0	300	600	911	176	30	10	230	1.725
2	150	2.5	36	0	300	600	806	193	33	12	122	1.476
3	150	2.5	36	0	300	600	829	188	32	11	138	1.528
4	150	2.5	36	0	300	600	811	184	32	12	114	1.474
5	150	2.5	35	0	300	600	808	189	35	11	112	1.465
6	150	2.5	35	0	300	600	811	192	36	11	108	1.466
7	150	4.5	64	0	300	600	1720	429	53	10	260	6.149
8	150	4.6	64	0	300	600	1802	469	57	9	281	6.345
9	150	4.6	65	0	300	600	1765	480	62	10	215	6.231
10	150	4.6	65	0	300	600	1751	485	63	10	189	6.157
11	150	4.5	64	0	300	600	1733	490	64	10	201	6.096
12	150	4.6	64	0	300	600	1734	491	66	10	148	6.084
13	150	5.9	84	0	300	600	2435	693	88	9	257	11.424
14	150	5.9	84	0	300	600	2485	696	76	9	197	11.674
15	150	6.0	85	0	300	600	2515	694	80	9	188	11.888
16	150	5.9	84	0	300	600	2530	694	79	9	197	11.998
17	150	5.9	83	0	300	600	2573	694	76	8	205	12.736
18	150	5.8	82	0	300	600	2553	701	76	8	136	12.035
19	150	2.5	35	0	300	600	1019	202	25	9	140	1.879
20	150	2.5	35	0	300	600	1003	209	33	9	99	1.807
21	150	2.4	35	0	300	600	1033	213	33	9	159	1.889
22	150	2.5	35	0	300	600	956	204	34	10	109	1.723
23	150	2.4	35	0	300	600	952	208	35	10	110	1.696
24	150	2.5	36	0	300	600	933	208	35	10	125	1.673

Location: **VA21A-sub1-A**

Drop	Radius	Load	Stress	Dist. 1	Dist. 2	Dist. 3	Def. 1	Def. 2	Def. 3	Eo	Offset	Energy
	mm	kN	kPa	mm	mm	mm	Micron	Micron	Micron	MPa	Micron	Joule
1	150	2.5	36	0	300	600	1010	211	21	9	390	1.821
2	150	2.5	36	0	300	600	786	200	30	12	72	1.298
3	150	2.5	36	0	300	600	778	197	31	12	62	1.279
4	150	2.5	36	0	300	600	768	196	34	12	37	1.219
5	150	2.5	36	0	300	600	741	193	35	13	7	1.210
6	150	2.5	36	0	300	600	761	193	34	12	6	1.201
7	150	4.6	65	0	300	600	1528	463	59	11	205	5.169
8	150	4.5	64	0	300	600	1593	444	62	11	186	5.527
9	150	4.6	65	0	300	600	1582	462	63	11	178	5.197
10	150	4.5	64	0	300	600	1574	445	63	11	31	5.147
11	150	4.5	63	0	300	600	1747	454	57	9	110	5.906
12	150	4.5	64	0	300	600	1804	448	53	9	103	6.110
13	150	5.9	83	0	300	600	2276	576	56	10	334	10.549
14	150	6.0	84	0	300	600	2337	579	52	9	279	10.707
15	150	5.9	83	0	300	600	2288	588	51	10	11	10.632
16	150	5.9	84	0	300	600	2225	568	58	10	114	10.160
17	150	5.9	84	0	300	600	2278	568	56	10	41	10.405
18	150	5.9	84	0	300	600	2299	570	54	10	9	10.494
19	150	2.4	35	0	300	600	983	158	26	9	164	1.724
20	150	2.5	35	0	300	600	968	170	27	10	111	1.672
21	150	2.5	35	0	300	600	951	163	27	10	108	1.647
22	150	2.5	35	0	300	600	952	167	28	10	96	1.638
23	150	2.4	35	0	300	600	943	166	28	10	80	1.609
24	150	2.5	35	0	300	600	937	166	28	10	85	1.599

Location: **VA21A-sub1-B**

Drop	Radius	Load	Stress	Dist. 1	Dist. 2	Dist. 3	Def. 1	Def. 2	Def. 3	Eo	Offset	Energy
	mm	kN	kPa	mm	mm	mm	Micron	Micron	Micron	MPa	Micron	Joule
1	150	2.4	35	0	300	600	901	190	28	10	210	1.717
2	150	2.5	35	0	300	600	822	194	30	11	117	1.512
3	150	2.5	35	0	300	600	808	201	32	11	92	1.475
4	150	2.5	35	0	300	600	801	198	31	12	87	1.453
5	150	2.5	36	0	300	600	797	200	32	12	88	1.455
6	150	2.6	36	0	300	600	792	199	31	12	82	1.437
7	150	4.5	64	0	300	600	1660	455	55	10	209	5.977
8	150	4.5	64	0	300	600	1716	470	57	10	167	6.124
9	150	4.5	64	0	300	600	1751	473	57	10	134	6.242
10	150	4.5	64	0	300	600	1771	485	57	10	116	6.321
11	150	4.5	64	0	300	600	1770	482	59	10	100	6.286
12	150	4.5	64	0	300	600	1788	484	58	9	108	6.338
13	150	5.9	83	0	300	600	2352	655	71	9	144	11.044
14	150	5.9	84	0	300	600	2455	678	70	9	153	11.537
15	150	5.9	84	0	300	600	2448	695	64	9	199	11.449
16	150	5.9	84	0	300	600	2419	695	67	9	117	11.354
17	150	5.9	84	0	300	600	2473	695	62	9	133	11.525
18	150	5.9	84	0	300	600	2491	701	63	9	122	11.693
19	150	2.6	36	0	300	600	1034	217	26	9	123	1.940
20	150	2.5	35	0	300	600	997	232	34	9	84	1.824
21	150	2.5	35	0	300	600	980	226	33	9	81	1.796
22	150	2.5	35	0	300	600	965	225	34	10	71	1.762
23	150	2.5	35	0	300	600	980	224	35	9	76	1.778
24	150	2.5	35	0	300	600	980	227	35	9	80	1.770

Location: **VA21A-sub2-1**

Drop	Radius	Load	Stress	Dist. 1	Dist. 2	Dist. 3	Def. 1	Def. 2	Def. 3	Eo	Offset	Energy
	mm	kN	kPa	mm	mm	mm	Micron	Micron	Micron	MPa	Micron	Joule
1	150	2.6	36	0	300	600	1061	188	24	9	485	1.938
2	150	2.5	36	0	300	600	805	183	31	12	126	1.389
3	150	2.5	36	0	300	600	788	182	27	12	71	1.349
4	150	2.5	36	0	300	600	765	177	30	12	56	1.306
5	150	2.5	36	0	300	600	752	169	29	13	33	1.271
6	150	2.5	36	0	300	600	740	170	30	13	35	1.266
7	150	4.5	64	0	300	600	1553	414	52	11	263	5.374
8	150	4.5	64	0	300	600	1605	422	59	10	147	5.566
9	150	4.5	64	0	300	600	1594	430	61	11	92	5.553
10	150	4.5	64	0	300	600	1587	434	62	11	55	5.543
11	150	4.5	64	0	300	600	1577	432	61	11	49	5.490
12	150	4.5	64	0	300	600	1579	435	63	11	45	5.529
13	150	6.1	86	0	300	600	2041	607	73	11	239	9.418
14	150	6.0	84	0	300	600	2009	624	81	11	70	9.164
15	150	6.1	86	0	300	600	2024	634	81	11	0	9.375
16	150	6.0	86	0	300	600	2046	633	81	11	-34	9.520
17	150	6.0	85	0	300	600	2027	629	80	11	-52	9.371
18	150	6.0	85	0	300	600	2026	637	81	11	-38	9.389
19	150	2.5	35	0	300	600	904	193	27	10	106	1.668
20	150	2.5	35	0	300	600	820	196	30	11	11	1.478
21	150	2.5	35	0	300	600	798	193	31	12	-8	1.438
22	150	2.5	35	0	300	600	788	193	30	12	-5	1.414
23	150	2.5	35	0	300	600	776	195	31	12	-7	1.390
24	150	2.5	35	0	300	600	782	193	31	12	-11	1.383

Location: **VA21A-sub2-5**

Drop	Radius	Load	Stress	Dist. 1	Dist. 2	Dist. 3	Def. 1	Def. 2	Def. 3	Eo	Offset	Energy
	mm	kN	kPa	mm	mm	mm	Micron	Micron	Micron	MPa	Micron	Joule
1	150	2.5	36	0	300	600	1065	281	22	9	238	2.074
2	150	2.5	35	0	300	600	954	273	31	10	80	1.792
3	150	2.5	35	0	300	600	919	269	33	10	20	1.712
4	150	2.5	35	0	300	600	918	268	33	10	13	1.706
5	150	2.5	35	0	300	600	916	270	35	10	8	1.688
6	150	2.5	35	0	300	600	908	270	35	10	3	1.680
7	150	4.5	64	0	300	600	1792	662	51	9	172	6.511
8	150	4.5	63	0	300	600	1857	675	61	9	129	6.740
9	150	4.5	63	0	300	600	1854	670	59	9	84	6.751
10	150	4.5	63	0	300	600	1900	673	61	9	92	6.875
11	150	4.5	63	0	300	600	1900	686	62	9	60	6.859
12	150	4.5	64	0	300	600	1897	684	63	9	109	6.827
13	150	5.9	84	0	300	600	2345	927	71	9	239	10.832
14	150	5.9	84	0	300	600	2368	935	72	9	202	10.983
15	150	6.0	85	0	300	600	2402	922	74	9	157	11.184
16	150	6.0	85	0	300	600	2414	937	75	9	94	11.149
17	150	5.9	84	0	300	600	2436	934	73	9	152	11.129
18	150	6.0	84	0	300	600	2444	941	75	9	115	11.236
19	150	2.4	35	0	300	600	1132	314	27	8	26	2.115
20	150	2.4	35	0	300	600	1038	312	32	9	-69	1.912
21	150	2.5	35	0	300	600	1018	315	33	9	-82	1.871
22	150	2.5	35	0	300	600	1009	317	34	9	-76	1.852
23	150	2.5	35	0	300	600	997	322	35	9	-92	1.835
24	150	2.4	35	0	300	600	997	324	36	9	-89	1.821

Location: **VA21A-sub2-9**

Drop	Radius	Load	Stress	Dist. 1	Dist. 2	Dist. 3	Def. 1	Def. 2	Def. 3	Eo	Offset	Energy
	mm	kN	kPa	mm	mm	mm	Micron	Micron	Micron	MPa	Micron	Joule
1	150	2.5	35	0	300	600	1033	273	28	9	194	2.006
2	150	2.5	36	0	300	600	934	280	36	10	158	1.756
3	150	2.5	36	0	300	600	876	264	40	11	70	1.604
4	150	2.5	36	0	300	600	868	262	41	11	43	1.574
5	150	2.5	36	0	300	600	861	264	42	11	38	1.547
6	150	2.5	35	0	300	600	846	263	42	11	5	1.510
7	150	4.5	64	0	300	600	1690	565	68	10	62	6.059
8	150	4.5	64	0	300	600	1815	593	71	9	62	6.503
9	150	4.5	64	0	300	600	1828	602	72	9	27	6.549
10	150	4.5	64	0	300	600	1849	608	70	9	16	6.608
11	150	4.5	64	0	300	600	1814	622	64	9	237	6.546
12	150	4.6	64	0	300	600	1706	599	72	10	99	6.116
13	150	6.0	85	0	300	600	2238	792	85	10	147	10.553
14	150	6.0	85	0	300	600	2314	799	79	10	58	10.881
15	150	6.0	85	0	300	600	2336	813	76	10	156	11.002
16	150	6.0	85	0	300	600	2262	810	70	10	361	10.603
17	150	6.0	85	0	300	600	2080	785	80	11	89	9.809
18	150	6.0	85	0	300	600	2088	789	83	11	62	9.819
19	150	2.5	35	0	300	600	978	295	35	9	98	1.857
20	150	2.5	35	0	300	600	843	277	38	11	-14	1.564
21	150	2.5	35	0	300	600	824	277	41	11	-25	1.523
22	150	2.5	35	0	300	600	828	278	41	11	-22	1.524
23	150	2.5	35	0	300	600	830	277	42	11	-25	1.534
24	150	2.5	35	0	300	600	818	271	43	11	-52	1.500

Location: **vA21A-sub2-3h-9**

Drop	Radius	Load	Stress	Dist. 1	Dist. 2	Dist. 3	Def. 1	Def. 2	Def. 3	Eo	Offset	Energy
	mm	kN	kPa	mm	mm	mm	Micron	Micron	Micron	MPa	Micron	Joule
1	150	2.6	36	0	300	600	797	272	31	12	170	1.533
2	150	2.5	35	0	300	600	698	273	39	13	31	1.321
3	150	2.5	36	0	300	600	710	267	39	13	56	1.349
4	150	2.5	36	0	300	600	672	253	37	14	25	1.261
5	150	2.5	35	0	300	600	683	258	38	13	33	1.284
6	150	2.5	35	0	300	600	673	262	35	14	27	1.263
7	150	4.3	61	0	300	600	1295	557	66	12	33	4.500
8	150	4.3	61	0	300	600	1273	548	73	13	-51	4.395
9	150	4.2	60	0	300	600	1351	568	70	12	2	4.603
10	150	4.3	61	0	300	600	1397	578	71	11	-12	4.848
11	150	4.3	60	0	300	600	1391	559	70	11	115	4.848
12	150	4.3	61	0	300	600	1277	544	78	13	29	4.428
13	150	6.1	86	0	300	600	1787	756	111	13	13	8.575
14	150	5.8	82	0	300	600	1771	737	100	12	18	8.419
15	150	6.0	86	0	300	600	1731	719	94	13	-170	8.275
16	150	6.0	85	0	300	600	1854	744	92	12	45	8.836
17	150	5.9	84	0	300	600	1761	724	91	13	-66	8.404
18	150	6.0	85	0	300	600	1830	740	86	12	-7	8.712
19	150	2.5	35	0	300	600	797	253	26	12	44	1.507
20	150	2.5	36	0	300	600	763	239	31	12	14	1.420
21	150	2.5	35	0	300	600	761	242	36	12	-21	1.399
22	150	2.5	35	0	300	600	759	241	35	12	-22	1.401
23	150	2.5	35	0	300	600	751	237	34	12	-16	1.381
24	150	2.5	35	0	300	600	755	239	35	12	-13	1.384

Location: **vA21A-sub2-3h-5**

Drop	Radius	Load	Stress	Dist. 1	Dist. 2	Dist. 3	Def. 1	Def. 2	Def. 3	Eo	Offset	Energy
	mm	kN	kPa	mm	mm	mm	Micron	Micron	Micron	MPa	Micron	Joule
1	150	2.5	35	0	300	600	1085	226	32	8	306	2.065
2	150	2.5	35	0	300	600	943	229	42	10	122	1.721
3	150	2.4	35	0	300	600	819	225	42	11	7	1.458
4	150	2.5	35	0	300	600	830	226	44	11	11	1.486
5	150	2.5	35	0	300	600	821	222	43	11	-7	1.463
6	150	2.5	35	0	300	600	803	220	43	11	-28	1.406
7	150	4.5	63	0	300	600	1630	520	74	10	13	5.741
8	150	4.5	64	0	300	600	1652	523	87	10	-88	5.799
9	150	4.5	64	0	300	600	1735	519	77	10	-25	6.088
10	150	4.5	64	0	300	600	1715	515	76	10	-22	6.041
11	150	4.5	64	0	300	600	1646	513	70	10	111	5.807
12	150	4.5	64	0	300	600	1562	519	80	11	30	5.464
13	150	6.0	85	0	300	600	2080	723	102	11	-43	9.610
14	150	6.0	85	0	300	600	2111	747	101	11	-119	9.729
15	150	5.9	84	0	300	600	2114	735	99	10	-107	9.537
16	150	6.0	85	0	300	600	2113	747	95	11	-131	9.653
17	150	6.0	85	0	300	600	2112	748	96	11	-148	9.568
18	150	5.9	84	0	300	600	2110	745	96	10	-156	9.505
19	150	2.5	35	0	300	600	994	239	32	9	39	1.838
20	150	2.5	35	0	300	600	916	240	39	10	-56	1.629
21	150	2.5	35	0	300	600	871	239	40	11	-81	1.582
22	150	2.5	35	0	300	600	873	240	41	11	-68	1.582
23	150	2.5	35	0	300	600	867	239	41	11	-68	1.567
24	150	2.5	35	0	300	600	869	243	42	11	-70	1.587

Location: **vA21A-sub2-3h-1**

Drop	Radius	Load	Stress	Dist. 1	Dist. 2	Dist. 3	Def. 1	Def. 2	Def. 3	Eo	Offset	Energy
	mm	kN	kPa	mm	mm	mm	Micron	Micron	Micron	MPa	Micron	Joule
1	150	2.5	35	0	300	600	632	154	25	15	222	1.270
2	150	2.5	36	0	300	600	540	169	32	18	97	1.013
3	150	2.5	36	0	300	600	509	169	40	19	33	0.897
4	150	2.5	36	0	300	600	507	171	41	19	29	0.877
5	150	2.5	36	0	300	600	508	173	42	19	29	0.863
6	150	2.5	36	0	300	600	508	173	43	19	27	0.852
7	150	4.6	65	0	300	600	1112	403	69	15	101	3.924
8	150	4.6	65	0	300	600	1160	423	83	15	104	4.056
9	150	4.6	65	0	300	600	1171	423	86	15	73	4.068
10	150	4.6	66	0	300	600	1185	431	90	15	65	4.132
11	150	4.6	66	0	300	600	1190	432	89	15	49	4.130
12	150	4.6	65	0	300	600	1184	433	86	14	43	4.091
13	150	6.1	86	0	300	600	1550	588	100	15	93	7.205
14	150	6.2	87	0	300	600	1570	589	105	15	131	7.350
15	150	6.2	88	0	300	600	1512	585	114	15	47	7.033
16	150	6.2	88	0	300	600	1514	586	117	15	30	7.030
17	150	6.2	87	0	300	600	1510	588	117	15	29	6.996
18	150	6.1	87	0	300	600	1490	584	118	15	20	6.817
19	150	2.5	35	0	300	600	643	193	46	14	28	1.144
20	150	2.5	36	0	300	600	593	190	47	16	-1	1.027
21	150	2.5	36	0	300	600	585	191	47	16	5	1.008
22	150	2.5	35	0	300	600	581	194	47	16	2	0.996
23	150	2.5	35	0	300	600	576	193	48	16	-4	0.986
24	150	2.5	36	0	300	600	574	195	48	17	12	0.982

Location: **vA21A-sub2-9days-1**

Drop	Radius	Load	Stress	Dist. 1	Dist. 2	Dist. 3	Def. 1	Def. 2	Def. 3	Eo	Offset	Energy
	mm	kN	kPa	mm	mm	mm	Micron	Micron	Micron	MPa	Micron	Joule
1	150	2.6	37	0	300	600	108	47	17	90	27	0.139
2	150	2.5	35	0	300	600	92	44	16	100	15	0.087
3	150	2.4	35	0	300	600	91	43	16	101	74	0.091
4	150	2.4	35	0	300	600	90	42	15	102	61	0.090
5	150	2.5	35	0	300	600	96	40	14	96	16	0.087
6	150	2.6	37	0	300	600	115	45	16	85	9	0.102
7	150	4.7	66	0	300	600	257	112	37	68	34	0.652
8	150	4.7	67	0	300	600	228	106	37	77	0	0.519
9	150	4.7	66	0	300	600	245	117	42	71	21	0.585
10	150	4.7	67	0	300	600	231	104	36	76	9	0.520
11	150	4.7	66	0	300	600	226	102	35	77	-22	0.488
12	150	4.7	66	0	300	600	251	105	36	69	13	0.513
13	150	6.3	89	0	300	600	360	154	50	65	64	1.252
14	150	6.3	89	0	300	600	348	158	53	67	-28	1.219
15	150	6.3	88	0	300	600	346	160	55	67	-38	1.174
16	150	6.3	89	0	300	600	345	159	54	68	-41	1.170
17	150	6.3	89	0	300	600	343	158	54	68	0	1.164
18	150	6.3	89	0	300	600	345	163	55	68	-7	1.211
19	150	2.5	36	0	300	600	113	49	17	84	8	0.108
20	150	2.5	36	0	300	600	106	47	17	89	-3	0.096
21	150	2.5	36	0	300	600	111	47	17	85	0	0.096
22	150	2.5	35	0	300	600	106	49	17	87	0	0.094
23	150	2.5	35	0	300	600	105	47	17	88	-1	0.096
24	150	2.5	36	0	300	600	107	47	17	89	5	0.100

Location: **vA21A-sub2-9days-5**

Drop	Radius	Load	Stress	Dist. 1	Dist. 2	Dist. 3	Def. 1	Def. 2	Def. 3	Eo	Offset	Energy
	mm	kN	kPa	mm	mm	mm	Micron	Micron	Micron	MPa	Micron	Joule
1	150	2.7	39	0	300	600	110	58	18	93	13	0.175
2	150	2.5	36	0	300	600	85	51	17	111	2	0.101
3	150	2.5	36	0	300	600	84	51	17	113	0	0.096
4	150	2.5	36	0	300	600	76	48	16	125	-4	0.082
5	150	2.5	36	0	300	600	78	50	17	122	8	0.085
6	150	2.5	36	0	300	600	80	50	17	118	-5	0.093
7	150	4.7	67	0	300	600	228	127	37	77	26	0.675
8	150	4.7	66	0	300	600	206	122	38	84	0	0.564
9	150	4.6	66	0	300	600	203	121	37	86	-3	0.549
10	150	4.7	67	0	300	600	210	127	39	84	3	0.574
11	150	4.7	67	0	300	600	210	125	38	84	-7	0.564
12	150	4.7	66	0	300	600	208	125	39	84	-6	0.565
13	150	6.3	89	0	300	600	336	187	52	70	25	1.395
14	150	6.4	90	0	300	600	336	191	56	71	7	1.378
15	150	6.3	90	0	300	600	336	193	57	71	0	1.348
16	150	6.3	90	0	300	600	341	195	58	69	5	1.374
17	150	6.3	90	0	300	600	347	197	59	68	10	1.397
18	150	6.4	90	0	300	600	350	198	59	68	6	1.408
19	150	2.5	36	0	300	600	100	58	18	95	1	0.125
20	150	2.6	36	0	300	600	95	57	18	100	-4	0.113
21	150	2.5	36	0	300	600	91	56	18	104	-13	0.102
22	150	2.5	36	0	300	600	92	56	18	103	-16	0.102
23	150	2.5	36	0	300	600	92	55	17	103	-5	0.107
24	150	2.5	36	0	300	600	95	57	18	100	-4	0.111

Location: **vA21A-sub2-9days-9**

Drop	Radius	Load	Stress	Dist. 1	Dist. 2	Dist. 3	Def. 1	Def. 2	Def. 3	Eo	Offset	Energy
	mm	kN	kPa	mm	mm	mm	Micron	Micron	Micron	MPa	Micron	Joule
1	150	2.7	38	0	300	600	110	47	16	91	23	0.134
2	150	2.6	37	0	300	600	86	39	14	113	2	0.072
3	150	2.7	38	0	300	600	83	38	14	121	-3	0.063
4	150	2.6	37	0	300	600	83	38	14	117	1	0.072
5	150	2.6	37	0	300	600	80	38	14	122	-3	0.066
6	150	2.6	36	0	300	600	82	38	14	116	-3	0.072
7	150	4.8	67	0	300	600	244	102	32	72	38	0.646
8	150	4.8	67	0	300	600	286	99	34	62	80	0.751
9	150	4.8	68	0	300	600	236	96	33	76	29	0.531
10	150	4.8	67	0	300	600	227	94	33	78	13	0.481
11	150	4.8	68	0	300	600	226	96	34	79	16	0.479
12	150	4.8	67	0	300	600	222	94	32	79	-6	0.455
13	150	6.4	90	0	300	600	382	152	49	62	55	1.398
14	150	6.3	90	0	300	600	371	151	50	64	18	1.277
15	150	6.3	90	0	300	600	369	152	51	64	21	1.251
16	150	6.3	90	0	300	600	367	154	52	65	6	1.240
17	150	6.4	90	0	300	600	363	154	52	65	-9	1.211
18	150	6.4	90	0	300	600	360	155	53	66	-3	1.204
19	150	2.5	35	0	300	600	94	40	14	98	8	0.082
20	150	2.5	35	0	300	600	94	40	15	98	-4	0.091
21	150	2.5	36	0	300	600	96	42	15	99	-1	0.093
22	150	2.5	35	0	300	600	95	42	15	97	-3	0.090
23	150	2.5	35	0	300	600	94	42	15	98	-1	0.088
24	150	2.5	35	0	300	600	94	40	14	98	-7	0.086

Appendix 6

Dynatest 3031 LWD
Data Report

Project: Pit 3
Data File: pit 3

Test Results

Location: loc9-lift1

Drop	Radius	Load	Stress	Dist. 1	Dist. 2	Dist. 3	Def. 1	Def. 2	Def. 3	Eo	Offset	Energy
	mm	kN	kPa	mm	mm	mm	Micron	Micron	Micron	MPa	Micron	Joule
1	150	2.6	37	0	300	600	543	161	12	18	68	0.472
2	150	2.5	36	0	300	600	494	145	11	19	-71	0.343
3	150	2.6	37	0	300	600	472	144	12	21	-15	0.329
4	150	2.6	37	0	300	600	463	145	14	21	-32	0.303
5	150	2.5	36	0	300	600	476	142	13	20	20	0.354
6	150	2.6	37	0	300	600	457	143	13	21	-21	0.300
7	150	4.7	66	0	300	600	948	273	17	18	45	1.872
8	150	4.7	67	0	300	600	953	277	23	19	76	1.616
9	150	4.8	67	0	300	600	945	285	23	19	84	1.652
10	150	4.8	67	0	300	600	933	288	22	19	43	1.633
11	150	4.7	66	0	300	600	965	282	26	18	51	1.760
12	150	4.7	67	0	300	600	979	284	24	18	120	1.686
13	150	6.3	89	0	300	600	1244	344	28	19	343	3.151
14	150	6.4	91	0	300	600	1325	342	30	18	131	3.940
15	150	6.3	89	0	300	600	2092	333	33	11	2092	4.696
16	150	6.2	88	0	300	600	1223	342	31	19	769	3.533
17	150	6.2	88	0	300	600	1175	328	26	20	199	2.533
18	150	6.3	89	0	300	600	1219	342	30	19	68	2.653
19	150	2.6	36	0	300	600	591	156	12	16	41	0.467
20	150	2.6	36	0	300	600	527	134	10	18	-44	0.398
21	150	2.7	38	0	300	600	512	133	10	20	20	0.414
22	150	2.6	37	0	300	600	514	142	13	19	19	0.374
23	150	2.6	37	0	300	600	499	142	12	20	5	0.358
24	150	2.7	38	0	300	600	512	142	12	20	22	0.367

Location: locD-lift2

Drop	Radius	Load	Stress	Dist. 1	Dist. 2	Dist. 3	Def. 1	Def. 2	Def. 3	Eo	Offset	Energy
	mm	kN	kPa	mm	mm	mm	Micron	Micron	Micron	MPa	Micron	Joule
1	150	6.3	88	0	300	600	1085	1		21	80	2.552
2	150	6.3	89	0	300	600	1044			22	78	2.338
3	150	6.3	89	0	300	600	1020			23	51	2.238
4	150	6.4	90	0	300	600	1018			23	55	2.235
5	150	6.3	89	0	300	600	1005			23	56	2.163
6	150	6.3	89	0	300	600	1007			23	54	2.175

Location: locE-lift2

Drop	Radius	Load	Stress	Dist. 1	Dist. 2	Dist. 3	Def. 1	Def. 2	Def. 3	Eo	Offset	Energy
	mm	kN	kPa	mm	mm	mm	Micron	Micron	Micron	MPa	Micron	Joule
1	150	6.4	90	0	300	600	952			25	64	2.393
2	150	6.3	90	0	300	600	914			26	41	2.153
3	150	6.3	90	0	300	600	905			26	30	2.060
4	150	6.2	88	0	300	600	908			26	45	2.051
5	150	6.2	88	0	300	600	899			26	25	2.021
6	150	6.3	89	0	300	600	898			26	34	2.009

Location: locA-lift4

Drop	Radius	Load	Stress	Dist. 1	Dist. 2	Dist. 3	Def. 1	Def. 2	Def. 3	Eo	Offset	Energy
	mm	kN	kPa	mm	mm	mm	Micron	Micron	Micron	MPa	Micron	Joule
1	150	6.0	85	0	300	600	357			63	22	0.796
2	150	6.2	87	0	300	600	338			68	38	0.688
3	150	6.2	88	0	300	600	334			69	66	0.651
4	150	6.2	88	0	300	600	325			71	35	0.619
5	150	6.2	88	0	300	600	324			72	5	0.637
6	150	6.2	88	0	300	600	326			71	43	0.620

Location: **locB-lift4**

Drop	Radius	Load	Stress	Dist. 1	Dist. 2	Dist. 3	Def. 1	Def. 2	Def. 3	Eo	Offset	Energy
	mm	kN	kPa	mm	mm	mm	Micron	Micron	Micron	MPa	Micron	Joule
1	150	6.2	88	0	300	600	467			50	-13	1.143
2	150	6.2	88	0	300	600	453			51	-18	1.065
3	150	6.3	89	0	300	600	447			52	15	1.081
4	150	6.3	89	0	300	600	440	1		53	11	1.057
5	150	6.3	89	0	300	600	441			53	12	1.040
6	150	6.3	89	0	300	600	443			53	13	1.054

Location: **locC-lift4**

Drop	Radius	Load	Stress	Dist. 1	Dist. 2	Dist. 3	Def. 1	Def. 2	Def. 3	Eo	Offset	Energy
	mm	kN	kPa	mm	mm	mm	Micron	Micron	Micron	MPa	Micron	Joule
1	150	6.1	87	0	300	600	384			60	10	0.912
2	150	6.2	87	0	300	600	379			60	21	0.860
3	150	6.2	88	0	300	600	381			61	23	0.873
4	150	6.2	88	0	300	600	382			61	23	0.861
5	150	6.2	87	0	300	600	380			60	22	0.851
6	150	6.2	88	0	300	600	381			61	25	0.850

Location: **loc1-lift5**

Drop	Radius	Load	Stress	Dist. 1	Dist. 2	Dist. 3	Def. 1	Def. 2	Def. 3	Eo	Offset	Energy
	mm	kN	kPa	mm	mm	mm	Micron	Micron	Micron	MPa	Micron	Joule
1	150	2.6	36	0	300	600	174	64	18	54	7	0.135
2	150	2.6	36	0	300	600	158	59	17	60	3	0.113
3	150	2.6	37	0	300	600	157	56	16	62	0	0.101
4	150	2.6	36	0	300	600	155	55	16	61	-40	0.081
5	150	2.6	36	0	300	600	158	56	16	60	-19	0.077
6	150	2.6	36	0	300	600	154	55	17	62	-40	0.073
7	150	4.7	66	0	300	600	365	117	33	48	22	0.573
8	150	4.7	67	0	300	600	340	116	33	52	-3	0.499
9	150	4.7	66	0	300	600	338	115	33	51	-5	0.479
10	150	4.7	67	0	300	600	337	114	33	52	-5	0.476
11	150	4.7	66	0	300	600	332	115	33	52	-18	0.447
12	150	4.7	67	0	300	600	333	115	33	53	-15	0.445
13	150	6.3	89	0	300	600	475	157	42	49	-17	1.000
14	150	6.3	89	0	300	600	470	158	43	50	5	0.986
15	150	6.3	89	0	300	600	471	158	43	50	-3	0.929
16	150	6.3	90	0	300	600	465	160	45	51	-5	0.965
17	150	6.3	89	0	300	600	464	159	43	50	0	0.943
18	150	6.3	89	0	300	600	461	159	44	51	7	0.946
19	150	2.5	36	0	300	600	161	59	16	59	1	0.105
20	150	2.5	36	0	300	600	166	58	16	57	-11	0.082
21	150	2.5	36	0	300	600	172	58	16	55	-6	0.084
22	150	2.5	36	0	300	600	170	59	17	56	-5	0.083
23	150	2.5	36	0	300	600	168	58	17	56	-9	0.083
24	150	2.5	36	0	300	600	161	58	16	59	-10	0.077

Location: **loc5-lift5**

Drop	Radius	Load	Stress	Dist. 1	Dist. 2	Dist. 3	Def. 1	Def. 2	Def. 3	Eo	Offset	Energy
	mm	kN	kPa	mm	mm	mm	Micron	Micron	Micron	MPa	Micron	Joule
1	150	2.6	37	0	300	600	161	80	24	60	6	0.101
2	150	2.5	36	0	300	600	135	73	22	70	-12	0.073
3	150	2.5	36	0	300	600	136	72	22	70	-2	0.089
4	150	2.5	36	0	300	600	136	73	22	70	-2	0.090
5	150	2.5	36	0	300	600	136	72	23	70	-1	0.089
6	150	2.5	36	0	300	600	135	72	23	70	-3	0.087
7	150	4.7	67	0	300	600	279	143	42	63	5	0.461
8	150	4.7	66	0	300	600	277	145	44	63	3	0.436
9	150	4.7	67	0	300	600	276	148	46	64	2	0.436
10	150	4.7	66	0	300	600	276	147	47	63	1	0.432
11	150	4.7	66	0	300	600	274	147	46	63	-2	0.421
12	150	4.7	66	0	300	600	275	149	46	63	-1	0.422
13	150	6.3	89	0	300	600	379	199	60	62	7	0.885
14	150	6.3	89	0	300	600	379	203	62	62	2	0.871
15	150	6.3	89	0	300	600	375	203	63	62	-3	0.860
16	150	6.3	89	0	300	600	376	205	63	62	-3	0.854
17	150	6.3	89	0	300	600	377	206	64	62	-4	0.853
18	150	6.3	88	0	300	600	376	206	64	62	-3	0.840
19	150	2.5	36	0	300	600	144	77	23	66	-2	0.102
20	150	2.5	35	0	300	600	140	75	23	66	-4	0.095
21	150	2.5	36	0	300	600	140	74	23	68	-4	0.094
22	150	2.5	35	0	300	600	140	75	23	66	-4	0.093
23	150	2.5	35	0	300	600	139	75	23	66	-3	0.094
24	150	2.5	36	0	300	600	139	73	22	68	-5	0.090

Location: **loc9-lift5**

Drop	Radius	Load	Stress	Dist. 1	Dist. 2	Dist. 3	Def. 1	Def. 2	Def. 3	Eo	Offset	Energy
	mm	kN	kPa	mm	mm	mm	Micron	Micron	Micron	MPa	Micron	Joule
1	150	2.6	37	0	300	600	169	62	18	58	22	0.126
2	150	2.5	36	0	300	600	155	58	19	61	0	0.093
3	150	2.5	36	0	300	600	143	58	18	66	-25	0.077
4	150	2.5	36	0	300	600	151	58	19	63	-10	0.082
5	150	2.5	36	0	300	600	146	57	18	65	-28	0.067
6	150	2.5	36	0	300	600	149	58	19	64	-11	0.082
7	150	4.6	65	0	300	600	335	114	32	51	-15	0.530
8	150	4.6	66	0	300	600	314	119	35	55	-27	0.460
9	150	4.6	65	0	300	600	314	120	36	54	-40	0.462
10	150	4.6	65	0	300	600	318	123	36	54	1	0.490
11	150	4.6	65	0	300	600	317	120	36	54	-24	0.473
12	150	4.6	65	0	300	600	316	120	35	54	-27	0.467
13	150	6.2	88	0	300	600	459	166	45	50	-39	1.041
14	150	6.2	88	0	300	600	464	172	48	50	-63	1.046
15	150	6.2	87	0	300	600	463	171	48	49	-16	1.035
16	150	6.2	87	0	300	600	464	173	49	49	1	1.057
17	150	6.3	89	0	300	600	464	173	49	50	-37	1.033
18	150	6.2	88	0	300	600	464	174	49	50	-25	1.016
19	150	2.5	36	0	300	600	161	63	19	59	-22	0.090
20	150	2.5	35	0	300	600	170	62	18	54	-9	0.092
21	150	2.5	35	0	300	600	156	62	17	59	-13	0.073
22	150	2.5	36	0	300	600	157	63	18	60	-12	0.074
23	150	2.5	35	0	300	600	151	61	19	61	-49	0.068
24	150	2.5	36	0	300	600	154	62	19	62	-22	0.072

Location: **loc1-lift6**

Drop	Radius	Load	Stress	Dist. 1	Dist. 2	Dist. 3	Def. 1	Def. 2	Def. 3	Eo	Offset	Energy
	mm	kN	kPa	mm	mm	mm	Micron	Micron	Micron	MPa	Micron	Joule
1	150	2.6	36	0	300	600	135	57	20	70	44	0.143
2	150	2.6	36	0	300	600	125	45	16	76	6	0.091
3	150	2.5	36	0	300	600	121	44	16	78	18	0.090
4	150	2.6	37	0	300	600	122	45	16	80	8	0.090
5	150	2.6	36	0	300	600	117	45	16	81	0	0.079
6	150	2.6	36	0	300	600	118	45	16	80	1	0.079
7	150	4.7	66	0	300	600	255	90	32	68	21	0.440
8	150	4.6	66	0	300	600	255	90	33	68	17	0.422
9	150	4.6	65	0	300	600	249	90	35	69	20	0.416
10	150	4.6	65	0	300	600	249	94	34	69	20	0.401
11	150	4.6	66	0	300	600	247	89	33	70	19	0.401
12	150	4.6	66	0	300	600	240	92	34	72	16	0.381
13	150	6.2	88	0	300	600	337	127	46	69	31	0.819
14	150	6.3	89	0	300	600	342	126	46	69	17	0.804
15	150	6.2	88	0	300	600	339	129	48	68	22	0.798
16	150	6.2	88	0	300	600	338	127	47	69	17	0.796
17	150	6.2	88	0	300	600	339	125	46	68	10	0.789
18	150	6.3	88	0	300	600	339	130	47	68	14	0.795
19	150	2.5	36	0	300	600	123	46	16	77	5	0.096
20	150	2.5	36	0	300	600	116	46	16	82	0	0.083
21	150	2.5	36	0	300	600	115	46	16	82	-2	0.078
22	150	2.5	35	0	300	600	114	47	17	81	-2	0.073
23	150	2.5	35	0	300	600	111	46	17	83	0	0.071
24	150	2.5	36	0	300	600	106	45	16	89	-2	0.059

Location: **loc5-lift6**

Drop	Radius	Load	Stress	Dist. 1	Dist. 2	Dist. 3	Def. 1	Def. 2	Def. 3	Eo	Offset	Energy
	mm	kN	kPa	mm	mm	mm	Micron	Micron	Micron	MPa	Micron	Joule
1	150	2.6	37	0	300	600	119	51	20	82	16	0.105
2	150	2.6	36	0	300	600	99	57	20	96	11	0.067
3	150	2.5	35	0	300	600	92	57	20	100	-17	0.049
4	150	2.5	36	0	300	600	104	54	19	91	13	0.080
5	150	2.5	36	0	300	600	100	54	19	95	-9	0.069
6	150	2.5	36	0	300	600	100	53	19	95	4	0.061
7	150	4.6	65	0	300	600	205	112	35	83	4	0.380
8	150	4.7	66	0	300	600	199	111	38	87	10	0.312
9	150	4.6	65	0	300	600	190	107	36	90	8	0.314
10	150	4.6	65	0	300	600	184	108	36	93	2	0.323
11	150	4.6	65	0	300	600	183	104	35	94	-2	0.330
12	150	4.6	65	0	300	600	186	103	35	92	-2	0.320
13	150	6.2	87	0	300	600	272	143	46	84	4	0.700
14	150	6.2	88	0	300	600	270	138	46	86	-8	0.693
15	150	6.2	88	0	300	600	273	138	46	85	-9	0.698
16	150	6.3	89	0	300	600	271	138	47	86	-1	0.710
17	150	6.2	88	0	300	600	268	139	48	86	-1	0.695
18	150	6.3	89	0	300	600	270	139	47	87	-7	0.694
19	150	2.5	36	0	300	600	101	54	18	94	-4	0.075
20	150	2.5	35	0	300	600	97	53	18	95	-4	0.066
21	150	2.5	36	0	300	600	96	53	18	99	-6	0.070
22	150	2.5	35	0	300	600	95	52	18	97	-7	0.066
23	150	2.5	36	0	300	600	101	53	18	94	-5	0.073
24	150	2.5	36	0	300	600	100	53	18	95	-4	0.074

Location: **loc9-lift6**

Drop	Radius	Load	Stress	Dist. 1	Dist. 2	Dist. 3	Def. 1	Def. 2	Def. 3	Eo	Offset	Energy
	mm	kN	kPa	mm	mm	mm	Micron	Micron	Micron	MPa	Micron	Joule
1	150	2.5	36	0	300	600	155	57	19	61	24	0.150
2	150	2.5	36	0	300	600	130	54	19	73	0	0.096
3	150	2.5	36	0	300	600	119	54	18	80	-12	0.079
4	150	2.5	36	0	300	600	122	55	19	78	-7	0.085
5	150	2.5	36	0	300	600	119	55	19	80	-15	0.075
6	150	2.5	36	0	300	600	123	54	19	77	-5	0.080
7	150	4.7	67	0	300	600	273	108	34	65	10	0.502
8	150	4.7	66	0	300	600	259	109	36	67	0	0.479
9	150	4.7	66	0	300	600	258	109	37	67	-3	0.466
10	150	4.7	66	0	300	600	267	109	36	65	-14	0.475
11	150	4.7	66	0	300	600	282	111	36	62	-17	0.495
12	150	4.7	66	0	300	600	286	110	36	61	9	0.505
13	150	6.3	89	0	300	600	396	150	48	59	5	1.029
14	150	6.3	89	0	300	600	398	150	49	59	-4	1.010
15	150	6.3	89	0	300	600	398	149	50	59	-13	1.008
16	150	6.3	89	0	300	600	402	151	51	58	-1	1.024
17	150	6.3	88	0	300	600	401	150	50	58	0	1.002
18	150	6.3	89	0	300	600	402	150	50	58	4	1.008
19	150	2.5	36	0	300	600	154	57	19	62	-5	0.119
20	150	2.5	36	0	300	600	147	59	19	64	-4	0.109
21	150	2.5	36	0	300	600	147	58	19	64	-3	0.106
22	150	2.5	36	0	300	600	144	58	20	66	-10	0.103
23	150	2.5	36	0	300	600	148	59	19	64	-3	0.107
24	150	2.5	36	0	300	600	144	58	19	66	-6	0.104

Location: **loc1-lift6-2nd compaction**

Drop	Radius	Load	Stress	Dist. 1	Dist. 2	Dist. 3	Def. 1	Def. 2	Def. 3	Eo	Offset	Energy
	mm	kN	kPa	mm	mm	mm	Micron	Micron	Micron	MPa	Micron	Joule
1	150	2.6	36	0	300	600	371	48	19	26	179	0.487
2	150	2.6	37	0	300	600	253	47	18	38	39	0.230
3	150	2.6	37	0	300	600	243	47	18	40	41	0.184
4	150	2.6	37	0	300	600	303	48	17	32	66	0.211
5	150	2.6	36	0	300	600	220	48	18	43	-10	0.171
6	150	2.6	37	0	300	600	235	49	19	41	-15	0.164
7	150	4.7	67	0	300	600	443	98	37	40	42	0.759
8	150	4.8	67	0	300	600	423	96	36	42	-5	0.658
9	150	4.8	67	0	300	600	423	96	36	42	-6	0.644
10	150	4.8	67	0	300	600	418	97	36	42	-2	0.639
11	150	4.7	67	0	300	600	417	97	36	42	-23	0.638
12	150	4.8	67	0	300	600	409	97	37	43	-11	0.611
13	150	6.4	90	0	300	600	543	134	46	44	-6	1.237
14	150	6.4	91	0	300	600	528	133	47	45	-2	1.144
15	150	6.4	90	0	300	600	512	134	47	46	22	1.102
16	150	6.3	90	0	300	600	522	135	48	45	22	1.094
17	150	6.4	90	0	300	600	509	136	48	47	16	1.073
18	150	6.4	90	0	300	600	517	137	50	46	-11	1.092
19	150	2.5	36	0	300	600	240	49	19	39	-2	0.178
20	150	2.5	36	0	300	600	238	48	19	40	-21	0.171
21	150	2.6	36	0	300	600	243	50	19	39	17	0.174
22	150	2.6	36	0	300	600	231	49	19	41	12	0.159
23	150	2.5	36	0	300	600	256	49	18	37	25	0.189
24	150	2.6	36	0	300	600	248	49	19	38	-17	0.155

Location: **loc5-lift6-2nd compaction**

Drop	Radius	Load	Stress	Dist. 1	Dist. 2	Dist. 3	Def. 1	Def. 2	Def. 3	Eo	Offset	Energy
	mm	kN	kPa	mm	mm	mm	Micron	Micron	Micron	MPa	Micron	Joule
1	150	2.5	36	0	300	600	197	49	18	48	24	0.168
2	150	2.5	36	0	300	600	206	48	18	46	53	0.177
3	150	2.5	36	0	300	600	186	48	17	51	15	0.142
4	150	2.5	36	0	300	600	195	49	17	49	20	0.142
5	150	2.6	36	0	300	600	185	50	17	51	6	0.133
6	150	2.5	36	0	300	600	187	49	17	51	12	0.133
7	150	4.7	67	0	300	600	398	99	34	44	69	0.747
8	150	4.8	67	0	300	600	368	97	35	48	30	0.630
9	150	4.7	67	0	300	600	360	96	34	49	26	0.605
10	150	4.8	68	0	300	600	361	99	35	50	28	0.590
11	150	4.7	67	0	300	600	352	98	35	50	24	0.569
12	150	4.7	66	0	300	600	343	98	35	51	18	0.542
13	150	6.3	89	0	300	600	489	138	48	48	66	1.224
14	150	6.4	91	0	300	600	477	140	48	50	52	1.149
15	150	6.3	89	0	300	600	458	136	48	51	44	1.074
16	150	6.3	90	0	300	600	448	134	48	53	15	1.034
17	150	6.4	91	0	300	600	441	136	48	54	29	1.019
18	150	6.4	90	0	300	600	442	136	48	54	20	1.020
19	150	2.5	36	0	300	600	189	49	18	50	16	0.152
20	150	2.5	36	0	300	600	169	52	18	56	0	0.122
21	150	2.5	36	0	300	600	168	52	18	56	3	0.116
22	150	2.5	36	0	300	600	165	51	18	57	2	0.109
23	150	2.5	36	0	300	600	165	52	18	57	-2	0.106
24	150	2.6	36	0	300	600	166	51	18	57	-1	0.104

Location: **loc9-lift6-2nd compaction**

Drop	Radius	Load	Stress	Dist. 1	Dist. 2	Dist. 3	Def. 1	Def. 2	Def. 3	Eo	Offset	Energy
	mm	kN	kPa	mm	mm	mm	Micron	Micron	Micron	MPa	Micron	Joule
1	150	2.6	36	0	300	600	778	41	20	12	422	1.086
2	150	2.5	36	0	300	600	325	46	19	29	32	0.285
3	150	2.6	36	0	300	600	290	48	20	33	10	0.222
4	150	2.5	36	0	300	600	269	48	19	35	-9	0.185
5	150	2.5	36	0	300	600	269	48	19	35	25	0.194
6	150	2.6	36	0	300	600	259	50	20	37	-8	0.170
7	150	4.7	67	0	300	600	501	95	38	35	67	0.875
8	150	4.7	66	0	300	600	460	93	37	38	19	0.762
9	150	4.7	67	0	300	600	451	90	38	39	6	0.771
10	150	4.7	67	0	300	600	442	90	37	40	16	0.707
11	150	4.8	67	0	300	600	442	93	38	40	10	0.678
12	150	4.7	67	0	300	600	407	95	40	43	-22	0.595
13	150	6.4	90	0	300	600	529	142	53	45	58	1.221
14	150	6.3	90	0	300	600	519	140	56	46	23	1.186
15	150	6.3	90	0	300	600	510	137	54	46	72	1.176
16	150	6.4	90	0	300	600	492	138	56	48	40	1.105
17	150	6.2	88	0	300	600	464	136	60	50	0	1.088
18	150	6.4	90	0	300	600	454	142	55	52	9	1.012
19	150	2.5	36	0	300	600	190	52	20	50	-5	0.129
20	150	2.5	36	0	300	600	165	50	19	57	-29	0.090
21	150	2.5	36	0	300	600	145	50	19	65	-23	0.075
22	150	2.5	36	0	300	600	103	51	18	92	-32	0.058
23	150	2.6	36	0	300	600	108	51	18	88	-16	0.064
24	150	2.6	36	0	300	600	124	51	18	76	-18	0.063

Location: **locBTW1&2-lift6-2nd compaction-3hr**

Drop	Radius	Load	Stress	Dist. 1	Dist. 2	Dist. 3	Def. 1	Def. 2	Def. 3	Eo	Offset	Energy
	mm	kN	kPa	mm	mm	mm	Micron	Micron	Micron	MPa	Micron	Joule
1	150	2.6	36	0	300	600	196			48	33	0.167
2	150	2.5	36	0	300	600	158			60	14	0.158
3	150	2.6	37	0	300	600	163			60	-4	0.138
4	150	2.6	36	0	300	600	170			56	-1	0.115
5	150	2.6	37	0	300	600	166			59	-10	0.100
6	150	2.6	36	0	300	600	169			56	-4	0.099
7	150	4.7	67	0	300	600	329			54	-18	0.400
8	150	4.7	67	0	300	600	341			52	10	0.487
9	150	4.7	67	0	300	600	360			49	12	0.533
10	150	4.7	67	0	300	600	336			52	-12	0.485
11	150	4.7	67	0	300	600	339			52	-8	0.454
12	150	4.7	66	0	300	600	374			46	28	0.572
13	150	6.3	90	0	300	600	470			50	-9	0.948
14	150	6.4	90	0	300	600	462			51	-11	0.915
15	150	6.3	89	0	300	600	448			52	-16	0.922
16	150	6.3	88	0	300	600	437			53	-9	0.911
17	150	6.2	88	0	300	600	430			54	-14	0.871
18	150	2.5	35	0	300	600	183			50	-3	0.118
19	150	2.5	36	0	300	600	178			53	13	0.164
20	150	2.5	35	0	300	600	166			56	6	0.157
21	150	2.7	38	0	300	600	168			60	3	0.156
22	150	2.7	38	0	300	600	168			60	-4	0.144
23	150	2.6	37	0	300	600	170			57	-4	0.147
24	150	2.5	35	0	300	600	182			51	50	0.149

Location: **locBTW7&8-lift6-2nd compaction-3hr**

Drop	Radius	Load	Stress	Dist. 1	Dist. 2	Dist. 3	Def. 1	Def. 2	Def. 3	Eo	Offset	Energy
	mm	kN	kPa	mm	mm	mm	Micron	Micron	Micron	MPa	Micron	Joule
1	150	2.6	37	0	300	600	86			113	-12	0.047
2	150	2.6	36	0	300	600	90			105	-5	0.056
3	150	2.6	36	0	300	600	89			106	-7	0.054
4	150	2.6	36	0	300	600	90			105	-7	0.055
5	150	2.5	36	0	300	600	89			106	-6	0.055
6	150	2.6	36	0	300	600	90			105	-3	0.058
7	150	4.7	67	0	300	600	184			96	-2	0.281
8	150	4.8	67	0	300	600	186			95	-5	0.264
9	150	4.7	66	0	300	600	188			92	-3	0.271
10	150	4.8	68	0	300	600	193			93	-7	0.284
11	150	4.7	67	0	300	600	194			91	-1	0.275
12	150	4.7	67	0	300	600	183			96	-13	0.225
13	150	6.4	90	0	300	600	281			84	22	0.542
14	150	6.3	89	0	300	600	267			88	-23	0.543
15	150	6.4	91	0	300	600	277			86	-6	0.585
16	150	6.4	90	0	300	600	277			86	-6	0.592
17	150	6.4	90	0	300	600	279			85	-20	0.595
18	150	6.3	90	0	300	600	280			85	-27	0.582
19	150	2.5	36	0	300	600	98			97	-3	0.063
20	150	2.6	37	0	300	600	98			99	-3	0.060
21	150	2.6	37	0	300	600	98			99	-2	0.059
22	150	2.6	37	0	300	600	99			98	-1	0.060
23	150	2.6	37	0	300	600	99			98	-3	0.060

Location: **loc1-lift6-44hrs**

Drop	Radius	Load	Stress	Dist. 1	Dist. 2	Dist. 3	Def. 1	Def. 2	Def. 3	Eo	Offset	Energy
	mm	kN	kPa	mm	mm	mm	Micron	Micron	Micron	MPa	Micron	Joule
1	150	2.5	36	0	300	600	170	64	17	56	43	0.157
2	150	2.6	36	0	300	600	142	58	16	67	-8	0.074
3	150	2.6	36	0	300	600	135	58	16	70	-15	0.064
4	150	2.6	36	0	300	600	130	58	17	73	-30	0.063
5	150	2.6	36	0	300	600	128	58	16	74	-33	0.056
6	150	2.6	36	0	300	600	130	57	16	73	-58	0.045
7	150	4.7	67	0	300	600	275	125	33	64	55	0.421
8	150	4.8	67	0	300	600	259	119	32	68	-36	0.345
9	150	4.8	67	0	300	600	260	121	34	68	25	0.362
10	150	4.8	68	0	300	600	250	120	35	72	-8	0.329
11	150	4.8	67	0	300	600	256	120	35	69	28	0.391
12	150	4.7	66	0	300	600	252	119	34	69	13	0.352
13	150	6.3	90	0	300	600	360	165	47	66	3	0.848
14	150	6.4	90	0	300	600	350	166	49	68	6	0.792
15	150	6.4	90	0	300	600	347	165	50	68	-7	0.744
16	150	6.4	90	0	300	600	349	164	50	68	14	0.733
17	150	6.3	90	0	300	600	351	164	50	68	29	0.743
18	150	6.3	90	0	300	600	343	164	50	69	0	0.745
19	150	2.5	36	0	300	600	135	62	19	70	3	0.107
20	150	2.5	36	0	300	600	126	60	19	75	-7	0.085
21	150	2.5	36	0	300	600	133	59	19	71	-2	0.076
22	150	2.5	36	0	300	600	140	60	19	68	-8	0.066
23	150	2.5	36	0	300	600	141	60	19	67	-11	0.065
24	150	2.5	36	0	300	600	142	59	19	67	-9	0.069

Location: **loc5-lift6-44hrs**

Drop	Radius	Load	Stress	Dist. 1	Dist. 2	Dist. 3	Def. 1	Def. 2	Def. 3	Eo	Offset	Energy
	mm	kN	kPa	mm	mm	mm	Micron	Micron	Micron	MPa	Micron	Joule
1	150	2.6	37	0	300	600	301	61	17	32	80	0.343
2	150	2.6	36	0	300	600	216	56	15	44	13	0.177
3	150	2.5	36	0	300	600	209	55	16	45	7	0.163
4	150	2.5	36	0	300	600	199	56	16	48	2	0.142
5	150	2.5	36	0	300	600	205	56	16	46	1	0.149
6	150	2.5	36	0	300	600	204	57	16	46	5	0.146
7	150	4.7	66	0	300	600	425	113	29	41	42	0.793
8	150	4.7	67	0	300	600	409	113	30	43	21	0.696
9	150	4.7	66	0	300	600	401	112	30	43	7	0.650
10	150	4.7	66	0	300	600	400	115	31	43	10	0.650
11	150	4.7	66	0	300	600	392	114	31	44	10	0.626
12	150	4.7	66	0	300	600	390	113	30	45	8	0.615
13	150	6.3	89	0	300	600	543	158	40	43	47	1.348
14	150	6.4	90	0	300	600	518	160	41	46	18	1.185
15	150	6.3	90	0	300	600	509	159	41	47	13	1.139
16	150	6.3	90	0	300	600	503	160	41	47	3	1.133
17	150	6.3	90	0	300	600	497	159	42	48	-7	1.084
18	150	6.3	90	0	300	600	494	160	42	48	-4	1.072
19	150	2.5	35	0	300	600	230	61	16	40	13	0.184
20	150	2.5	36	0	300	600	209	59	15	45	6	0.154
21	150	2.5	36	0	300	600	202	60	16	47	-7	0.142
22	150	2.5	36	0	300	600	201	60	16	47	-4	0.141
23	150	2.5	36	0	300	600	202	60	16	47	1	0.146
24	150	2.5	36	0	300	600	199	60	16	48	-2	0.138

Location: **loc9-lift6-44hrs**

Drop	Radius	Load	Stress	Dist. 1	Dist. 2	Dist. 3	Def. 1	Def. 2	Def. 3	Eo	Offset	Energy
	mm	kN	kPa	mm	mm	mm	Micron	Micron	Micron	MPa	Micron	Joule
1	150	2.5	36	0	300	600	237	50	15	40	46	0.216
2	150	2.5	36	0	300	600	169	47	14	56	-4	0.087
3	150	2.5	36	0	300	600	169	47	14	56	-7	0.088
4	150	2.6	36	0	300	600	165	48	14	57	-15	0.101
5	150	2.5	36	0	300	600	171	49	15	55	-12	0.075
6	150	2.5	36	0	300	600	166	47	14	57	-35	0.086
7	150	4.7	66	0	300	600	364	101	29	48	71	0.765
8	150	4.7	66	0	300	600	319	101	30	54	34	0.633
9	150	4.7	66	0	300	600	319	101	30	54	41	0.610
10	150	4.7	66	0	300	600	311	99	29	56	32	0.610
11	150	4.7	66	0	300	600	310	103	30	56	29	0.591
12	150	4.7	66	0	300	600	310	101	30	56	23	0.572
13	150	6.3	89	0	300	600	408	138	40	57	-43	0.860
14	150	6.3	90	0	300	600	436	141	41	54	31	0.899
15	150	6.4	90	0	300	600	428	140	42	55	24	0.879
16	150	6.3	90	0	300	600	413	141	42	57	-1	0.868
17	150	6.3	89	0	300	600	417	140	41	56	-5	0.837
18	150	6.4	90	0	300	600	427	143	44	55	-6	0.891
19	150	2.5	36	0	300	600	168	54	17	56	-2	0.110
20	150	2.5	36	0	300	600	155	54	17	61	-18	0.079
21	150	2.5	36	0	300	600	162	53	16	59	-18	0.067
22	150	2.5	36	0	300	600	163	52	16	58	-12	0.077
23	150	2.5	36	0	300	600	160	53	16	59	-23	0.082
24	150	2.5	36	0	300	600	154	52	17	62	-7	0.085

Appendix 7

Olson LWD data, Pits 1, 2, and 3

Soil type	height (cm)	lift	Loc	time after compaction	File Name	Plate Diameter (mm)	Possion's Ratio	Stress Distribution Para	Force 1 (N)	Disp 1 (mm)	Force 2 (N)	Disp 2 (mm)	Force 3 (N)	Disp 3 (mm)	Force 4 (N)	Disp 4 (mm)	Force 5 (N)	Disp 5 (mm)	Force 6 (N)	Disp 6 (mm)	Force ave (N)	Force ave (kN)	Disp ave (mm)	E ave (MPa)
Crushed Stone	61.0	0	A	0	PITI1.NDE	300	0.35	3.14	8614.8	1.099	8227.0	0.752	8183.4	0.685	8166.3	0.666	8280.3	0.705	8309.4	0.665	8252.0	8.3	0.679	45.3
Crushed Stone	61.0	0	B	0	PITI2.NDE	300	0.35	3.14	9046.3	1.010	8391.8	0.642	8294.8	0.619	8227.0	0.578	8156.7	0.509	8144.6	0.512	8176.1	8.2	0.533	57.3
ALF	20.3	1	6	0	PITI4.NDE	300	0.35	3.14	4568.9	0.986	4506.1	0.939	4537.4	0.940	4477.3	0.931	4547.6	0.922	4459.4	0.896	4494.8	4.5	0.916	18.3
ALF	48.3	1	6	0	PITI5.NDE	300	0.35	3.14	7068.3	1.289	7090.1	1.354	7145.9	1.386	7111.9	1.367	7128.9	1.338	7102.2	1.346	7114.3	7.1	1.350	19.6
ALF	61.0	1	6	0	PITI6.NDE	300	0.35	3.14	7863.3	1.422	8025.8	1.480	8100.9	1.273	8064.5	1.279	7999.1	1.375	8054.9	1.366	8039.5	8.0	1.340	22.4
ALF	20.3	1	6	0	PITI7.NDE	300	0.35	3.14	4447.7	0.951	4503.8	0.932	4560.0	0.942	4523.4	0.909	4442.4	0.968	4507.6	0.900	4491.1	4.5	0.926	18.1
ALF	20.3	2	B	0	PITI8.NDE	300	0.35	3.14	4169.7	2.071	4385.5	1.576	4506.9	1.446	4537.4	1.379	4563.9	1.323	4617.6	1.303	4573.0	4.6	1.335	12.8
ALF	48.3	2	B	0	PITI9.NDE	300	0.35	3.14	6937.4	2.044	6988.3	2.233	7005.2	2.188	7073.1	2.185	7291.3	1.887	7206.4	1.829	7190.3	7.2	1.967	13.7
ALF	61.0	2	B	0	PITI10.NDE	300	0.35	3.14	8132.5	1.908	8222.1	1.908	8149.4	2.079	8105.8	2.041	8205.1	1.964	8340.9	1.909	8217.3	8.2	1.971	15.5
ALF	20.3	2	B	0	PITI11.NDE	300	0.35	3.14	4576.0	1.478	4591.0	1.243	4690.4	1.183	4714.2	1.214	4736.5	1.181	4775.5	1.131	4742.0	4.7	1.175	15.0
ALF	20.3	2	F	0	PITI12.NDE	300	0.35	3.14	4252.8	2.096	4319.0	1.600	4366.5	1.522	4290.2	1.493	4371.4	1.564	4386.9	1.590	4349.5	4.3	1.549	10.5
ALF	48.3	2	F	0	PITI13.NDE	300	0.35	3.14	6753.2	1.868	6804.1	2.080	6702.3	2.170	6624.8	2.197	6692.6	2.180	6765.3	2.190	6694.2	6.7	2.189	11.4
ALF	61.0	2	F	0	PITI14.NDE	300	0.35	3.14	7703.4	2.334	7611.2	2.404	7574.9	2.293	7608.9	2.396	7533.6	2.382	7652.5	2.259	7598.3	7.6	2.346	12.1
ALF	20.3	2	F	0	PITI15.NDE	300	0.35	3.14	4223.3	1.758	4154.7	1.680	4255.1	1.706	4253.1	1.673	4243.9	1.690	4264.5	1.656	4253.9	4.3	1.673	9.5
ALF	20.3	3	2	2	PITI16.NDE	300	0.35	3.14	4145.3	2.213	4345.5	2.007	4412.8	1.996	4315.4	1.906	4324.1	1.837	4329.2	1.840	4322.9	4.3	1.861	8.7
ALF	48.3	3	2	2	PITI17.NDE	300	0.35	3.14	6784.7	2.215	6714.4	2.295	6702.3	2.308	6631.9	2.265	6787.1	2.277	6775.0	2.316	6731.3	6.7	2.286	11.0
ALF	61.0	3	2	2	PITI18.NDE	300	0.35	3.14	7596.8	2.349	7511.9	2.453	7589.5	2.483	7657.3	2.362	7703.4	2.317	7732.5	2.422	7697.7	7.7	2.367	12.1
ALF	20.3	3	2	2	PITI19.NDE	300	0.35	3.14	4291.4	1.566	4240.7	1.695	4268.1	1.716	4329.6	1.658	4335.8	1.698	4335.8	1.736	4333.7	4.3	1.697	9.5
ALF	20.3	3	6	2	PITI20.NDE	300	0.35	3.14	4244.1	2.155	4243.6	2.347	4422.0	2.104	4229.8	1.810	4358.0	1.783	4250.9	1.741	4279.6	4.3	1.778	9.0
ALF	48.3	3	6	2	PITI21.NDE	300	0.35	3.14	6663.5	2.238	6304.7	2.154	6447.8	2.329	6445.3	2.313	6476.9	2.288	6586.0	2.334	6502.7	6.5	2.312	10.5
ALF	61.0	3	6	2	PITI22.NDE	300	0.35	3.14	7402.8	2.453	7504.6	2.393	7448.9	2.360	7480.4	2.405	7519.2	2.401	7499.8	2.424	7499.8	7.5	2.410	11.6
ALF	20.3	3	6	2	PITI23.NDE	300	0.35	3.14	4142.0	1.834	4115.7	1.539	4186.0	1.553	4187.7	1.526	4153.9	1.592	4201.0	1.536	4180.9	4.2	1.551	10.0
ALF	20.3	3	7	2	PITI24.NDE	300	0.35	3.14	4120.3	2.368	4242.2	1.964	4156.4	2.030	4197.1	1.717	4208.5	1.715	4208.8	1.626	4204.8	4.2	1.686	9.3
ALF	48.3	3	7	2	PITI25.NDE	300	0.35	3.14	6527.8	2.225	6469.6	2.357	6481.7	2.400	6535.0	2.353	6605.4	2.307	6425.9	2.256	6522.1	6.5	2.306	10.5
ALF	61.0	3	7	2	PITI26.NDE	300	0.35	3.14	7359.2	2.340	7412.5	2.408	7511.9	2.399	7533.6	2.406	7499.8	2.397	7451.3	2.349	7494.9	7.5	2.384	11.7
ALF	20.3	3	7	2	PITI27.NDE	300	0.35	3.14	4136.3	2.107	4200.5	1.817	4205.4	1.728	4215.0	1.713	4391.3	1.695	4261.8	1.634	4289.4	4.3	1.681	9.5
ALF	20.3	5	A	0	PITII1.NDE	300	0.35	3.14	4161.0	2.607	4447.9	2.064	4508.6	2.189	4381.3	1.956	4413.8	2.005	4570.9	2.156	4455.3	4.5	2.039	8.1
ALF	61.0	5	A	0	PITII2.NDE	300	0.35	3.14	7764.0	2.283	7817.3	2.249	7778.5	2.231	7785.8	2.293	7725.2	2.263	7686.4	2.216	7732.5	7.7	2.257	12.8
ALF	20.3	5	A	0	PITII3.NDE	300	0.35	3.14	4318.1	2.270	4332.1	2.183	4214.6	2.128	4244.9	2.136	4288.5	2.178	4252.4	2.129	4261.9	4.3	2.147	7.4
ALF	20.3	5	B	0	PITII4.NDE	300	0.35	3.14	4091.9	2.624	4522.6	1.809	4526.8	1.727	4446.0	1.677	4429.6	1.645	4496.9	1.629	4457.5	4.5	1.650	10.1
ALF	61.0	5	B	0	PITII5.NDE	300	0.35	3.14	7725.2	2.246	7751.9	2.318	7834.3	2.376	7698.5	2.325	7742.1	2.374	7722.8	2.349	7721.1	7.7	2.350	12.2
ALF	48.3	5	B	0	PITII6.NDE	300	0.35	3.14	6616.0	2.730	6606.3	2.736	6589.1	2.765	6559.3	2.773	6620.8	2.772	6566.3	2.742	6582.1	6.6	2.762	8.9
ALF	20.3	5	B	0	PITII7.NDE	300	0.35	3.14	4382.8	1.708	4283.9	1.704	4351.3	1.677	4316.4	1.672	4298.5	1.671	4343.0	1.682	4319.3	4.3	1.675	9.6
ALF	20.3	5	C	0	PITII8.NDE	300	0.35	3.14	4509.3	2.356	4539.3	1.870	4536.2	1.817	4861.3	2.261	4667.1	1.977	4446.5	1.827	4658.3	4.7	2.022	8.6
ALF	48.3	5	C	0	PITII9.NDE	300	0.35	3.14	6985.8	2.610	6896.1	2.645	6869.6	2.658	6845.3	2.665	6857.4	2.670	6876.8	2.696	6859.8	6.9	2.677	9.5
ALF	20.3	5	C	0	PITII10.NDE	300	0.35	3.14	4394.7	1.765	4398.3	1.722	4336.5	1.685	4331.7	1.718	4366.1	1.719	4362.4	1.705	4353.4	4.4	1.714	9.5
ALF	20.3	6	2	0.5	PITII11.NDE	300	0.35	3.14	4168.5	2.170	4270.3	1.993	4253.6	1.914	4230.5	1.936	4257.4	1.914	4268.4	1.904	4252.1	4.3	1.918	8.3
ALF	48.3	6	2	0.5	PITII12.NDE	300	0.35	3.14	6600.4	2.595	6544.7	2.579	6571.4	2.608	6576.2	2.554	6602.9	2.424	6571.4	2.367	6583.5	6.6	2.448	10.0
ALF	20.3	6	2	0.5	PITII13.NDE	300	0.35	3.14	4119.5	2.021	4148.4	2.002	4133.4	1.985	4179.2	1.996	4147.9	1.958	4106.3	1.954	4144.5	4.1	1.969	7.8

ALF	20.3	6	6	0.5	PITII14.NDE	300	0.35	3.14	4008.0	2.987	4346.1	2.257	4345.0	2.101	4329.4	2.056	4342.8	2.016	4356.1	2.010	4342.8	4.3	2.027	8.0
ALF	48.3	6	6	0.5	PITII15.NDE	300	0.35	3.14	6772.6	2.349	6823.5	2.500	6743.5	2.410	6741.0	2.492	6726.5	2.422	6702.3	2.356	6723.3	6.7	2.423	10.3
ALF	20.3	6	6	0.5	PITII16.NDE	300	0.35	3.14	4278.5	2.063	4337.7	2.077	4285.8	2.024	4308.9	2.005	4366.8	2.051	4271.5	1.979	4315.7	4.3	2.012	8.0
ALF	20.3	6	7	0.5	PITII17.NDE	300	0.35	3.14	3848.0	2.321	4260.3	2.410	4356.9	2.321	4322.1	2.186	4336.9	2.080	4301.4	2.032	4320.1	4.3	2.099	7.7
ALF	48.3	6	7	0.5	PITII18.NDE	300	0.35	3.14	6762.9	2.287	6678.0	2.240	6792.0	2.254	6733.8	2.271	6678.0	2.211	6733.8	2.246	6715.2	6.7	2.243	11.2
ALF	20.3	6	7	0.5	PITII19.NDE	300	0.35	3.14	4275.6	2.063	4266.4	2.052	4361.9	2.063	4226.9	2.009	4281.0	2.011	4265.9	2.018	4257.9	4.3	2.013	7.9
ALF	20.3	6	2	16	PITII20.NDE	300	0.35	3.14	4237.3	2.177	4410.2	1.608	4414.1	1.519	4428.9	1.496	4407.0	1.496	4464.4	1.530	4433.4	4.4	1.507	11.0
ALF	48.3	6	2	16	PITII21.NDE	300	0.35	3.14	6830.8	2.318	6881.7	2.394	6893.8	2.431	6898.6	2.433	6889.0	2.442	6891.3	2.439	6893.0	6.9	2.438	10.5
ALF	20.3	6	2	16	PITII22.NDE	300	0.35	3.14	4300.6	1.626	4409.3	1.622	4333.3	1.580	4312.3	1.566	4398.8	1.593	4363.6	1.569	4358.2	4.4	1.576	10.3
ALF	20.3	6	6	16	PITII23.NDE	300	0.35	3.14	4055.0	2.217	4551.8	1.853	4529.9	1.699	4525.3	1.628	4475.1	1.575	4530.6	1.577	4510.4	4.5	1.593	10.5
ALF	48.3	6	6	16	PITII24.NDE	300	0.35	3.14	6871.9	2.393	6886.5	2.443	6884.0	2.434	6876.8	2.446	6758.0	2.421	6864.6	2.464	6833.1	6.8	2.443	10.4
ALF	20.3	6	6	16	PITII25.NDE	300	0.35	3.14	4389.9	1.653	4433.5	1.606	4378.2	1.569	4371.6	1.558	4477.3	1.604	4450.2	1.597	4433.0	4.4	1.587	10.4
ALF	20.3	6	7	16	PITII26.NDE	300	0.35	3.14	4206.1	2.629	4570.2	1.676	4590.0	1.559	4576.7	1.527	4601.5	1.489	4556.6	1.492	4578.3	4.6	1.502	11.4
ALF	48.3	6	7	16	PITII27.NDE	300	0.35	3.14	6934.9	2.184	6876.8	2.210	6910.7	2.253	6971.4	2.264	6964.1	2.277	6891.3	2.242	6942.3	6.9	2.261	11.4
ALF	20.3	6	7	16	PITII28.NDE	300	0.35	3.14	4419.6	1.545	4441.4	1.502	4391.3	1.473	4381.6	1.481	4447.5	1.487	4435.8	1.462	4421.6	4.4	1.477	11.2
VA21a	20.3	7	A	16	PITII29.NDE	300	0.35	3.14	4282.2	2.296	4229.4	1.939	4296.2	1.914	4312.5	1.896	4305.0	1.876	4308.9	1.872	4308.8	4.3	1.881	8.5
VA21a	48.3	7	A	16	PITII30.NDE	300	0.35	3.14	6801.6	2.517	6782.3	2.592	6796.8	2.626	6719.3	2.648	6753.2	2.669	6680.5	2.675	6717.6	6.7	2.664	9.4
VA21a	20.3	7	A	16	PITII31.NDE	300	0.35	3.14	4252.6	1.953	4252.8	1.906	4264.7	1.888	4279.7	1.910	4278.5	1.881	4232.8	1.878	4263.7	4.3	1.890	8.4
VA21a	20.3	7	B	16	PITII32.NDE	300	0.35	3.14	4372.1	1.600	4369.7	1.290	4382.8	1.323	4409.5	1.317	4393.7	1.323	4398.5	1.345	4400.6	4.4	1.329	12.3
VA21a	48.3	7	B	16	PITII33.NDE	300	0.35	3.14	6961.6	1.874	6913.2	2.055	6918.0	2.086	6903.4	2.036	6947.1	2.053	6947.1	2.083	6932.6	6.9	2.057	12.6
VA21a	20.3	7	B	16	PITII34.NDE	300	0.35	3.14	4260.1	1.557	4342.5	1.455	4369.0	1.498	4413.3	1.573	4393.7	1.528	4396.8	1.505	4401.3	4.4	1.535	10.7
VA21a	20.3	8	2	1	PITII35.NDE	300	0.35	3.14	4324.8	1.704	4271.8	1.314	4347.9	1.287	4441.7	1.295	4398.8	1.272	4378.9	1.267	4406.5	4.4	1.278	12.8
VA21a	48.3	8	2	1	PITII36.NDE	300	0.35	3.14	6927.8	1.718	6952.0	1.805	6925.3	1.825	6930.1	1.834	6942.2	1.848	6881.7	1.834	6918.0	6.9	1.839	14.0
VA21a	20.3	8	2	1	PITII37.NDE	300	0.35	3.14	4270.8	1.282	4373.0	1.280	4385.9	1.287	4402.2	1.303	4336.5	1.292	4312.7	1.271	4350.5	4.4	1.288	12.6
VA21a	20.3	8	6	1	PITII38.NDE	300	0.35	3.14	4435.8	1.885	4341.5	1.482	4400.5	1.462	4395.1	1.445	4468.4	1.460	4430.0	1.452	4431.2	4.4	1.452	11.4
VA21a	48.3	8	6	1	PITII39.NDE	300	0.35	3.14	6973.7	1.930	6930.1	1.983	6903.4	1.999	6915.5	2.025	6927.8	2.057	6903.4	2.081	6915.6	6.9	2.055	12.5
VA21a	20.3	8	6	1	PITII40.NDE	300	0.35	3.14	4405.3	1.478	4414.8	1.447	4421.6	1.442	4427.6	1.424	4407.0	1.429	4407.8	1.424	4414.1	4.4	1.426	11.5
VA21a	20.3	8	7	1	PITII41.NDE	300	0.35	3.14	4550.0	0.873	4448.7	0.890	4413.3	0.887	4464.8	0.900	4412.1	0.897	4453.1	0.891	4443.3	4.4	0.896	18.5
VA21a	48.3	8	7	1	PITII42.NDE	300	0.35	3.14	7095.0	1.322	7039.2	1.364	7053.8	1.381	7031.9	1.411	7017.4	1.419	7000.4	1.426	7016.6	7.0	1.419	18.4
VA21a	20.3	8	7	1	PITII43.NDE	300	0.35	3.14	4437.8	0.967	4490.4	0.936	4365.9	0.904	4451.6	0.917	4447.3	0.933	4421.4	0.931	4440.1	4.4	0.927	17.8
VA21a	20.3	8	2	4	PITII44.NDE	300	0.35	3.14	4453.6	1.353	4488.4	1.088	4395.6	1.196	4542.8	1.146	4556.6	1.117	4442.9	1.198	4514.1	4.5	1.153	14.6
VA21a	48.3	8	2	4	PITII45.NDE	300	0.35	3.14		1.458	6995.6	1.504	7041.6	1.542	7099.8	1.586	7070.7	1.596	7080.4	1.621	7083.6	7.1	1.601	16.5
VA21a	20.3	8	2	4	PITII46.NDE	300	0.35	3.14	4452.1	1.176	4423.3	1.167	4431.2	1.168	4430.0	1.149	4462.5	1.167	4464.8	1.168	4452.4	4.5	1.162	14.3
VA21a	20.3	8	6	4	PITII47.NDE	300	0.35	3.14	4417.9	1.575	4388.6	1.457	4461.5	1.335	4378.4	1.491	4448.7	1.434	4422.8	1.542	4416.6	4.4	1.489	11.1
VA21a	48.3	8	6	4	PITII48.NDE	300	0.35	3.14	6956.8	1.792	6981.0	1.792	7036.8	1.842	7010.1	1.864	7082.8	1.875	7061.0	1.885	7051.3	7.1	1.874	14.0
VA21a	20.3	8	6	4	PITII49.NDE	300	0.35	3.14	4424.5	1.362	4421.8	1.354	4422.3	1.385	4446.3	1.357	4454.6	1.346	4451.9	1.332	4450.9	4.5	1.345	12.3
VA21a	20.3	8	7	4	PITII50.NDE	300	0.35	3.14	4775.9	1.421	4606.7	1.067	4594.4	1.102	4562.4	1.106	4687.9	1.125	4534.5	1.050	4594.9	4.6	1.093	15.7
VA21a	48.3	8	7	4	PITII51.NDE	300	0.35	3.14	7162.8	1.430	7121.6	1.469	7174.9	1.488	7085.3	1.503	7124.0	1.514	7116.8	1.507	7108.7	7.1	1.508	17.6
VA21a	20.3	8	7	4	PITII52.NDE	300	0.35	3.14	4559.0	1.082	4508.6	1.138	4489.0	1.033	4486.5	1.002	4475.1	0.980	4498.2	0.985	4486.6	4.5	0.989	16.9
VA21a	61.0	8	6	122	PITII56.NDE	300	0.35	3.14	8428.2	1.305	8008.8	0.909	7977.3	0.818	8083.9	0.802	8156.7	0.787	8234.3	0.804	8158.3	8.2	0.798	38.1
VA21a	20.3	8	2	216	PITII57.NDE	300	0.35	3.14	4760.9	0.401	4644.5	0.269	4764.5	0.262	4763.6	0.254	4759.0	0.252	4738.8	0.256	4753.8	4.8	0.254	69.7
VA21a	48.3	8	2	216	PITII58.NDE	300	0.35	3.14	7291.3	0.420	7354.3	0.411	7206.4	0.402	7361.6	0.406	7177.4	0.408	7276.7	0.408	7271.9	7.3	0.408	66.5
VA21a	61.0	8	2	216	PITII59.NDE	300	0.35	3.14	8222.1	0.471	8178.4	0.480	8248.7	0.458	8367.5	0.463	8435.4	0.472	8372.4	0.481	8391.8	8.4	0.472	66.2
VA21a	20.3	8	2	216	PITII60.NDE	300	0.35	3.14	4735.2	0.266	4647.2	0.291	4639.7	0.353	4648.0	0.291			4698.1	0.388	4673.0	4.7	0.339	52.3
VA21a	20.3	8	6	216	PITII61.NDE	300	0.35	3.14	4995.1	0.928	4551.0	0.328	4625.5	0.296	4627.1	0.293	4621.5	0.281	4623.2	0.267	4623.9	4.6	0.280	61.5

VA21a	48.3	8	6	216	PITII62.NDE	300	0.35	3.14	7356.8	0.417	7453.7	0.411	7521.5	0.414	7531.3	0.400	7444.0	0.394	7468.3	0.400	7481.2	7.5	0.398	70.0
VA21a	61.0	8	6	216	PITII63.NDE	300	0.35	3.14	8343.3	0.479	8268.1	0.478	8239.1	0.448	8299.7	0.461	8282.7	0.446	8345.7	0.459	8309.4	8.3	0.455	68.0
VA21a	20.3	8	6	216	PITII64.NDE	300	0.35	3.14	4740.1	0.258	4743.2	0.251	4825.9	0.251	4750.0	0.248	4585.9	0.240	4692.8	0.242	4676.2	4.7	0.243	71.6
VA21a	20.3	8	7	216	PITII65.NDE	300	0.35	3.14	5072.4	1.549	4762.4	0.504	4600.9	0.333	4679.3	0.279	4707.5	0.262	4654.0	0.251	4680.3	4.7	0.264	66.1
VA21a	48.3	8	7	216	PITII66.NDE	300	0.35	3.14	7417.4	0.425	7398.0	0.411	7516.7	0.414	7499.8	0.413	7315.5	0.397	7451.3	0.401	7422.2	7.4	0.404	68.5
VA21a	61.0	8	7	216	PITII67.NDE	300	0.35	3.14	8328.8	0.475	8168.8	0.517	8323.9	0.487	8285.1	0.447	8348.1	0.456	8275.4	0.451	8302.9	8.3	0.452	68.5
VA21a	20.3	8	7	216	PITII68.NDE	300	0.35	3.14	4712.9	0.260	4746.6	0.251	4761.6	0.254	4797.0	0.253	4748.0	0.252	4752.6	0.247	4765.9	4.8	0.251	70.8

HPC	20.3	1	6	0	PIII1.NDE	300	0.35	4.00	4775.3	0.932	4766.0	1.029	4734.5	1.033	4706.1	1.084	4666.2	1.119	4654.3	1.088	4675.5	4.7	1.097	12.5
HPC	48.3	1	6	0	PIII2.NDE	300	0.35	4.00	7730.0	1.371	7831.8	1.391	7861.0	1.397	7873.1	1.407	7902.1	1.407	7868.3	1.441	7881.1	7.9	1.419	16.3
HPC	20.3	1	6	0	PIII3.NDE	300	0.35	4.00	4835.6	1.044	4904.7	1.178	4966.0	1.190	4951.2	1.109	4906.1	1.152	4959.4	1.210	4938.9	4.9	1.157	12.5
HPC	20.3	1	7	0	PIII4.NDE	300	0.35	4.00	4570.2	1.327	4548.3	1.171	4574.8	1.175	4565.3	1.234	4662.5	1.190	4606.5	1.122	4611.4	4.6	1.182	11.4
HPC	48.3	1	7	0	PIII5.NDE	300	0.35	4.00	7305.9	1.513	7267.1	1.602	7153.2	2.157	7078.0	1.754	7223.5	1.692	7240.4	1.948	7180.6	7.2	1.798	11.7
HPC	20.3	1	7	0	PIII6.NDE	300	0.35	4.00	4433.1	1.337	4357.8	1.575	4434.2	1.349	4450.0	1.318	4528.2	1.193	4454.8	1.204	4477.6	4.5	1.238	10.6
HPC	48.3	2	D	65	PIII7.NDE	300	0.35	4.00	8098.5	0.872	8127.5	0.952	7996.7	0.942	8239.1	0.955	8164.0	0.956	8142.1	0.949	8181.7	8.2	0.953	25.1
HPC	48.3	2	E	65	PIII8.NDE	300	0.35	4.00	8304.5	0.891	8290.0	1.290	8248.7	1.100	8236.6	1.078	8256.0	1.134	8309.4	1.097	8267.3	8.3	1.103	21.9
HPC	48.3	2	F	65	PIII0.NDE	300	0.35	4.00	8091.2	1.057	8256.0	0.908	7991.8	0.924	8270.6	0.946	8287.5	0.878	8309.4	0.854	8289.1	8.3	0.893	27.2
HPC	48.3	4	A	0	PIII9.NDE	300	0.35	4.00	8767.5	1.196	8549.4	1.001	8532.3	0.975	8515.4	0.948	8433.0	0.938	8447.6	0.923	8465.3	8.5	0.936	26.4
HPC	48.3	4	B	0	PIII10.NDE	300	0.35	4.00	8896.0	1.318	8578.4	1.082	8893.5	1.111	8740.8	1.054	8399.0	1.007	8343.3	0.981	8494.4	8.5	1.014	24.5
HPC	48.3	4	C	0	PIII11.NDE	300	0.35	4.00	8942.0	1.592	8520.2	1.129	8532.3	1.064	8493.5	1.024	8583.3	1.017	8496.0	0.999	8524.3	8.5	1.013	24.6
HPC	20.3	5	2	0	PIII12.NDE	300	0.35	4.00	4899.1	0.700	4977.6	0.696	5058.3	0.707	5010.9	0.710	4993.2	0.773	4982.7	0.717	4995.6	5.0	0.733	20.0
HPC	48.3	5	2	0	PIII13.NDE	300	0.35	4.00	7674.3	0.924	7613.7	0.880	7582.2	0.852	7528.8	0.864	7574.9	0.813	7616.1	0.827	7573.3	7.6	0.835	26.6
HPC	20.3	5	2	0	PIII14.NDE	300	0.35	4.00	5006.7	0.691	4832.9	0.694	4950.0	0.707	5071.4	0.725	5064.1	0.727	5063.5	0.727	5066.3	5.1	0.726	20.4
HPC	20.3	5	6	0	PIII15.NDE	300	0.35	4.00	5148.0	1.813	4713.2	0.623	4647.2	0.567	4657.9	0.547	4621.3	0.531	4628.6	0.548	4635.9	4.6	0.542	25.0
HPC	48.3	5	6	0	PIII16.NDE	300	0.35	4.00	7465.8	0.766	7393.1	0.753	7419.8	0.747	7318.0	0.733	7305.9	0.717	7133.8	0.732	7252.5	7.3	0.727	29.2
HPC	20.3	5	6	0	PIII17.NDE	300	0.35	4.00	4753.2	0.538	4568.3	0.527	4576.0	0.544	4622.5	0.547	4684.6	0.556	4654.3	0.543	4653.8	4.7	0.549	24.8
HPC	20.3	5	7	0	PIII18.NDE	300	0.35	4.00	4923.5	0.892	4644.5	0.624	4654.3	0.593	4674.1	0.578	4602.6	0.561	4652.4	0.559	4643.0	4.6	0.566	24.0
HPC	48.3	5	7	0	PIII19.NDE	300	0.35	4.00	7468.3	0.840	7485.2	0.815	7434.3	0.809	7504.6	0.801	7473.1	0.788	7504.6	0.744	7494.1	7.5	0.778	28.2
HPC	20.3	5	7	0	PIII20.NDE	300	0.35	4.00	4626.9	0.561	4659.1	0.551	4633.6	0.547	4645.1	0.549	4617.2	0.540	4648.9	0.538	4637.1	4.6	0.543	25.0
VA21a	20.3	6	2	0	PIII21.NDE	300	0.35	3.14	4760.5	0.729	4588.8	0.427	4613.0	0.385	4641.2	0.369	4510.5	0.378	4648.2	0.365	4600.0	4.6	0.371	46.2
VA21a	48.3	6	2	0	PIII22.NDE	300	0.35	3.14	7376.1	0.492	7342.2	0.517	7410.1	0.510	7436.8	0.510	7431.9	0.512	7446.4	0.511	7438.4	7.4	0.511	54.2
VA21a	61.0	6	2	0	PIII23.NDE	300	0.35	3.14	8314.2	0.550	8350.6	0.553	8389.4	0.557	8520.2	0.540	8357.9	0.555	8500.8	0.553	8459.6	8.5	0.549	57.4
VA21a	20.3	6	2	0	PIII24.NDE	300	0.35	3.14	4622.5	0.373	4686.8	0.357	4697.9	0.356	4608.6	0.350	4639.5	0.351	4658.6	0.345	4635.6	4.6	0.349	49.5
VA21a	20.3	6	6	0	PIII25.NDE	300	0.35	3.14	4584.4	0.587	4686.5	0.384	4696.4	0.359	4685.3	0.362	4683.3	0.358	4642.8	0.348	4670.5	4.7	0.356	48.9
VA21a	48.3	6	6	0	PIII26.NDE	300	0.35	3.14	7407.6	0.473	7414.9	0.497	7417.4	0.496	7334.9	0.494	7533.6	0.498	7536.1	0.490	7468.2	7.5	0.494	56.3
VA21a	61.0	6	6	0	PIII27.NDE	300	0.35	3.14	8353.0	0.522	8420.9	0.517	8406.3	0.514	8365.1	0.510	8433.0	0.501	8469.3	0.504	8422.5	8.4	0.505	62.1
VA21a	20.3	6	6	0	PIII28.NDE	300	0.35	3.14	4725.5	0.341	4782.0	0.336	4621.8	0.329	4754.9	0.341	4689.6	0.324	4712.1	0.329	4718.9	4.7	0.331	53.1
VA21a	20.3	6	7	0	PIII29.NDE	300	0.35	3.14	5004.8	1.299	4841.9	0.862	5090.6	0.930	5002.6	0.910	4904.9	0.734	4497.2	0.611	4801.6	4.8	0.752	24.3
VA21a	48.3	6	7	0	PIII30.NDE	300	0.35	3.14	7327.6	0.687	7347.0	0.717	7342.2	0.697	7400.4	0.633	7395.5	0.631	7422.2	0.597	7406.0	7.4	0.620	44.5
VA21a	61.0	6	7	0	PIII31.NDE	300	0.35	3.14	8205.1	0.632	8311.8	0.641	8355.4	0.603	8377.2	0.589	8399.0	0.603	8374.8	0.631	8383.7	8.4	0.607	51.4
VA21a	20.3	6	7	0	PIII32.NDE	300	0.35	3.14	4679.3	0.463	4536.0	0.479	4652.8	0.499	4698.1	0.521	4794.1	0.542	4668.5	0.505	4720.3	4.7	0.523	33.7
VA21a	20.3	6	2	1.5	PIII33.NDE	300	0.35	3.14	4651.6	1.463	4827.3	0.882	4697.7	0.779	4923.5	0.708	4897.6	0.658	4811.4	0.622	4877.5	4.9	0.663	27.5
VA21a	48.3	6	2	1.5	PIII34.NDE	300	0.35	3.14	7458.5	0.882	7560.3	0.842	7446.4	0.842	7407.6	0.807	7424.6	0.787	7427.0	0.704	7419.8	7.4	0.766	36.2
VA21a	61.0	6	2	1.5	PIII35.NDE	300	0.35	3.14	8496.0	0.767	8377.2	0.735	8406.3	0.725	8374.8	0.718	8343.3	0.700	8403.9	0.695	8374.0	8.4	0.704	44.3
VA21a	20.3	6	2	1.5	PIII36.NDE	300	0.35	3.14	4628.8	0.557	4731.5	0.562	4625.1	0.552	4694.0	0.566	4741.5	0.554	4736.1	0.543	4723.9	4.7	0.554	31.7

VA21a	20.3	6	6	1.5	PIII37.NDE	300	0.35	3.14	5020.1	1.676	4707.3	0.704	4715.6	0.605	4756.3	0.573	4604.4	0.520	4647.0	0.527	4669.2	4.7	0.540	32.2
VA21a	48.3	6	6	1.5	PIII38.NDE	300	0.35	3.14	7482.8	0.708	7458.5	0.704	7524.0	0.720	7288.8	0.759	7313.1	0.643	7332.5	0.650	7311.5	7.3	0.684	40.1
VA21a	61.0	6	6	1.5	PIII39.NDE	300	0.35	3.14	8370.0	0.653	8365.1	0.728	8396.6	0.658	8462.0	0.596	8323.9	0.619	8319.1	0.580	8368.4	8.4	0.598	52.1
VA21a	20.3	6	6	1.5	PIII40.NDE	300	0.35	3.14	4682.4	0.442	4667.8	0.407	4773.8	0.417	4670.8	0.414	4670.3	0.412	4544.9	0.397	4628.6	4.6	0.408	42.3
VA21a	20.3	6	7	1.5	PIII41.NDE	300	0.35	3.14	4731.5	1.609	4854.8	0.857	4811.8	0.755	4750.0	0.720	4759.7	0.718	4726.0	0.632	4745.2	4.7	0.690	25.7
VA21a	48.3	6	7	1.5	PIII42.NDE	300	0.35	3.14	7393.1	0.735	7395.5	0.766	7339.8	0.763	7407.6	0.726	7318.0	0.751	7354.3	0.712	7360.0	7.4	0.730	37.6
VA21a	61.0	6	7	1.5	PIII43.NDE	300	0.35	3.14	8265.8	0.689	8323.9	0.678	8311.8	0.698	8333.6	0.764	8403.9	0.723	8386.9	0.715	8374.8	8.4	0.734	42.5
VA21a	20.3	6	7	1.5	PIII44.NDE	300	0.35	3.14	4612.3	0.553	4660.1	0.605	4648.2	0.520	4614.5	0.566	4680.6	0.569	4645.8	0.591	4647.0	4.6	0.575	30.1
VA21a	20.3	6	7&8	4	PIII45.NDE	300	0.35	3.14	4660.1	0.302	4662.2	0.293	4991.1	0.587	5094.6	0.619	5682.2	0.747	4587.6	0.430	5121.5	5.1	0.599	32.9
VA21a	48.3	6	7&8	4	PIII46.NDE	300	0.35	3.14	7393.1	0.391	7354.3	0.395	7322.8	0.393	7339.8	0.408	7334.9	0.404	7354.3	0.404	7343.0	7.3	0.405	67.5
VA21a	61.0	6	7&8	4	PIII47.NDE	300	0.35	3.14	8294.8	0.414	8338.5	0.423	8416.0	0.435	8396.6	0.439	8348.1	0.438	8294.8	0.444	8346.5	8.3	0.441	70.6
VA21a	20.3	6	7&8	4	PIII48.NDE	300	0.35	3.14	4661.0	0.295	4651.6	0.307	4690.2	0.293	4698.4	0.317	4673.4	0.286	4662.8	0.295	4678.2	4.7	0.299	58.3
VA21a	20.3	6	1&2	4	PIII49.NDE	300	0.35	3.14	5103.6	1.665	4658.6	0.542	4627.6	0.527	4626.9	0.476	4604.8	0.456	4559.3	0.433	4597.0	4.6	0.455	37.7
VA21a	48.3	6	1&2	4	PIII50.NDE	300	0.35	3.14	7490.0	0.567	7364.0	0.589	7344.6	0.567	7318.0	0.562	7296.1	0.558	7354.3	0.561	7322.8	7.3	0.560	48.7
VA21a	61.0	6	1&2	4	PIII51.NDE	300	0.35	3.14	8282.7	0.494	8292.4	0.531	8333.6	0.519	8403.9	0.527	8350.6	0.521	8304.5	0.483	8353.0	8.4	0.510	61.1
VA21a	20.3	6	1&2	4	PIII52.NDE	300	0.35	3.14	4735.0	0.370	4677.3	0.351	4671.8	0.348	4702.3	0.342	4695.0	0.346	4635.6	0.350	4677.6	4.7	0.346	50.4
VA21a	20.3	6	2	45	PIII53.NDE	300	0.35	3.14	4574.3	0.456	4600.0	0.459	4590.2	0.455	4549.5	0.453	4516.3	0.437	4578.9	0.440	4548.2	4.5	0.443	38.2
VA21a	48.3	6	2	45	PIII54.NDE	300	0.35	3.14	7361.6	0.497	7410.1	0.492	7414.9	0.497	7405.2	0.494	7431.9	0.495	7419.8	0.505	7418.9	7.4	0.498	55.5
VA21a	61.0	6	2	45	PIII55.NDE	300	0.35	3.14	8306.9	0.616	8440.3	0.610	8321.5	0.589	8273.0	0.671	8224.5	0.733	8229.3	0.753	8242.3	8.2	0.719	42.8
VA21a	20.3	6	2	45	PIII56.NDE	300	0.35	3.14	4545.6	0.453	4618.4	0.429	4609.2	0.427	4606.5	0.414	4627.8	0.404	4577.5	0.402	4603.9	4.6	0.407	42.2
VA21a	20.3	6	6	45	PIII57.NDE	300	0.35	3.14	4726.9	0.619	4685.8	0.509	4647.0	0.477	4645.3	0.477	4663.2	0.465	4681.4	0.471	4663.3	4.7	0.471	36.9
VA21a	48.3	6	6	45	PIII58.NDE	300	0.35	3.14	7373.7	0.572	7322.8	0.621	7424.6	0.617	7402.8	0.609	7395.5	0.577	7511.9	0.598	7436.8	7.4	0.594	46.6
VA21a	61.0	6	6	45	PIII59.NDE	300	0.35	3.14	8377.2	0.554	8435.4	0.575	8326.3	0.606	8243.9	0.616	8263.3	0.598	8243.9	0.592	8250.4	8.3	0.602	51.1
VA21a	20.3	6	6	45	PIII60.NDE	300	0.35	3.14	4600.0	0.516	4594.6	0.462	4603.6	0.452	4632.2	0.421	4653.8	0.423	4636.1	0.404	4640.7	4.6	0.416	41.6
VA21a	20.3	6	7	45	PIII61.NDE	300	0.35	3.14	4621.8	0.457	4627.1	0.450	4552.0	0.448	4624.7	0.443	4608.6	0.449	4624.2	0.438	4619.2	4.6	0.443	38.8
VA21a	48.3	6	7	45	PIII62.NDE	300	0.35	3.14	7402.8	0.546	7359.2	0.532	7381.0	0.563	7373.7	0.556	7364.0	0.554	7456.1	0.545	7397.9	7.4	0.552	49.9
VA21a	61.0	6	7	45	PIII63.NDE	300	0.35	3.14	8500.8	0.556	8534.8	0.571	8510.6	0.574	8517.9	0.594	8408.8	0.610	8469.3	0.613	8465.3	8.5	0.606	52.1
VA21a	20.3	6	7	45	PIII64.NDE	300	0.35	3.14	4619.6	0.467	4613.0	0.442	4653.5	0.435	4609.6	0.431	4594.2	0.431	4616.5	0.430	4606.8	4.6	0.431	39.8

Appendix 8

Zorn LWD data, Pits 1, 2, and 3

Soil type	Height	Pit	Lift	Loc	time after compaction	Test #	Date	time	Possoin's ratio	D1	D2	D3	D ave	A	E	CV in def
[-]	[cm]	[-]	[-]	[-]	[hr]	[-]	[-]	[-]	[-]	[mm]	[mm]	[mm]	[mm]	[-]	[MPa]	[%]
Stone	31.8	1	0	A	0	394	2015.07.17	14:01:29	0.35	0.555	0.535	0.526	0.539	3.141593	48.88	2.8%
Stone	72.4	1	0	A	0	395	2015.07.17	14:05:14	0.35	0.698	0.67	0.644	0.671	3.141593	39.26	4.0%
Stone	31.8	1	0	A	0	396	2015.07.17	14:06:18	0.35	0.449	0.444	0.435	0.443	3.141593	59.48	1.6%
Stone	72.4	1	0	B	0	397	2015.07.17	14:08:12	0.35	0.642	0.62	0.612	0.625	3.141593	42.15	2.5%
ALF	31.8	1	1	4	0	434	2015.07.22	13:36:56	0.35	1.458	1.418	1.379	1.418	3.141593	18.56	2.8%
ALF	72.4	1	1	4	0	435	2015.07.22	13:38:03	0.35	1.786	1.799	1.762	1.782	3.141593	14.77	1.1%
ALF	31.8	1	1	4	0	436	2015.07.22	13:38:58	0.35	1.259	1.266	1.259	1.261	3.141593	20.87	0.3%
ALF	31.8	1	2	A	0	452	2015.07.24	8:06:44	0.35	1.996	1.933	1.913	1.947	3.141593	13.52	2.2%
ALF	72.4	1	2	A	0	453	2015.07.24	8:07:23	0.35	2.648	2.828	2.796	2.757	3.141593	9.55	3.5%
ALF	31.8	1	2	A	0	454	2015.07.24	8:07:48	0.35	1.777	1.754	1.714	1.748	3.141593	15.06	1.8%
ALF	31.8	1	2	E	0	455	2015.07.24	8:12:21	0.35	1.909	1.813	1.768	1.830	3.141593	14.39	3.9%
ALF	72.4	1	2	E	0	456	2015.07.24	8:14:05	0.35	2.651	2.469	2.458	2.526	3.141593	10.42	4.3%
ALF	31.8	1	2	E	0	457	2015.07.24	8:14:36	0.35	1.714	1.685	1.665	1.688	3.141593	15.60	1.5%
ALF	31.8	1	3	3	2	467	2015.07.24	15:10:10	0.35	2.256	2.207	2.212	2.225	3.141593	11.83	1.2%
ALF	72.4	1	3	3	2	468	2015.07.24	15:11:14	0.35	3.5	3.531	3.546	3.526	3.141593	7.47	0.7%
ALF	31.8	1	3	3	2	469	2015.07.24	15:13:08	0.35	2.107	2.06	2.043	2.070	3.141593	12.72	1.6%
ALF	31.8	1	3	4	2	470	2015.07.24	15:17:09	0.35	2.449	2.378	2.356	2.394	3.141593	11.00	2.0%
ALF	72.4	1	3	4	2	471	2015.07.24	15:18:56	0.35	3.768	3.702	3.592	3.687	3.141593	7.14	2.4%
ALF	31.8	1	3	4	2	472	2015.07.24	15:19:34	0.35	2.183	2.18	2.201	2.188	3.141593	12.03	0.5%
ALF	31.8	1	3	8	2	473	2015.07.24	15:24:03	0.35	2.604	2.598	2.668	2.623	3.141593	10.04	1.5%
ALF	72.4	1	3	8	2	474	2015.07.24	15:25:41	0.35	4.348	4.169	4.075	4.197	3.141593	6.27	3.3%
ALF	31.8	1	3	8	2	475	2015.07.24	15:28:09	0.35	2.496	2.435	2.438	2.456	3.141593	10.72	1.4%
ALF	31.8	2	5	D	0	316	2015.07.13	10:36:49	0.35	2.161	2.129	2.136	2.142	3.141593	12.29	0.8%
ALF	72.4	2	5	D	0	317	2015.07.13	10:37:55	0.35	3.442	3.461	3.381	3.428	3.141593	7.68	1.2%
ALF	31.8	2	5	D	0	318	2015.07.13	10:38:51	0.35	2.149	2.125	2.135	2.136	3.141593	12.32	0.6%
ALF	31.8	2	5	B	0	319	2015.07.13	10:42:58	0.35	2.049	2.047	2.044	2.047	3.141593	12.86	0.1%
ALF	72.4	2	5	B	0	320	2015.07.13	10:44:15	0.35	3.275	3.273	3.267	3.272	3.141593	8.05	0.1%
ALF	31.8	2	5	B	0	321	2015.07.13	10:45:15	0.35	2.097	2.094	2.1	2.097	3.141593	12.56	0.1%
ALF	31.8	2	5	C	0	322	2015.07.13	10:47:10	0.35	2.085	2.079	2.042	2.069	3.141593	12.73	1.1%
ALF	72.4	2	5	C	0	323	2015.07.13	10:48:43	0.35	3.487	3.519	3.511	3.506	3.141593	7.51	0.5%
ALF	31.8	2	5	C	0	324	2015.07.13	10:52:29	0.35	2.104	2.076	2.062	2.081	3.141593	12.65	1.0%
ALF	31.8	2	6	3	0.5	325	2015.07.13	16:16:20	0.35	2.329	2.306	2.32	2.318	3.141593	11.36	0.5%
ALF	72.4	2	6	3	0.5	326	2015.07.13	16:19:37	0.35	3.736	3.746	3.714	3.732	3.141593	7.06	0.4%
ALF	31.8	2	6	3	0.5	327	2015.07.13	16:20:57	0.35	2.385	2.415	2.389	2.396	3.141593	10.99	0.7%
ALF	31.8	2	6	4	0.5	328	2015.07.13	16:24:31	0.35	2.834	2.826	2.836	2.832	3.141593	9.30	0.2%
ALF	72.4	2	6	4	0.5	329	2015.07.13	16:26:57	0.35	4.371	4.351	4.3	4.341	3.141593	6.07	0.8%
ALF	31.8	2	6	4	0.5	330	2015.07.13	16:27:55	0.35	2.753	2.738	2.809	2.767	3.141593	9.52	1.4%

ALF	31.8	2	6	8	0.5	331	2015.07.13	16:30:43	0.35	2.721	2.71	2.675	2.702	3.141593	9.74	0.9%
ALF	72.4	2	6	8	0.5	332	2015.07.13	16:33:04	0.35	4.262	4.328	4.339	4.310	3.141593	6.11	1.0%
ALF	31.8	2	6	8	0.5	333	2015.07.13	16:33:54	0.35	2.757	2.753	2.741	2.750	3.141593	9.57	0.3%
ALF	31.8	2	6	3	16	334	2015.07.14	7:33:23	0.35	1.85	1.831	1.822	1.834	3.141593	14.35	0.8%
ALF	72.4	2	6	3	16	335	2015.07.14	7:35:10	0.35	2.883	2.868	2.889	2.880	3.141593	9.14	0.4%
ALF	31.8	2	6	3	16	336	2015.07.14	7:36:29	0.35	1.915	1.887	1.911	1.904	3.141593	13.83	0.8%
ALF	31.8	2	6	4	16	337	2015.07.14	7:39:36	0.35	2.21	2.157	2.129	2.165	3.141593	12.16	1.9%
ALF	72.4	2	6	4	16	338	2015.07.14	7:41:28	0.35	3.293	3.288	3.311	3.297	3.141593	7.99	0.4%
ALF	31.8	2	6	4	16	339	2015.07.14	7:43:57	0.35	2.155	2.172	2.176	2.168	3.141593	12.15	0.5%
ALF	31.8	2	6	8	16	340	2015.07.14	7:46:36	0.35	2.424	2.44	2.375	2.413	3.141593	10.91	1.4%
ALF	72.4	2	6	8	16	341	2015.07.14	7:47:47	0.35	3.792	3.782	3.806	3.793	3.141593	6.94	0.3%
ALF	31.8	2	6	8	16	342	2015.07.14	7:49:35	0.35	2.494	2.451	2.47	2.472	3.141593	10.65	0.9%
ALF	31.8	2	6		21	343	2015.07.14	12:30:57	0.35	2.396	2.354	2.369	2.373	3.141593	11.10	0.9%
ALF	72.4	2	6		21	344	2015.07.14	12:31:42	0.35	3.509	3.587	3.547	3.548	3.141593	7.42	1.1%
ALF	31.8	2	6		21	345	2015.07.14	12:33:09	0.35	2.42	2.401	2.411	2.411	3.141593	10.92	0.4%
ALF	31.8	2	6		21	346	2015.07.14	12:40:44	0.35	2.291	2.241	2.234	2.255	3.141593	11.67	1.4%
ALF	72.4	2	6		21	347	2015.07.14	12:42:05	0.35	3.519	3.537	3.523	3.526	3.141593	7.47	0.3%
ALF	31.8	2	6		21	348	2015.07.14	12:42:51	0.35	2.185	2.165	2.157	2.169	3.141593	12.14	0.7%
ALF	31.8	2	6		21	349	2015.07.14	12:47:06	0.35	2.049	2.076	2.098	2.074	3.141593	12.69	1.2%
ALF	72.4	2	6		21	350	2015.07.14	12:47:58	0.35	3.439	3.45	3.418	3.436	3.141593	7.66	0.5%
ALF	31.8	2	6		21	351	2015.07.14	12:48:57	0.35	2.222	2.194	2.172	2.196	3.141593	11.99	1.1%
VA21a	31.8	2	7	B	16	354	2015.07.15	7:25:11	0.35	2.281	2.275	2.278	2.278	3.141593	11.56	0.1%
VA21a	72.4	2	7	B	16	355	2015.07.15	7:26:08	0.35	3.575	3.62	3.583	3.593	3.141593	7.33	0.7%
VA21a	31.8	2	7	B	16	356	2015.07.15	7:27:11	0.35	2.338	2.316	2.33	2.328	3.141593	11.31	0.5%
VA21a	31.8	2	7	C	16	357	2015.07.15	7:43:13	0.35	1.901	1.877	1.866	1.881	3.141593	14.00	1.0%
VA21a	72.4	2	7	C	16	358	2015.07.15	7:44:41	0.35	3.057	3.012	3.056	3.042	3.141593	8.66	0.8%
VA21a	31.8	2	7	C	16	359	2015.07.15	7:45:22	0.35	2.004	1.983	1.966	1.984	3.141593	13.27	1.0%
VA21a	31.8	2	8	3	1	360	2015.07.15	12:13:10	0.35	1.949	1.859	1.879	1.896	3.141593	13.89	2.5%
VA21a	72.4	2	8	3	1	361	2015.07.15	12:13:59	0.35	2.6	2.528	2.54	2.556	3.141593	10.30	1.5%
VA21a	31.8	2	8	3	1	362	2015.07.15	12:14:42	0.35	1.637	1.627	1.606	1.623	3.141593	16.22	1.0%
VA21a	31.8	2	8	4	1	363	2015.07.15	12:16:42	0.35	1.484	1.486	1.481	1.484	3.141593	17.75	0.2%
VA21a	72.4	2	8	4	1	364	2015.07.15	12:17:51	0.35	2.171	2.193	2.205	2.190	3.141593	12.02	0.8%
VA21a	31.8	2	8	4	1	365	2015.07.15	12:18:33	0.35	1.413	1.429	1.416	1.419	3.141593	18.55	0.6%
VA21a	31.8	2	8	8	1	366	2015.07.15	12:20:50	0.35	1.602	1.599	1.597	1.599	3.141593	16.46	0.2%
VA21a	72.4	2	8	8	1	367	2015.07.15	12:22:33	0.35	2.333	2.299	2.242	2.291	3.141593	11.49	2.0%
VA21a	31.8	2	8	8	1	368	2015.07.15	12:23:40	0.35	1.465	1.457	1.437	1.453	3.141593	18.12	1.0%
VA21a	31.8	2	8	3	4	369	2015.07.15	14:36:58	0.35	1.529	1.548	1.538	1.538	3.141593	17.12	0.6%
VA21a	72.4	2	8	3	4	370	2015.07.15	14:38:20	0.35	2.212	2.246	2.238	2.232	3.141593	11.80	0.8%
VA21a	31.8	2	8	3	4	371	2015.07.15	14:39:09	0.35	1.498	1.487	1.5	1.495	3.141593	17.61	0.5%
VA21a	31.8	2	8	4	4	372	2015.07.15	14:41:44	0.35	1.378	1.357	1.378	1.371	3.141593	19.21	0.9%
VA21a	72.4	2	8	4	4	373	2015.07.15	14:44:00	0.35	2.011	2.013	2.036	2.020	3.141593	13.03	0.7%

VA21a	31.8	2	8	4	4	374	2015.07.15	14:46:13	0.35	1.318	1.308	1.314	1.313	3.141593	20.05	0.4%
VA21a	31.8	2	8	8	4	375	2015.07.15	14:48:35	0.35	1.44	1.453	1.472	1.455	3.141593	18.10	1.1%
VA21a	72.4	2	8	8	4	376	2015.07.15	14:50:15	0.35	2.214	2.193	2.254	2.220	3.141593	11.86	1.4%
VA21a	31.8	2	8	8	4	377	2015.07.15	14:51:22	0.35	1.495	1.504	1.481	1.493	3.141593	17.63	0.8%
VA21a	72.4	2	8	3	122	402	2015.07.20	13:00:55	0.35	0.854	0.811	0.836	0.834	3.141593	31.58	2.6%
VA21a	31.8	2	8	3	216	458	2015.07.24	8:37:28	0.35	0.357	0.344	0.325	0.342	3.141593	76.99	4.7%
VA21a	72.4	2	8	3	216	459	2015.07.24	8:38:18	0.35	0.508	0.494	0.493	0.498	3.141593	52.84	1.7%
VA21a	31.8	2	8	3	216	460	2015.07.24	8:39:26	0.35	0.327	0.327	0.327	0.327	3.141593	80.52	0.0%
VA21a	31.8	2	8	4	216	461	2015.07.24	8:43:43	0.35	0.319	0.329	0.342	0.330	3.141593	79.79	3.5%
VA21a	72.4	2	8	4	216	462	2015.07.24	8:44:32	0.35	0.558	0.541	0.553	0.551	3.141593	47.82	1.6%
VA21a	31.8	2	8	4	216	463	2015.07.24	8:45:43	0.35	0.348	0.367	0.339	0.351	3.141593	74.94	4.1%
VA21a	31.8	2	8	8	216	464	2015.07.24	8:49:51	0.35	0.372	0.354	0.35	0.359	3.141593	73.41	3.3%
VA21a	72.4	2	8	8	216	465	2015.07.24	8:50:46	0.35	0.591	0.567	0.601	0.586	3.141593	44.91	3.0%
VA21a	31.8	2	8	8	216	466	2015.07.24	8:51:24	0.35	0.374	0.367	0.369	0.370	3.141593	71.16	1.0%
HPC	31.8	3	1	4	0	388	2015.07.17	10:47:30	0.35	1.254	1.278	1.276	1.269	4	16.29	1.0%
HPC	72.4	3	1	4	0	389	2015.07.17	10:48:46	0.35	1.751	1.743	1.745	1.746	4	11.84	0.2%
HPC	31.8	3	1	4	0	390	2015.07.17	10:50:41	0.35	1.279	1.263	1.264	1.269	4	16.30	0.7%
HPC	72.4	3	2	A	0	398	2015.07.17	16:20:47	0.35	2.318	2.339	2.151	2.269	4	9.11	4.5%
HPC	72.4	3	2	B	0	399	2015.07.17	16:22:18	0.35	1.315	1.296	1.249	1.287	4	16.07	2.6%
HPC	72.4	3	2	D	65	400	2015.07.20	8:45:56	0.35	1.434	1.441	1.433	1.436	4	14.40	0.3%
HPC	72.4	3	2	E	65	401	2015.07.20	9:28:00	0.35	1.433	1.413	1.413	1.420	4	14.57	0.8%
HPC	31.8	3	4	A	0	403	2015.07.20	15:10:18	0.35	1.306	1.28	1.228	1.271	4	16.27	3.1%
HPC	72.4	3	4	B	0	404	2015.07.20	15:12:45	0.35	1.23	1.279	1.264	1.258	4	16.44	2.0%
HPC	31.8	3	4	C	0	405	2015.07.20	15:15:45	0.35	1.072	1.059	1.038	1.056	4	19.58	1.6%
HPC	31.8	3	5	3	0	406	2015.07.21	11:07:32	0.35	0.842	0.83	0.85	0.841	4	24.60	1.2%
HPC	72.4	3	5	3	0	407	2015.07.21	11:08:40	0.35	1.13	1.14	1.147	1.139	4	18.16	0.8%
HPC	31.8	3	5	3	0	408	2015.07.21	11:09:22	0.35	0.836	0.826	0.825	0.829	4	24.95	0.7%
HPC	31.8	3	5	4	0	409	2015.07.21	11:12:38	0.35	0.919	0.872	0.864	0.885	4	23.37	3.4%
HPC	72.4	3	5	4	0	410	2015.07.21	11:14:27	0.35	1.158	1.137	1.127	1.141	4	18.13	1.4%
HPC	31.8	3	5	4	0	411	2015.07.21	11:15:16	0.35	0.802	0.794	0.788	0.795	4	26.02	0.9%
HPC	31.8	3	5	8	0	412	2015.07.21	11:17:19	0.35	1.008	0.975	0.968	0.984	4	21.02	2.2%
HPC	72.4	3	5	8	0	413	2015.07.21	11:18:02	0.35	1.222	1.203	1.194	1.206	4	17.14	1.2%
HPC	31.8	3	5	8	0	414	2015.07.21	11:22:25	0.35	0.857	0.859	0.86	0.859	4	24.08	0.2%
VA21a	31.8	3	6	3	0	416	2015.07.22	10:16:04	0.35	0.435	0.433	0.414	0.427	3.141593	61.62	2.7%
VA21a	72.4	3	6	3	0	417	2015.07.22	10:17:07	0.35	0.55	0.544	0.535	0.543	3.141593	48.49	1.4%
VA21a	31.8	3	6	3	0	418	2015.07.22	10:18:14	0.35	0.374	0.389	0.372	0.378	3.141593	69.60	2.5%
VA21a	31.8	3	6	4	0	419	2015.07.22	10:21:55	0.35	0.586	0.568	0.539	0.564	3.141593	46.66	4.2%
VA21a	72.4	3	6	4	0	420	2015.07.22	10:22:34	0.35	0.694	0.694	0.664	0.684	3.141593	38.49	2.5%
VA21a	31.8	3	6	4	0	421	2015.07.22	10:25:12	0.35	0.465	0.454	0.446	0.455	3.141593	57.87	2.1%
VA21a	31.8	3	6	8	0	422	2015.07.22	10:28:50	0.35	0.474	0.463	0.458	0.465	3.141593	56.62	1.8%

VA21a	72.4	3	6	8	0	423	2015.07.22	10:29:31	0.35	0.605	0.612	0.607	0.608	3.141593	43.31	0.6%
VA21a	31.8	3	6	8	0	424	2015.07.22	10:30:22	0.35	0.421	0.421	0.424	0.422	3.141593	62.39	0.4%
VA21a	31.8	3	6	3		425	2015.07.22	12:40:50	0.35	0.477	0.466	0.452	0.465	3.141593	56.62	2.7%
VA21a	72.4	3	6	3		426	2015.07.22	12:42:05	0.35	0.59	0.586	0.58	0.585	3.141593	44.98	0.9%
VA21a	31.8	3	6	3		427	2015.07.22	12:43:30	0.35	0.41	0.417	0.414	0.414	3.141593	63.65	0.8%
VA21a	31.8	3	6	4		428	2015.07.22	12:45:21	0.35	0.635	0.623	0.597	0.618	3.141593	42.58	3.1%
VA21a	72.4	3	6	4		429	2015.07.22	12:47:26	0.35	0.717	0.671	0.675	0.688	3.141593	38.29	3.7%
VA21a	31.8	3	6	4		430	2015.07.22	12:49:40	0.35	0.479	0.484	0.48	0.481	3.141593	54.74	0.6%
VA21a	31.8	3	6	8		431	2015.07.22	12:52:27	0.35	0.679	0.65	0.616	0.648	3.141593	40.61	4.9%
VA21a	72.4	3	6	8		432	2015.07.22	12:53:20	0.35	0.782	0.758	0.734	0.758	3.141593	34.74	3.2%
VA21a	31.8	3	6	8		433	2015.07.22	12:54:08	0.35	0.525	0.515	0.5	0.513	3.141593	51.29	2.5%
VA21a	31.8	3	6	7-8	4	437	2015.07.22	15:21:41	0.35	0.393	0.388	0.373	0.385	3.141593	68.45	2.7%
VA21a	72.4	3	6	7-8	4	438	2015.07.22	15:22:42	0.35	0.5	0.488	0.487	0.492	3.141593	53.55	1.5%
VA21a	31.8	3	6	7-8	4	439	2015.07.22	15:24:25	0.35	0.348	0.345	0.339	0.344	3.141593	76.54	1.3%
VA21a	31.8	3	6	1-2	4	440	2015.07.22	15:28:09	0.35	0.528	0.487	0.481	0.499	3.141593	52.80	5.1%
VA21a	72.4	3	6	1-2	4	441	2015.07.22	15:28:54	0.35	0.606	0.596	0.613	0.605	3.141593	43.52	1.4%
VA21a	31.8	3	6	1-2	4	442	2015.07.22	15:29:23	0.35	0.436	0.441	0.436	0.438	3.141593	60.16	0.7%
VA21a	31.8	3	6	3	45	443	2015.07.24	7:47:24	0.35	0.426	0.431	0.422	0.426	3.141593	61.76	1.1%
VA21a	72.4	3	6	3	45	444	2015.07.24	7:49:06	0.35	0.564	0.536	0.53	0.543	3.141593	48.46	3.3%
VA21a	31.8	3	6	3	45	445	2015.07.24	7:50:10	0.35	0.384	0.38	0.396	0.387	3.141593	68.10	2.2%
VA21a	31.8	3	6	4	45	446	2015.07.24	7:55:28	0.35	0.543	0.52	0.505	0.523	3.141593	50.38	3.7%
VA21a	72.4	3	6	4	45	447	2015.07.24	7:58:41	0.35	0.669	0.661	0.641	0.657	3.141593	40.08	2.2%
VA21a	31.8	3	6	4	45	448	2015.07.24	7:59:14	0.35	0.462	0.448	0.457	0.456	3.141593	57.78	1.6%
VA21a	31.8	3	6	8	45	449	2015.07.24	8:00:27	0.35	0.469	0.463	0.449	0.460	3.141593	57.20	2.2%
VA21a	72.4	3	6	8	45	450	2015.07.24	8:01:52	0.35	0.594	0.596	0.595	0.595	3.141593	44.25	0.2%
VA21a	31.8	3	6	8	45	451	2015.07.24	8:02:26	0.35	0.436	0.426	0.425	0.429	3.141593	61.38	1.4%

Appendix 9

Resilient Modulus test data

Sample ID	[-]	HPC_01	HPC_01 (base)	HPC_02	HPC_02 (base)	HPC__All Pit 3	HPC__Ave Pit 3
Achieved MC	[%]	30.5%	30.5%	31.1%	31.1%	30.8%	30.8%
Achieved DD	[pcf]	89.9	89.9	88.9	88.9	89.4	89.4
	[kg/m3]	1440.4	1440.4	1423.8	1423.8	1432.1	1432.1
Pa	[kPa]	101.3	101.3	101.3	101.3	101.3	101.3
k1	[-]	600.6	572.5	603.8	779.0	583.2	583.4
k2	[-]	0.086	0.157	0.015	0.131	0.094	0.095
k3	[-]	-2.262	-1.820	-2.160	-2.342	-1.788	-1.789
SSE	[MPa^2]	14.2	4.4	38.9	4.6	822.5	259.0
Sqr(SSE)	[MPa]	3.8	2.1	6.2	2.1	28.7	16.09
R^2	[MPa^2]	98.0%	97.7%	94.9%	99.5%	70.6%	81.0%
R^2_adj	[MPa^2]	97.4%	95.4%	93.5%	99.1%	68.6%	78.3%
Max Sample-to-Sample CV of M_R at a given stress state	[%]						18.7%
Average Sample-to-Sample CV of M_R at a given stress state	[%]						5.3%

Sample ID	[-]	HPC_04	HPC_04 (base)	HPC_05	HPC_05 (base)	HPC__All OPT	HPC__Ave OPT
Achieved MC	[%]	23.8%	23.8%	25.2%	25.2%	24.5%	24.5%
Achieved DD	[pcf]	93.6	93.6	93.6	93.6	93.6	93.6
	[kg/m3]	1499.7	1499.7	1498.7	1498.7	1499.2	1499.2
Pa	[kPa]	101.3	101.3	101.3	101.3	101.3	101.3
k1	[-]	908.2	1017.2	896.8	1065.5	888.7	888.8
k2	[-]	0.150	0.325	0.101	0.388	0.378	0.378
k3	[-]	-1.105	-0.926	-0.799	-1.186	-0.841	-0.843
SSE	[MPa^2]	117.0	348.4	22.6	223.1	4766.3	2261.6
Sqr(SSE)	[MPa]	10.8	18.7	4.7	14.9	69.0	47.56
R^2	[MPa^2]	81.1%	86.2%	92.2%	93.7%	67.7%	26.8%
R^2_adj	[MPa^2]	75.9%	82.4%	90.1%	92.0%	66.1%	16.4%
Max Sample-to-Sample CV of M_R at a given stress state	[%]						6.4%
Average Sample-to-Sample CV of M_R at a given stress state	[%]						2.4%

Sample ID	[-]	VA21a_ 01	VA21a_ 02	VA21a__All OMC	VA21a__Ave OMC
Achieved MC	[%]	4.0%	3.4%	3.7%	3.7%
Achieved DD	[pcf]	156.4	150.5	153.4	153.4
	[kg/m3]	2505.4	2410.6	2458.0	2458.0
Pa	[kPa]	101.3	101.3	101.3	101.3
k1	[-]	522.1	701.5	599.2	590.6
k2	[-]	0.912	0.745	0.815	0.824
k3	[-]	-0.061	0.000	0.000	0.000
SSE	[MPa^2]	1011.7	4771.5	12628.2	2765.0
Sqr(SSE)	[MPa]	31.8	69.1	112.4	52.58
R^2	[MPa^2]	98.9%	93.8%	92.6%	96.6%
R^2_adj	[MPa^2]	98.5%	92.1%	91.8%	95.7%
Max Sample-to-Sample CV of M_R at a given stress state	[%]				47.9%
Average Sample-to-Sample CV of M_R at a given stress state	[%]				17.6%

Sample ID	[-]	ALF_01	ALF_02	ALF_03	ALF__all OPT	ALF__ave OPT
Achieved MC	[%]	12.0%	12.2%	11.4%	11.9%	11.9%
Achieved DD	[pcf]	118.3	117.9	120.4	118.9	118.9
	[kg/m3]	1895.4	1888.9	1928.5	1904.3	1904.3
Pa	[kPa]	101.3	101.3	101.3	101.3	101.3
k1	[-]	1369.1	2041.3	1430.7	1439.5	1437.4
k2	[-]	0.609	0.275	0.366	0.425	0.429
k3	[-]	-4.584	-4.528	-3.579	-3.727	-3.717
SSE	[MPa^2]	543.1	374.1	272.4	7747.0	131.6
Sqr(SSE)	[MPa]	23.3	19.3	16.5	88.0	11.5
R^2	[MPa^2]	93.6%	94.0%	95.0%	70.0%	98.1%
R^2_adj	[MPa^2]	91.8%	91.7%	93.6%	67.8%	97.6%
Max Sample-to-Sample CV of M_R at a given stress state	[%]					32.5%
Average Sample-to-Sample CV of M_R at a given stress state	[%]					16.2%

Sample ID	[-]	ALF_04	ALF_05	ALF__all OPT_4 hr*	ALF__aveOPT_4 hr*
Achieved MC	[%]	10.8%	11.8%	11.3%	11.3%
Achieved DD	[pcf]	119.2	118.8	119.0	119.0
	[kg/m3]	1908.7	1903.3	1906.0	1906.0
Pa	[kPa]	101.3	101.3	101.3	101.3
k1	[-]	1248.1	606.2	927.1	927.1
k2	[-]	0.444	0.021	0.232	0.232
k3	[-]	-3.375	-1.140	-2.257	-2.257
SSE	[MPa^2]	175.2	67.6	7070.0	209.2
Sqr(SSE)	[MPa]	13.2	8.2	84.08	14.46
R^2	[MPa^2]	96.4%	80.0%	41.5%	89.2%
R^2_adj	[MPa^2]	95.4%	74.6%	34.4%	86.5%
Max Sample-to-Sample CV of M_R at a given stress state	[%]				52.8%
Average Sample-to-Sample CV of M_R at a given stress state	[%]				29.6%

* Solver doesn't converge

Sample ID	[-]	ALF_07	ALF_07 (base)	ALF_08	ALF_08 (base)	ALF__all Pit 2	ALF__ave Pit 2
Achieved MC	[%]	14.4%	14.4%	14.9%	14.9%	14.6%	14.6%
Achieved DD	[pcf]	116.5	116.5	116.6	116.6	116.5	116.5
	[kg/m3]	1866.1	1866.1	1867.8	1867.8	1867.0	1867.0
Pa	[kPa]	101.3	101.3	101.3	101.3	101.3	101.3
k1	[-]	215.0	264.8	171.3	190.8	178.5	177.6
k2	[-]	0.000	0.646	0.000	0.811	0.487	0.485
k3	[-]	-0.494	-0.936	0.000	-0.925	0.000	0.000
SSE	[MPa^2]	57.9	4.5	53.7	6.3	983.1	384.1
Sqr(SSE)	[MPa]	7.6	2.1	7.3	2.5	31.4	19.60
R^2	[MPa^2]	10.6%	98.4%	0.0%	98.1%	61.8%	58.7%
R^2_adj	[MPa^2]	-16.2%	97.2%	-27.3%	96.7%	59.4%	52.8%
Max Sample-to-Sample CV of M_R at a given stress state	[%]						27.9%
Average Sample-to-Sample CV of M_R at a given stress state	[%]						13.2%

Sample ID	[-]	ALF_10	ALF_MC 7%_PC85%
Achieved MC	[%]	7.3%	7.3%
Achieved DD	[pcf]	104.3	104.3
	[kg/m3]	1670.6	1670.6
Pa	[kPa]	101.3	101.3
k1	[-]	1233.4	1233.4
k2	[-]	0.313	0.313
k3	[-]	-3.212	-3.212
SSE	[MPa^2]	818.1	818.1
Sqr(SSE)	[MPa]	28.6	28.6
R^2	[MPa^2]	83.5%	83.5%
R^2_adj	[MPa^2]	79.1%	79.1%
Max Sample-to-Sample CV of M_R at a given stress state	[%]		
Average Sample-to-Sample CV of M_R at a given stress state	[%]		

Sample ID	[-]	ALF_11	ALF_12	ALF_12 (base)	ALF_all~Pit1	ALF_ave~Pit1
Achieved MC	[%]	8.9%	9.9%	9.9%	9.4%	9.4%
Achieved DD	[pcf]	111.2	110.0	110.0	110.6	110.6
	[kg/m3]	1781.0	1761.3	1761.3	1771.2	1771.2
Pa	[kPa]	101.3	101.3	101.3	101.3	101.3
k1	[-]	967.8	966.7	592.3	673.2	793.9
k2	[-]	0.380	0.451	0.665	0.620	0.601
k3	[-]	-3.105	-3.102	-0.948	-1.171	-2.023
SSE	[MPa^2]	295.7	191.1	972.3	5919.7	1635.8
Sqr(SSE)	[MPa]	17.2	13.8	31.2	76.9	40.44
R^2	[MPa^2]	89.7%	93.3%	88.5%	69.4%	66.2%
R^2_adj	[MPa^2]	86.8%	91.5%	85.3%	67.3%	61.4%
Max Sample-to-Sample CV of M_R at a given stress state	[%]					5.0%
Average Sample-to-Sample CV of M_R at a given stress state	[%]					1.8%

HPC_01	Target		Measured								
Sequence	Confining pressure [kPa]	Maximum axial stress [kPa]	Confining pressure [kPa]	Maximum axial stress [kPa]	Cyclic stress [kPa]	Contact stress [kPa]	MR [MPa]	Last 5 cycles Mr_Sd [MPa]	Last 5 cycles CV [%]	First invariant (θ) [kPa]	Second invariant (τ) [kPa]
0	41.4	27.6	42.5	27.7	24.4	3.3	48.2	0.1	0.28%	155.3	13.1
1	41.4	13.8	43.0	14.0	12.0	2.1	55.9	0.6	1.06%	143.0	6.6
2	41.4	27.6	42.6	27.8	24.5	3.3	48.9	0.2	0.40%	155.5	13.1
3	41.4	41.4	42.7	41.6	36.9	4.8	42.2	0.2	0.40%	169.6	19.6
4	41.4	55.2	42.5	55.5	49.4	6.1	36.4	0.1	0.27%	183.0	26.2
5	41.4	68.9	42.6	69.3	61.8	7.4	32.7	0.1	0.16%	197.0	32.7
6	27.6	13.8	29.0	13.9	12.1	1.9	51.6	0.6	1.24%	101.1	6.6
7	27.6	27.6	29.1	27.8	24.5	3.3	46.3	0.3	0.75%	115.0	13.1
8	27.6	41.4	29.1	41.5	36.9	4.6	41.5	0.2	0.44%	128.7	19.6
9	27.6	55.2	29.0	55.3	49.3	6.0	37.6	0.1	0.15%	142.2	26.1
10	27.6	68.9	29.0	69.1	61.8	7.3	34.3	0.0	0.11%	156.1	32.6
11	13.8	13.8	15.6	13.9	12.0	1.9	49.8	0.6	1.18%	60.7	6.6
12	13.8	27.6	15.7	27.7	24.5	3.2	45.1	0.3	0.65%	74.7	13.1
13	13.8	41.4	15.6	41.4	36.8	4.6	40.8	0.1	0.27%	88.3	19.5
14	13.8	55.2	15.7	55.2	49.3	5.9	37.1	0.1	0.19%	102.2	26.0
15	13.8	68.9	15.6	69.1	61.7	7.4	34.1	0.1	0.23%	116.0	32.6

HPC_01 (base)	Target		Measured								
Sequence	**Confining pressure [kPa]**	**Maximum axial stress [kPa]**	**Confining pressure [kPa]**	**Maximum axial stress [kPa]**	**Cyclic stress [kPa]**	**Contact stress [kPa]**	**MR [MPa]**	**Last 5 cycles Mr_Sd [MPa]**	**Last 5 cycles CV [%]**	**First invariant (θ) [kPa]**	**Second invariant (τ) [kPa]**
0	103.4	103.4	103.9	104.0	92.8	11.2	33.9	0.0	0.12%	415.7	49.0
1	20.7	20.7	22.3	20.8	18.2	2.6	46.8	0.2	0.52%	87.8	9.8
2	20.7	41.4	22.3	41.5	36.8	4.7	42.9	0.1	0.19%	108.4	19.5
3	20.7	62.1	22.2	62.4	55.7	6.7	37.9	0.2	0.41%	129.1	29.4
4	34.5	34.5	35.7	34.7	30.6	4.0	47.9	0.2	0.51%	141.8	16.3
5	34.5	68.9	35.8	69.1	61.6	7.5	38.5	0.1	0.13%	176.6	32.6
6	34.5	103.4	35.8	103.7	92.8	10.9	31.7	0.0	0.08%	211.0	48.9
7	68.9	68.9	69.8	69.3	61.7	7.6	40.0	0.1	0.22%	278.6	32.6
8	68.9	137.9	Test terminated due to excess permanent deformation.								
9	68.9	206.8									
10	103.4	68.9									
11	103.4	103.4									
12	103.4	206.8									
13	137.9	103.4									
14	137.9	137.9									
15	137.9	275.8									

HPC_02	Target		Measured								
Sequence	Confining pressure [kPa]	Maximum axial stress [kPa]	Confining pressure [kPa]	Maximum axial stress [kPa]	Cyclic stress [kPa]	Contact stress [kPa]	MR [MPa]	Last 5 cycles Mr_Sd [MPa]	Last 5 cycles CV [%]	First invariant (θ) [kPa]	Second invariant (τ) [kPa]
0	41.4	27.6	42.6	27.9	24.5	3.4	46.1	0.2	0.53%	155.7	13.1
1	41.4	13.8	42.7	13.9	11.9	2.0	57.0	0.9	1.51%	142.0	6.6
2	41.4	27.6	42.5	27.9	24.5	3.4	47.8	0.1	0.20%	155.4	13.1
3	41.4	41.4	42.6	41.6	36.9	4.7	39.8	0.1	0.19%	169.4	19.6
4	41.4	55.2	42.6	55.4	49.3	6.1	34.9	0.1	0.17%	183.2	26.1
5	41.4	68.9	42.8	69.2	61.7	7.5	32.1	0.0	0.15%	197.6	32.6
6	27.6	13.8	28.9	13.9	12.0	1.9	52.3	0.2	0.37%	100.7	6.6
7	27.6	27.6	29.0	27.8	24.4	3.4	46.9	0.4	0.77%	114.7	13.1
8	27.6	41.4	29.0	41.5	36.8	4.7	42.1	0.1	0.22%	128.6	19.6
9	27.6	55.2	29.0	55.3	49.2	6.1	38.3	0.1	0.18%	142.2	26.1
10	27.6	68.9	29.2	69.0	61.6	7.4	34.8	0.1	0.20%	156.7	32.5
11	13.8	13.8	15.6	13.8	11.9	1.9	51.3	0.6	1.15%	60.7	6.5
12	13.8	27.6	15.7	27.6	24.3	3.3	46.9	0.1	0.28%	74.6	13.0
13	13.8	41.4	15.6	41.6	37.0	4.5	42.6	0.2	0.36%	88.5	19.6
14	13.8	55.2	15.7	55.4	49.3	6.0	38.7	0.1	0.32%	102.3	26.1
15	13.8	68.9	15.7	69.0	61.7	7.3	35.4	0.1	0.21%	116.0	32.5

HPC_02 (base)	Target		Measured								
Sequence	**Confining pressure [kPa]**	**Maximum axial stress [kPa]**	**Confining pressure [kPa]**	**Maximum axial stress [kPa]**	**Cyclic stress [kPa]**	**Contact stress [kPa]**	**MR [MPa]**	**Last 5 cycles Mr_Sd [MPa]**	**Last 5 cycles CV [%]**	**First invariant (θ) [kPa]**	**Second invariant (τ) [kPa]**
0	103.4	103.4	103.9	105.1	92.8	12.3	38.5	0.0	0.09%	416.8	49.5
1	20.7	20.7	22.3	21.8	18.2	3.7	61.0	0.4	0.67%	88.8	10.3
2	20.7	41.4	22.3	42.6	36.9	5.7	52.2	0.1	0.19%	109.5	20.1
3	20.7	62.1	22.1	63.3	55.5	7.8	44.1	0.1	0.16%	129.8	29.9
4	34.5	34.5	35.8	35.7	30.7	5.0	58.6	0.1	0.17%	143.2	16.9
5	34.5	68.9	35.8	70.2	61.7	8.5	44.6	0.1	0.15%	177.7	33.1
6	34.5	103.4	35.7	104.7	92.8	11.9	35.3	0.0	0.06%	211.9	49.4
7	68.9	68.9	69.8	70.4	61.8	8.6	45.7	0.1	0.14%	279.8	33.2
8	68.9	137.9	69.8	139.7	124.2	15.4	27.8	0.0	0.05%	349.2	65.8
9	68.9	206.8	Test terminated due to excess permanent deformation.								
10	103.4	68.9									
11	103.4	103.4									
12	103.4	206.8									
13	137.9	103.4									
14	137.9	137.9									
15	137.9	275.8									

HPC_04	Target		Measured								
Sequence	Confining pressure [kPa]	Maximum axial stress [kPa]	Confining pressure [kPa]	Maximum axial stress [kPa]	Cyclic stress [kPa]	Contact stress [kPa]	MR [MPa]	Mr_Sd [MPa]	Last 5 cycles CV [%]	First invariant (θ) [kPa]	Second invariant (τ) [kPa]
0	41.4	27.6	42.6	27.6	24.9	2.8	80.5	0.3	0.37%	155.3	13.0
1	41.4	13.8	42.6	13.7	12.2	1.5	86.3	1.0	1.11%	141.4	6.5
2	41.4	27.6	42.6	27.6	24.7	2.9	84.1	0.5	0.64%	155.5	13.0
3	41.4	41.4	42.6	41.4	37.1	4.3	79.4	0.5	0.66%	169.2	19.5
4	41.4	55.2	42.6	55.2	49.5	5.7	78.3	0.2	0.20%	183.2	26.0
5	41.4	68.9	42.7	68.9	61.7	7.2	77.4	0.2	0.21%	196.9	32.5
6	27.6	13.8	28.9	13.7	12.1	1.5	92.9	1.8	1.88%	100.4	6.4
7	27.6	27.6	29.0	27.5	24.7	2.7	83.3	0.6	0.69%	114.5	13.0
8	27.6	41.4	29.0	41.3	37.1	4.2	79.0	0.3	0.44%	128.2	19.5
9	27.6	55.2	29.1	55.1	49.6	5.5	76.3	0.1	0.16%	142.4	26.0
10	27.6	68.9	28.8	68.9	61.9	7.0	74.7	0.1	0.14%	155.4	32.5
11	13.8	13.8	15.6	13.7	12.2	1.4	81.2	1.6	1.98%	60.6	6.4
12	13.8	27.6	15.6	27.5	24.7	2.8	74.2	0.4	0.47%	74.2	13.0
13	13.8	41.4	15.6	41.3	37.1	4.2	71.1	0.3	0.44%	88.1	19.5
14	13.8	55.2	15.5	55.1	49.6	5.6	69.1	0.2	0.25%	101.5	26.0
15	13.8	68.9	15.6	68.9	61.8	7.1	68.2	0.3	0.37%	115.7	32.5

HPC_04 (base)	Target		Measured								
Sequence	Confining pressure [kPa]	Maximum axial stress [kPa]	Confining pressure [kPa]	Maximum axial stress [kPa]	Cyclic stress [kPa]	Contact stress [kPa]	MR [MPa]	Mr_Sd [MPa]	Last 5 cycles CV [%]	First invariant (θ) [kPa]	Second invariant (τ) [kPa]
0	103.4	103.4	104.0	103.5	92.7	10.8	109.4	0.2	0.15%	415.6	48.8
1	20.7	20.7	22.2	20.5	18.4	2.0	99.3	1.2	1.17%	87.0	9.6
2	20.7	41.4	22.3	41.2	37.1	4.1	92.8	0.3	0.33%	108.0	19.4
3	20.7	62.1	22.2	61.9	55.8	6.1	88.4	0.4	0.46%	128.4	29.2
4	34.5	34.5	35.8	34.2	30.9	3.4	98.4	0.5	0.50%	141.6	16.1
5	34.5	68.9	35.7	68.7	61.7	7.1	92.9	0.2	0.17%	175.8	32.4
6	34.5	103.4	35.9	103.4	92.9	10.5	85.6	0.1	0.13%	211.1	48.7
7	68.9	68.9	69.8	69.0	61.9	7.1	101.7	0.3	0.26%	278.3	32.5
8	68.9	137.9	70.0	138.0	123.9	14.1	91.2	0.0	0.05%	347.9	65.0
9	68.9	206.8	70.0	207.0	186.0	21.1	82.8	0.1	0.10%	417.1	97.6
10	103.4	68.9	104.0	69.1	61.7	7.4	122.8	0.2	0.15%	381.2	32.6
11	103.4	103.4	104.1	103.6	92.8	10.8	115.0	0.1	0.05%	415.8	48.8
12	103.4	206.8	103.9	207.3	186.3	21.0	93.6	0.1	0.06%	518.9	97.7
13	137.9	103.4	138.1	103.8	92.7	11.0	123.8	0.3	0.26%	518.1	48.9
14	137.9	137.9	138.1	138.2	123.7	14.5	118.0	0.1	0.09%	552.7	65.2
15	137.9	275.8	138.2	276.4	248.3	28.2	96.1	0.1	0.06%	691.1	130.3

HPC_05	Target		Measured								
Sequence	Confining pressure [kPa]	Maximum axial stress [kPa]	Confining pressure [kPa]	Maximum axial stress [kPa]	Cyclic stress [kPa]	Contact stress [kPa]	MR [MPa]	Mr_Sd [MPa]	Last 5 cycles CV [%]	First invariant (θ) [kPa]	Second invariant (τ) [kPa]
0	41.4	27.6	41.2	27.5	24.5	3.0	84.1	1.1	1.26%	151.1	13.0
1	41.4	13.8	41.3	13.7	12.1	1.5	89.2	1.2	1.35%	137.5	6.4
2	41.4	27.6	41.1	27.6	24.6	2.9	85.8	0.4	0.41%	150.9	13.0
3	41.4	41.4	41.2	41.4	37.0	4.3	80.6	0.2	0.28%	164.9	19.5
4	41.4	55.2	41.2	55.1	49.5	5.6	80.2	0.4	0.45%	178.8	26.0
5	41.4	68.9	41.9	68.8	61.8	7.1	79.7	0.2	0.29%	194.6	32.5
6	27.6	13.8	28.5	13.5	12.1	1.4	87.1	0.8	0.89%	98.9	6.4
7	27.6	27.6	28.4	27.4	24.5	3.0	82.1	0.6	0.75%	112.6	12.9
8	27.6	41.4	28.7	41.3	37.0	4.3	81.0	0.2	0.26%	127.2	19.4
9	27.6	55.2	28.8	55.0	49.3	5.7	79.1	0.3	0.33%	141.3	25.9
10	27.6	68.9	28.6	68.8	61.8	7.1	77.7	0.1	0.19%	154.6	32.4
11	13.8	13.8	15.2	13.5	12.0	1.5	83.7	1.1	1.26%	59.0	6.4
12	13.8	27.6	15.1	27.4	24.5	2.9	79.6	0.6	0.70%	72.7	12.9
13	13.8	41.4	15.1	41.2	37.0	4.2	76.9	0.6	0.74%	86.5	19.4
14	13.8	55.2	15.2	55.0	49.4	5.6	74.4	0.3	0.37%	100.5	25.9
15	13.8	68.9	15.2	68.8	61.8	7.0	72.3	0.2	0.21%	114.3	32.4

HPC_05 (base)	Target		Measured								
Sequence	Confining pressure [kPa]	Maximum axial stress [kPa]	Confining pressure [kPa]	Maximum axial stress [kPa]	Cyclic stress [kPa]	Contact stress [kPa]	MR [MPa]	Mr_Sd [MPa]	Last 5 cycles CV [%]	First invariant (θ) [kPa]	Second invariant (τ) [kPa]
0	103.4	103.4	103.0	103.9	92.9	11.0	113.9	0.3	0.24%	413.0	49.0
1	20.7	20.7	22.0	20.6	18.2	2.4	97.1	0.8	0.85%	86.5	9.7
2	20.7	41.4	22.0	41.4	37.0	4.4	93.5	0.2	0.26%	107.4	19.5
3	20.7	62.1	22.0	62.1	55.7	6.4	89.5	0.2	0.18%	128.2	29.3
4	34.5	34.5	35.1	34.5	30.7	3.8	99.1	0.8	0.83%	139.9	16.3
5	34.5	68.9	35.2	69.0	61.7	7.2	94.5	0.2	0.26%	174.7	32.5
6	34.5	103.4	35.3	103.5	92.7	10.7	86.0	0.1	0.08%	209.4	48.8
7	68.9	68.9	68.6	69.2	61.8	7.3	105.4	0.1	0.13%	275.1	32.6
8	68.9	137.9	68.6	138.2	123.7	14.4	92.5	0.2	0.23%	343.9	65.1
9	68.9	206.8	68.7	207.3	186.1	21.2	80.8	0.0	0.05%	413.3	97.7
10	103.4	68.9	103.1	69.3	61.8	7.6	129.4	0.3	0.20%	378.6	32.7
11	103.4	103.4	102.9	103.8	92.8	11.0	119.2	0.3	0.25%	412.6	48.9
12	103.4	206.8	102.9	207.4	186.0	21.4	91.2	0.0	0.05%	516.0	97.8
13	137.9	103.4	137.4	103.9	92.6	11.3	129.5	0.4	0.33%	516.1	49.0
14	137.9	137.9	137.4	138.5	123.8	14.7	119.9	0.2	0.18%	550.7	65.3
15	137.9	275.8	137.5	276.7	248.2	28.4	87.8	0.0	0.04%	689.0	130.4

ALF_01	Target		Measured								
Sequence	**Confining pressure [kPa]**	**Maximum axial stress [kPa]**	**Confining pressure [kPa]**	**Maximum axial stress [kPa]**	**Cyclic stress [kPa]**	**Contact stress [kPa]**	**MR [MPa]**	**Last 5 cycles Mr_Sd [MPa]**	**Last 5 cycles CV [%]**	**First invariant (θ) [kPa]**	**Second invariant (τ) [kPa]**
0	41.4	27.6	43.0	27.5	24.2	3.3	90.7	1.6	1.82%	156.5	13.0
1	41.4	13.8	43.3	13.8	11.9	1.9	133.5	2.2	1.68%	143.8	6.5
2	41.4	27.6	42.9	27.6	24.0	3.6	93.6	1.1	1.18%	156.3	13.0
3	41.4	41.4	43.0	41.3	36.9	4.4	81.4	0.3	0.34%	170.2	19.5
4	41.4	55.2	42.8	55.2	49.2	6.0	73.3	0.5	0.70%	183.6	26.0
5	41.4	68.9	43.0	68.9	61.6	7.3	67.2	0.2	0.33%	197.8	32.5
6	27.6	13.8	29.3	13.7	11.9	1.8	112.5	2.8	2.47%	101.7	6.5
7	27.6	27.6	29.3	27.6	24.3	3.3	80.8	1.2	1.50%	115.6	13.0
8	27.6	41.4	29.3	41.4	36.6	4.8	66.5	0.4	0.55%	129.3	19.5
9	27.6	55.2	29.5	55.2	49.3	5.8	59.8	0.3	0.54%	143.8	26.0
10	27.6	68.9	29.5	68.8	61.6	7.2	57.8	0.3	0.56%	157.2	32.4
11	13.8	13.8	15.9	13.6	11.9	1.7	83.8	2.2	2.61%	61.2	6.4
12	13.8	27.6	16.0	27.5	23.9	3.5	60.2	0.3	0.43%	75.6	12.9
13	13.8	41.4	15.9	41.3	36.6	4.7	50.8	0.1	0.24%	89.1	19.5
14	13.8	55.2	15.8	55.0	49.3	5.7	47.0	0.2	0.38%	102.5	25.9
15	13.8	68.9	15.9	68.7	61.7	7.0	45.6	0.1	0.20%	116.5	32.4

ALF_02	Target		Measured								
Sequence	**Confining pressure [kPa]**	**Maximum axial stress [kPa]**	**Confining pressure [kPa]**	**Maximum axial stress [kPa]**	**Cyclic stress [kPa]**	**Contact stress [kPa]**	**MR [MPa]**	**Mr_Sd [MPa]**	**Last 5 cycles CV [%]**	**First invariant (θ) [kPa]**	**Second invariant (τ) [kPa]**
0	41.4	27.6	42.6	27.4	24.3	3.1	139.2	1.7	1.25%	155.1	12.9
1	41.4	13.8	42.5	13.5	11.9	1.5					
2	41.4	27.6	42.4	27.4	24.4	3.0	140.2	1.5	1.06%	154.7	12.9
3	41.4	41.4	42.7	41.2	36.8	4.4	95.5	0.4	0.46%	169.2	19.4
4	41.4	55.2	42.6	55.0	49.3	5.6	85.9	0.3	0.31%	182.8	25.9
5	41.4	68.9	42.9	68.5	61.6	7.0	77.3	0.1	0.12%	197.2	32.3
6	27.6	13.8	28.8	13.4	12.1	1.3					
7	27.6	27.6	28.8	27.2	24.5	2.8	130.4	0.3	0.20%	113.8	12.8
8	27.6	41.4	28.8	41.1	36.9	4.2	94.2	0.3	0.30%	127.4	19.4
9	27.6	55.2	29.0	54.8	49.1	5.7	78.8	0.3	0.41%	141.7	25.8
10	27.6	68.9	28.9	68.6	61.7	6.9	71.9	0.3	0.43%	155.5	32.3
11	13.8	13.8	15.8	13.3	11.8	1.5					
12	13.8	27.6	15.6	27.2	24.3	2.9	112.0	1.3	1.12%	73.9	12.8
13	13.8	41.4	15.5	41.0	37.0	4.0	84.8	0.3	0.33%	87.5	19.3
14	13.8	55.2	15.5	54.8	49.1	5.7	71.7	0.3	0.47%	101.1	25.8
15	13.8	68.9	15.2	68.5	61.6	6.8	65.7	0.1	0.22%	114.2	32.3

ALF_03	Target		Measured								
Sequence	**Confining pressure [kPa]**	**Maximum axial stress [kPa]**	**Confining pressure [kPa]**	**Maximum axial stress [kPa]**	**Cyclic stress [kPa]**	**Contact stress [kPa]**	**MR [MPa]**	**Last 5 cycles Mr_Sd [MPa]**	**Last 5 cycles CV [%]**	**First invariant (θ) [kPa]**	**Second invariant (τ) [kPa]**
0	41.4	27.6	42.6	34.3	24.5	9.8	96.5	0.5	0.47%	162.0	16.2
1	41.4	13.8	42.8	20.5	12.0	8.6	119.8	1.4	1.17%	148.9	9.7
2	41.4	27.6	42.8	34.4	24.6	9.8	98.3	0.2	0.25%	162.8	16.2
3	41.4	41.4	42.5	48.3	36.9	11.4	83.8	0.5	0.58%	175.8	22.8
4	41.4	55.2	42.3	62.1	49.5	12.6	75.0	0.2	0.22%	188.8	29.3
5	41.4	68.9	42.7	75.7	61.7	14.1	70.7	0.1	0.18%	203.8	35.7
6	27.6	13.8	29.1	20.5	11.9	8.5	113.7	1.8	1.58%	107.7	9.7
7	27.6	27.6	29.1	34.4	24.4	9.9	88.1	0.3	0.30%	121.5	16.2
8	27.6	41.4	29.0	48.2	37.0	11.2	73.2	0.2	0.26%	135.2	22.7
9	27.6	55.2	28.9	62.0	49.3	12.7	65.7	0.1	0.19%	148.8	29.2
10	27.6	68.9	29.1	75.7	61.7	14.0	63.1	0.2	0.29%	163.1	35.7
11	13.8	13.8	15.6	20.4	12.0	8.4	95.8	1.4	1.41%	67.1	9.6
12	13.8	27.6	15.7	34.2	24.4	9.8	74.7	0.4	0.59%	81.4	16.1
13	13.8	41.4	15.6	48.1	36.9	11.2	62.6	0.2	0.39%	94.8	22.7
14	13.8	55.2	15.6	61.8	49.3	12.5	57.4	0.2	0.32%	108.6	29.1
15	13.8	68.9	15.6	75.6	61.7	13.9	55.9	0.0	0.09%	122.4	35.6

ALF_04_4hr	Target		Measured								
Sequence	Confining pressure [kPa]	Maximum axial stress [kPa]	Confining pressure [kPa]	Maximum axial stress [kPa]	Cyclic stress [kPa]	Contact stress [kPa]	MR [MPa]	Mr_Sd [MPa]	Last 5 cycles CV [%]	First invariant (θ) [kPa]	Second invariant (τ) [kPa]
0	41.4	27.6	42.3	27.7	24.7	3.0	98.7	1.0	0.98%	154.6	13.1
1	41.4	13.8	42.4	13.8	11.8	2.0	119.4	3.2	2.67%	140.8	6.5
2	41.4	27.6	42.2	27.6	24.4	3.2	99.0	0.9	0.92%	154.1	13.0
3	41.4	41.4	42.5	41.5	36.9	4.6	86.0	0.6	0.66%	168.9	19.6
4	41.4	55.2	42.5	55.3	49.3	5.9	77.2	0.1	0.11%	182.9	26.0
5	41.4	68.9	43.0	69.1	61.7	7.3	71.9	0.2	0.30%	198.0	32.6
6	27.6	13.8	28.9	13.7	11.8	1.9	106.8	2.6	2.45%	100.5	6.5
7	27.6	27.6	28.8	27.5	24.3	3.2	85.4	0.3	0.35%	114.0	13.0
8	27.6	41.4	29.0	41.4	36.9	4.5	73.1	0.3	0.35%	128.4	19.5
9	27.6	55.2	28.9	55.2	49.2	6.0	65.7	0.2	0.29%	141.9	26.0
10	27.6	68.9	28.9	68.9	61.8	7.1	63.5	0.2	0.24%	155.6	32.5
11	13.8	13.8	15.5	13.6	11.9	1.7	86.5	1.2	1.42%	60.1	6.4
12	13.8	27.6	15.7	27.5	24.4	3.1	70.4	0.4	0.51%	74.5	13.0
13	13.8	41.4	15.6	41.3	36.8	4.5	61.2	0.2	0.32%	88.2	19.5
14	13.8	55.2	15.5	55.1	49.1	6.0	56.7	0.2	0.36%	101.5	26.0
15	13.8	68.9	15.6	68.7	61.6	7.2	55.5	0.2	0.28%	115.4	32.4

ALF_05 _5hr	Target		Measured								
Sequence	Confining pressure [kPa]	Maximum axial stress [kPa]	Confining pressure [kPa]	Maximum axial stress [kPa]	Cyclic stress [kPa]	Contact stress [kPa]	MR [MPa]	Mr_Sd [MPa]	Last 5 cycles CV [%]	First invariant (θ) [kPa]	Second invariant (τ) [kPa]
0	41.4	27.6	42.6	27.4	24.4	3.0	53.5	0.2	0.33%	155.3	12.9
1	41.4	13.8	42.7	13.6	12.0	1.7	54.5	0.7	1.36%	141.8	6.4
2	41.4	27.6	42.5	27.4	24.3	3.1	53.4	0.3	0.50%	154.9	12.9
3	41.4	41.4	42.6	41.3	36.9	4.4	51.8	0.2	0.43%	169.0	19.5
4	41.4	55.2	42.4	55.1	49.3	5.8	49.4	0.1	0.27%	182.3	26.0
5	41.4	68.9	42.6	68.8	61.7	7.1	48.2	0.2	0.36%	196.7	32.4
6	27.6	13.8	29.0	13.6	12.0	1.6	59.6	0.8	1.30%	100.5	6.4
7	27.6	27.6	29.0	27.3	24.3	3.0	54.0	0.3	0.64%	114.3	12.9
8	27.6	41.4	29.0	41.2	36.8	4.4	49.0	0.1	0.30%	128.2	19.4
9	27.6	55.2	29.0	55.1	49.3	5.8	46.6	0.2	0.38%	142.1	26.0
10	27.6	68.9	28.9	68.7	61.7	7.0	46.7	0.1	0.25%	155.4	32.4
11	13.8	13.8	15.5	13.5	11.9	1.7	60.5	0.5	0.80%	60.1	6.4
12	13.8	27.6	15.5	27.3	24.4	2.9	52.4	0.3	0.56%	73.9	12.9
13	13.8	41.4	15.5	41.2	36.9	4.3	46.7	0.2	0.52%	87.7	19.4
14	13.8	55.2	15.7	55.0	49.3	5.7	44.7	0.2	0.40%	102.1	25.9
15	13.8	68.9	15.6	68.7	61.7	7.0	45.0	0.1	0.31%	115.5	32.4

ALF_07	Target		Measured								
Sequence	Confining pressure [kPa]	Maximum axial stress [kPa]	Confining pressure [kPa]	Maximum axial stress [kPa]	Cyclic stress [kPa]	Contact stress [kPa]	MR [MPa]	Mr_Sd [MPa]	Last 5 cycles CV [%]	First invariant (θ) [kPa]	Second invariant (τ) [kPa]
0	41.4	27.6	42.8	27.5	24.5	3.1	19.2	0.1	0.77%	156.0	13.0
1	41.4	13.8	42.6	13.7	12.1	1.7	22.4	0.2	0.76%	141.4	6.5
2	41.4	27.6	42.5	27.4	24.3	3.1	19.1	0.1	0.78%	154.9	12.9
3	41.4	41.4	42.7	41.4	36.9	4.5	17.9	0.1	0.61%	169.5	19.5
4	41.4	55.2	42.6	55.2	49.4	5.8	19.2	0.1	0.42%	183.1	26.0
6	27.6	13.8	29.0	13.7	12.0	1.7	24.3	0.4	1.64%	100.6	6.5
7	27.6	27.6	28.9	27.7	24.7	3.0	19.8	0.2	0.80%	114.3	13.0
8	27.6	41.4	29.1	41.2	36.8	4.4	17.5	0.1	0.57%	128.6	19.4
9	27.6	55.2	29.0	55.2	49.3	5.9	19.6	0.1	0.70%	142.1	26.0
10	27.6	68.9	29.1	68.9	61.8	7.1	21.7	0.1	0.39%	156.3	32.5
11	13.8	13.8	15.5	13.6	12.0	1.6	23.3	0.3	1.12%	60.0	6.4
12	13.8	27.6	15.9	27.4	24.4	3.0	17.6	0.1	0.54%	75.0	12.9
13	13.8	41.4	15.7	41.2	36.8	4.4	17.5	0.1	0.61%	88.2	19.4
14	13.8	55.2	15.7	55.1	49.5	5.6	19.7	0.1	0.39%	102.2	26.0
15	13.8	68.9	15.6	69.0	61.8	7.1	21.5	0.1	0.59%	115.8	32.5

ALF_07 (base)	Target		Measured								
Sequence	**Confining pressure [kPa]**	**Maximum axial stress [kPa]**	**Confining pressure [kPa]**	**Maximum axial stress [kPa]**	**Cyclic stress [kPa]**	**Contact stress [kPa]**	**MR [MPa]**	**Mr_Sd [MPa]**	**Last 5 cycles CV [%]**	**First invariant (θ) [kPa]**	**Second invariant (τ) [kPa]**
0	103.4	103.4	103.8	101.6	92.9	8.8	40.1	0.1	0.22%	412.9	47.9
1	20.7	20.7	22.2	18.4	18.3	0.1	22.8	0.1	0.46%	85.1	8.7
2	20.7	41.4	22.2	39.2	37.0	2.2	22.5	0.1	0.57%	105.9	18.5
3	20.7	62.1	22.4	60.0	55.8	4.2	25.1	0.1	0.22%	127.2	28.3
4	34.5	34.5	35.8	32.2	30.7	1.5	29.3	0.1	0.42%	139.5	15.2
5	34.5	68.9	35.9	66.8	61.8	5.0	28.3	0.1	0.30%	174.4	31.5
6	34.5	103.4	35.9	101.5	93.1	8.4	30.8	0.1	0.28%	209.1	47.9
7	68.9	68.9	69.7	66.9	61.8	5.1	39.9	0.1	0.25%	276.1	31.6
8	68.9	137.9	69.9	136.1	124.0	12.1	37.2	0.1	0.16%	345.6	64.1
9	68.9	206.8	Test terminated due to excess permanent deformation								
10	103.4	68.9									
11	103.4	103.4									
12	103.4	206.8									
13	137.9	103.4									
14	137.9	137.9									
15	137.9	275.8									

ALF_08	Target		Measured								
Sequence	Confining pressure [kPa]	Maximum axial stress [kPa]	Confining pressure [kPa]	Maximum axial stress [kPa]	Cyclic stress [kPa]	Contact stress [kPa]	MR [MPa]	Mr_Sd [MPa]	Last 5 cycles CV [%]	First invariant (θ) [kPa]	Second invariant (τ) [kPa]
0	41.4	27.6	42.8	27.5	24.4	3.1	14.9	0.1	0.36%	155.9	13.0
1	41.4	13.8	42.5	13.7	12.0	1.8	17.1	0.2	0.97%	141.2	6.5
2	41.4	27.6	42.7	27.6	24.4	3.2	15.2	0.1	0.89%	155.7	13.0
3	41.4	41.4	42.7	41.4	37.0	4.5	14.9	0.1	0.48%	169.6	19.5
4	41.4	55.2	42.7	55.4	49.5	5.9	16.7	0.1	0.41%	183.3	26.1
5	41.4	68.9	42.7	69.2	61.9	7.3	18.8	0.1	0.57%	197.5	32.6
6	27.6	13.8	28.9	13.6	12.0	1.6	19.2	0.1	0.62%	100.4	6.4
7	27.6	27.6	28.9	27.4	24.4	3.0	15.0	0.1	0.58%	114.1	12.9
8	27.6	41.4	28.9	41.2	36.8	4.4	15.7	0.1	0.43%	128.1	19.4
9	27.6	55.2	29.0	55.2	49.3	5.9	17.8	0.1	0.78%	142.3	26.0
10	27.6	68.9	28.9	69.0	61.8	7.1	20.0	0.1	0.37%	155.6	32.5
11	13.8	13.8	15.6	13.6	12.0	1.7	19.8	0.2	1.04%	60.4	6.4
12	13.8	27.6	15.5	27.5	24.5	3.0	15.5	0.1	0.71%	73.9	13.0
13	13.8	41.4	15.6	41.3	36.8	4.4	16.0	0.1	0.50%	88.1	19.5
14	13.8	55.2	15.6	55.1	49.4	5.8	18.4	0.1	0.54%	102.0	26.0
15	13.8	68.9	15.6	68.9	61.7	7.2	20.3	0.1	0.29%	115.6	32.5

ALF_08 (base)	Target		Measured								
Sequence	**Confining pressure [kPa]**	**Maximum axial stress [kPa]**	**Confining pressure [kPa]**	**Maximum axial stress [kPa]**	**Cyclic stress [kPa]**	**Contact stress [kPa]**	**MR [MPa]**	**Mr_Sd [MPa]**	**Last 5 cycles CV [%]**	**First invariant (θ) [kPa]**	**Second invariant (τ) [kPa]**
0	103.4	103.4	103.7	103.9	92.6	11.3	33.3	0.1	0.29%	415.0	49.0
1	20.7	20.7	22.1	20.8	18.1	2.7	15.3	0.2	1.01%	87.2	9.8
2	20.7	41.4	22.2	41.7	37.0	4.7	16.4	0.1	0.55%	108.4	19.6
3	20.7	62.1	22.1	62.4	55.7	6.7	19.6	0.1	0.39%	128.7	29.4
4	34.5	34.5	36.0	34.7	30.7	4.0	22.4	0.1	0.33%	142.7	16.4
5	34.5	68.9	35.8	69.1	61.6	7.5	22.5	0.1	0.41%	176.7	32.6
6	34.5	103.4	35.9	104.0	93.0	11.0	25.9	0.1	0.41%	211.7	49.0
7	68.9	68.9	69.6	69.2	61.6	7.7	34.3	0.1	0.30%	278.2	32.6
8	68.9	137.9	69.8	138.5	123.8	14.7	32.3	0.1	0.19%	347.9	65.3
9	68.9	206.8	Test terminated due to excess permanent deformation								
10	103.4	68.9									
11	103.4	103.4									
12	103.4	206.8									
13	137.9	103.4									
14	137.9	137.9									
15	137.9	275.8									

ALF_11	Target		Measured								
Sequence	Confining pressure [kPa]	Maximum axial stress [kPa]	Confining pressure [kPa]	Maximum axial stress [kPa]	Cyclic stress [kPa]	Contact stress [kPa]	MR [MPa]	Mr_Sd [MPa]	Last 5 cycles CV [%]	First invariant (θ) [kPa]	Second invariant (τ) [kPa]
0	41.4	27.6	42.4	27.5	24.5	3.0	73.7	0.5	0.65%	154.8	13.0
1	41.4	13.8	42.8	13.7	12.0	1.8	91.3	1.2	1.30%	142.1	6.5
2	41.4	27.6	42.7	27.5	24.5	3.0	75.2	0.4	0.51%	155.6	13.0
3	41.4	41.4	42.5	41.4	37.0	4.4	65.5	0.1	0.18%	168.9	19.5
4	41.4	55.2	42.6	55.1	49.3	5.7	62.1	0.2	0.28%	182.9	26.0
5	41.4	68.9	42.3	68.9	61.7	7.2	60.0	0.1	0.17%	195.8	32.5
6	27.6	13.8	28.9	13.7	12.2	1.5	87.4	0.8	0.86%	100.5	6.5
7	27.6	27.6	28.8	27.4	24.4	3.0	69.5	0.4	0.51%	113.8	12.9
8	27.6	41.4	29.0	41.2	36.9	4.3	59.9	0.2	0.33%	128.1	19.4
9	27.6	55.2	28.9	55.1	49.4	5.7	55.1	0.2	0.30%	141.8	26.0
10	27.6	68.9	28.8	68.8	61.8	7.1	53.4	0.1	0.20%	155.1	32.4
11	13.8	13.8	15.4	13.7	12.1	1.5	73.1	1.7	2.32%	60.0	6.4
12	13.8	27.6	15.6	27.5	24.5	2.9	53.9	0.3	0.50%	74.2	12.9
13	13.8	41.4	15.7	41.1	36.9	4.3	47.3	0.1	0.29%	88.2	19.4
14	13.8	55.2	15.9	55.0	49.4	5.6	45.0	0.2	0.35%	102.6	25.9
15	13.8	68.9	15.8	68.8	61.8	7.0	44.6	0.1	0.16%	116.2	32.4

ALF_12	Target		Measured								
Sequence	**Confining pressure [kPa]**	**Maximum axial stress [kPa]**	**Confining pressure [kPa]**	**Maximum axial stress [kPa]**	**Cyclic stress [kPa]**	**Contact stress [kPa]**	**MR [MPa]**	**Mr_Sd [MPa]**	**Last 5 cycles CV [%]**	**First invariant (θ) [kPa]**	**Second invariant (τ) [kPa]**
0	41.4	27.6	42.6	27.5	24.4	3.1	77.2	0.4	0.54%	155.4	13.0
1	41.4	13.8	42.4	13.8	12.1	1.7	93.4	0.7	0.73%	141.1	6.5
2	41.4	27.6	42.4	27.7	24.6	3.1	78.2	0.5	0.68%	154.7	13.0
3	41.4	41.4	42.4	41.4	36.9	4.5	68.9	0.4	0.51%	168.5	19.5
4	41.4	55.2	42.4	55.3	49.5	5.7	63.9	0.1	0.17%	182.6	26.1
5	41.4	68.9	42.5	69.0	61.8	7.3	61.8	0.2	0.35%	196.7	32.5
6	27.6	13.8	28.9	13.7	12.0	1.7	87.0	0.6	0.69%	100.4	6.5
7	27.6	27.6	28.8	27.5	24.5	3.0	69.4	0.3	0.42%	114.0	13.0
8	27.6	41.4	28.8	41.4	37.0	4.3	59.2	0.2	0.26%	127.6	19.5
9	27.6	55.2	28.8	55.1	49.4	5.8	54.8	0.1	0.17%	141.5	26.0
10	27.6	68.9	28.7	68.8	61.6	7.2	53.8	0.1	0.19%	154.8	32.4
11	13.8	13.8	15.4	13.5	11.9	1.6	68.1	1.0	1.43%	59.7	6.4
12	13.8	27.6	15.5	27.5	24.5	3.0	55.1	0.2	0.39%	74.0	13.0
13	13.8	41.4	15.6	41.3	37.0	4.4	48.5	0.1	0.26%	88.2	19.5
14	13.8	55.2	15.5	55.1	49.4	5.7	46.0	0.1	0.18%	101.6	26.0
15	13.8	68.9	15.5	68.8	61.8	7.0	45.5	0.1	0.20%	115.1	32.4

ALF_12 (base)	Target		Measured								
Sequence	Confining pressure [kPa]	Maximum axial stress [kPa]	Confining pressure [kPa]	Maximum axial stress [kPa]	Cyclic stress [kPa]	Contact stress [kPa]	MR [MPa]	Mr_Sd [MPa]	Last 5 cycles CV [%]	First invariant (θ) [kPa]	Second invariant (τ) [kPa]
0	103.4	103.4	104.0	103.7	92.8	10.9	98.4	0.1	0.11%	415.6	48.9
1	20.7	20.7	22.2	20.6	18.2	2.3	70.1	0.7	1.02%	87.1	9.7
2	20.7	41.4	22.1	41.3	36.9	4.4	57.8	0.2	0.32%	107.8	19.5
3	20.7	62.1	22.2	62.1	55.5	6.5	52.8	0.1	0.24%	128.7	29.3
4	34.5	34.5	35.6	34.5	30.8	3.7	68.2	0.1	0.17%	141.5	16.3
5	34.5	68.9	35.9	68.9	61.7	7.2	59.6	0.1	0.23%	176.7	32.5
6	34.5	103.4	35.6	103.4	92.8	10.6	57.7	0.0	0.08%	210.3	48.7
7	68.9	68.9	69.6	69.1	61.8	7.3	82.6	0.1	0.16%	277.8	32.6
8	68.9	137.9	69.6	138.2	123.9	14.3	75.3	0.1	0.12%	347.0	65.1
9	68.9	206.8	69.6	207.2	186.1	21.1	73.4	0.1	0.10%	416.0	97.7
10	103.4	68.9	103.8	69.2	61.8	7.4	113.8	0.2	0.19%	380.6	32.6
11	103.4	103.4	103.8	103.8	92.8	11.0	102.8	0.2	0.21%	415.2	48.9
12	103.4	206.8	103.8	207.3	185.9	21.4	94.0	0.1	0.07%	518.8	97.7
13	137.9	103.4	138.1	103.9	92.8	11.1	124.5	0.3	0.21%	518.1	49.0
14	137.9	137.9	138.1	138.5	123.9	14.6	118.7	0.2	0.16%	552.7	65.3
15	137.9	275.8	138.1	276.7	248.3	28.4	110.0	0.1	0.09%	690.9	130.4

ALF_10	Target		Measured								
Sequence	Confining pressure [kPa]	Maximum axial stress [kPa]	Confining pressure [kPa]	Maximum axial stress [kPa]	Cyclic stress [kPa]	Contact stress [kPa]	MR [MPa]	Mr_Sd [MPa]	Last 5 cycles CV [%]	First invariant (θ) [kPa]	Second invariant (τ) [kPa]
0	41.4	27.6	42.8	27.9	24.6	3.3	88.6	0.6	0.67%	156.4	13.2
1	41.4	13.8	42.5	14.1	12.1	1.9	105.0	1.6	1.57%	141.4	6.6
2	41.4	27.6	42.5	28.0	24.6	3.3	91.0	1.0	1.10%	155.5	13.2
3	41.4	41.4	42.5	41.7	37.0	4.7	81.7	0.4	0.51%	169.2	19.7
4	41.4	55.2	42.5	55.5	49.4	6.2	75.2	0.1	0.18%	183.1	26.2
5	41.4	68.9	42.5	69.3	61.6	7.6	72.0	0.2	0.31%	196.9	32.6
6	27.6	13.8	28.9	14.0	12.2	1.8	121.1	1.6	1.31%	100.8	6.6
7	27.6	27.6	29.1	27.8	24.4	3.4	86.0	0.6	0.75%	115.0	13.1
8	27.6	41.4	29.0	41.6	36.9	4.6	71.9	0.2	0.29%	128.5	19.6
9	27.6	55.2	29.1	55.4	49.3	6.1	65.6	0.2	0.27%	142.8	26.1
10	27.6	68.9	29.0	69.2	61.7	7.5	63.8	0.2	0.25%	156.3	32.6
11	13.8	13.8	15.5	13.9	11.9	2.0	92.1	2.6	2.87%	60.4	6.5
12	13.8	27.6	15.6	27.8	24.6	3.2	68.2	0.4	0.65%	74.7	13.1
13	13.8	41.4	15.5	41.6	37.0	4.6	59.2	0.2	0.29%	88.0	19.6
14	13.8	55.2	15.4	55.4	49.4	6.0	55.3	0.2	0.32%	101.5	26.1
15	13.8	68.9	15.5	69.2	61.7	7.4	54.8	0.1	0.22%	115.7	32.6

VA21a_01	Target		Measured								
Sequence	Confining pressure [kPa]	Maximum axial stress [kPa]	Confining pressure [kPa]	Maximum axial stress [kPa]	Cyclic stress [kPa]	Contact stress [kPa]	MR [MPa]	Mr_Sd [MPa]	Last 5 cycles CV [%]	First invariant (θ) [kPa]	Second invariant (τ) [kPa]
0	103.4	103.4	103.3	100.8	93.0	7.8	122.7	0.3	0.22%	410.6	47.5
1	20.7	20.7	20.6	17.9	18.5	-0.6	35.0	0.2	0.68%	79.5	8.4
2	20.7	41.4	20.5	38.6	37.1	1.5	46.6	0.2	0.41%	100.2	18.2
3	20.7	62.1	20.5	59.3	55.8	3.6	57.4	0.2	0.31%	120.9	28.0
4	34.5	34.5	34.3	31.7	30.9	0.8	60.5	0.1	0.22%	134.7	15.0
5	34.5	68.9	34.3	66.1	61.9	4.2	76.4	0.2	0.32%	169.2	31.2
6	34.5	103.4	34.3	100.8	93.1	7.7	91.6	0.1	0.15%	203.8	47.5
7	68.9	68.9	68.6	66.2	62.0	4.3	137.5	0.2	0.14%	272.1	31.2
8	68.9	137.9	68.6	135.3	124.1	11.2	162.6	0.2	0.09%	341.2	63.8
9	68.9	206.8	68.5	204.4	186.3	18.1	188.5	0.4	0.19%	410.1	96.4
10	103.4	68.9	103.0	66.2	61.9	4.3	180.0	0.3	0.16%	375.3	31.2
11	103.4	103.4	103.0	100.8	93.0	7.8	195.2	0.4	0.20%	409.9	47.5
12	103.4	206.8	103.0	204.4	186.3	18.1	235.3	0.2	0.07%	513.3	96.4
13	137.9	103.4	137.3	100.7	92.9	7.8	214.9	0.3	0.16%	512.7	47.5
14	137.9	137.9	137.4	135.4	124.1	11.3	231.8	0.3	0.12%	547.5	63.8
15	137.9	275.8	137.4	273.4	248.4	25.0	279.0	0.3	0.12%	685.7	128.9

VA21a_02	Target		Measured								
Sequence	Confining pressure [kPa]	Maximum axial stress [kPa]	Confining pressure [kPa]	Maximum axial stress [kPa]	Cyclic stress [kPa]	Contact stress [kPa]	MR [MPa]	Mr_Sd [MPa]	Last 5 cycles CV [%]	First invariant (θ) [kPa]	Second invariant (τ) [kPa]
0	103.4	103.4	103.5	103.7	93.1	10.6	183.1	0.3	0.17%	414.1	48.9
1	20.7	20.7	22.0	20.8	18.6	2.2	70.8	0.3	0.37%	86.7	9.8
2	20.7	41.4	21.9	41.6	37.2	4.4	79.6	0.2	0.20%	107.2	19.6
3	20.7	62.1	22.0	62.2	55.7	6.5	89.4	0.3	0.29%	128.3	29.3
4	34.5	34.5	35.7	34.6	30.9	3.7	95.2	0.3	0.33%	141.8	16.3
5	34.5	68.9	35.6	69.0	61.8	7.2	113.9	0.2	0.16%	176.0	32.5
6	34.5	103.4	35.6	103.6	93.1	10.5	129.2	0.1	0.05%	210.5	48.8
7	68.9	68.9	69.4	69.1	61.9	7.2	148.0	0.4	0.25%	277.4	32.6
8	68.9	137.9	69.8	138.2	124.2	14.0	192.4	0.3	0.17%	347.5	65.1
9	68.9	206.8	69.8	207.1	186.2	21.0	213.8	0.2	0.10%	416.6	97.6
10	103.4	68.9	103.5	69.1	61.9	7.2	153.0	0.4	0.28%	379.7	32.6
11	103.4	103.4	103.5	103.7	93.1	10.6	189.0	0.3	0.18%	414.2	48.9
12	103.4	206.8	103.8	207.3	186.3	21.0	259.1	0.3	0.11%	518.7	97.7
13	137.9	103.4	137.4	103.7	93.1	10.6	202.8	0.7	0.34%	515.8	48.9
14	137.9	137.9	137.4	138.3	124.2	14.1	240.7	0.3	0.12%	550.4	65.2
15	137.9	275.8	137.3	276.3	248.3	28.0	326.1	0.5	0.14%	688.3	130.2

Appendix 10

BVT Dynatest Spectral Analysis

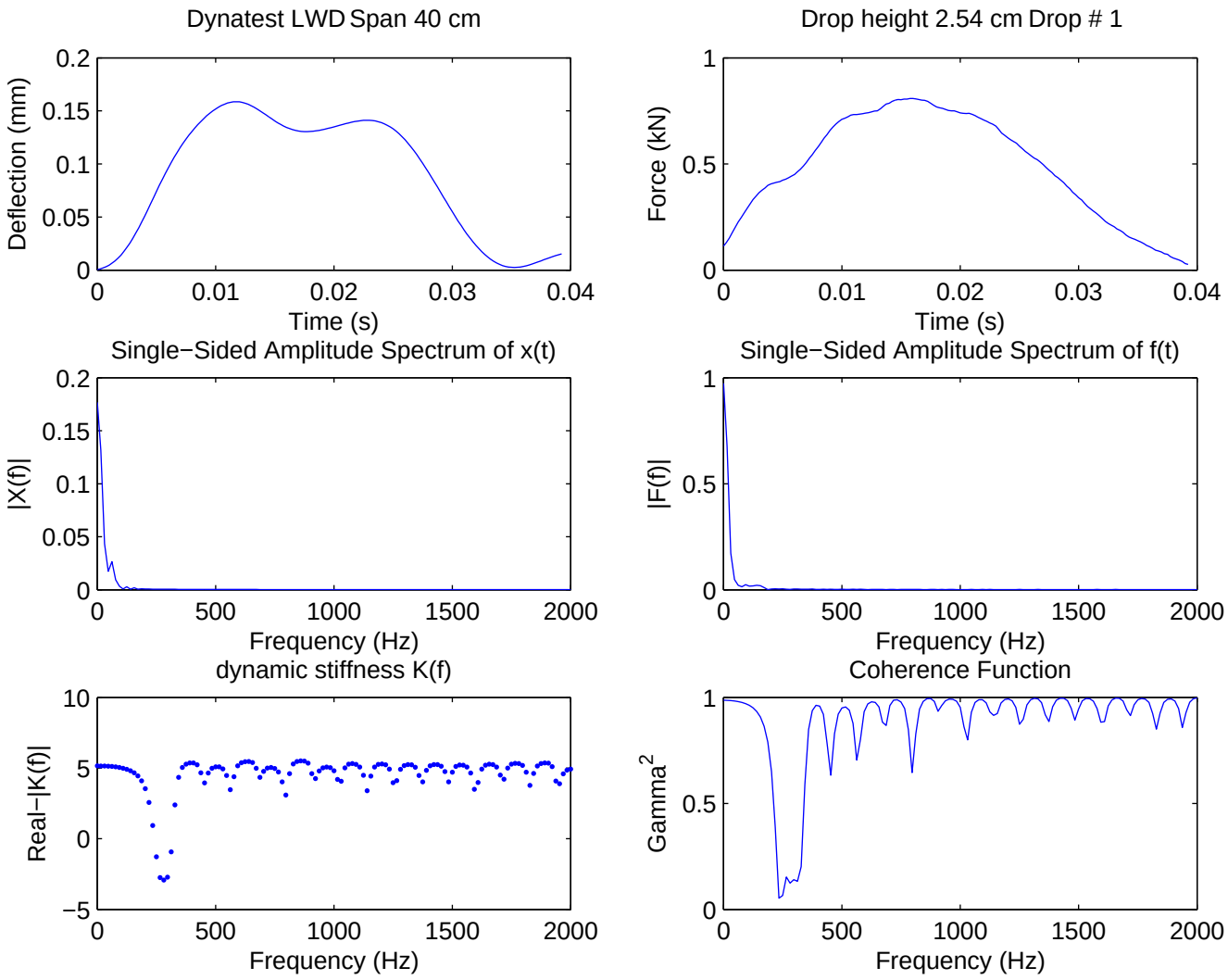
Dynatest LWD Span 40 cm
Deflection (mm)
Time (s)
Drop height 2.54 cm Drop # 1
Force (kN)
Time (s)
Single−Sided Amplitude Spectrum of x(t)
|X(f)|
Frequency (Hz)
Single−Sided Amplitude Spectrum of f(t)
|F(f)|
Frequency (Hz)
dynamic stiffness K(f)
Real−|K(f)|
Frequency (Hz)
Coherence Function
Gamma2
Frequency (Hz)

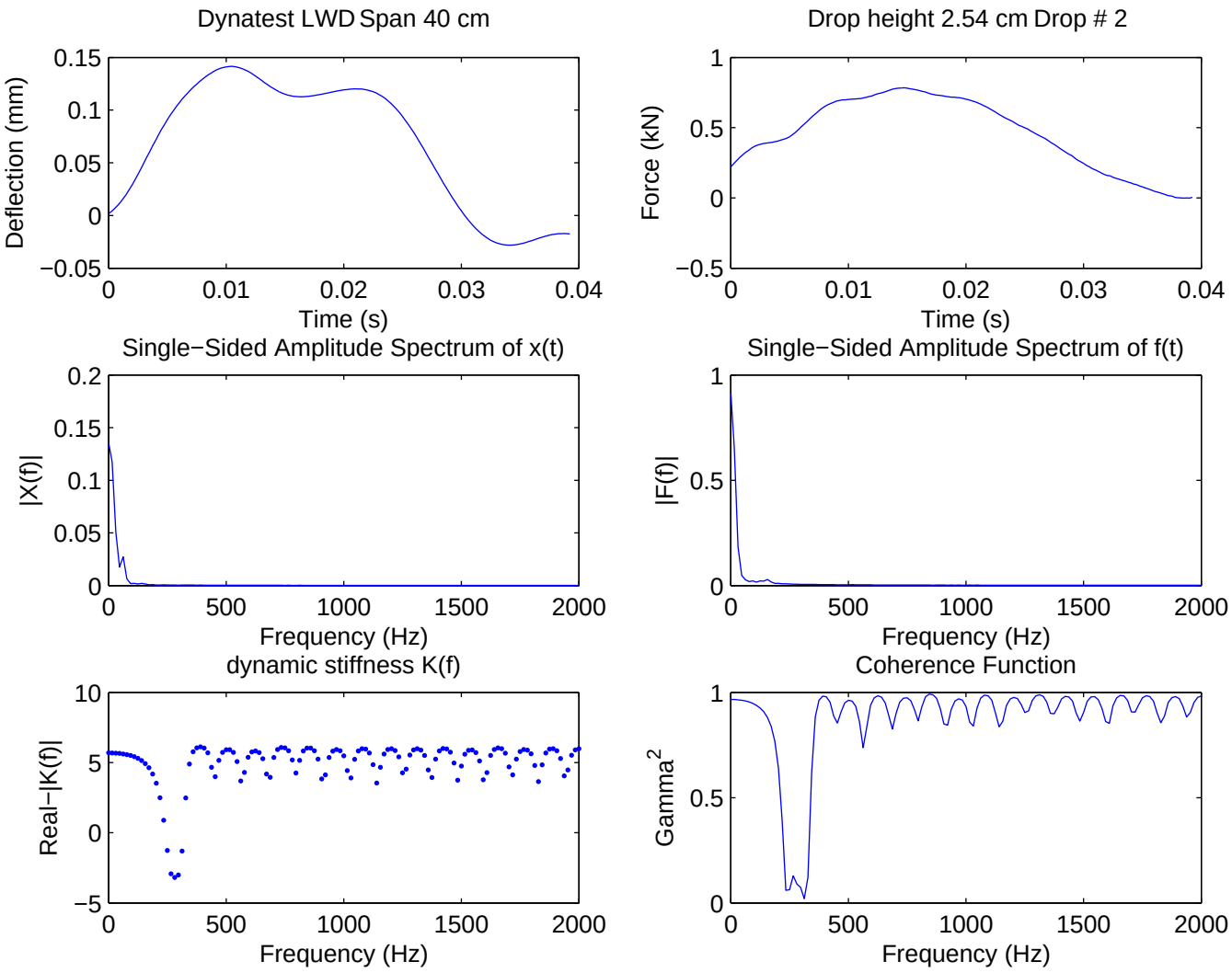
Dynatest LWD Span 40 cm
Deflection (mm)
0.15
0.1
0.05
0
−0.05
0
0.01
0.02
0.03
0.04
Time (s)
Drop height 2.54 cm Drop # 2
Force (kN)
1
0.5
0
−0.5
0
0.01
0.02
0.03
0.04
Time (s)
Single−Sided Amplitude Spectrum of x(t)
|X(f)|
0.2
0.15
0.1
0.05
0
0
500
1000
1500
2000
Frequency (Hz)
Single−Sided Amplitude Spectrum of f(t)
|F(f)|
1
0.5
0
0
500
1000
1500
2000
Frequency (Hz)
dynamic stiffness K(f)
Real−|K(f)|
10
5
0
−5
0
500
1000
1500
2000
Frequency (Hz)
Coherence Function
Gamma^2
1
0.5
0
0
500
1000
1500
2000
Frequency (Hz)

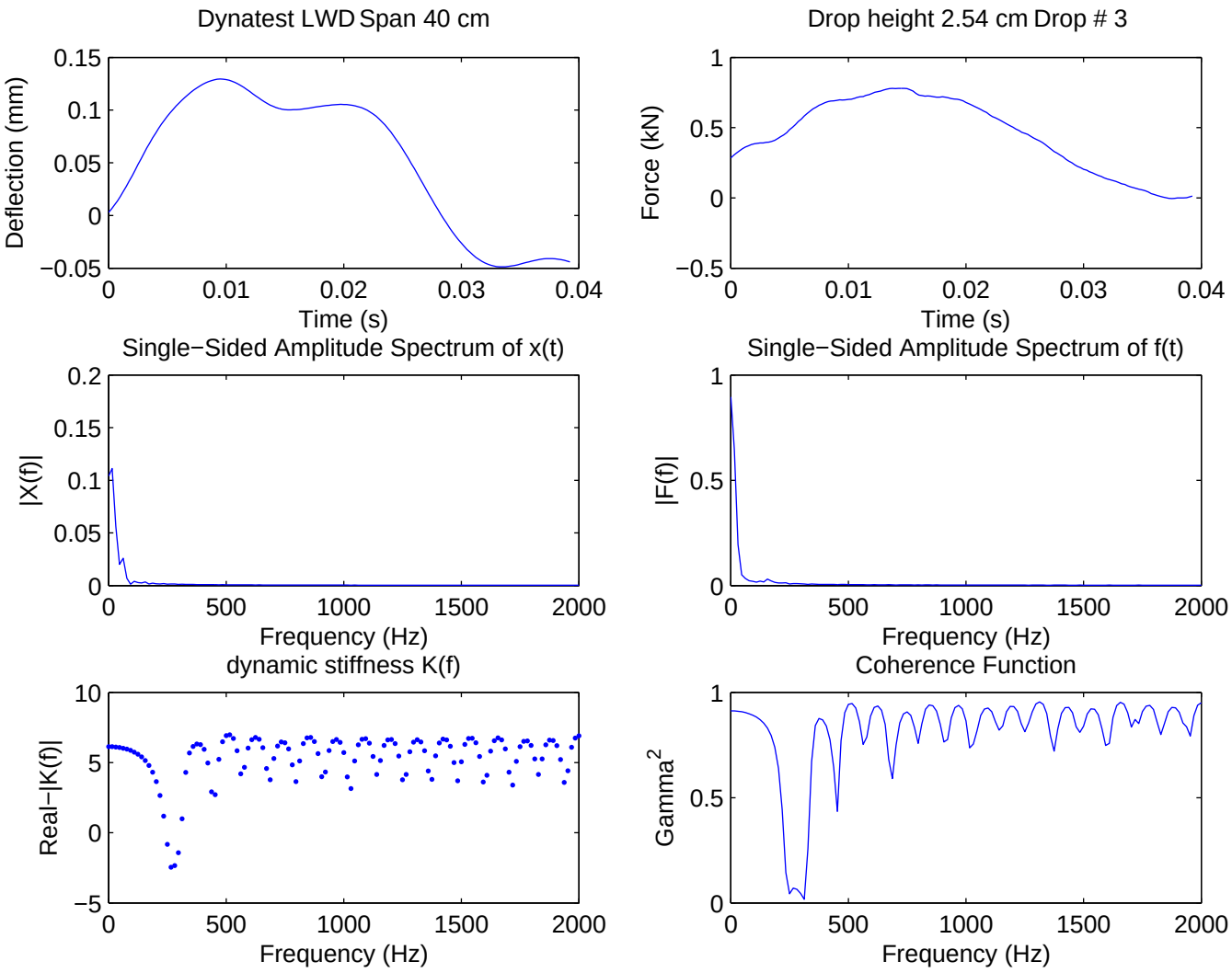
Dynatest LWD Span 40 cm
Deflection (mm)
0.15
0.1
0.05
0
−0.05
0
0.01
0.02
0.03
0.04
Time (s)
Drop height 2.54 cm Drop # 3
Force (kN)
1
0.5
0
−0.5
0
0.01
0.02
0.03
0.04
Time (s)
Single−Sided Amplitude Spectrum of x(t)
|X(f)|
0.2
0.15
0.1
0.05
0
0
500
1000
1500
2000
Frequency (Hz)
Single−Sided Amplitude Spectrum of f(t)
|F(f)|
1
0.5
0
0
500
1000
1500
2000
Frequency (Hz)
dynamic stiffness K(f)
Real−|K(f)|
10
5
0
−5
0
500
1000
1500
2000
Frequency (Hz)
Coherence Function
Gamma^2
1
0.5
0
0
500
1000
1500
2000
Frequency (Hz)

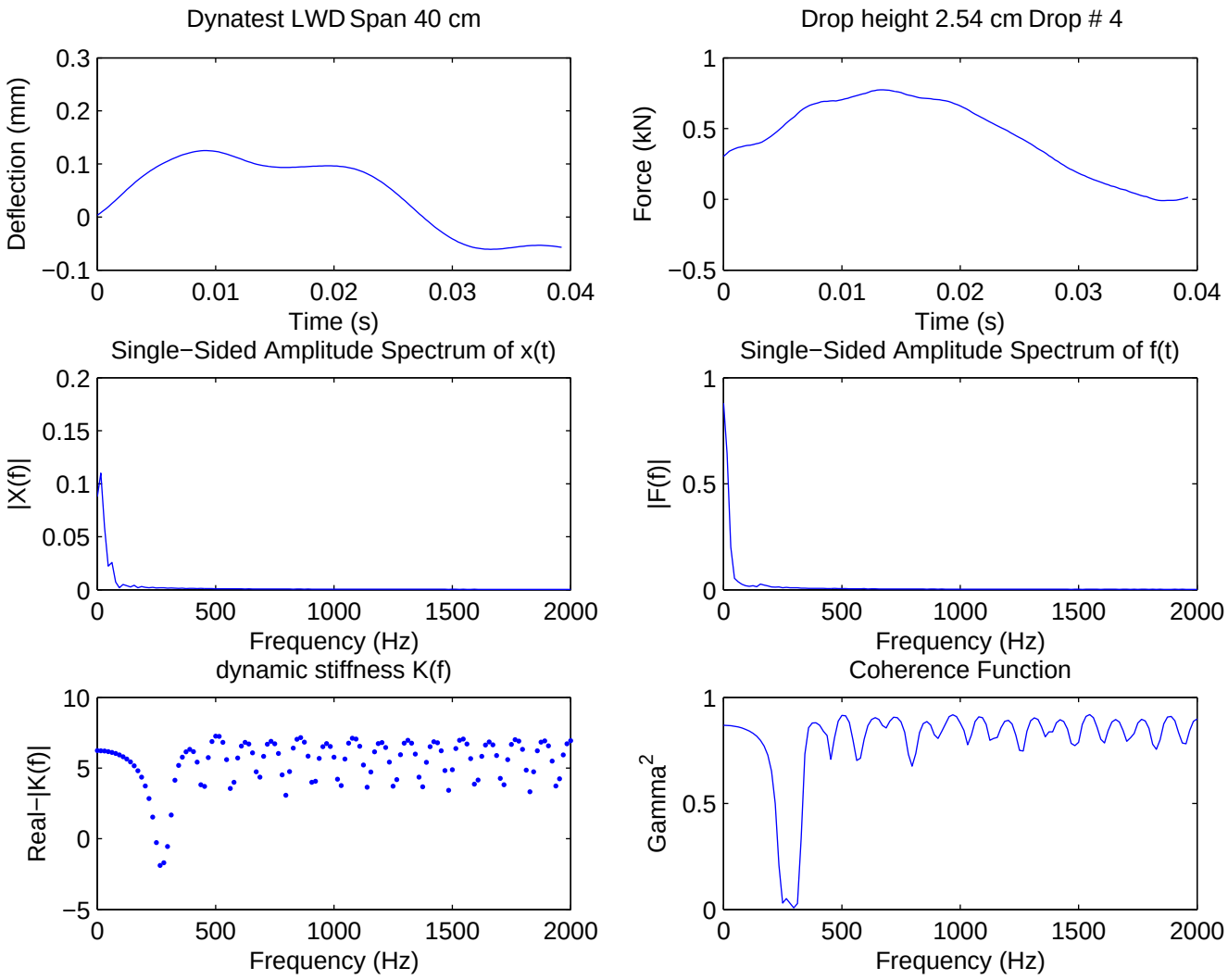
Dynatest LWD Span 40 cm
Deflection (mm)
Time (s)
Drop height 2.54 cm Drop # 4
Force (kN)
Time (s)
Single−Sided Amplitude Spectrum of x(t)
|X(f)|
Frequency (Hz)
Single−Sided Amplitude Spectrum of f(t)
|F(f)|
Frequency (Hz)
dynamic stiffness K(f)
Real−|K(f)|
Frequency (Hz)
Coherence Function
Gamma2
Frequency (Hz)

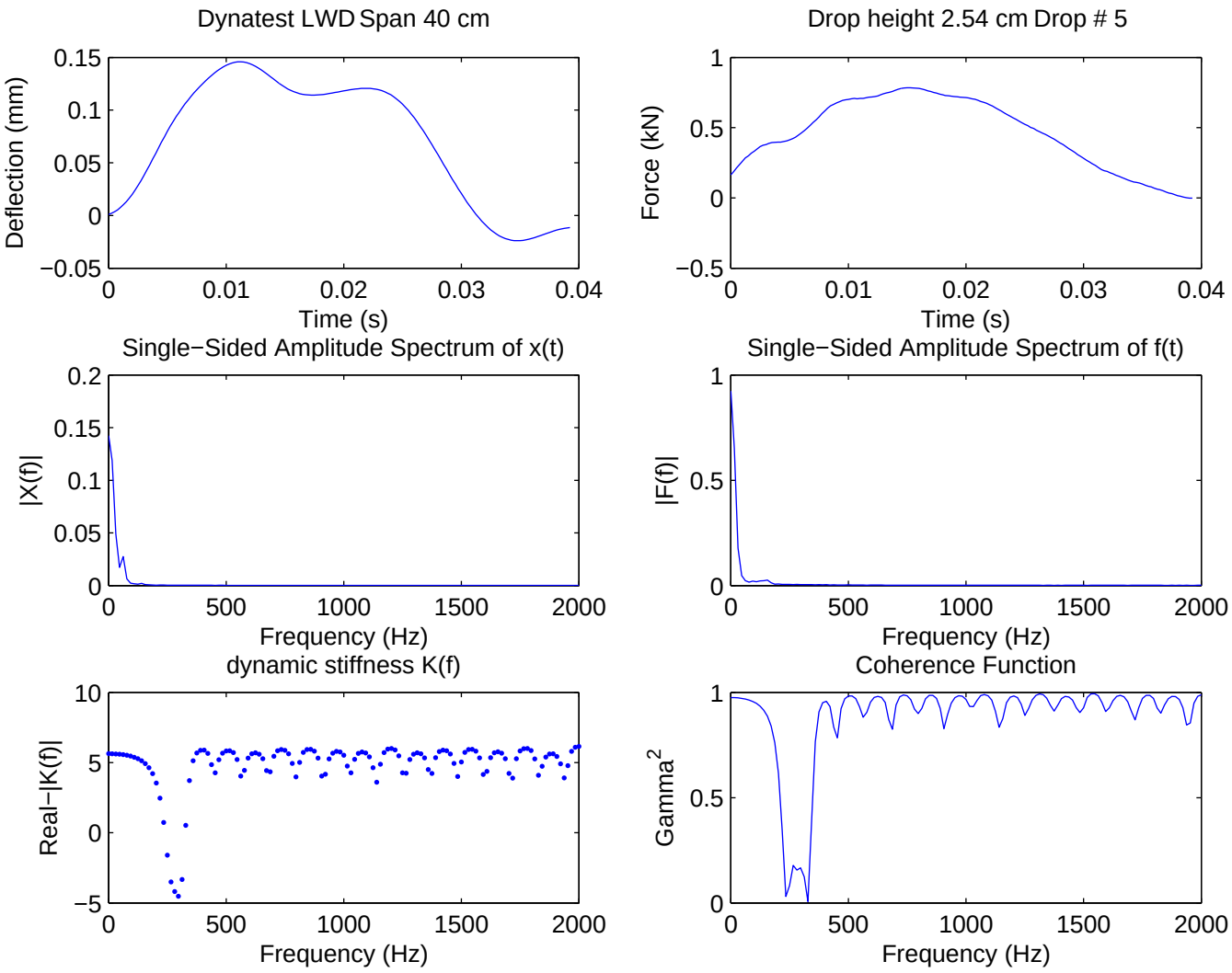
Dynatest LWD Span 40 cm
Deflection (mm)
Time (s)
Drop height 2.54 cm Drop # 5
Force (kN)
Time (s)
Single−Sided Amplitude Spectrum of x(t)
|X(f)|
Frequency (Hz)
Single−Sided Amplitude Spectrum of f(t)
|F(f)|
Frequency (Hz)
dynamic stiffness K(f)
Real−|K(f)|
Frequency (Hz)
Coherence Function
Gamma2
Frequency (Hz)

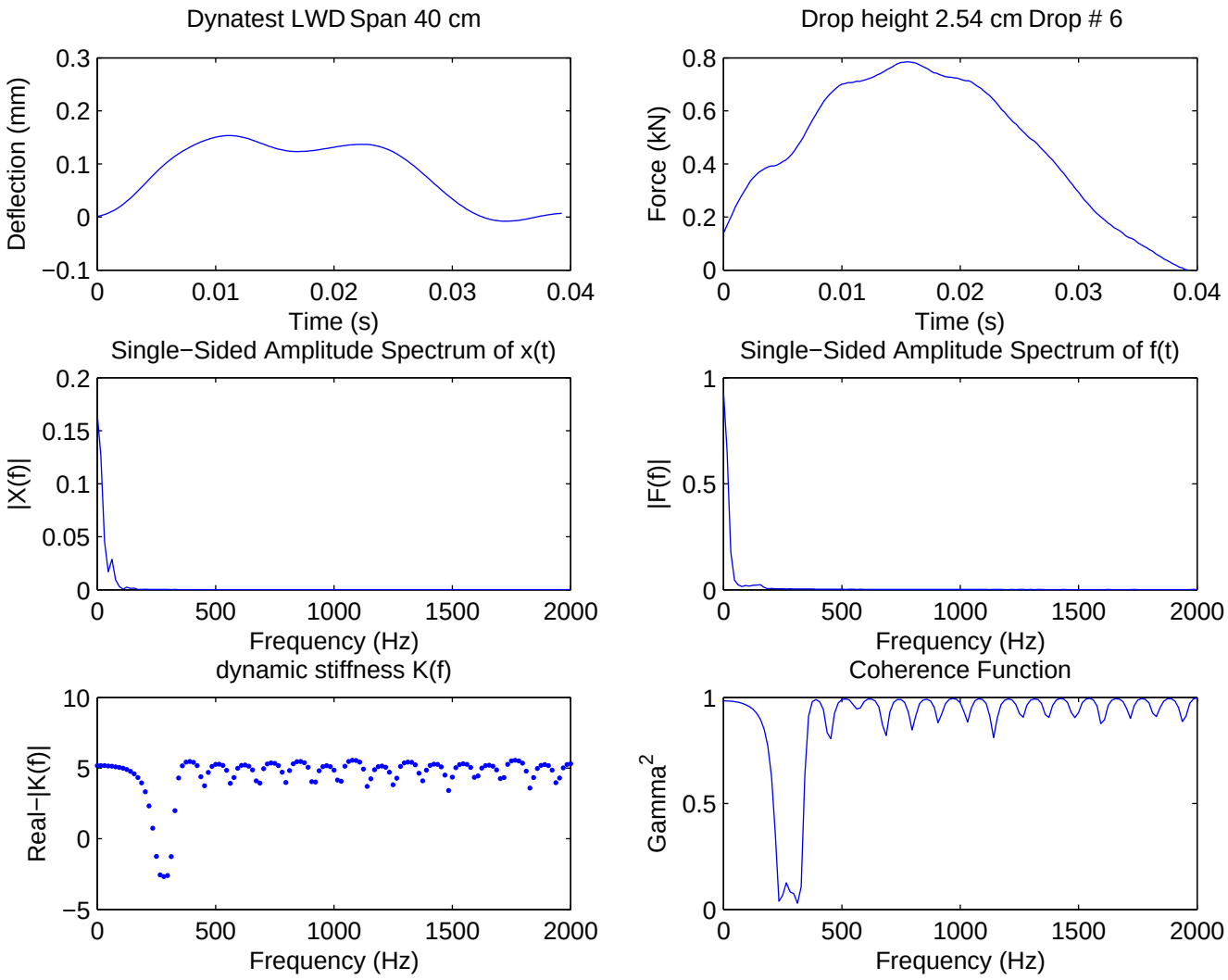
Dynatest LWD Span 40 cm
Deflection (mm)
Time (s)
Drop height 2.54 cm Drop # 6
Force (kN)
Time (s)
Single−Sided Amplitude Spectrum of x(t)
|X(f)|
Frequency (Hz)
Single−Sided Amplitude Spectrum of f(t)
|F(f)|
Frequency (Hz)
dynamic stiffness K(f)
Real−|K(f)|
Frequency (Hz)
Coherence Function
Gamma2
Frequency (Hz)

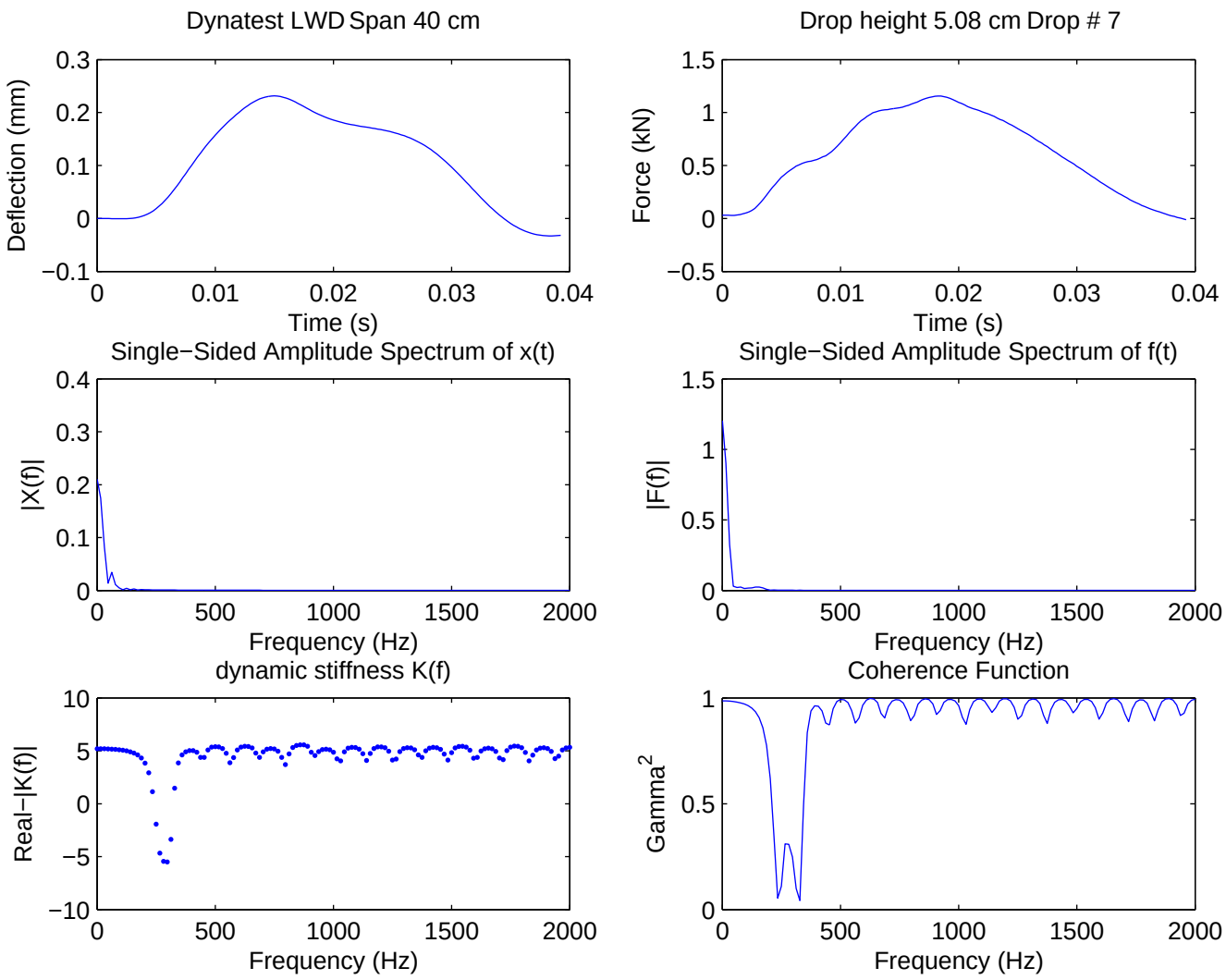
Dynatest LWD Span 40 cm
Deflection (mm)
Time (s)
Drop height 5.08 cm Drop # 7
Force (kN)
Time (s)
Single−Sided Amplitude Spectrum of x(t)
|X(f)|
Frequency (Hz)
Single−Sided Amplitude Spectrum of f(t)
|F(f)|
Frequency (Hz)
dynamic stiffness K(f)
Real−|K(f)|
Frequency (Hz)
Coherence Function
Gamma2
Frequency (Hz)

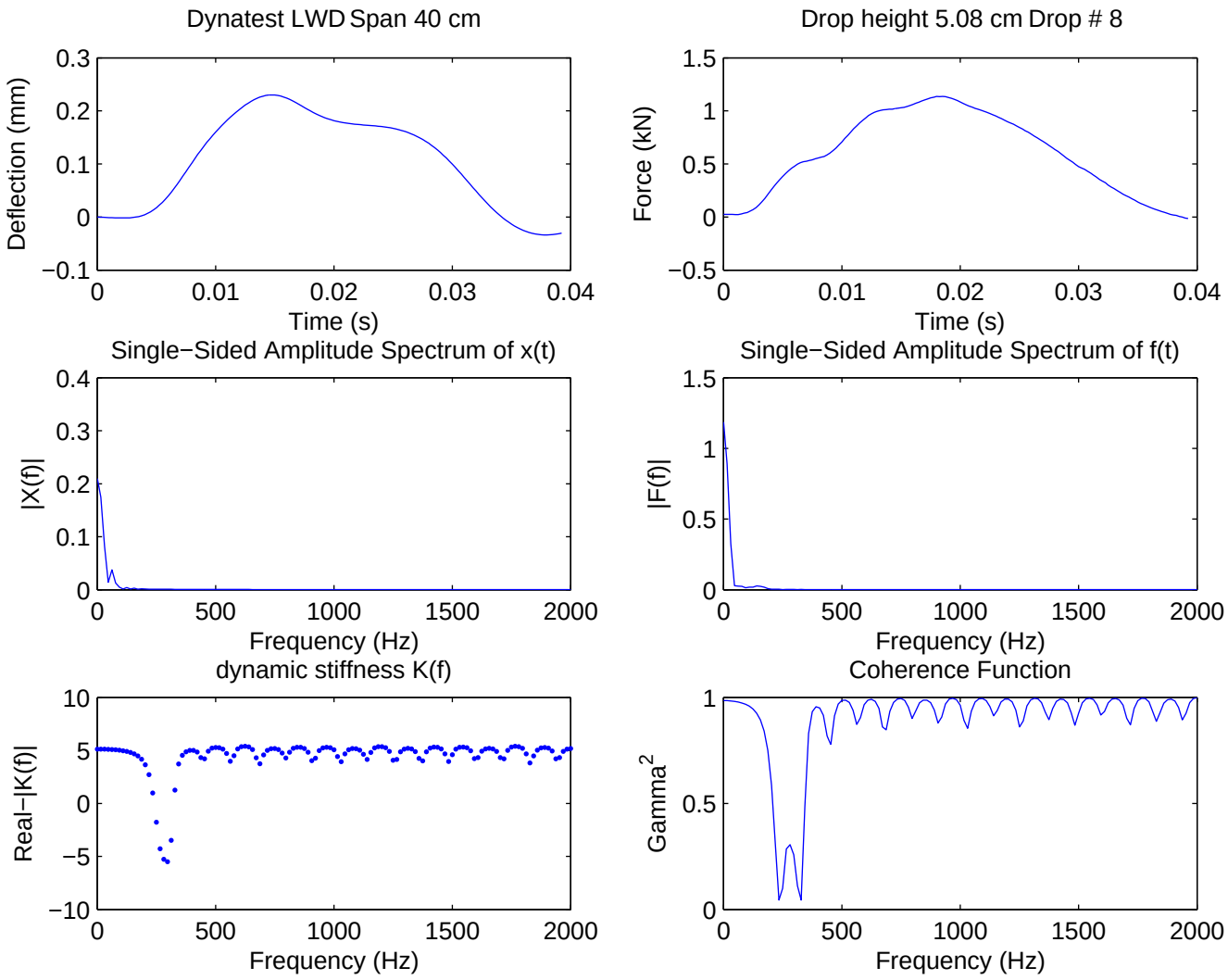
Dynatest LWD Span 40 cm
Deflection (mm)
Time (s)
Drop height 5.08 cm Drop # 8
Force (kN)
Time (s)
Single−Sided Amplitude Spectrum of x(t)
|X(f)|
Frequency (Hz)
Single−Sided Amplitude Spectrum of f(t)
|F(f)|
Frequency (Hz)
dynamic stiffness K(f)
Real−|K(f)|
Frequency (Hz)
Coherence Function
Gamma2
Frequency (Hz)

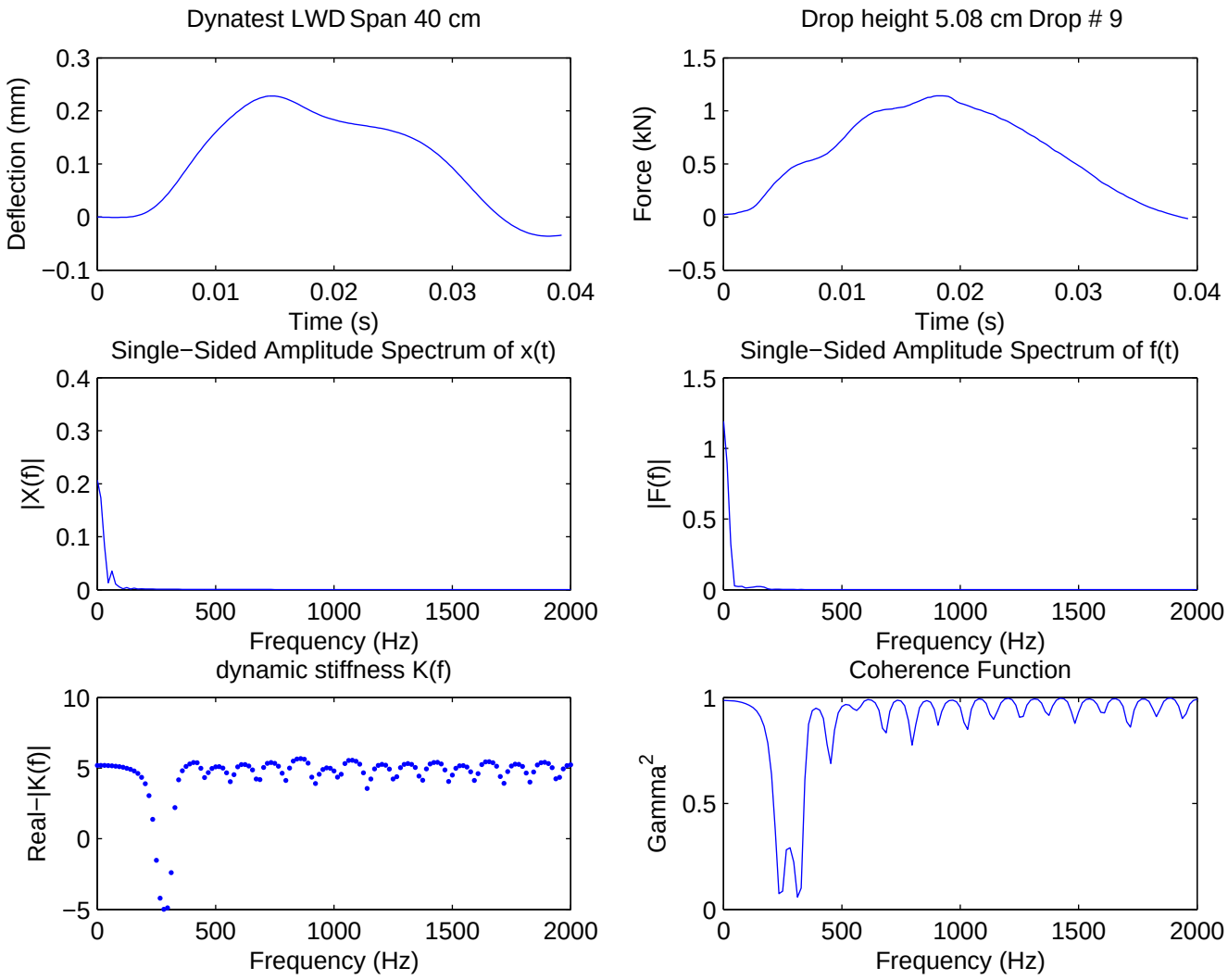
Dynatest LWD Span 40 cm
Deflection (mm)
Time (s)
Drop height 5.08 cm Drop # 9
Force (kN)
Time (s)
Single−Sided Amplitude Spectrum of x(t)
|X(f)|
Frequency (Hz)
Single−Sided Amplitude Spectrum of f(t)
|F(f)|
Frequency (Hz)
dynamic stiffness K(f)
Real−|K(f)|
Frequency (Hz)
Coherence Function
Gamma2
Frequency (Hz)

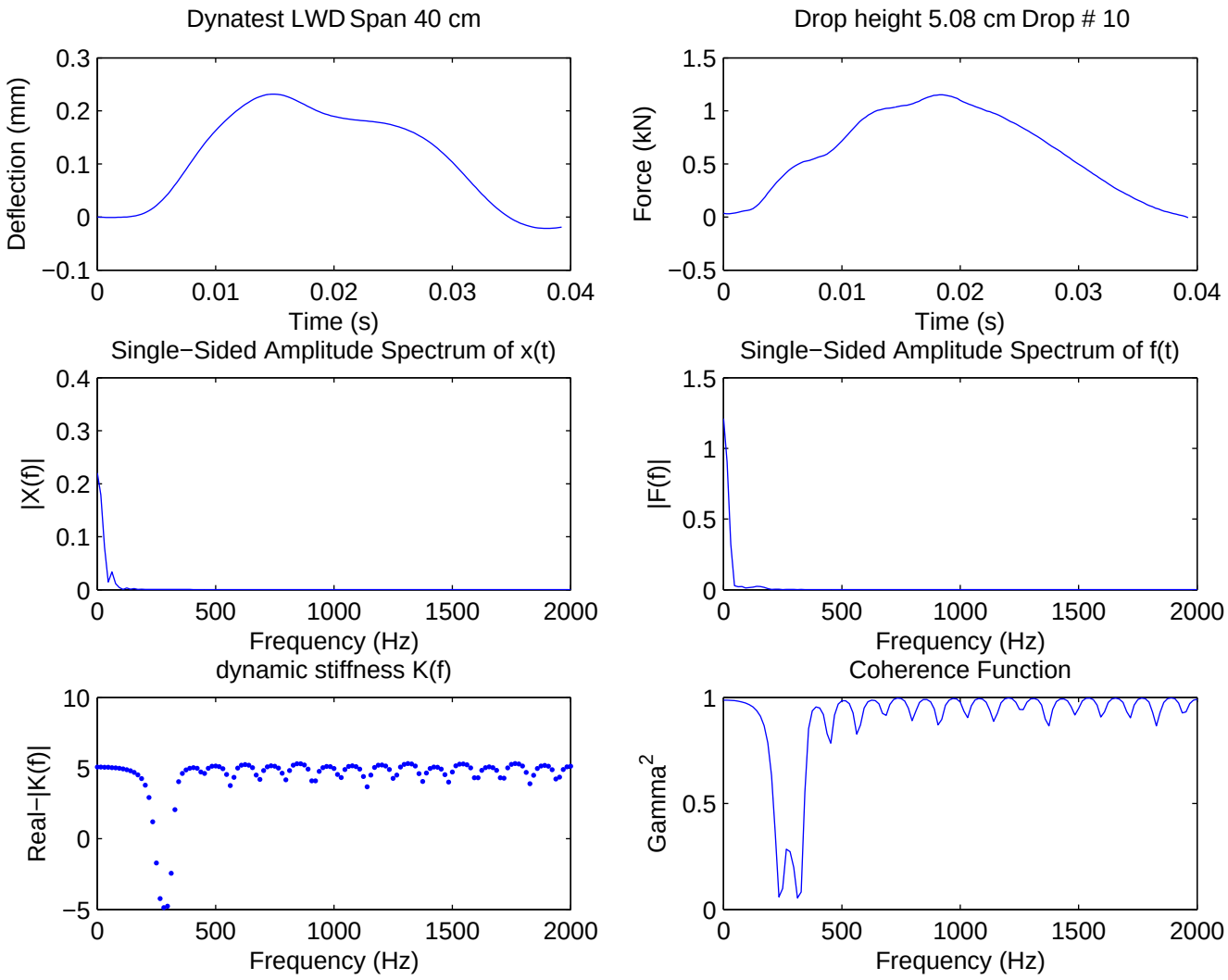
Dynatest LWD Span 40 cm
Deflection (mm)
Time (s)
Drop height 5.08 cm Drop # 10
Force (kN)
Time (s)
Single−Sided Amplitude Spectrum of x(t)
|X(f)|
Frequency (Hz)
Single−Sided Amplitude Spectrum of f(t)
|F(f)|
Frequency (Hz)
dynamic stiffness K(f)
Real−|K(f)|
Frequency (Hz)
Coherence Function
Gamma2
Frequency (Hz)

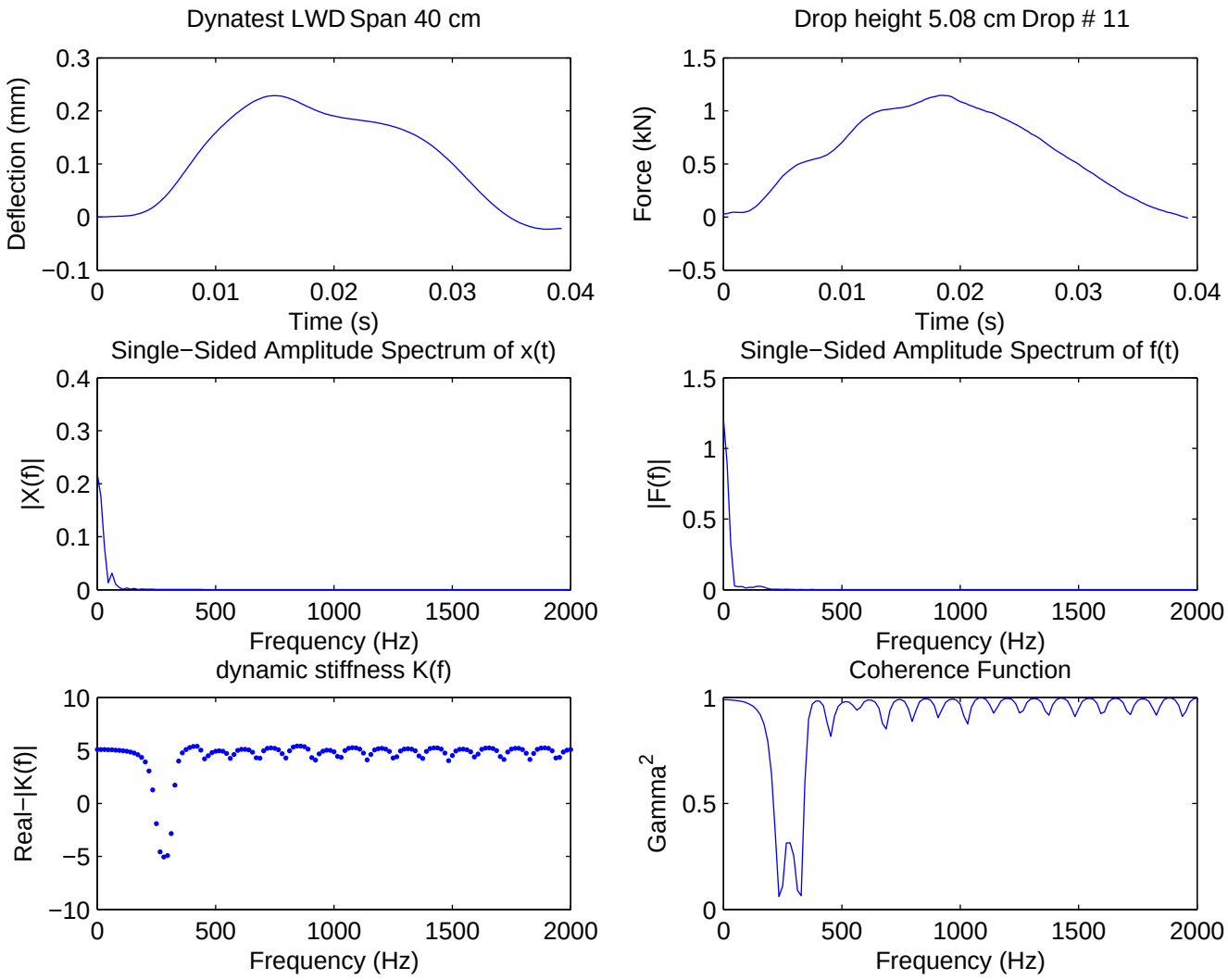
Dynatest LWD Span 40 cm
Deflection (mm)
Time (s)
Drop height 5.08 cm Drop # 11
Force (kN)
Time (s)
Single−Sided Amplitude Spectrum of x(t)
|X(f)|
Frequency (Hz)
Single−Sided Amplitude Spectrum of f(t)
|F(f)|
Frequency (Hz)
dynamic stiffness K(f)
Real−|K(f)|
Frequency (Hz)
Coherence Function
Gamma2
Frequency (Hz)

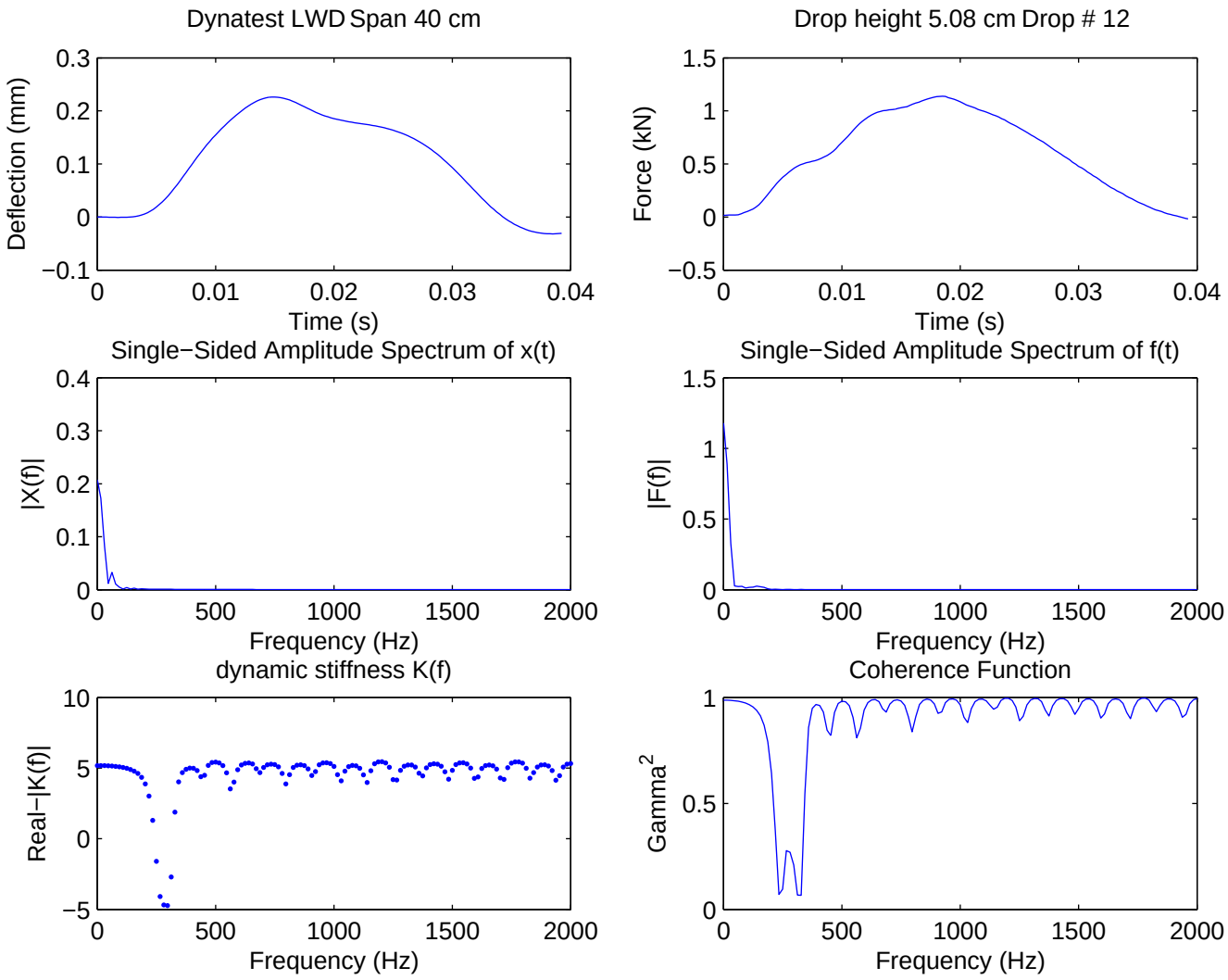
Dynatest LWD Span 40 cm
Deflection (mm)
Time (s)
Drop height 5.08 cm Drop # 12
Force (kN)
Time (s)
Single−Sided Amplitude Spectrum of x(t)
|X(f)|
Frequency (Hz)
Single−Sided Amplitude Spectrum of f(t)
|F(f)|
Frequency (Hz)
dynamic stiffness K(f)
Real−|K(f)|
Frequency (Hz)
Coherence Function
Gamma2
Frequency (Hz)

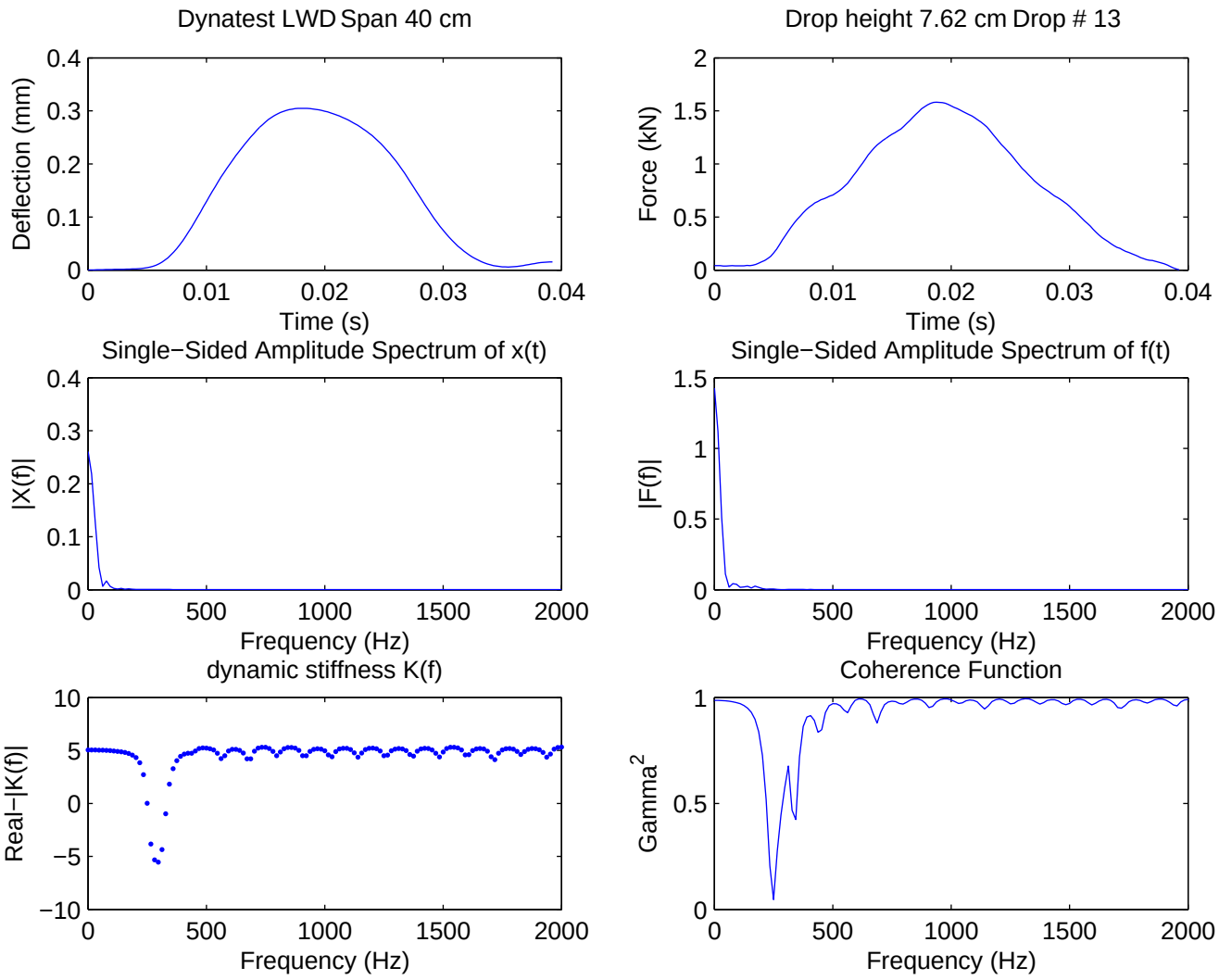
Dynatest LWD Span 40 cm
Deflection (mm)
Time (s)
Drop height 7.62 cm Drop # 13
Force (kN)
Time (s)
Single−Sided Amplitude Spectrum of x(t)
|X(f)|
Frequency (Hz)
Single−Sided Amplitude Spectrum of f(t)
|F(f)|
Frequency (Hz)
dynamic stiffness K(f)
Real−|K(f)|
Frequency (Hz)
Coherence Function
Gamma2
Frequency (Hz)

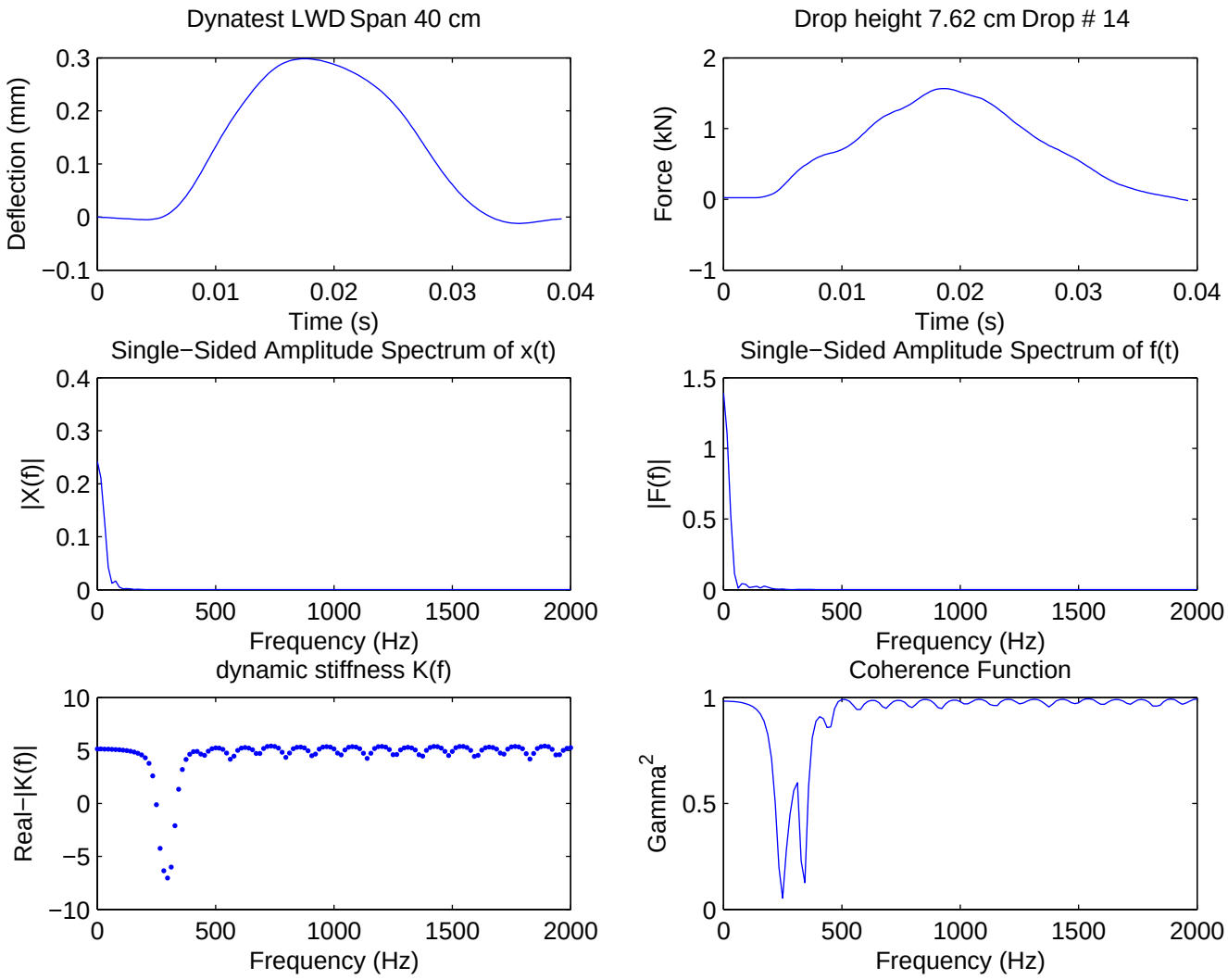
Dynatest LWD Span 40 cm
Deflection (mm)
Time (s)
Drop height 7.62 cm Drop # 14
Force (kN)
Time (s)
Single−Sided Amplitude Spectrum of x(t)
|X(f)|
Frequency (Hz)
Single−Sided Amplitude Spectrum of f(t)
|F(f)|
Frequency (Hz)
dynamic stiffness K(f)
Real−|K(f)|
Frequency (Hz)
Coherence Function
Gamma2
Frequency (Hz)

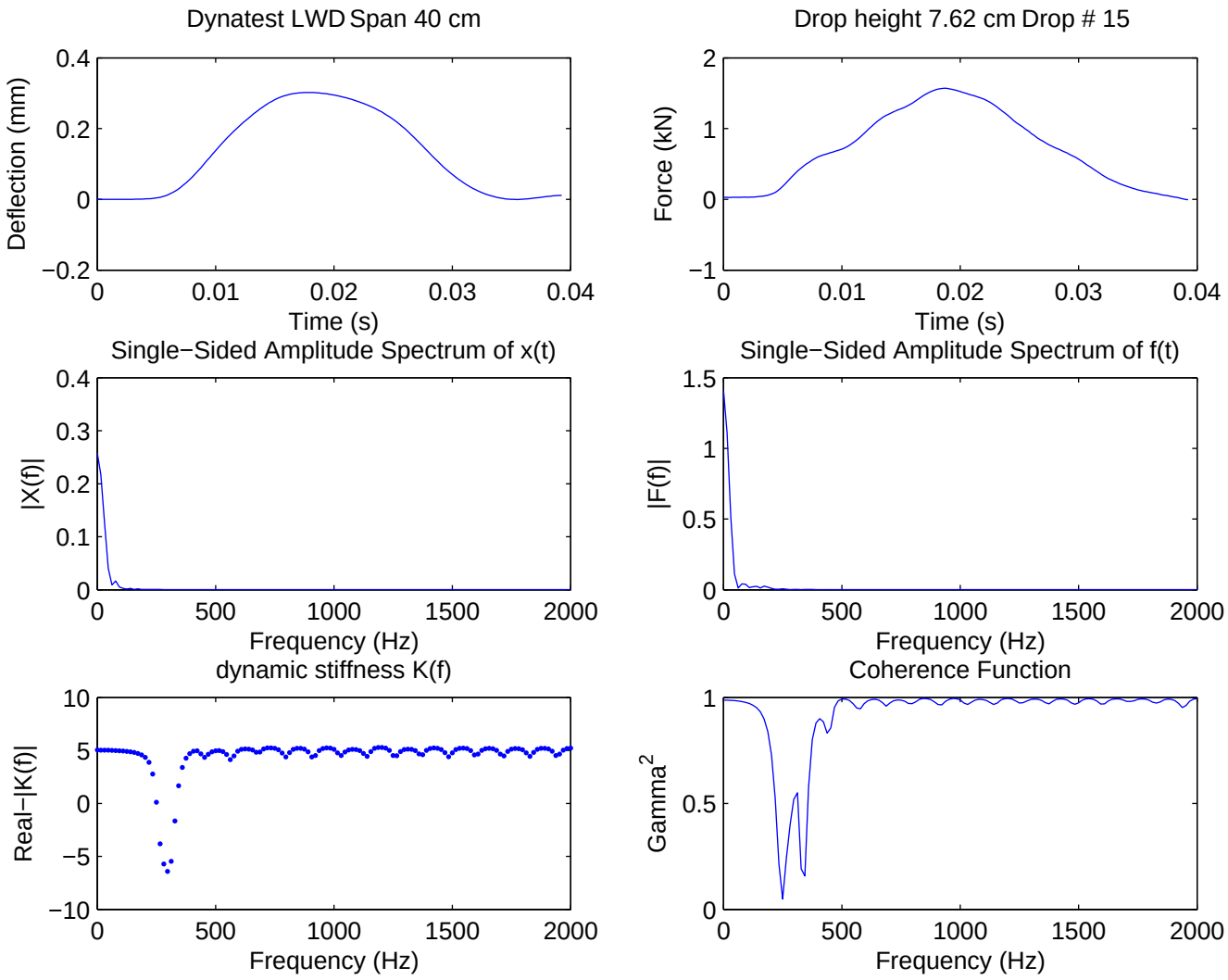
Dynatest LWD Span 40 cm
Deflection (mm)
Time (s)
Drop height 7.62 cm Drop # 15
Force (kN)
Time (s)
Single−Sided Amplitude Spectrum of x(t)
|X(f)|
Frequency (Hz)
Single−Sided Amplitude Spectrum of f(t)
|F(f)|
Frequency (Hz)
dynamic stiffness K(f)
Real−|K(f)|
Frequency (Hz)
Coherence Function
Gamma2
Frequency (Hz)

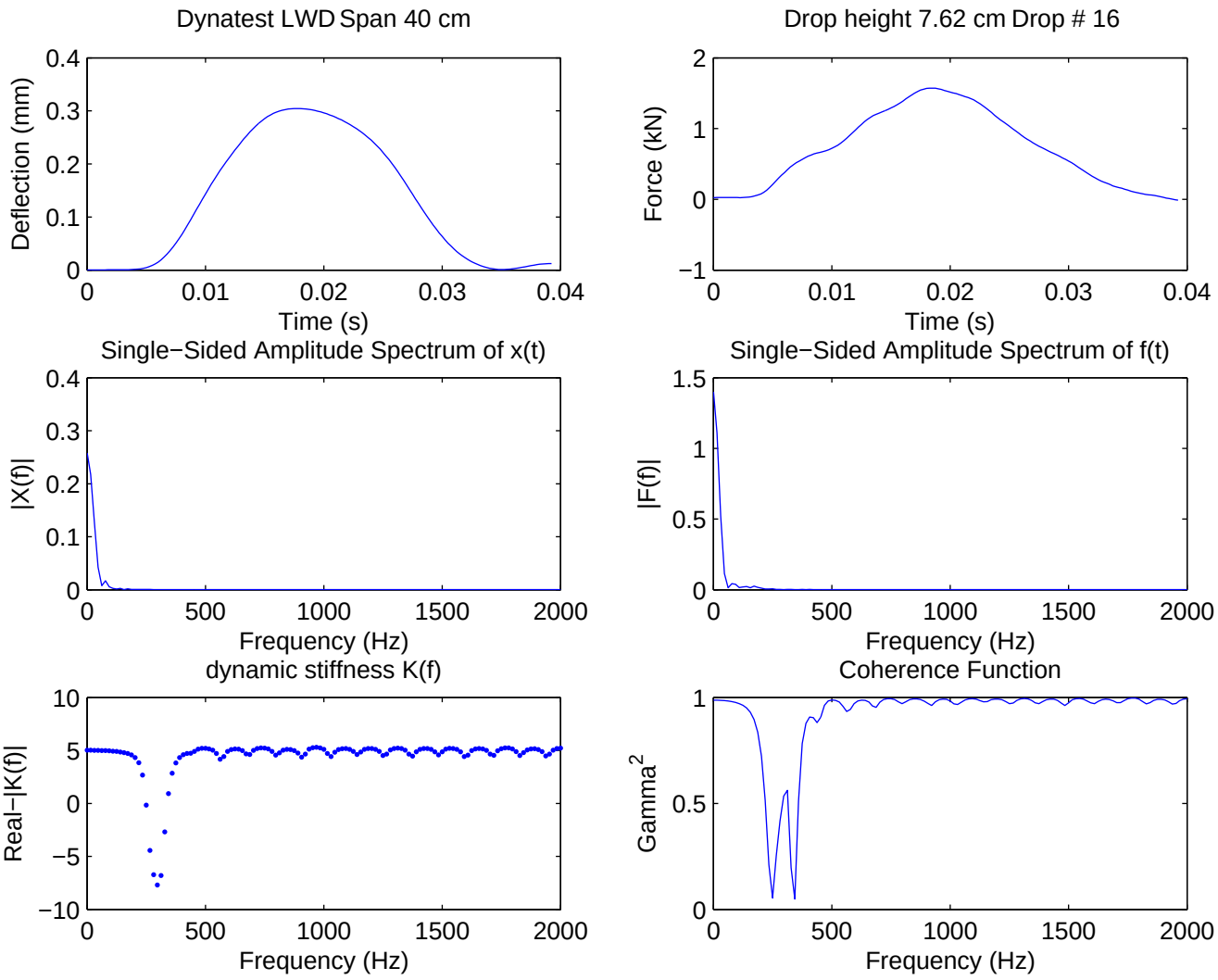
Dynatest LWD Span 40 cm
Deflection (mm)
Time (s)
Drop height 7.62 cm Drop # 16
Force (kN)
Time (s)
Single−Sided Amplitude Spectrum of x(t)
|X(f)|
Frequency (Hz)
Single−Sided Amplitude Spectrum of f(t)
|F(f)|
Frequency (Hz)
dynamic stiffness K(f)
Real−|K(f)|
Frequency (Hz)
Coherence Function
Gamma2
Frequency (Hz)

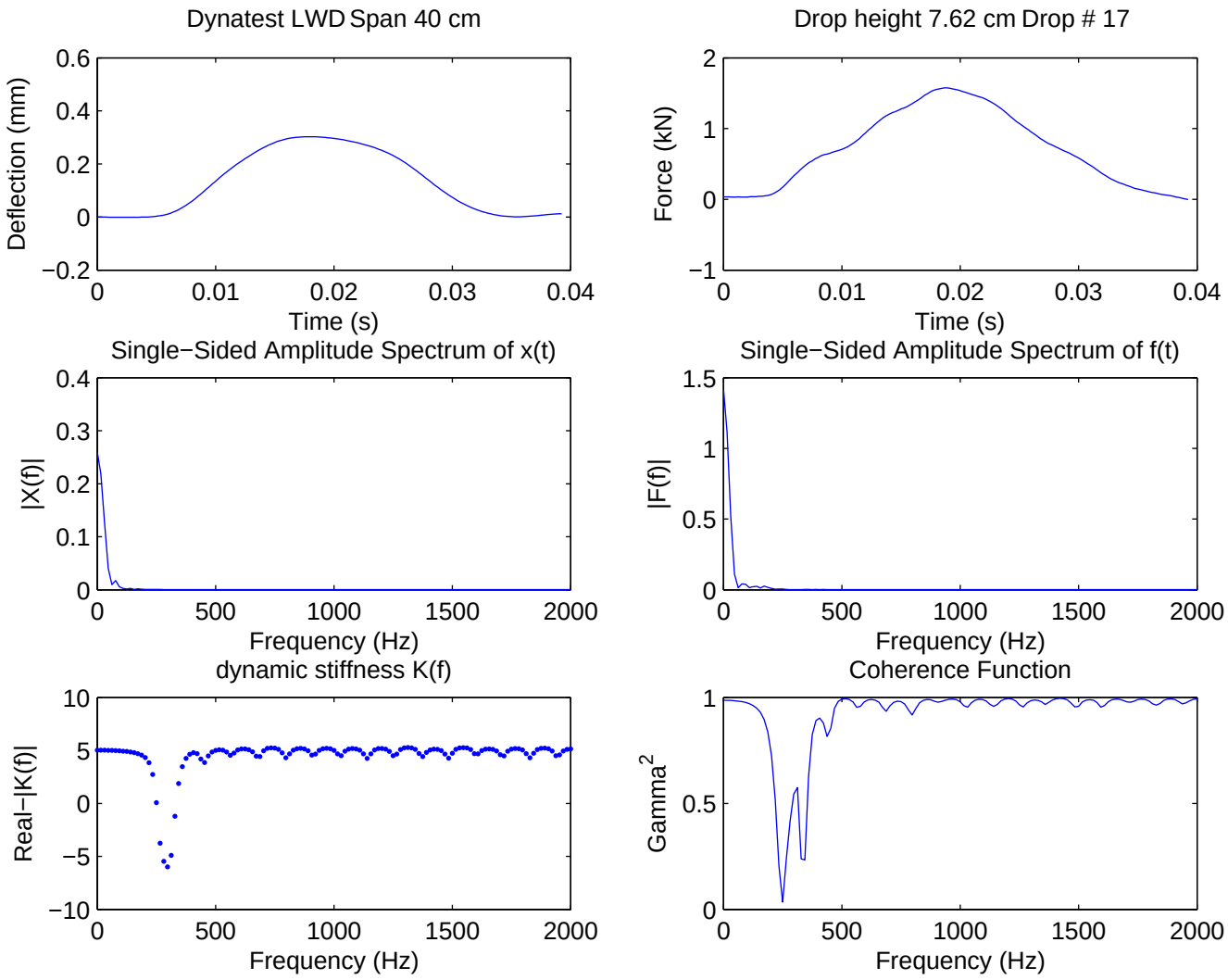
Dynatest LWD Span 40 cm
Deflection (mm)
Time (s)
Drop height 7.62 cm Drop # 17
Force (kN)
Time (s)
Single−Sided Amplitude Spectrum of x(t)
|X(f)|
Frequency (Hz)
Single−Sided Amplitude Spectrum of f(t)
|F(f)|
Frequency (Hz)
dynamic stiffness K(f)
Real−|K(f)|
Frequency (Hz)
Coherence Function
Gamma2
Frequency (Hz)

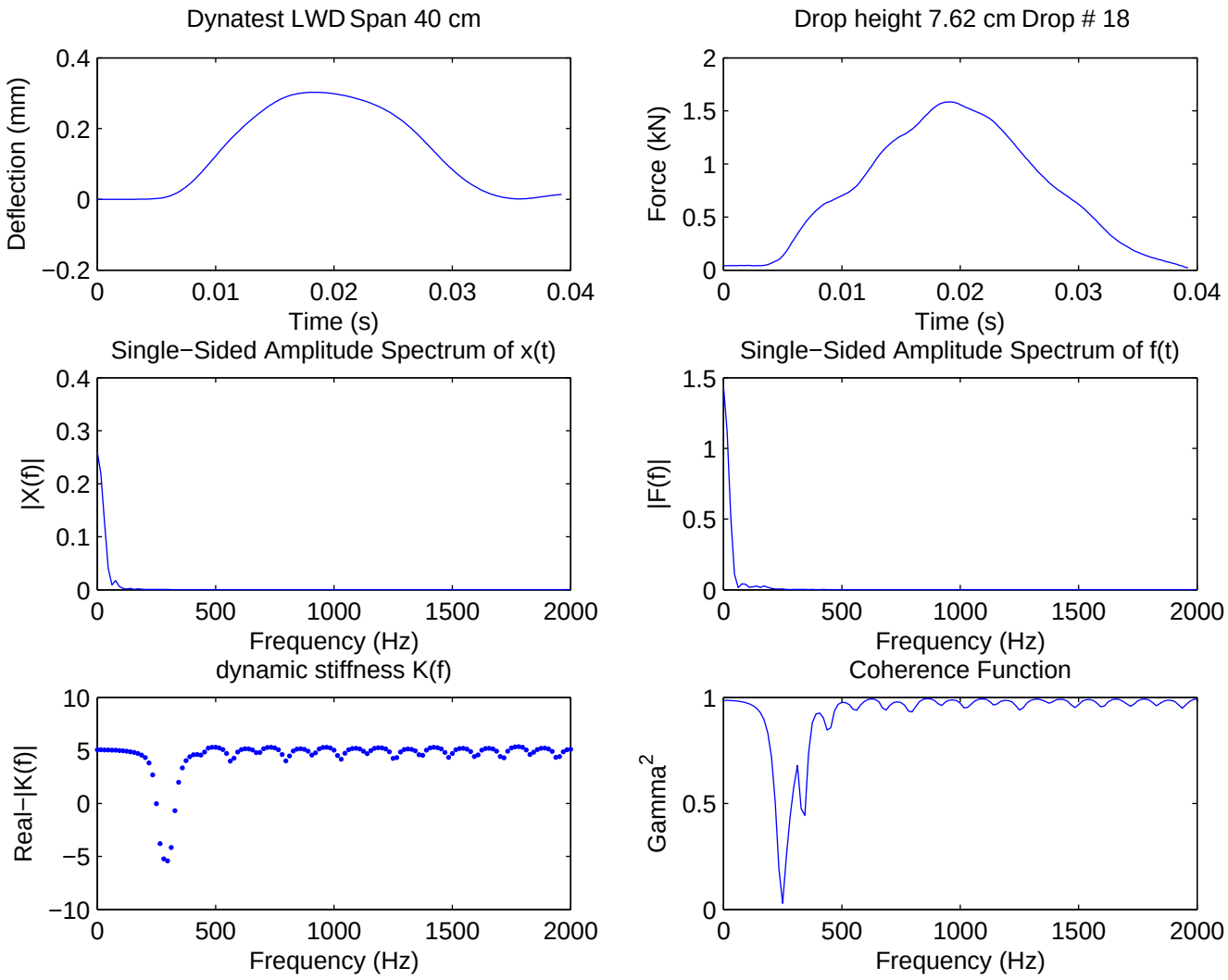
Dynatest LWD Span 40 cm
Deflection (mm)
Time (s)
Drop height 7.62 cm Drop # 18
Force (kN)
Time (s)
Single−Sided Amplitude Spectrum of x(t)
|X(f)|
Frequency (Hz)
Single−Sided Amplitude Spectrum of f(t)
|F(f)|
Frequency (Hz)
dynamic stiffness K(f)
Real−|K(f)|
Frequency (Hz)
Coherence Function
Gamma2
Frequency (Hz)

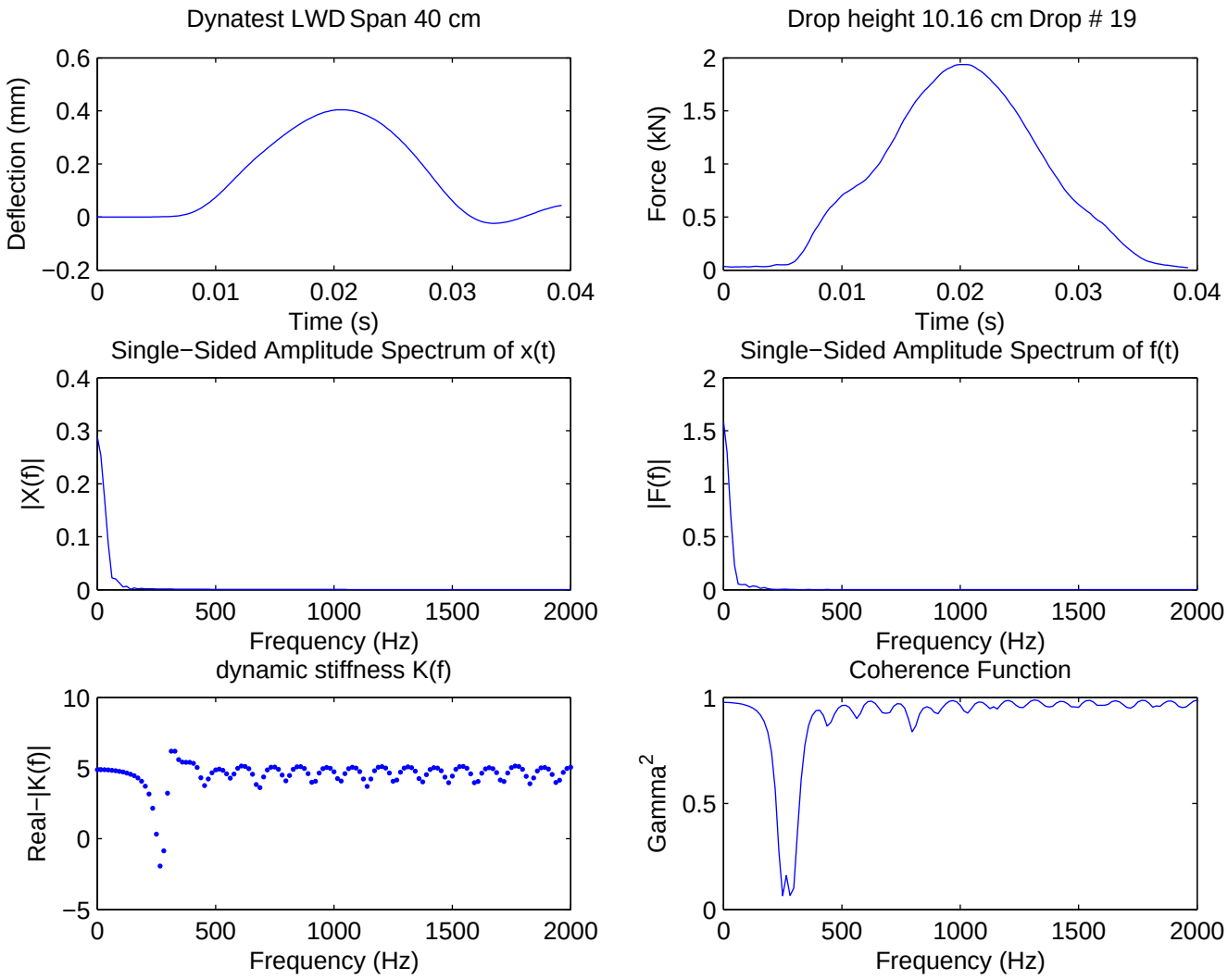
Dynatest LWD Span 40 cm
Deflection (mm)
Time (s)
Drop height 10.16 cm Drop # 19
Force (kN)
Time (s)
Single−Sided Amplitude Spectrum of x(t)
|X(f)|
Frequency (Hz)
Single−Sided Amplitude Spectrum of f(t)
|F(f)|
Frequency (Hz)
dynamic stiffness K(f)
Real−|K(f)|
Frequency (Hz)
Coherence Function
Gamma2
Frequency (Hz)

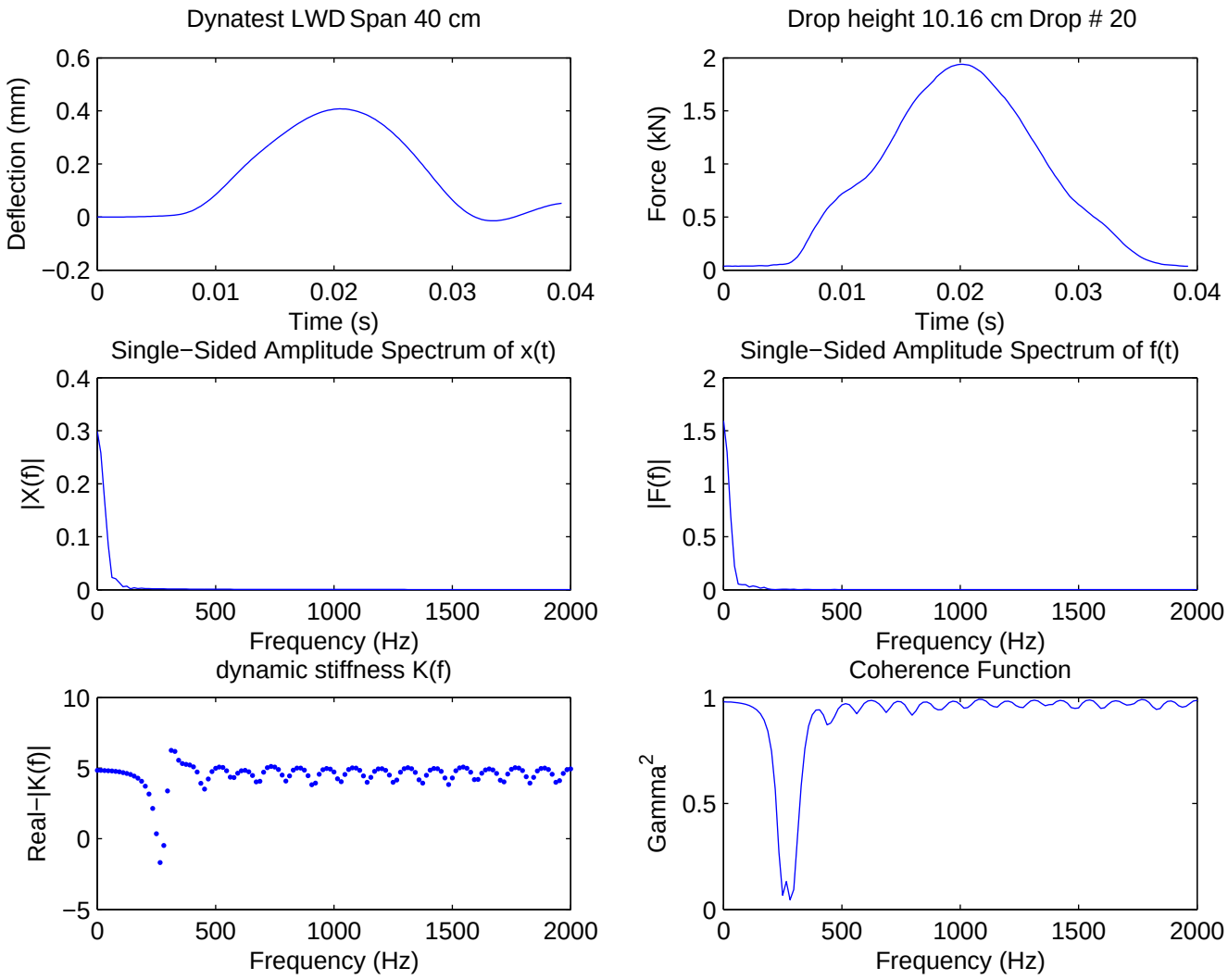
Dynatest LWD Span 40 cm
Deflection (mm)
Time (s)
Drop height 10.16 cm Drop # 20
Force (kN)
Time (s)
Single−Sided Amplitude Spectrum of x(t)
|X(f)|
Frequency (Hz)
Single−Sided Amplitude Spectrum of f(t)
|F(f)|
Frequency (Hz)
dynamic stiffness K(f)
Real−|K(f)|
Frequency (Hz)
Coherence Function
Gamma2
Frequency (Hz)

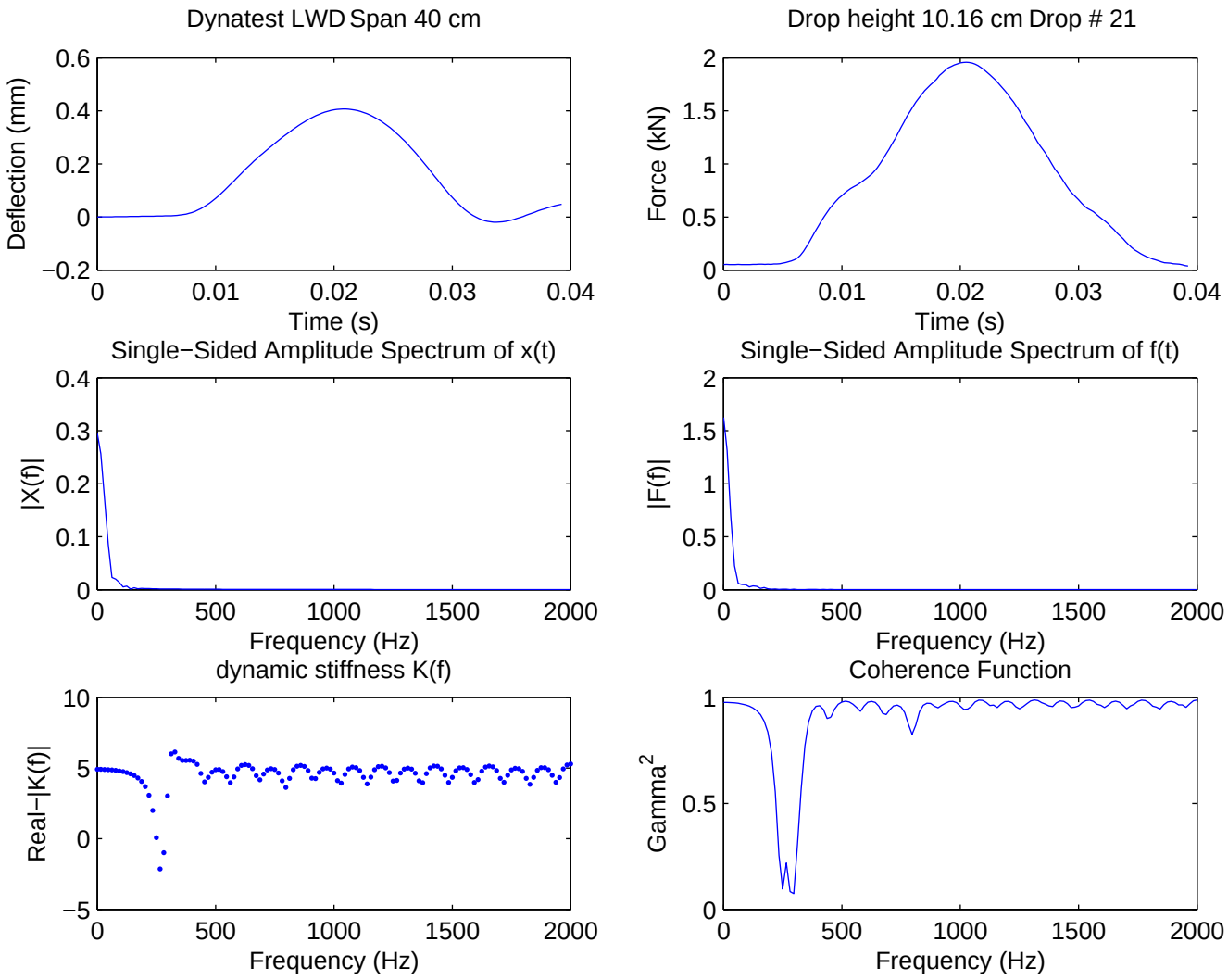
Dynatest LWD Span 40 cm
Deflection (mm)
Time (s)
Drop height 10.16 cm Drop # 21
Force (kN)
Time (s)
Single−Sided Amplitude Spectrum of x(t)
|X(f)|
Frequency (Hz)
Single−Sided Amplitude Spectrum of f(t)
|F(f)|
Frequency (Hz)
dynamic stiffness K(f)
Real−|K(f)|
Frequency (Hz)
Coherence Function
Gamma2
Frequency (Hz)

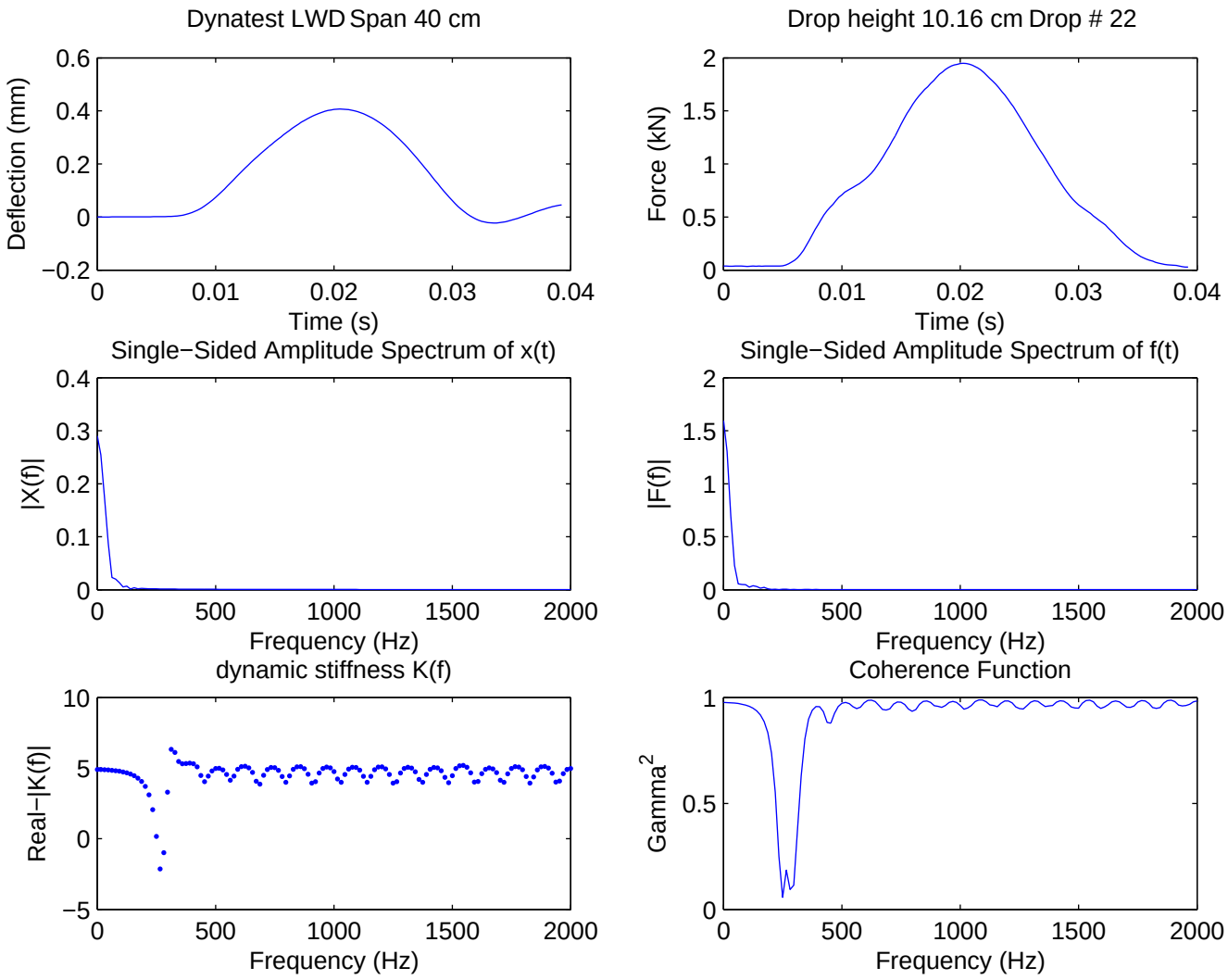
Dynatest LWD Span 40 cm
Deflection (mm)
Time (s)
Drop height 10.16 cm Drop # 22
Force (kN)
Time (s)
Single−Sided Amplitude Spectrum of x(t)
|X(f)|
Frequency (Hz)
Single−Sided Amplitude Spectrum of f(t)
|F(f)|
Frequency (Hz)
dynamic stiffness K(f)
Real−|K(f)|
Frequency (Hz)
Coherence Function
Gamma2
Frequency (Hz)

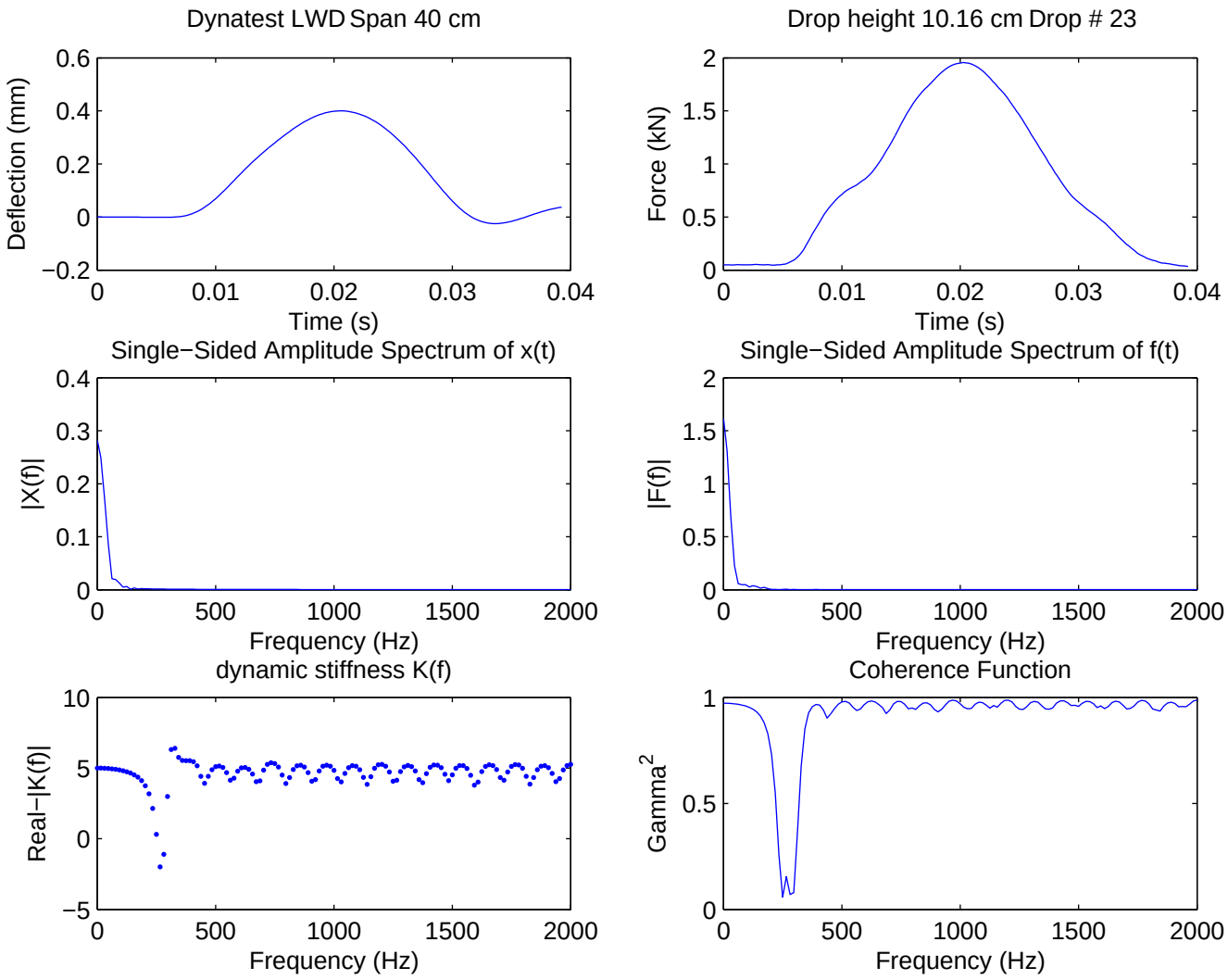
Dynatest LWD Span 40 cm
Deflection (mm)
Time (s)
Drop height 10.16 cm Drop # 23
Force (kN)
Time (s)
Single−Sided Amplitude Spectrum of x(t)
|X(f)|
Frequency (Hz)
Single−Sided Amplitude Spectrum of f(t)
|F(f)|
Frequency (Hz)
dynamic stiffness K(f)
Real−|K(f)|
Frequency (Hz)
Coherence Function
Gamma2
Frequency (Hz)

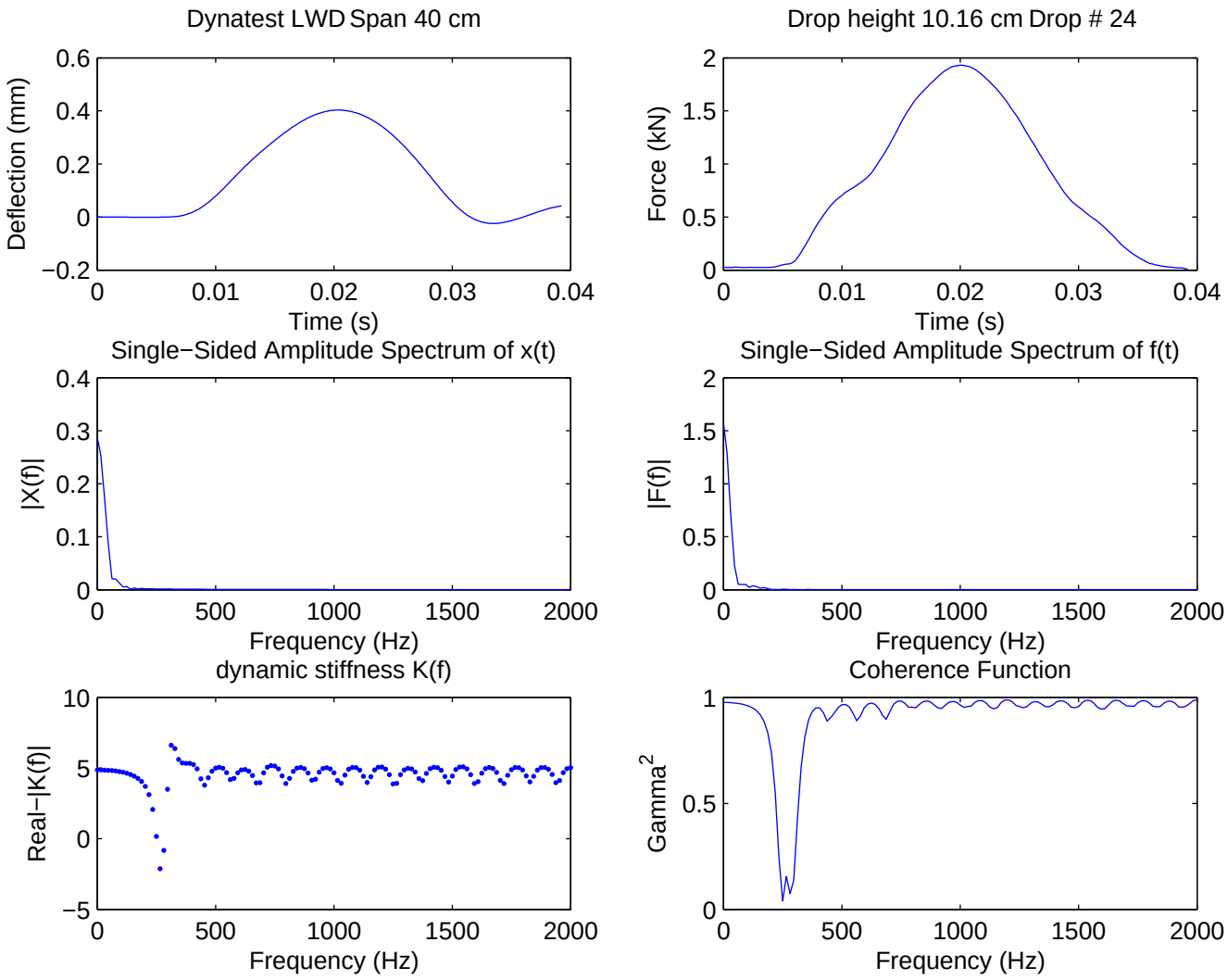
Dynatest LWD Span 40 cm
Deflection (mm)
Time (s)
Drop height 10.16 cm Drop # 24
Force (kN)
Time (s)
Single−Sided Amplitude Spectrum of x(t)
|X(f)|
Frequency (Hz)
Single−Sided Amplitude Spectrum of f(t)
|F(f)|
Frequency (Hz)
dynamic stiffness K(f)
Real−|K(f)|
Frequency (Hz)
Coherence Function
Gamma2
Frequency (Hz)

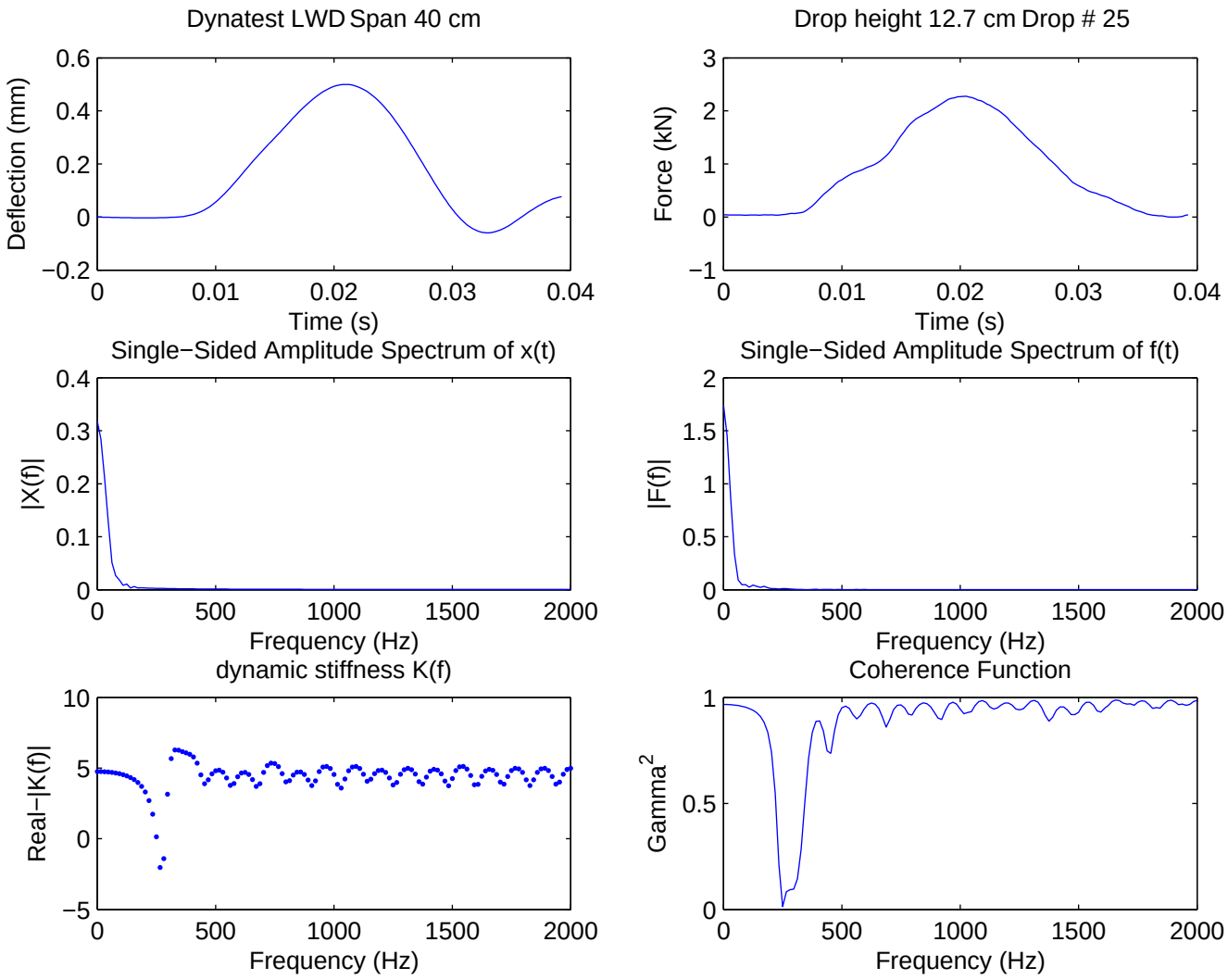
Dynatest LWD Span 40 cm
Deflection (mm)
Time (s)
Drop height 12.7 cm Drop # 25
Force (kN)
Time (s)
Single−Sided Amplitude Spectrum of x(t)
|X(f)|
Frequency (Hz)
Single−Sided Amplitude Spectrum of f(t)
|F(f)|
Frequency (Hz)
dynamic stiffness K(f)
Real−|K(f)|
Frequency (Hz)
Coherence Function
Gamma2
Frequency (Hz)

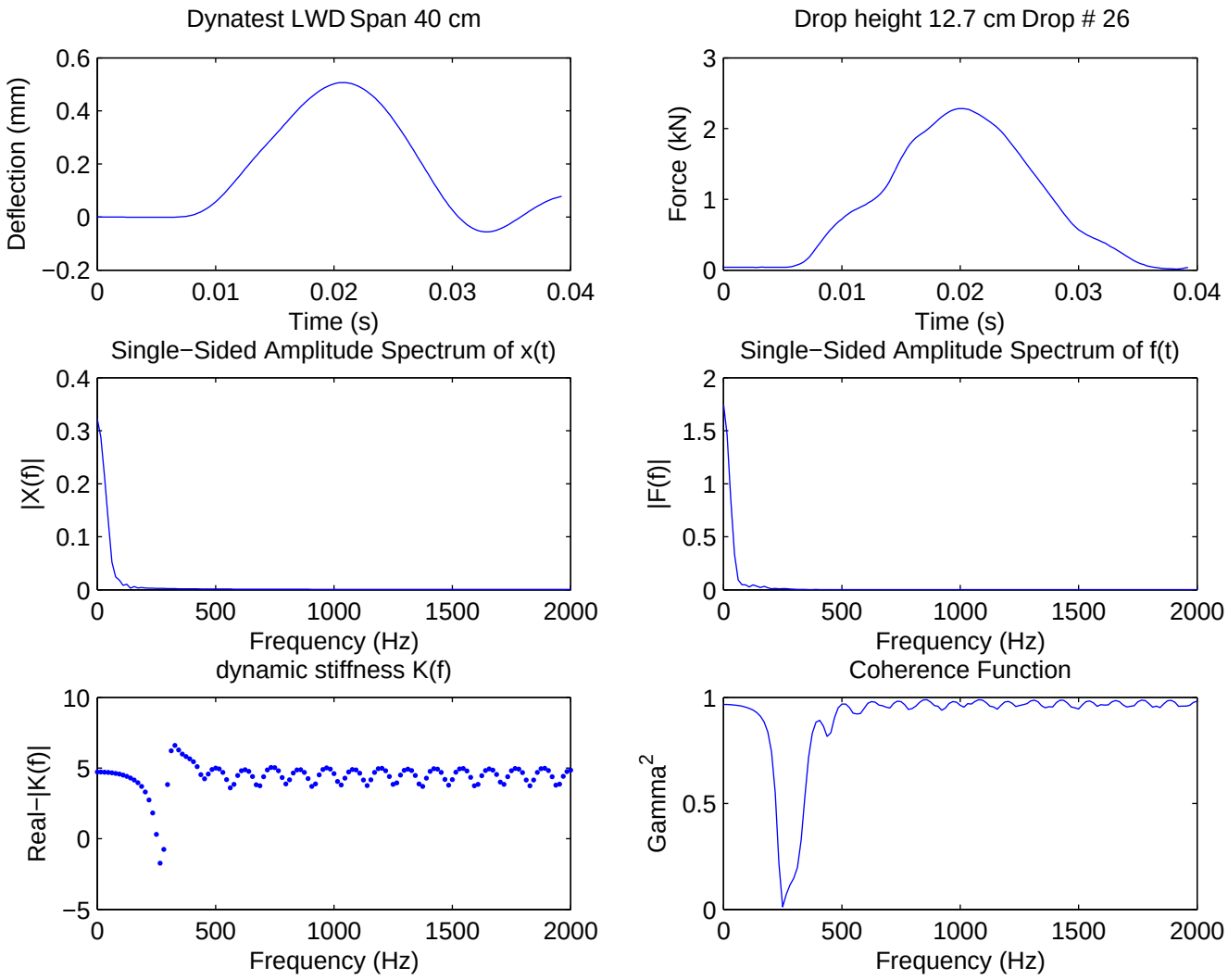
Dynatest LWD Span 40 cm
Deflection (mm)
Time (s)
Drop height 12.7 cm Drop # 26
Force (kN)
Time (s)
Single−Sided Amplitude Spectrum of x(t)
|X(f)|
Frequency (Hz)
Single−Sided Amplitude Spectrum of f(t)
|F(f)|
Frequency (Hz)
dynamic stiffness K(f)
Real−|K(f)|
Frequency (Hz)
Coherence Function
Gamma2
Frequency (Hz)

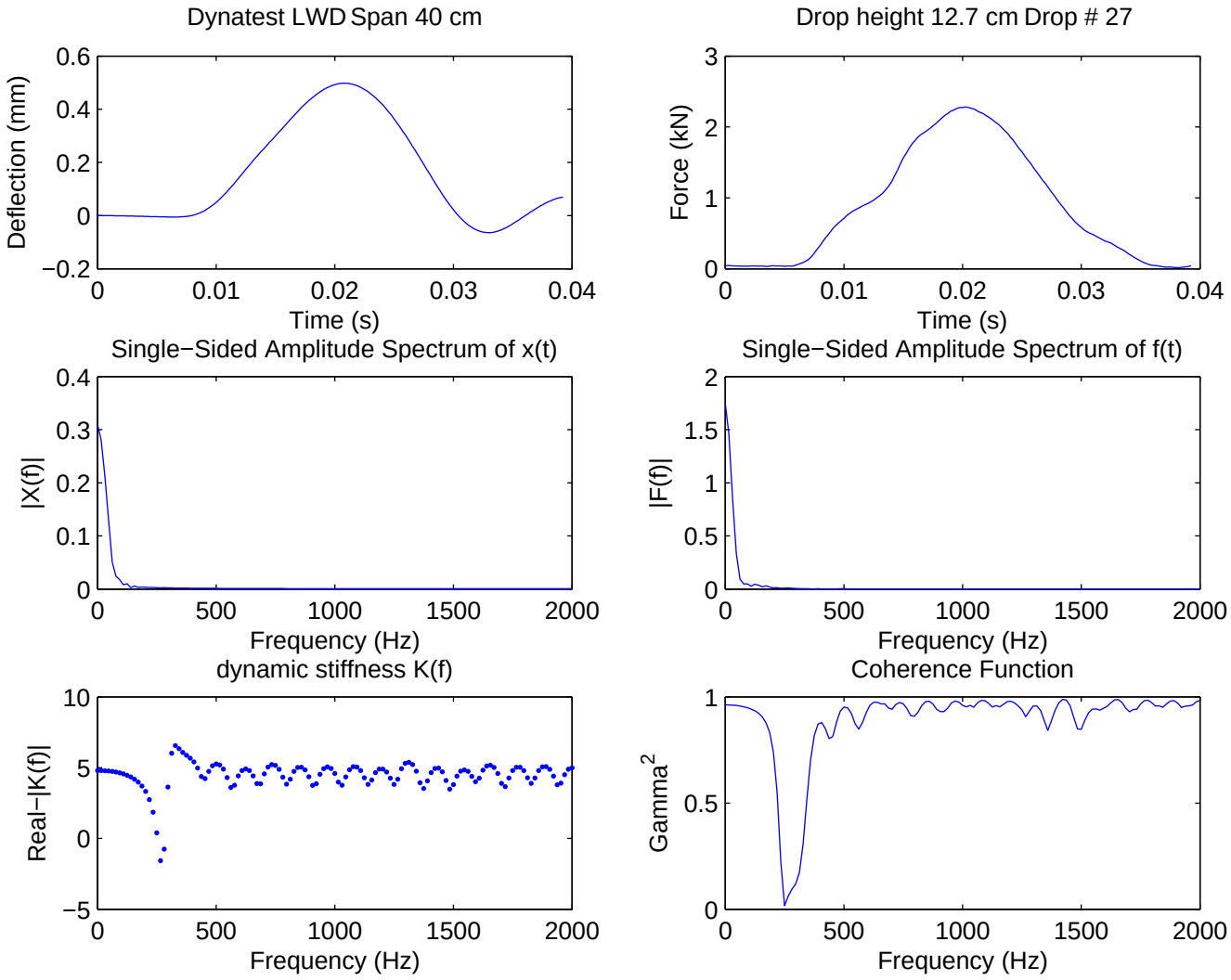
Dynatest LWD Span 40 cm
Deflection (mm)
Time (s)
Drop height 12.7 cm Drop # 27
Force (kN)
Time (s)
Single−Sided Amplitude Spectrum of x(t)
|X(f)|
Frequency (Hz)
Single−Sided Amplitude Spectrum of f(t)
|F(f)|
Frequency (Hz)
dynamic stiffness K(f)
Real−|K(f)|
Frequency (Hz)
Coherence Function
Gamma2
Frequency (Hz)

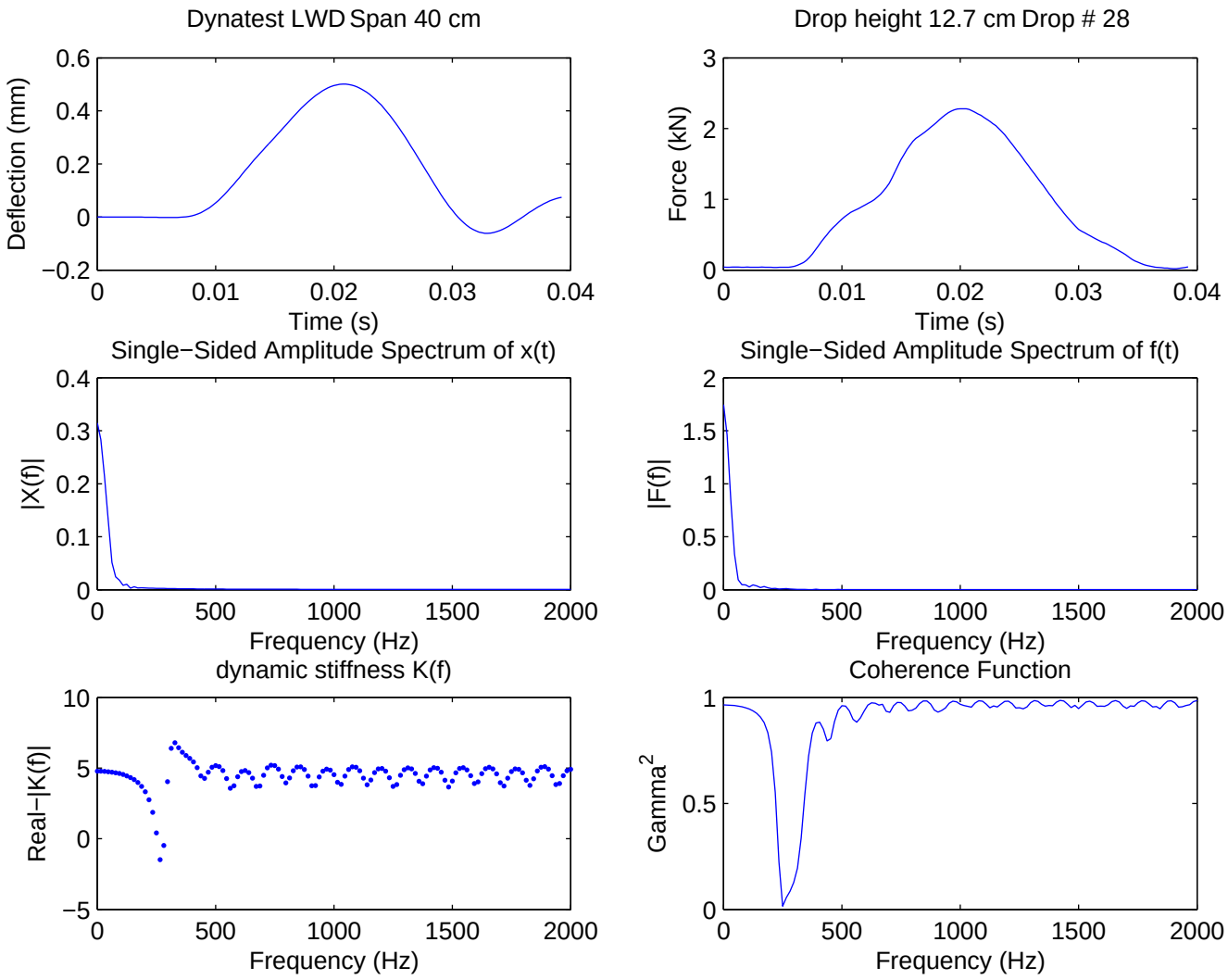
Dynatest LWD Span 40 cm
Deflection (mm)
Time (s)
Drop height 12.7 cm Drop # 28
Force (kN)
Time (s)
Single−Sided Amplitude Spectrum of x(t)
|X(f)|
Frequency (Hz)
Single−Sided Amplitude Spectrum of f(t)
|F(f)|
Frequency (Hz)
dynamic stiffness K(f)
Real−|K(f)|
Frequency (Hz)
Coherence Function
Gamma2
Frequency (Hz)

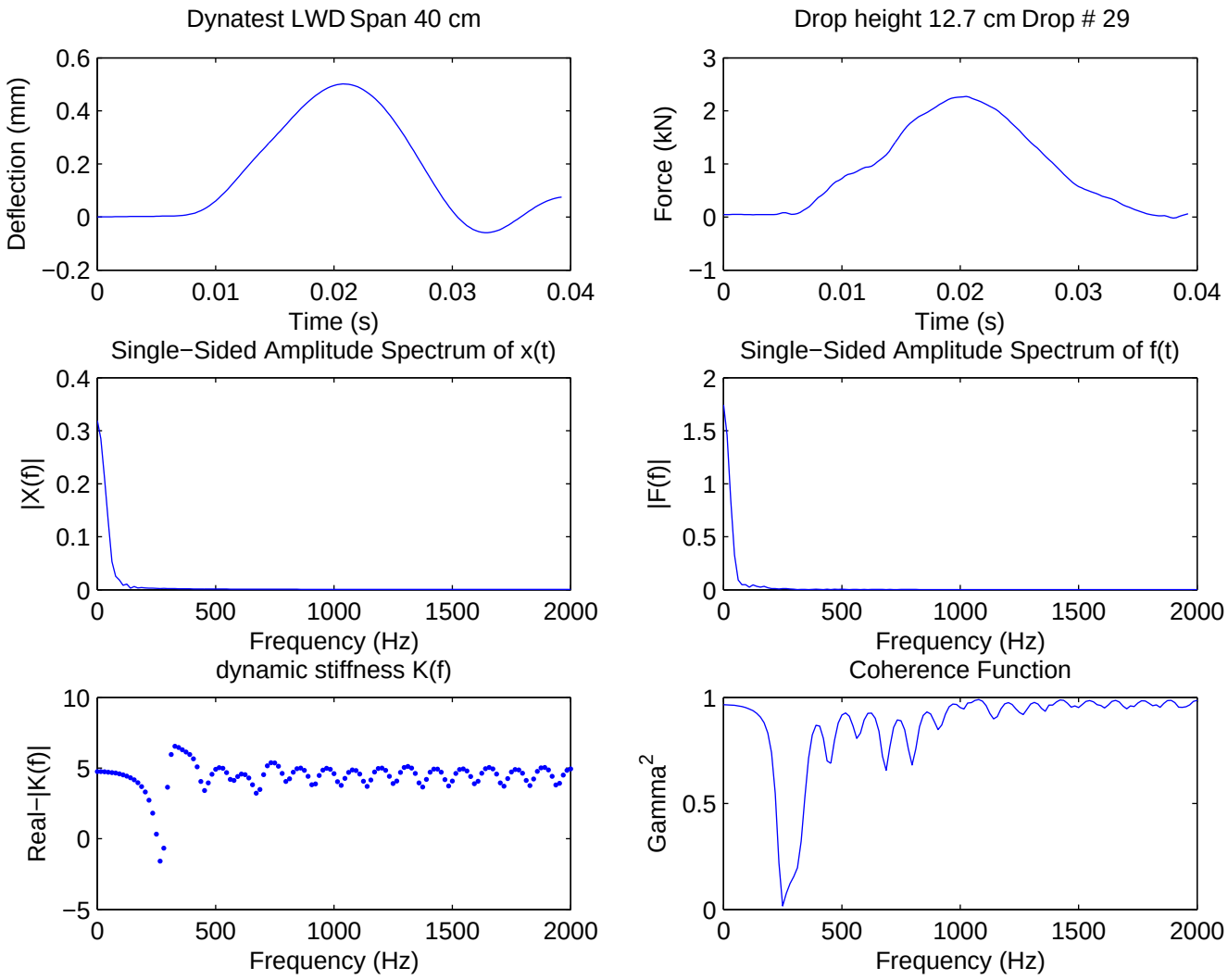
Dynatest LWD Span 40 cm
Deflection (mm)
Time (s)
Drop height 12.7 cm Drop # 29
Force (kN)
Time (s)
Single−Sided Amplitude Spectrum of x(t)
|X(f)|
Frequency (Hz)
Single−Sided Amplitude Spectrum of f(t)
|F(f)|
Frequency (Hz)
dynamic stiffness K(f)
Real−|K(f)|
Frequency (Hz)
Coherence Function
Gamma2
Frequency (Hz)

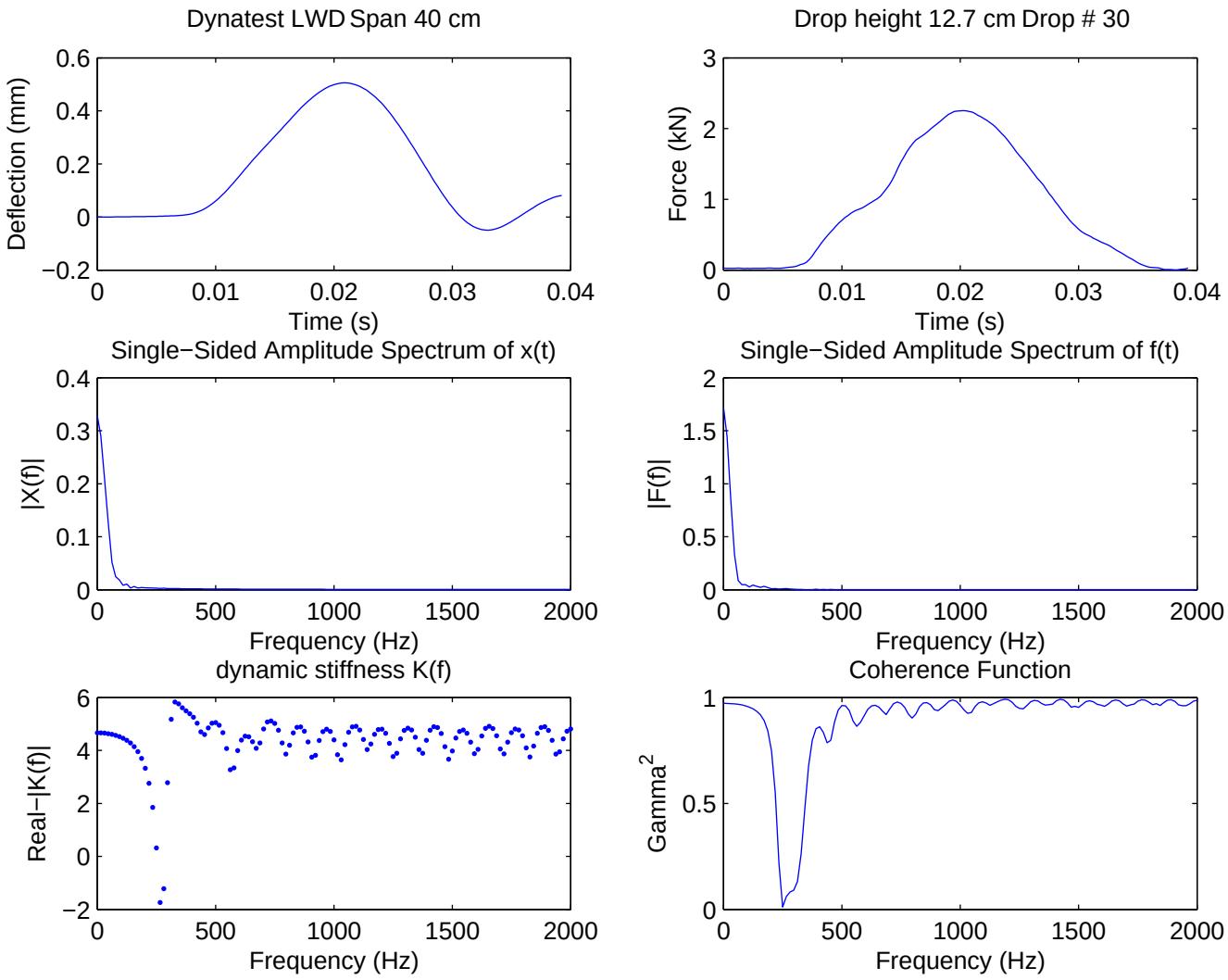
Dynatest LWD Span 40 cm
Deflection (mm)
Time (s)
Drop height 12.7 cm Drop # 30
Force (kN)
Time (s)
Single−Sided Amplitude Spectrum of x(t)
|X(f)|
Frequency (Hz)
Single−Sided Amplitude Spectrum of f(t)
|F(f)|
Frequency (Hz)
dynamic stiffness K(f)
Real−|K(f)|
Frequency (Hz)
Coherence Function
Gamma2
Frequency (Hz)

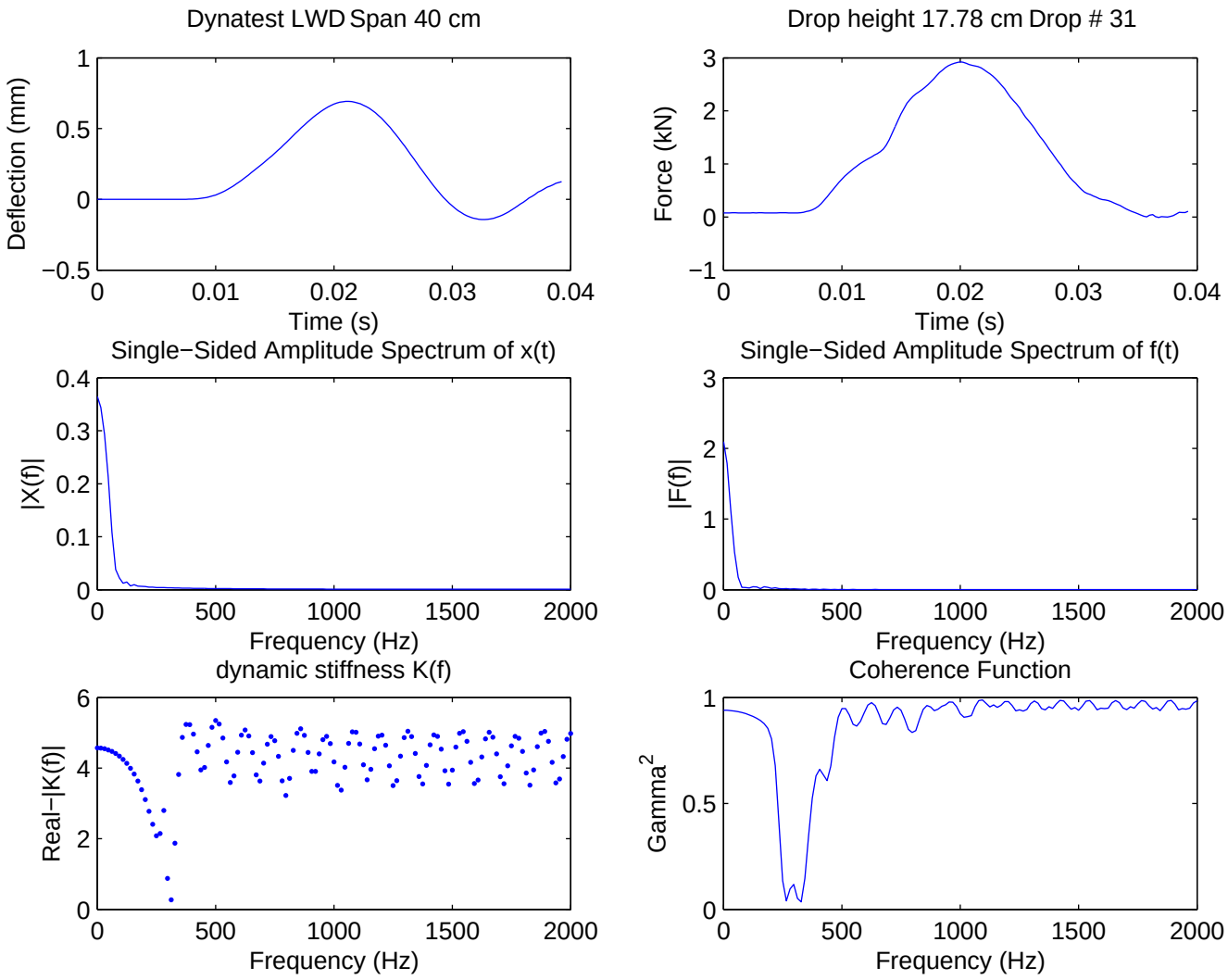
Dynatest LWD Span 40 cm
Deflection (mm)
Time (s)
Drop height 17.78 cm Drop # 31
Force (kN)
Time (s)
Single−Sided Amplitude Spectrum of x(t)
|X(f)|
Frequency (Hz)
Single−Sided Amplitude Spectrum of f(t)
|F(f)|
Frequency (Hz)
dynamic stiffness K(f)
Real−|K(f)|
Frequency (Hz)
Coherence Function
Gamma2
Frequency (Hz)

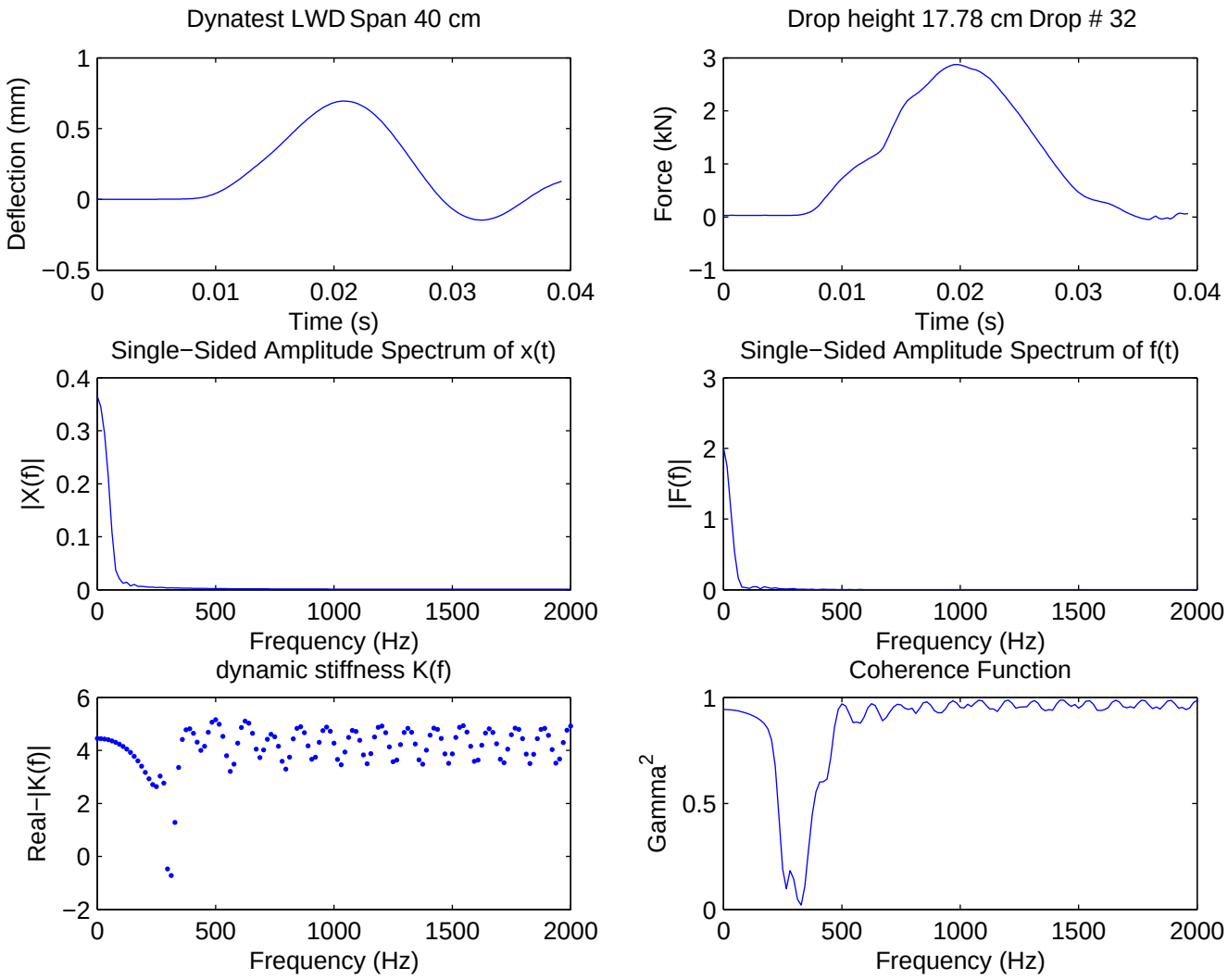
Dynatest LWD Span 40 cm
Deflection (mm)
Time (s)
Drop height 17.78 cm Drop # 32
Force (kN)
Time (s)
Single−Sided Amplitude Spectrum of x(t)
|X(f)|
Frequency (Hz)
Single−Sided Amplitude Spectrum of f(t)
|F(f)|
Frequency (Hz)
dynamic stiffness K(f)
Real−|K(f)|
Frequency (Hz)
Coherence Function
Gamma2
Frequency (Hz)

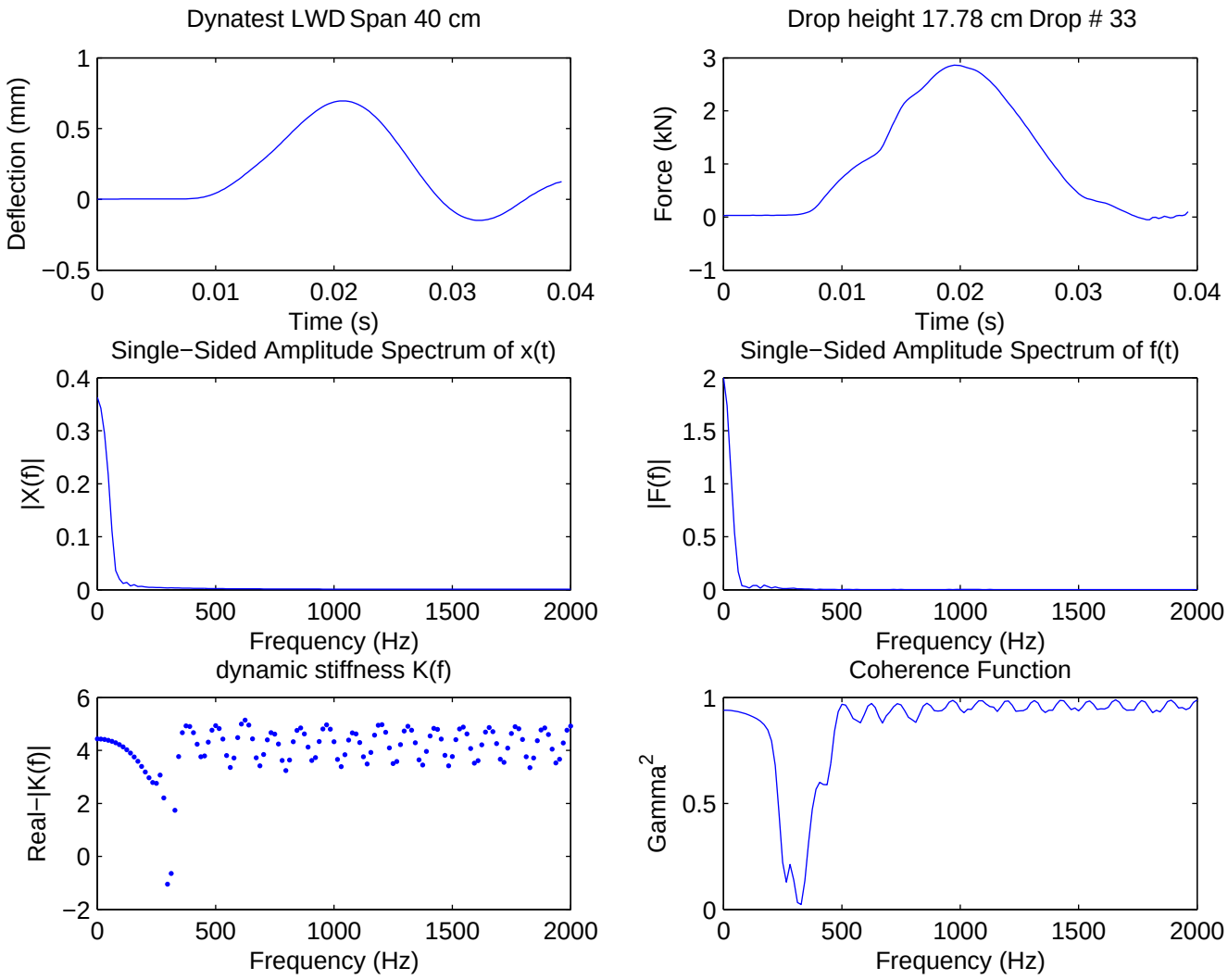
Dynatest LWD Span 40 cm
Deflection (mm)
Time (s)
Drop height 17.78 cm Drop # 33
Force (kN)
Time (s)
Single−Sided Amplitude Spectrum of x(t)
|X(f)|
Frequency (Hz)
Single−Sided Amplitude Spectrum of f(t)
|F(f)|
Frequency (Hz)
dynamic stiffness K(f)
Real−|K(f)|
Frequency (Hz)
Coherence Function
Gamma2
Frequency (Hz)

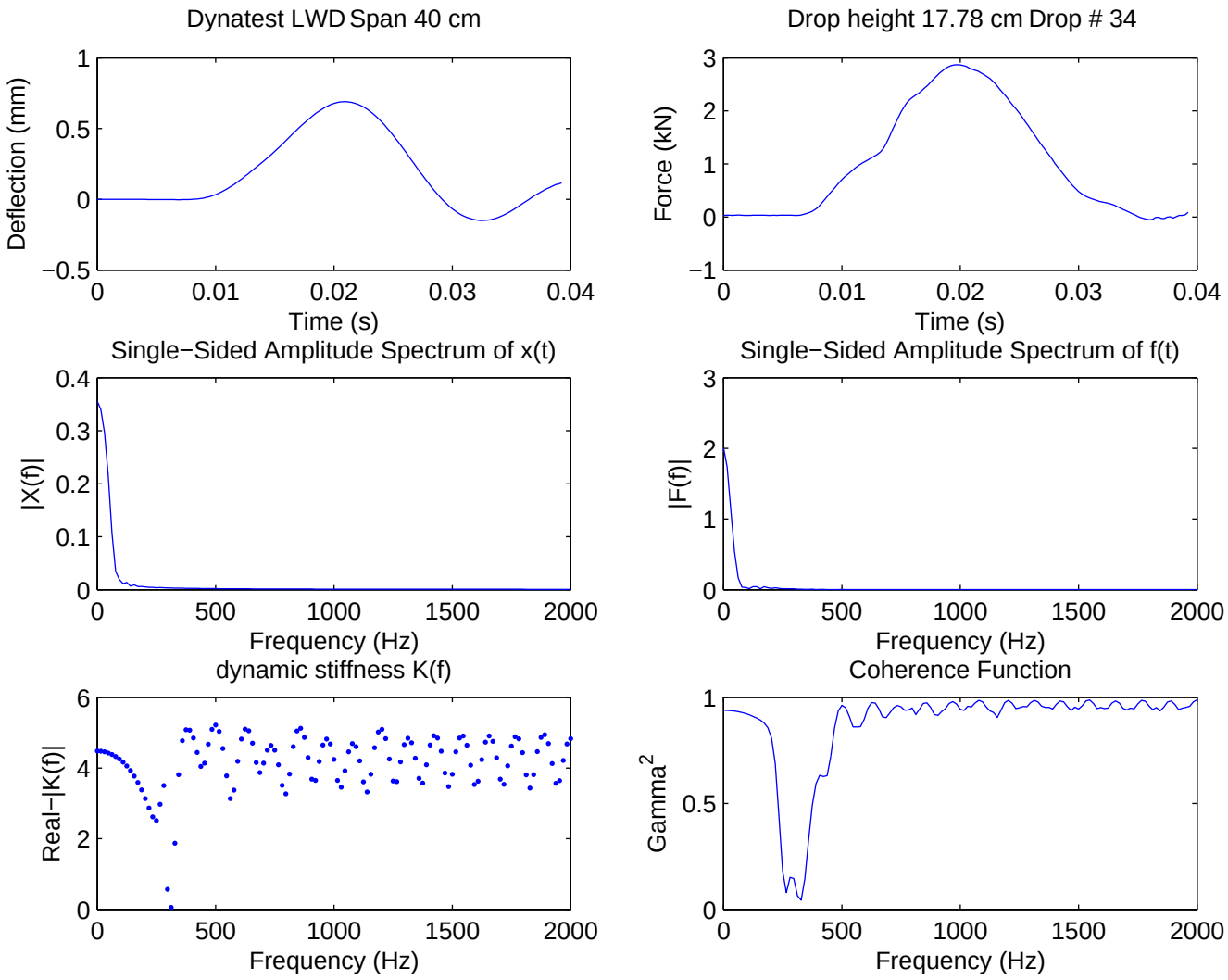
Dynatest LWD Span 40 cm
Deflection (mm)
Time (s)
Drop height 17.78 cm Drop # 34
Force (kN)
Time (s)
Single−Sided Amplitude Spectrum of x(t)
|X(f)|
Frequency (Hz)
Single−Sided Amplitude Spectrum of f(t)
|F(f)|
Frequency (Hz)
dynamic stiffness K(f)
Real−|K(f)|
Frequency (Hz)
Coherence Function
Gamma2
Frequency (Hz)

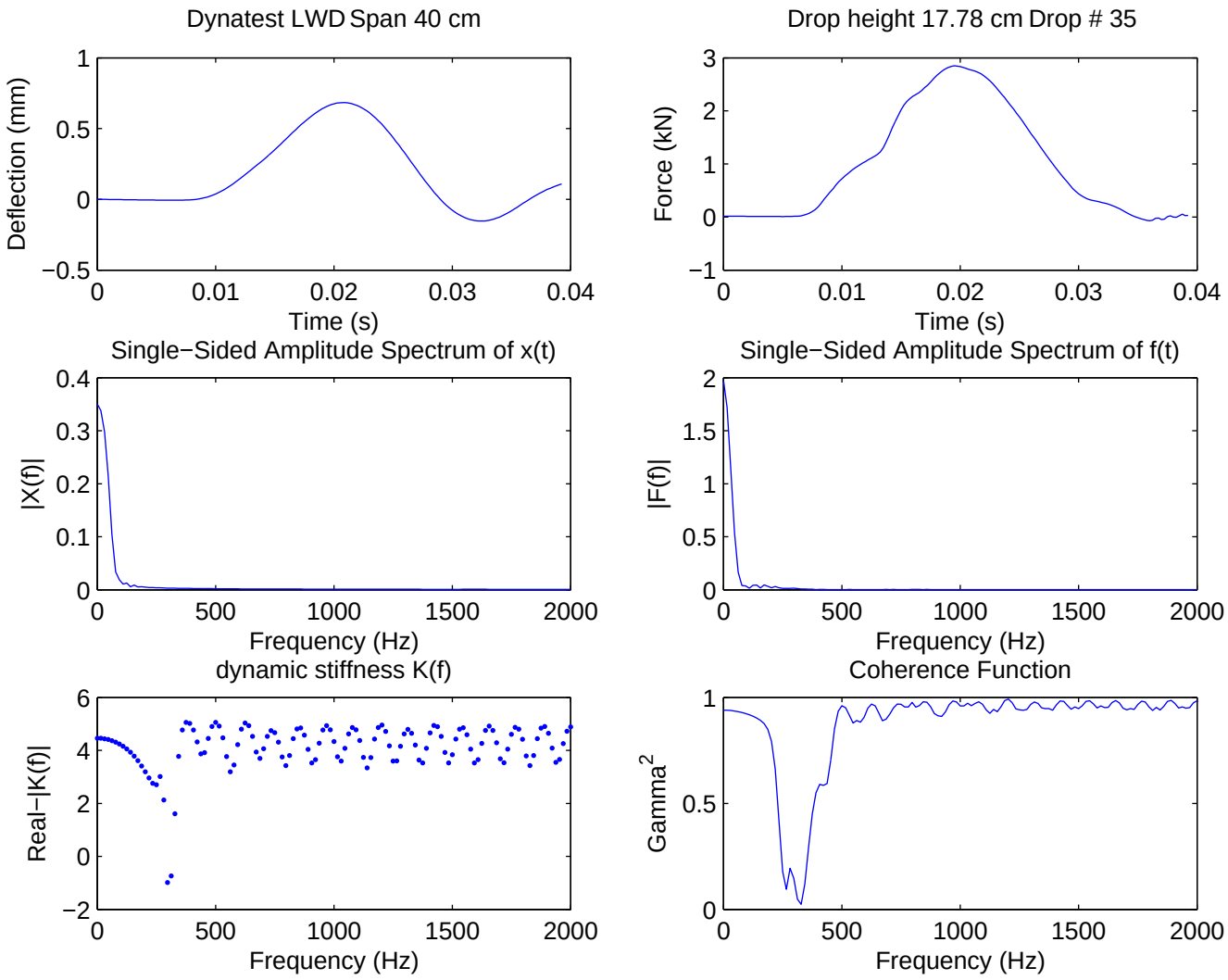
Dynatest LWD Span 40 cm
Deflection (mm)
Time (s)
Drop height 17.78 cm Drop # 35
Force (kN)
Time (s)
Single−Sided Amplitude Spectrum of x(t)
|X(f)|
Frequency (Hz)
Single−Sided Amplitude Spectrum of f(t)
|F(f)|
Frequency (Hz)
dynamic stiffness K(f)
Real−|K(f)|
Frequency (Hz)
Coherence Function
Gamma2
Frequency (Hz)

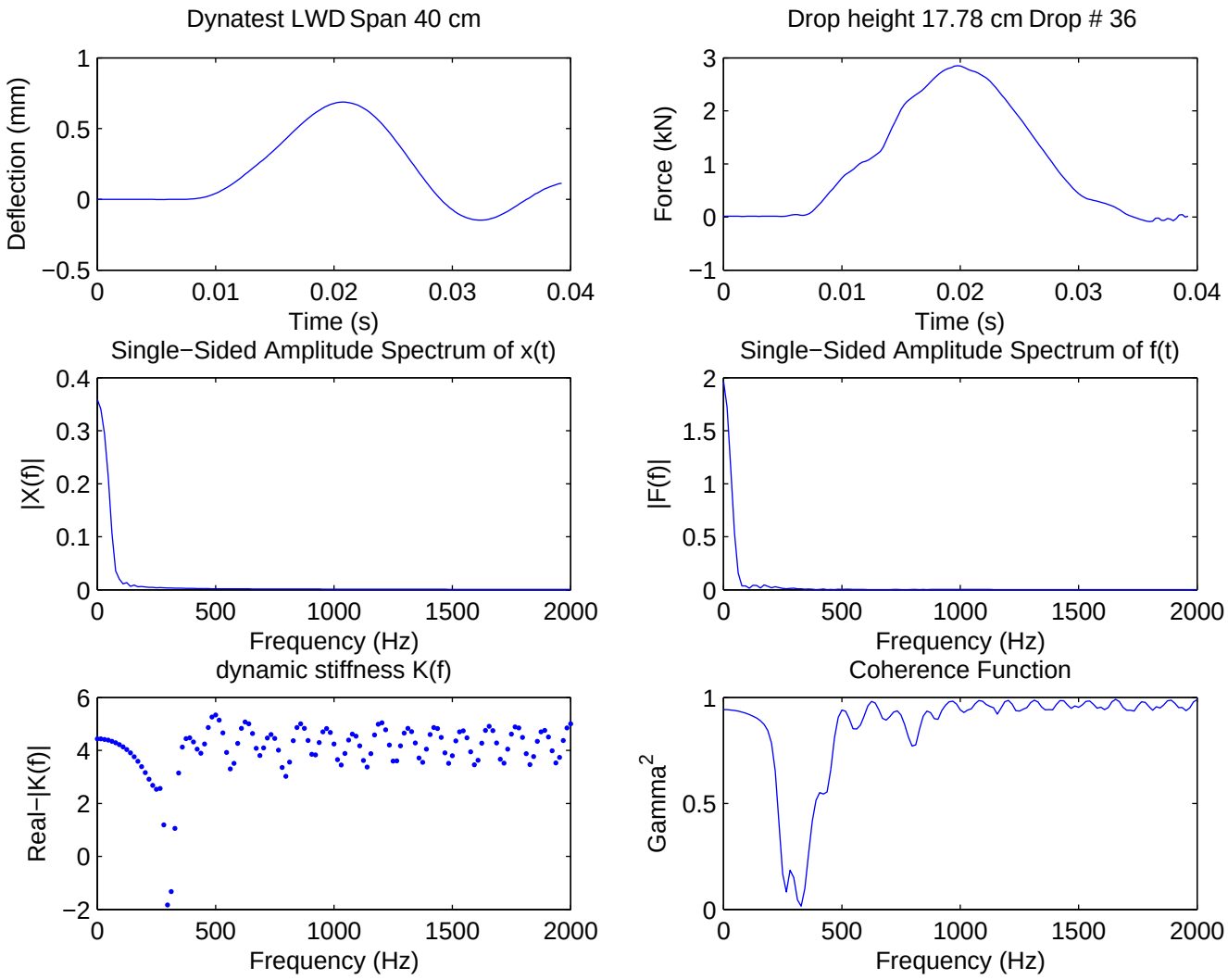
Dynatest LWD Span 40 cm
Deflection (mm)
Time (s)
Drop height 17.78 cm Drop # 36
Force (kN)
Time (s)
Single−Sided Amplitude Spectrum of x(t)
|X(f)|
Frequency (Hz)
Single−Sided Amplitude Spectrum of f(t)
|F(f)|
Frequency (Hz)
dynamic stiffness K(f)
Real−|K(f)|
Frequency (Hz)
Coherence Function
Gamma2
Frequency (Hz)

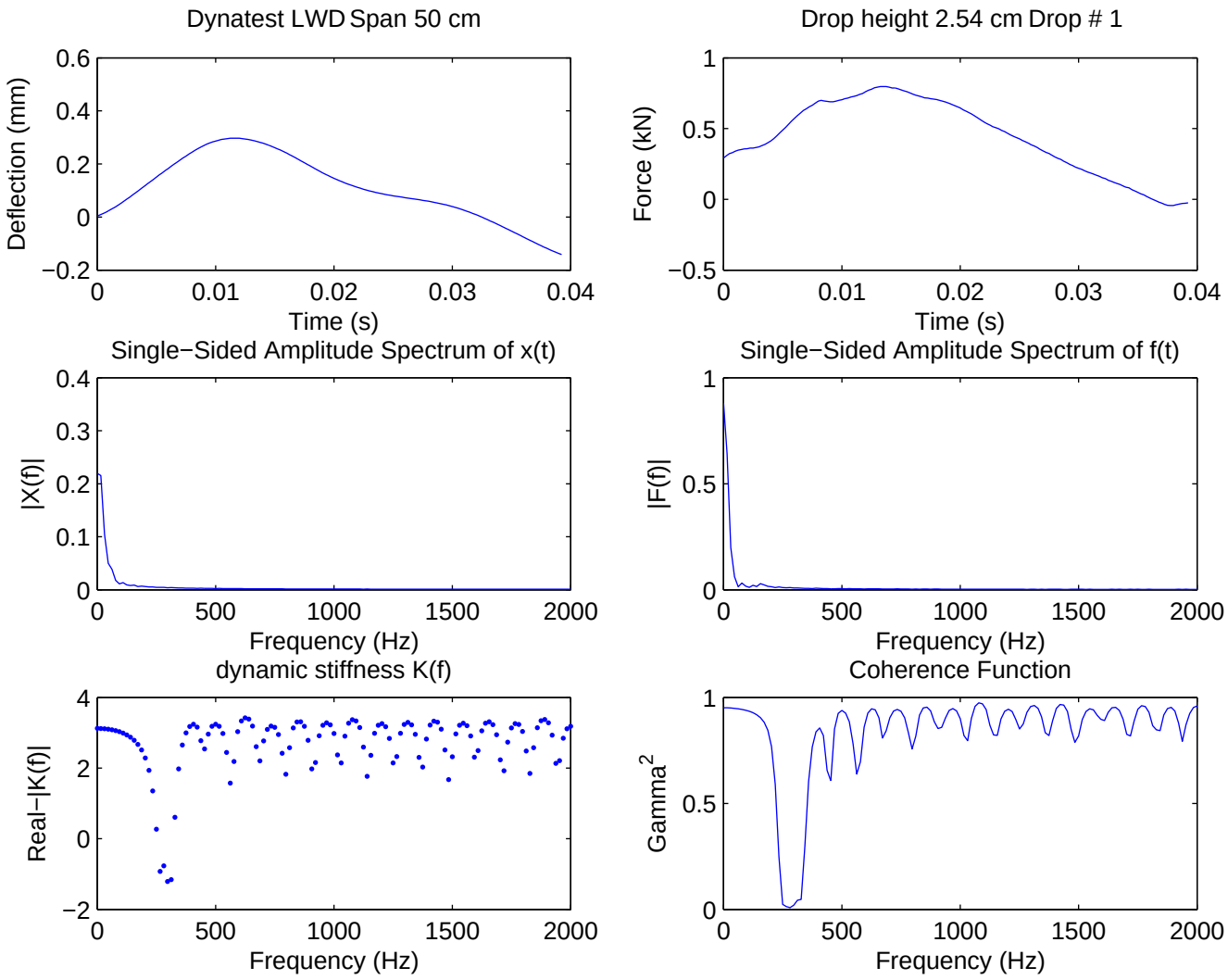
Dynatest LWD Span 50 cm
Deflection (mm)
Time (s)
Drop height 2.54 cm Drop # 1
Force (kN)
Time (s)
Single−Sided Amplitude Spectrum of x(t)
|X(f)|
Frequency (Hz)
Single−Sided Amplitude Spectrum of f(t)
|F(f)|
Frequency (Hz)
dynamic stiffness K(f)
Real−|K(f)|
Frequency (Hz)
Coherence Function
Gamma2
Frequency (Hz)

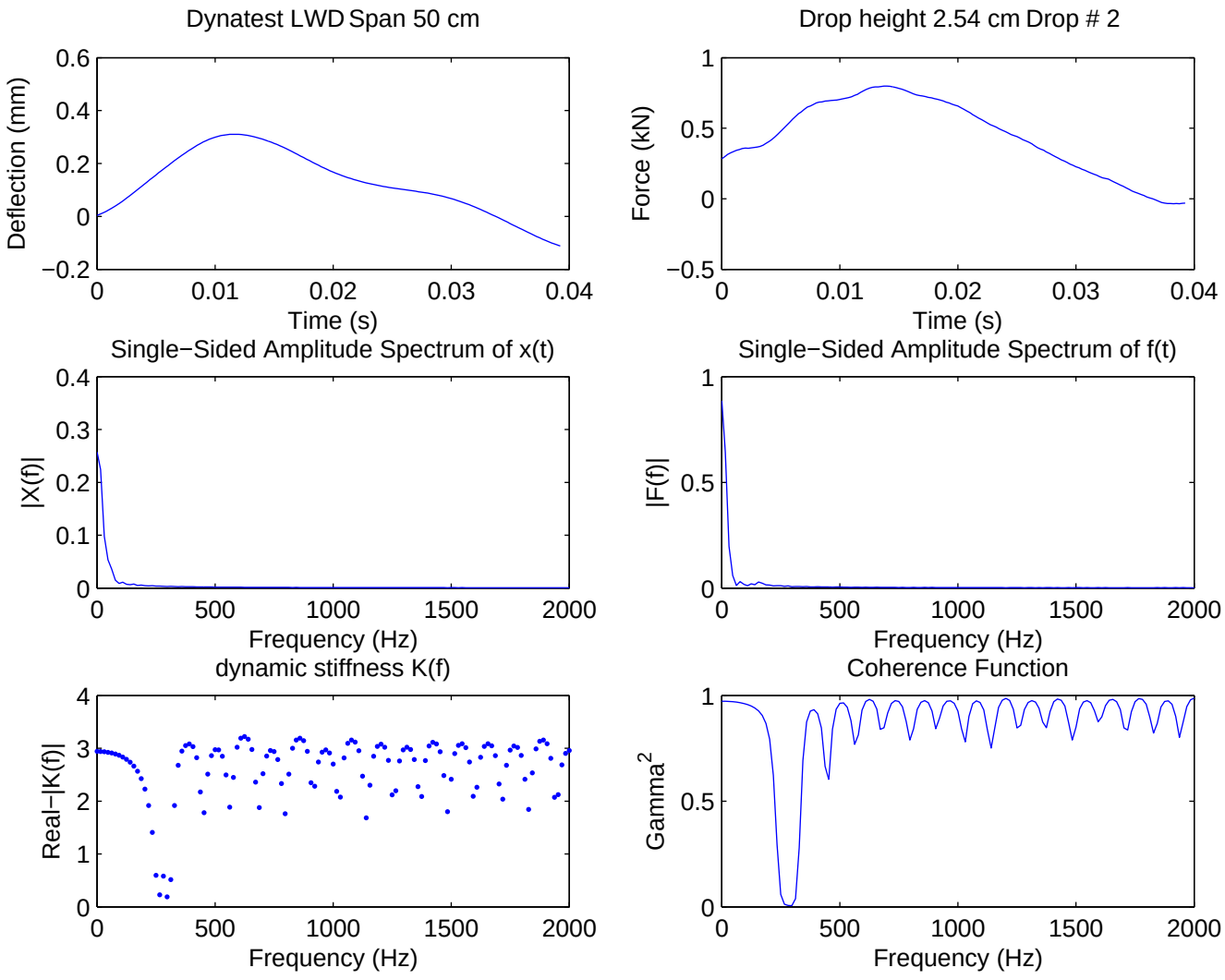
Dynatest LWD Span 50 cm
Deflection (mm)
Time (s)
Drop height 2.54 cm Drop # 2
Force (kN)
Time (s)
Single−Sided Amplitude Spectrum of x(t)
|X(f)|
Frequency (Hz)
Single−Sided Amplitude Spectrum of f(t)
|F(f)|
Frequency (Hz)
dynamic stiffness K(f)
Real−|K(f)|
Frequency (Hz)
Coherence Function
Gamma2
Frequency (Hz)

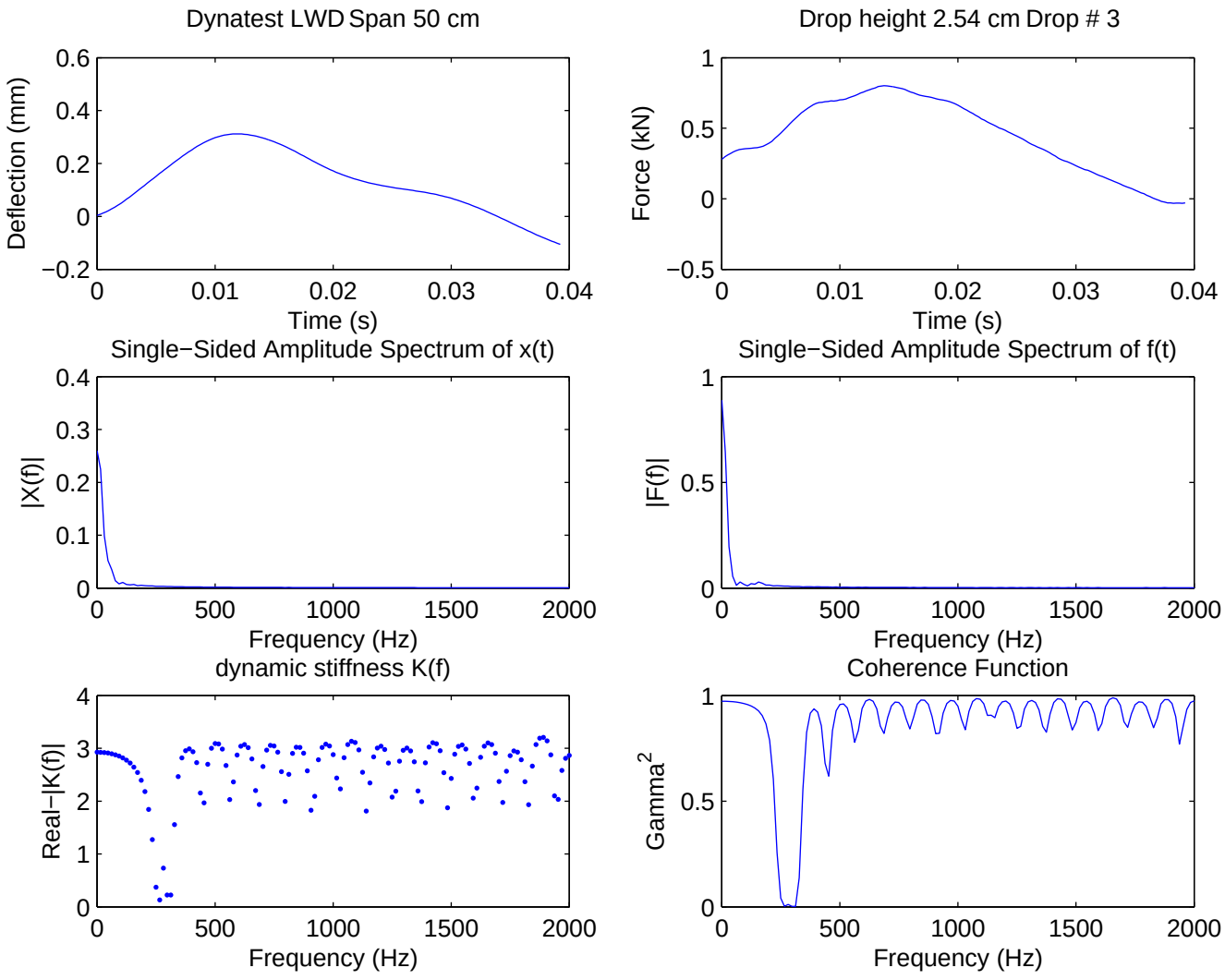
Dynatest LWD Span 50 cm
Deflection (mm)
Time (s)
Drop height 2.54 cm Drop # 3
Force (kN)
Time (s)
Single−Sided Amplitude Spectrum of x(t)
|X(f)|
Frequency (Hz)
Single−Sided Amplitude Spectrum of f(t)
|F(f)|
Frequency (Hz)
dynamic stiffness K(f)
Real−|K(f)|
Frequency (Hz)
Coherence Function
Gamma2
Frequency (Hz)

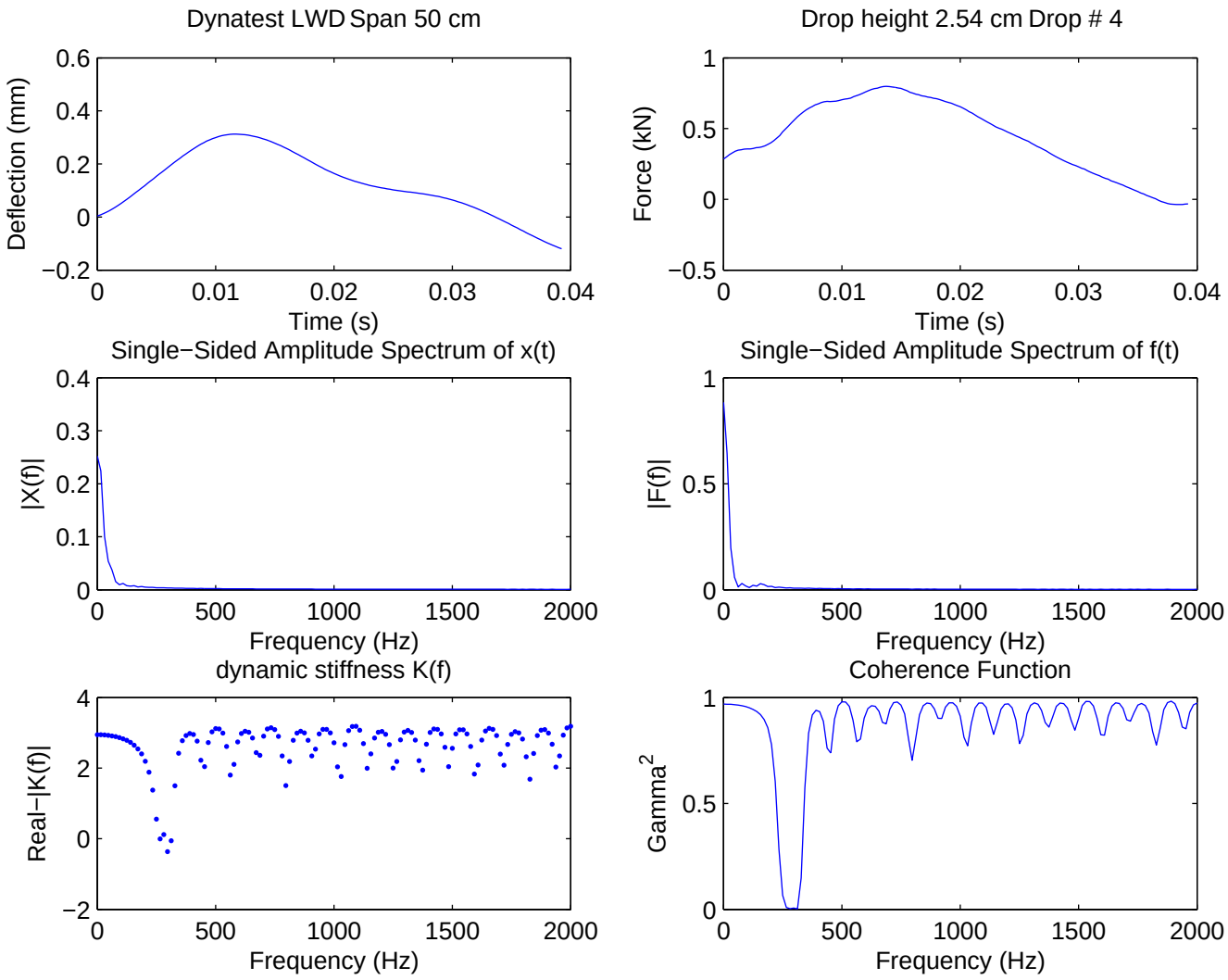
Dynatest LWD Span 50 cm
Deflection (mm)
Time (s)
Drop height 2.54 cm Drop # 4
Force (kN)
Time (s)
Single−Sided Amplitude Spectrum of x(t)
|X(f)|
Frequency (Hz)
Single−Sided Amplitude Spectrum of f(t)
|F(f)|
Frequency (Hz)
dynamic stiffness K(f)
Real−|K(f)|
Frequency (Hz)
Coherence Function
Gamma2
Frequency (Hz)

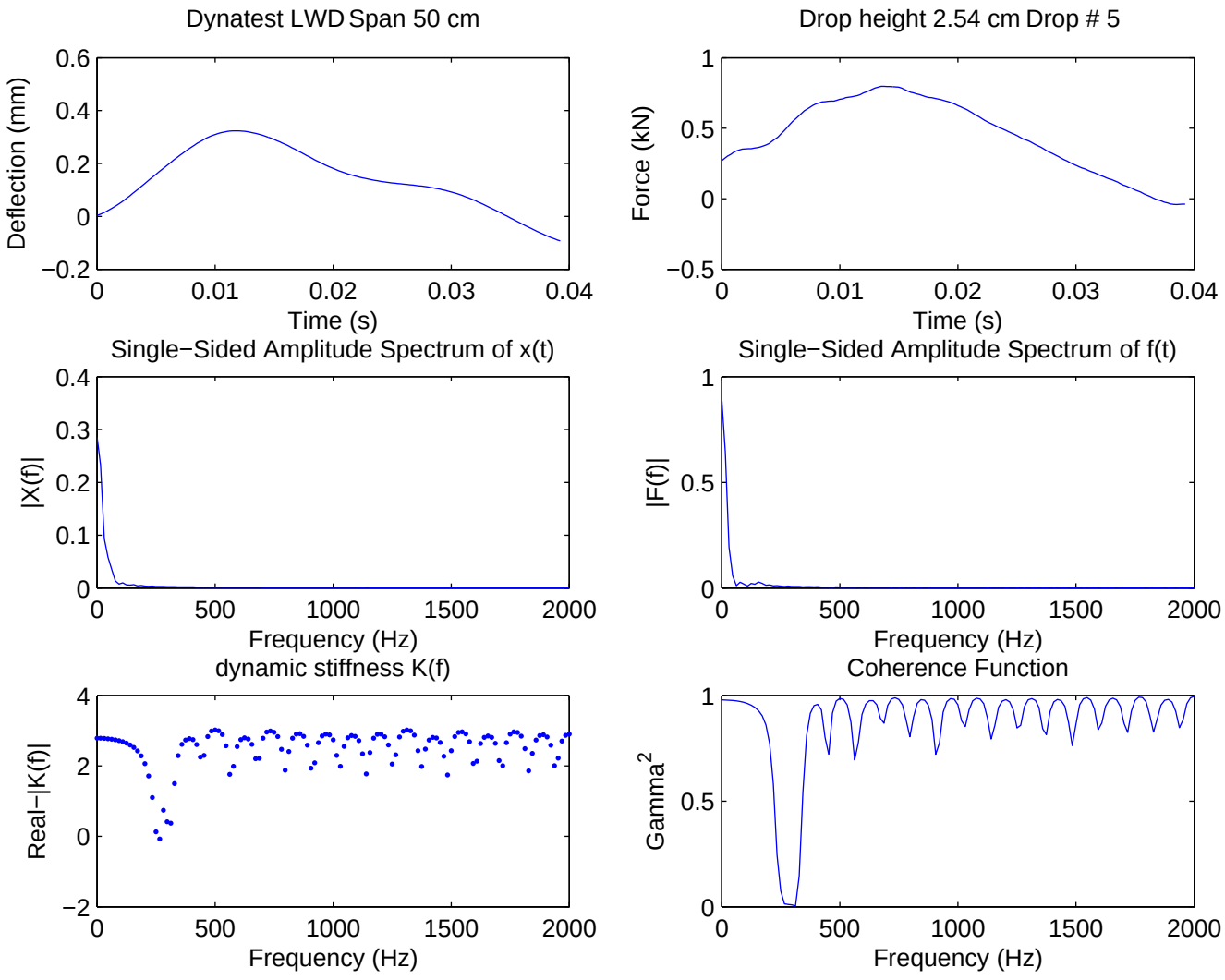
Dynatest LWD Span 50 cm
Deflection (mm)
Time (s)
Drop height 2.54 cm Drop # 5
Force (kN)
Time (s)
Single−Sided Amplitude Spectrum of x(t)
|X(f)|
Frequency (Hz)
Single−Sided Amplitude Spectrum of f(t)
|F(f)|
Frequency (Hz)
dynamic stiffness K(f)
Real−|K(f)|
Frequency (Hz)
Coherence Function
Gamma2
Frequency (Hz)

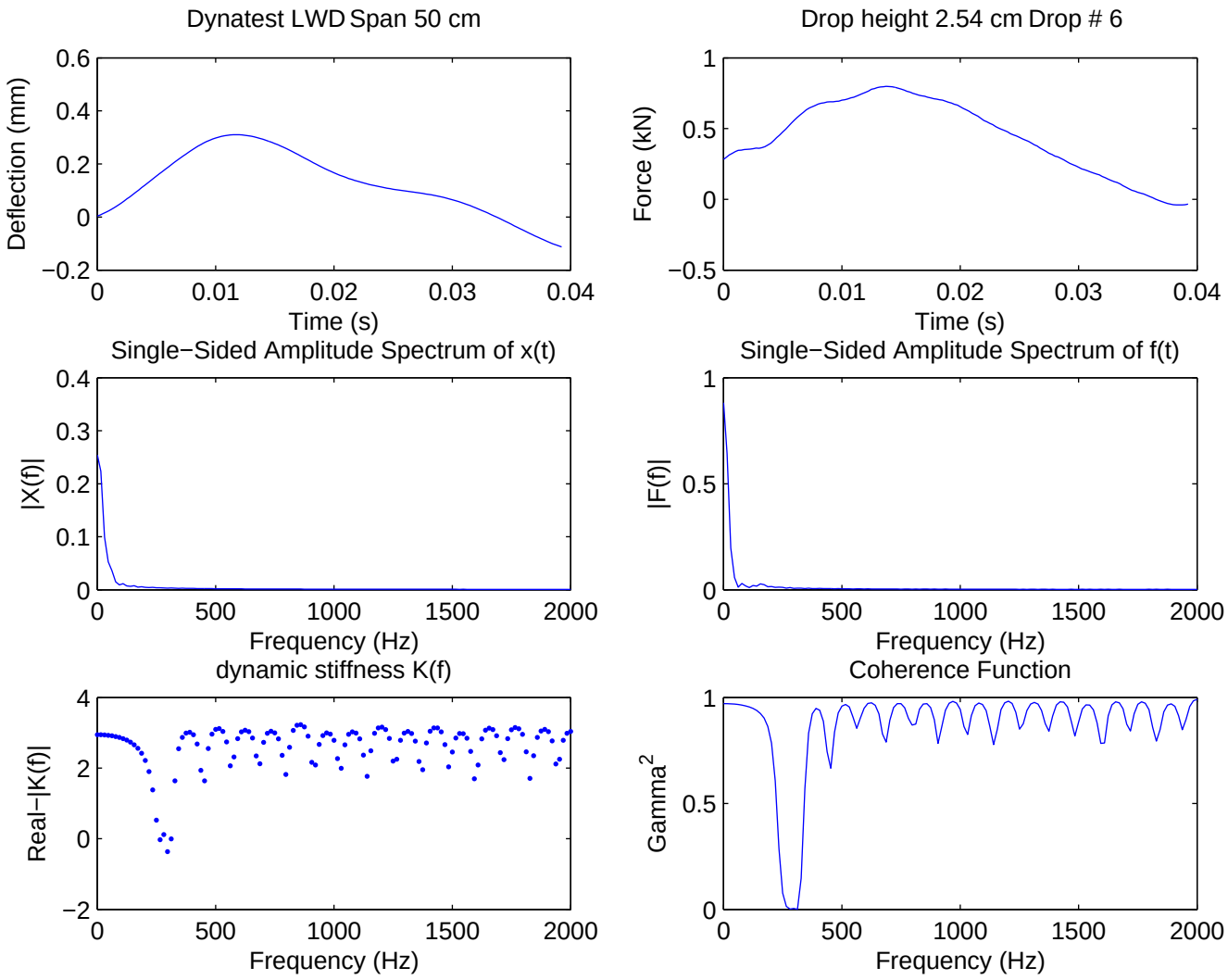
Dynatest LWD Span 50 cm
Deflection (mm)
Time (s)
Drop height 2.54 cm Drop # 6
Force (kN)
Time (s)
Single−Sided Amplitude Spectrum of x(t)
|X(f)|
Frequency (Hz)
Single−Sided Amplitude Spectrum of f(t)
|F(f)|
Frequency (Hz)
dynamic stiffness K(f)
Real−|K(f)|
Frequency (Hz)
Coherence Function
Gamma2
Frequency (Hz)

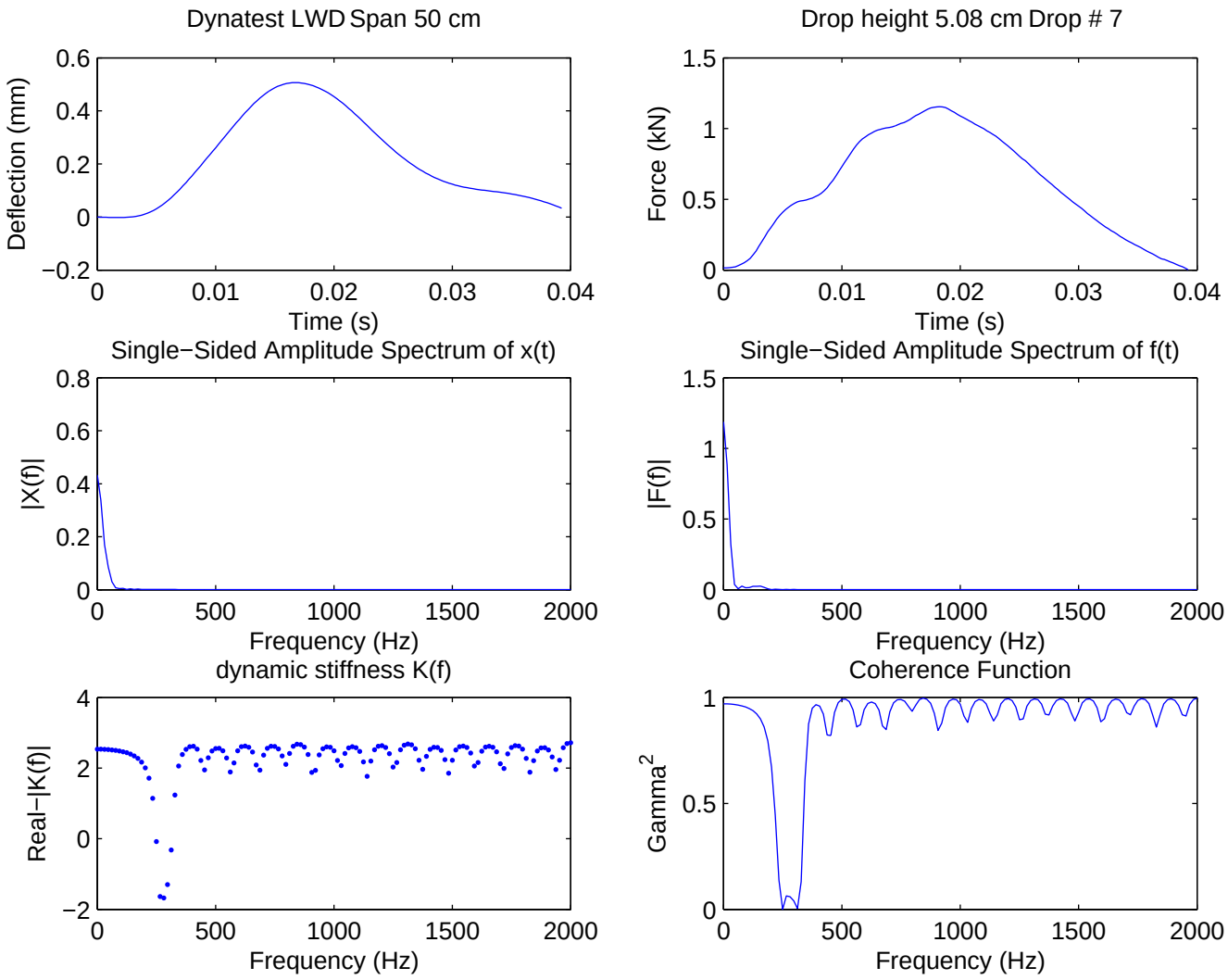
Dynatest LWD Span 50 cm
Deflection (mm)
Time (s)
Drop height 5.08 cm Drop # 7
Force (kN)
Time (s)
Single−Sided Amplitude Spectrum of x(t)
|X(f)|
Frequency (Hz)
Single−Sided Amplitude Spectrum of f(t)
|F(f)|
Frequency (Hz)
dynamic stiffness K(f)
Real−|K(f)|
Frequency (Hz)
Coherence Function
Gamma2
Frequency (Hz)

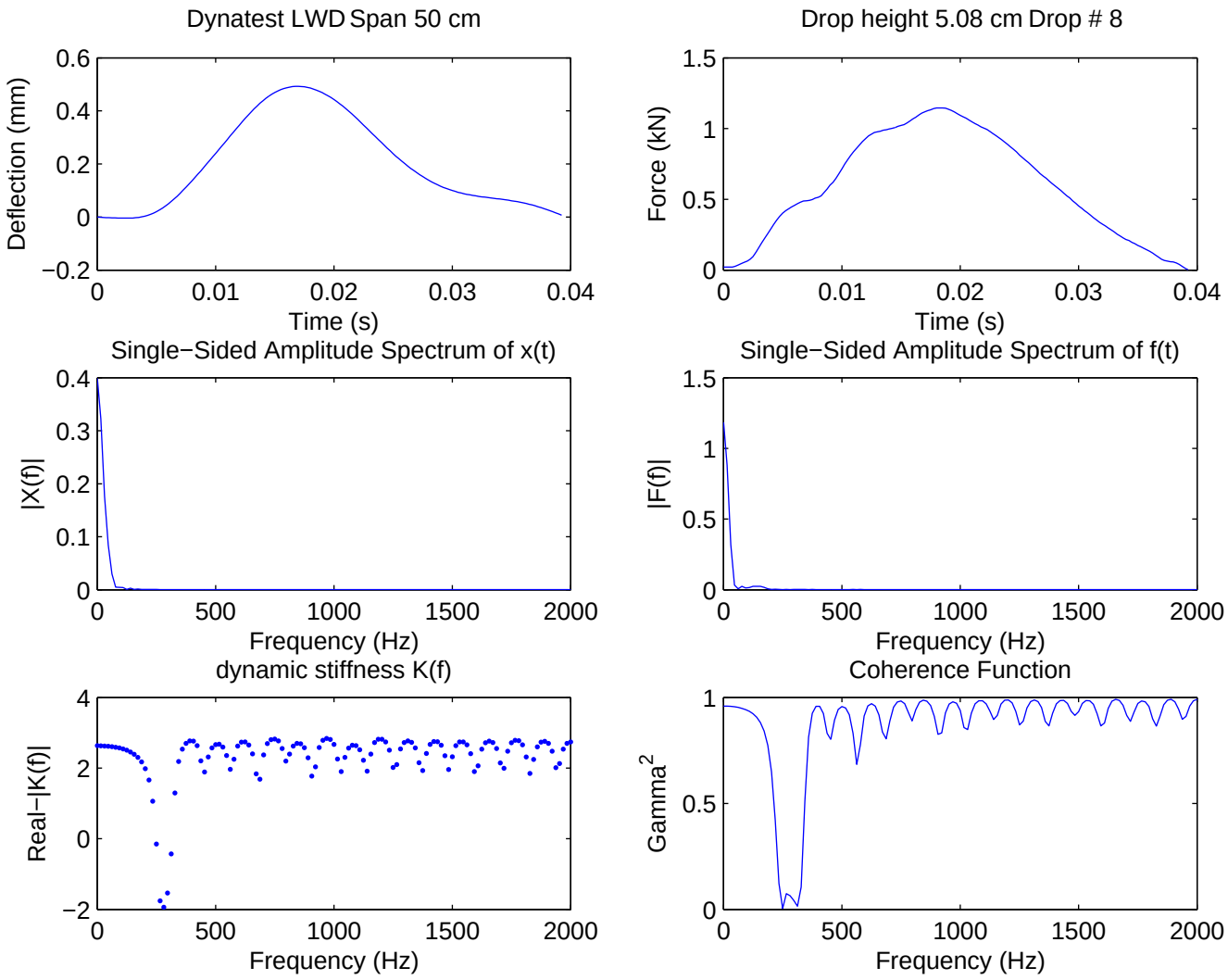
Dynatest LWD Span 50 cm
Deflection (mm)
Time (s)
Drop height 5.08 cm Drop # 8
Force (kN)
Time (s)
Single−Sided Amplitude Spectrum of x(t)
|X(f)|
Frequency (Hz)
Single−Sided Amplitude Spectrum of f(t)
|F(f)|
Frequency (Hz)
dynamic stiffness K(f)
Real−|K(f)|
Frequency (Hz)
Coherence Function
Gamma2
Frequency (Hz)

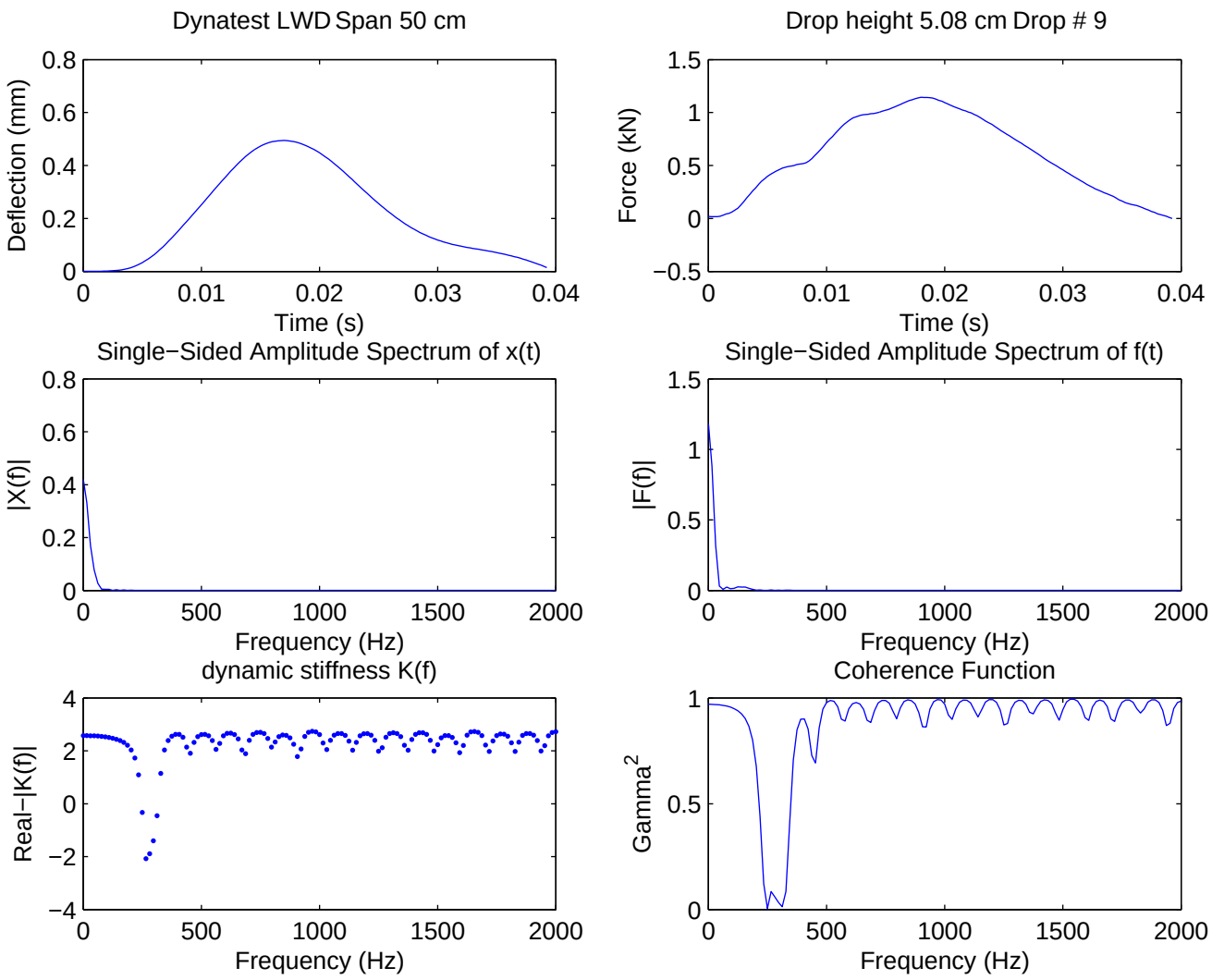
Dynatest LWD Span 50 cm
Deflection (mm)
Time (s)
Drop height 5.08 cm Drop # 9
Force (kN)
Time (s)
Single−Sided Amplitude Spectrum of x(t)
|X(f)|
Frequency (Hz)
Single−Sided Amplitude Spectrum of f(t)
|F(f)|
Frequency (Hz)
dynamic stiffness K(f)
Real−|K(f)|
Frequency (Hz)
Coherence Function
Gamma2
Frequency (Hz)

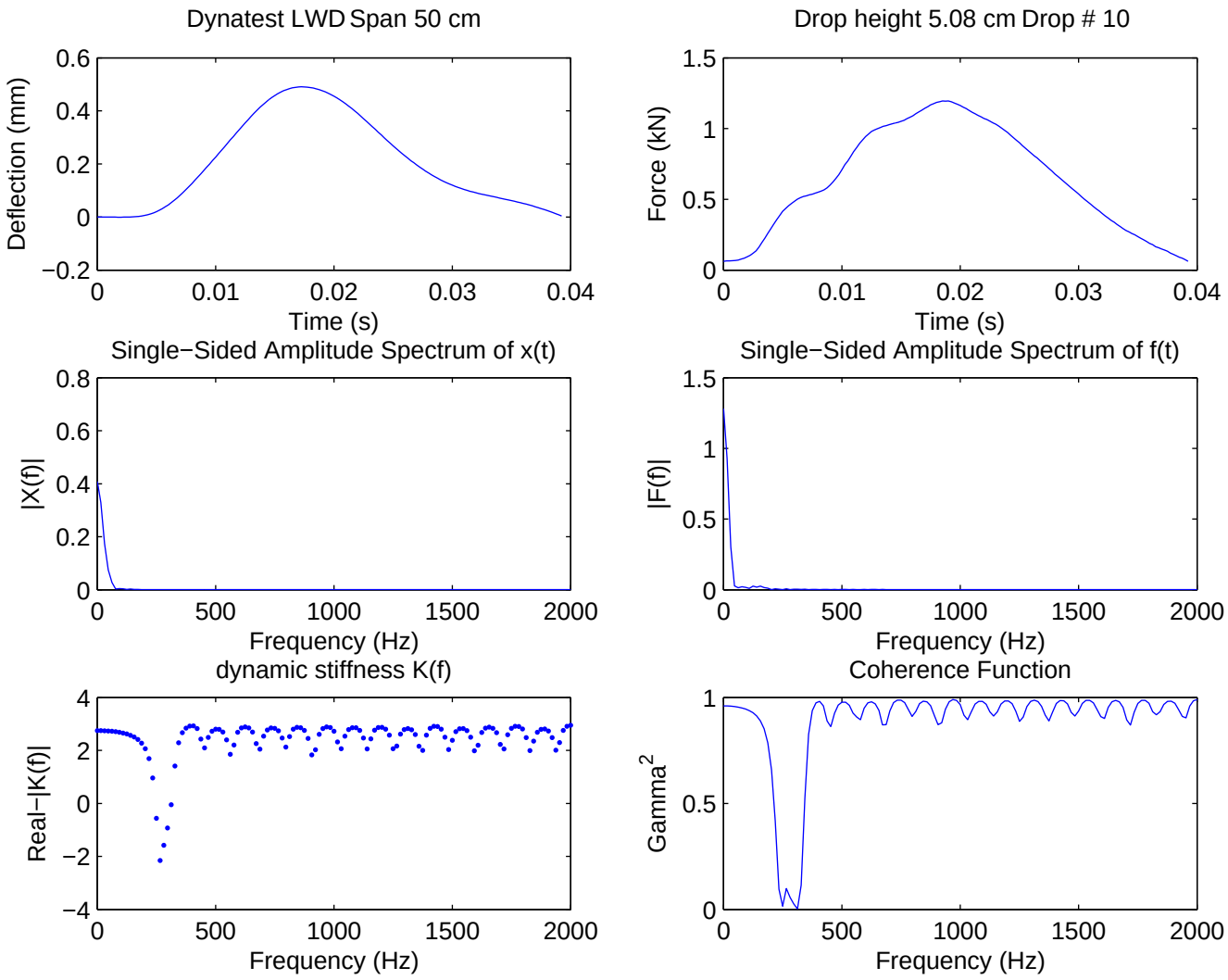
Dynatest LWD Span 50 cm
Deflection (mm)
Time (s)
Drop height 5.08 cm Drop # 10
Force (kN)
Time (s)
Single−Sided Amplitude Spectrum of x(t)
|X(f)|
Frequency (Hz)
Single−Sided Amplitude Spectrum of f(t)
|F(f)|
Frequency (Hz)
dynamic stiffness K(f)
Real−|K(f)|
Frequency (Hz)
Coherence Function
Gamma2
Frequency (Hz)

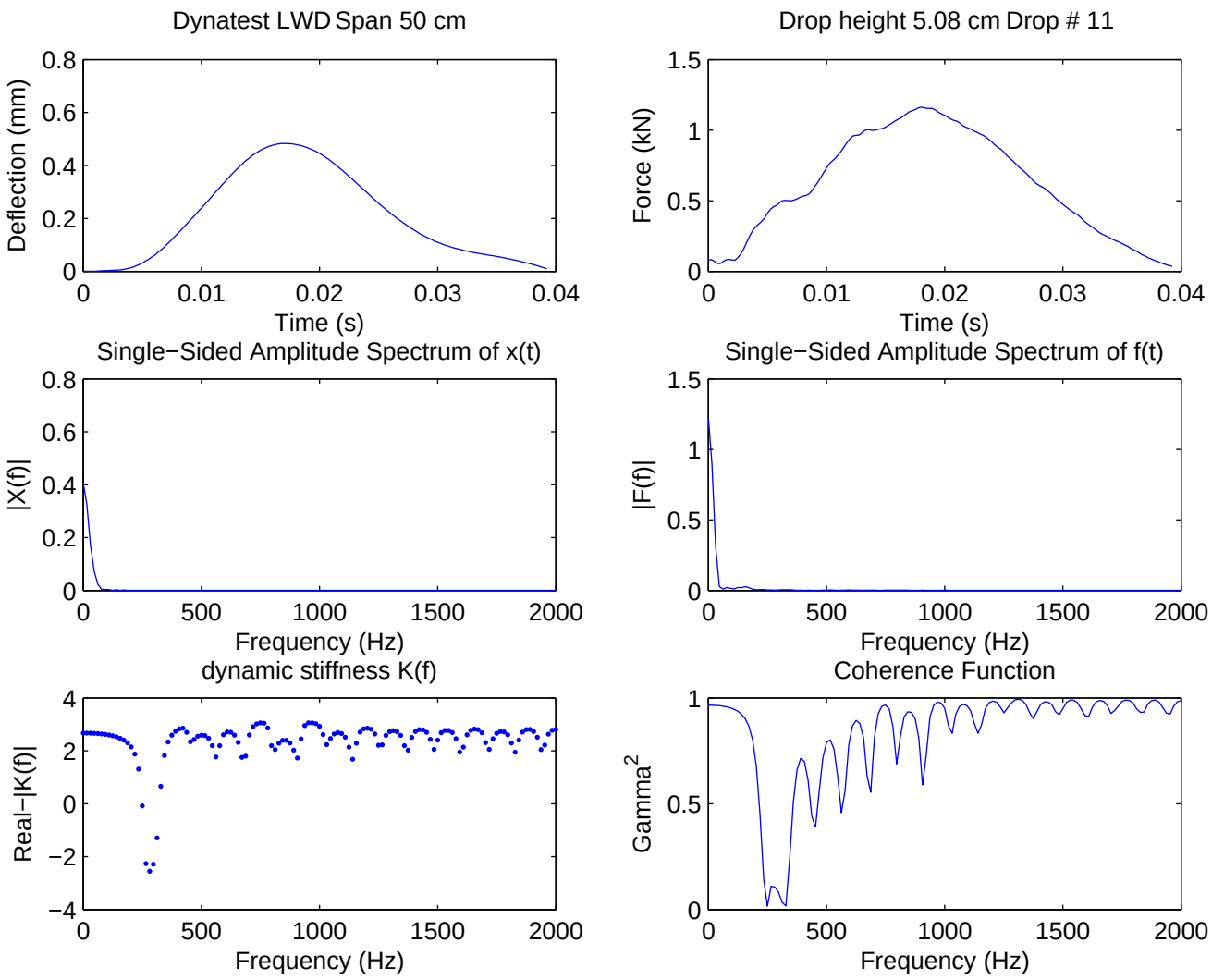
Dynatest LWD Span 50 cm
Deflection (mm)
Time (s)
Drop height 5.08 cm Drop # 11
Force (kN)
Time (s)
Single−Sided Amplitude Spectrum of x(t)
|X(f)|
Frequency (Hz)
Single−Sided Amplitude Spectrum of f(t)
|F(f)|
Frequency (Hz)
dynamic stiffness K(f)
Real−|K(f)|
Frequency (Hz)
Coherence Function
Gamma2
Frequency (Hz)

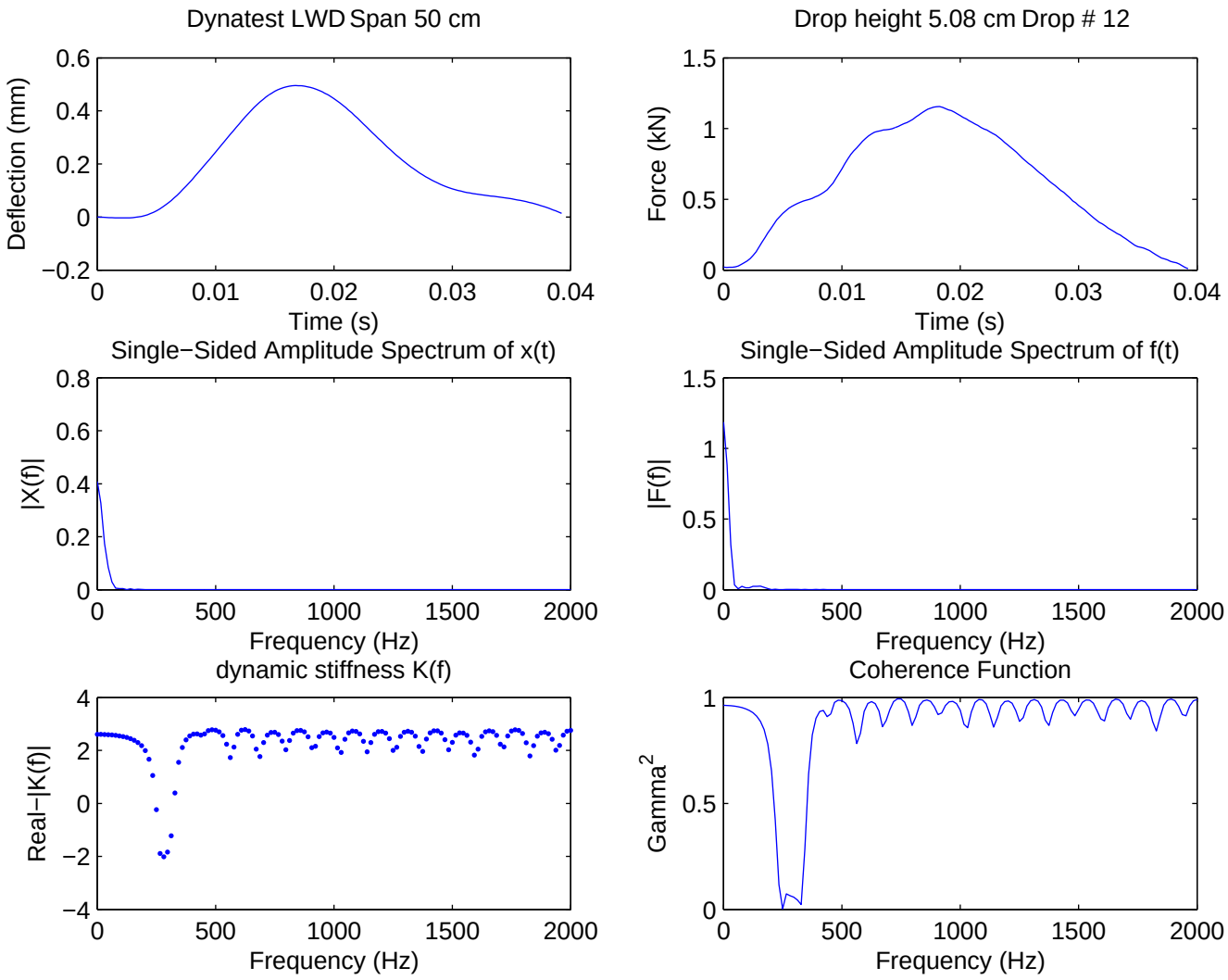
Dynatest LWD Span 50 cm
Deflection (mm)
Time (s)
Drop height 5.08 cm Drop # 12
Force (kN)
Time (s)
Single−Sided Amplitude Spectrum of x(t)
|X(f)|
Frequency (Hz)
Single−Sided Amplitude Spectrum of f(t)
|F(f)|
Frequency (Hz)
dynamic stiffness K(f)
Real−|K(f)|
Frequency (Hz)
Coherence Function
Gamma2
Frequency (Hz)

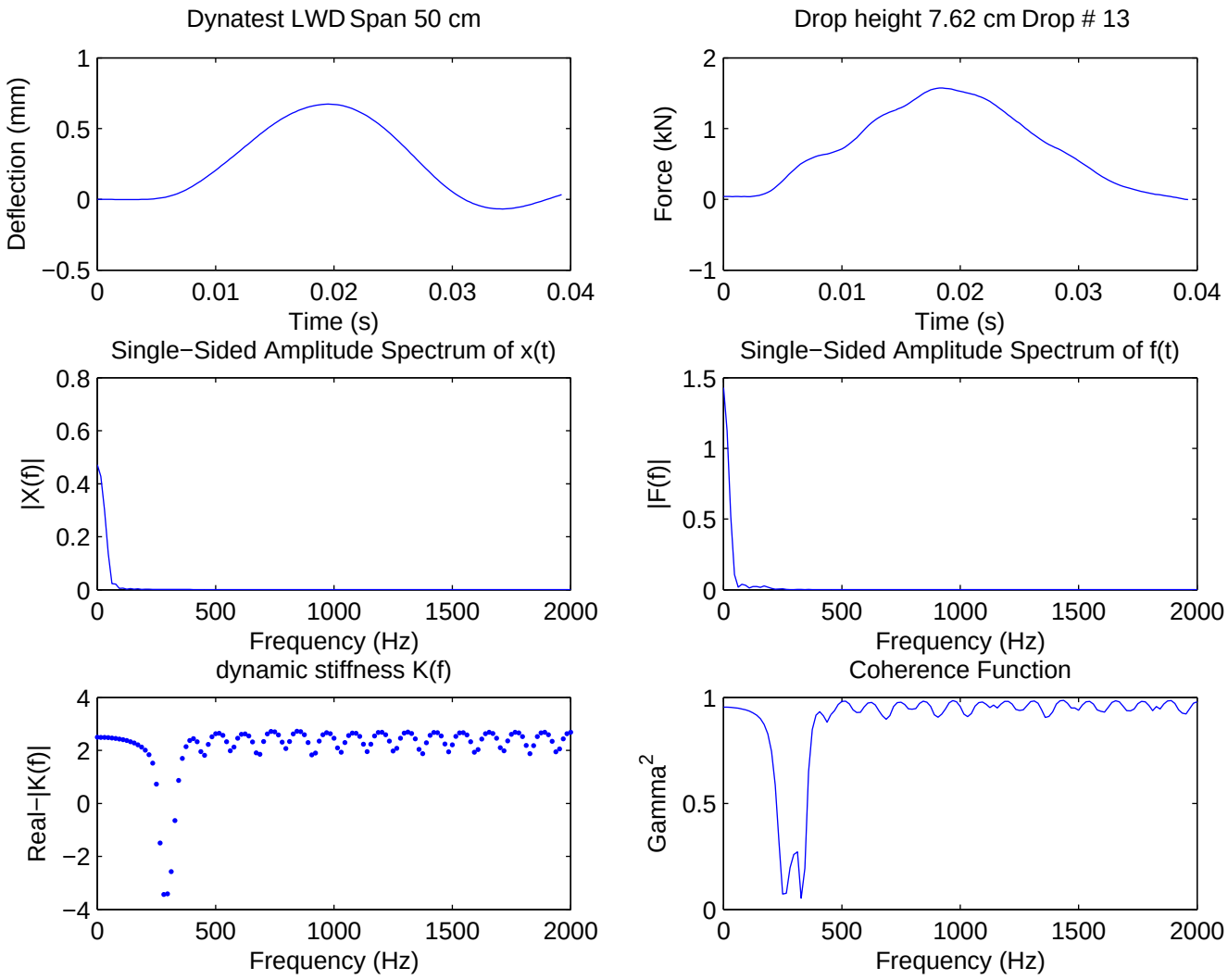
Dynatest LWD Span 50 cm
Deflection (mm)
Time (s)
Drop height 7.62 cm Drop # 13
Force (kN)
Time (s)
Single−Sided Amplitude Spectrum of x(t)
|X(f)|
Frequency (Hz)
Single−Sided Amplitude Spectrum of f(t)
|F(f)|
Frequency (Hz)
dynamic stiffness K(f)
Real−|K(f)|
Frequency (Hz)
Coherence Function
Gamma2
Frequency (Hz)

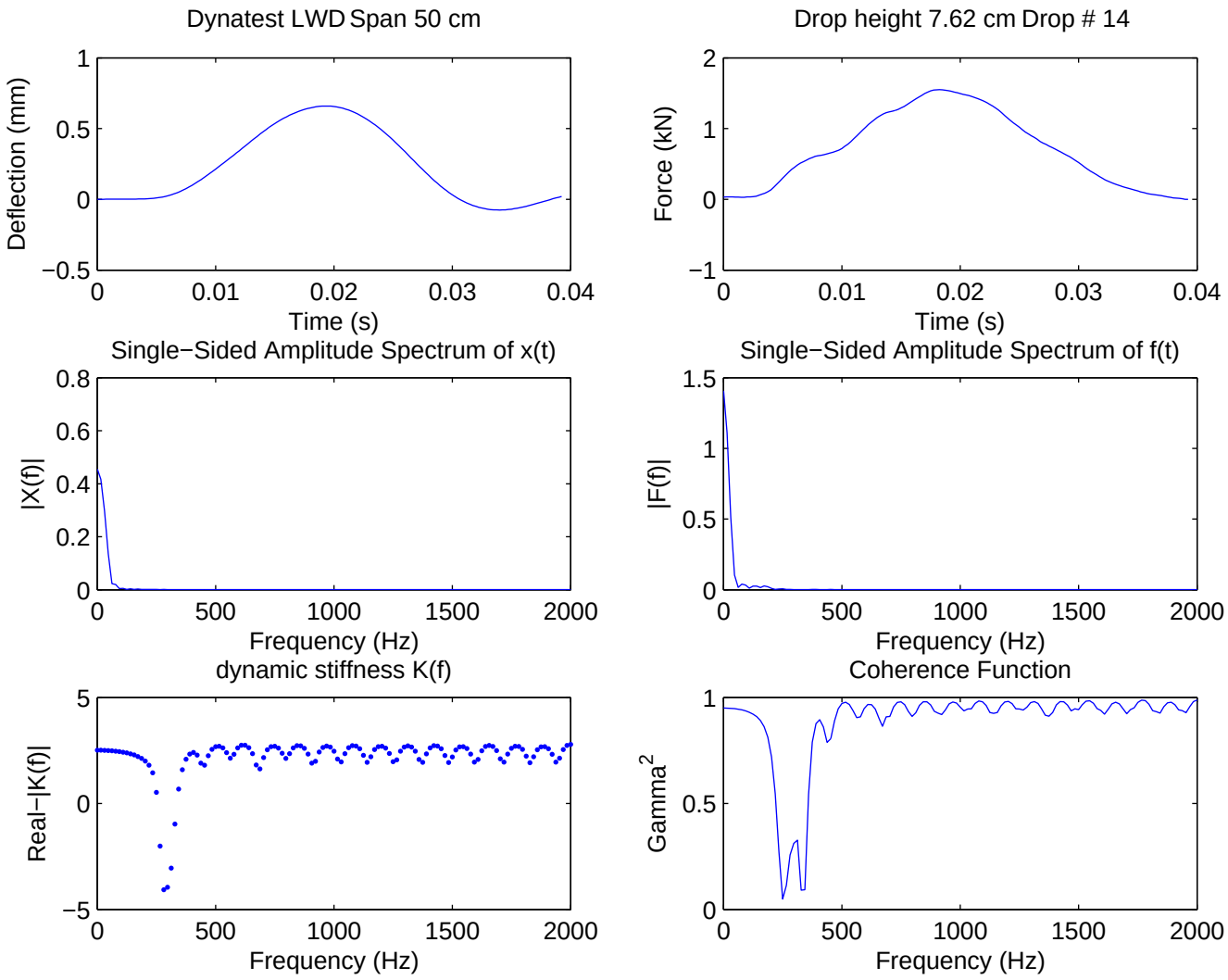
Dynatest LWD Span 50 cm
Deflection (mm)
Time (s)
Drop height 7.62 cm Drop # 14
Force (kN)
Time (s)
Single−Sided Amplitude Spectrum of x(t)
|X(f)|
Frequency (Hz)
Single−Sided Amplitude Spectrum of f(t)
|F(f)|
Frequency (Hz)
dynamic stiffness K(f)
Real−|K(f)|
Frequency (Hz)
Coherence Function
Gamma2
Frequency (Hz)

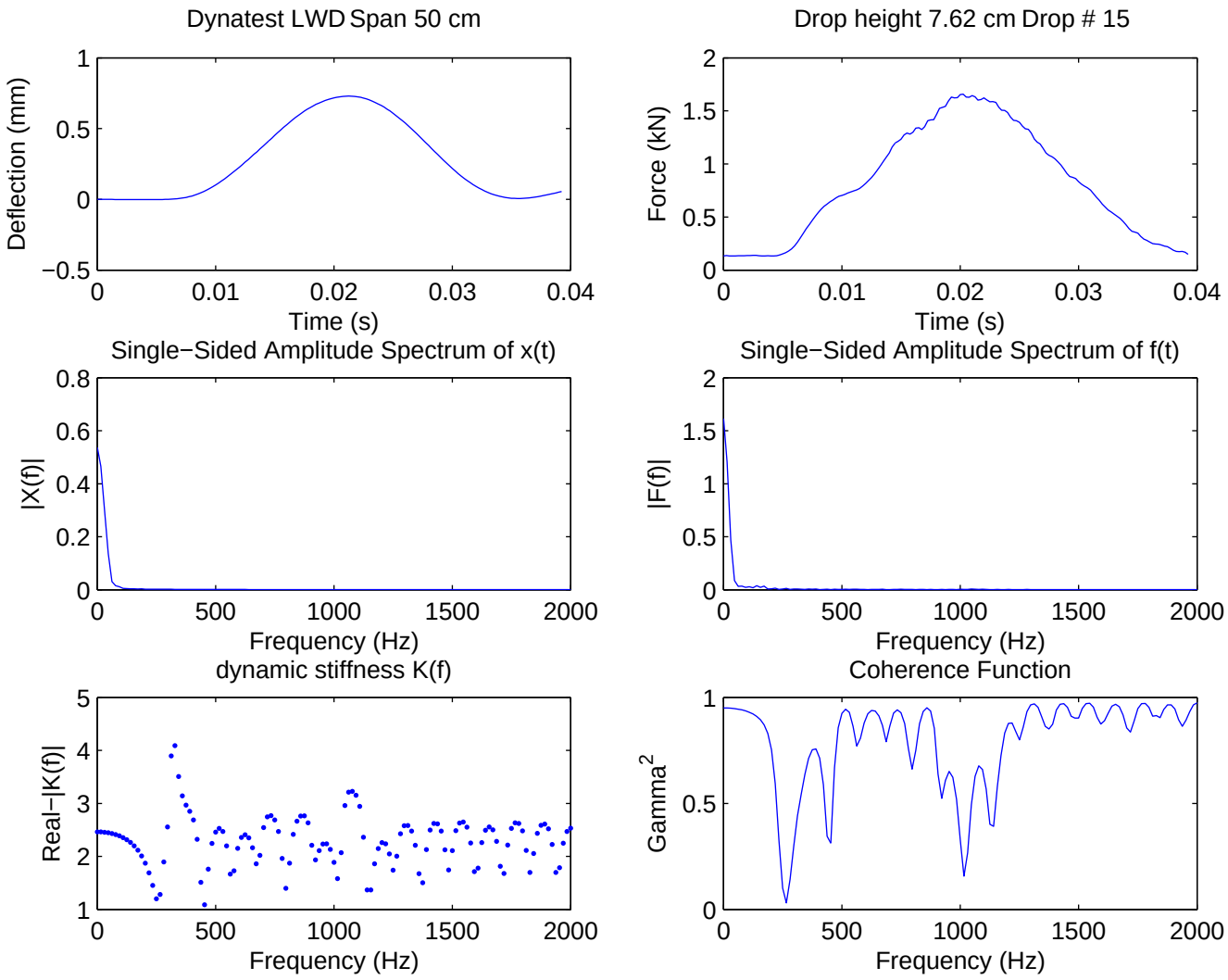
Dynatest LWD Span 50 cm
Deflection (mm)
Time (s)
Drop height 7.62 cm Drop # 15
Force (kN)
Time (s)
Single−Sided Amplitude Spectrum of x(t)
|X(f)|
Frequency (Hz)
Single−Sided Amplitude Spectrum of f(t)
|F(f)|
Frequency (Hz)
dynamic stiffness K(f)
Real−|K(f)|
Frequency (Hz)
Coherence Function
Gamma2
Frequency (Hz)

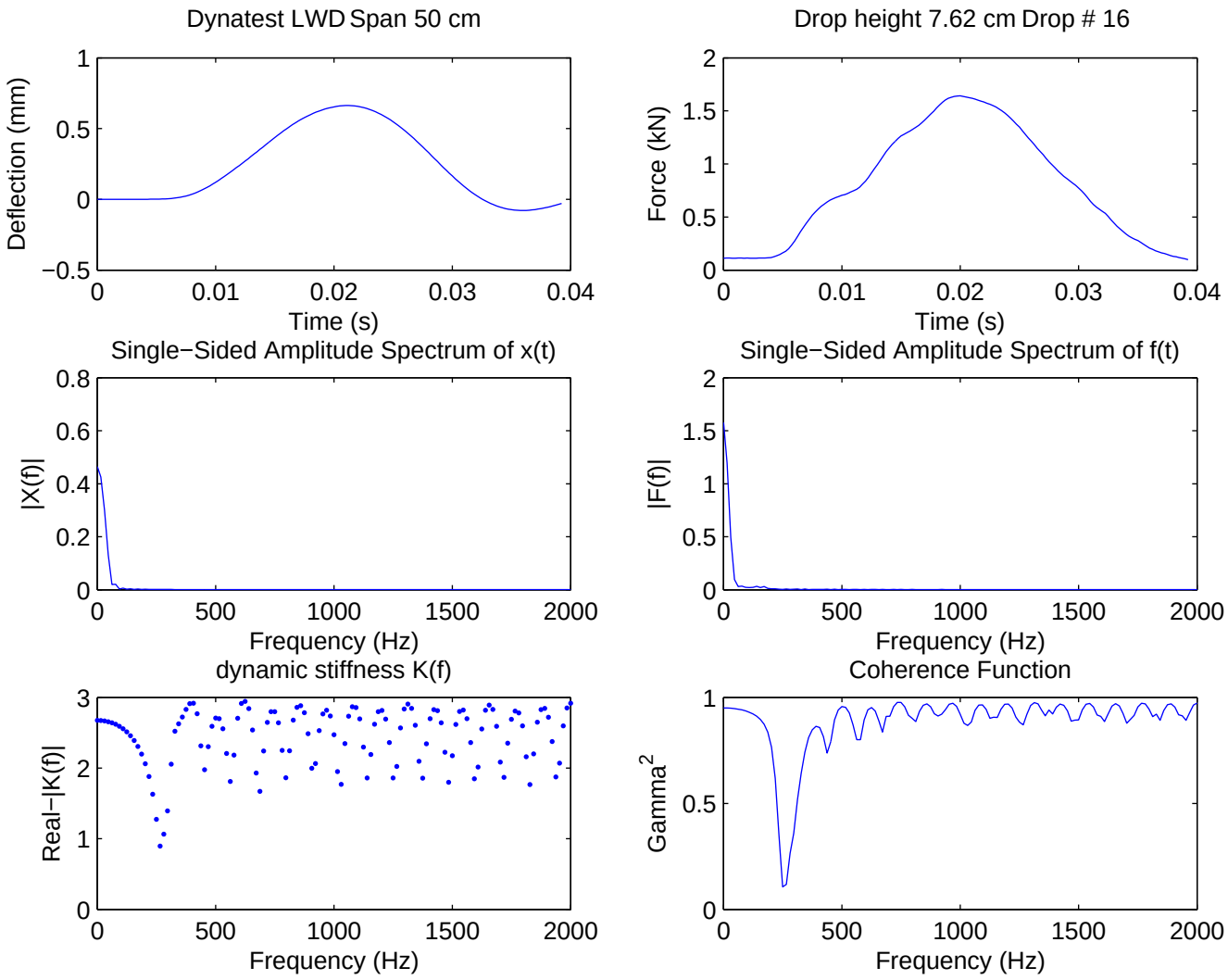
Dynatest LWD Span 50 cm
Deflection (mm)
Time (s)
Drop height 7.62 cm Drop # 16
Force (kN)
Time (s)
Single−Sided Amplitude Spectrum of x(t)
|X(f)|
Frequency (Hz)
Single−Sided Amplitude Spectrum of f(t)
|F(f)|
Frequency (Hz)
dynamic stiffness K(f)
Real−|K(f)|
Frequency (Hz)
Coherence Function
Gamma2
Frequency (Hz)

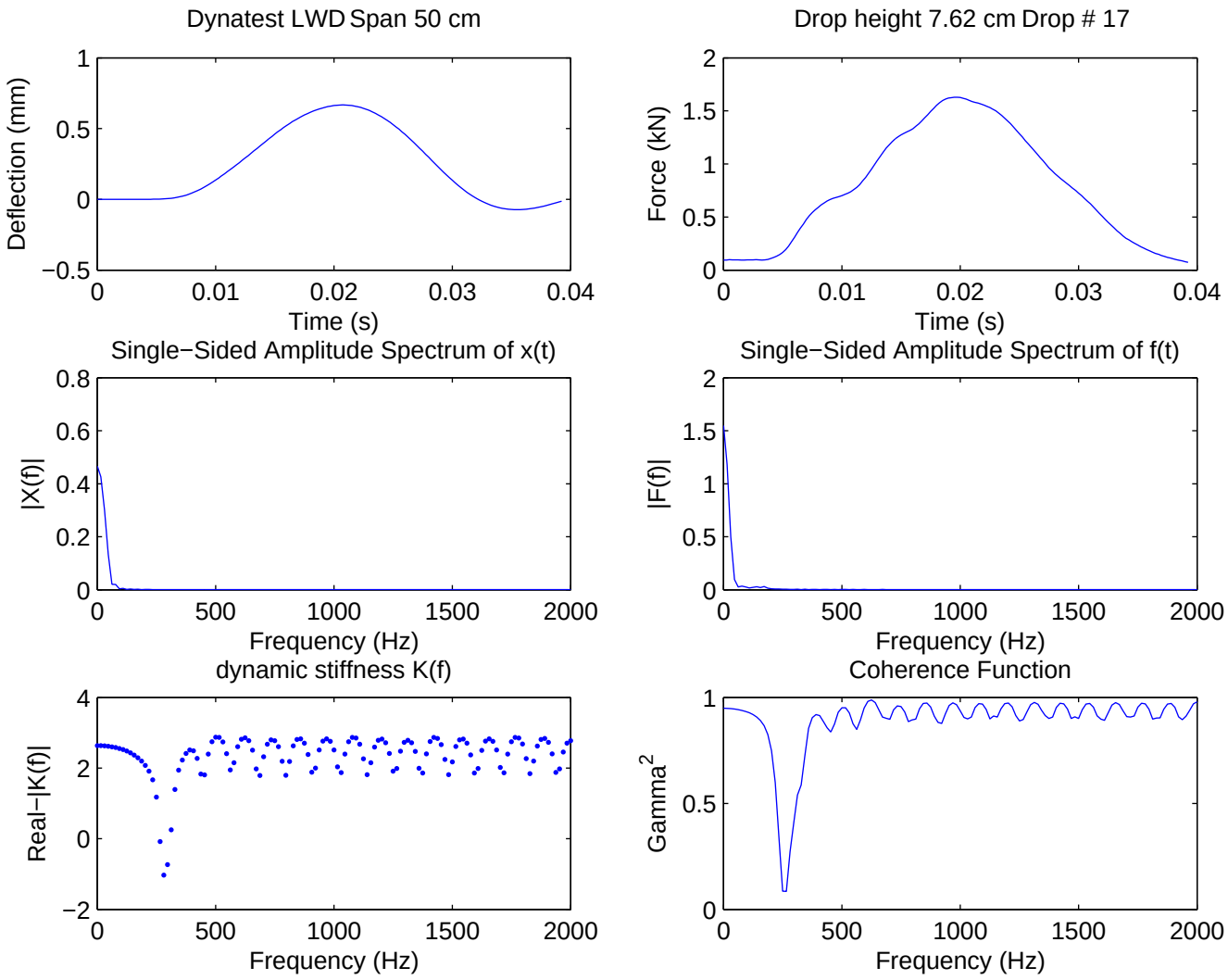
Dynatest LWD Span 50 cm
Deflection (mm)
Time (s)
Drop height 7.62 cm Drop # 17
Force (kN)
Time (s)
Single−Sided Amplitude Spectrum of x(t)
|X(f)|
Frequency (Hz)
Single−Sided Amplitude Spectrum of f(t)
|F(f)|
Frequency (Hz)
dynamic stiffness K(f)
Real−|K(f)|
Frequency (Hz)
Coherence Function
Gamma2
Frequency (Hz)

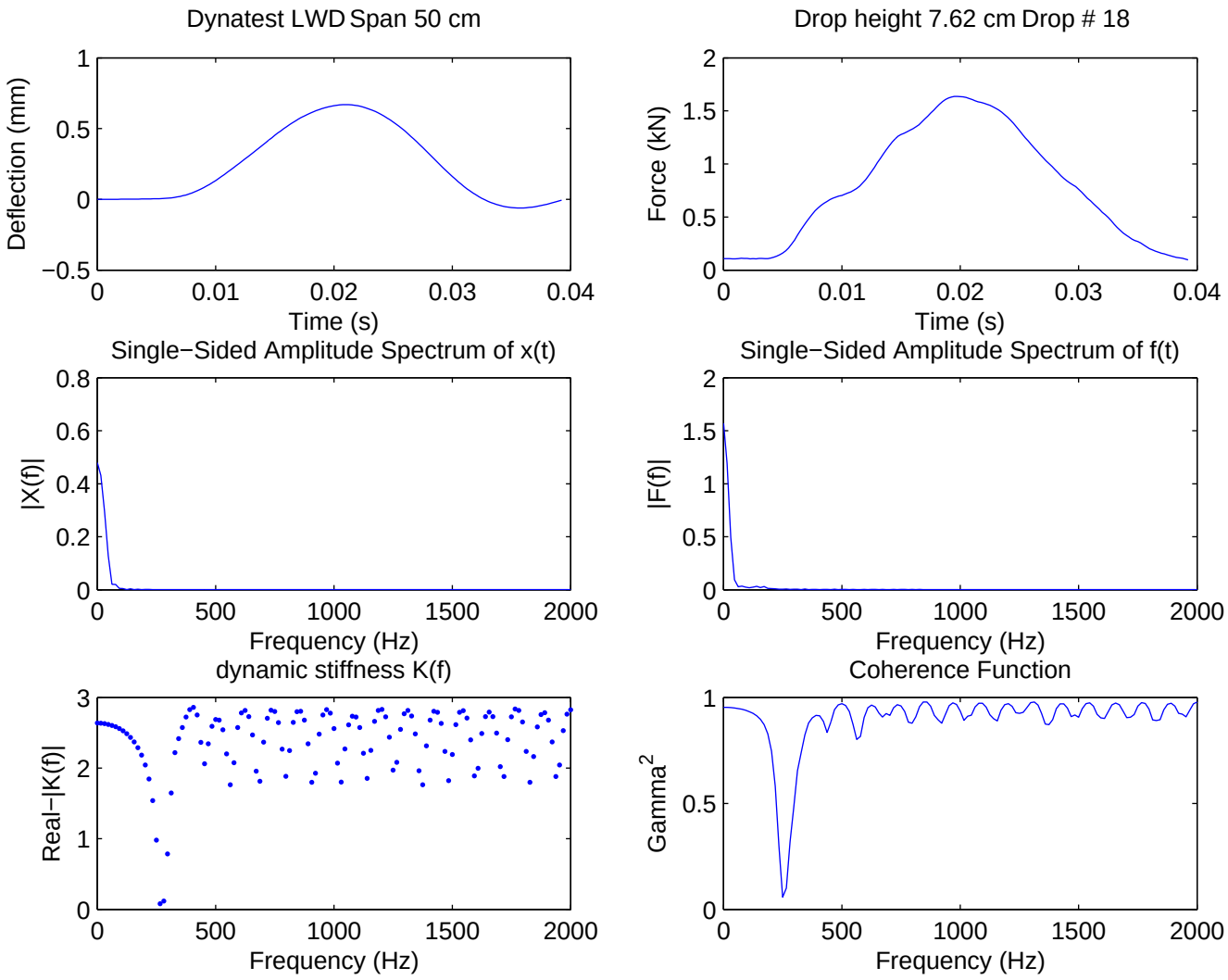
Dynatest LWD Span 50 cm
Deflection (mm)
Time (s)
Drop height 7.62 cm Drop # 18
Force (kN)
Time (s)
Single−Sided Amplitude Spectrum of x(t)
|X(f)|
Frequency (Hz)
Single−Sided Amplitude Spectrum of f(t)
|F(f)|
Frequency (Hz)
dynamic stiffness K(f)
Real−|K(f)|
Frequency (Hz)
Coherence Function
Gamma2
Frequency (Hz)

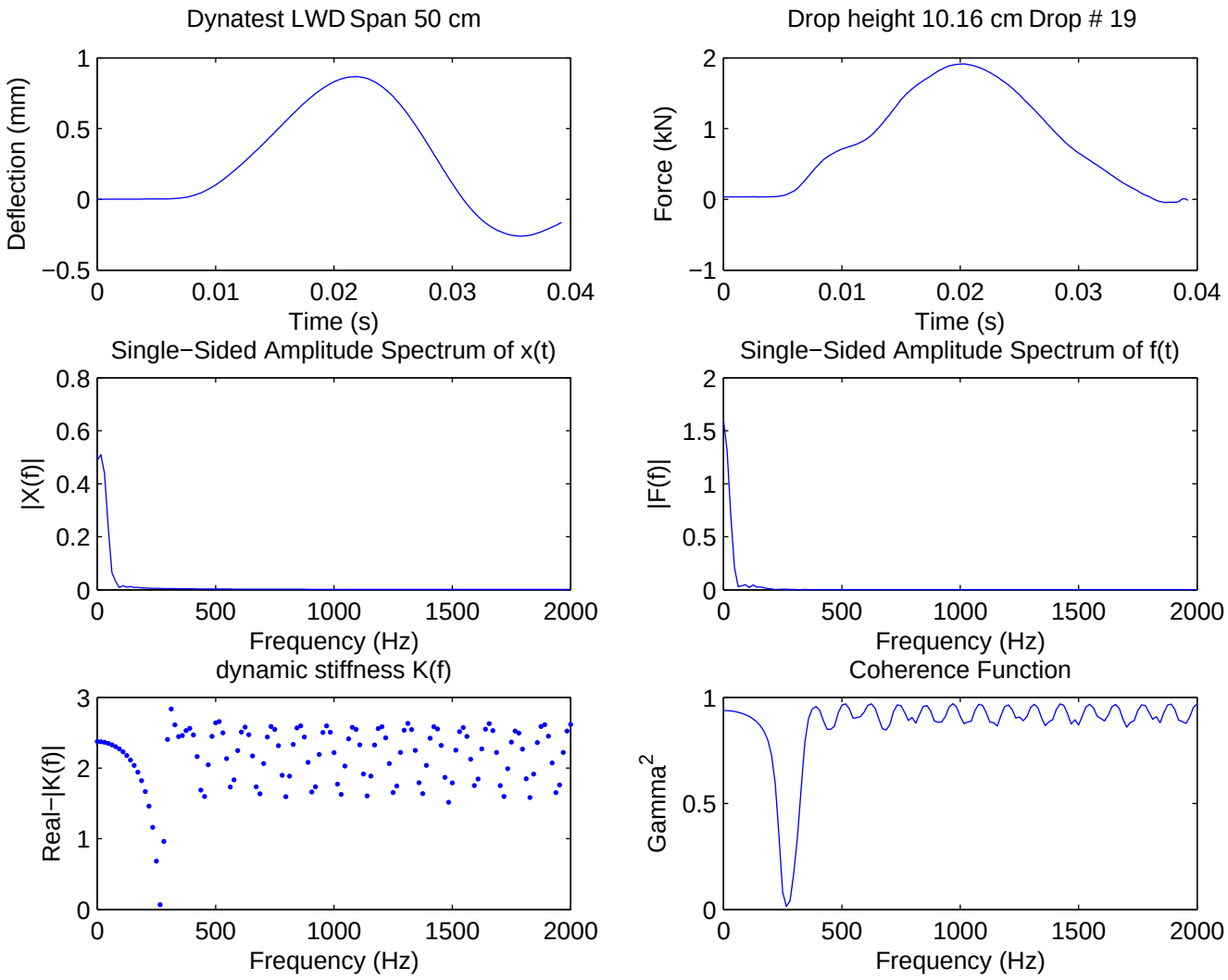
Dynatest LWD Span 50 cm
Deflection (mm)
Time (s)
Drop height 10.16 cm Drop # 19
Force (kN)
Time (s)
Single−Sided Amplitude Spectrum of x(t)
|X(f)|
Frequency (Hz)
Single−Sided Amplitude Spectrum of f(t)
|F(f)|
Frequency (Hz)
dynamic stiffness K(f)
Real−|K(f)|
Frequency (Hz)
Coherence Function
Gamma2
Frequency (Hz)

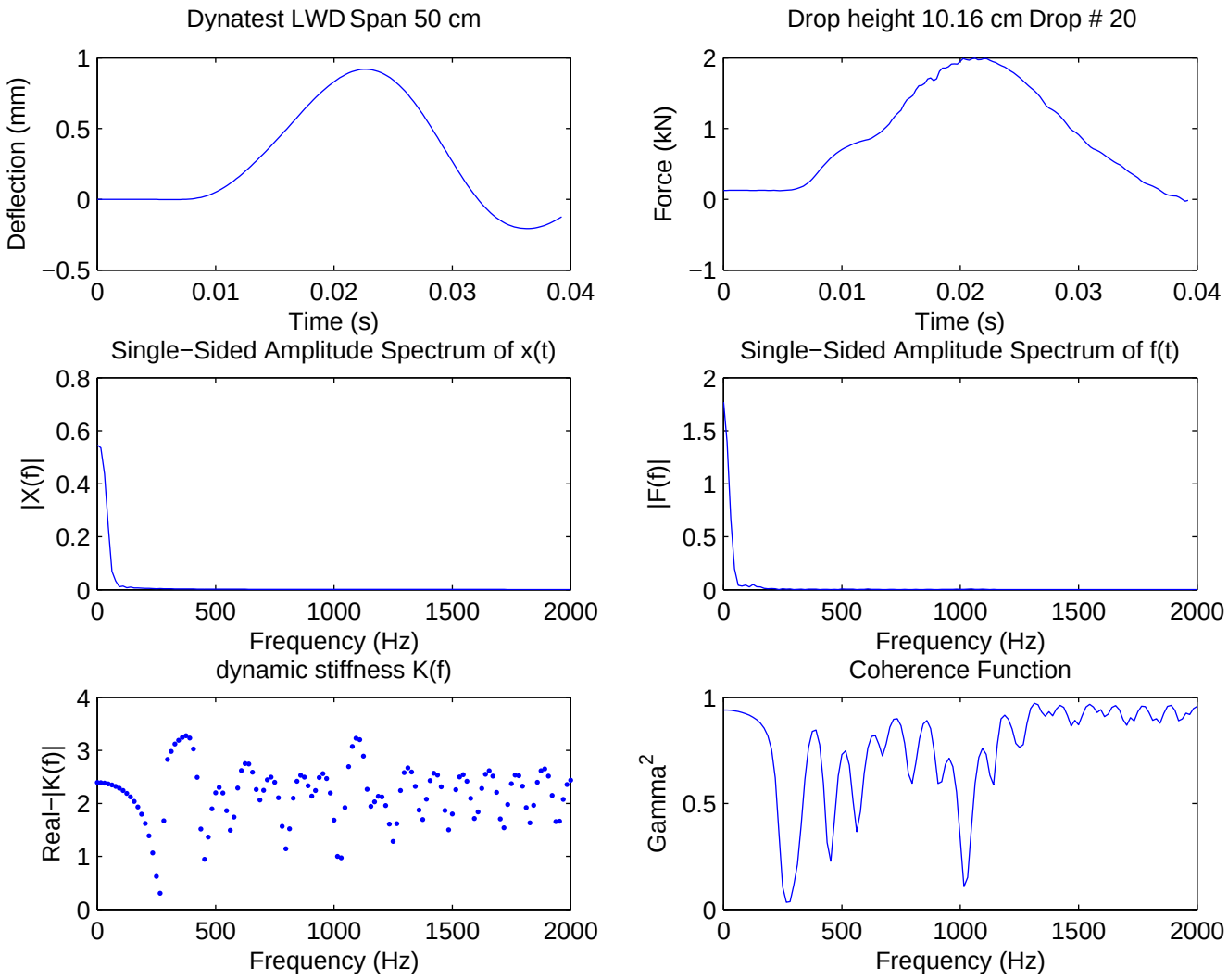
Dynatest LWD Span 50 cm
Deflection (mm)
Time (s)
Drop height 10.16 cm Drop # 20
Force (kN)
Time (s)
Single−Sided Amplitude Spectrum of x(t)
|X(f)|
Frequency (Hz)
Single−Sided Amplitude Spectrum of f(t)
|F(f)|
Frequency (Hz)
dynamic stiffness K(f)
Real−|K(f)|
Frequency (Hz)
Coherence Function
Gamma2
Frequency (Hz)

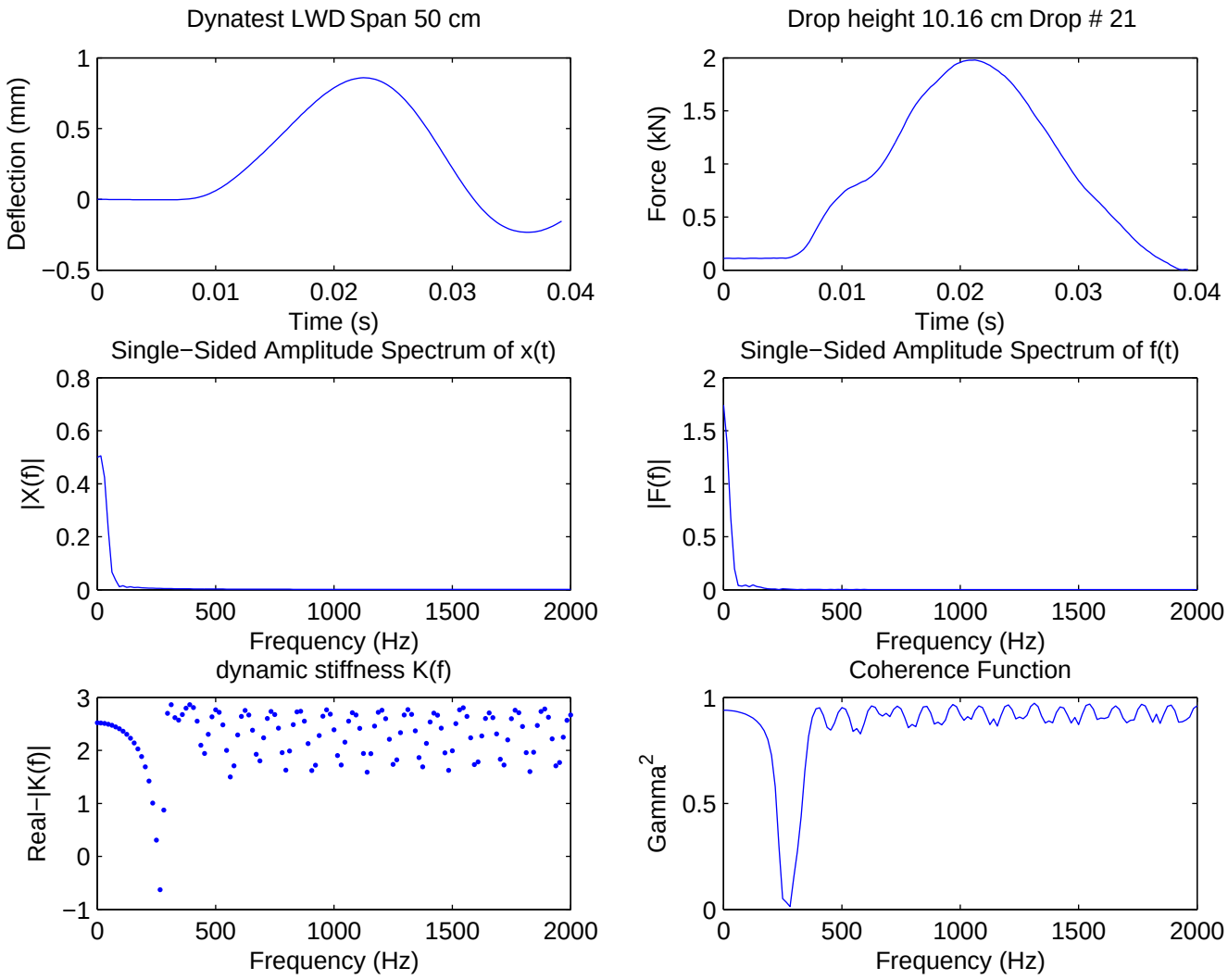
Dynatest LWD Span 50 cm
Deflection (mm)
Time (s)
Drop height 10.16 cm Drop # 21
Force (kN)
Time (s)
Single−Sided Amplitude Spectrum of x(t)
|X(f)|
Frequency (Hz)
Single−Sided Amplitude Spectrum of f(t)
|F(f)|
Frequency (Hz)
dynamic stiffness K(f)
Real−|K(f)|
Frequency (Hz)
Coherence Function
Gamma2
Frequency (Hz)

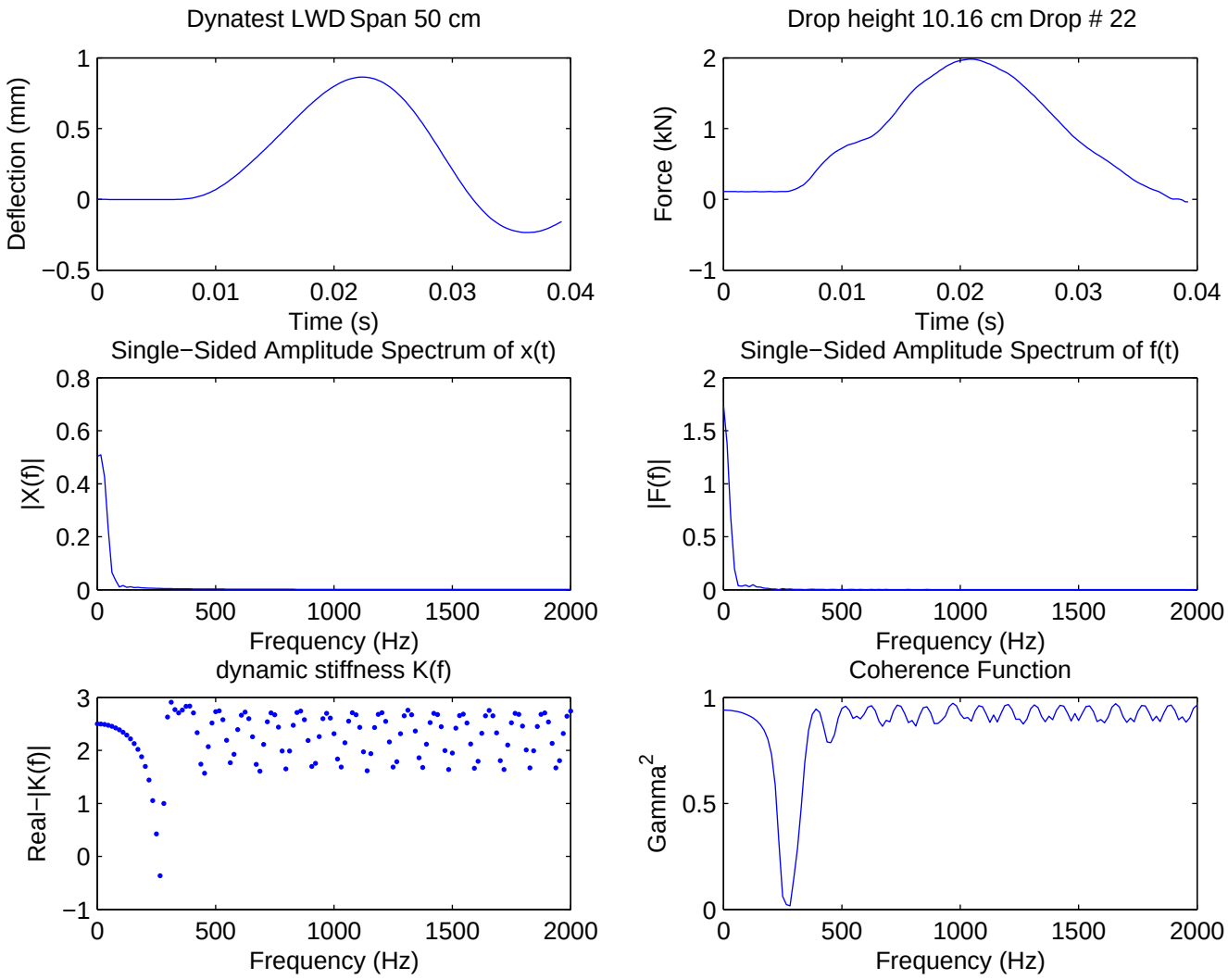
Dynatest LWD Span 50 cm
Deflection (mm)
Time (s)
Drop height 10.16 cm Drop # 22
Force (kN)
Time (s)
Single−Sided Amplitude Spectrum of x(t)
|X(f)|
Frequency (Hz)
Single−Sided Amplitude Spectrum of f(t)
|F(f)|
Frequency (Hz)
dynamic stiffness K(f)
Real−|K(f)|
Frequency (Hz)
Coherence Function
Gamma2
Frequency (Hz)

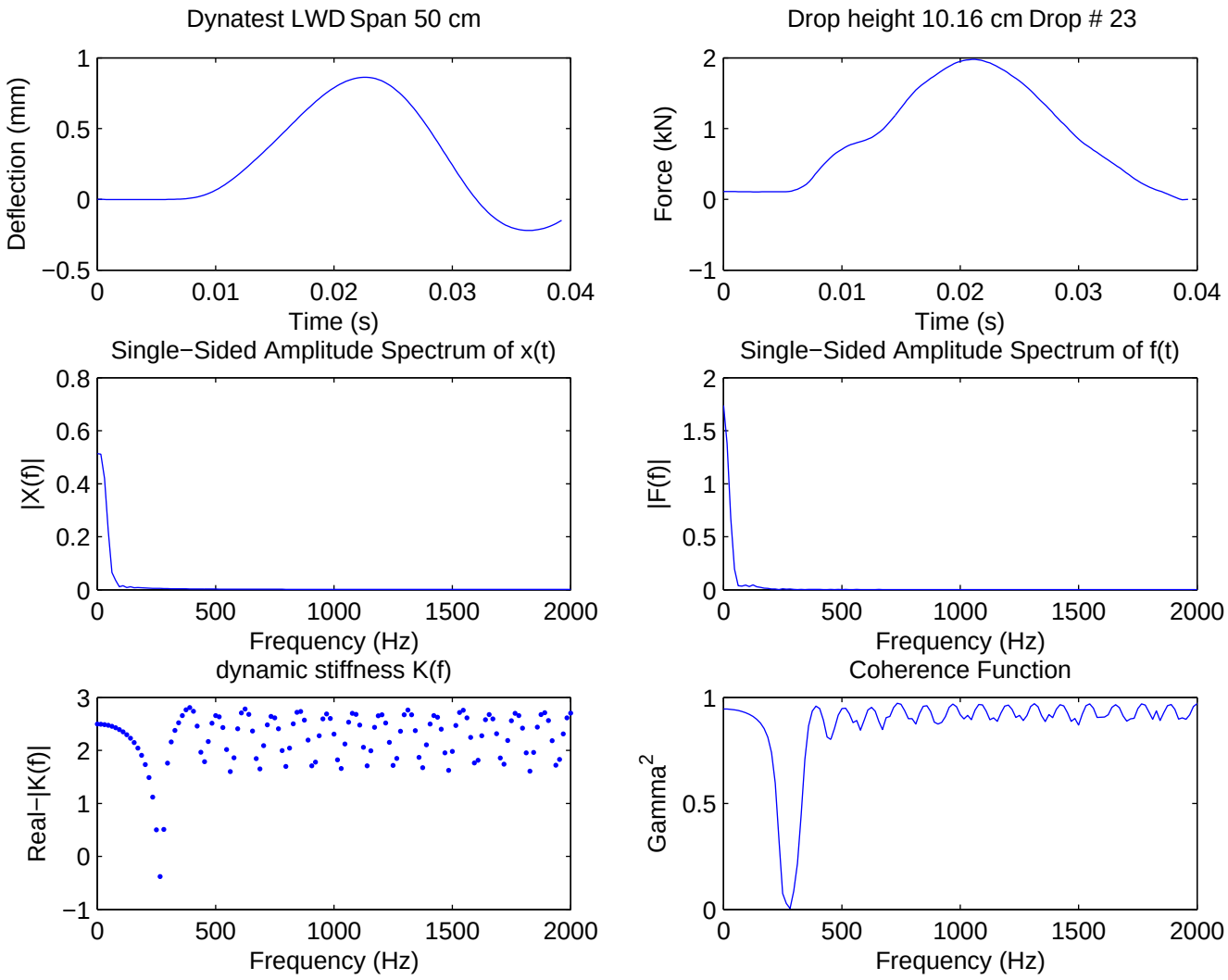
Dynatest LWD Span 50 cm
Deflection (mm)
Time (s)
Drop height 10.16 cm Drop # 23
Force (kN)
Time (s)
Single−Sided Amplitude Spectrum of x(t)
|X(f)|
Frequency (Hz)
Single−Sided Amplitude Spectrum of f(t)
|F(f)|
Frequency (Hz)
dynamic stiffness K(f)
Real−|K(f)|
Frequency (Hz)
Coherence Function
Gamma2
Frequency (Hz)

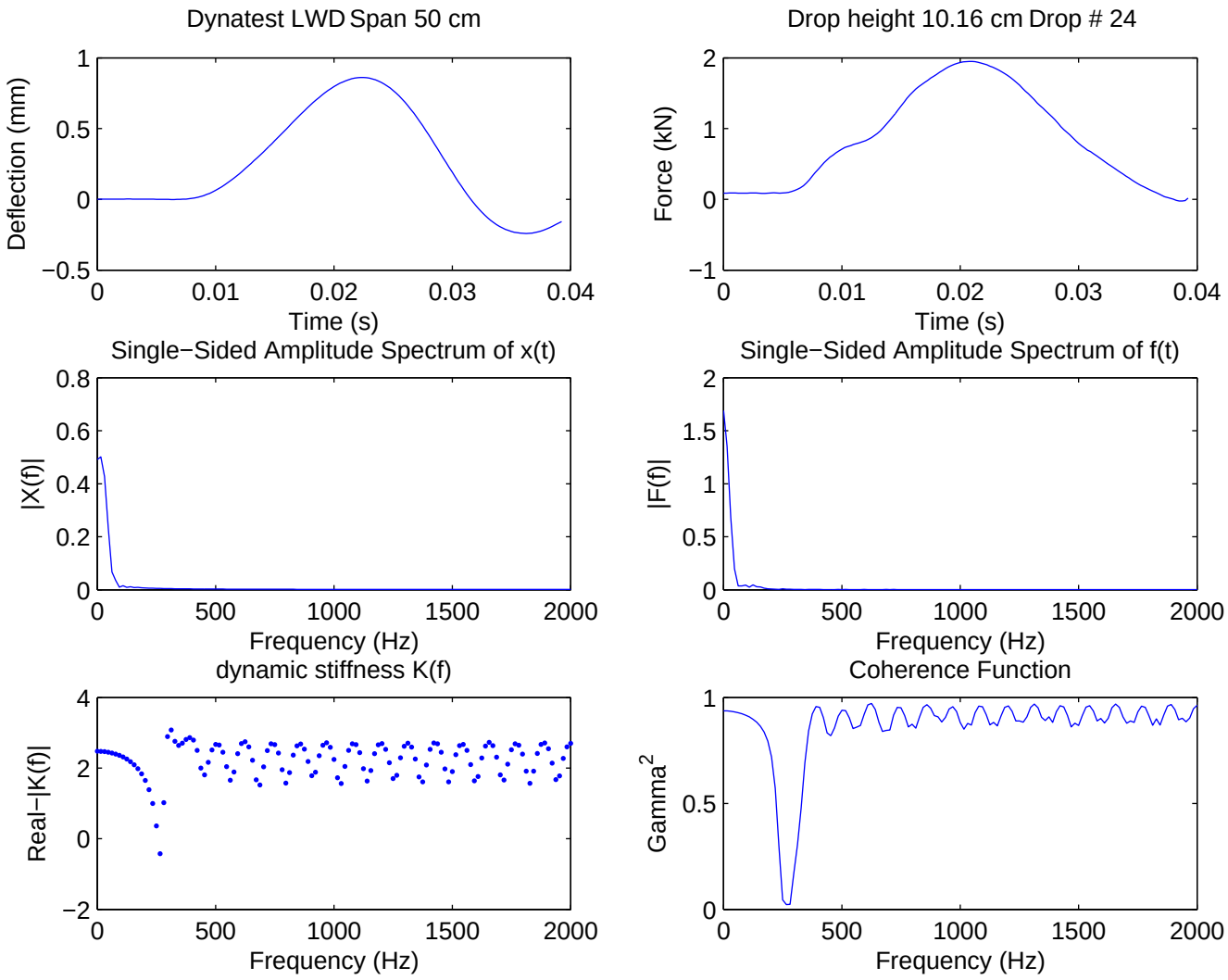
Dynatest LWD Span 50 cm
Deflection (mm)
Time (s)
Drop height 10.16 cm Drop # 24
Force (kN)
Time (s)
Single−Sided Amplitude Spectrum of x(t)
|X(f)|
Frequency (Hz)
Single−Sided Amplitude Spectrum of f(t)
|F(f)|
Frequency (Hz)
dynamic stiffness K(f)
Real−|K(f)|
Frequency (Hz)
Coherence Function
Gamma2
Frequency (Hz)

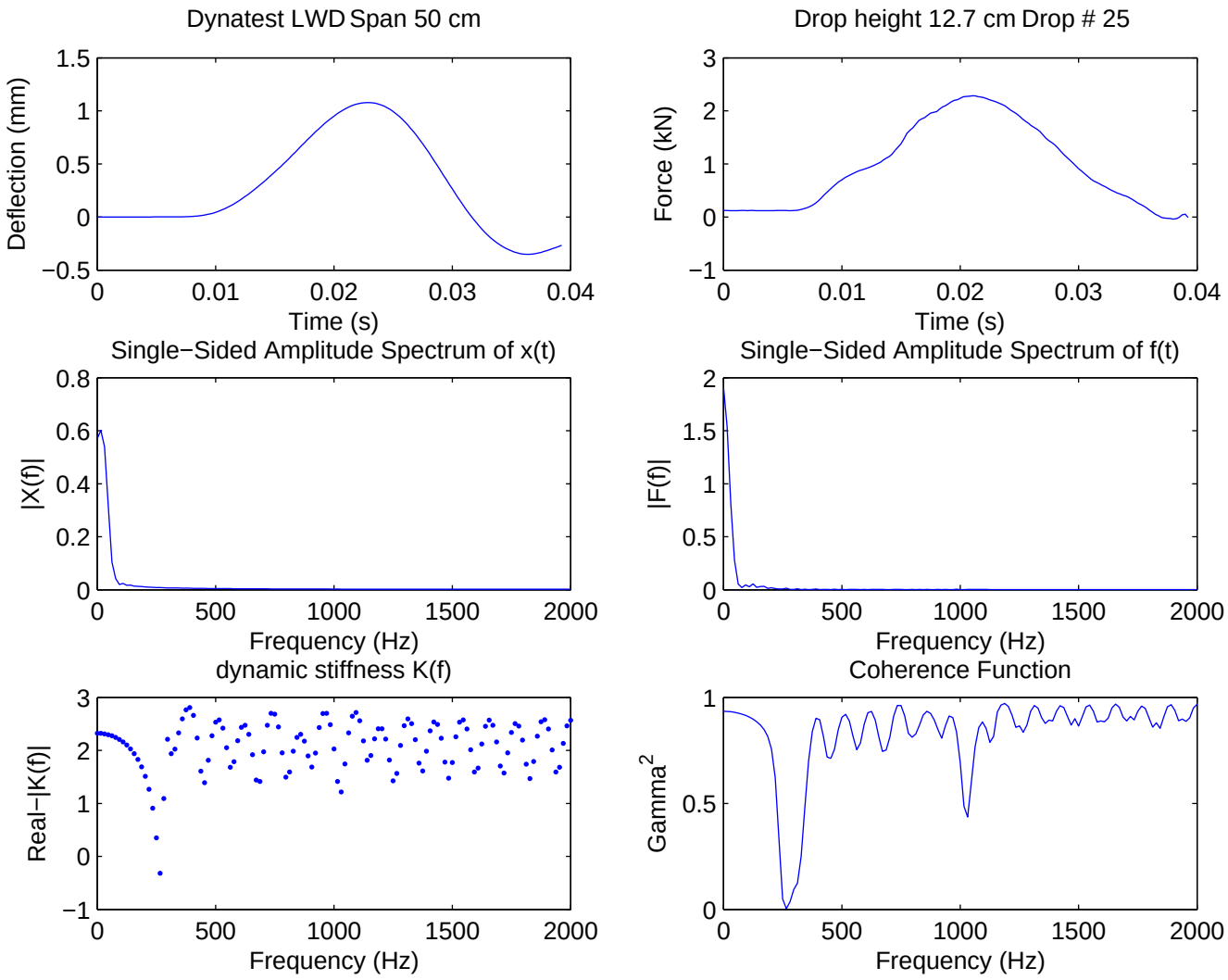
Dynatest LWD Span 50 cm
Deflection (mm)
Time (s)
Drop height 12.7 cm Drop # 25
Force (kN)
Time (s)
Single−Sided Amplitude Spectrum of x(t)
|X(f)|
Frequency (Hz)
Single−Sided Amplitude Spectrum of f(t)
|F(f)|
Frequency (Hz)
dynamic stiffness K(f)
Real−|K(f)|
Frequency (Hz)
Coherence Function
Gamma2
Frequency (Hz)

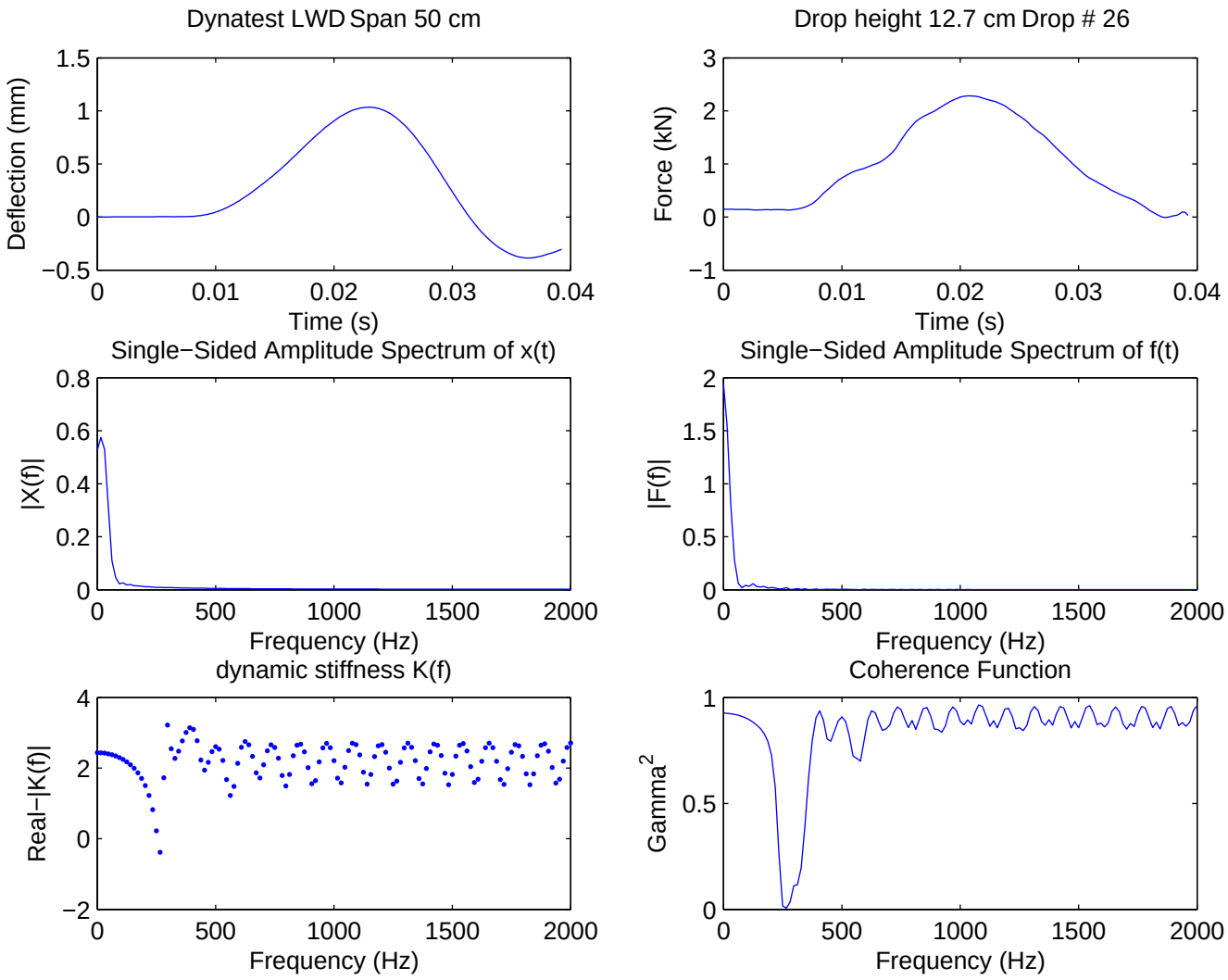
Dynatest LWD Span 50 cm
Deflection (mm)
Time (s)
Drop height 12.7 cm Drop # 26
Force (kN)
Time (s)
Single−Sided Amplitude Spectrum of x(t)
|X(f)|
Frequency (Hz)
Single−Sided Amplitude Spectrum of f(t)
|F(f)|
Frequency (Hz)
dynamic stiffness K(f)
Real−|K(f)|
Frequency (Hz)
Coherence Function
Gamma2
Frequency (Hz)

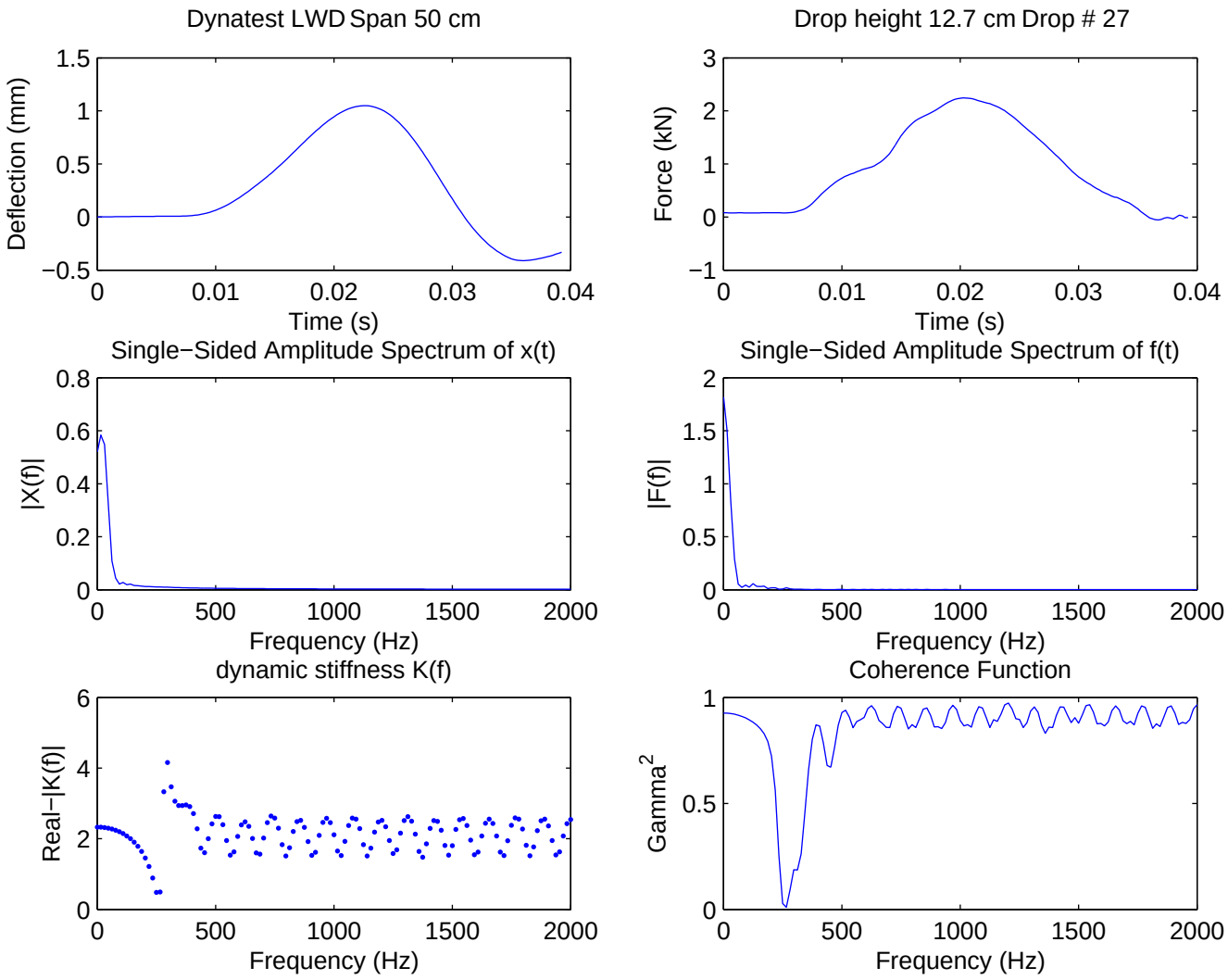
Dynatest LWD Span 50 cm
Deflection (mm)
Time (s)
Drop height 12.7 cm Drop # 27
Force (kN)
Time (s)
Single−Sided Amplitude Spectrum of x(t)
|X(f)|
Frequency (Hz)
Single−Sided Amplitude Spectrum of f(t)
|F(f)|
Frequency (Hz)
dynamic stiffness K(f)
Real−|K(f)|
Frequency (Hz)
Coherence Function
Gamma2
Frequency (Hz)

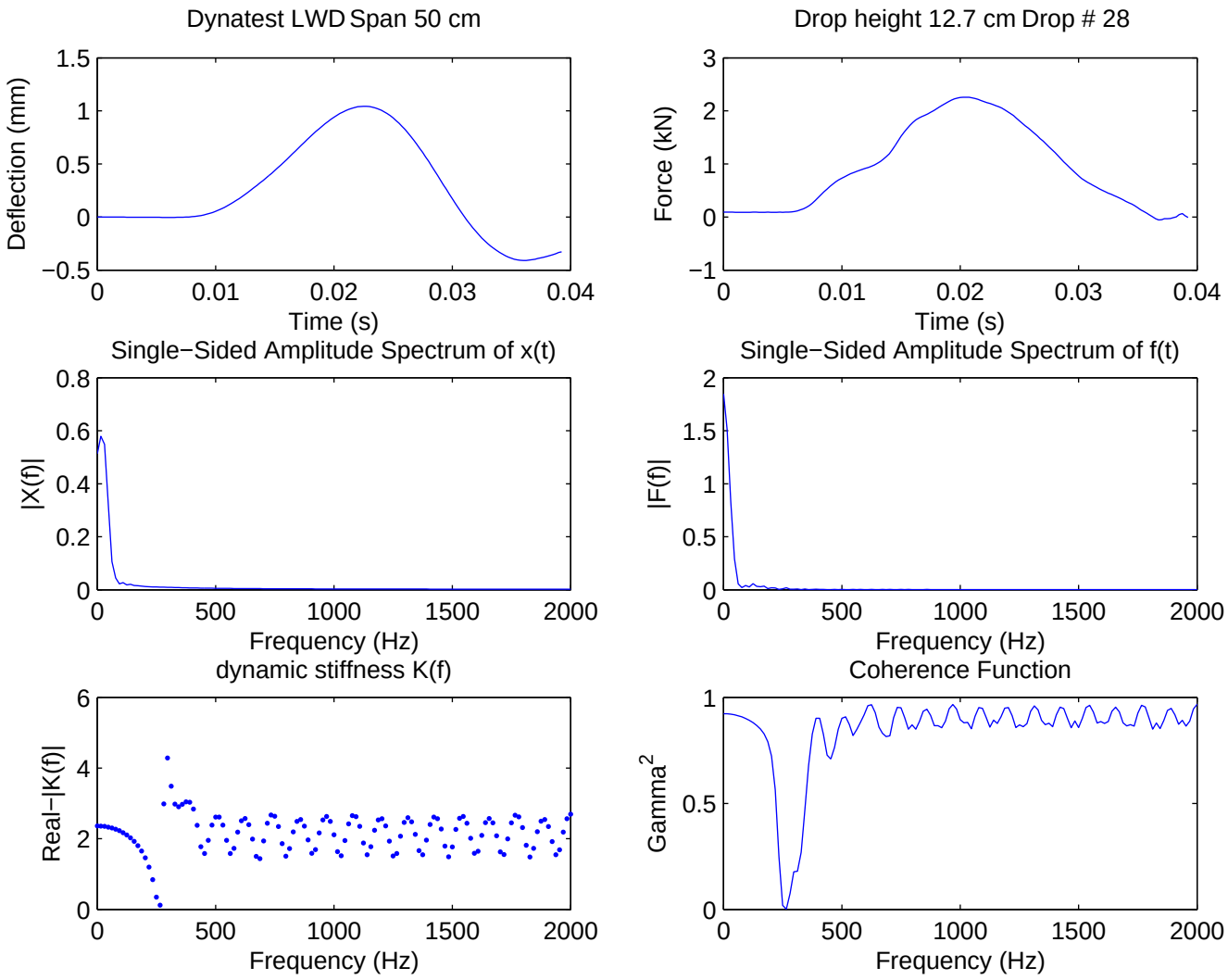
Dynatest LWD Span 50 cm
Deflection (mm)
Time (s)
Drop height 12.7 cm Drop # 28
Force (kN)
Time (s)
Single−Sided Amplitude Spectrum of x(t)
|X(f)|
Frequency (Hz)
Single−Sided Amplitude Spectrum of f(t)
|F(f)|
Frequency (Hz)
dynamic stiffness K(f)
Real−|K(f)|
Frequency (Hz)
Coherence Function
Gamma2
Frequency (Hz)

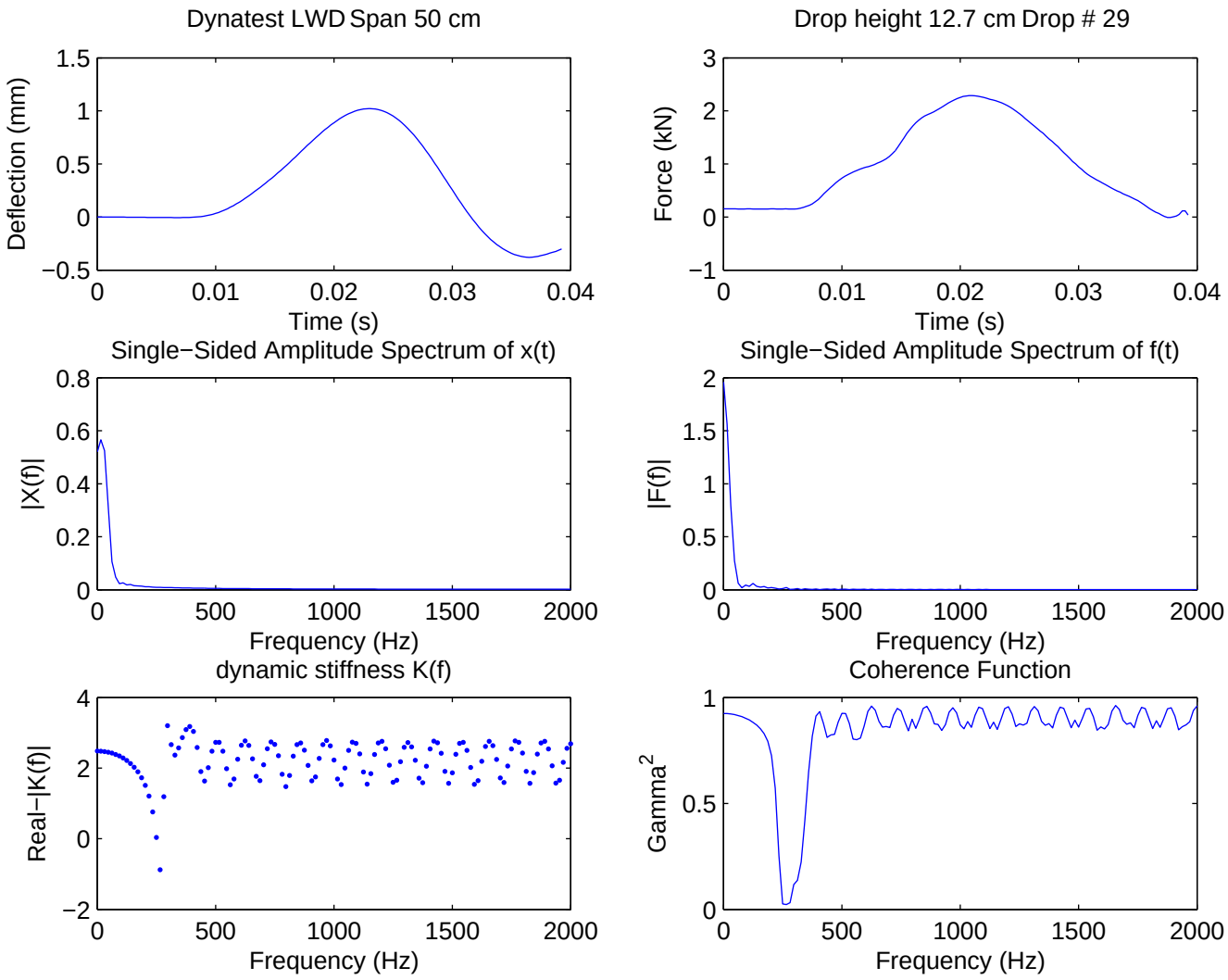
Dynatest LWD Span 50 cm
Deflection (mm)
Time (s)
Drop height 12.7 cm Drop # 29
Force (kN)
Time (s)
Single−Sided Amplitude Spectrum of x(t)
|X(f)|
Frequency (Hz)
Single−Sided Amplitude Spectrum of f(t)
|F(f)|
Frequency (Hz)
dynamic stiffness K(f)
Real−|K(f)|
Frequency (Hz)
Coherence Function
Gamma2
Frequency (Hz)

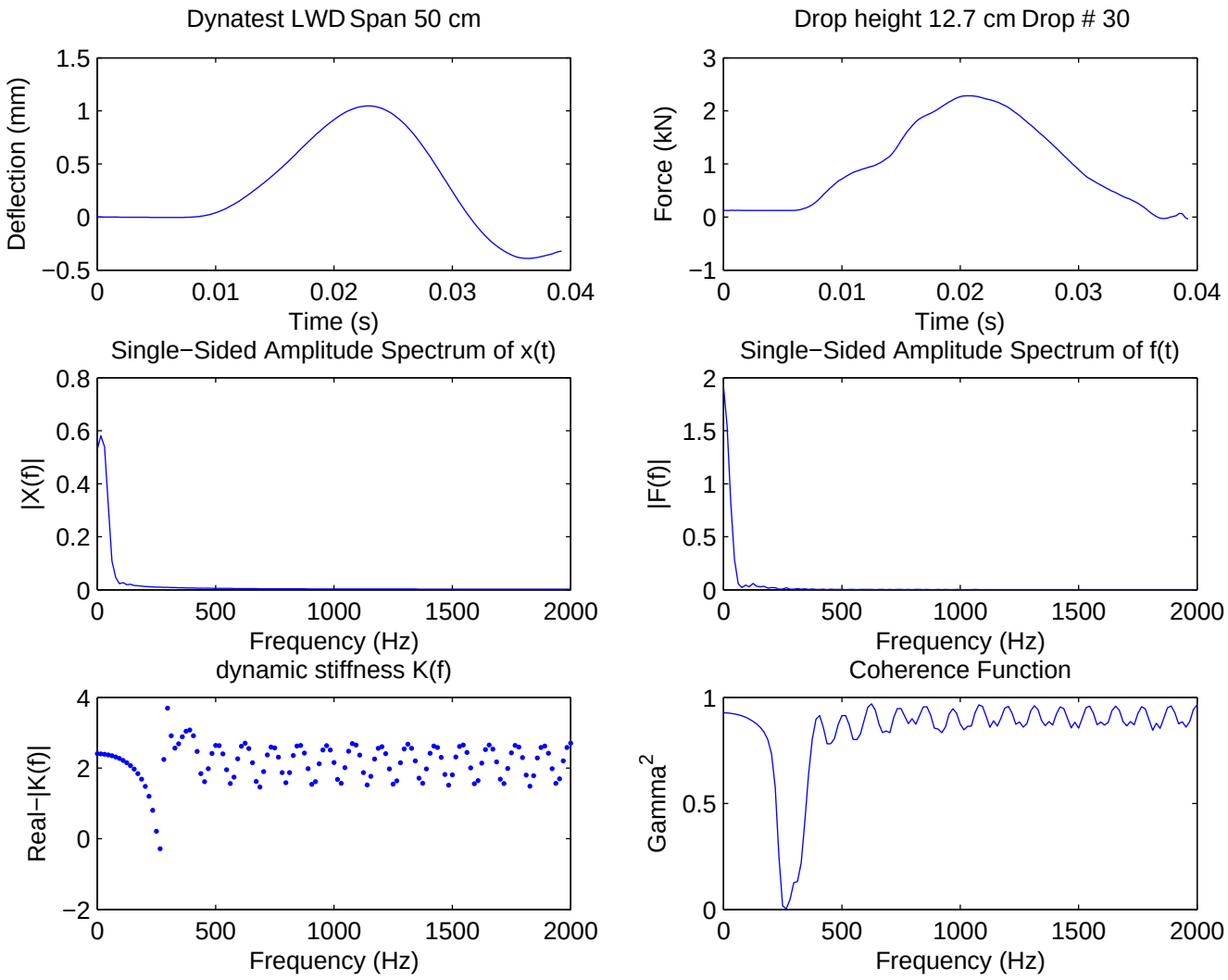
Dynatest LWD Span 50 cm
Deflection (mm)
Time (s)
Drop height 12.7 cm Drop # 30
Force (kN)
Time (s)
Single−Sided Amplitude Spectrum of x(t)
|X(f)|
Frequency (Hz)
Single−Sided Amplitude Spectrum of f(t)
|F(f)|
Frequency (Hz)
dynamic stiffness K(f)
Real−|K(f)|
Frequency (Hz)
Coherence Function
Gamma2
Frequency (Hz)

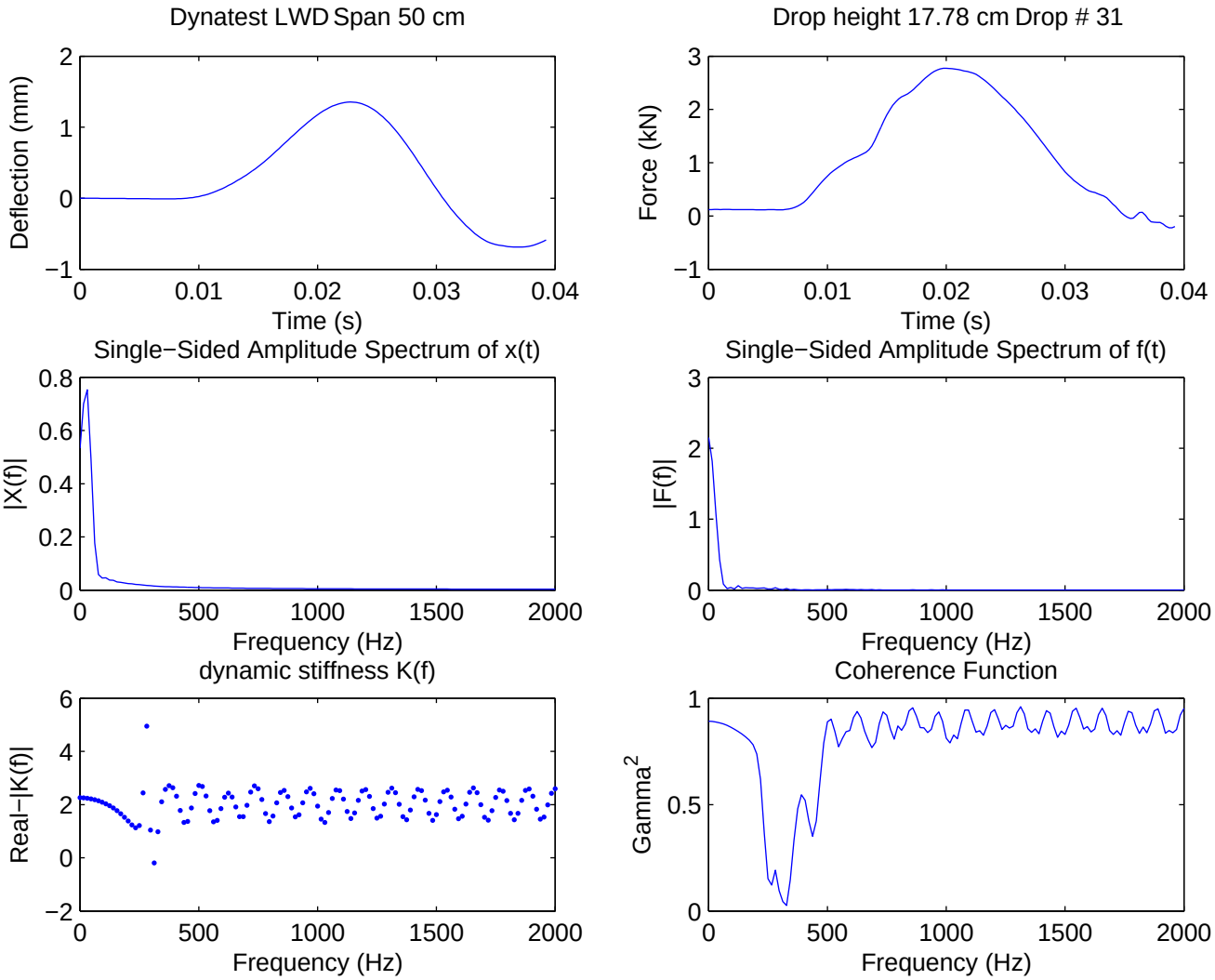
Dynatest LWD Span 50 cm
Deflection (mm)
Time (s)
Drop height 17.78 cm Drop # 31
Force (kN)
Time (s)
Single−Sided Amplitude Spectrum of x(t)
|X(f)|
Frequency (Hz)
Single−Sided Amplitude Spectrum of f(t)
|F(f)|
Frequency (Hz)
dynamic stiffness K(f)
Real−|K(f)|
Frequency (Hz)
Coherence Function
Gamma2
Frequency (Hz)

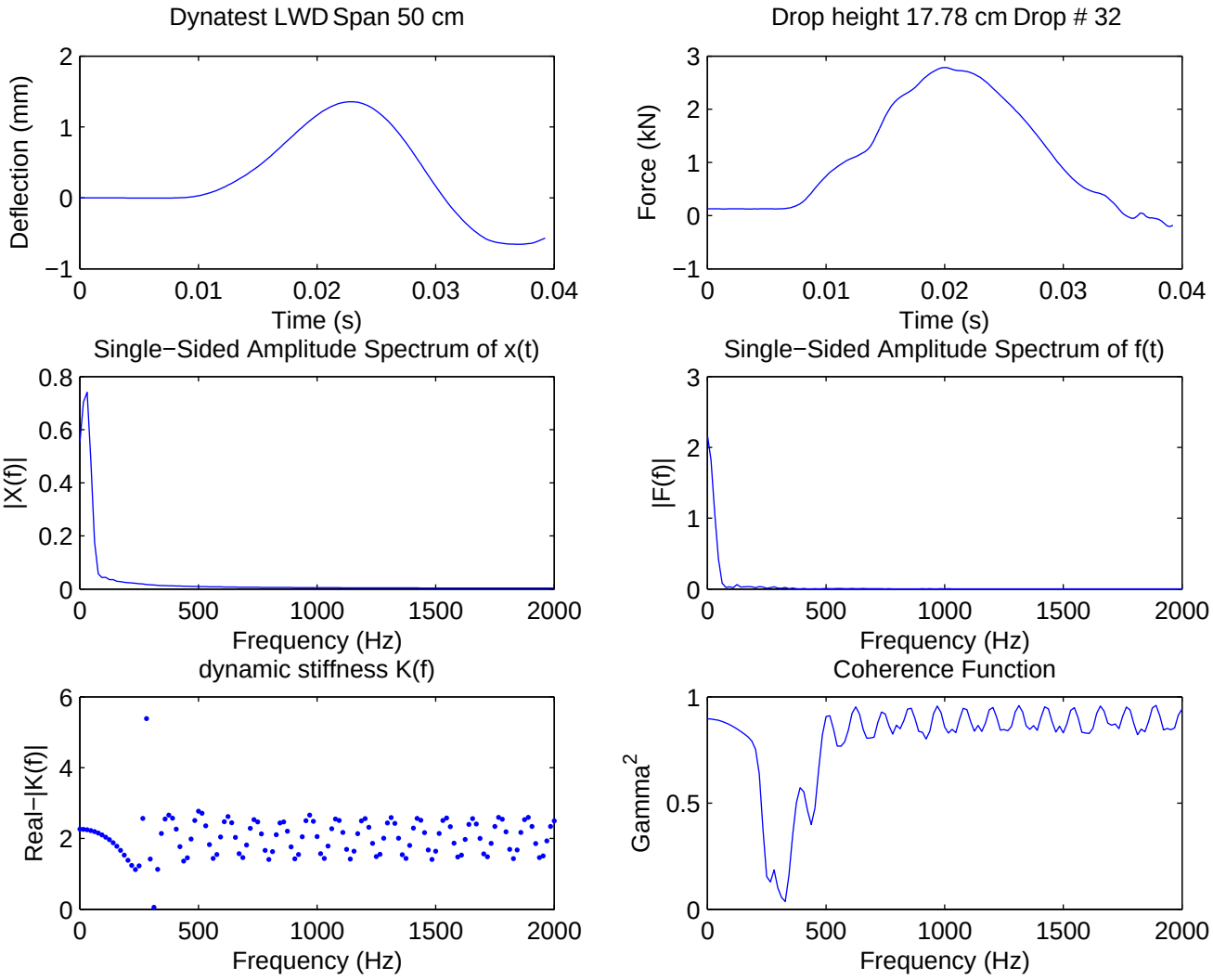
Dynatest LWD Span 50 cm
Deflection (mm)
Time (s)
Drop height 17.78 cm Drop # 32
Force (kN)
Time (s)
Single−Sided Amplitude Spectrum of x(t)
|X(f)|
Frequency (Hz)
Single−Sided Amplitude Spectrum of f(t)
|F(f)|
Frequency (Hz)
dynamic stiffness K(f)
Real−|K(f)|
Frequency (Hz)
Coherence Function
Gamma2
Frequency (Hz)

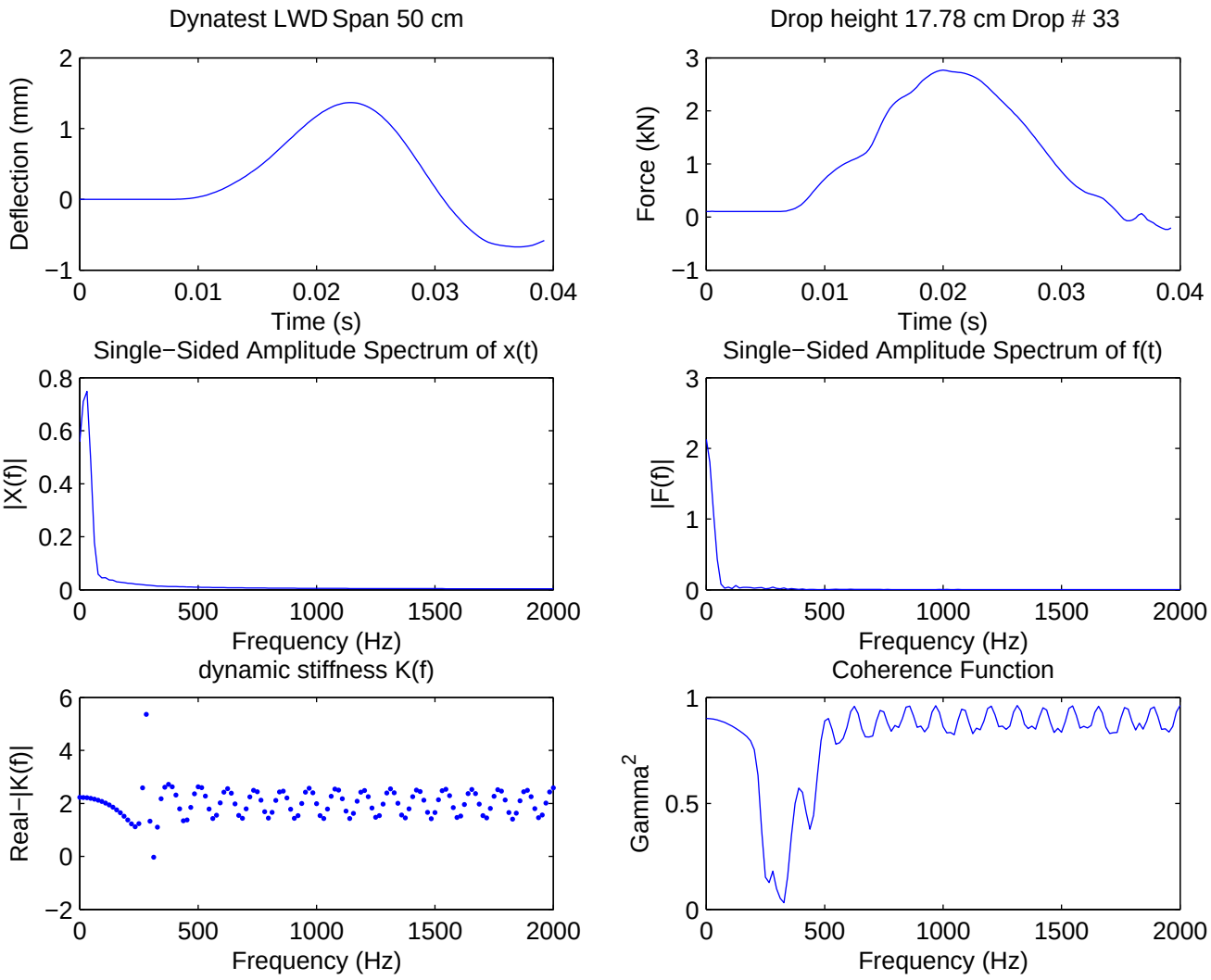
Dynatest LWD Span 50 cm
Deflection (mm)
Time (s)
Drop height 17.78 cm Drop # 33
Force (kN)
Time (s)
Single−Sided Amplitude Spectrum of x(t)
|X(f)|
Frequency (Hz)
Single−Sided Amplitude Spectrum of f(t)
|F(f)|
Frequency (Hz)
dynamic stiffness K(f)
Real−|K(f)|
Frequency (Hz)
Coherence Function
Gamma2
Frequency (Hz)

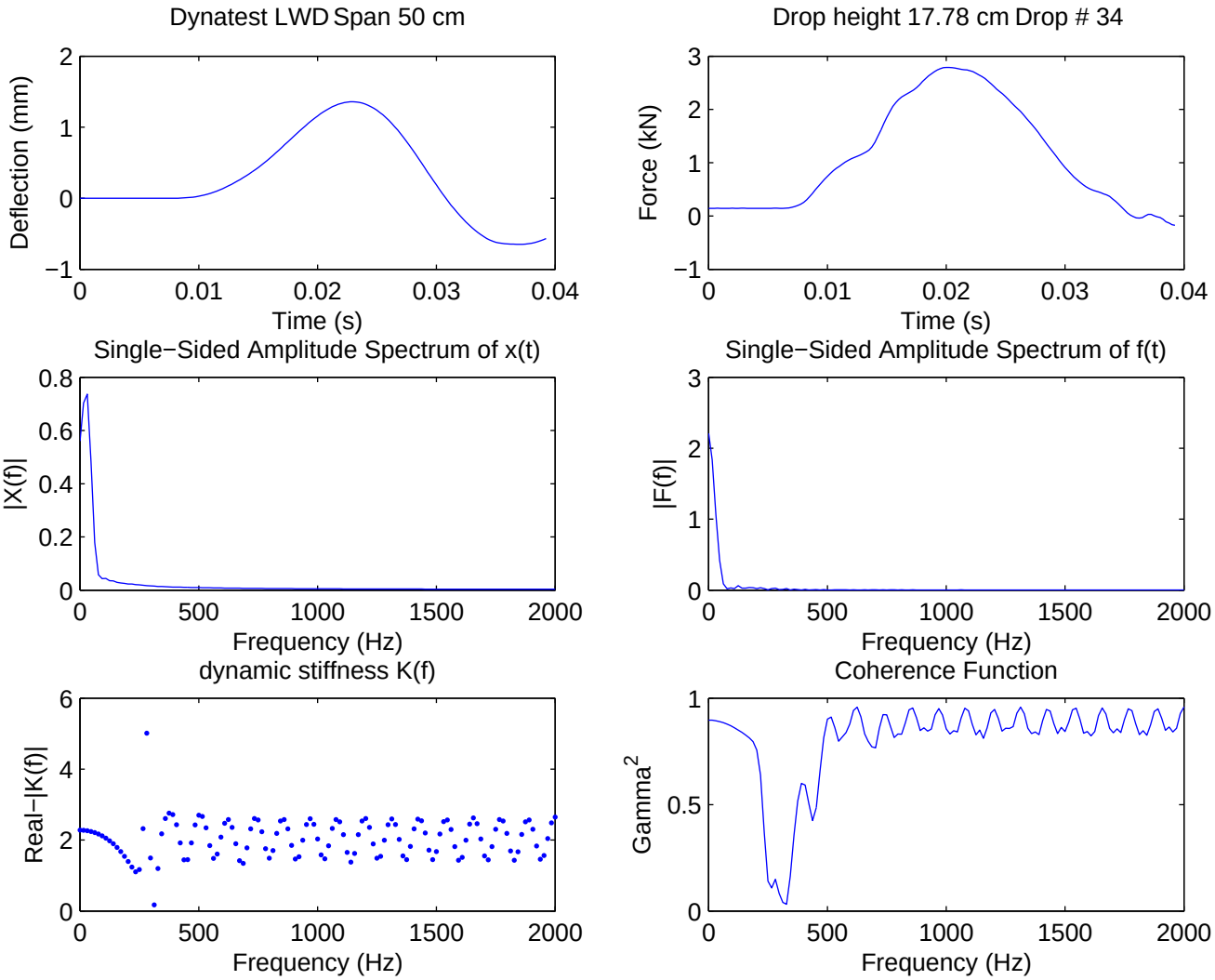
Dynatest LWD Span 50 cm
Deflection (mm)
Time (s)
Drop height 17.78 cm Drop # 34
Force (kN)
Time (s)
Single−Sided Amplitude Spectrum of x(t)
|X(f)|
Frequency (Hz)
Single−Sided Amplitude Spectrum of f(t)
|F(f)|
Frequency (Hz)
dynamic stiffness K(f)
Real−|K(f)|
Frequency (Hz)
Coherence Function
Gamma2
Frequency (Hz)

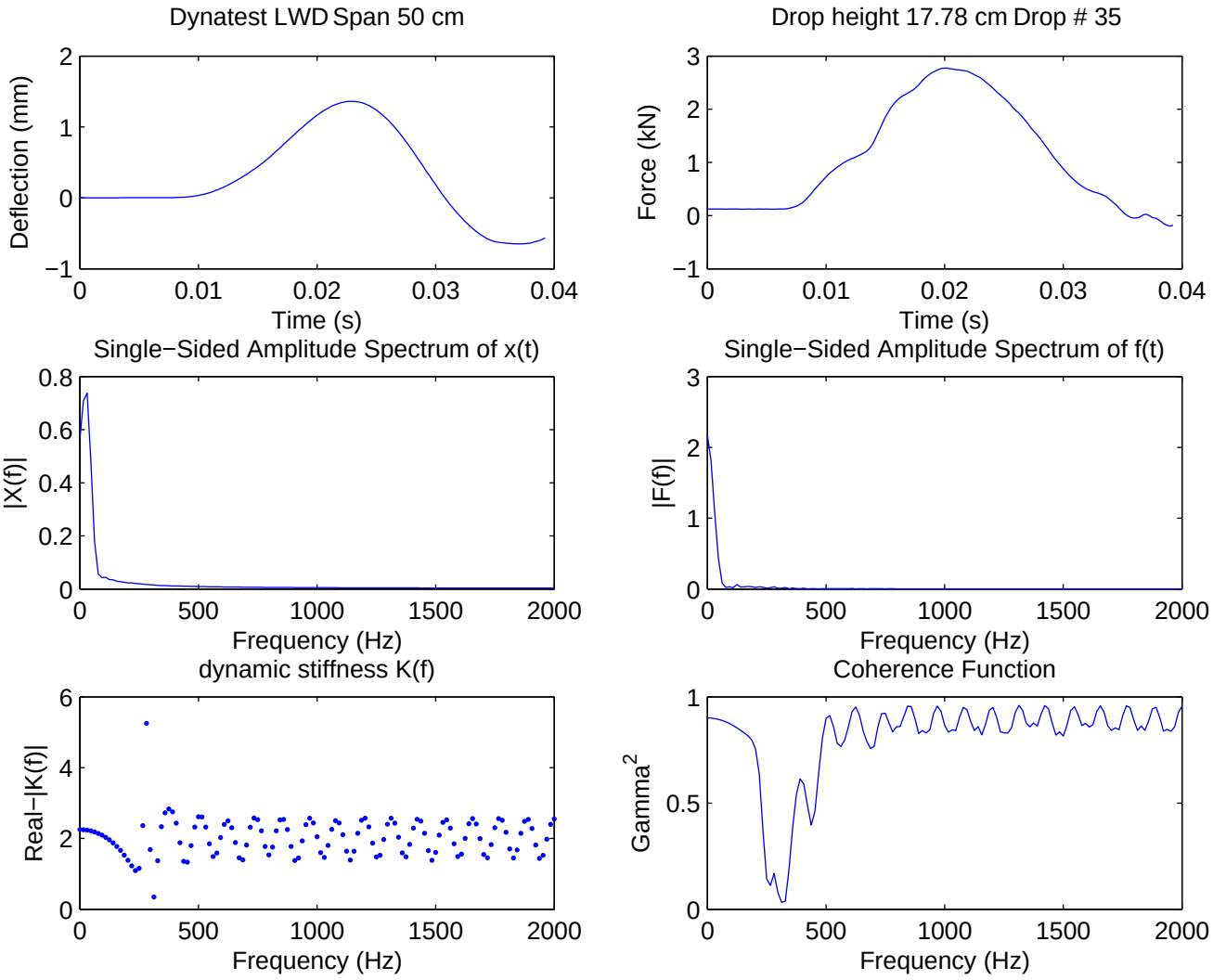
Dynatest LWD Span 50 cm
Deflection (mm)
Time (s)
Drop height 17.78 cm Drop # 35
Force (kN)
Time (s)
Single−Sided Amplitude Spectrum of x(t)
|X(f)|
Frequency (Hz)
Single−Sided Amplitude Spectrum of f(t)
|F(f)|
Frequency (Hz)
dynamic stiffness K(f)
Real−|K(f)|
Frequency (Hz)
Coherence Function
Gamma2
Frequency (Hz)

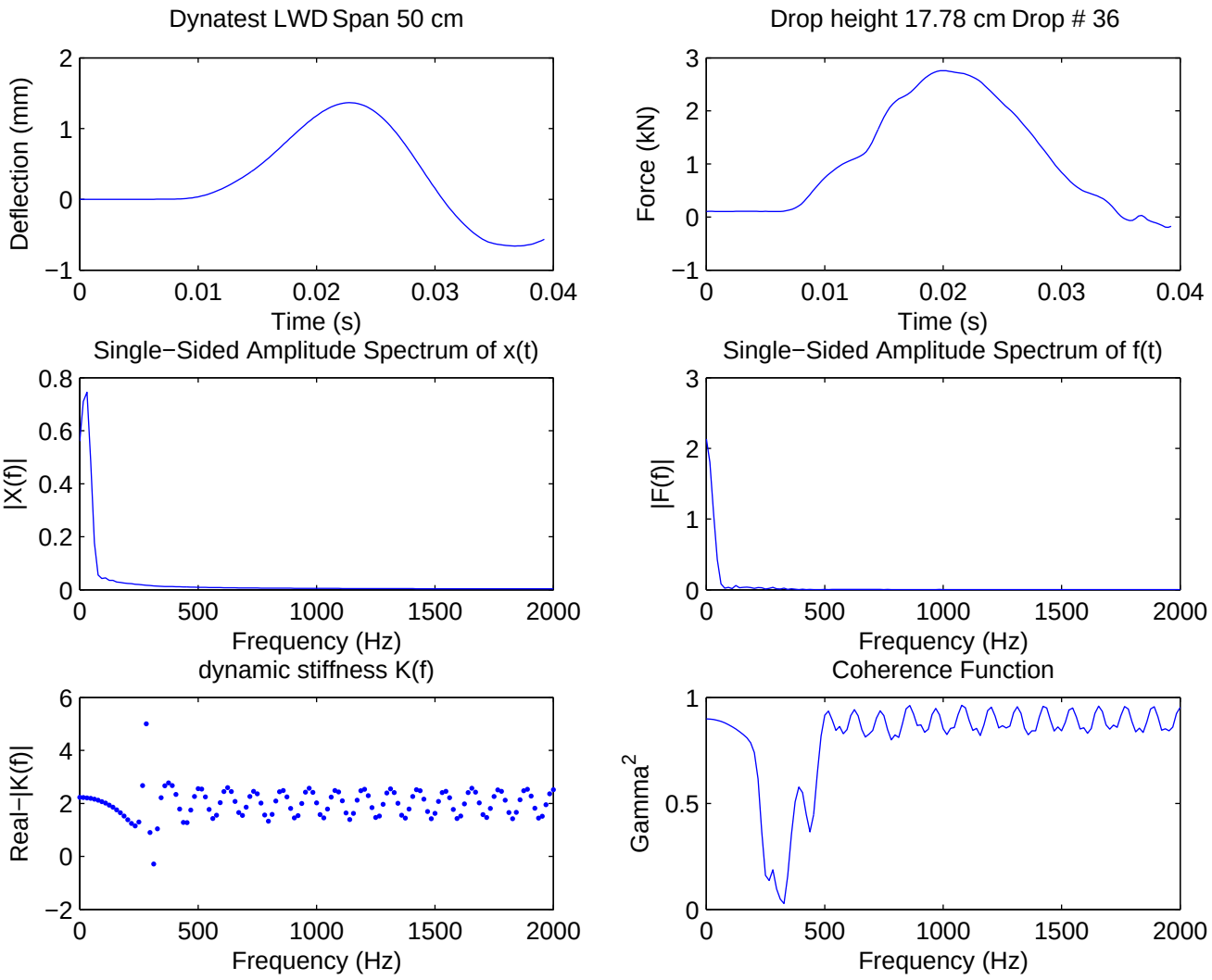
Dynatest LWD Span 50 cm
Deflection (mm)
Time (s)
Drop height 17.78 cm Drop # 36
Force (kN)
Time (s)
Single−Sided Amplitude Spectrum of x(t)
|X(f)|
Frequency (Hz)
Single−Sided Amplitude Spectrum of f(t)
|F(f)|
Frequency (Hz)
dynamic stiffness K(f)
Real−|K(f)|
Frequency (Hz)
Coherence Function
Gamma2
Frequency (Hz)

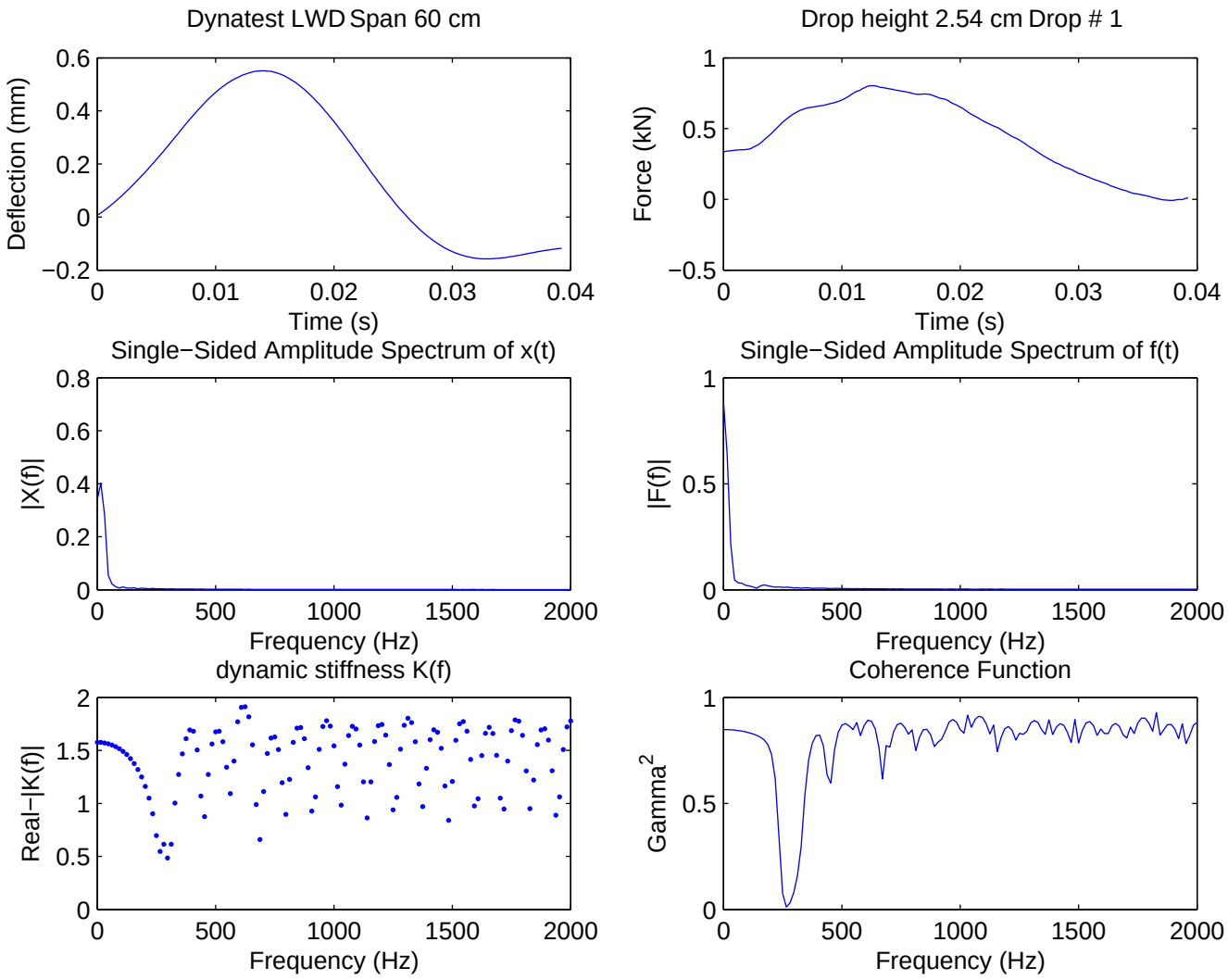
Dynatest LWD Span 60 cm
Deflection (mm)
Time (s)
Drop height 2.54 cm Drop # 1
Force (kN)
Time (s)
Single−Sided Amplitude Spectrum of x(t)
|X(f)|
Frequency (Hz)
Single−Sided Amplitude Spectrum of f(t)
|F(f)|
Frequency (Hz)
dynamic stiffness K(f)
Real−|K(f)|
Frequency (Hz)
Coherence Function
Gamma2
Frequency (Hz)

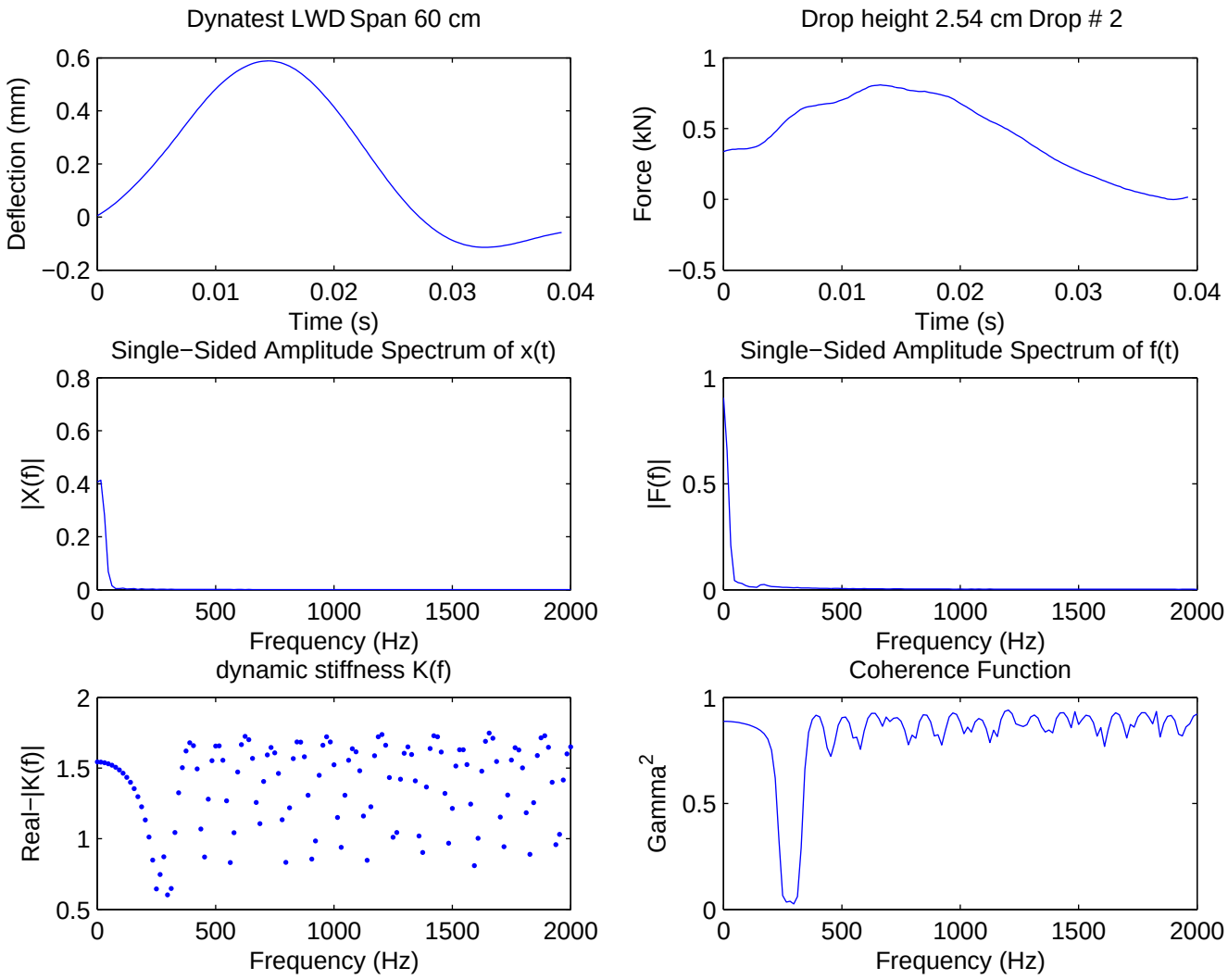
Dynatest LWD Span 60 cm
Deflection (mm)
Time (s)
Drop height 2.54 cm Drop # 2
Force (kN)
Time (s)
Single−Sided Amplitude Spectrum of x(t)
|X(f)|
Frequency (Hz)
Single−Sided Amplitude Spectrum of f(t)
|F(f)|
Frequency (Hz)
dynamic stiffness K(f)
Real−|K(f)|
Frequency (Hz)
Coherence Function
Gamma2
Frequency (Hz)

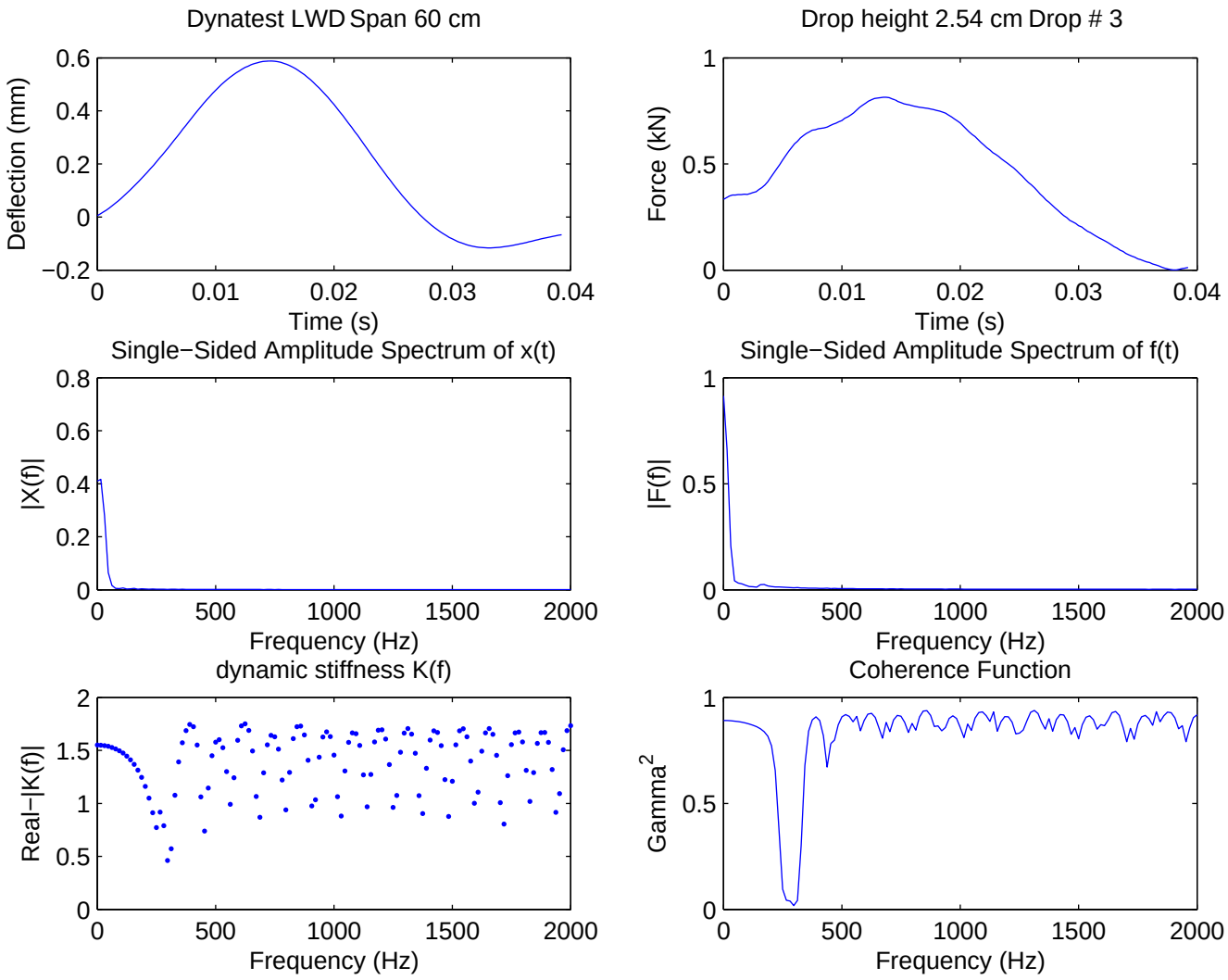
Dynatest LWD Span 60 cm
Deflection (mm)
Time (s)
Drop height 2.54 cm Drop # 3
Force (kN)
Time (s)
Single−Sided Amplitude Spectrum of x(t)
|X(f)|
Frequency (Hz)
Single−Sided Amplitude Spectrum of f(t)
|F(f)|
Frequency (Hz)
dynamic stiffness K(f)
Real−|K(f)|
Frequency (Hz)
Coherence Function
Gamma2
Frequency (Hz)

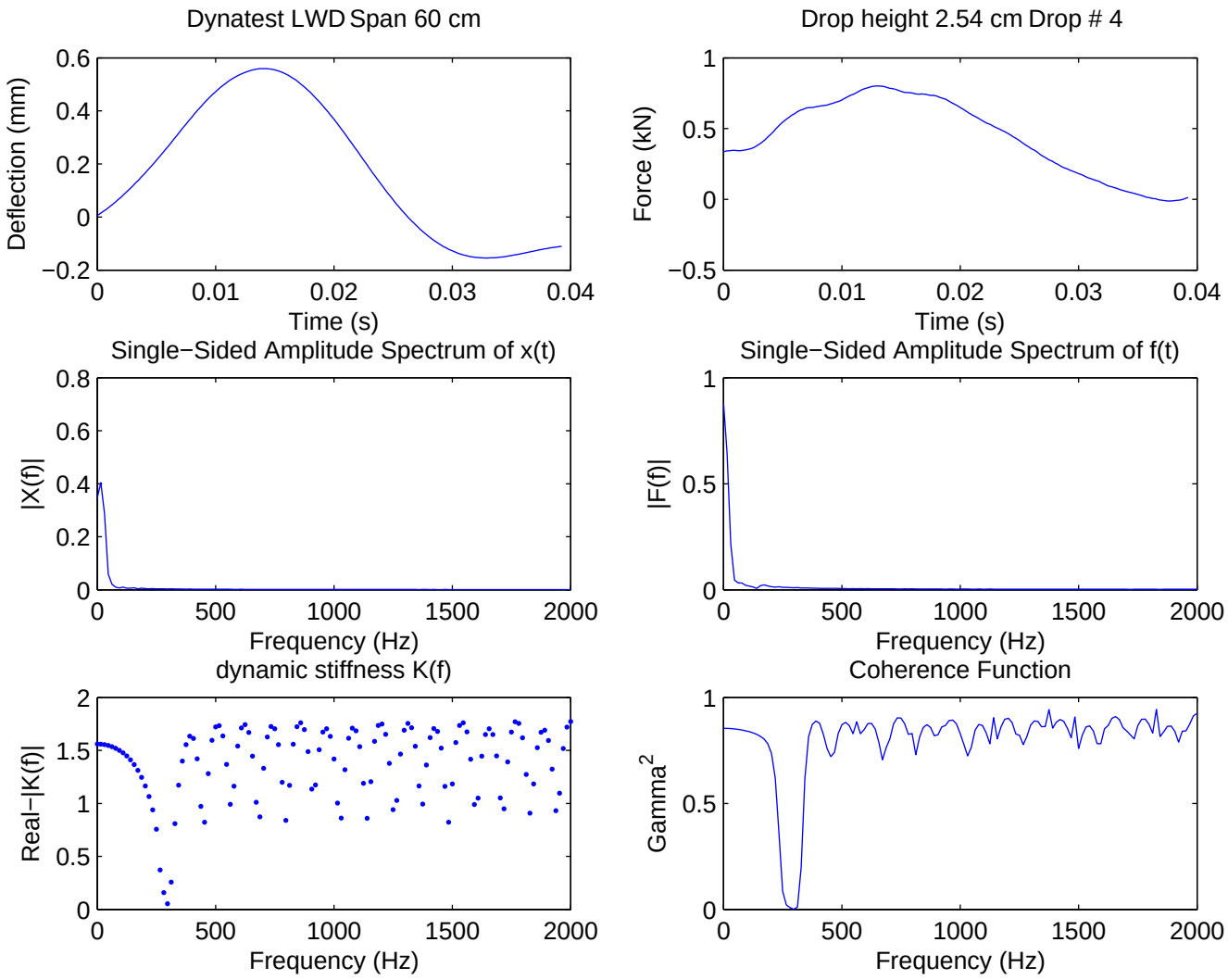
Dynatest LWD Span 60 cm
Deflection (mm)
Time (s)
Drop height 2.54 cm Drop # 4
Force (kN)
Time (s)
Single−Sided Amplitude Spectrum of x(t)
|X(f)|
Frequency (Hz)
Single−Sided Amplitude Spectrum of f(t)
|F(f)|
Frequency (Hz)
dynamic stiffness K(f)
Real−|K(f)|
Frequency (Hz)
Coherence Function
Gamma2
Frequency (Hz)

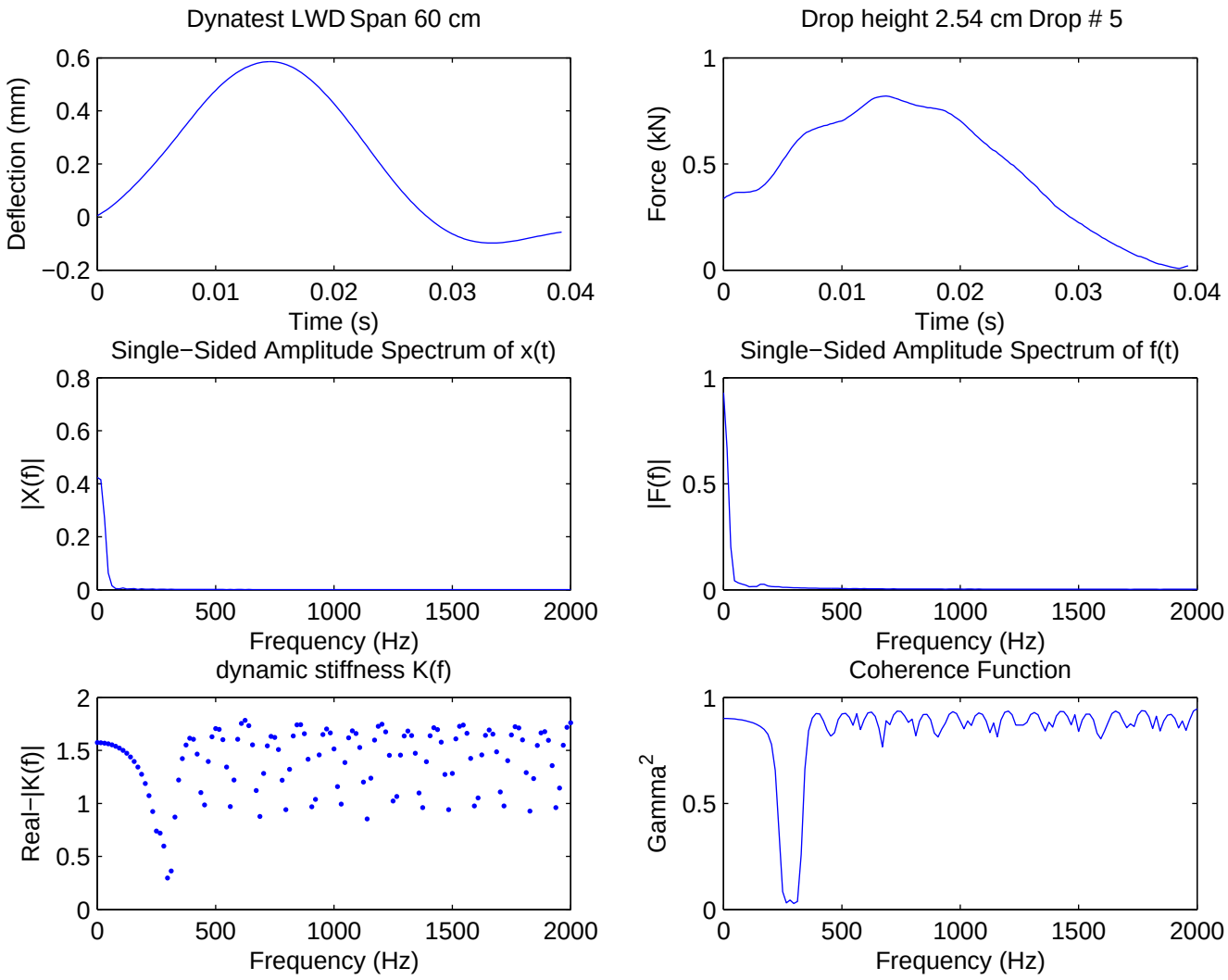
Dynatest LWD Span 60 cm
Deflection (mm)
Time (s)
Drop height 2.54 cm Drop # 5
Force (kN)
Time (s)
Single−Sided Amplitude Spectrum of x(t)
|X(f)|
Frequency (Hz)
Single−Sided Amplitude Spectrum of f(t)
|F(f)|
Frequency (Hz)
dynamic stiffness K(f)
Real−|K(f)|
Frequency (Hz)
Coherence Function
Gamma2
Frequency (Hz)

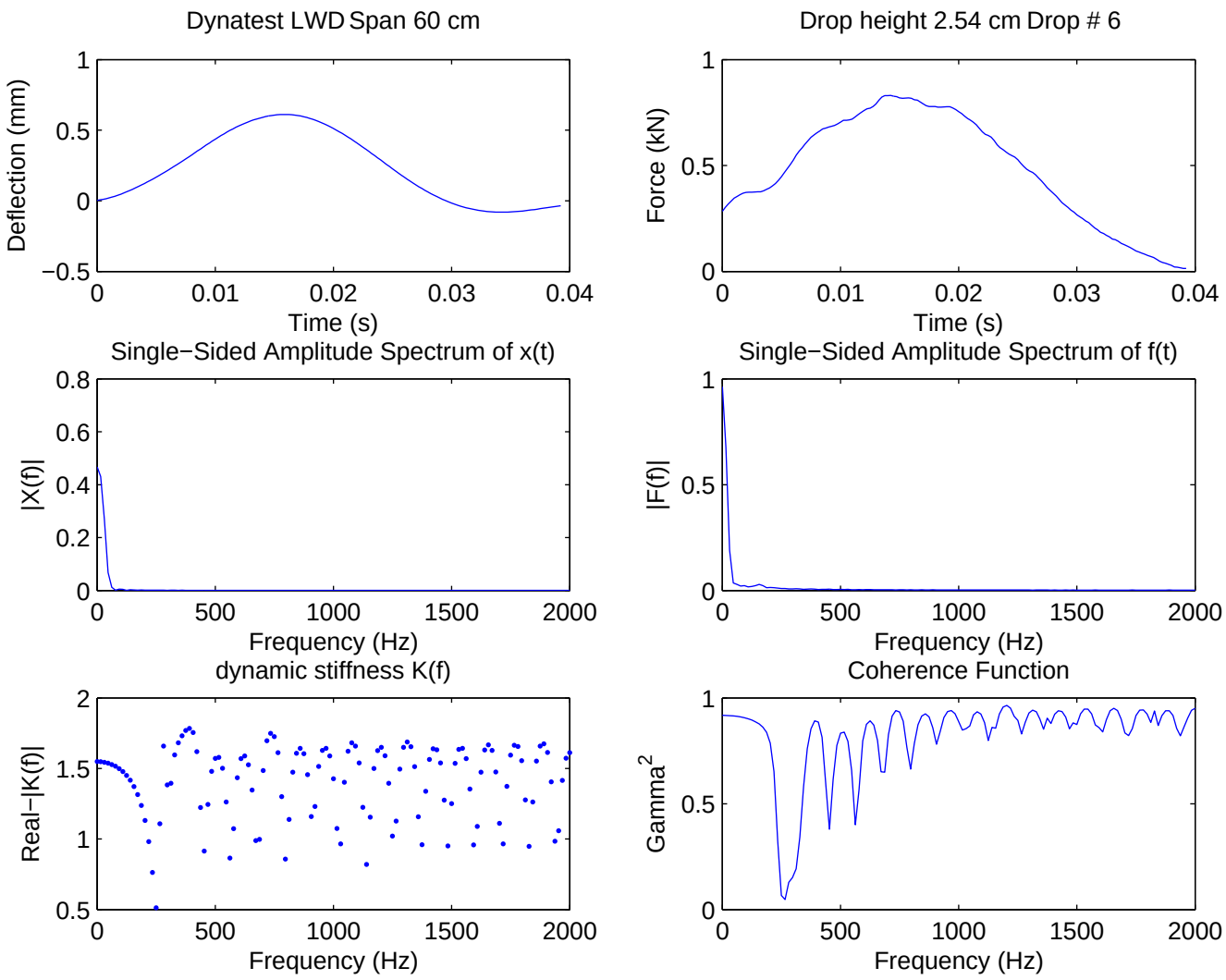
Dynatest LWD Span 60 cm
Deflection (mm)
Time (s)
Drop height 2.54 cm Drop # 6
Force (kN)
Time (s)
Single−Sided Amplitude Spectrum of x(t)
|X(f)|
Frequency (Hz)
Single−Sided Amplitude Spectrum of f(t)
|F(f)|
Frequency (Hz)
dynamic stiffness K(f)
Real−|K(f)|
Frequency (Hz)
Coherence Function
Gamma2
Frequency (Hz)

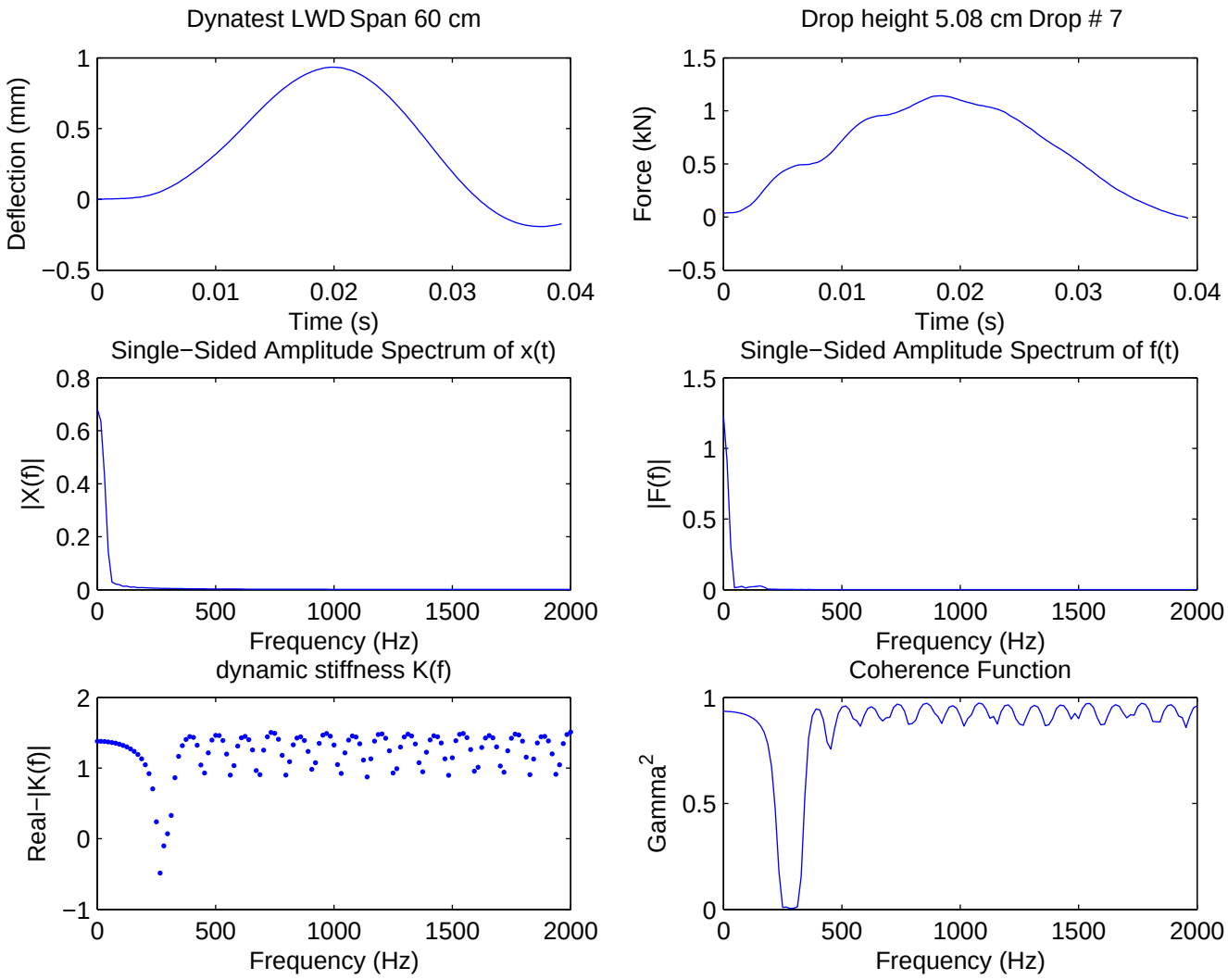
Dynatest LWD Span 60 cm
Deflection (mm)
Time (s)
Drop height 5.08 cm Drop # 7
Force (kN)
Time (s)
Single−Sided Amplitude Spectrum of x(t)
|X(f)|
Frequency (Hz)
Single−Sided Amplitude Spectrum of f(t)
|F(f)|
Frequency (Hz)
dynamic stiffness K(f)
Real−|K(f)|
Frequency (Hz)
Coherence Function
Gamma2
Frequency (Hz)

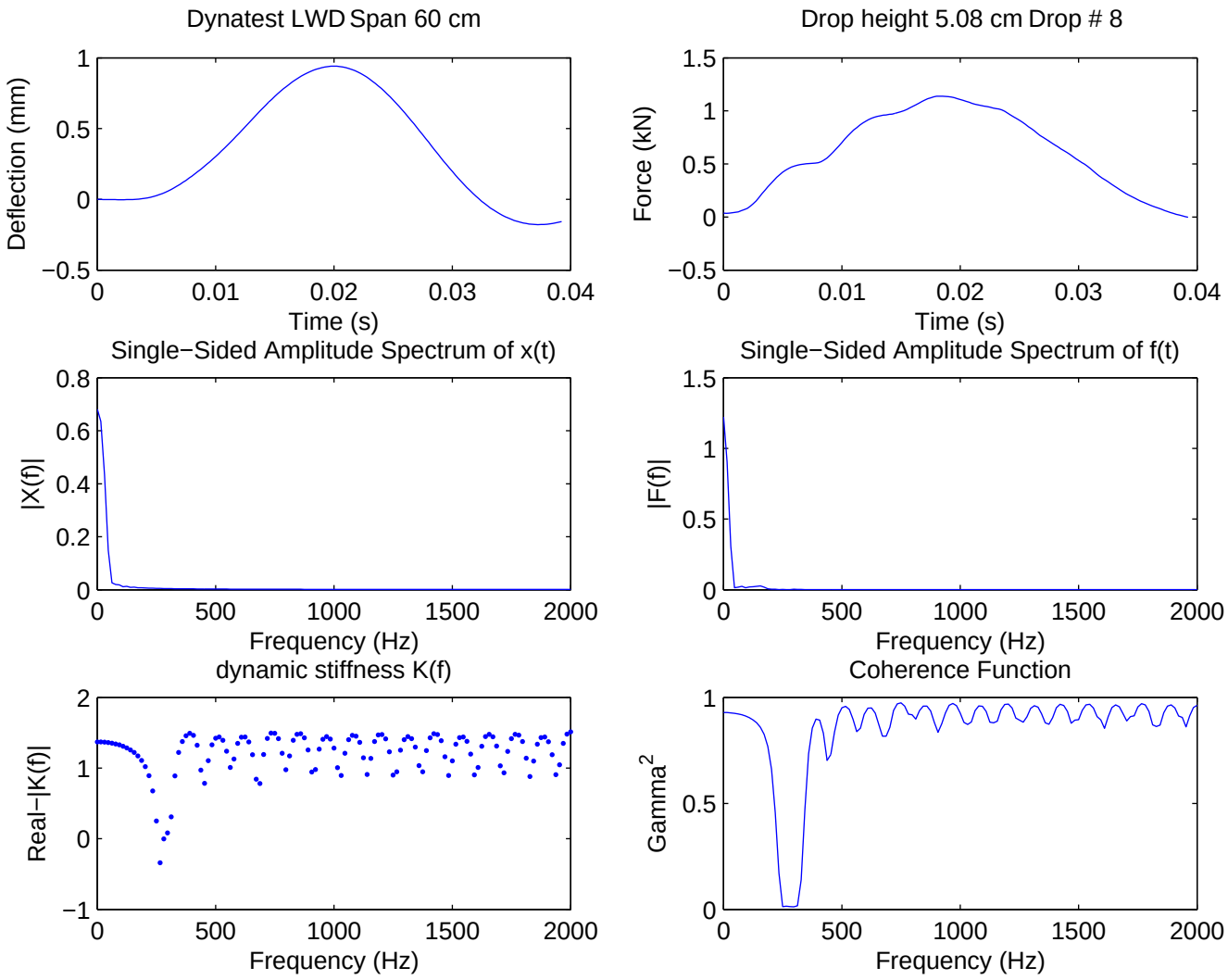
Dynatest LWD Span 60 cm
Deflection (mm)
Time (s)
Drop height 5.08 cm Drop # 8
Force (kN)
Time (s)
Single−Sided Amplitude Spectrum of x(t)
|X(f)|
Frequency (Hz)
Single−Sided Amplitude Spectrum of f(t)
|F(f)|
Frequency (Hz)
dynamic stiffness K(f)
Real−|K(f)|
Frequency (Hz)
Coherence Function
Gamma2
Frequency (Hz)

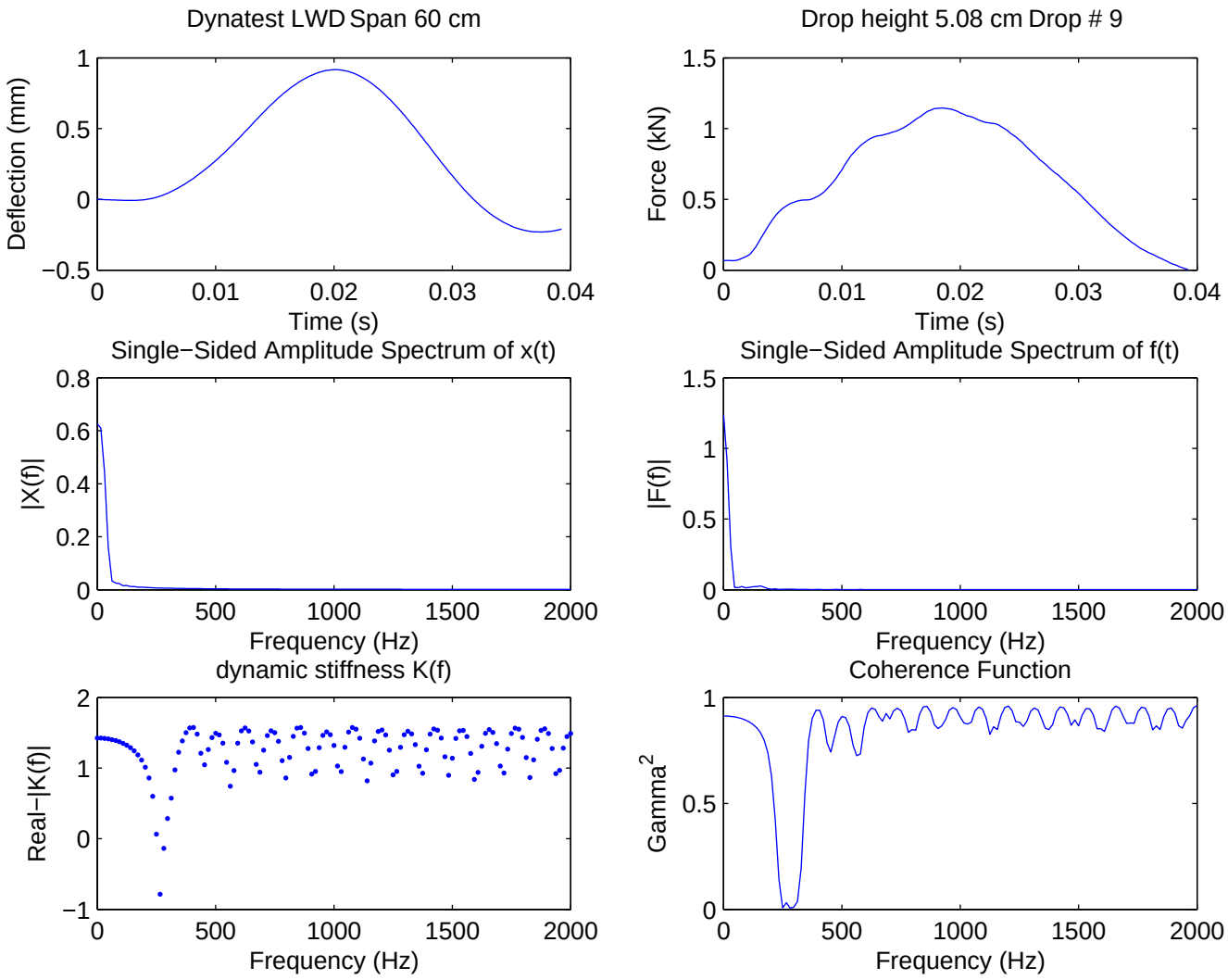
Dynatest LWD Span 60 cm
Deflection (mm)
Time (s)
Drop height 5.08 cm Drop # 9
Force (kN)
Time (s)
Single−Sided Amplitude Spectrum of x(t)
|X(f)|
Frequency (Hz)
Single−Sided Amplitude Spectrum of f(t)
|F(f)|
Frequency (Hz)
dynamic stiffness K(f)
Real−|K(f)|
Frequency (Hz)
Coherence Function
Gamma2
Frequency (Hz)

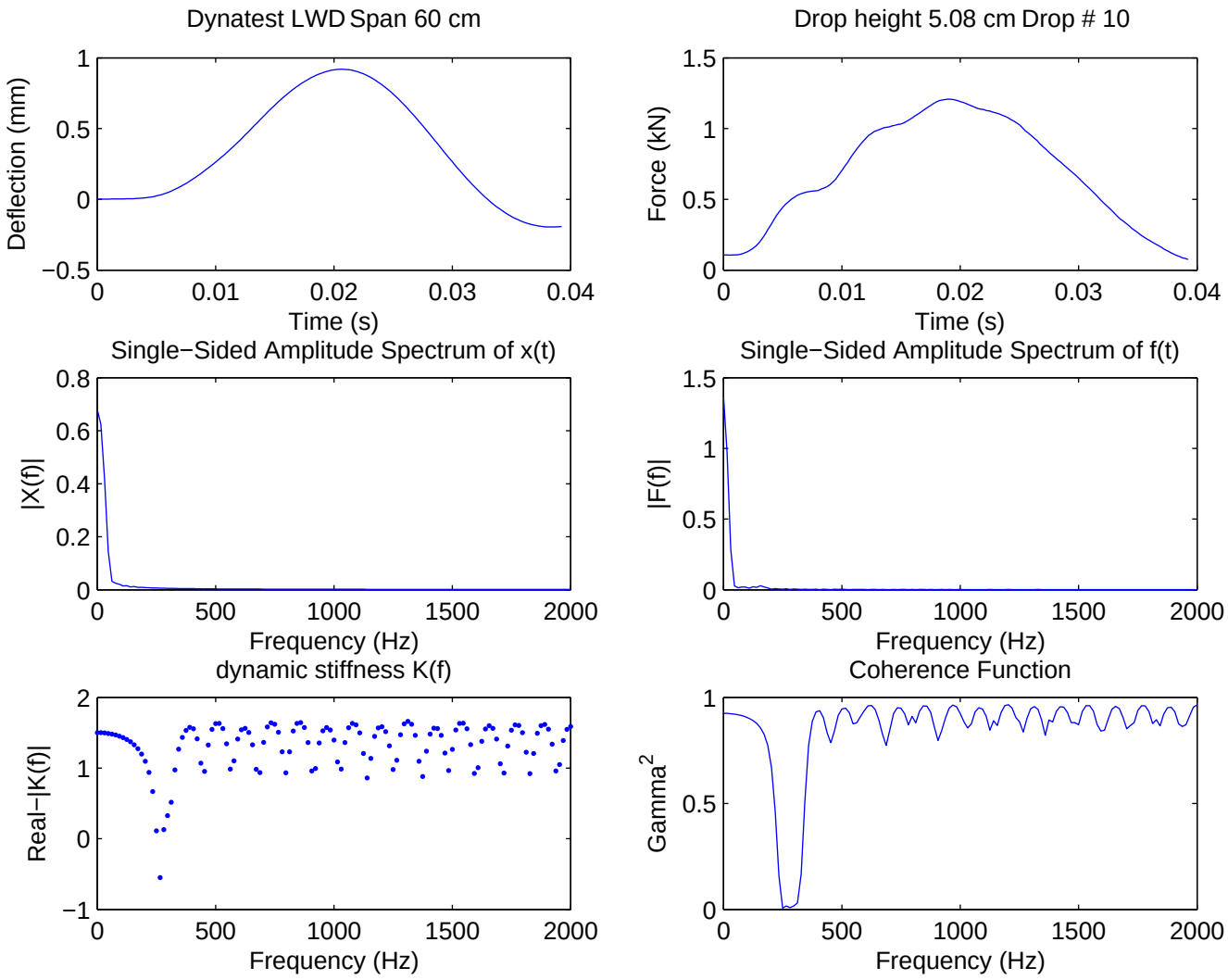
Dynatest LWD Span 60 cm
Deflection (mm)
Time (s)
Drop height 5.08 cm Drop # 10
Force (kN)
Time (s)
Single−Sided Amplitude Spectrum of x(t)
|X(f)|
Frequency (Hz)
Single−Sided Amplitude Spectrum of f(t)
|F(f)|
Frequency (Hz)
dynamic stiffness K(f)
Real−|K(f)|
Frequency (Hz)
Coherence Function
Gamma2
Frequency (Hz)

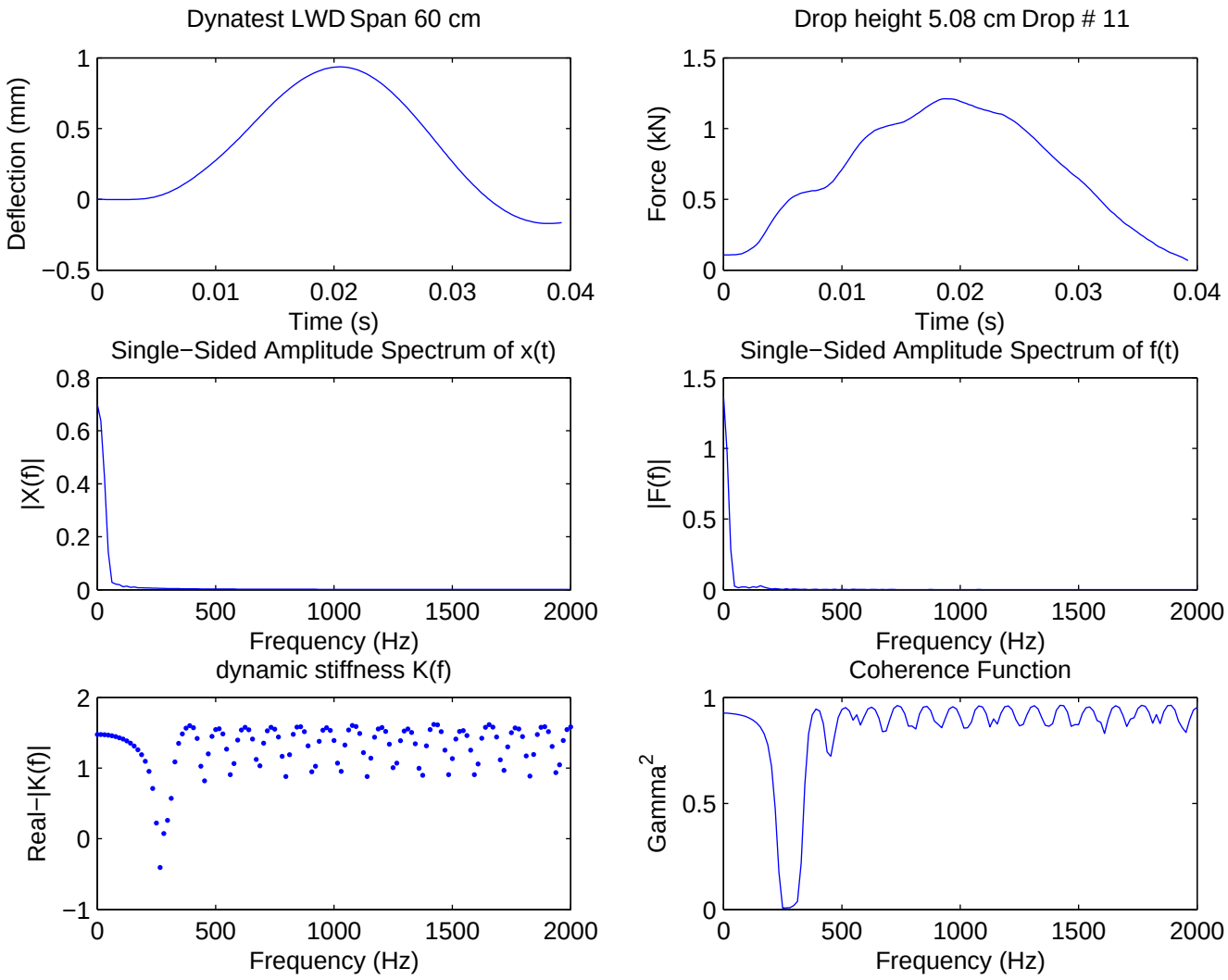
Dynatest LWD Span 60 cm
Deflection (mm)
Time (s)
Drop height 5.08 cm Drop # 11
Force (kN)
Time (s)
Single−Sided Amplitude Spectrum of x(t)
|X(f)|
Frequency (Hz)
Single−Sided Amplitude Spectrum of f(t)
|F(f)|
Frequency (Hz)
dynamic stiffness K(f)
Real−|K(f)|
Frequency (Hz)
Coherence Function
Gamma2
Frequency (Hz)

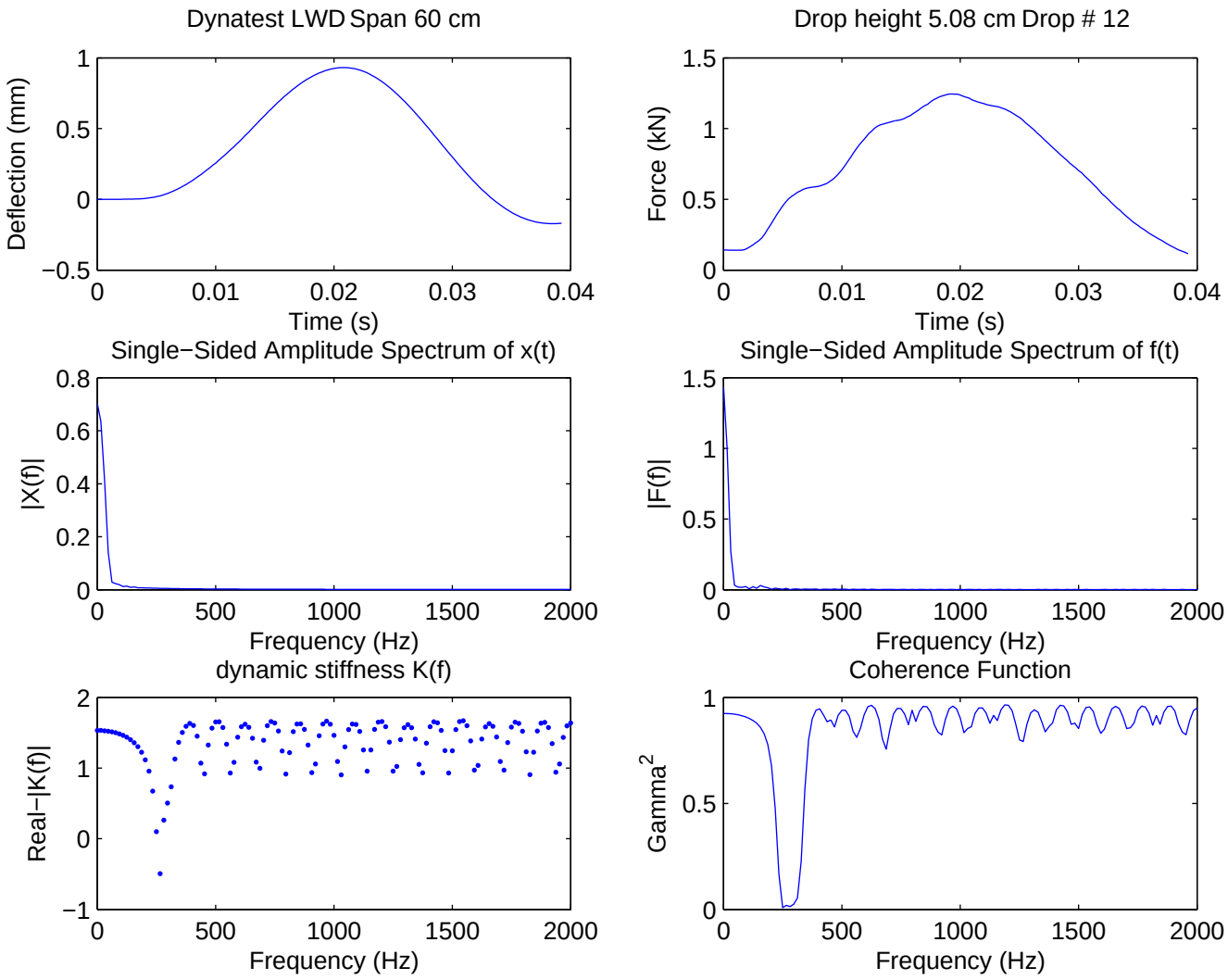
Dynatest LWD Span 60 cm
Deflection (mm)
Time (s)
Drop height 5.08 cm Drop # 12
Force (kN)
Time (s)
Single−Sided Amplitude Spectrum of x(t)
|X(f)|
Frequency (Hz)
Single−Sided Amplitude Spectrum of f(t)
|F(f)|
Frequency (Hz)
dynamic stiffness K(f)
Real−|K(f)|
Frequency (Hz)
Coherence Function
Gamma2
Frequency (Hz)

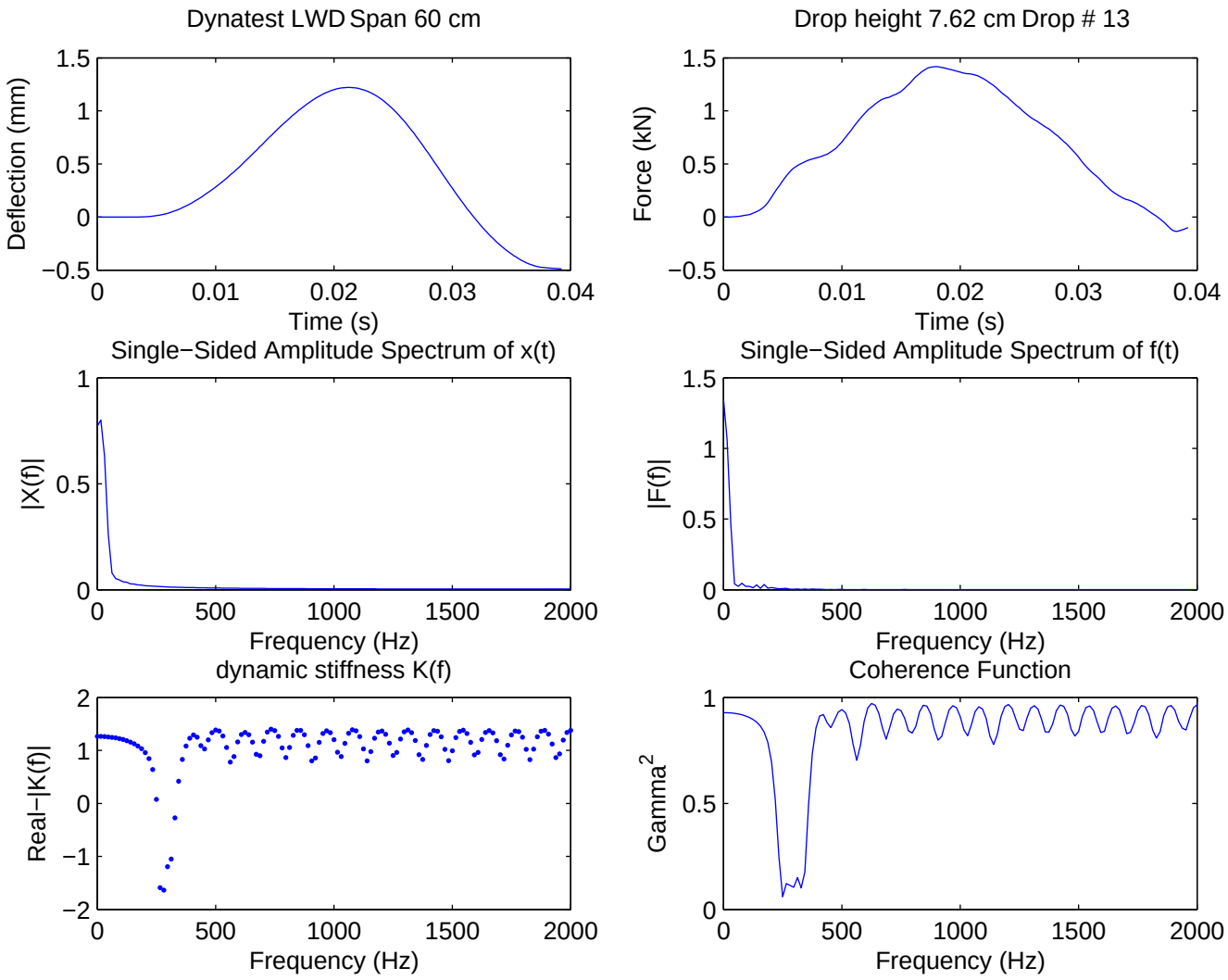
Dynatest LWD Span 60 cm
Deflection (mm)
Time (s)
Drop height 7.62 cm Drop # 13
Force (kN)
Time (s)
Single−Sided Amplitude Spectrum of x(t)
|X(f)|
Frequency (Hz)
Single−Sided Amplitude Spectrum of f(t)
|F(f)|
Frequency (Hz)
dynamic stiffness K(f)
Real−|K(f)|
Frequency (Hz)
Coherence Function
Gamma2
Frequency (Hz)

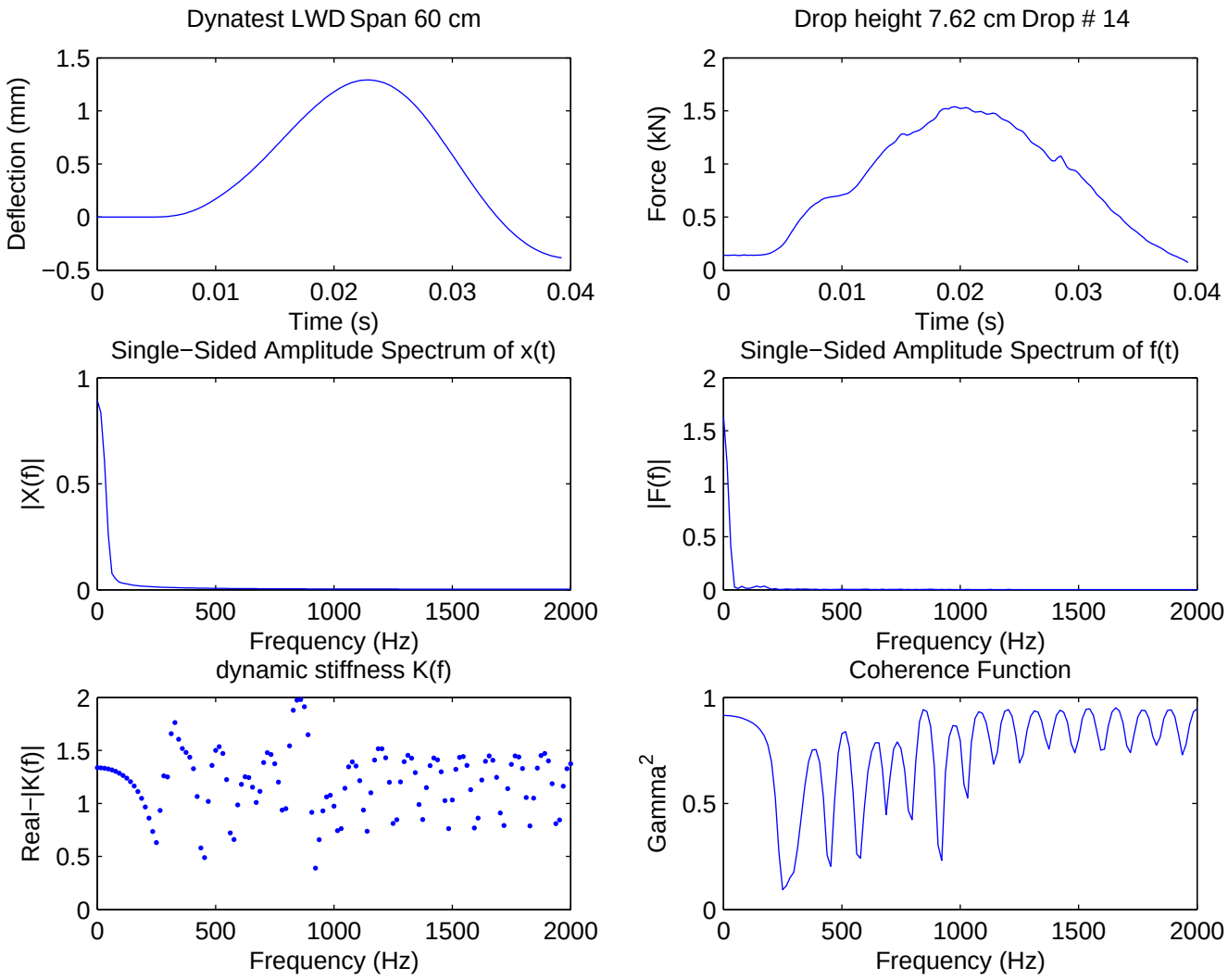
Dynatest LWD Span 60 cm
Deflection (mm)
Time (s)
Drop height 7.62 cm Drop # 14
Force (kN)
Time (s)
Single−Sided Amplitude Spectrum of x(t)
|X(f)|
Frequency (Hz)
Single−Sided Amplitude Spectrum of f(t)
|F(f)|
Frequency (Hz)
dynamic stiffness K(f)
Real−|K(f)|
Frequency (Hz)
Coherence Function
Gamma2
Frequency (Hz)

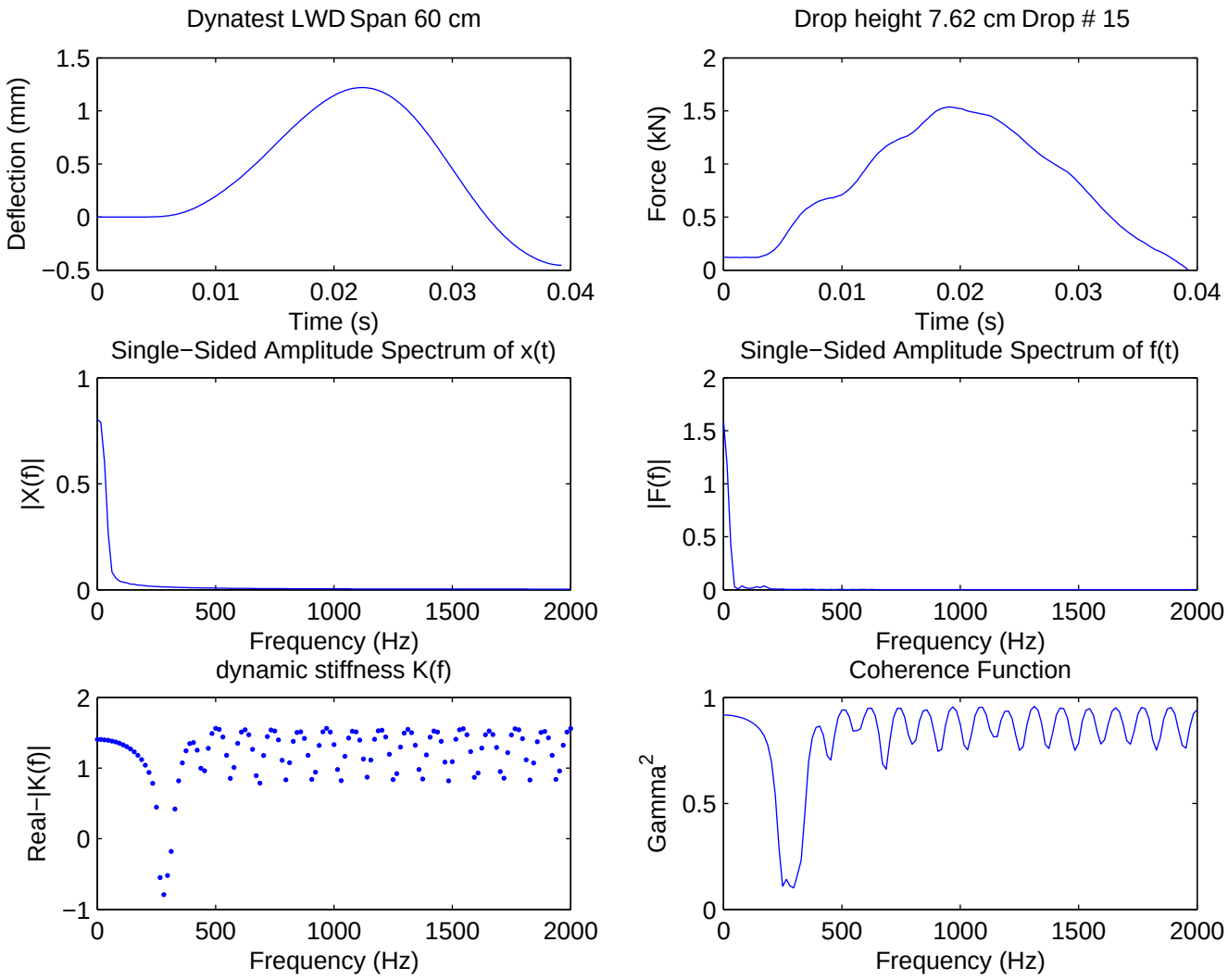
Dynatest LWD Span 60 cm
Deflection (mm)
Time (s)
Drop height 7.62 cm Drop # 15
Force (kN)
Time (s)
Single−Sided Amplitude Spectrum of x(t)
|X(f)|
Frequency (Hz)
Single−Sided Amplitude Spectrum of f(t)
|F(f)|
Frequency (Hz)
dynamic stiffness K(f)
Real−|K(f)|
Frequency (Hz)
Coherence Function
Gamma2
Frequency (Hz)

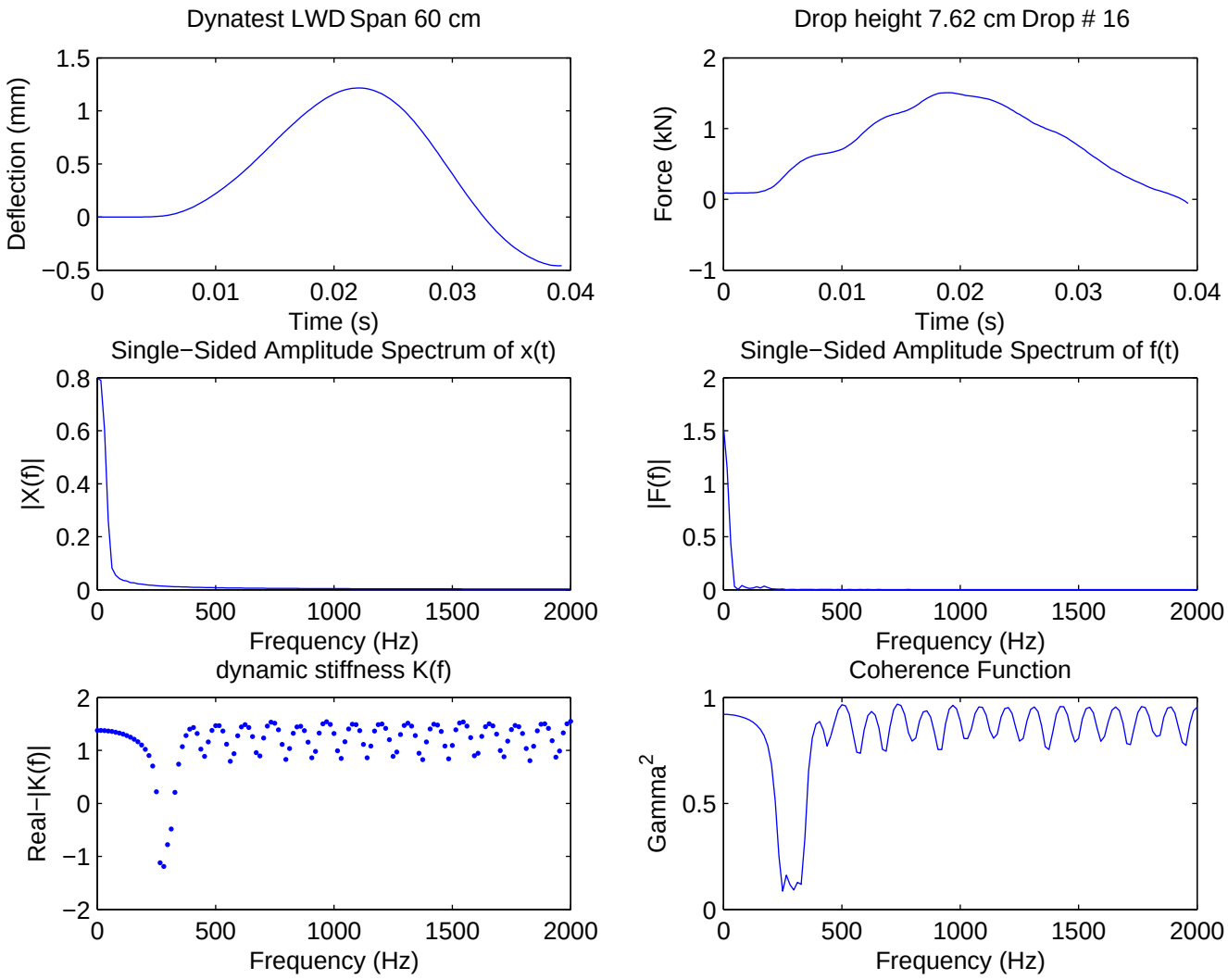
Dynatest LWD Span 60 cm
Deflection (mm)
Time (s)
Drop height 7.62 cm Drop # 16
Force (kN)
Time (s)
Single−Sided Amplitude Spectrum of x(t)
|X(f)|
Frequency (Hz)
Single−Sided Amplitude Spectrum of f(t)
|F(f)|
Frequency (Hz)
dynamic stiffness K(f)
Real−|K(f)|
Frequency (Hz)
Coherence Function
Gamma2
Frequency (Hz)

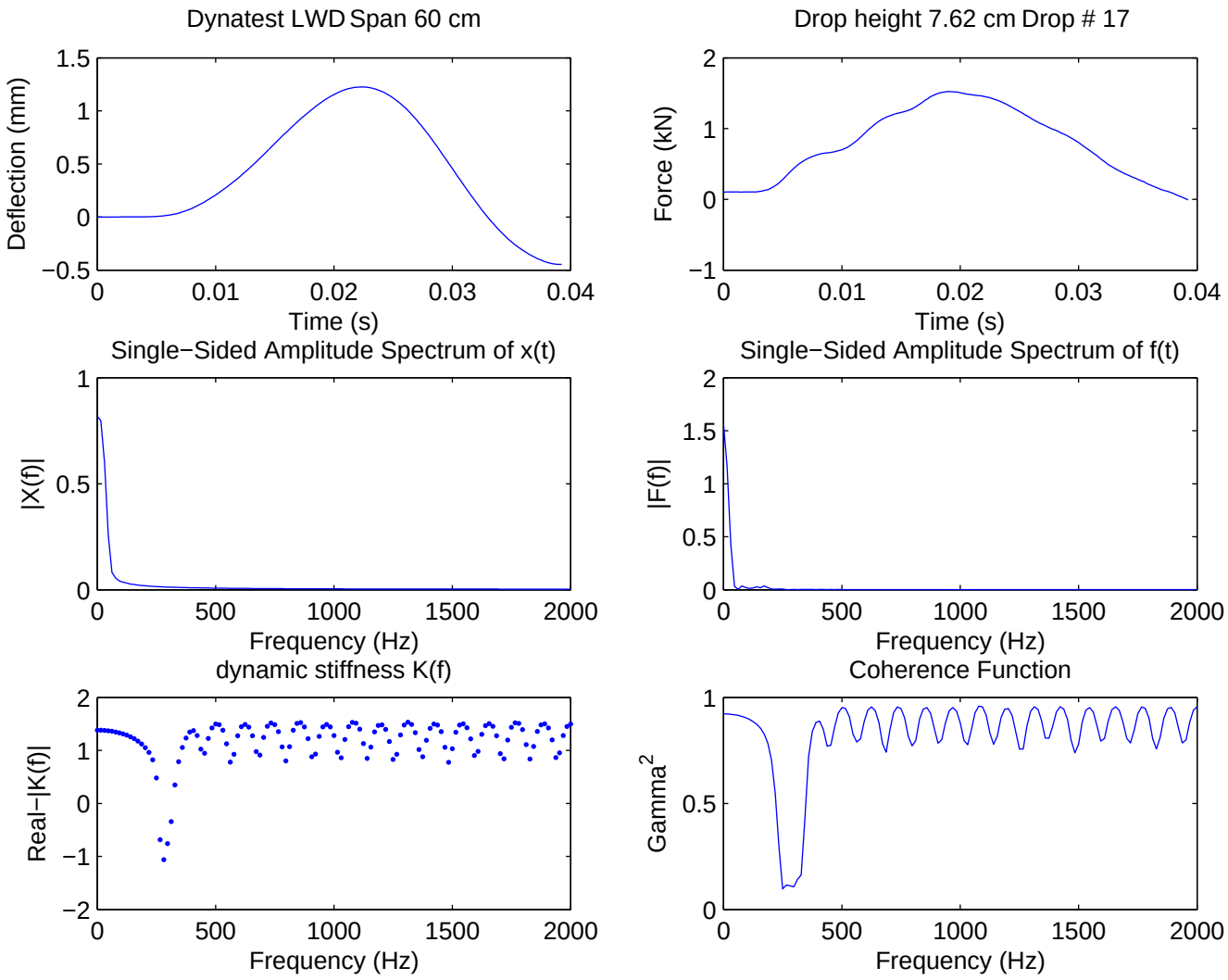
Dynatest LWD Span 60 cm
Deflection (mm)
Time (s)
Drop height 7.62 cm Drop # 17
Force (kN)
Time (s)
Single−Sided Amplitude Spectrum of x(t)
|X(f)|
Frequency (Hz)
Single−Sided Amplitude Spectrum of f(t)
|F(f)|
Frequency (Hz)
dynamic stiffness K(f)
Real−|K(f)|
Frequency (Hz)
Coherence Function
Gamma2
Frequency (Hz)

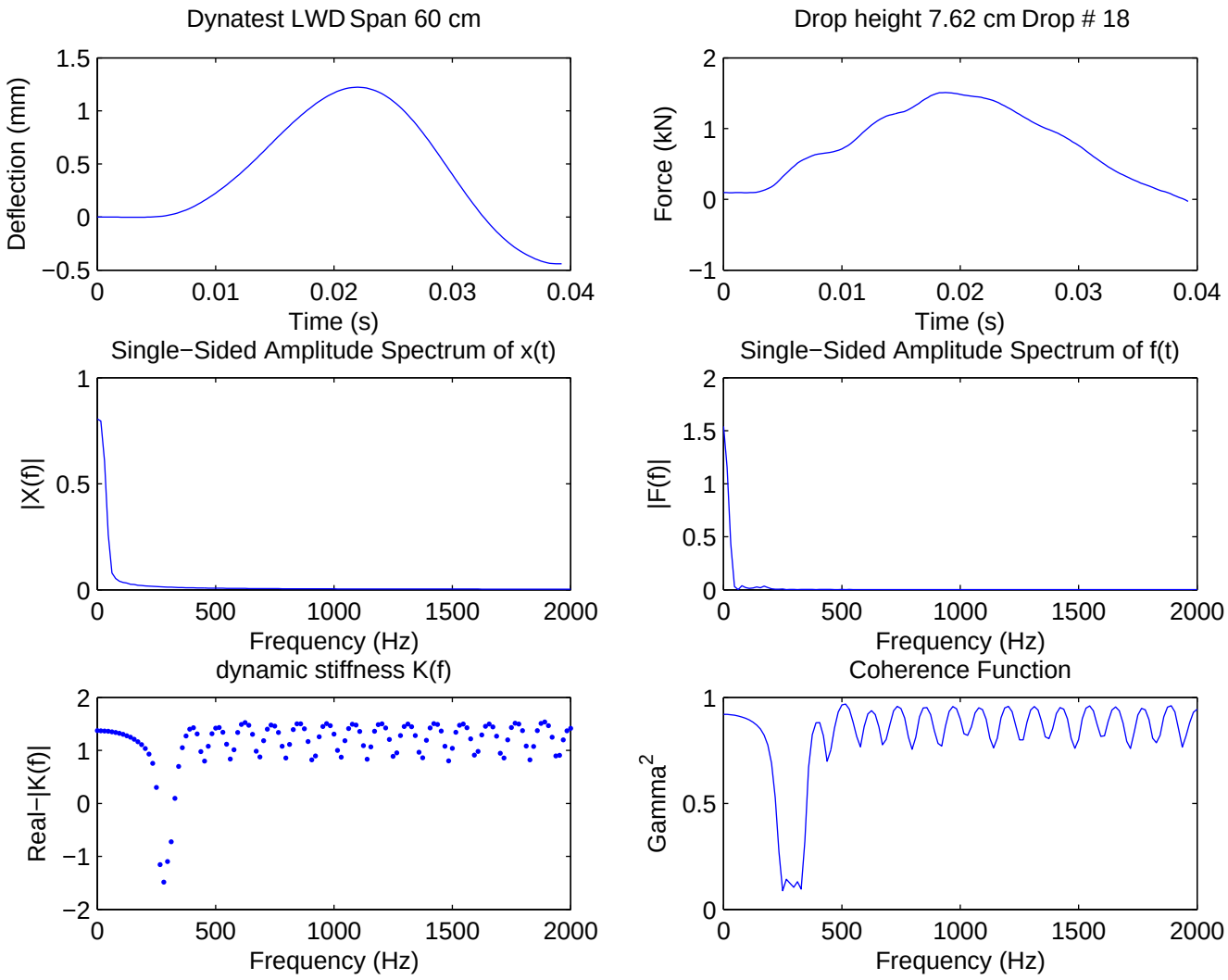
Dynatest LWD Span 60 cm
Deflection (mm)
Time (s)
Drop height 7.62 cm Drop # 18
Force (kN)
Time (s)
Single−Sided Amplitude Spectrum of x(t)
|X(f)|
Frequency (Hz)
Single−Sided Amplitude Spectrum of f(t)
|F(f)|
Frequency (Hz)
dynamic stiffness K(f)
Real−|K(f)|
Frequency (Hz)
Coherence Function
Gamma2
Frequency (Hz)

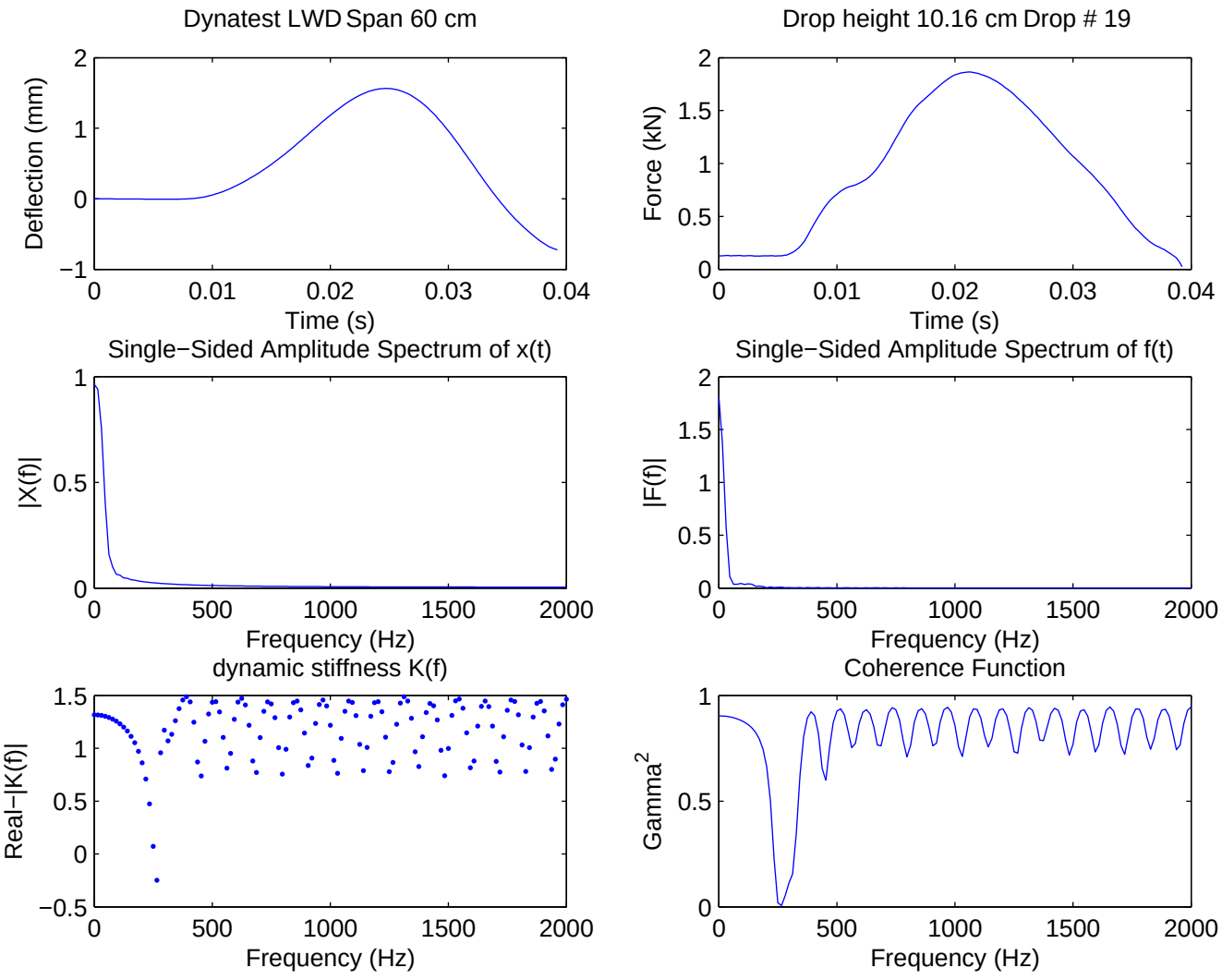
Dynatest LWD Span 60 cm
Deflection (mm)
Time (s)
Drop height 10.16 cm Drop # 19
Force (kN)
Time (s)
Single−Sided Amplitude Spectrum of x(t)
|X(f)|
Frequency (Hz)
Single−Sided Amplitude Spectrum of f(t)
|F(f)|
Frequency (Hz)
dynamic stiffness K(f)
Real−|K(f)|
Frequency (Hz)
Coherence Function
Gamma2
Frequency (Hz)

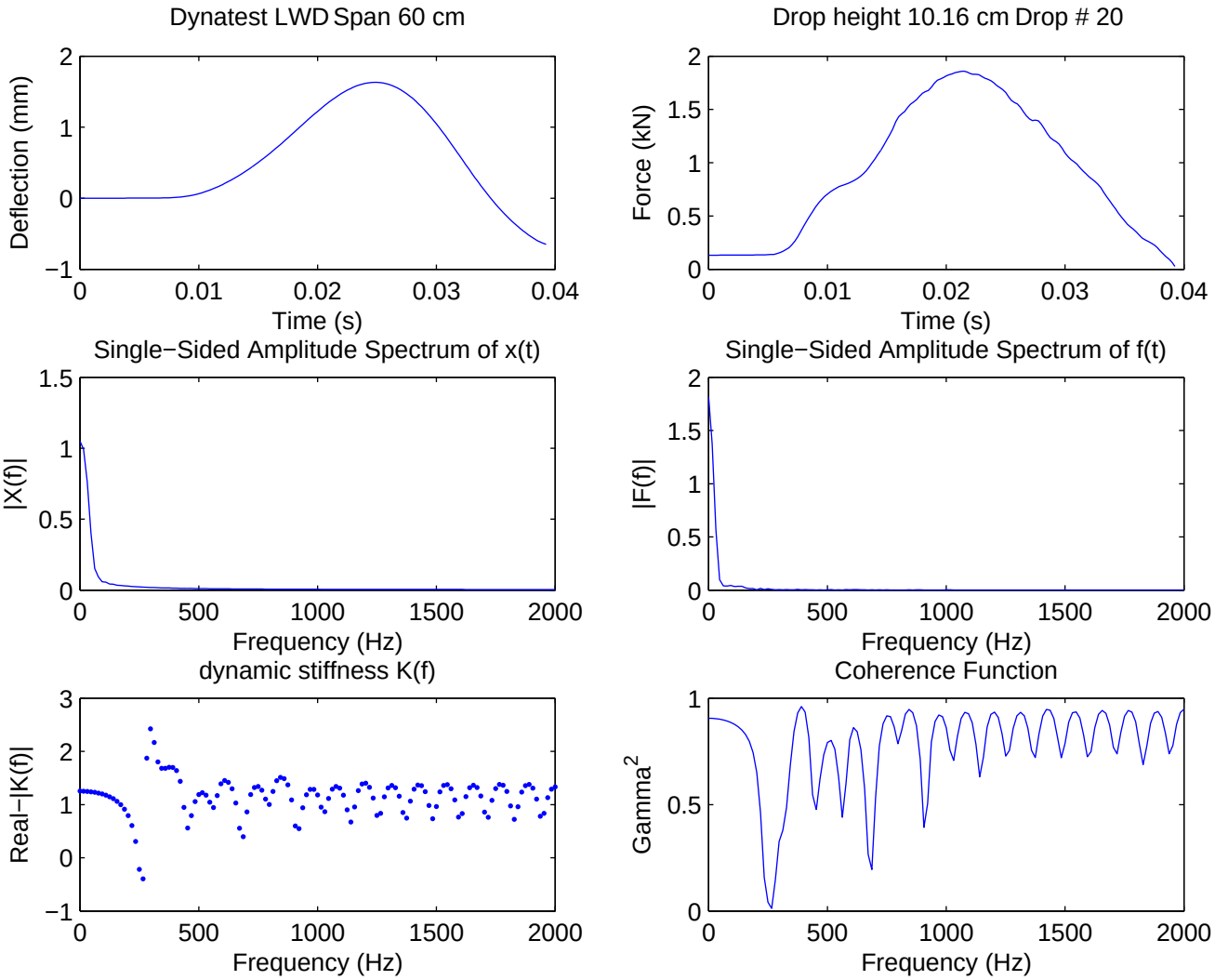
Dynatest LWD Span 60 cm
Deflection (mm)
Time (s)
Drop height 10.16 cm Drop # 20
Force (kN)
Time (s)
Single−Sided Amplitude Spectrum of x(t)
|X(f)|
Frequency (Hz)
Single−Sided Amplitude Spectrum of f(t)
|F(f)|
Frequency (Hz)
dynamic stiffness K(f)
Real−|K(f)|
Frequency (Hz)
Coherence Function
Gamma2
Frequency (Hz)

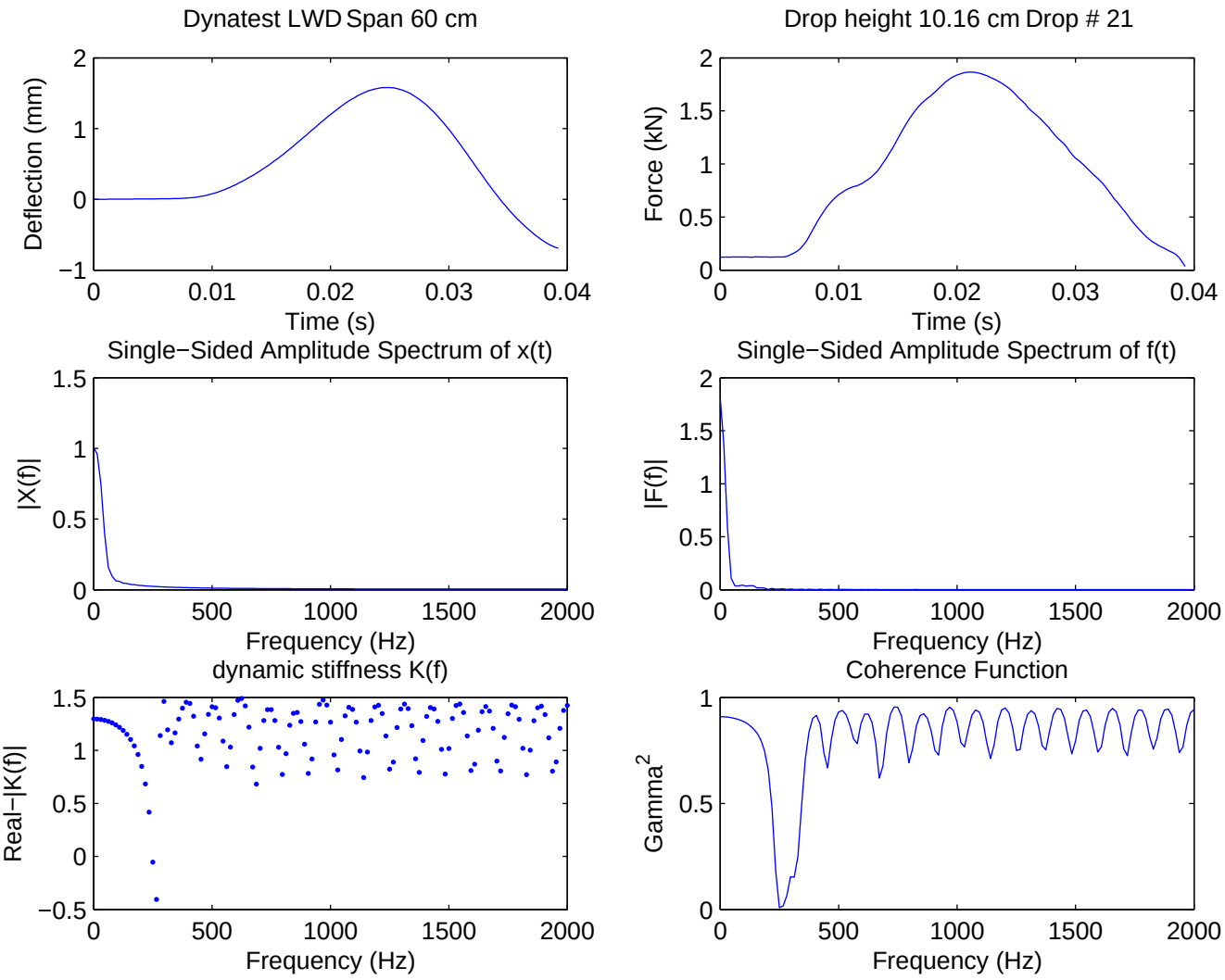
Dynatest LWD Span 60 cm
Deflection (mm)
Time (s)
Drop height 10.16 cm Drop # 21
Force (kN)
Time (s)
Single−Sided Amplitude Spectrum of x(t)
|X(f)|
Frequency (Hz)
Single−Sided Amplitude Spectrum of f(t)
|F(f)|
Frequency (Hz)
dynamic stiffness K(f)
Real−|K(f)|
Frequency (Hz)
Coherence Function
Gamma2
Frequency (Hz)

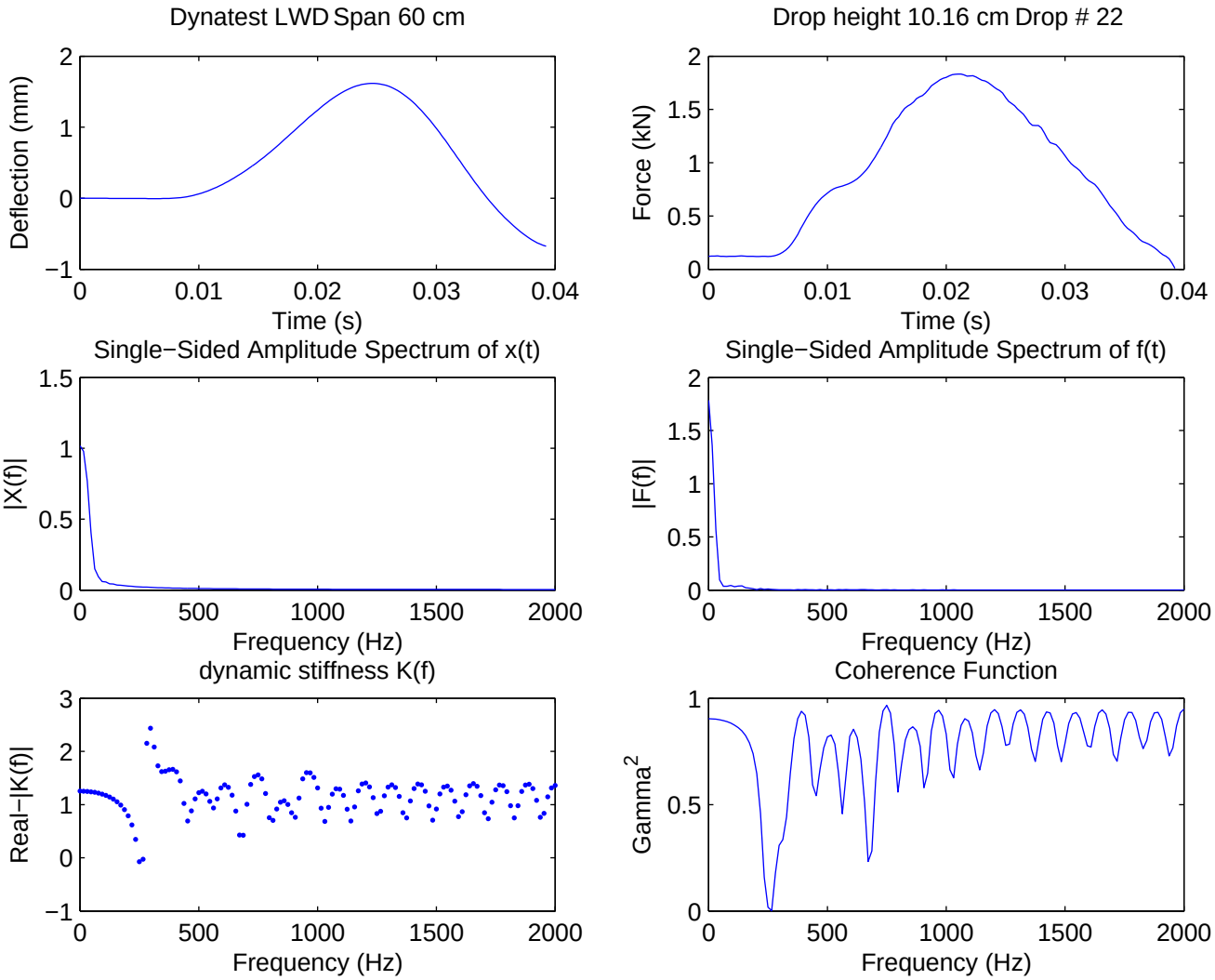
Dynatest LWD Span 60 cm
Deflection (mm)
Time (s)
Drop height 10.16 cm Drop # 22
Force (kN)
Time (s)
Single−Sided Amplitude Spectrum of x(t)
|X(f)|
Frequency (Hz)
Single−Sided Amplitude Spectrum of f(t)
|F(f)|
Frequency (Hz)
dynamic stiffness K(f)
Real−|K(f)|
Frequency (Hz)
Coherence Function
Gamma2
Frequency (Hz)

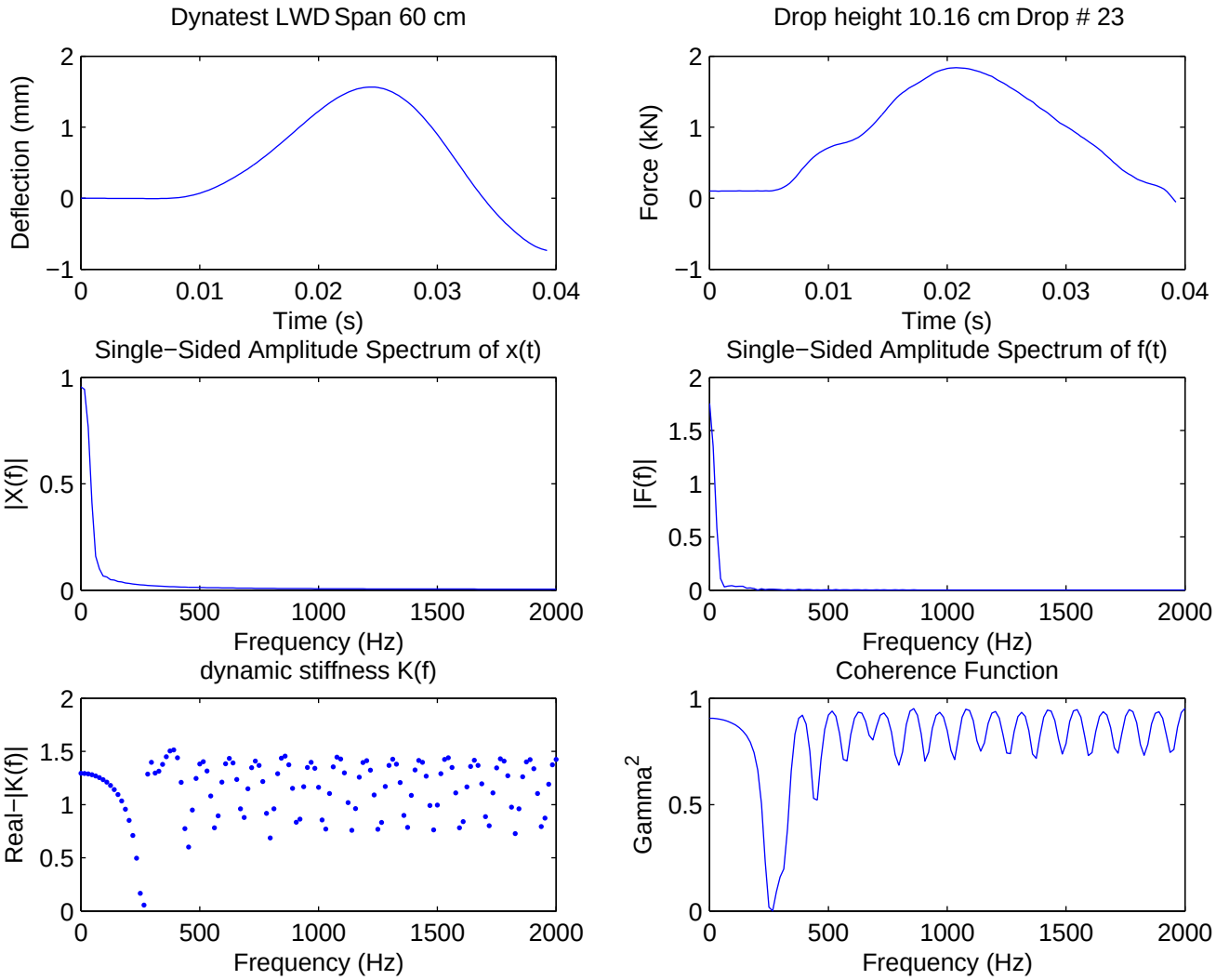
Dynatest LWD Span 60 cm
Deflection (mm)
Time (s)
Drop height 10.16 cm Drop # 23
Force (kN)
Time (s)
Single−Sided Amplitude Spectrum of x(t)
|X(f)|
Frequency (Hz)
Single−Sided Amplitude Spectrum of f(t)
|F(f)|
Frequency (Hz)
dynamic stiffness K(f)
Real−|K(f)|
Frequency (Hz)
Coherence Function
Gamma2
Frequency (Hz)

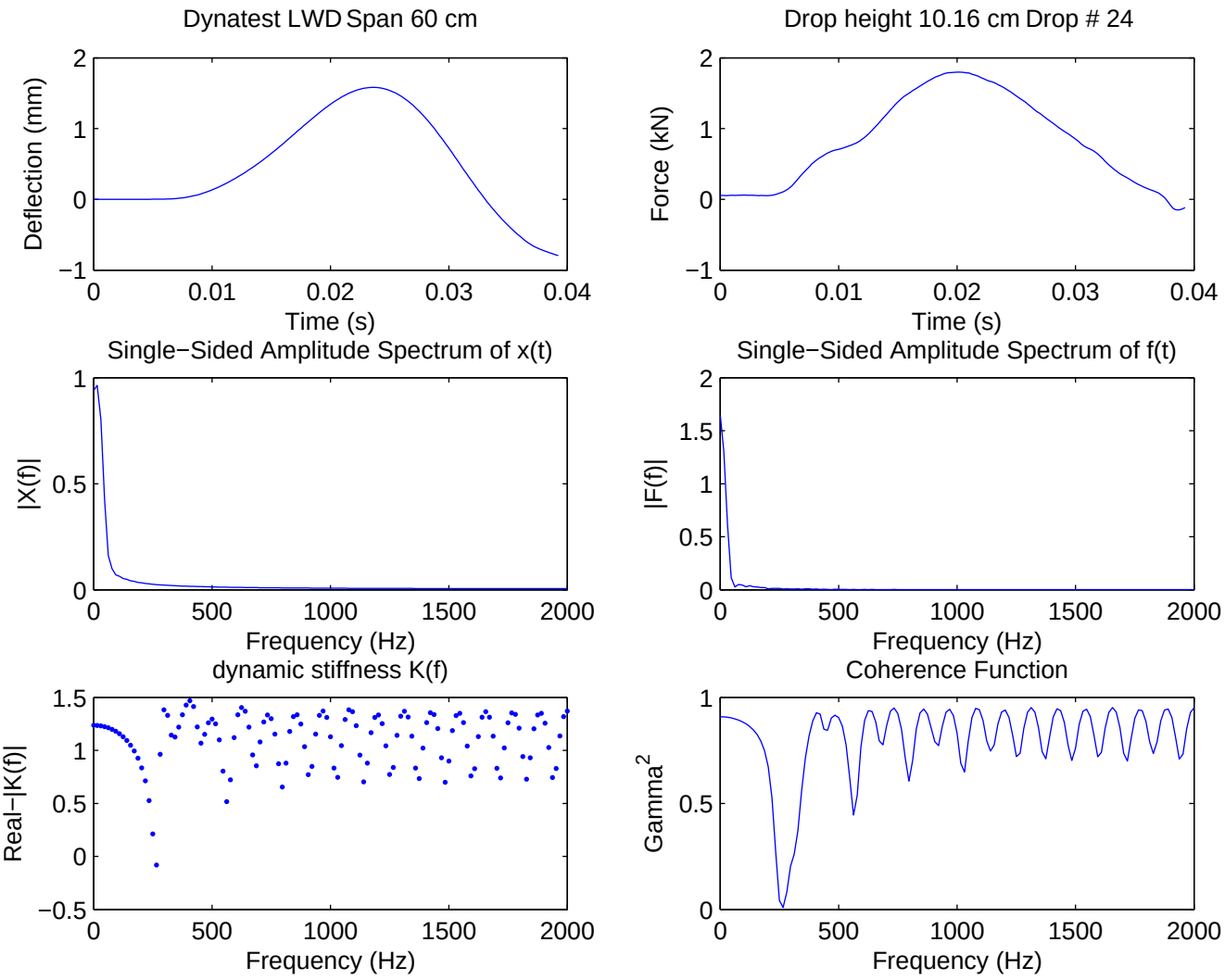
Dynatest LWD Span 60 cm
Deflection (mm)
Time (s)
Drop height 10.16 cm Drop # 24
Force (kN)
Time (s)
Single−Sided Amplitude Spectrum of x(t)
|X(f)|
Frequency (Hz)
Single−Sided Amplitude Spectrum of f(t)
|F(f)|
Frequency (Hz)
dynamic stiffness K(f)
Real−|K(f)|
Frequency (Hz)
Coherence Function
Gamma2
Frequency (Hz)

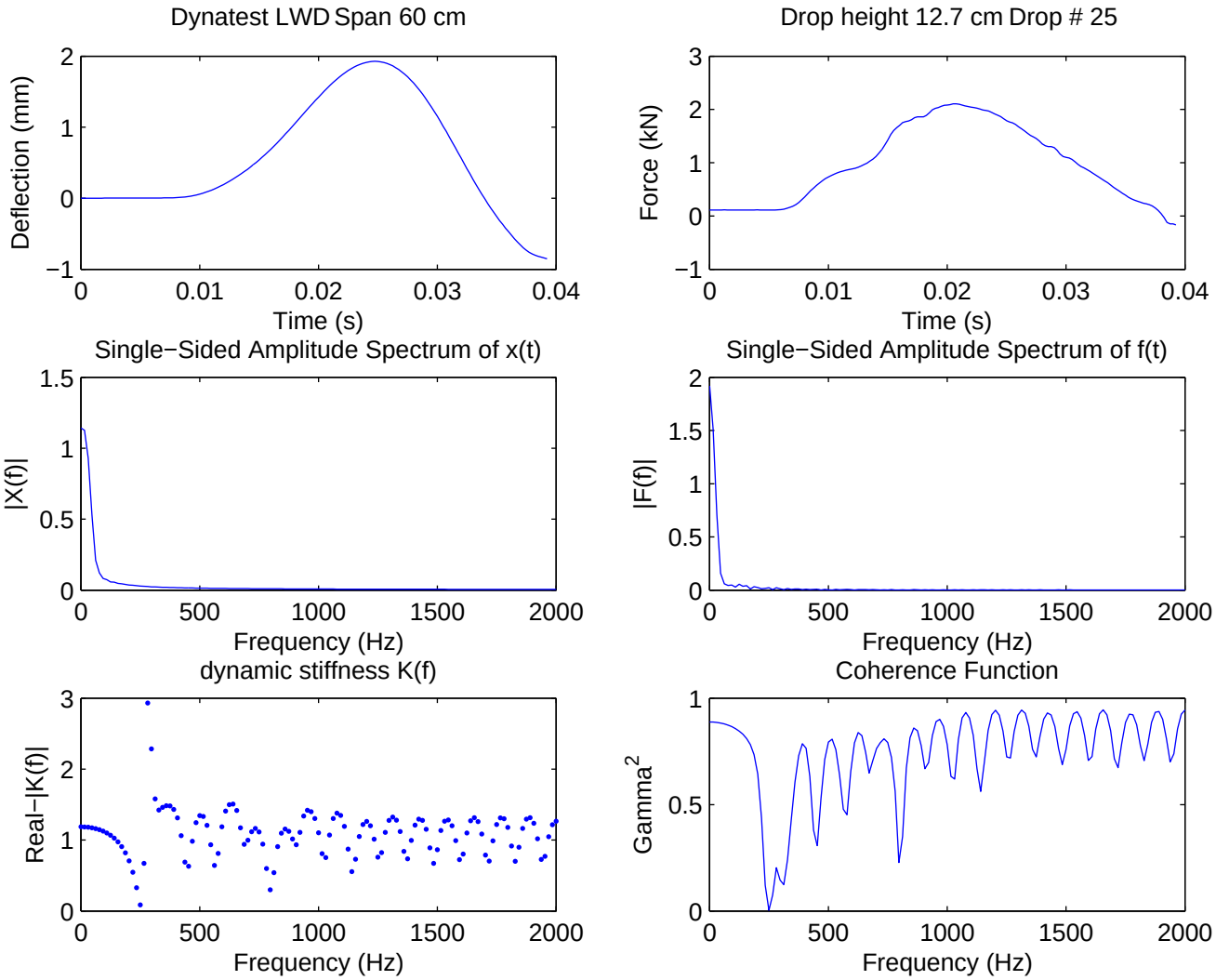
Dynatest LWD Span 60 cm
Deflection (mm)
Time (s)
Drop height 12.7 cm Drop # 25
Force (kN)
Time (s)
Single−Sided Amplitude Spectrum of x(t)
|X(f)|
Frequency (Hz)
Single−Sided Amplitude Spectrum of f(t)
|F(f)|
Frequency (Hz)
dynamic stiffness K(f)
Real−|K(f)|
Frequency (Hz)
Coherence Function
Gamma2
Frequency (Hz)

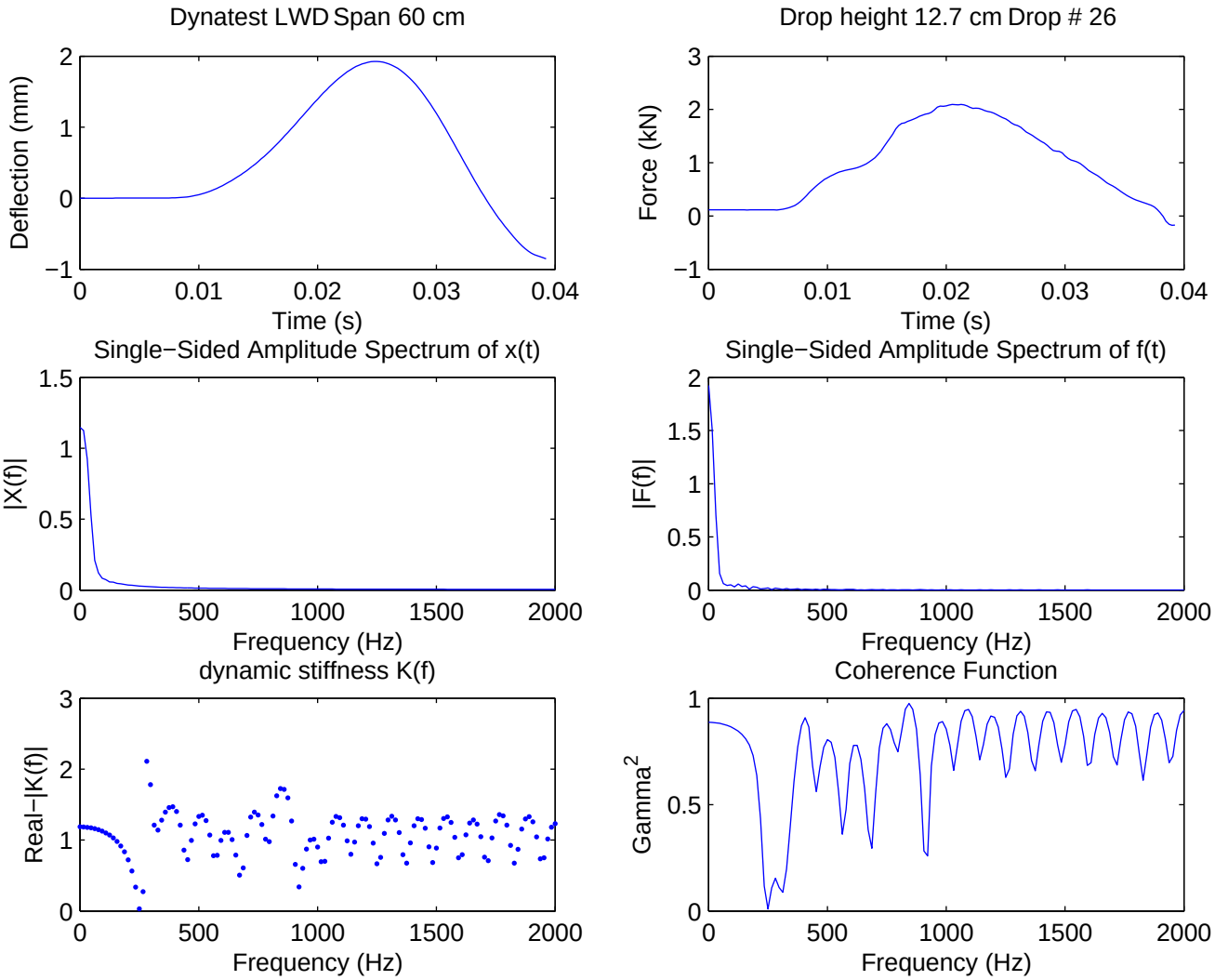
Dynatest LWD Span 60 cm
Deflection (mm)
Time (s)
Drop height 12.7 cm Drop # 26
Force (kN)
Time (s)
Single−Sided Amplitude Spectrum of x(t)
|X(f)|
Frequency (Hz)
Single−Sided Amplitude Spectrum of f(t)
|F(f)|
Frequency (Hz)
dynamic stiffness K(f)
Real−|K(f)|
Frequency (Hz)
Coherence Function
Gamma2
Frequency (Hz)

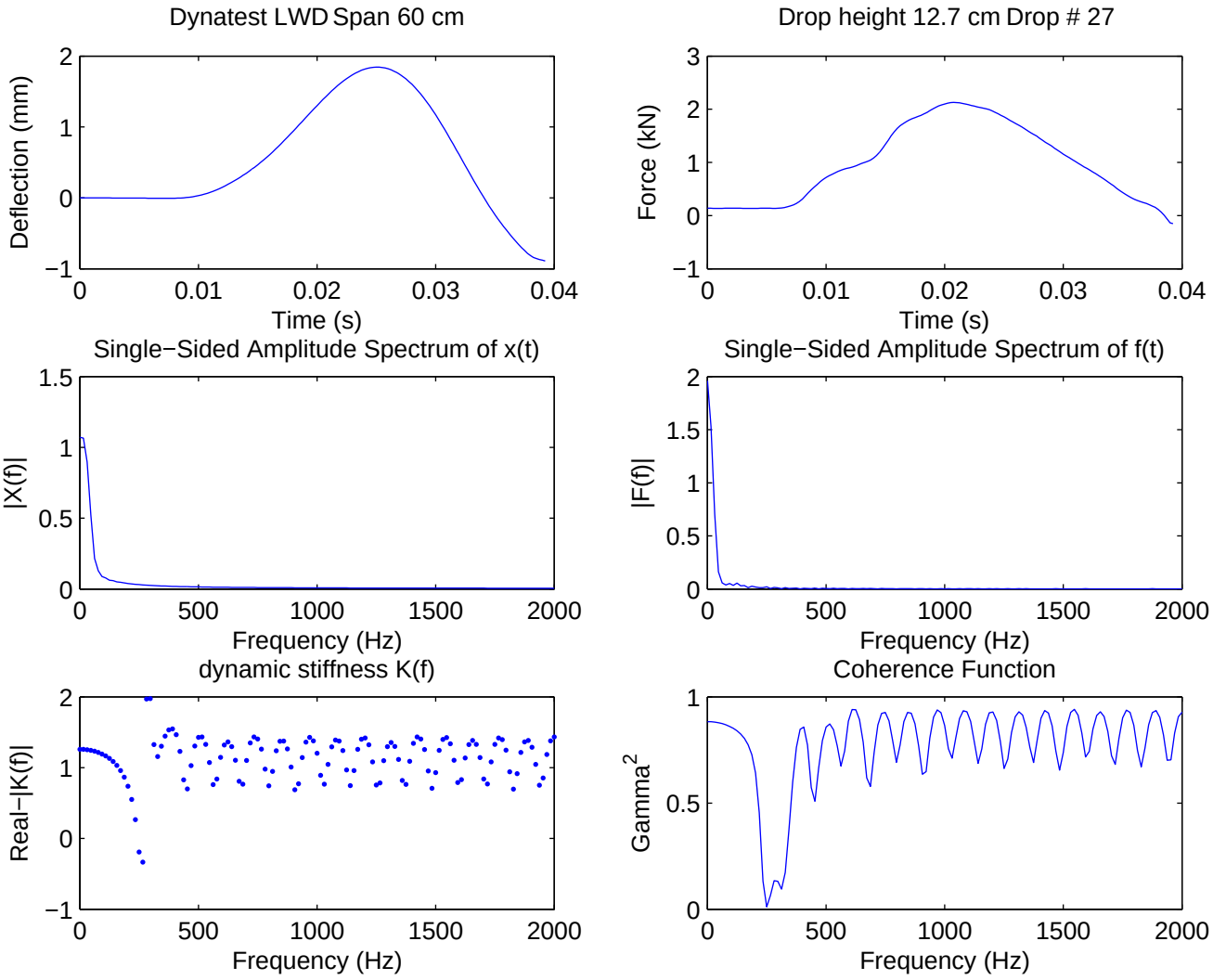
Dynatest LWD Span 60 cm
Deflection (mm)
Time (s)
Drop height 12.7 cm Drop # 27
Force (kN)
Time (s)
Single−Sided Amplitude Spectrum of x(t)
|X(f)|
Frequency (Hz)
Single−Sided Amplitude Spectrum of f(t)
|F(f)|
Frequency (Hz)
dynamic stiffness K(f)
Real−|K(f)|
Frequency (Hz)
Coherence Function
Gamma2
Frequency (Hz)

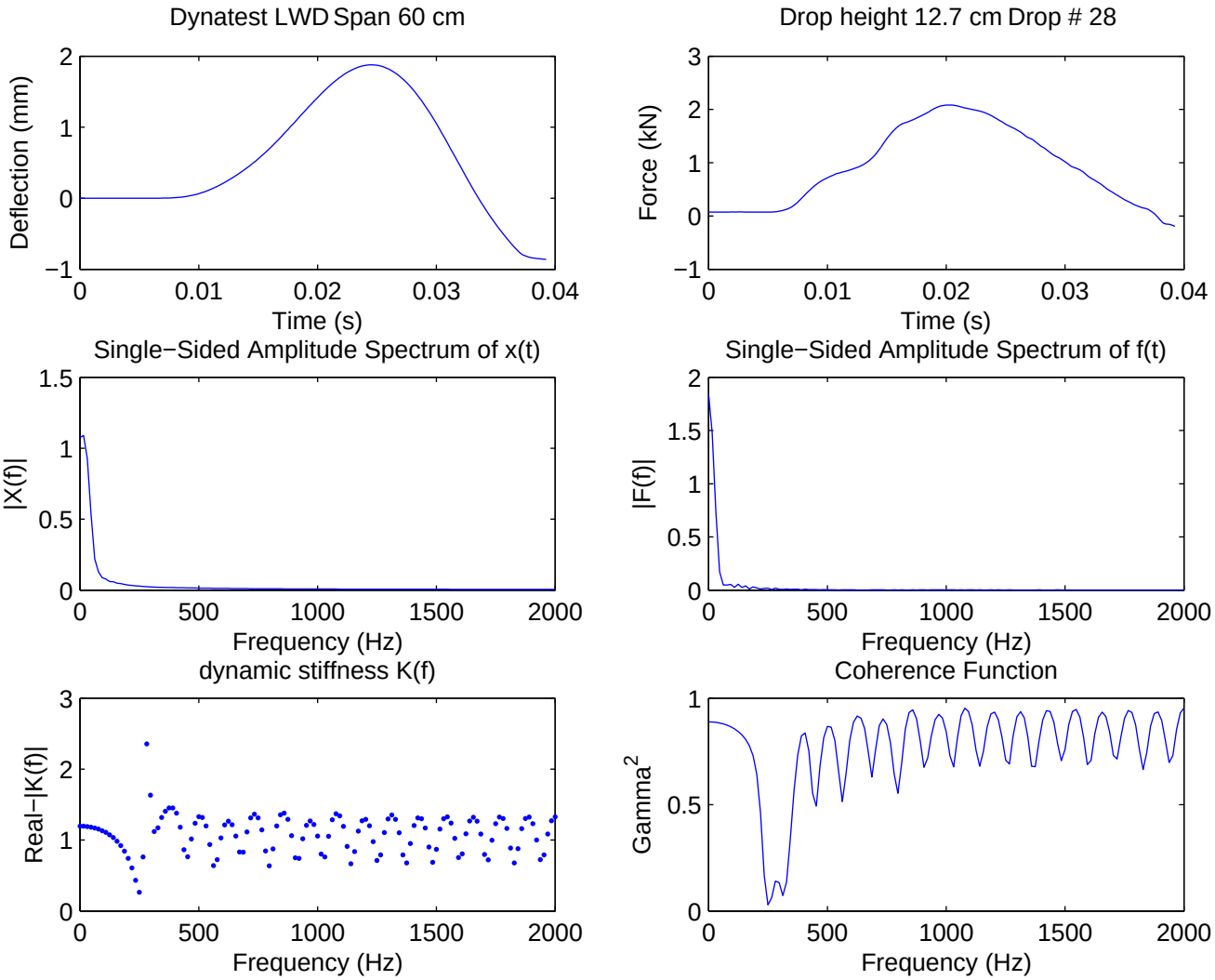
Dynatest LWD Span 60 cm
Deflection (mm)
Time (s)
Drop height 12.7 cm Drop # 28
Force (kN)
Time (s)
Single−Sided Amplitude Spectrum of x(t)
|X(f)|
Frequency (Hz)
Single−Sided Amplitude Spectrum of f(t)
|F(f)|
Frequency (Hz)
dynamic stiffness K(f)
Real−|K(f)|
Frequency (Hz)
Coherence Function
Gamma2
Frequency (Hz)

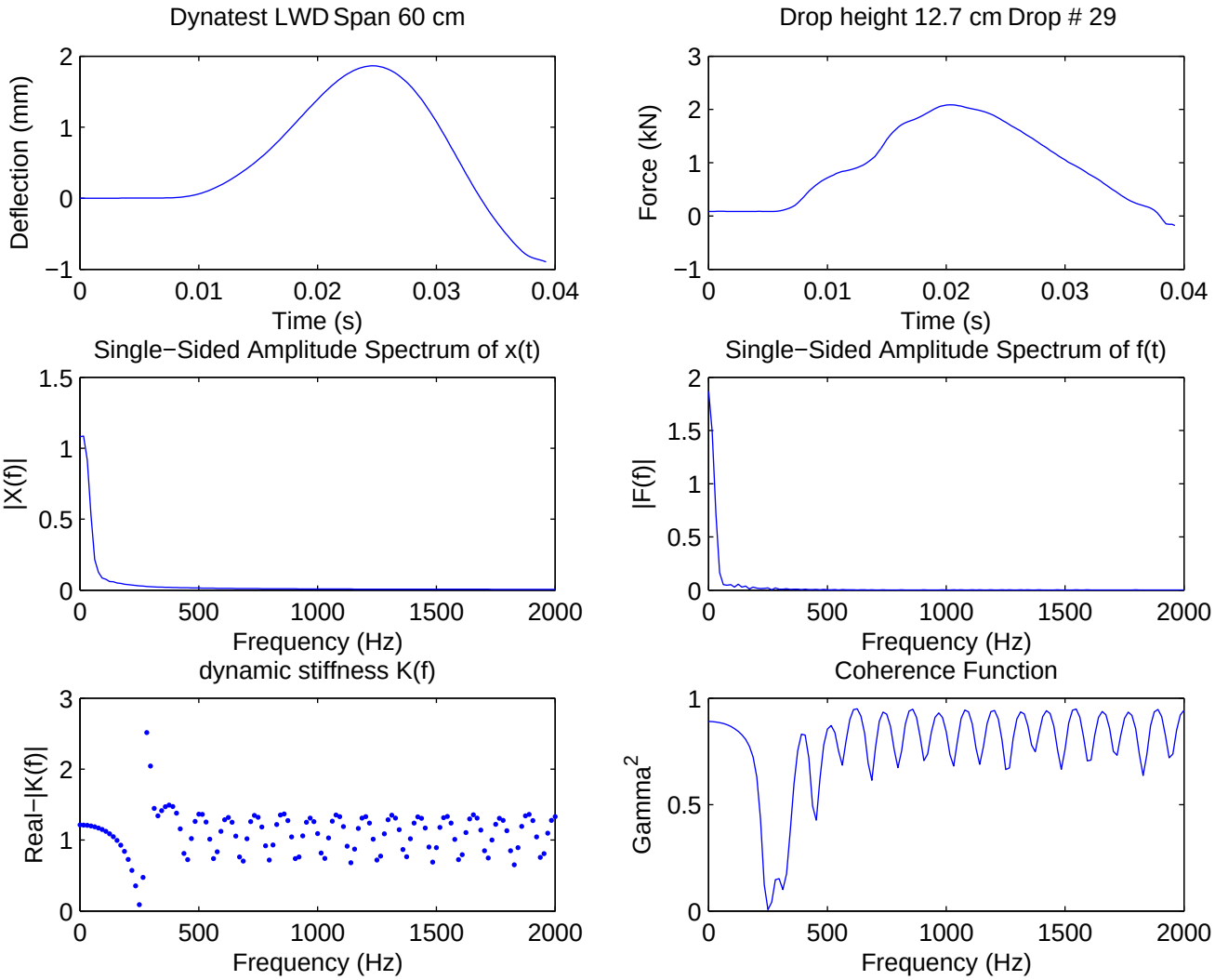
Dynatest LWD Span 60 cm
Deflection (mm)
Time (s)
Drop height 12.7 cm Drop # 29
Force (kN)
Time (s)
Single−Sided Amplitude Spectrum of x(t)
|X(f)|
Frequency (Hz)
Single−Sided Amplitude Spectrum of f(t)
|F(f)|
Frequency (Hz)
dynamic stiffness K(f)
Real−|K(f)|
Frequency (Hz)
Coherence Function
Gamma2
Frequency (Hz)

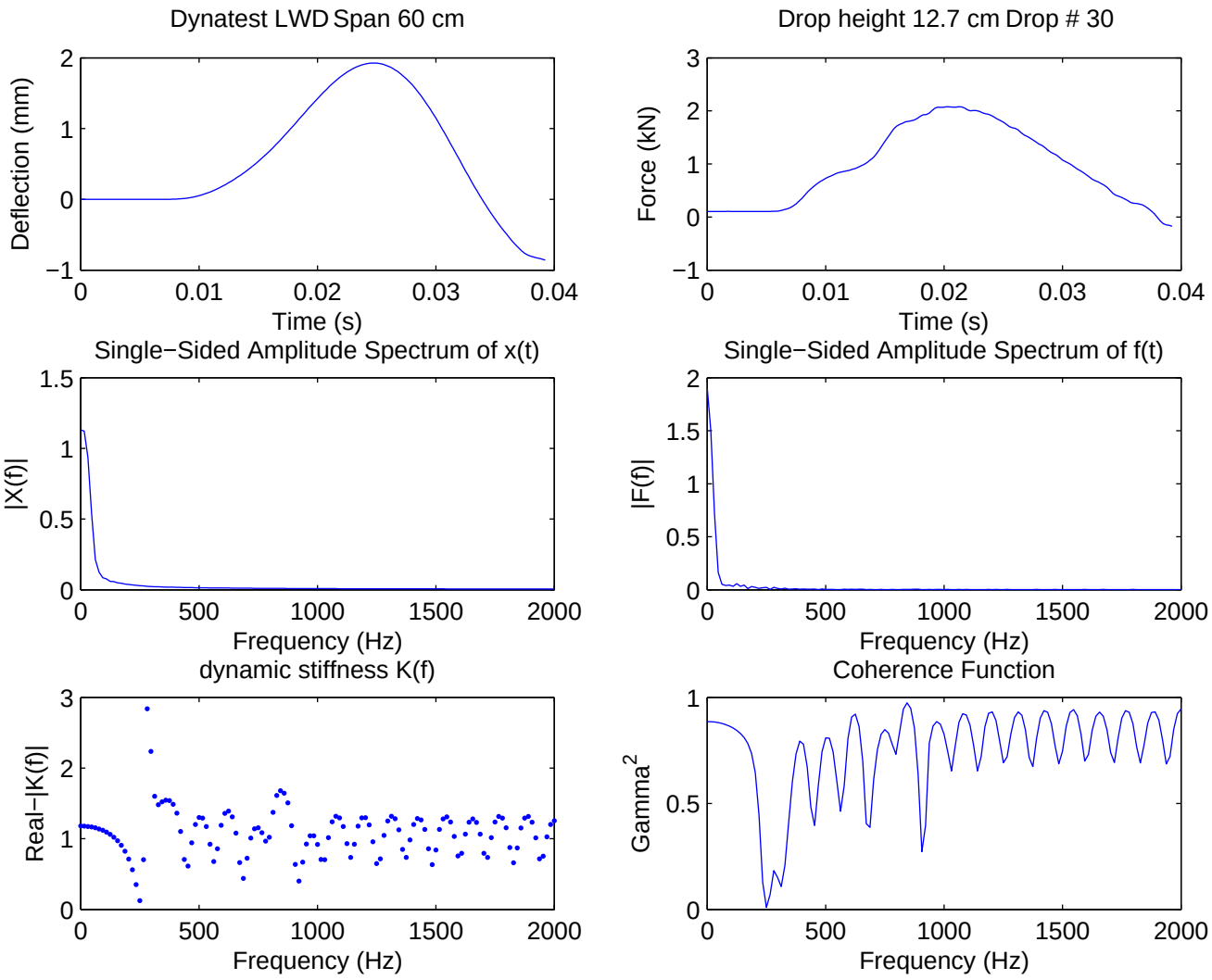
Dynatest LWD Span 60 cm
Deflection (mm)
Time (s)
Drop height 12.7 cm Drop # 30
Force (kN)
Time (s)
Single−Sided Amplitude Spectrum of x(t)
|X(f)|
Frequency (Hz)
Single−Sided Amplitude Spectrum of f(t)
|F(f)|
Frequency (Hz)
dynamic stiffness K(f)
Real−|K(f)|
Frequency (Hz)
Coherence Function
Gamma2
Frequency (Hz)

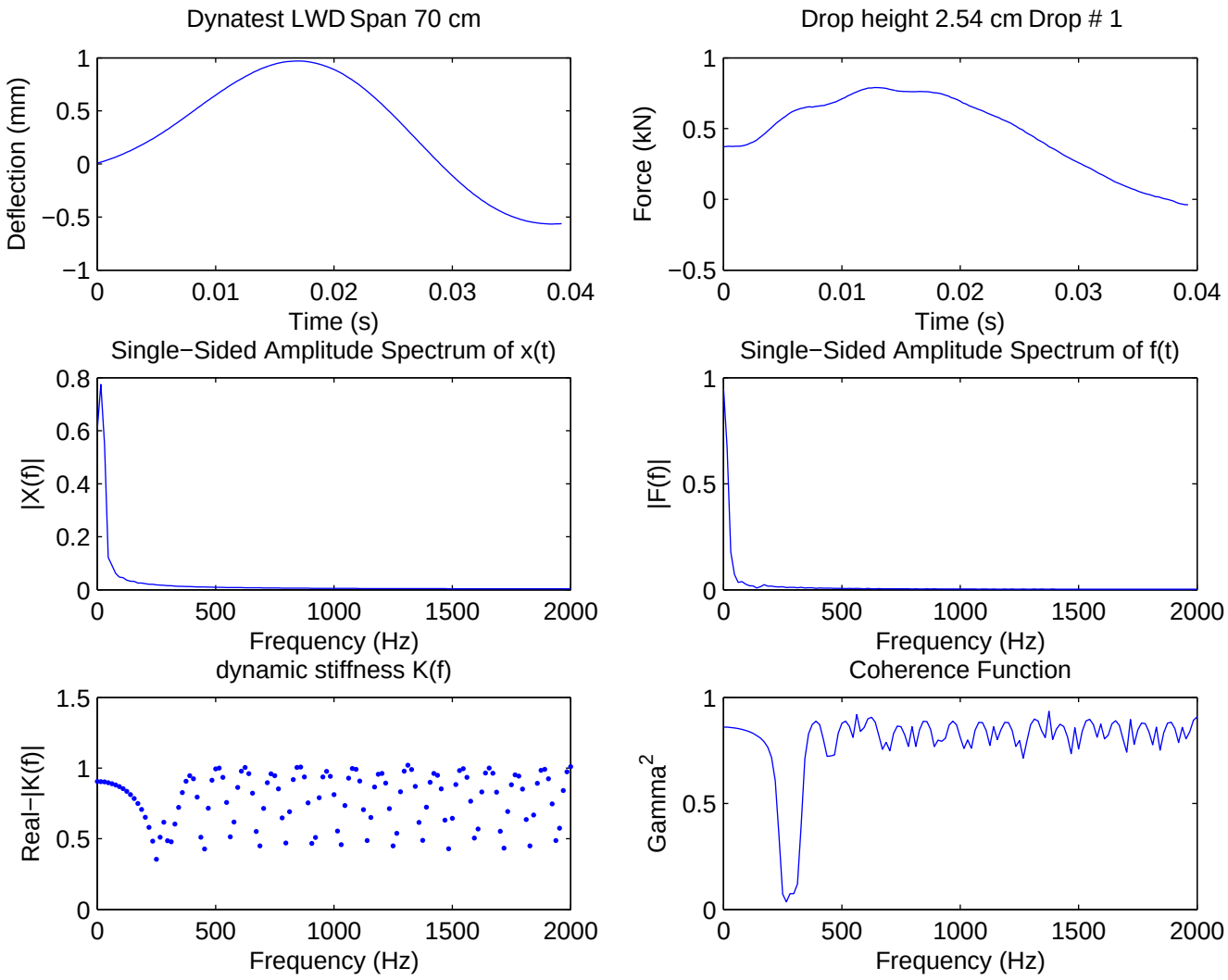
Dynatest LWD Span 70 cm
Deflection (mm)
Time (s)
Drop height 2.54 cm Drop # 1
Force (kN)
Time (s)
Single−Sided Amplitude Spectrum of x(t)
|X(f)|
Frequency (Hz)
Single−Sided Amplitude Spectrum of f(t)
|F(f)|
Frequency (Hz)
dynamic stiffness K(f)
Real−|K(f)|
Frequency (Hz)
Coherence Function
Gamma2
Frequency (Hz)

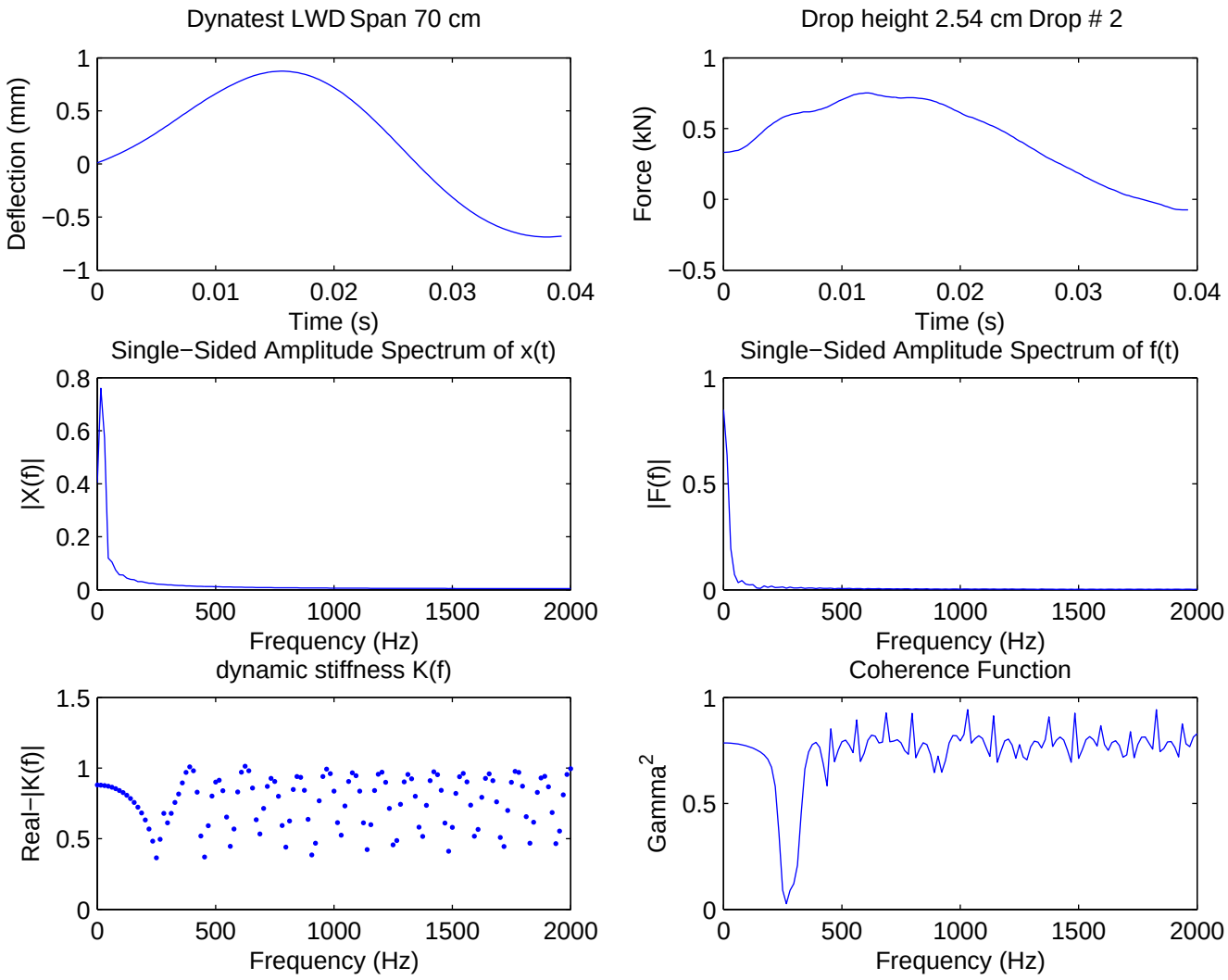
Dynatest LWD Span 70 cm
Deflection (mm)
Time (s)
Drop height 2.54 cm Drop # 2
Force (kN)
Time (s)
Single−Sided Amplitude Spectrum of x(t)
|X(f)|
Frequency (Hz)
Single−Sided Amplitude Spectrum of f(t)
|F(f)|
Frequency (Hz)
dynamic stiffness K(f)
Real−|K(f)|
Frequency (Hz)
Coherence Function
Gamma2
Frequency (Hz)

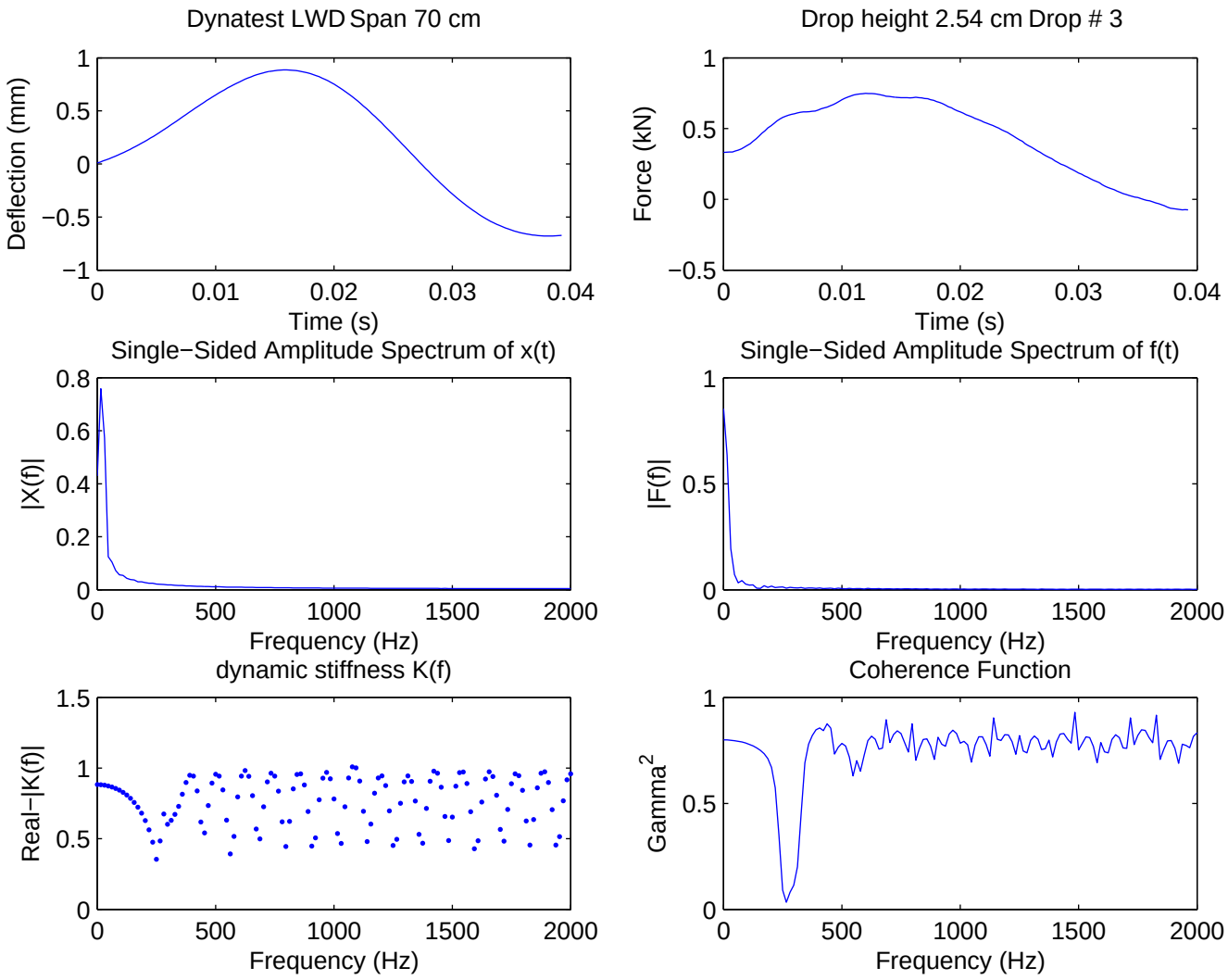
Dynatest LWD Span 70 cm
Deflection (mm)
Time (s)
Drop height 2.54 cm Drop # 3
Force (kN)
Time (s)
Single−Sided Amplitude Spectrum of x(t)
|X(f)|
Frequency (Hz)
Single−Sided Amplitude Spectrum of f(t)
|F(f)|
Frequency (Hz)
dynamic stiffness K(f)
Real−|K(f)|
Frequency (Hz)
Coherence Function
Gamma2
Frequency (Hz)

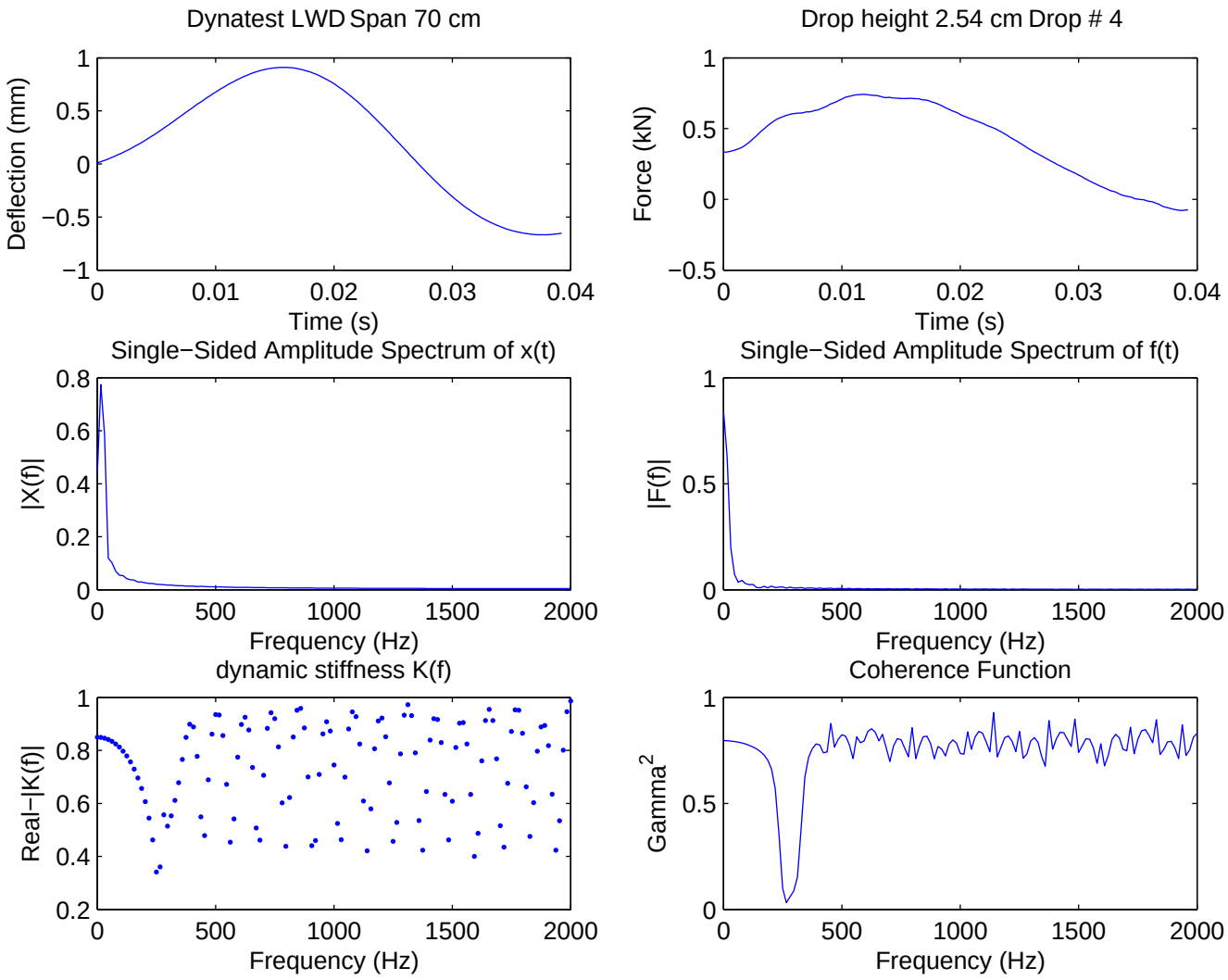
Dynatest LWD Span 70 cm
Deflection (mm)
Time (s)
Drop height 2.54 cm Drop # 4
Force (kN)
Time (s)
Single−Sided Amplitude Spectrum of x(t)
|X(f)|
Frequency (Hz)
Single−Sided Amplitude Spectrum of f(t)
|F(f)|
Frequency (Hz)
dynamic stiffness K(f)
Real−|K(f)|
Frequency (Hz)
Coherence Function
Gamma2
Frequency (Hz)

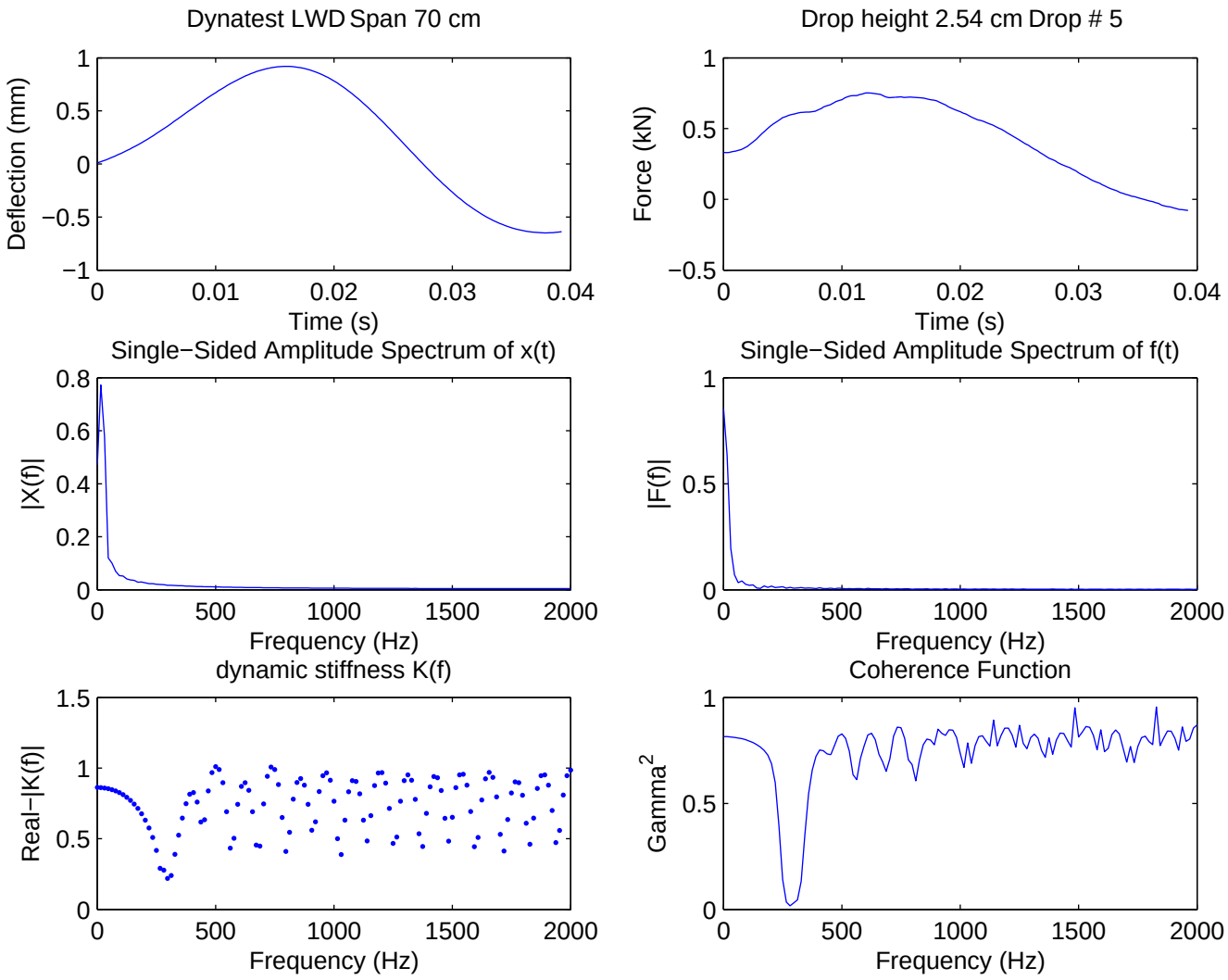
Dynatest LWD Span 70 cm
Deflection (mm)
Time (s)
Drop height 2.54 cm Drop # 5
Force (kN)
Time (s)
Single−Sided Amplitude Spectrum of x(t)
|X(f)|
Frequency (Hz)
Single−Sided Amplitude Spectrum of f(t)
|F(f)|
Frequency (Hz)
dynamic stiffness K(f)
Real−|K(f)|
Frequency (Hz)
Coherence Function
Gamma2
Frequency (Hz)

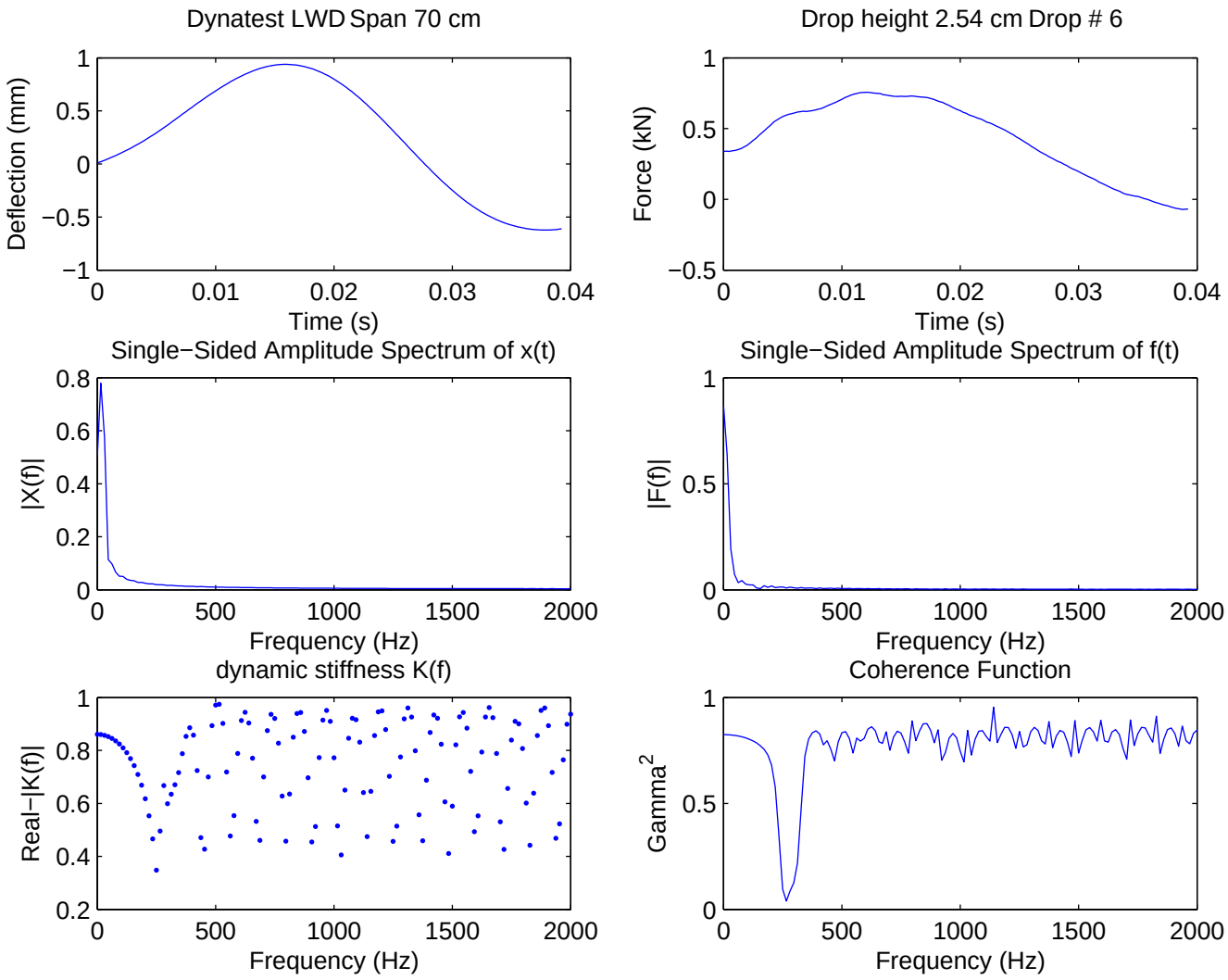
Dynatest LWD Span 70 cm
Deflection (mm)
Time (s)
Drop height 2.54 cm Drop # 6
Force (kN)
Time (s)
Single−Sided Amplitude Spectrum of x(t)
|X(f)|
Frequency (Hz)
Single−Sided Amplitude Spectrum of f(t)
|F(f)|
Frequency (Hz)
dynamic stiffness K(f)
Real−|K(f)|
Frequency (Hz)
Coherence Function
Gamma2
Frequency (Hz)

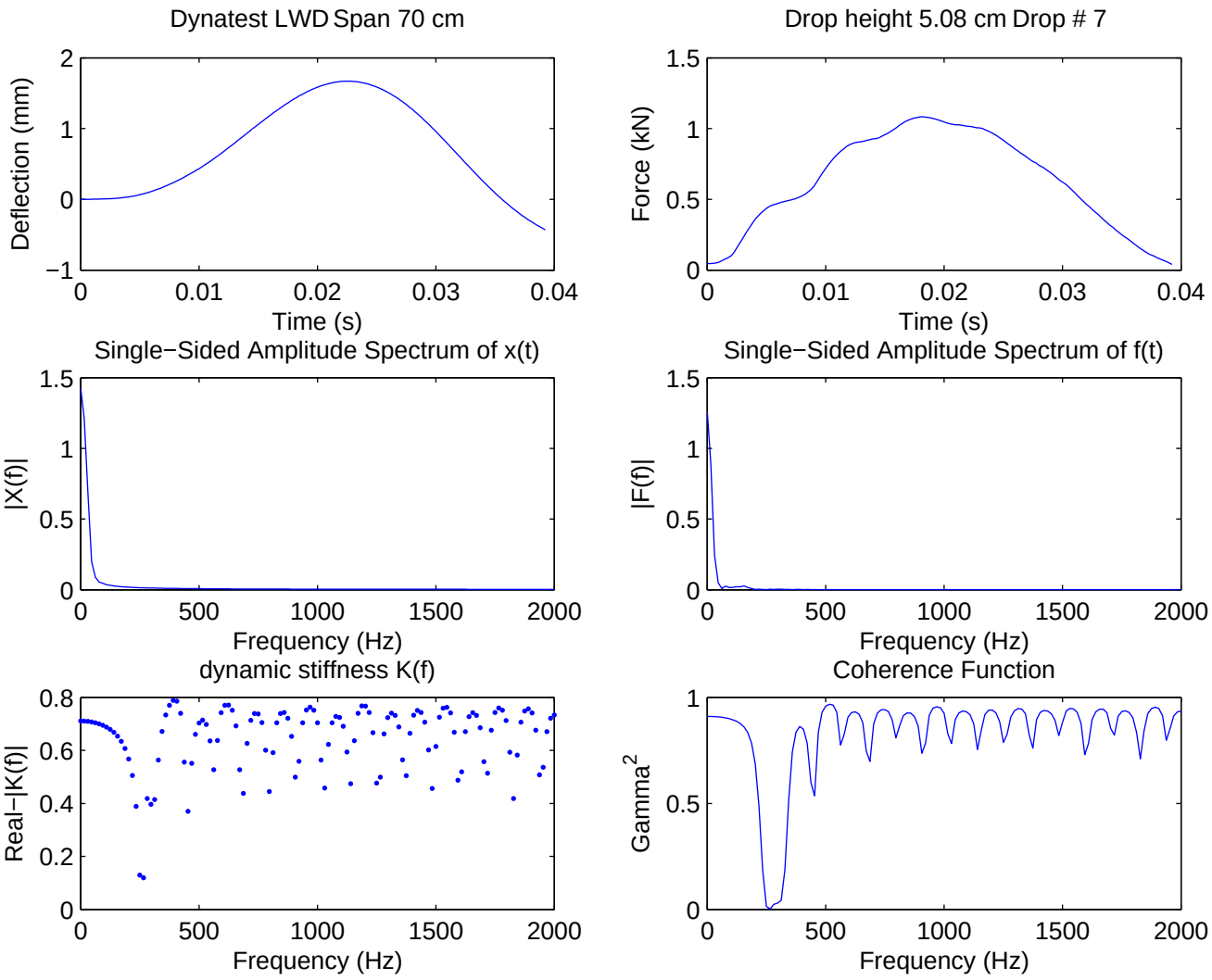
Dynatest LWD Span 70 cm
Deflection (mm)
Time (s)
Drop height 5.08 cm Drop # 7
Force (kN)
Time (s)
Single−Sided Amplitude Spectrum of x(t)
|X(f)|
Frequency (Hz)
Single−Sided Amplitude Spectrum of f(t)
|F(f)|
Frequency (Hz)
dynamic stiffness K(f)
Real−|K(f)|
Frequency (Hz)
Coherence Function
Gamma2
Frequency (Hz)

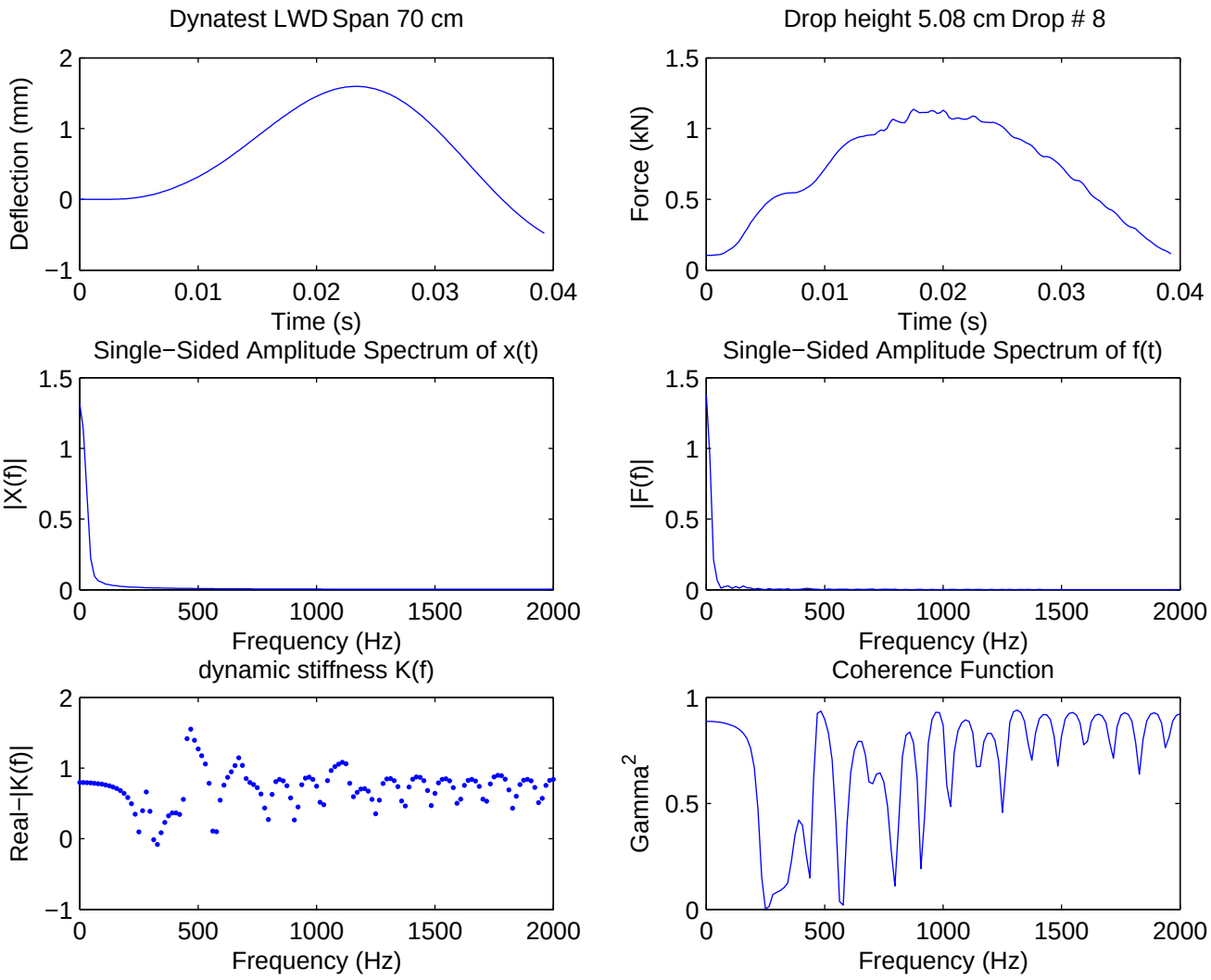
Dynatest LWD Span 70 cm
Deflection (mm)
Time (s)
Drop height 5.08 cm Drop # 8
Force (kN)
Time (s)
Single−Sided Amplitude Spectrum of x(t)
|X(f)|
Frequency (Hz)
Single−Sided Amplitude Spectrum of f(t)
|F(f)|
Frequency (Hz)
dynamic stiffness K(f)
Real−|K(f)|
Frequency (Hz)
Coherence Function
Gamma2
Frequency (Hz)

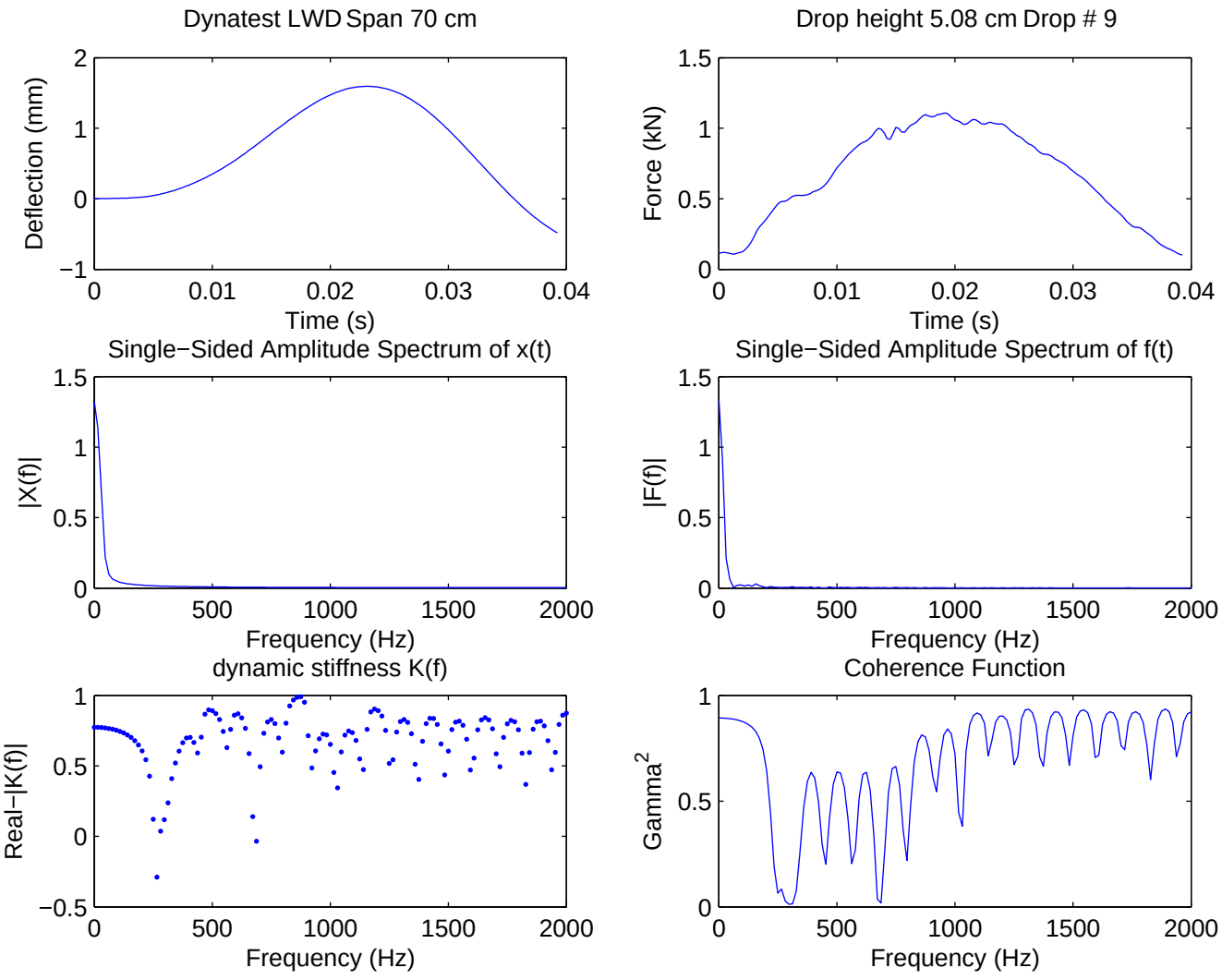
Dynatest LWD Span 70 cm
Deflection (mm)
Time (s)
Drop height 5.08 cm Drop # 9
Force (kN)
Time (s)
Single−Sided Amplitude Spectrum of x(t)
|X(f)|
Frequency (Hz)
Single−Sided Amplitude Spectrum of f(t)
|F(f)|
Frequency (Hz)
dynamic stiffness K(f)
Real−|K(f)|
Frequency (Hz)
Coherence Function
Gamma2
Frequency (Hz)

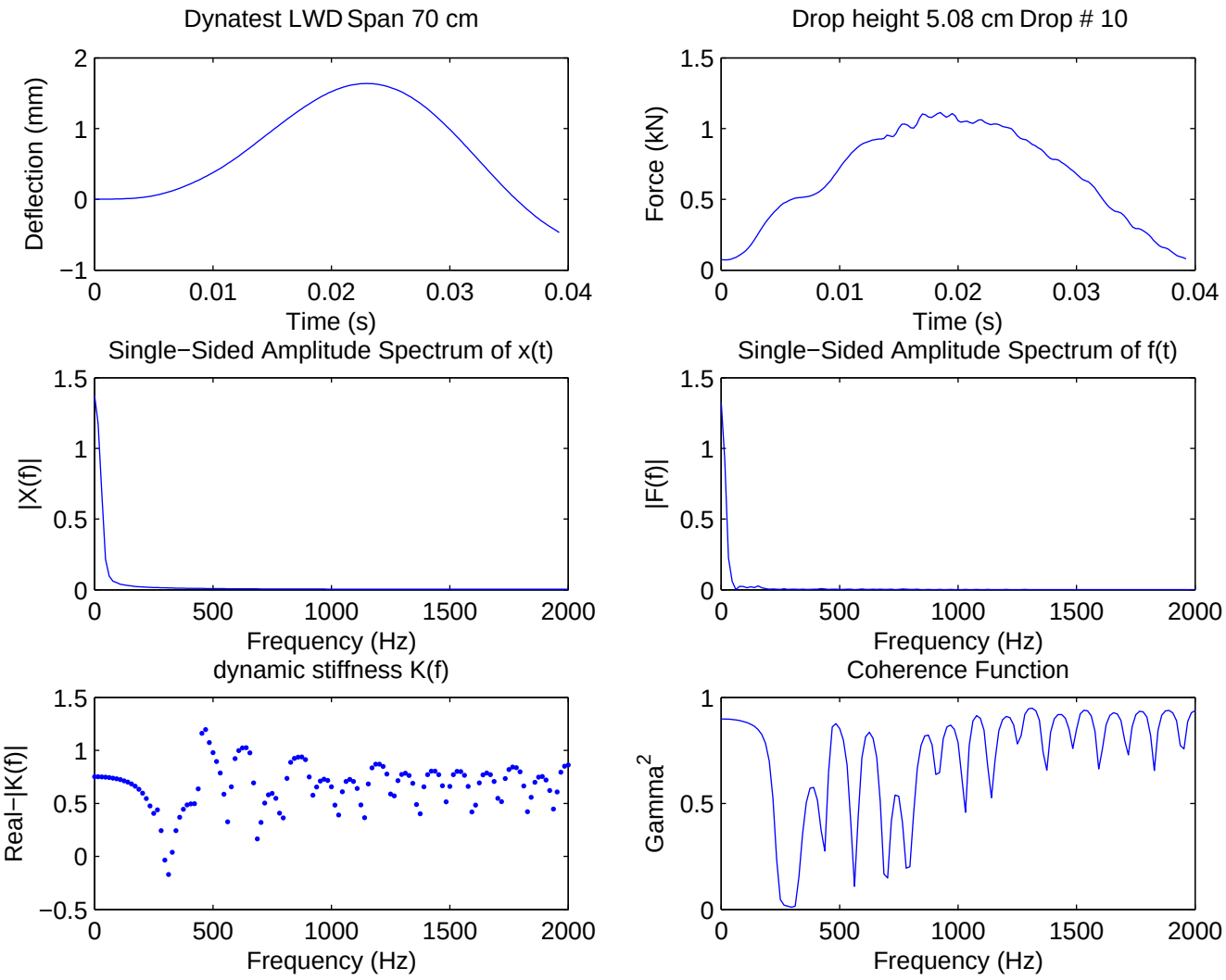
Dynatest LWD Span 70 cm
Deflection (mm)
Time (s)
Drop height 5.08 cm Drop # 10
Force (kN)
Time (s)
Single−Sided Amplitude Spectrum of x(t)
|X(f)|
Frequency (Hz)
Single−Sided Amplitude Spectrum of f(t)
|F(f)|
Frequency (Hz)
dynamic stiffness K(f)
Real−|K(f)|
Frequency (Hz)
Coherence Function
Gamma2
Frequency (Hz)

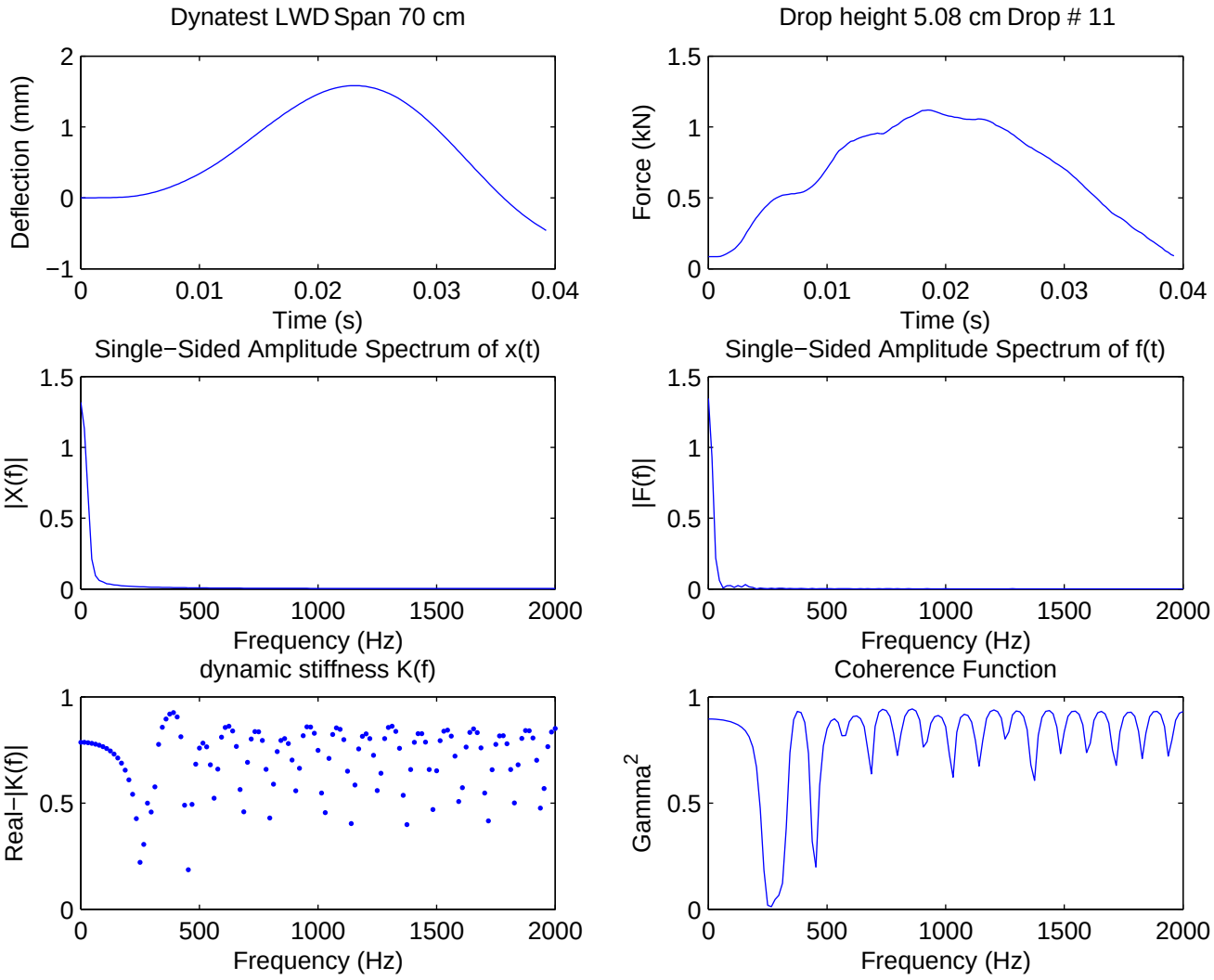
Dynatest LWD Span 70 cm
Deflection (mm)
Time (s)
Drop height 5.08 cm Drop # 11
Force (kN)
Time (s)
Single−Sided Amplitude Spectrum of x(t)
|X(f)|
Frequency (Hz)
Single−Sided Amplitude Spectrum of f(t)
|F(f)|
Frequency (Hz)
dynamic stiffness K(f)
Real−|K(f)|
Frequency (Hz)
Coherence Function
Gamma2
Frequency (Hz)

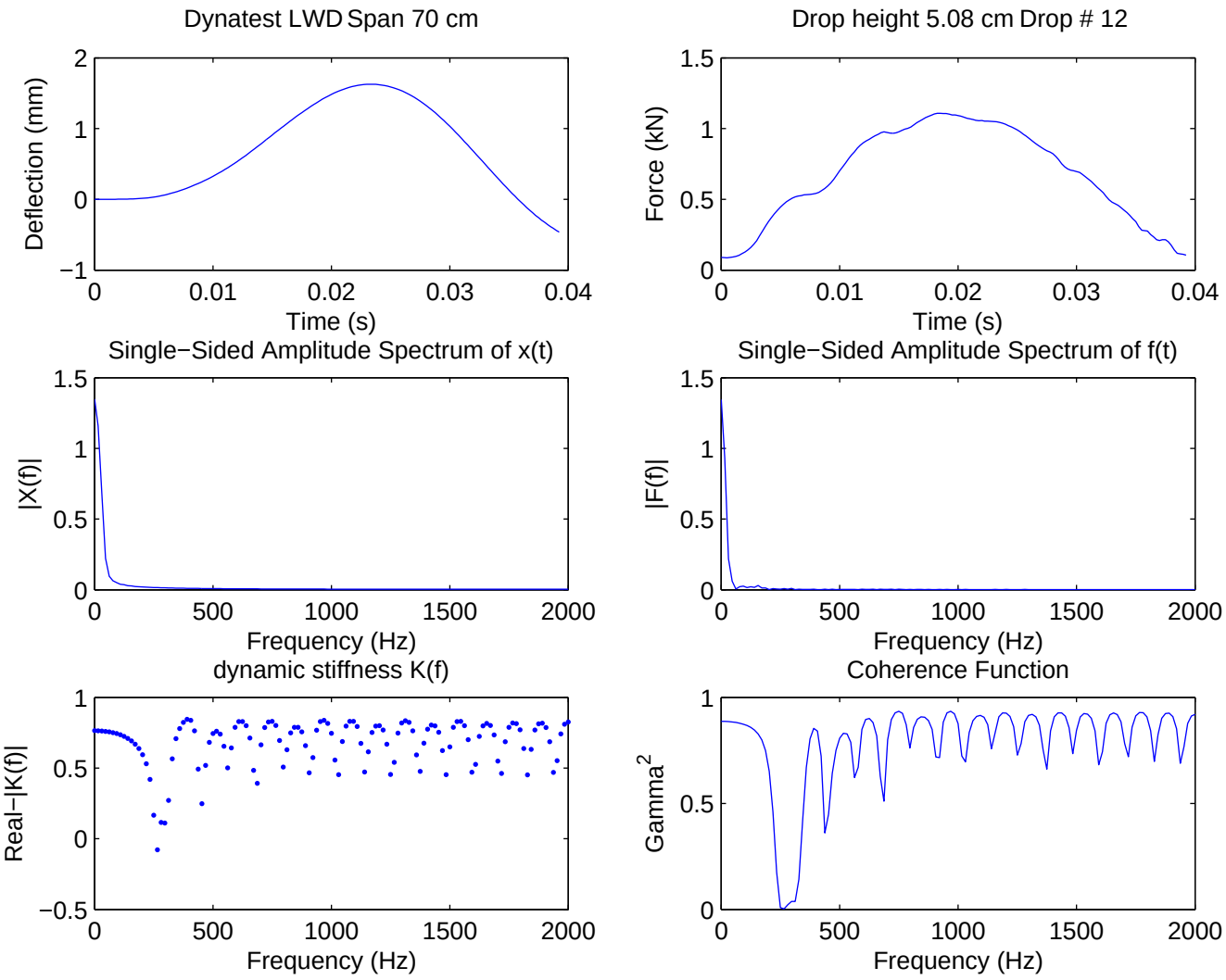
Dynatest LWD Span 70 cm
Deflection (mm)
Time (s)
Drop height 5.08 cm Drop # 12
Force (kN)
Time (s)
Single−Sided Amplitude Spectrum of x(t)
|X(f)|
Frequency (Hz)
Single−Sided Amplitude Spectrum of f(t)
|F(f)|
Frequency (Hz)
dynamic stiffness K(f)
Real−|K(f)|
Frequency (Hz)
Coherence Function
Gamma2
Frequency (Hz)

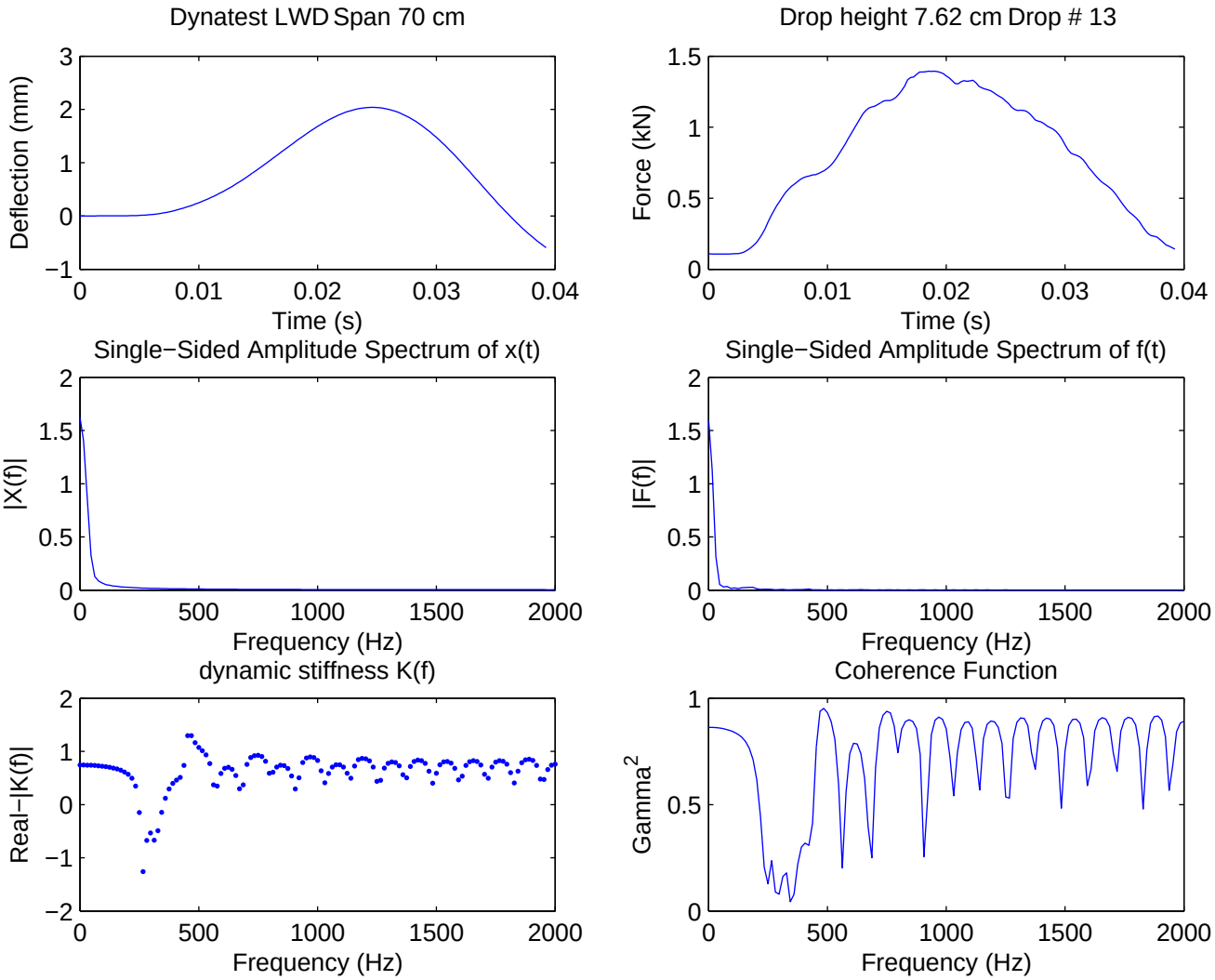
Dynatest LWD Span 70 cm
Deflection (mm)
Time (s)
Drop height 7.62 cm Drop # 13
Force (kN)
Time (s)
Single−Sided Amplitude Spectrum of x(t)
|X(f)|
Frequency (Hz)
Single−Sided Amplitude Spectrum of f(t)
|F(f)|
Frequency (Hz)
dynamic stiffness K(f)
Real−|K(f)|
Frequency (Hz)
Coherence Function
Gamma2
Frequency (Hz)

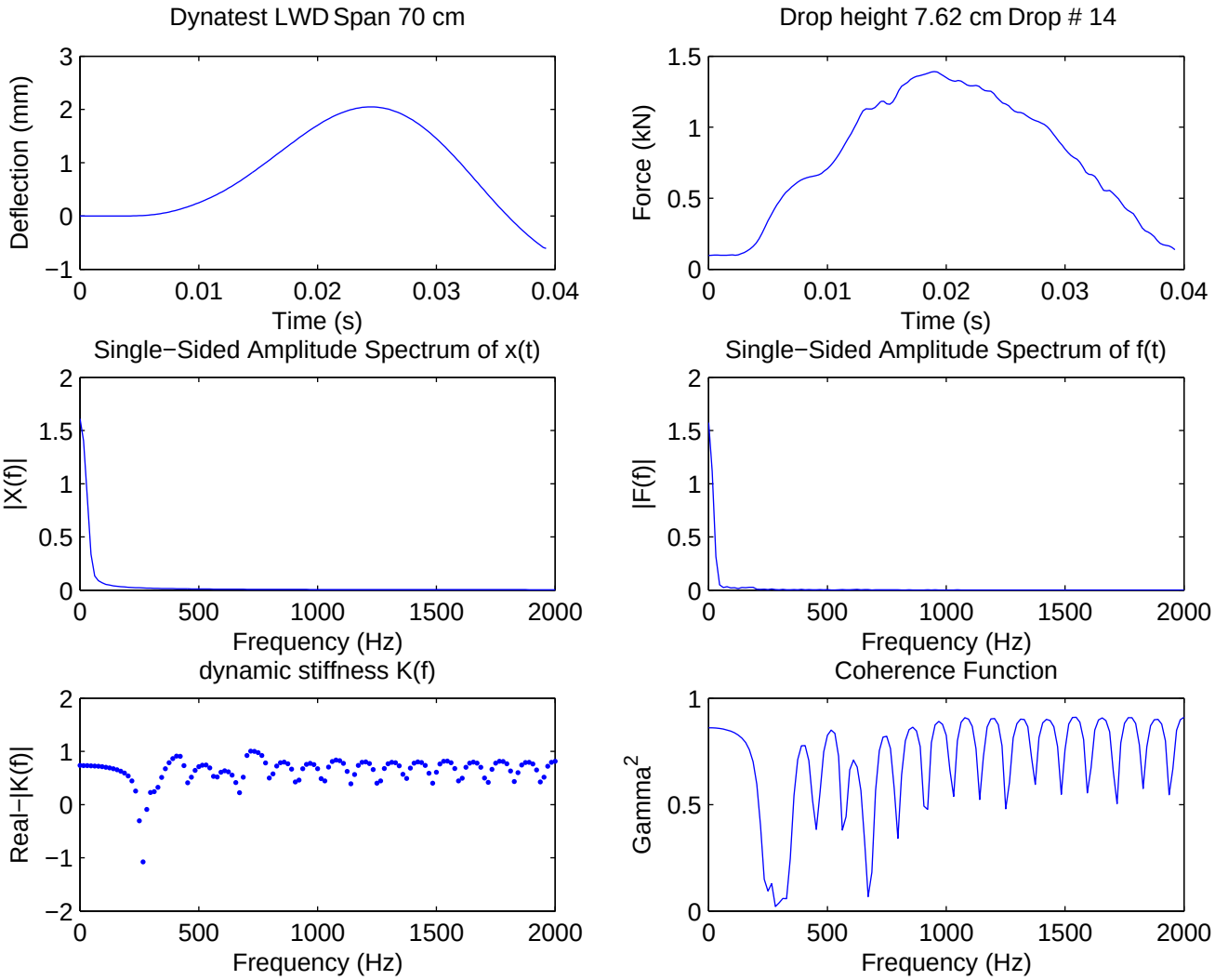
Dynatest LWD Span 70 cm
Deflection (mm)
Time (s)
Drop height 7.62 cm Drop # 14
Force (kN)
Time (s)
Single−Sided Amplitude Spectrum of x(t)
|X(f)|
Frequency (Hz)
Single−Sided Amplitude Spectrum of f(t)
|F(f)|
Frequency (Hz)
dynamic stiffness K(f)
Real−|K(f)|
Frequency (Hz)
Coherence Function
Gamma2
Frequency (Hz)

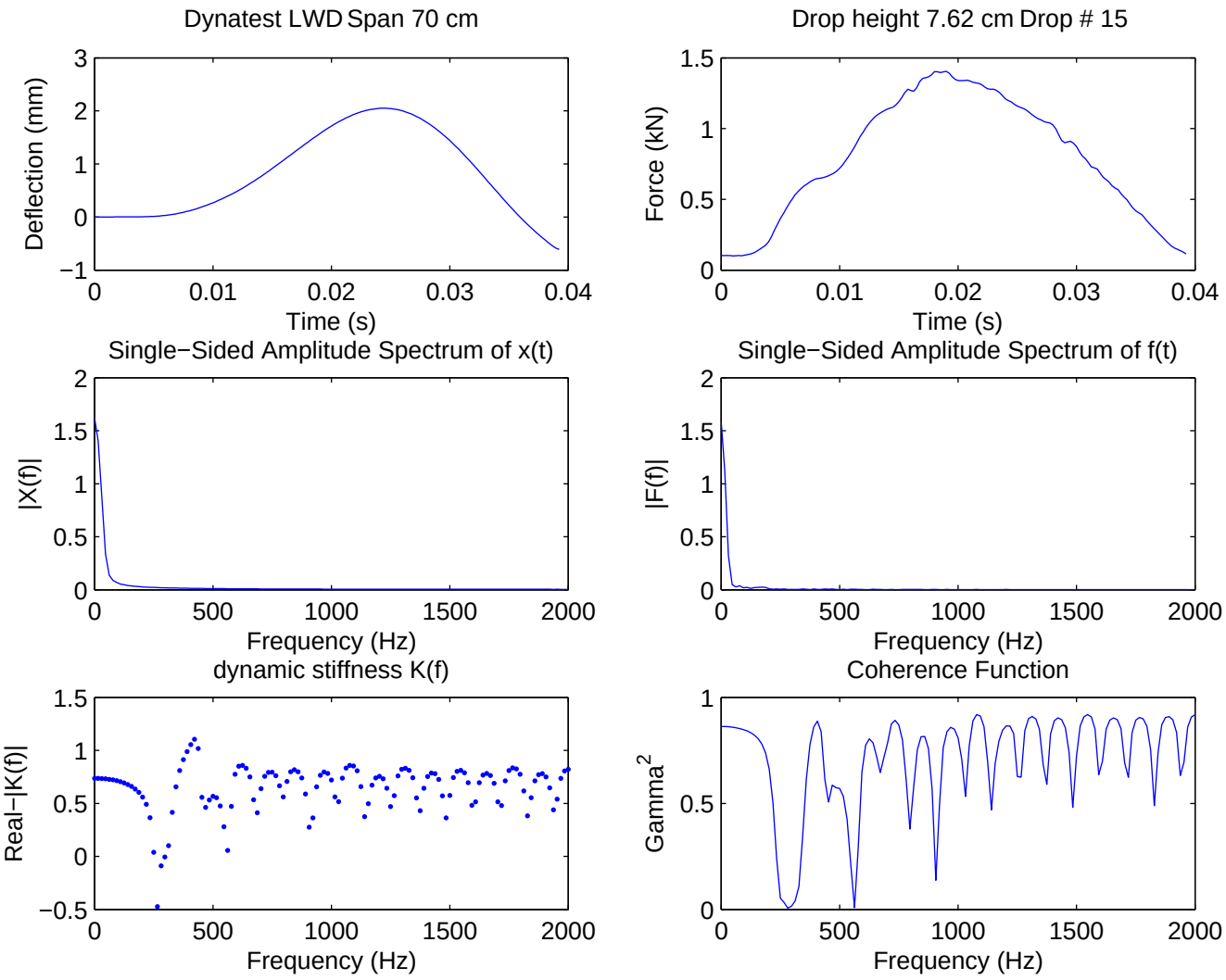
Dynatest LWD Span 70 cm
Deflection (mm)
Time (s)
Drop height 7.62 cm Drop # 15
Force (kN)
Time (s)
Single−Sided Amplitude Spectrum of x(t)
|X(f)|
Frequency (Hz)
Single−Sided Amplitude Spectrum of f(t)
|F(f)|
Frequency (Hz)
dynamic stiffness K(f)
Real−|K(f)|
Frequency (Hz)
Coherence Function
Gamma2
Frequency (Hz)

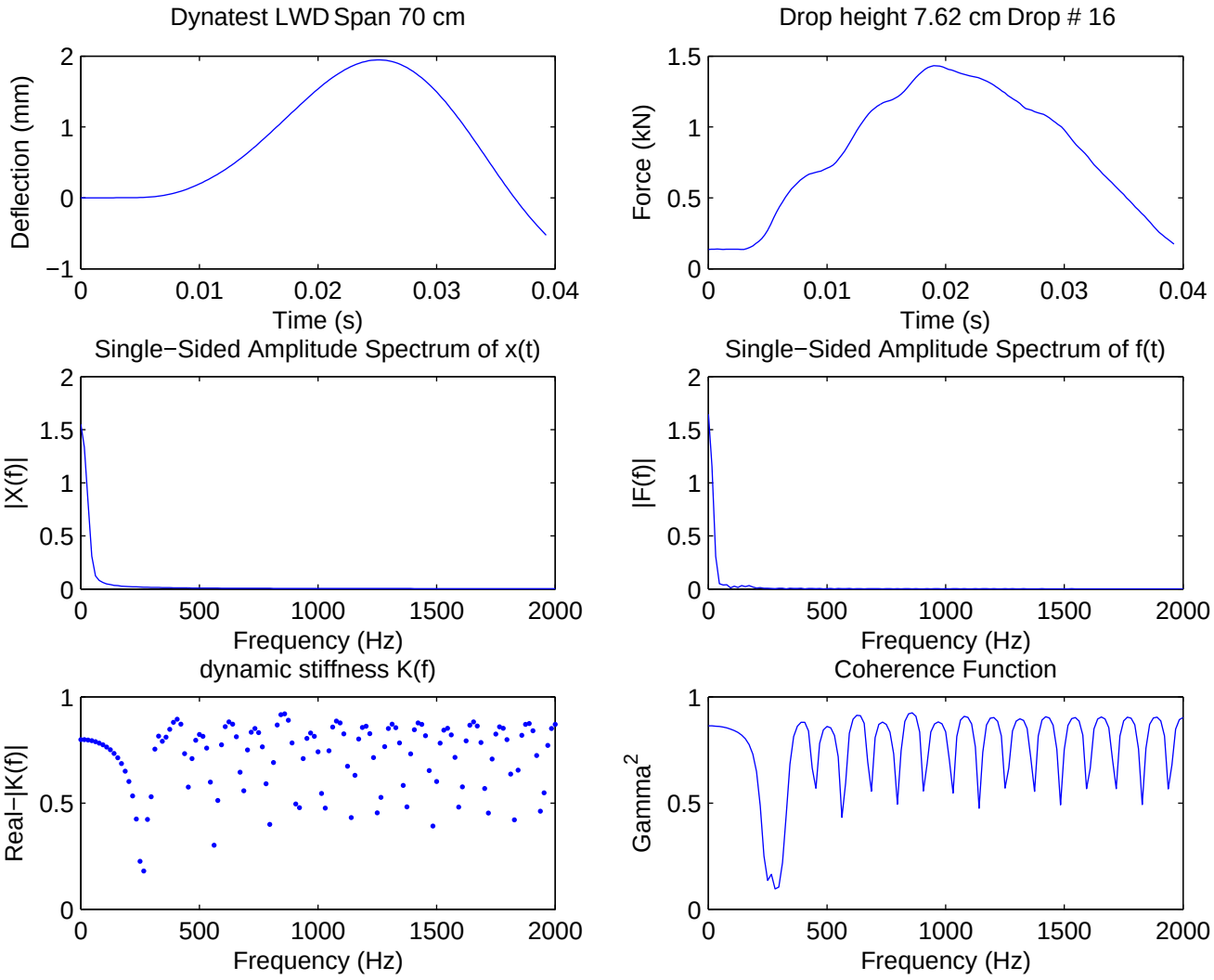
Dynatest LWD Span 70 cm
Deflection (mm)
Time (s)
Drop height 7.62 cm Drop # 16
Force (kN)
Time (s)
Single−Sided Amplitude Spectrum of x(t)
|X(f)|
Frequency (Hz)
Single−Sided Amplitude Spectrum of f(t)
|F(f)|
Frequency (Hz)
dynamic stiffness K(f)
Real−|K(f)|
Frequency (Hz)
Coherence Function
Gamma2
Frequency (Hz)

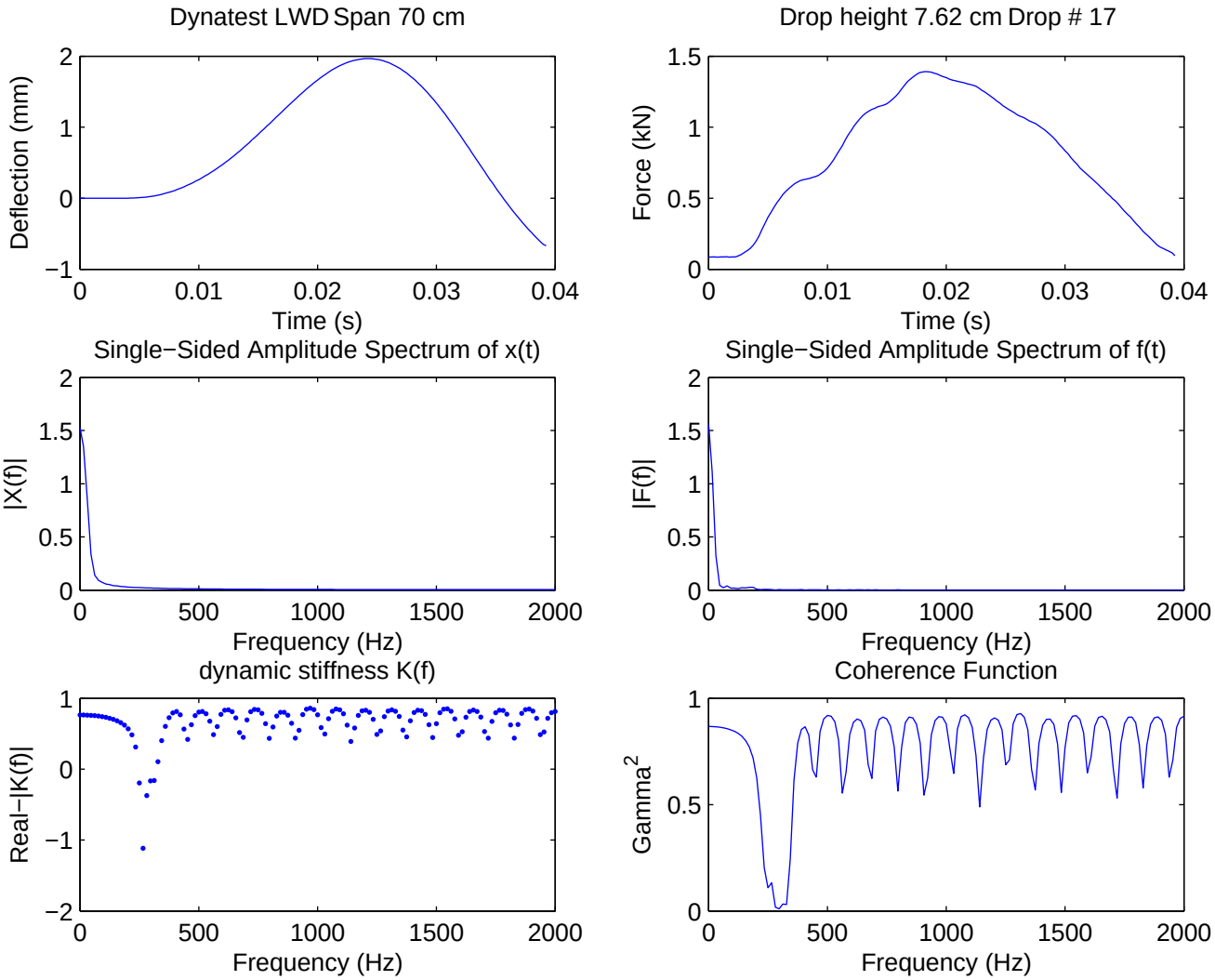
Dynatest LWD Span 70 cm
Deflection (mm)
Time (s)
Drop height 7.62 cm Drop # 17
Force (kN)
Time (s)
Single−Sided Amplitude Spectrum of x(t)
|X(f)|
Frequency (Hz)
Single−Sided Amplitude Spectrum of f(t)
|F(f)|
Frequency (Hz)
dynamic stiffness K(f)
Real−|K(f)|
Frequency (Hz)
Coherence Function
Gamma2
Frequency (Hz)

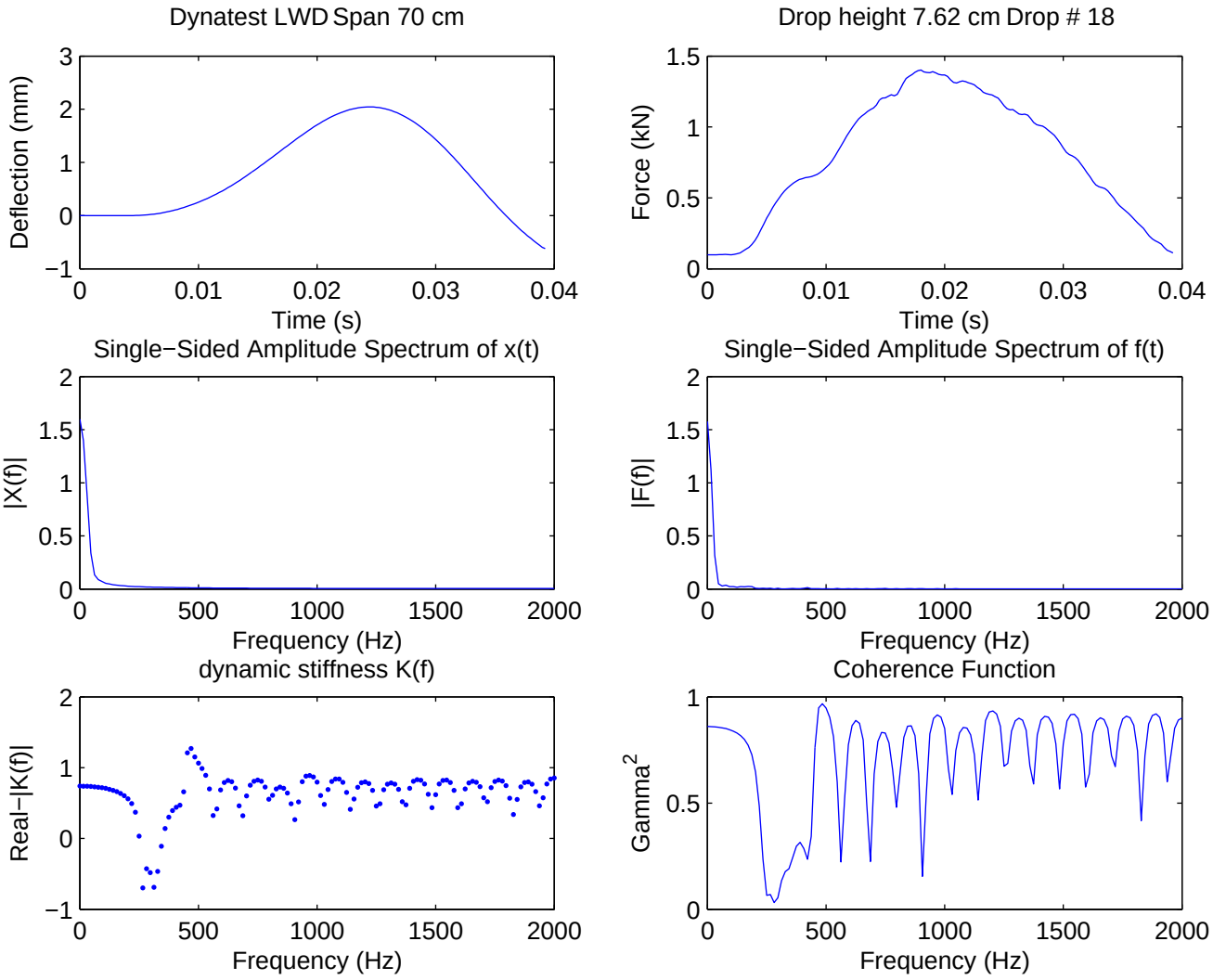
Dynatest LWD Span 70 cm
Deflection (mm)
Time (s)
Drop height 7.62 cm Drop # 18
Force (kN)
Time (s)
Single−Sided Amplitude Spectrum of x(t)
|X(f)|
Frequency (Hz)
Single−Sided Amplitude Spectrum of f(t)
|F(f)|
Frequency (Hz)
dynamic stiffness K(f)
Real−|K(f)|
Frequency (Hz)
Coherence Function
Gamma2
Frequency (Hz)

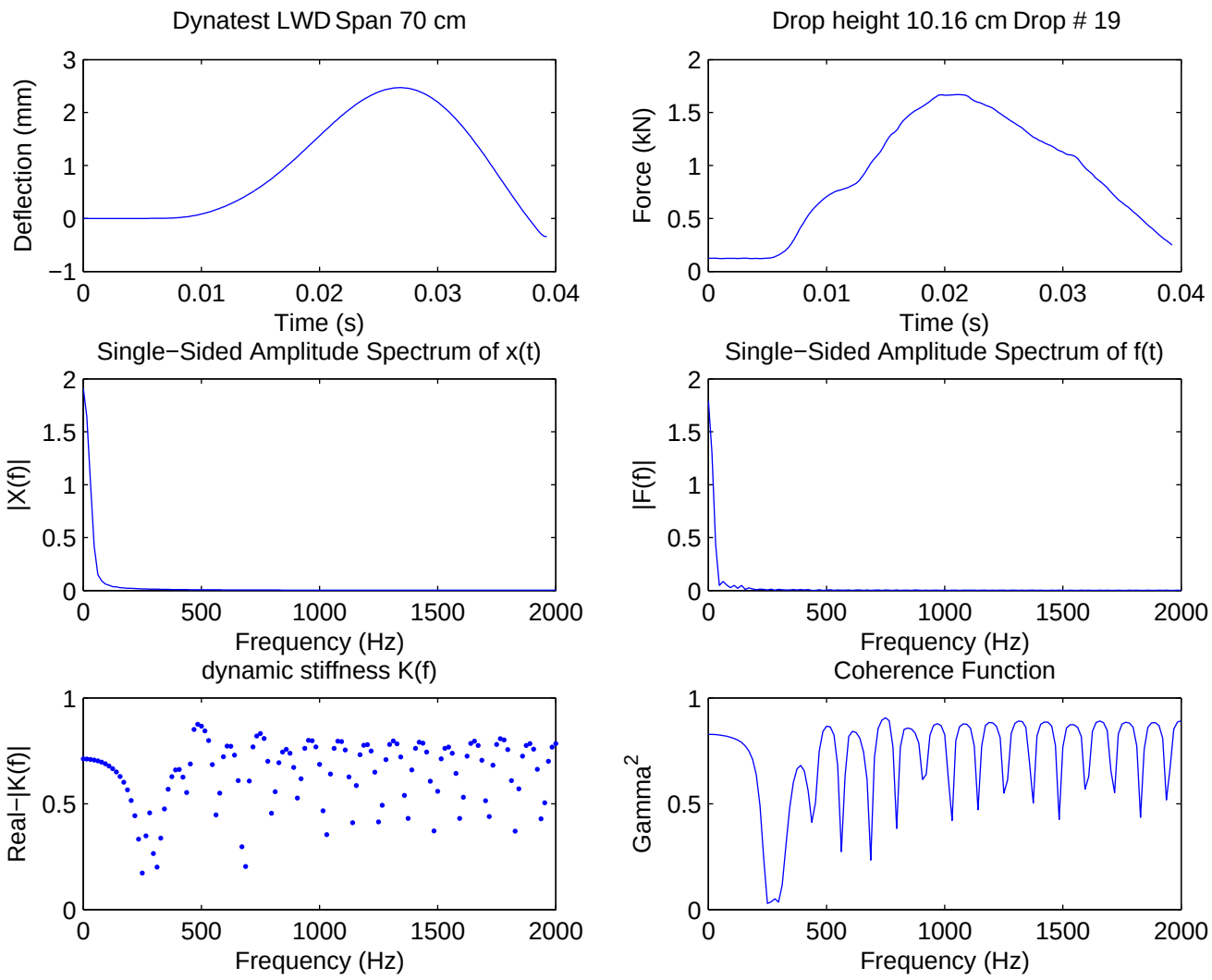
Dynatest LWD Span 70 cm
Deflection (mm)
Time (s)
Drop height 10.16 cm Drop # 19
Force (kN)
Time (s)
Single−Sided Amplitude Spectrum of x(t)
|X(f)|
Frequency (Hz)
Single−Sided Amplitude Spectrum of f(t)
|F(f)|
Frequency (Hz)
dynamic stiffness K(f)
Real−|K(f)|
Frequency (Hz)
Coherence Function
Gamma2
Frequency (Hz)

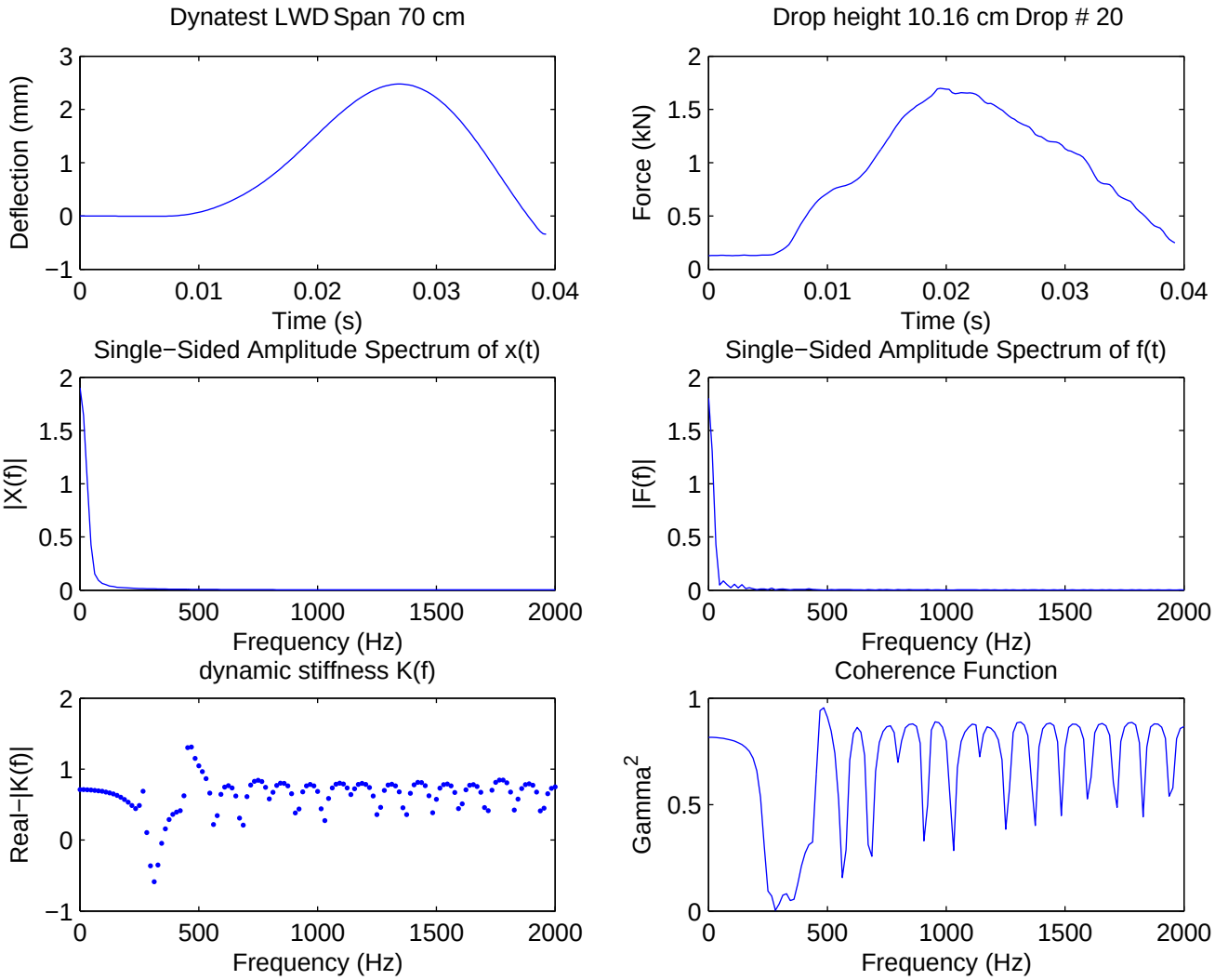
Dynatest LWD Span 70 cm
Deflection (mm)
Time (s)
Drop height 10.16 cm Drop # 20
Force (kN)
Time (s)
Single−Sided Amplitude Spectrum of x(t)
|X(f)|
Frequency (Hz)
Single−Sided Amplitude Spectrum of f(t)
|F(f)|
Frequency (Hz)
dynamic stiffness K(f)
Real−|K(f)|
Frequency (Hz)
Coherence Function
Gamma2
Frequency (Hz)

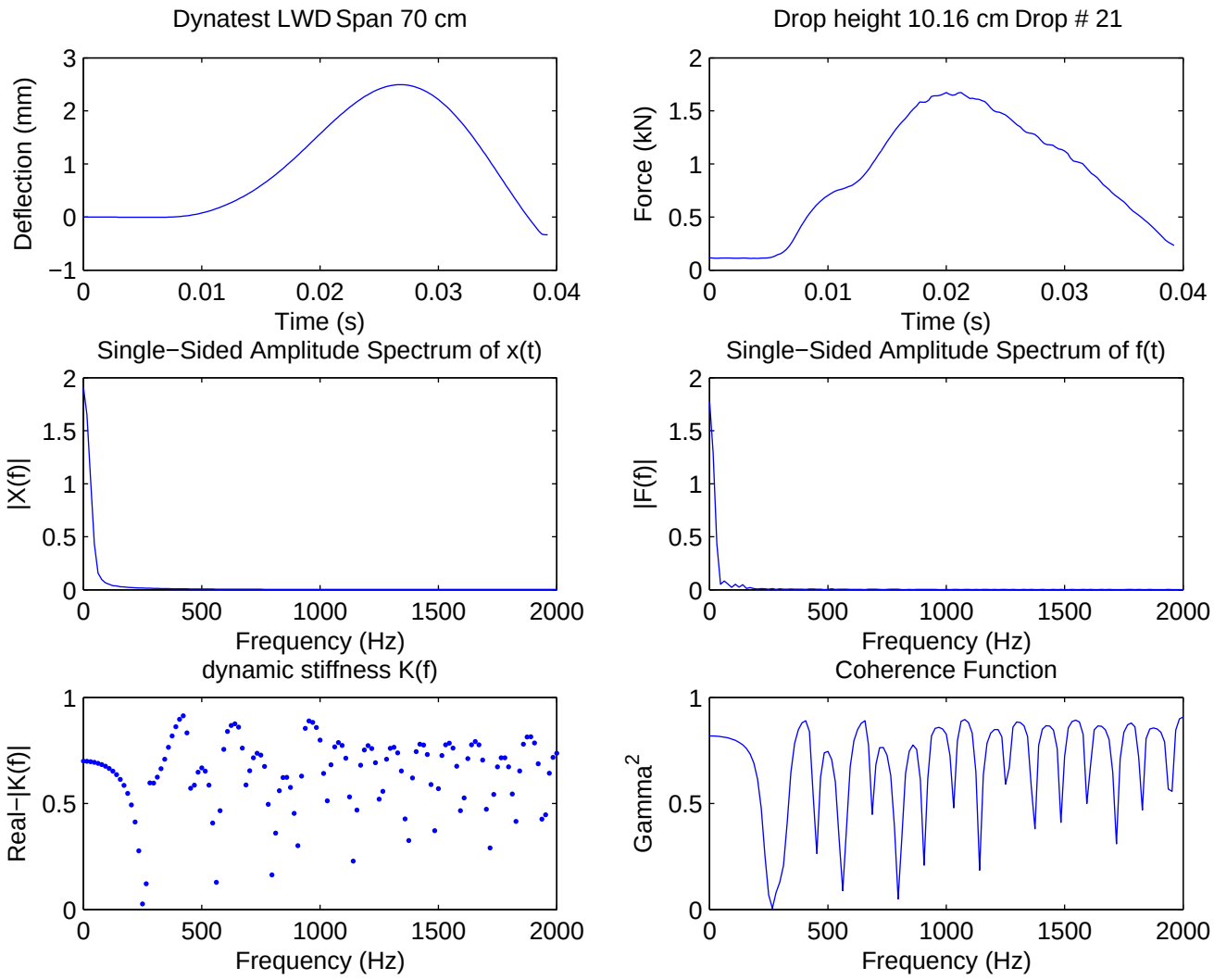
Dynatest LWD Span 70 cm
Deflection (mm)
Time (s)
Drop height 10.16 cm Drop # 21
Force (kN)
Time (s)
Single−Sided Amplitude Spectrum of x(t)
|X(f)|
Frequency (Hz)
Single−Sided Amplitude Spectrum of f(t)
|F(f)|
Frequency (Hz)
dynamic stiffness K(f)
Real−|K(f)|
Frequency (Hz)
Coherence Function
Gamma2
Frequency (Hz)

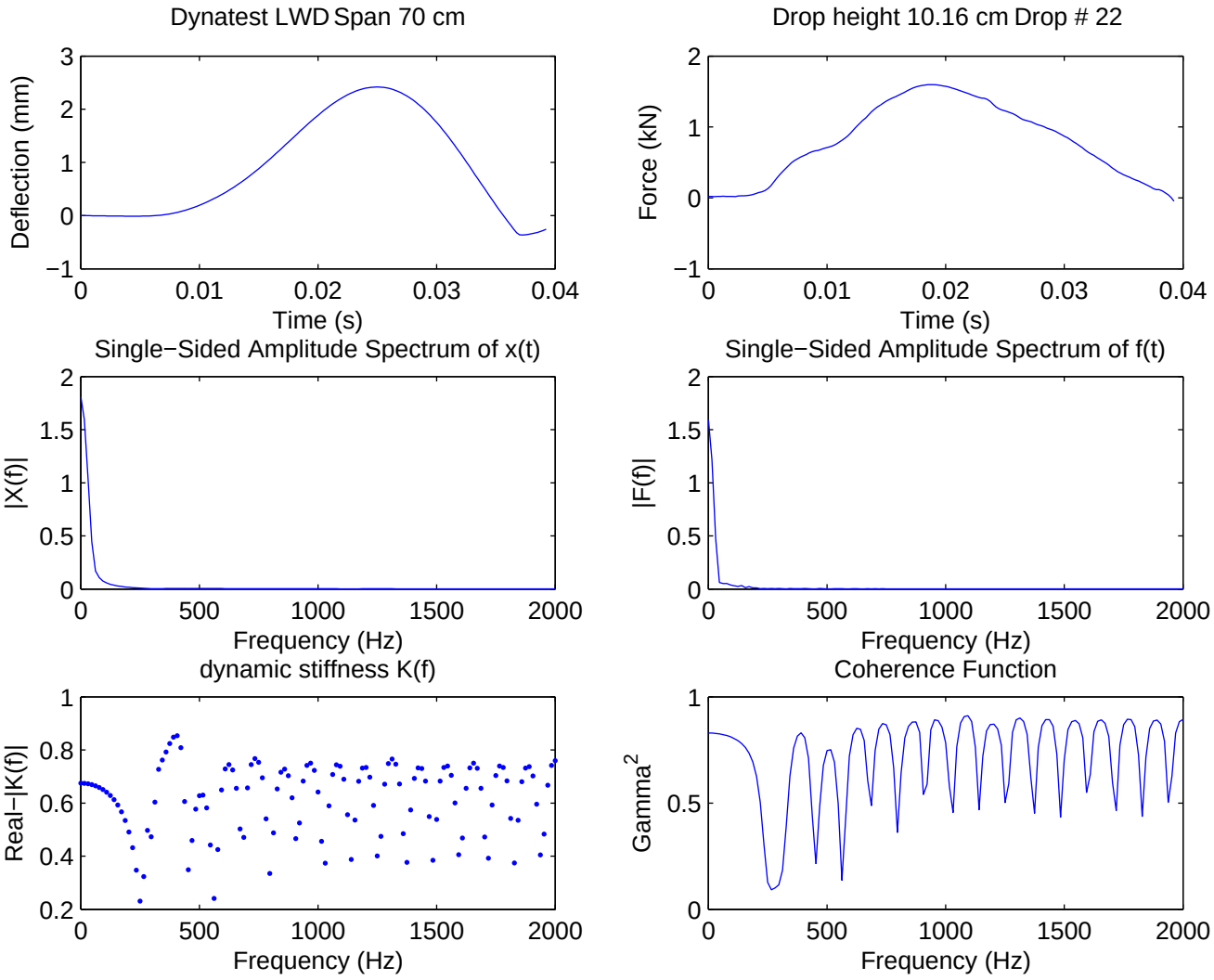
Dynatest LWD Span 70 cm
Deflection (mm)
Time (s)
Drop height 10.16 cm Drop # 22
Force (kN)
Time (s)
Single−Sided Amplitude Spectrum of x(t)
|X(f)|
Frequency (Hz)
Single−Sided Amplitude Spectrum of f(t)
|F(f)|
Frequency (Hz)
dynamic stiffness K(f)
Real−|K(f)|
Frequency (Hz)
Coherence Function
Gamma2
Frequency (Hz)

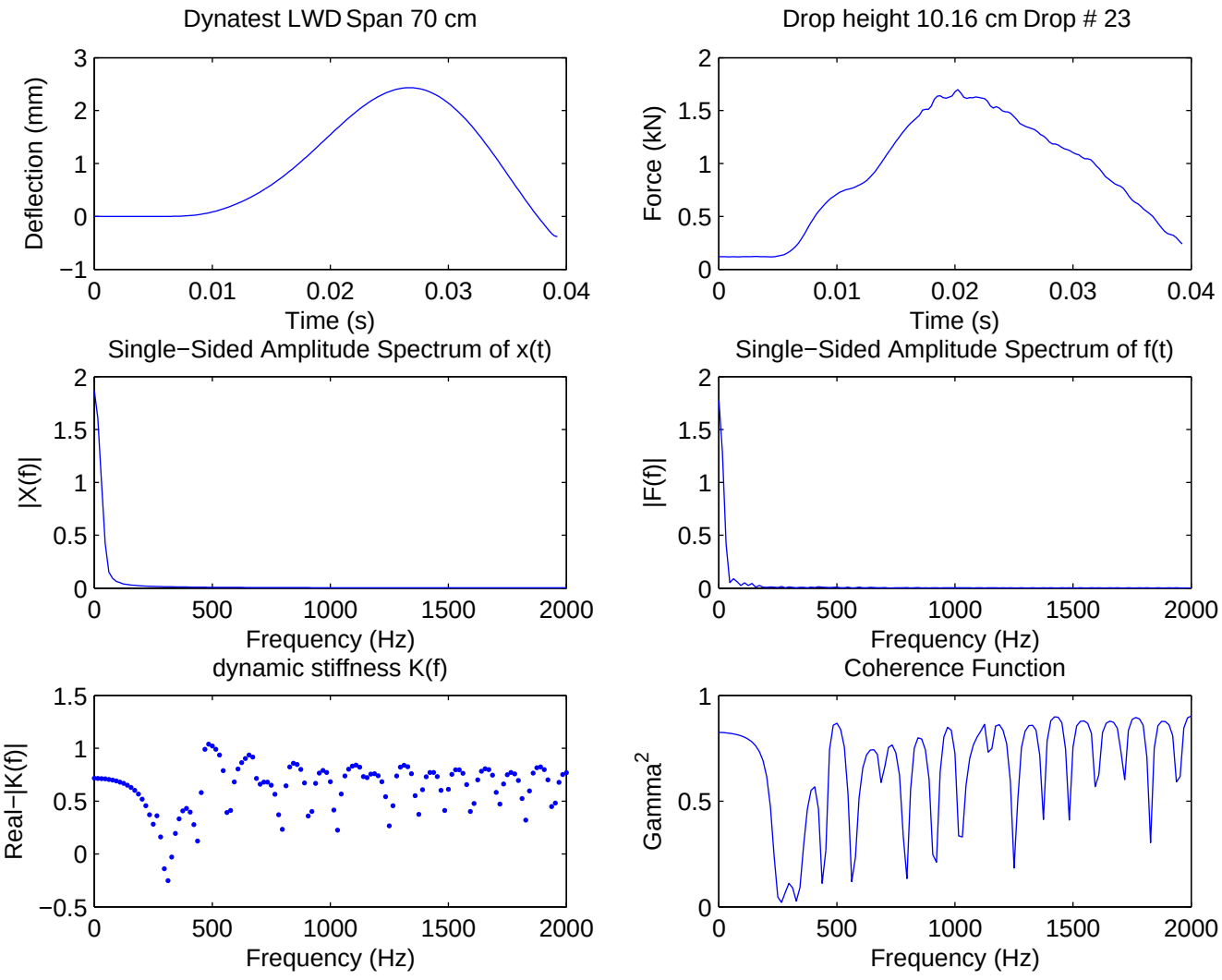
Dynatest LWD Span 70 cm
Deflection (mm)
Time (s)
Drop height 10.16 cm Drop # 23
Force (kN)
Time (s)
Single−Sided Amplitude Spectrum of x(t)
|X(f)|
Frequency (Hz)
Single−Sided Amplitude Spectrum of f(t)
|F(f)|
Frequency (Hz)
dynamic stiffness K(f)
Real−|K(f)|
Frequency (Hz)
Coherence Function
Gamma2
Frequency (Hz)

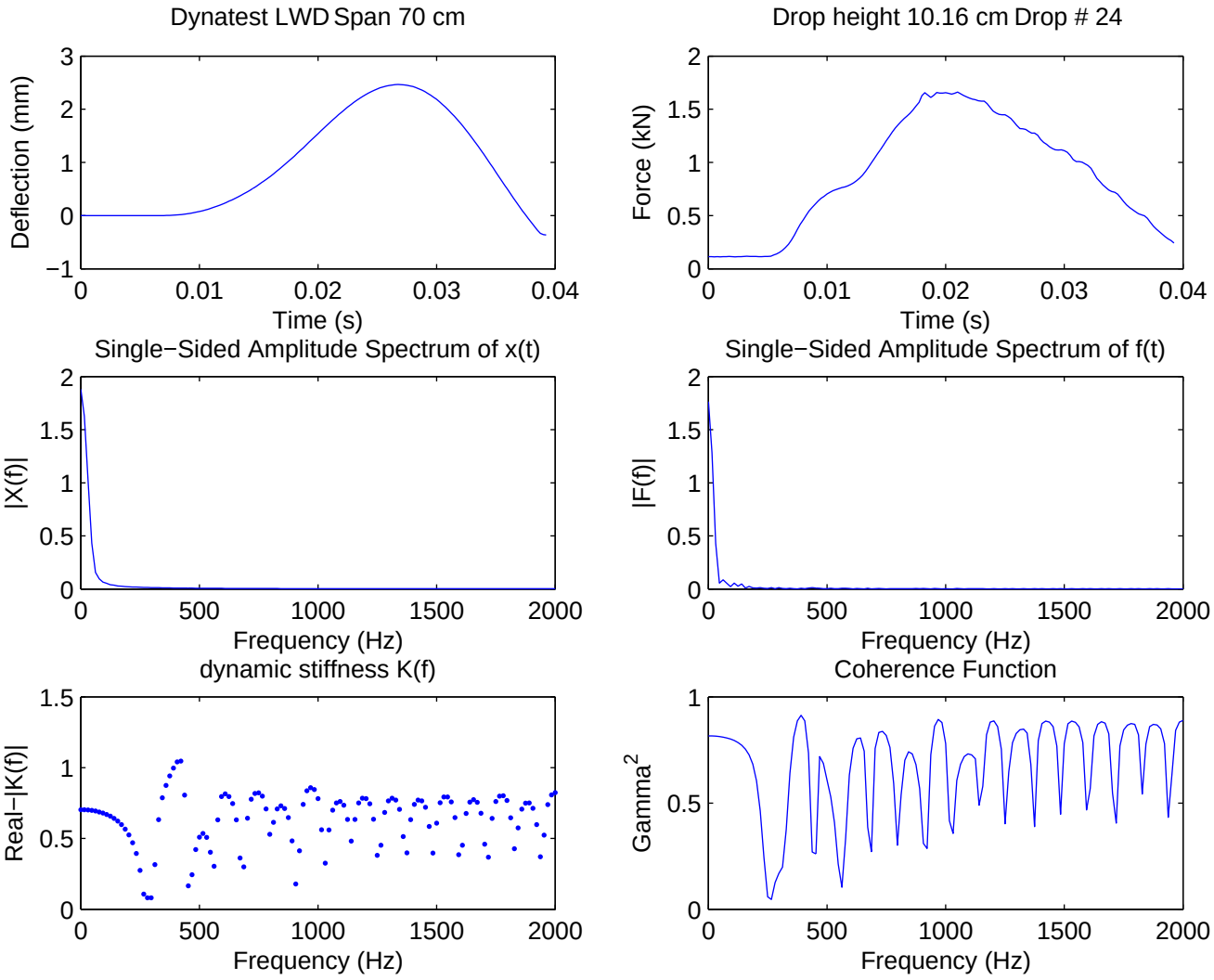
Dynatest LWD Span 70 cm
Deflection (mm)
Time (s)
Drop height 10.16 cm Drop # 24
Force (kN)
Time (s)
Single−Sided Amplitude Spectrum of x(t)
|X(f)|
Frequency (Hz)
Single−Sided Amplitude Spectrum of f(t)
|F(f)|
Frequency (Hz)
dynamic stiffness K(f)
Real−|K(f)|
Frequency (Hz)
Coherence Function
Gamma2
Frequency (Hz)

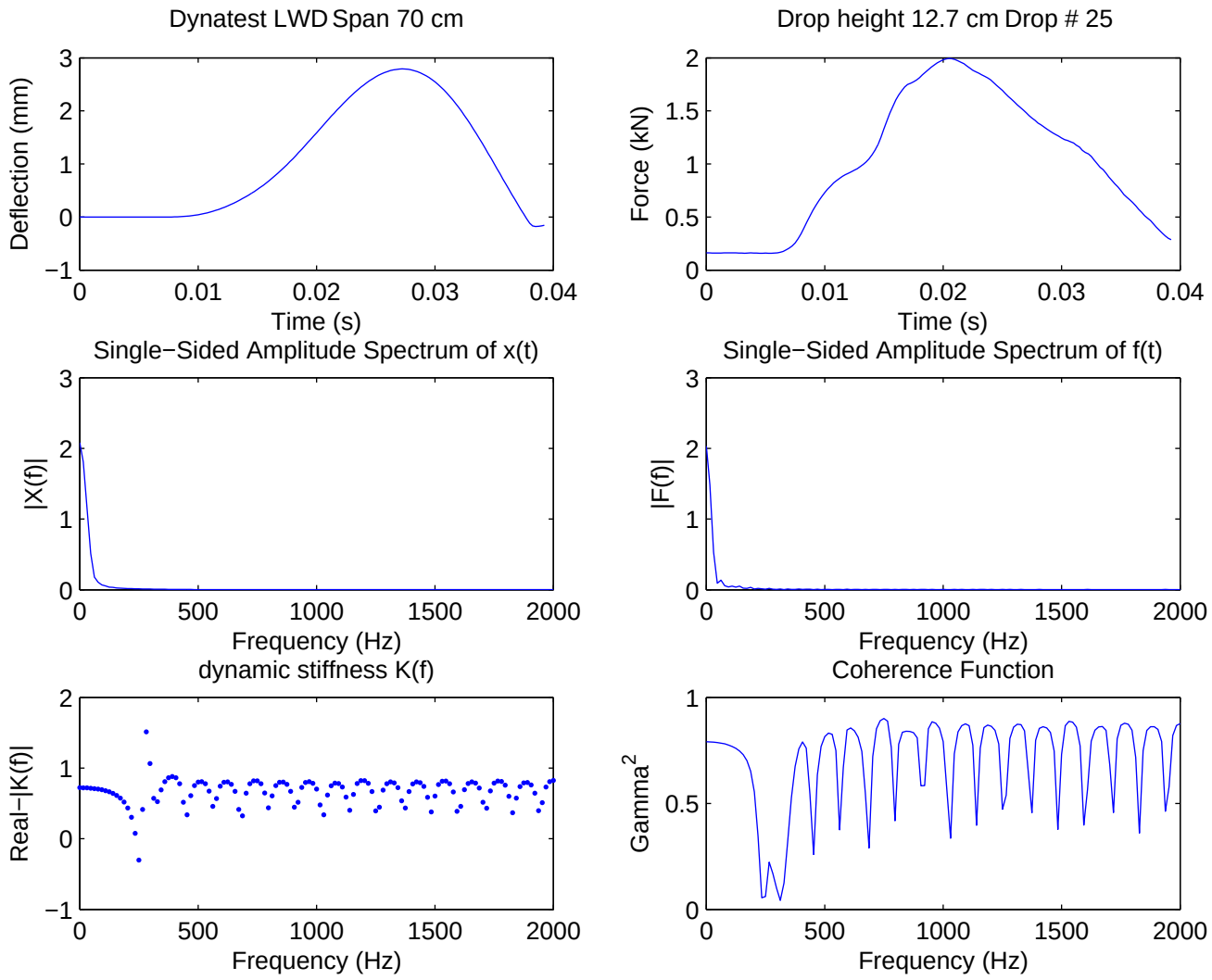
Dynatest LWD Span 70 cm
Deflection (mm)
Time (s)
Drop height 12.7 cm Drop # 25
Force (kN)
Time (s)
Single−Sided Amplitude Spectrum of x(t)
|X(f)|
Frequency (Hz)
Single−Sided Amplitude Spectrum of f(t)
|F(f)|
Frequency (Hz)
dynamic stiffness K(f)
Real−|K(f)|
Frequency (Hz)
Coherence Function
Gamma2
Frequency (Hz)

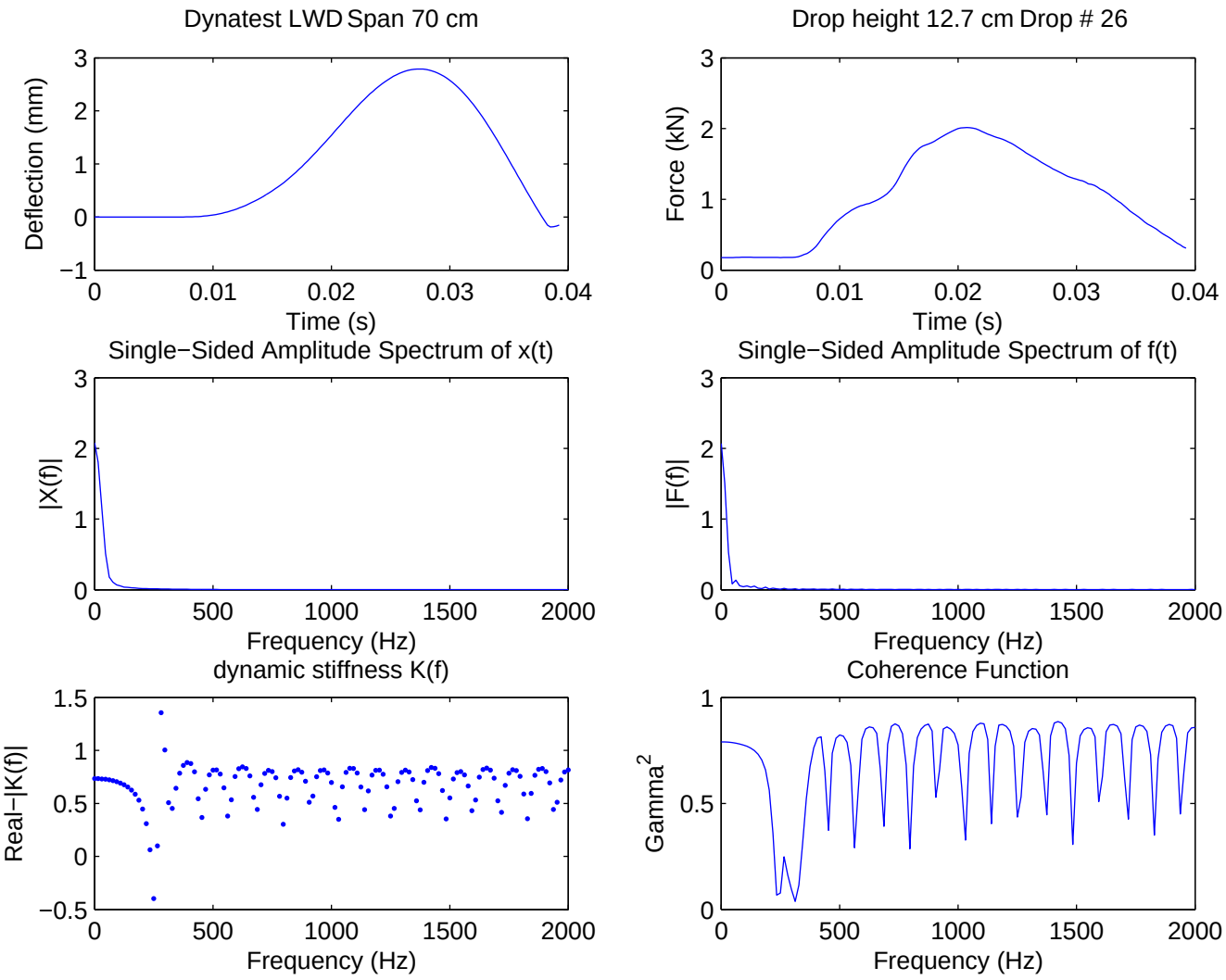
Dynatest LWD Span 70 cm
Deflection (mm)
Time (s)
Drop height 12.7 cm Drop # 26
Force (kN)
Time (s)
Single−Sided Amplitude Spectrum of x(t)
|X(f)|
Frequency (Hz)
Single−Sided Amplitude Spectrum of f(t)
|F(f)|
Frequency (Hz)
dynamic stiffness K(f)
Real−|K(f)|
Frequency (Hz)
Coherence Function
Gamma2
Frequency (Hz)

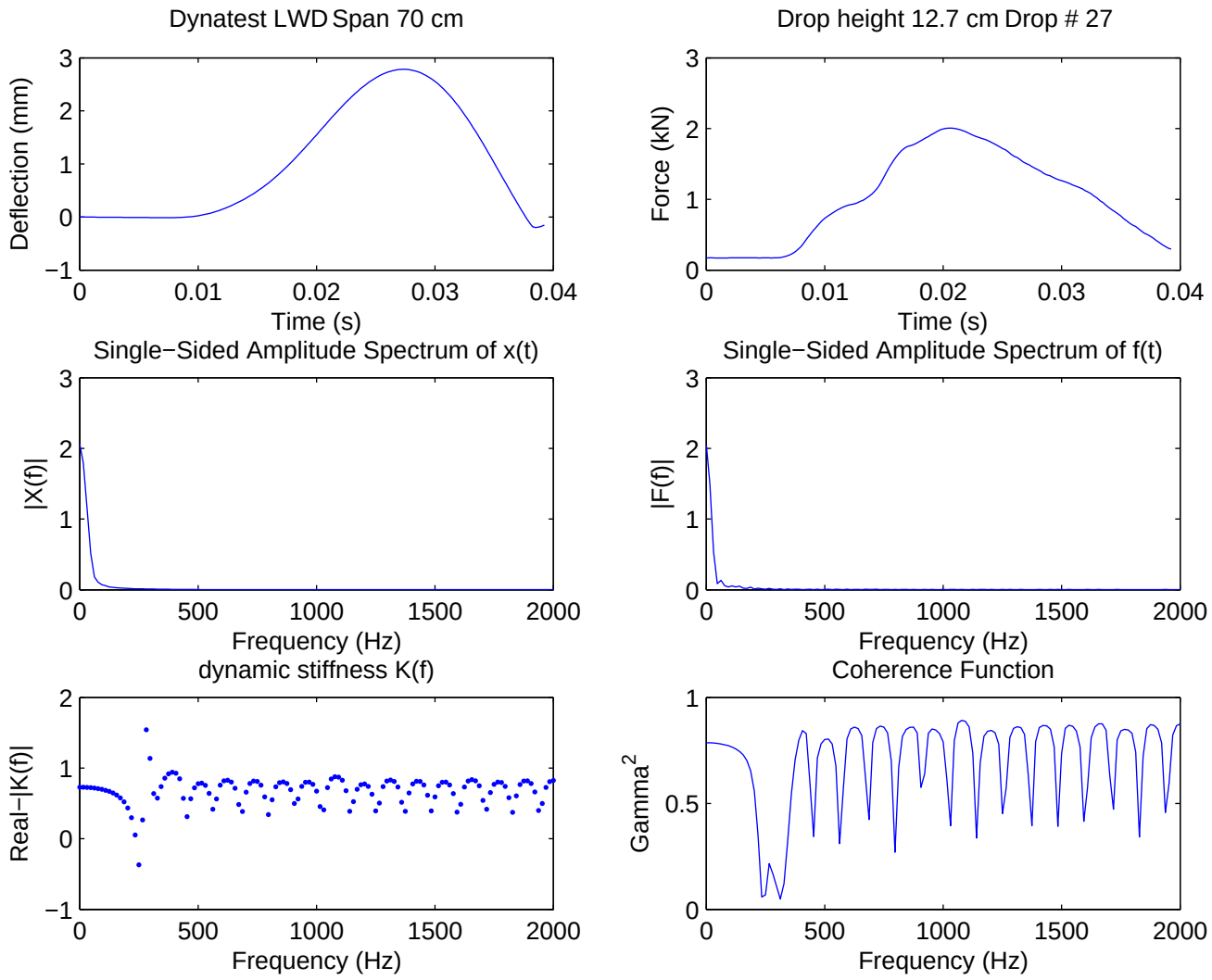
Dynatest LWD Span 70 cm
Deflection (mm)
Time (s)
Drop height 12.7 cm Drop # 27
Force (kN)
Time (s)
Single−Sided Amplitude Spectrum of x(t)
|X(f)|
Frequency (Hz)
Single−Sided Amplitude Spectrum of f(t)
|F(f)|
Frequency (Hz)
dynamic stiffness K(f)
Real−|K(f)|
Frequency (Hz)
Coherence Function
Gamma2
Frequency (Hz)

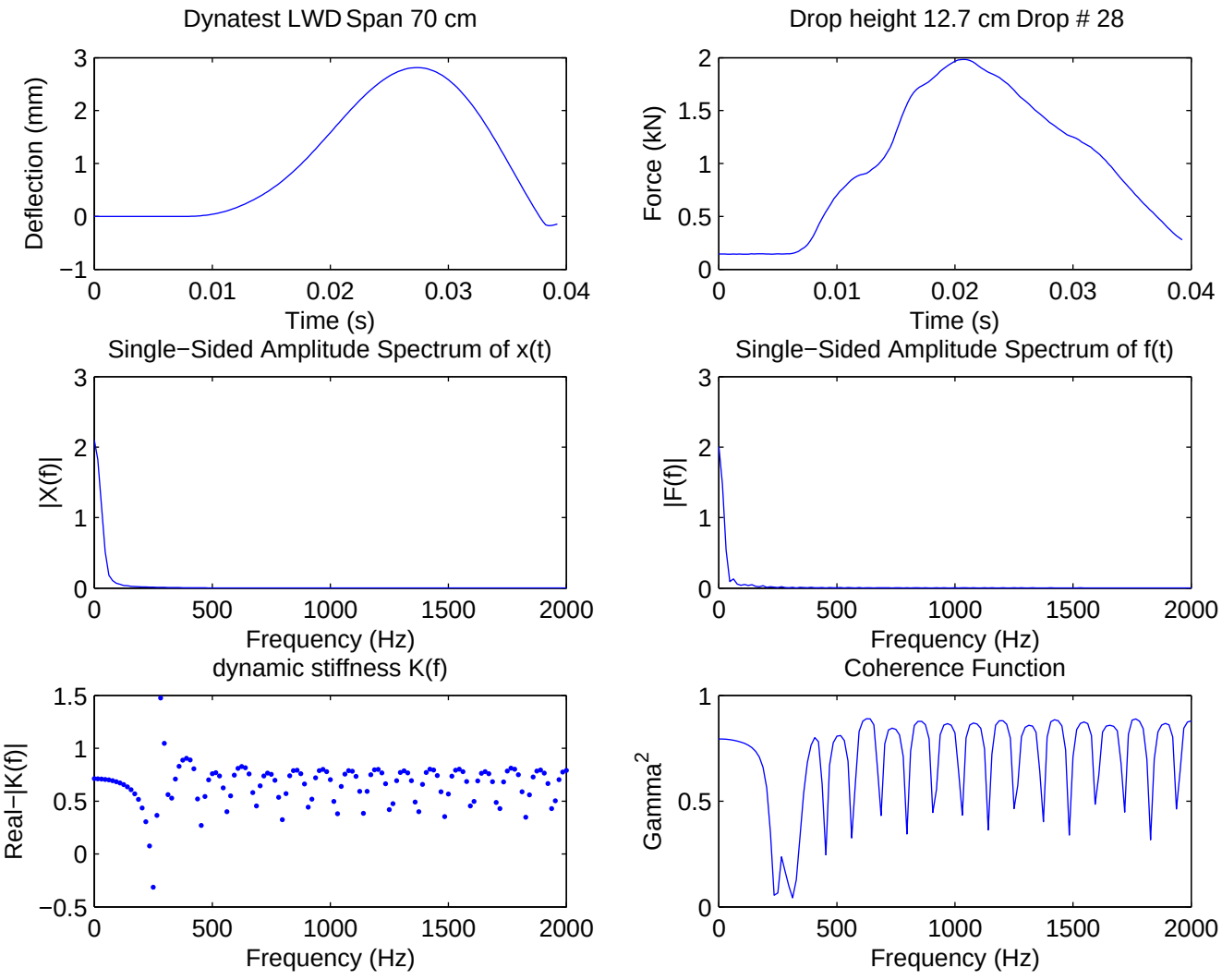
Dynatest LWD Span 70 cm
Deflection (mm)
Time (s)
Drop height 12.7 cm Drop # 28
Force (kN)
Time (s)
Single−Sided Amplitude Spectrum of x(t)
|X(f)|
Frequency (Hz)
Single−Sided Amplitude Spectrum of f(t)
|F(f)|
Frequency (Hz)
dynamic stiffness K(f)
Real−|K(f)|
Frequency (Hz)
Coherence Function
Gamma2
Frequency (Hz)

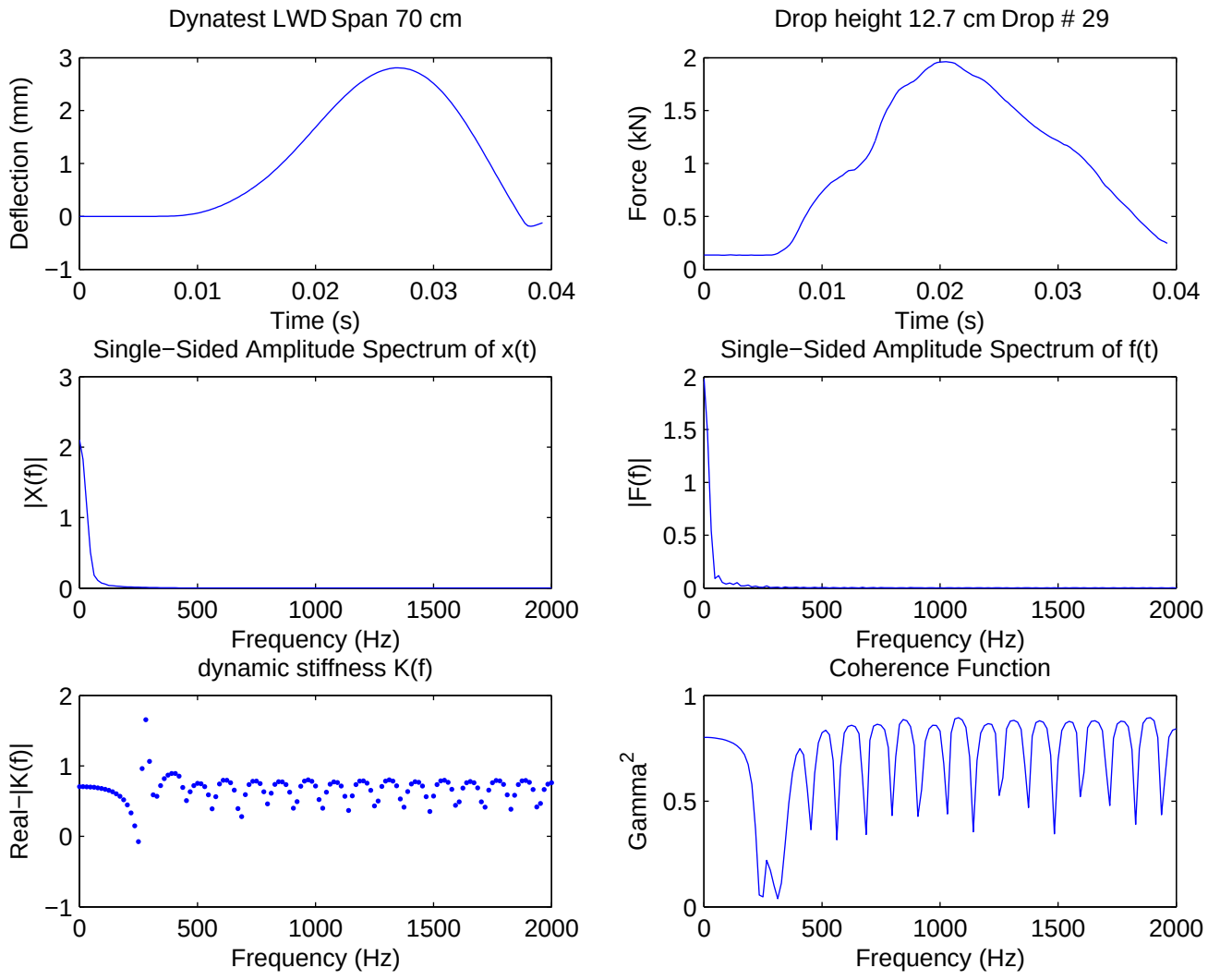
Dynatest LWD Span 70 cm
Deflection (mm)
Time (s)
Drop height 12.7 cm Drop # 29
Force (kN)
Time (s)
Single−Sided Amplitude Spectrum of x(t)
|X(f)|
Frequency (Hz)
Single−Sided Amplitude Spectrum of f(t)
|F(f)|
Frequency (Hz)
dynamic stiffness K(f)
Real−|K(f)|
Frequency (Hz)
Coherence Function
Gamma2
Frequency (Hz)

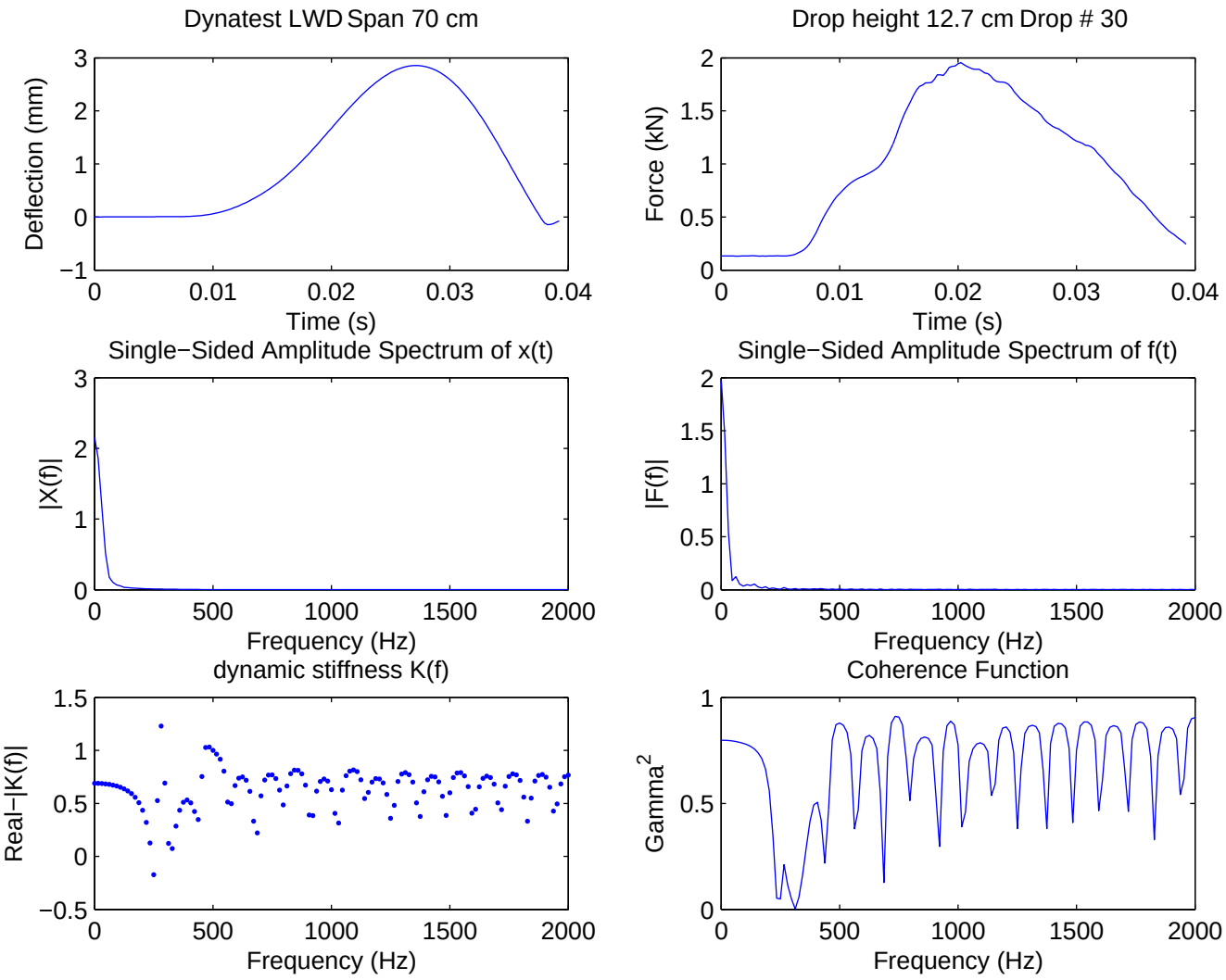
Dynatest LWD Span 70 cm
Deflection (mm)
Time (s)
Drop height 12.7 cm Drop # 30
Force (kN)
Time (s)
Single−Sided Amplitude Spectrum of x(t)
|X(f)|
Frequency (Hz)
Single−Sided Amplitude Spectrum of f(t)
|F(f)|
Frequency (Hz)
dynamic stiffness K(f)
Real−|K(f)|
Frequency (Hz)
Coherence Function
Gamma2
Frequency (Hz)

Chapter 7. References

1. Andrei, D. (2003). "Development of a predictive model for the resilient modulus of unbound materials." PhD diss., Arizona State University.
2. Bendat, J. S., & Piersol, A. G. (2011). *Random data: analysis and measurement procedures* (Vol. 729). John Wiley & Sons.
3. Bishop, A. W. (1960). *The principles of effective stress*. Norges Geotekniske Institutt.
4. Black, W. P. M. (1962). A Method of Estimating the California Bearing Ratio of Cohesive Soils from Plasticity Data*. *Geotechnique*, *12*(4), 271-282.
5. Davich, P., Camargo, F., Larsen, B., Roberson, R., & Siekmeier, J. (2006).*Validation of DCP and LWD moisture specifications for granular materials* (No. MN/RC-2006-20).
6. Decagon.com. Gs-1 Manual
7. Fleming, P. R., Frost, M. W., & Rogers, C. D. F. (2000). A comparison of devices for measuring stiffness in situ.
8. Fredlund, D. G., & Xing, A. (1994). "Equations for the soil-water characteristic curve." *Canadian Geotechnical Journal*, *31*(4), 521-532.
9. Geokon Instruction manual, Model 3500, 3510, 3515, 3600 earth pressure cells.
10. Gu, F., Sahin, H., Luo, X., Luo, R., & Lytton, R. L. (2014). "Estimation of Resilient Modulus of Unbound Aggregates Using Performance-Related Base Course Properties." *Journal of Materials in Civil Engineering*.
11. Guzina, B., & Osburn, R. (2002). Effective tool for enhancing elastostatic pavement diagnosis. *Transportation Research Record: Journal of the Transportation Research Board*, (1806), 30-37.
12. Hoffmann, O., Guzina, B., & Drescher, A. (2004). Stiffness estimates using portable deflectometers. *Transportation Research Record: Journal of the Transportation Research Board*, (1869), 59-66.
13. Khalili, N., and Khabbaz, M. H. (1998). "A unique relationship of chi for the determination of the shear strength of unsaturated soils." *Geotechnique* 48, no. 5.
14. Liang, R. Y., Rabab'ah, S., & Khasawneh, M. (2008). "Predicting moisture-dependent resilient modulus of cohesive soils using soil suction concept." *Journal of Transportation Engineering*, *134*(1), 34-40.
15. Lytton, R. L. (*1995).*"Foundations and pavements on unsaturated soils." *Proceedings of the first International Conference on Unsaturated Soils, unsat'95, Paris, France. 6-8 September 1995. Volume 3.*
16. Mooney, M. A., & Miller, P. K. (2009). Analysis of lightweight deflectometer test based on in situ stress and strain response. *Journal of Geotechnical and Geoenvironmental Engineering*.
17. Morgenstern, N. R. (1979). Properties of compacted soils. In *Contribution to panel discussion, Session IV, Proc., 6th Panamerican Conf. on Soil Mechanics and Foundation Engineering* (Vol. 3, pp. 349-354).

18. Nazzal, M. (2014). *Non-nuclear methods for compaction control of unbound materials* (No. Project 20-05, Topic 44-10).
19. Nazarian, S., Mazari, M., Abdallah, I. N., Puppala, A. J., & Mohammad, L. N. (2011). Modulus-based construction specification for compaction of earthwork and unbound aggregate. *Phase*, *1*, 10-84.
20. Perera, Y. Y., Zapata, C. E., Houston, W. N., & Houston, S. L. (2005). Prediction of the soil–water characteristic curve based on grain-size-distribution and index properties. *Advances in pavement engineering (ed. EM Rathje), Geotechnical Special Publication*, 130, 49-60.
21. Puppala, A. J., Transportation Research Board, & National Cooperative Highway Research Program Synthesis Program. (2009). *NCHRP Synthesis 382: Estimating Stiffness of Subgrade and Unbound Materials for Pavement Design*.
22. Roberson, R., & Siekmeier, J. (2002). Determining material moisture characteristics for pavement drainage and mechanistic empirical design. *Research Bulletin. Minnesota Department of Transportation. Office of Materials and Road Research*.
23. Senseney, C. T., Grasmick, J., & Mooney, M. A. (2014). Sensitivity of lightweight deflectometer deflections to layer stiffness via finite element analysis. *Canadian Geotechnical Journal*, *52*(999), 1-10.
24. Senseney, C. T., Krahenbuhl, R. A., & Mooney, M. A. (2012). Genetic algorithm to optimize layer parameters in light weight deflectometer backcalculation. *International Journal of Geomechanics*, *13*(4), 473-476.
25. Senseney, C., & Mooney, M. (2010). Characterization of Two-Layer Soil System Using a Lightweight Deflectometer with Radial Sensors. *Transportation Research Record: Journal of the Transportation Research Board*, (2186), 21-28.
26. Siekmeier, J. A. (2011). Unsaturated Soil Mechanics Implementation During Pavement Construction Quality Assurance. In *Proceeding of the 59 th Annual Geotechnical Engineering Conference* (pp. 179-188).
27. Siekmeier, J., Pinta, C., Merth, S., Jensen, J., Davich, P., Camargo, F., & Beyer, M. (2009). *Using the dynamic cone penetrometer and light weight deflectometer for construction quality assurance* (No. MN/RC 2009-12).
28. Siekmeier, J. A., Young, D., & Beberg, D. (2000). Comparison of the dynamic cone penetrometer with other tests during subgrade and granular base characterization in Minnesota. *ASTM Special Technical Publication*, *1375*, 175-188.
29. Stamp, D. H., & Mooney, M. A. (2013). Influence of lightweight deflectometer characteristics on deflection measurement. *Geotechnical Testing Journal*,*36*(2), 216-226.
30. Terzaghi, K., Peck, R. B., & Mesri, G. (1996). *Soil mechanics in engineering practice*. John Wiley & Sons.
31. Troxler RoadReader Model 3440 Moisture-Density Gauge, Manual of Operation and Instruction (2015). *Troxler Electronic Laboratories, Inc.* www.troxlerlabs.com.
32. Uzan, J. (1985). "Characterization of granular material." Transportation Research Record 1022, Transportation Research Board, Washington, DC, 52–59.

33. Vanapalli, S. K., Fredlund, D. G., & Pufahl, D. E. (1999). The influence of soil structure and stress history on the soil–water characteristics of a compacted till.*Geotechnique*, *49*(2), 143-159.
34. Vennapusa, P. K., & White, D. J. (2009). Comparison of light weight deflectometer measurements for pavement foundation materials. *ASTM geotechnical testing journal*, *32*(3), 239-251.
35. Yan, K. Z., Xu, H. B., & Shen, G. H. (2013). "Novel Approach to Resilient Modulus Using Routine Subgrade Soil Properties." *International Journal of Geomechanics*.